AGARD-R-710

AGARD

ADVISORY GROUP FOR AEROSPACE RESEARCH & DEVELOPMENT

7 RUE ANCELLE 92200 NEUILLY SUR SEINE FRANCE

AGARD REPORT No.710

Special Course on V/STOL Aerodynamics

NORTH ATLANTIC TREATY ORGANIZATION

NOTICE

THIS DOCUMENT HAS BEEN REPRODUCED FROM THE BEST COPY FURNISHED US BY THE SPONSORING AGENCY. ALTHOUGH IT IS RECOGNIZED THAT CERTAIN PORTIONS ARE ILLEGIBLE, IT IS BEING RELEASED IN THE INTEREST OF MAKING AVAILABLE AS MUCH INFORMATION AS POSSIBLE.

NORTH ATLANTIC TREATY ORGANIZATION

ADVISORY GROUP FOR AEROSPACE RESEARCH AND DEVELOPMENT

(ORGANISATION DU TRAITE DE L'ATLANTIQUE NORD)

AGARD Report No.710

SPECIAL COURSE ON V/STOL AERODYNAMICS

The material assembled in this book was prepared under the combined sponsorship of the Fluid Dynamics Panel, the von Kármán Institute and the Consultant and Exchange Program of AGARD and r ed as an AGARD Special Course at the von Kármán Institute, Rhode-St-Genèse, Belgiu . 14–18 May 1984 and 4–8 June 1984 at NASA Ames Research Center, Moffett Field, CA, USA.

THE MISSION OF AGARD

The mission of AGARD is to bring together the leading personalities of the NATO nations in the fields of science and technology relating to aerospace for the following purposes:

- Exchanging of scientific and technical information;
- Continuously stimulating advances in the aerospace sciences relevant to strengthening the common defence posture;
- Improving the co-operation among member nations in aerospace research and development;
- Providing scientific and technical advice and assistance to the North Atlantic Military Committee in the field of aerospace research and development;
- Rendering scientific and technical assistance, as requested, to other NATO bodies and to member nations in connection with research and development problems in the aerospace field;
- Providing assistance to member nations for the purpose of increasing their scientific and technical potential;
- Recommending effective ways for the member nations to use their research and development capabilities for the common benefit of the NATO community.

The highest authority within AGARD is the National Delegates Board consisting of officially appointed senior representatives from each member nation. The mission of AGARD is carried out through the Panels which are composed of experts appointed by the National Delegates, the Consultant and Exchange Programme and the Aerospace Applications Studies Programme. The results of AGARD work are reported to the member nations and the NATO Authorities through the AGARD series of publications of which this is one.

Participation in AGARD activities is by invitation only and is normally limited to citizens of the NATO nations.

Published April 1984

ISBN 92-835-1472-6

Printed by Specialised Printing Services Limited
40 Chigwell Lane, Loughton, Essex IG10 3TZ

PREFACE

The aim of the Special Course on V/STOL Aerodynamics was to outline and discuss the additional knowledge of aerodynamics needed to embark on the design of V/STOL aircraft. The influence of V/STOL features on wing design, layout considerations, engine and air intake considerations, effects of jet effluxes, wind tunnel and flight testing, manoeuvrability and control, performance assessment and special aspects of flight aerodynamics were discussed by nine lecturers at the course which was presented on 14–18 May 1984 at the von Kármán Institute Belgium, and on 4–8 June 1984 at the NASA Ames Research Center, USA under the joint sponsorship of the Institute, NASA, and the Fluid Dynamics Panel of AGARD.

SPECIAL COURSE STAFF

SPECIAL COURSE DIRECTOR: Mr C.' ?ore
Briti: erospace Kingston-Brough Division
Richmo.d Road
Kingston-upon-Thames
Surrey KT2 5QS
UK

LECTURERS

Mr W.P.Nelms
Aircraft Aerodynamics Branch
NASA Ames Research Center
Moffett Field
California 94035
USA

Dr D.R.Kotansky
McDonnell Aircraft Company
McDonnell Douglas Corporation
P.O. Box 516
St Louis
MO 63066
USA

Mr J.Fletcher
Head of Advanced Projects
British Aerospace PLC
Warton Division
Preston, Lancs PR4 1AX
UK

Dr J.A.Franklin
Chief, Flight Dynamics and Controls
NASA Ames Research Center
Moffett Field
California 94035
USA

Mr W.J.Lewis
Rolls Royce Ltd
Bristol Engine Division
P.O. Box 3
Filton
Bristol BS12 7QE
UK

Mr D.Koenig
Low Speed Aircraft Research Branch
Mail Code N 247-1
NASA Ames Research Center
Moffett Field
California 94035
USA

Mr D.C.Leyland
Deputy Chief Aerodynamicist
British Aerospace
Aircraft Group – Warton Division
Warton Aerodrome
Preston
Lancs PR4 1AX
UK

VKI COORDINATOR

Professor J.Sandford
Von Kármán Institute for Fluid Dynamics
Chaussée de Waterloo 72
B-1640 Rhode-Saint-Genèse
Belgium

AGARD REPRESENTATIVE

Mr R.H.Rollins, II
Executive, Fluid Dynamics Panel
AGARD
7 rue Ancelle
92200 Neuilly-sur-Seine
France

US COORDINATORS

Dr W.J. McCroskey
N 202A-1
Senior Staff Scientist
Ames Research Center
Moffett Field
CA 94035
USA

Dr G.K.Richey
Chief Scientist – Air Force Wright
Aeronautical Laboratories/FS
Wright Patterson AFB
Ohio 45433
USA

CONTENTS

V/STOL AERODYNAMICS – INTRODUCTION

by

C.L.Bore
Head of Research
British Aerospace PLC: Kingston
Richmond Road
Kingston-upon-Thames, Surrey KT2 5QS, UK.

Welcome to this Lecture Course on the Aerodynamics of V/STOL Aircraft. We have a lot of material to consider and discuss in the next five days, but I feel sure that with such an assembly of experienced aerodynamicists, both at the podium and in the audience, we will find the experience stimulating.

The special requirements of vertical take-off (and in practice more importantly, vertical landing) introduce a lot more complication into the aerodynamics. Indeed, if we were to consider every conceivable configuration in the time available, we would have to dig very shallowly. So immediately we excluded rotorcraft, and in view of the Fluid Dynamics Panel's Symposium on boundary layer control and high lift devices in Brussels in later May (21st-25th) it was decided to restrict consideration of high lift flaps.

When I was first asked to direct this course, my feelings were very mixed, for I knew that it would involve a lot of extra work, and my normal workload would not go away. However, I felt that the challenge was too big to miss. I knew that there was an important contribution that I could make, and that was to set up for the first time a lecture course in which the long experience of those actually responsible for the design of successful V/STOL aircraft would be brought out clearly. Even that would not be easy, for it remains a fact that we have so much work to do that we do not have much time to sit down and write lectures about it! That it why you will not find many reports by my colleagues in the published literature.

As soon as I wrote those words, I felt that they sounded a bit arrogant. Then, a few minutes later, I came across a quotation of Samuel Butler, which makes my sentiments seem almost respectable: "An art can only be learned in the workshop of those who are winning their bread by it."

Before going into the aims of the course and the programme of lectures, let us emphasise the main differences between a course and a symposium. In a symposium, we tend to ask people to write about their latest advances - the most recent triumphs that they have won. If no-one responds on a particular topic, then we cannot deal with it. Each lecturer tends to dwell on his own work, rather than going over the work of others. A course is different in several ways. The ground to be covered comes first, and all the topics have to be addressed. Some of these topics have roots in the past, so they will not deal exclusively with the latest triumphs of science or technology. Since we can afford only a limited number of lecturers, each one may have to cover ground that is not entirely his own speciality, and may have to include material from colleagues.

For this course, we assume that all participants are familiar with the aerodynamics of conventional aircraft, but not necessarily familiar with the whole field of V/STOL aerodynamics. When designing V/STOL aircraft (or STOVL aircraft) we find two important extensions of scope. Firstly we have to deal with the complicated airflows that occur at speeds below that for wing-borne flight, and secondly we find that we have to deal with quite unfamiliar configurations, aerodynamically - even if they may <u>look</u> familiar!

BASIC AIMS OF THE COURSE

- To provide a general appreciation of the special features of V/STOL aerodynamics.
- To concentrate on matters of practical importance, rather than those of mainly academic interest.
- To illustrate the approaches used by people who have experience in the aerodynamics of V/STOL.
- To compare the approaches used on either side of the Atlantic.

TOPICS TO BE COVERED

- Introduction.
- Review of Previous Symposiums.
- Influence of V/STOL on Wing Design.
- Layout Considerations: US View.
- Layout Considerations: European View.
- Engine and Air Intake Considerations.
- Effects Induced by Jet Effluxes.
- Manoeuvrability and Control.
- Wind Tunnel Testing.
- Other Ground-borne Testing.
- Performance Assessment: UK View.
- Performance Assessment: US View.
- Special Flight Aspects.
- Short Contributions and Discussion.

By the time we have worked through to the end of that menu, every one of us should know more about the subject as a whole! Already we have got to the end of the introduction, and now we are ready for the review of the previous symposiums.

INTRODUCTION AND REVIEW OF SOME JET INTERFERENCE PHENOMENA RELEVANT TO V/STOL AIRCRAFT

E. C. P. Ransom
Senior Lecturer in Aircraft Propulsion
School of Mechanical Aeronautical & Production Engineering,
Kingston Polytechnic
Kingston-upon-Thames, Surrey, U.K.

J. R. Smy
Aerodynamics Department
British Aerospace P.L.C.
Kingston-upon-Thames, Surrey, U.K.

SUMMARY

This introductory paper summarises and discusses aspects of some fluid flows relevant to V/STOL aircraft. The principal sources of reference are the contributions to AGARD conferences which have been specifically concerned with V/STOL aerodynamics. Initially consideration has been given to the behaviour of single axisymmetric jets discharging into stationary surroundings and the creation of the corresponding flow field. The effect that a change of fluid properties has on the flow field and plume development is then described and is extended to include jets discharging into a cross flow and into a coflowing stream. The aerodynamics of jets impinging on adjacent surfaces are reviewed with particular reference to induced lift losses generated during hovering in ground effect, to ground erosion and to recirculation. Internal fluid flows in thrust augmentors are described including the effect of losses, and the generation of unsteady flows which are used to enhance mixing rates. The paper concludes with a brief discussion of modelling techniques and wind tunnel methods including interference effects.

INTRODUCTION

This paper represents an attempt to summarize the results and conclusions of research work which has been carried out in order to gain a deeper understanding of the aerodynamics of V/STOL aircraft. The sources of reference used are principally those papers presented at conferences organised by the Fluid Dynamics Panel of AGARD. In particular there have been two Symposia specifically devoted to the aerodynamics of V/STOL aircraft and it is information from papers contributed to these conferences that have formed the basis of this lecture. They are:-

AGARD CP 143	"V/STOL Aerodynamics"	Delft: April 1974
AGARD CP 308	"Fluid Dynamics of Jets with applications to V/STOL"	Lisbon: November 1981

Another useful source of information is:-

AGARD CP 135	"V/STOL Propulsion Systems"	Schiersee: 1973

In addition it has been necessary to consult the following conference proceedings:-

AGARD CP 126	"Military Applications of V/STOL Aircraft"	Brussels: 1972
AGARD CP 22	"Fluid dynamics of Rotor and Fan Supported Aircraft at subsonic speeds"	Goettingen: 1967
AGARD CP 174	"Wind Tunnel Design and Testing Techniques"	London: October 1975
AGARD CP 187	"Flight/Ground Testing facilities Correlation"	Valloire: 1975

All forms of powered lift have been considered but inevitably the emphasis is on jet lift systems. It is left for later presentations to deal with detailed observations and reports of the most recent developments, here the authors have attempted only to highlight some of the more important features of flow of direct application to V/STOL aircraft.

Flow phenomena are considered under the following sub headings:-

1. Jet Structure
   - 1.1 Jets discharging into still air
   - 1.2 Jets discharging into a coflowing stream
   - 1.3 Jets discharging into a cross flow
2. Jets interacting with surfaces
3. Thrust Augmenters
4. Theoretical Models
5. Wind Tunnel Simulation

1. JET STRUCTURE

In order to understand the behaviour of jets and wakes in relation to their effect upon the flow field, and upon induced forces and moments on a V/STOL airframe, some knowledge of the basic properties of simple jets is essential. However the extrapolation of data obtained from basic jet research in order to predict effects on real aircraft may be misleading since the properties of jets produced by gas turbine engines may be very different from jets examined in the laboratory. Much of the fundamental data which has been widely reported and often used for full scale performance predictions, has been obtained using small scale experimental equipment. Table 1 (1) tabulates the jet Reynolds Numbers for a series of well known experiments. Often these are less than 1×10^6 whereas in practical application jet Reynolds Numbers are likely to be much greater. In addition although not quoted here, Mach Numbers for the model jet flows are also unrepresentative. A second effect is due to the different thermodynamic properties exhibited by jets used in model tests and the jets discharged by V/STOL aircraft. Unfortunately use of such data is often unavoidable, but it is not thought to be of great significance except of course where the data results from tests on water jets. A perhaps more important factor is the use of data obtained from cool jets of low initial turbulence, uniform velocity profiles and in the absence of jet swirl. In practice jets emanating from propulsion gas turbines are at elevated temperature, with high turbulence levels, non uniform velocity profiles and in many cases velocity components normal to the flow direction.

The following sections illustrate the basic parameters affecting jet flow. From this it is possible to gain some insight to the structure of the flow even when it is modified by the factors noted above.

It is helpful to consider Table 2 (2) which perhaps over simplifies the situation concerning jet interference phenomena. This identifies the link between independent variables, the flow field which arises as a result of the interaction between the jet and its surroundings and corresponding induced effects which are apparent on the surface of the airframe or the ground. For convenience, the following three categories of jet flow are considered:-

Free jets emanating into stationary surroundings

Jets discharging into a parallel flowing stream

Jets emanating into a crossflow

1.1 FREE JETS EMANATING INTO STATIONARY SURROUNDINGS

Fig.1 (3) illustrates the classic form of the axisymmetric free jet, emanating from a symmetrical plenum chamber with a large contraction ratio and a nozzle of short length. Two basic regions are commonly identified, the short potential core region which encloses a conical volume of constant velocity followed by a fully turbulent region.

The decay of axial velocity along the centre line for such a jet is shown in fig.2 (3) together with typical curve fit equations. In addition the variation of turbulence intensity with axial distance is also given. Such jets exhibit potential core lengths typically 6 nozzle diameters long.

The influence of plenum chamber and nozzle geometry on velocity decay is indicated in fig.3. The tests reported by ref.4 show how sensitive jet properties are to plenum shape. This has particular significance for wind tunnel models which simulate the action of lifting jets and where sufficient space for the installation of lifting jet nozzles is not available. Fig.4 (5) shows a design developed for use in such models which has achieved some success.

However as fig.4 shows, the decay of axial velocity apparently is sensitive to jet Mach or Reynolds Numbers. Bradbury (3) suggests that small changes in flow angle might be responsible for this behaviour although research has not conclusively demonstrated this. The evidence in support has been obtained from experiments in which square tabs are introduced at the nozzle exit.

Fig.5 (3) indicates the change in velocity decay created by the presence of different numbers of tabs. Measurements within the jet flow show that considerable variations of flow angle with circumferential location occur and for that reason it is perhaps not surprising that the presence of two tabs only have the greatest effect upon velocity decay.

Corresponding measurements of turbulence in jets show that in highly turbulent jets, the decay of axial velocity takes place more rapidly. Mathier and Charnay (6) present data showing the distribution of intensity of turbulence, and velocity across the jet and along its trajectory. They show that the distribution of temperature in a heated jet exhibits a similar distribution to that of velocity.

The flow field created by these jets is dominated by turbulent entrainment. Several practical measurements of entrainment have been carried out (7, 8, 9) using a variety of techniques. Ricou and Spalding (7) deduced the following relationships using jets of gases of different species over a range of temperatures.

$$\frac{m}{mj} = 0.32 \frac{x}{dj} \left(\frac{\rho_\infty}{\rho_j}\right)^{\frac{1}{2}} \qquad \text{——— 1}$$

where
- m = mass flow rate
- mj = mass flow rate at nozzle exit
- dj = nozzle diameter
- x = distance from nozzle
- ρ_∞ = density of entrained fluid
- ρ_j = density of jet fluid

The results indicate the bulk entrainment over the total length of jet studied, and do not reveal the distrubution of entrainment along the jet trajectory.

Fig.6 (2) compares this data with that obtained by Schwantes (8) for a sonic jet and Fig.7 (10) gives similar data obtained by a gas tracer technique for entrainment into a subsonic jet. This indicates that entrainment in the potential core region may be of a different magnitude to that in the fully developed region.

It was pointed out by Schwantes that the initial temperature affects the jet characteristics by increasing the turbulence levels and decay rates, and that there was a need for much more comprehensive examination of the effect of temperature on the flow field and its influence upon induced pressure distributions and forces. The comparison with the data obtained by Ricou and Spalding (7) is rather poor and a further examination of all the data available together with some more experimentation is clearly desirable.

One of the factors which arises from this work is that it is perhaps more important to know the point along the jet trajectory where entrainment is a maximum, rather than the total amount of entrainment. This is because high entrainment concentrated in the region close to the nozzle exit has a much more severe effect upon the extent and intensity of a pressure field adjacent to a surface than the same total entrainment spread more evenly along the trajectory. Apart from a brief comment by Williams and Wood (11) there appears to be little information about the forces and pressure distributions created by hot gas jets in cold surroundings.

Entrainment rates into free jets may be accelerated by increasing the number of turbulent eddies in the jet (12), by acoustic excitations (13), or by introducing unsteadiness into the jet flow by pulsations and or flapping (14, 15, 16). The objective of these techniques is to provide an efficient means of increasing the rate of mixing between the jet flow and the surroundings. This is of particular significance for the design of effective thrust augmentors which have applications in V/STOL aircraft (see Section3). The induced pressure distribution over a flat surface normal to the jet axis, may be calculated using a simple potential flow model with sinks distributed along the axis of the jet in proportion to the entrainment. It may be demonstrated that the pressure distribution is quite sensitive to changes of entrainment rate close to the nozzle exit (9).

The effect of jet velocity profile on the induced interference force has been demonstrated clearly by Mayson et al (18). In a coaxial jet rig changes in the velocity of flow in the core jet and annular jet are shown to have a significant influence upon the interference force. Fig.8.

1.2 JETS IN CO-FLOWING STREAM

Although this is not a primary problem in the design of V/STOL aircraft, it is an important flow regime which has application for all aircraft. Indeed some aspects may have particular significance for the designers of V/STOL aircraft. Zacharias (17) shows that boat tail angle affects jet plume properties by influencing the flow of entrained air. This is reflected in the magnitude of pressure drag created by the jet.

1.3 JETS IN CROSS FLOW

A jet discharging into a crossflow deflects downstream forming a curved trajectory and develops a pair of spreading contra rotating vortices. Although numerous attempts have been made at predicting the development of the normal jet using potential flow solutions none has yet proved to be entirely satisfactory. Bradbury (3) explains that the two approaches either lead to an assumption of very high entrainment rates (19) not apparent in jets discharging into still or coflowing streams or to drag coefficients which seem rather high.

Numerous experimental determinations of jet trajectory have been carried out and a selection of empirical equations which correlate particular jet properties are given in Table 3 (1). Clearly it is important to specify which property is under consideration in each equation, and this no doubt partly explains the discrepancy between the equations given in Table 3. For example the locus of maximum stagnation pressure is not coincident with the line connecting the vortex centres. (Fig 9). The reports however do not always state if wind tunnel wall and boundary layer effects have been taken into account. Nor do they report on the condition of the jet as regards velocity profile or turbulence.

When a crossflow passes over a surface, it normally establishes a boundary layer and a pressure distribution. In the case of aerodynamically shaped surfaces such as aerofoils the pressure distribtuion is exploited to provide lift forces. The presence of a jet discharging from a nozzle where the exit is coincident with the surface, considerably modifies the pressure distribution in the vicinity of the jet, with consequent change in both lift and drag forces. The pricipal influences upon the magnitude of pressures and forces are jet velocity and cross flow velocity although other features such as surface and nozzle geometry may have some effect. Data therefore is related to some function of the ratio between jet and cross flow velocity. Where density differences between jet and crossflow fluid exist it may be shown that momentum ratio is a significant variable.

There is some indication (2) that there is a change in flow characteristics occuring at velocity ratios around 6:1. Fig 10 shows a comparison between the pressure distribution of a flat surface and that over a wing obtained at identical flow conditions.

At velocity ratios in excess of 6, the pressure distributions exhibit considerable similarity but at lower velocity ratios similarity was not present. Mikolowsky (20) concluded that in the upper range of velocity ratios, the flow field was almost independent of surface geometry. In the lower range it was suggested that the flow field exhibited some of the characteristics of the jet flap. Use of an oil film technique to visualise the flow over the upper surface of the wing, indicated that the upper surface flow was affected by the jet, since streamlines tended to turn inwards towards the jet at the trailing edge of the wing.

Nearly all research effort has concentrated upon the characteristics of an axisymmetric jet, since this is the preferred configuration of V/STOL applications. Fig 11 shows the interference pressure fields generated by jets from nozzles of non circular and circular cross sections emerging into a crossflow.

Jets presenting a narrow edge to the crossflow create a pressure distribution in which the lateral spread is less than that due to the circular jet or the jet presenting a broad face.

In the latter case there is a larger blockage, and the distance over which the wake persists is much longer. Upstream of the jet, the area and intensity of the positive pressure zone is greater when the broad face is presented to the crossflow. (21, 22).

The position of the centre of pressure is also affected by nozzle shape. Compared with the circular nozzle, the centre of pressure for the narrow jet is between $\frac{1}{2}$ to $1\frac{1}{2}$ diameters upstream whereas for the broad faced jet centre of pressure moves downstream for all velocity ratios (21).

Another variable which is of concern to the designers of jet lift aircraft is angle of inclination of jet axis to the crossflow. Taylor and Watkins (23) present data for an axisymmetric jet discharging downstream at an angle measured with respect to an axis in the plane of the flat surface. The test rig has the nozzle exit flush with the flat surface so that viewed from above, the nozzle exit appears oval in shape.

Examination of pressure coefficient contours reveals that for a fixed velocity ratio and as the angle of inclination is reduced the low pressure field becomes less extensive in front of and to the sides of the jet. In addition the suction force coefficient reduced and the centre of pressure moved downstream. Further the effect of velocity ratio has been examined and there is apparently good correlation for suction force coefficient and centre of pressure with velocity ratio and jet inclination. (See Fig. 12 & 13).

2. IMPINGEMENT OF JETS ON TO A SURFACE

A flight regime of particular significance for jet lift STOVL aircraft is that during hover close to the ground. The flow beneath and around the airframe gives rise to a number of different but interrelated aerodynamic phenomena and these may be summarised as follows:-

Ground effect lift loss

Ground erosion

Recirculation

2.1 GROUND EFFECT LIFT LOSS

Single Jets

A single axisymmetric jet impacting normally to a surface exhibits three distinct regions (23).

(1) A free turbulent jet region in which the jet behaves in an identical way to a free jet. Depending upon the magnitude of the vertical height H and the nozzle exit diameter dj the region may include the potential core, a transition zone, and a fully developed zone.

(2) An impingement region in which the jet flow is deflected from a direction normal to the surface, to a direction approximately parallel to the surface.

(3) A wall jet region, in which the general flow direction is almost parallel to the wall.

For the configuration as shown in fig.14 where there are no surfaces adjacent to the nozzle exit, the flow around the jet is governed by the rate of entrainment into the jet. Research suggests that it is the wall jet which generates the major component of this entrainment (8, 25, 26). It is well known that the wall jet thickness δ approximately varies as the radius from the jet centre line, r, and the peak velocity varies as $1/r$ so that the rate of change of mass flow with radius dm/dr is constant.

Arbuckle and Searle (25,26) employed a similar technique to that first developed by Ricou and Spalding (7), to measure the entrainment into an axisymmetric jet impinging on to a normal surface. Using a jet of low initial turbulence and a potential core length of five jet diameters, the following relationship has been obtained:-

$$\frac{m}{m_J} = 0.68 \frac{r}{dj} \left(\frac{Tj}{T_\infty}\right)^{1/2} \qquad \text{——— 2}$$

where dj = initial jet diameter
Tj = temperature of jet fluid
Ti = temperature of entrained fluid

The above equation represents entrainment into all regions of the impinging jet.

Schwantes (8) from measurements of velocity in the wall jet created by an impinging jet with an initial Mach No. of 1 and a range of temperatures, obtained entrainment data (fig.15).

General agreement exists between data obtained from each source, including the effect of nozzle height and the effect of jet temperature.

The data from Arbuckle (25) and Searle (26) shows an increase in entrainment of about 20% as the vertical height increased from 1.5 to 10 nozzle diameters, although this effect is not included in equation (2). The data obtained by Schwantes (8) indicates a somewhat greater increase in entrainment for a height increase from 3 to 10 nozzle diameters. As already noted the data from each source are not strictly comparable since that obtained by Arbuckle and Searle includes entrainment into both free and wall jets.

The magnitude and distribution of the induced pressure field is affected by the configuration of the shape surrounding the nozzle, its location in relation to the nozzle exit, and the vertical distance from nozzle exit to the ground. This is illustrated in fig.16 (27).

Clearly what is happening is that entrained flow into the wall jet and free jet parts of the flow system is impeded by the presence of a baffle plate, and this has a corresponding effect upon the induced pressure field and hence lift loss.

The following considerations have been used by Welte (28) to show the relationship between the interference lift loss ΔL, the baffle plate areas and the height between nozzle exit and the ground, H (see fig.17).

For the case of an axisymmetric jet impinging normally on to a flat surface, a representative velocity V' at a point within the wall jet may be shown to be proportional to the jet diameter of the jet velocity vj and inversely proportional to the height h' above the surface such that

$$V' = V_j \frac{d_j}{h'} \qquad \text{——————} \quad 3$$

It may also be assumed that the total interference force ΔL, generated on lower surface of a baffle plate, positioned so that its underside is parallel to the surface upon which the jet is impacting, is proportional to the velocity, V', squared then

$$-\frac{\Delta L}{F} \sim \int_S \frac{V'^2}{F} . ds \qquad \text{——————} \quad 4$$

where F is the thrust developed by a fully expanded jet of area Sj.

Thus $$-\frac{\Delta L}{F} \sim \int \frac{V_j^2}{\rho_j S_j V_j^2} \cdot \frac{1}{(h'/d_j)^2} ds \qquad \text{——————} \quad 5$$

Hence $$-\frac{\Delta L}{F} \sim \frac{1}{(h'/d_j)^2} \cdot \frac{S - S_j}{S} \qquad \text{——————} \quad 6$$

Empirical relations of very similar form to that given above have been proposed. For example Hall (29) suggests the relationship

$$-\frac{\Delta L}{F} = 0.012 \left[\frac{(S/S_j)^{1/2} - 1}{h'/d_j} \right]^{2.3} \qquad \text{——————} \quad 7$$

Further simplification of equation (6), assuming that the baffle plate is circular with a diameter D gives

$$-\frac{\Delta L}{F} \sim \frac{D^2 - d_j^2}{h'^2} \qquad \text{——————} \quad 8$$

Wyatt (30) proposes the equation

$$-\frac{\Delta L}{F} = 0.012 \left(\frac{D - d_j}{h'} \right)^{2.3} \qquad \text{——————} \quad 9$$

which is valid only for axisymmetric jets.

Fig 18 shows data compared with equation 7.

It is clear that whilst such expressions indicate trends and the order of magnitude of lift losses there is sufficient differences between measurements and theory to indicate that factors not measured are influencing the lift losses. More accurate prediction of lift losses for simple configurations will await numerical solutions of the type employed by Khan (36).

Multiple Jets

The lift losses due to an array of several jets become more difficult to predict since the flow field generated by entrainment, impingement of wall jets and geometry creates a very complex system. Such a flow field is critically dependent upon the following factors:-

(1) the number of nozzles

(2) the arrangement of nozzles including the spacing, orientation and distance from the ground plane

(3) the shape of the surface adjacent to the nozzles over which the interference pressure distribution acts and its distance above the ground plane.

A jet fountain arises as a result of the collision of two (or more) wall jets. Fig 19 (37) illustrates this effect created when two jets impinge upon a ground plane.

Fig 20 illustrates a few of the simple arrangements and gives the relationship between lift loss and height above ground plane. It shows clearly the independent effects of entrainment and jet fountains and the corresponding change of lift. Finally in the last configuration, the combined effect of entrainment and a jet fountain is illustrated.

It has been found that the character of the upflow region is quite sensitive to small changes in nozzle and jet conditions, for example, differences in the angles of inclination of each of the nozzles or velocity differences between each jet.

Fig. 21 (31) shows the influence of the disposition of 8 axisymmetric jets located in a VTOL combat aircraft on the interference lift loss in ground effect at various heights. The wide variations in lift loss between each arrangment arises because of the different combinations of wall jet entrainment effects and jet fountains. Arrangement clearly has a very profound effect upon the magnitude of the lift loss and its variation with height.

Clearly it becomes very difficult to predict the magnitude of the lift loss for a multi jet configuration. The geometrical arrangement is very critical and significant variations in lift loss can occur with quite small changes in nozzle height. This latter effect is due to the way in which jets from adjacent nozzles merge or fail to merge at a given distance from nozzle exit.

Kotansky (37) presents methods by which the location of the wall jet stagnation line may be calculated. He also points out that although the flow field beneath a multi jet VTOL aircraft in hover may be idealised, the actual flow field may be very different. The two factors which strongly influence the character of the flow field are the presence of a cross wind and the transient motion of the aircraft. In the latter case analysis based upon steady state conditions is likely to be in serious error. Modification of theory to allow for the presence of a cross wind is difficult but important since it has significance for gas reingestion problems, stability and control.

2.2 GROUND EROSION

Shear Stress Distribution

More recently (24) attention has been paid to the measurement of the shear stress distribution in the impact and wall jet region of an impinging subsonic jet. This is because of the propensity for the flow to move solid objects within its path or, more seriously, to erode the ground surface. Such effects under a jet lift V/STOL aircraft can give rise to serious damage if solid objects or surface soil strike the aircraft or enter the engine intake. The tendency for a given jet to create such problems is related to the shear stress distribution in the impact and wall jet regions of the flow. Data is correlated in terms of a non dimensional parameter, the shear stress coefficient Ψ

$$\text{where} \quad \Psi = \frac{2J_w}{\rho V_j^2}\left(\frac{H}{d_j}\right)^2 \qquad \text{——————————10}$$

where J_w = wall shear stress
ρ = fluid density
V_j = velocity nozzle exit
H = distance from ground to nozzle exit
d_j = nozzle exit diameter

Ψ is a function of H/dj and the jet Reynolds Number. R_o

For the impact region (i.e. within the range r/H < 0.2) Borges (24) suggests the following empirical relationship:-

$$\Psi = 0.0576\left\{1 - \exp\left(-114\left(\frac{r}{H}\right)^2\right)\frac{H}{r}\right\} - 3.02\,\frac{r}{H}\left\{\exp\left(-114\left(\frac{r}{H}\right)^2\right)\right\} \qquad \text{——————11}$$

For the wall jet region it is shown that:-

$$\Psi = 0.214\,R_o^{-0.256}\left(\frac{r}{H}\right)^{0.878\,R_o^{0.0018}} \qquad \text{——————————12}$$

Fig (22) shows a comparison between data and equation (11) and (12).

The work also includes impingement data for jets with a range of incidence from 15 - 60°. The maximum shear stress coefficient Ψ_m was found to vary according to the law:-

$\Psi m = 0.46 \sin\phi^2$ where ϕ is the angle of incidence.

It may be shown that by using the definition of shear stress coefficient Ψ_m and substituting the relation B = H/sin ϕ where B is the distance measured along the jet from nozzle exit to point of impact, the maximum shear stress is:-

$$J_m = B^2 \tfrac{1}{2} \rho V_j^2 d_j \qquad \text{——————————13}$$

This clearly indicates that the maximum shear stress is a function of the distance between nozzle exit and point of impact irrespective of the angle of the jet.

2.3 RECIRCULATION

Recirculation describes the motion of air around a jet lift V/STOL aircraft when hovering in ground effect. Three mechanisms are apparent:-

1. Bouyarcy effects due to a wall jet at an elevated temperature causing the fluid in the wall jet to rise.

2. Impingement of two or more wall jets creating a jet fountain.

3. Interaction between a wall jet and a cross wind, in which the wall jet rolls up in a stable vortex sheet.

Each one of the above can create conditions in which the temperature of air entering the engine intake continues to increase, and this may give rise to unacceptable losses in engine thrust.

1. Bouyancy effects in wall jets

Limited experimental data is available for such flows at present (35) but work in progress has been reported by Borges (24), Gersten (38) and Krause (39). Gersten et al are carrying out theoretical studies using an integral technique allowing for bouyancy and entrainment effects. Abbot (40) has carried out tests designed to measure the spread of a hot ground sheet.

2. Impingement of wall jets

This topic has been dealt with in section 2.1 in relation to the effect upon lift losses. Clearly jet fountains may generate positive lift when they impinge upon parts of the airframe. However, such fountains when hot may cause undesirable heating of parts of the aircraft, and if located in strategic positions can recirculate into engine intakes.

3. Interaction of a wall jet with crosswind

Interaction between a wall jet and a crosswind gives rise to a rolled up vortex sheet as already described (fig 23). Schwantes (8) reports on the effects of wind velocity, initial jet Mach number, jet temperature and vertical height on the radius at which separation occurs. Using sonic jets with different initial temperatures the radius of separation is shown to be inversely proportional to the wind velocity Fig 24.

Initial jet temperature does not appear to have a very significant influence upon the radius of separation. On the other hand, jet Mach number is of some importance as indicated by fig 25. The more vigorous the wall jet the further it spreads before separation occurs. Finally fig 26 illustrates that increase in nozzle height above the ground at least up to H/dj ratios of 8, increases the distance covered by the wall jet before separation.

3. THRUST AUGMENTATION

Thrust augmentation ejector systems have a particular attraction for the designers of jet lift STOVL aircraft but it is the practical application of these devices which is proving to be difficult.

The reasons for wishing to use these devices are:-

1. There is a large difference in the power requirements between the cruise, and vertical landing. A successful thrust augmenter could allow an engine sized for the cruise conditions to produce additional lift thrust which would prove useful for STOVL manoeuvres.

2. The requirement for control jets at the extremities of the aircraft during hover manoeuvres which are powered by air bleed from the engine compressor. poses the problem of ducting air through their structural sections. A successful thrust augmenter would (a) reduce air bleed demand and (b) save weight and volume at critical parts of the air frame by reducing the size of ducting.

3. In the case of lift engines, an even lower powered engine could be used in conjunction with thrust augmentation to generate the required thrust.

The mode of operation of a thrust augmentor is by the transfer of energy within a carefully shaped duct from a high energy primary stream to a secondary flow entrained from the surroundings. The use of shear forces only between adjacent layers of fluid to achieve this energy transfer is a significant feature which indicates that the process cannot achieve high efficiencies. In a thrust augmentation ejector one or more streams of fluid are allowed to discharge into a duct. The duct extends upstream of the nozzle exit plane and is designed to facilitate the entry of a secondary flow of air from the surroundings. Mixing takes place within the duct between the inducing and induced flow during which momentum is conserved. The mixed flow is expelled from the duct giving a total thrust greater than that due to the primary jet acting alone.

The provision of a duct surrounding a mixing zone creates a region of pressure lower than that existing in the surrounding atmosphere. The difference between the pressure of the atmosphere and the pressure within the duct is responsible for maintaining the flow of secondary fluid, and the reduced pressure distributions acting over the upstream surfaces of the inlet is an important increment of thrust, which augments the thrust due to the primary flow. In addition the existence of the low pressure region at the exit of the primary nozzle or nozzles, may also allow an increase in primary jet velocity and hence momentum, and it is this which can generate a second component of thrust augmentation.

The thrust augmentation ratio Φ is the parameter which is used to compare the actual net thrust (Fact) of a given ejector with a thrust (Fisen) theoretically generated when all the primary fluid, including that required for boundary layer control purposes (if incorporated) is expanded isentropically from the same supply conditions to ambient pressure thus:-

$$\Phi = \frac{\text{Fact}}{\text{Fisen}} \qquad (14)$$

Care is needed in comparing values of thrust augmentation ratio given in different reports since the interpretation of Φ does vary.

The fundamental one dimensional equations expressing the conservation of mass, momentum and energy may be solved to yield ideal values of thrust augmentation Φ in terms of two area ratios i.e. A_1/A_0 and A_3/A_2 where A_0 is nozzle exit area, A_1 is the secondary flow inlet area, A_2 is the mixing tube area and A_3 is the ejector exit area. The results of such calculations are shown in fig.(27). The assumptions implied by this simple analysis includes that of uniform velocity profiles, and frictionless flow. Under ideal conditions thrust augmentation ratios of two appear to be easily achievable. When account is taken of losses, the reduction in performance can be significant.

Fig.28. shows the cumulative effect of non uniform velocity profiles, and friction losses in the nozzle, intake and duct, on an ejector with an area ratio 1.5. Clearly it is important to account for losses and to ascertain the relative effect each loss has on the thrust augmentation ratio.

Quinn shows very clearly that propellers are the best thrust augmenters see fig.29, because they are able to transmit energy to a fluid by normal forces action across blades, whereas ejector devices rely entirely on shear forces. Other features of the thrust augmentor must recommend their use to the designer, such as the absence of rotating parts or non circular sections.

From experimental work it is possible to gain some insight into the relative importance of the effect of variation in different paramenters. The following conclusions refer to investigations on simple axisymmetric configurations with constant area mixing tubes.

1. Mixing rates between streams are enhanced if the primary stream is heated.

2. Excessive mixing tube length reduces ejector performance, since the wall friction effect becomes significant.

The application of thrust augmentors to aircraft imposes very severe restrictions on size both of overall length and cross section area. Reduction in length requires that mixing rates between streams should be as rapid as possible, and further that the diffusion process should be carried out concurrently with mixing. It is also clear that it is not always convenient to employ ejectors of circular section because of aircraft design requirements.

Rapid Mixing

In order to reduce the overall length of thrust augmenters it is necessary to increase the rate at which mixing proceeds between the primary jet flow and secondary induced flow. This may be achieved by increasing the surface or interface area between the streams of fluid. Multiple nozzles arranged so as to distribute the primary flow evenly across a section is a technique which has been used. It has the disadvantage that these nozzles create additional skin friction losses at the entry to the secondary flow.

The same philosophy has also led to the use of primary nozzles with non circular cross sections. Usually such nozzles have greater friction losses as well as creating the same difficulties for the secondary flow.

An alternative approach to the problem of rapid mixing is to consider the turbulent structure of the jet and in particular that of the shear layers. Nozzles which can increase the production of eddies or intensify existing turbulence in the primary flow, enable mixing to be accomplished within a much shorter length. Hypermixing nozzles consist of a series of slots arranged so that adjacent slots have their axes inclined at a small angle to the mean flow direction.

In Fig 30 the spread rate of a hypermixing nozzle is compared with that of a slot jet. Initially the spread rate for the hypermixing nozzle is much more rapid but within a relatively short distance the spread rate returns to that of the plane jet.

Another technique which increases the spread rate and the rate of decay of axial velocity is to acoustically excite the jet. Quinn (12) reproduces data indicating the increase decay rate of a subsonic jet when subject to noise radiation. He also points out that self created noise in a highly underexpanded jet can improve the performance of short ejectors. The acoustic effect however, is most significant when the frequency generated by the primary jet is matched to the fundamental modes of the ejector mixing tube. Since subsonic jets emit a broad band noise spectrum, separate acoustic excitation is required if this technique is to be exploited.

Work has been carried out (14, 15) using unsteady jets of the types shown in figs 31 and 32. Using nozzles of the type shown in fig 31, Viets measured the mass augmentation ratio for several mixing duct lengths. It was shown that some performance advantage accrues when duct lengths are very short.

Binder and Didelle (15) compared data obtained from ejectors driven by pulsating nozzles and flapping nozzles with that from steady flow nozzles. The pulsating nozzle consisted of a supply where the flow to the nozzle was controlled by a variable speed motor driven butterfly valve. The arrangement for flapping nozzles is shown in fig.32.

The conclusions reached from these investigations were that such oscillation in the flow produced improvements in the performance particularly in respect of short ejectors. The thrust augmentation ratios given do not allow for the energy required to drive the devices which produce the pulsations or flapping. What is clear is that the imposition of unsteady flow in the primary stream accelerates mixing processes.

4. THEORETICAL MODELS

Models for estimating jet/fuselage interference

It is quite unrealistic to expect to test in a wind tunnel every model configuration at all flow conditions. Estimation methods will increasingly be required and fortunately the current growth in available computing power will make even the more exotic methods possible. The improved speed and power of computers may well permit significant progress to be made. That is not to say that earlier methods will not continue to be used where they are adequate and where their speed is vital as in basic project work.

The earliest methods were analytic mainly developed to jet-flaps. One possible approach was to use simple theory to correlate data to derive an empirical method e.g. Moorhouse (41). Figure 33 shows the types of jet-flap considered by Moorhouse and Figure 34 shows the result of his correlation of experimental data for a diversity of configuration types. His correlation gives:-

$$\Delta C_{L_{MAX}} = K_b\left\{\Delta C'_{L_{MAX}}(C_\mu) - C_j(\alpha_{S_0} + \delta)\right\} + C_j(\alpha_{S_0} + \delta)$$

$$\Delta C'_{L_{MAX}} = 55\pi\left\{\frac{B_0\alpha_{S_0} + D_0\delta}{1 + \frac{B_0}{2}}\right\}\left\{\frac{AR + 0.637C_j}{AR + 2 + 0.604\sqrt{C_j} + 0.877C_j}\right\}$$

where
- C_j = Momentum flux coeff
- AR = Aspect ratio
- B_0, D_0 = Fourier coeff
- δ = effective jet deflection angle
- α_{S_μ} = power-on stall angle of attack
- α_{S_0} = power-off stall angle of attack
- K_b = part span flap factor

Ashill (92) uses similar methods as part of a theoretical and experimental investigation of a jet-augmented flap. Gersten, Loehr and Beese (43) extended the idea to configurations near the ground, in ground effect. To extend such methods to direct jet lift and vectored thrust has proved difficult and attention turned at an early date to potential flow methods. In these, the basic assumption is made that the flow field is irrotational except in the jet plume or fan slipstream and by a representation of this by singularities, the external induced flow field can be predicted.

Two features of the jet have to be modelled, the blockage of the flow reproduced by replacing the jet by a solid surface and the entrainment. As first, attempts to represent the jet by only one of these were tried but it soon became clear that both effects had to be modelled. The simplest model is one using singularities distributed along the jet path. Unless an empirical jet centreline equation is used this will entail calculation of the jet path.

Typical of jet path prediction methods is one due to Campbell and Shetz (44) who consider the jet as being a stream tube subject to a perpendicular force due to the drag of the cross flow and a momentum transfer due to entrainment of free stream. In order to predict the entrainment they define an entrainment coeff. E* given by:-

$$E = A_j \rho_\infty E^*(V_j - V_\infty)$$

where
- A_j is jet area
- C is jet periphery
- ρ free stream density
- V_j jet velocity
- V_∞ free stream velocity

A & V_j are predicted from mass flow and C comes from the assumption that the jet cross section is elliptical in shape. They give an expression for E* as:-

$$E^* = .2\lambda^{-.6}\left(\frac{s}{d}\right)^{+.37} \qquad \text{or} \quad E^* = 0.8$$

whichever is greater and which unfortunately does not give a sensible far field or high jet velocity value.

Smy (45) uses a similar method but defined a length scale h by the ratio of jet momentum to dynamic pressure and assume a constant coefficient E* as:-

$$E = E^*\rho_\infty(V_j - V_\infty)h$$

with

$$E^* = \frac{0.16}{\lambda}\ \frac{h}{d}$$

where h is an equivalent width based on the ratio between jet momentum and free stream dynamic pressure. By using h an extra effect is introduced, that of the destruction of jet-wise momentum. This is introduced as it is clear that the other forces are insufficient to explain the rapid reduction in momentum in the initial jet direction.

Given the jet path it is necessary to define the singularities. It may either be assumed that they are derivable from the jet properties, for example by equating sink strength to entrainment rate, or by deducing them from a known empirical flow field, from the pressure around a jet emerging from a wall for example. Unfortunately it is unlikely that the two methods will give the same results. For a discussion of jet singularities see Bradbury (3).

More accurate results may be expected, particularly near the fan or nozzle, if the jet or wake surface is defined and singularities are modelled on this. Early attempts to derive the jet shape were those based on Chang-Lu (46) which take the time dependent roll up of a vortex ring to be the development of a jet boundary along its length. Fig 35 taken from Margason (47) shows such a set of cross sections. Figure 36 shows the resulting shape for the jet boundary computed by the author. Clearly this will not follow a jet trajectory but it is a simple matter to transfer these shapes to another centre line however derived. When such a shape is derived it is a simple matter to panel it for a surface singularity method. A refinement of this is due to Adler and Baron (48) who extend it to predict enlargments due to entrainment and the variation of jet velocity within the boundary. An alternative approach is to derive the jet shape with the trajectory and the singularity model and this has been done by Snel (19). Fig 37 shows the jet paths compared by computed data with that obtained by experiment. Fig 38 shows the resultant pressure distribution on a plate with a jet emerging into a crossflow. For a review of other potential field methods see Woolard (49). An alternative to a panel method is the use of a potential flow field method. Zacharias (17) used a finite element method to compute the flow on an afterbody with an entrainment velocity assumed on the jet boundary.

Higher order methods are clearly concerned with flows where turbulence and viscosity are the governing effects, and therefore it is necessary to look at solutions to 3-D Navier/Stokes equations. In the last few years several reports have appeared on these although at present they are probably limited to the simplest of geometric configurations.

Baker, Manhardt, Orzechowski and Yen (50) have derived a parabolized version of the time-averaged Navier/Stokes equations which are solved by a finite element method. It is clear that they are at least picking up the main features of the jet. Khan, McGirk and Whitelaw (36) have studied the case of a row of jets in cross flow. They also use the time averages equations with a finite difference solution and two equation turbulence models. They note that numerical errors are evident even with their finest grid but are not dominant and do not affect the overall characteristics.

In future it may be expected that these methods will become standard, probably in the form of Navier/Stokes grids embeded in large Euler grids covering the complete aircraft.

5. WIND TUNNEL TESTING

Despite advances in Computational Fluid Mechanics, methods capable of evaluating comprehensively the flow over jet or fan borne aircraft are not yet available, it will be necessary to rely for the foreseeable future, probably for ever, on wind-tunnel tests for basic data on V/STOL configurations. Apart from the difficulties common to all tunnel tests, there are three problems peculiar to powered models these are:-

1. Simulating the intake and exhaust flows of jets and fans
2. Scaling the model and the jet flows
3. Correcting the tunnel results for interference effects, and deciding model scale and technique.

Each of these problems has been addressed in AGARD and other symposia but still many problems remain. One clear message appears to be the need for specialised facilities, and over the years a number of specialized V/STOL tunnels have been constructed. These are typified as being of low speed and large size to enable realistically sized models to be tested, whilst minimising jet/tunnel interference. They are often of open circuit construction to eliminate the recirculation of the jet flow and may require a large supply of compressed air. An example of such a tunnel is shown in Fig 39.

Simulation of flows

For a conventional aircraft it is common still to smooth the inlets and nozzles and to test the model as such to obtain the aerodynamic characteristics. Later intake models may be constructed to study the detailed flow. With a V/STOL aircraft however in a semi or wholly jet-borne phase it is vital to simulate the powered system. The problem is compounded by the fact that vertical lift systems are often very difficult to model.

Fig 40 shows various types of engine installation and their exhaust properties. This is taken from Wulf and Melzer (51) which contains a discussion on engine simulation from which the following figures are taken. Fig 41 shows the strategy for choosing various models. Fig 42 shows the jet properties of the model and Fig 43 gives the advantages and disadvantages of these. It seems safe to say that the most common method up to now for jet lift aircraft has been the use of compressed air, to simulate the nozzle flow and with faired intakes. For conventional aircraft, model engines are popular. For a comparison of methods on a pylon mounted engine see Decker, Gillette and Teyeber (52). It is possible to simulate the mass flow, thrust or velocity by compressed air motors, or ejectors but the physical properties (specific heat, temperature, etc.) will be different to that of real exhausts. Correct simulation of gas exhaust properties may be achieved by passing the air through a combustion chamber up stream of the nozzle or by burning fuel in a small combustion chamber inside the model.

Typical model installations for air-blowing ejectors and tip fan are shown in Figs 44, 45 & 46.

Thrust scaling

If a model could be constructed to produce an efflux at the full scale temperature, composition and pressure, then it would be sufficient to produce a model propulsion system to exact scale to achieve the correct thrust, momentum ratio and velocity simultaneously. With correct pressure and scaled area the momentum ratio will be correct but temperature may affect the shape of the efflux as well as the rates of heat and mass transfer.

Tunnel interference

For references to this topic it is necessary to look at symposia on tunnel testing rather than V/STOL aerodynamics, for example AGARD CP 174, Wind Tunnel Design and Testing Techniques, London 1975. The symposium has been used as a basis for much of the work in this section and in particular the papers of Carbonara (53) and Cull (54). The primary difficulty is that the jet efflux or propulsive wake will in general strike the tunnel wall and may, if the efflux is sufficiently vigorous cause the forward stagnation point to move so far forward as to separate and cause a vortex to be formed which will surround the impact point and will cause considerable interference with the model. It is possible to correct for such effects within limits. The limits within which the flow is suitable for correction must depend on velocity ratios and tunnel/wall separation. In general the limit will differ for all types of model and must be investigated experimentally. Typical investigation include those of Tyler and Williamson (55) and Cull (54). Fig 47 shows some experimental data from Cull (55) for a multi jet lift model. By plotting the stagnation points relative to the model the velocity margins can be obtained.

Carbonara (53) discusses various criteria for establishing whether or not flow breakdown has occurred. This is summarised in Fig 48 which compares limiting conditions proposed by South (56) Turner (57, 58) Tyler and Williamson (55) Owen (59) and Heyson (60). The presence of a tunnel wall when examining the flow around model in ground effect is useful. It is important however to ensure that the modelling is correct, particularly with regard to the provision of a moving ground. Turner (57) investigated conditions under which a moving belt system should be used and fig 49 summarises his conclusions.

6. REFERENCES

1. Smy J. R.
   Ransom E.C.P.
   The Structure of Single Jets at Large Angles to a Crossflow.
   Prepared for Procurement Executive Ministry of Defence Contract No. K/A72C/352.
   British Aerospace Rept. No. HSA-KAD-R-GEN 2288. 1976.

2. Ransom E.C.P.
   Wood P.M.
   Jet Interference Literature Survey and Critical Review.
   Prepared for Procurement Executive Ministry of Defence Cont. No.AT/2055/04SRA.
   June 1975.

3. Bradbury L.J.S.
   General Review, Some aspects of jet aerodynamics and their implications for VTOL Research.
   AGARD FDP Conference "Fluid dynamics of jets with applications to V/STOL" C.P.308. November 1981.

4. Gentry G.L.
   Margason R.J.
   Jet Induced Lift Losses on VTOL Configurations hovering in and out of Ground Effect.
   NASA TN D-3166. 1966.

5. Hargreaves J.J.
   Design, development and calibration of a jet efflux plenum chamber model for use in V/STOL research models.
   British Aircraft Corporation Report AXR-23.

6. Mathieu J.
   Charn ay G.
   Structure and development turbulent jets.
   AGARD CP 308. 1981.

7. Ricou F.P.
   Spalding D.B.
   Measurements of entrainment by axisymmetric turbulent jets.
   Journal of Fluid Mechanics Vo. II part I. 1961.

8. Schwantes E.
   The propulsion of jet of a VTOL aircraft.
   AGARD CP 91. December 1971.

9. Ransom E.C.P.
   Barnes J.H.
   The calculations of jet interference pressure distribution using integral and numerical methods based on actual measurements of entrainment.
   AGARD CP 308. November 1981.

10. Ransom E.C.P.
    An investigation of the flow field and induced pressure field created by an axisymmetric free jet.
    PhD Thesis. October 1982.

11. Williams J
    Wood M.N.
    Aerodynamic interference effects with jet lift V/STOL aircraft under static and forward speed conditions.
    RAE TR 66403. 1966

12. Quinn B.
    Thrust Augmenting Ejectors.
    A Review of the application of Jet Mechanics to V/STOL Aircraft Propulsion.
    AGARD CP 308. November 1981.

13. Sato H.
    The Stability and Transition of a two dimensional jet.
    Journal of Fluid Mechanics Vol 7 p 53. 1960.

14. Viets H. — Unsteady Ejectors. AGARD CP308. November 1981.

15. Binder G. Didelle H. — Improvement of Ejector thrust augmentation by pulsating or flapping jets. AGARD CP308. November 1981.

16. Parikh P.G. — Resonant entrainment of a confined pulsed jet. AGARD CP308. November 1981.

17. Zacharias A. — An experimental and theoretical investigation of the interaction between the engine jet and the surrounding flow field with regard to the pressure drag on after bodies. AGARD CP308. November 1981.

18. Mayson I. Ogilvie F.B. Harris K.D. — An investigation under static external flow conditions of the axial force induced on circular flat plates surrounding simple uniform and co axial jets exhausting normally to the plate. HSA, Hatfield Research/1010/IM/FBO/KDH. December 1971.

19. Snel H. — A method for the calculation of the flow field induced by a jet exhausting perpendicularly into a cross flow. AGARD CP143. April 1974.

20. Mikolowsky W.J. McMahon H.M. — An experiemental investigation of a jet issuing from a wing in cross flow. Journal of Aircraft Vol 10 No.9. September 1973.

21. Mosher D.K. — An experimental investigation of a turbulent jet in a cross flow. PhD Thesis. Georgia Institute of Technology CIT-AER-70-7. December 1970.

22. Wu J.C. McMahon H.M. Mosher D.K. Wright M.A. — Experiemental and analytical investigations of jets exhausting into a deflecting stream. AIAP Paper No. 69-223. February 1969.

23. Taylor P Watkins D.J. — An investigation of inclined jets in a crosswind. AGARD CP308. November 1981.

24. Borges A.R.J. Viegas D.X. — Interaction of simple and multiple jets with a plane surface. AGARD CP308. November 1981.

25. Arbuckle J.A. — Investigation of density effects on entrainment by impinging jets. Cranfield Institute of Technology. MSc Thesis. May 1965.

26. Searle N. — Entrainment by axisymmetric jets impinging on a flat plate. Cranfield Institute of Technology. MSc Thesis. June 1964.

27. Skifstad J.G. — Aerodynamics of jets pertinent to VTOL aircraft. Journal of Aircraft, Vol No.3 May/June 1970.

28. Welte D. — Prediction of aerodynamic interference effects with jet-lift anf fan-lift aircraft. AGARD CP143. April 1974.

29. Hall G.R. — Scaling of VTOL Aerodynamic suckdown forces. Journal of Aircraft Vol.4 No.4. 1967.

30. Wyatt C.A. — Static Tests of ground effects on plan forms fitted with centrally located round lifting jet. ARC CPN 749. 1964.

31. Knott P.G. Hargreaves J.J. — A review of the lifting characteristics of some jet lift V/STOL configurations. AGARD CP143. April 1974.

32. Beltaos S. Rajaratnam N. — Impinging circular turbulent jets. J. Hyd Div ASCE Vol.100. pp 1313-1328. October 1967.

33. Barche J. — Jet lift problems of V/STOL aircraft. AGARD CP143. April 1974.

34. Barche J. — Jet Interactions with neighbouring surfaces. AGARD CP308. November 1981.

35. Cox M. Abbott W.A. — Studies of the flowfields created by single vertical jets directed downwards upon a horizontal surface. ARC CPN 912. 1967.

36. Khan Z.A. McGuirk J.J. Whitelaw J.H. — A Row of Jets in a Crossflow. AGARD CP308. November 1981.

37. Kotansky D.R. — The modelling and prediction of multiple Jet VTOL Aircraft Flow Fields in Ground Effect. AGARD CP308. November 1981.

38. Gersten K. Schulz-Hausmann F.U. Schilawa S. — Effects of Bouyancy and Entrainment on hot free jets and wall jets. AGARD CP308. November 1981.

39. Krause E. Hänel D. Hewedy N.I.I. — Investigations of Wall Jets. AGARD CP308. November 1981.

40. Abbott W.A. — Studies of flowfields Created by Vertical and Inclined Jets when stationary or moving over horizontal surfaces. ARC CPN 911. 1967.

41. Moorhouse D.J. — Predicting the Maximum Lift of Jet-Flapped Wings. AGARD CP143. April 1974.

42. Ashill P.R. — A theoretical and Experimental Investigation of the External flow Jet Augmented Flap. AGARD CP135. September 1973.

43. Gersten K Loehr R. Beese E. — Ground Effect on Airfoils with Flaps or Jet Flaps. AGARD CP143. April 1974.

44. Campbell J.F. Schetz J.A. — Analysis of the injection of a Heated Turbulent Jet into a Cross Flow. NASA TR R413. December 1973.

45. Smy J.R. — The Trajectory of a Heated, Buoyant Jet in a Non-Uniform Cross Flow. BAe Report BAe-KAD-GEN-N-2868. August 1982.

46. Chang-Lu Hsiu-Chen — Aufrollung eines zylindrischen Strahles Durch Querwind. Univ. Goettingen, Doctorial Dissertation. 1942.

47. Margason R.J — Analytic Description of Jet Wake Cross Sections for a Jet Normal to a Subsonic Free Stream. NASA SP218. September 1969.

48. Adler D Baron A — Prediction of a Three Dimensional Circular Turbulent Jet in Crossflow. AIAA Journal, Vol.17, No.2 pp.168-173. February 1979.

49. Woolard H.W. — U.S. Air Force V/STOL Aircraft Aerodynamic Prediction Methods. AGARD CP143. April 1974.

50. Baker A.J. Manhardt P.D. Orzechowski S.A. Yen K.T. — A Three Dimensional Finite Element Algorithm for Prediction of V/STOL Jet Induced Flowfields. AGARD CP308. November 1981.

51. Wulf R Melzer E — Wind tunnel testing with engine simulation for V/STOL airplanes. AGARD CP135. Shleirsee 1973.

52. Decker R. Gillette W.B. Tegeler D.C. — Nacelle Airframe integration: Model Testing for nacelle simulation and measurement accuracy. AGARD CP174. London 1975.

53. Carbonara M — Interference problems in V/STOL testing at low speeds. AGARD CP174. London 1975.

54. Cull M.J. — V/STOL wind tunnel model testing: An experimental assessment of flow breakdown using a multiple fan model. AGARD CP174. London 1975.

55. Tyler R.A. Williamson R.G. — Experience with the NRC 10 ft. x 20 ft. V/STOL Engine model Testing. Canadian Aeronautics and Space Journal No.10 pp 191-199. September 1972.

56. South P. — Measurements of flow breakdown in rectangular wind tunnel working sections. NRC Aero Report LR513. November 1968.

57. Turner T.R. — Endless-belt technique for ground simulations. NASA SP116 paper 23. April 1966.

58. Turner T.R. — A moving belt ground plane for wind tunnel ground simulation and results for two jet flap configurations. NASA TN D4228. November 1967.

59. Owen T.B. Limiting test conditions in wind tunnels used for V/STOL model testing. La Ws Paper No. 37. January 1972.

60. Heyson H.H. Theoretical study of conditions limited V/STOL testing in wind tunnels with solid floor. NASA TN D5819. 1970.

TABLE 1. (1)

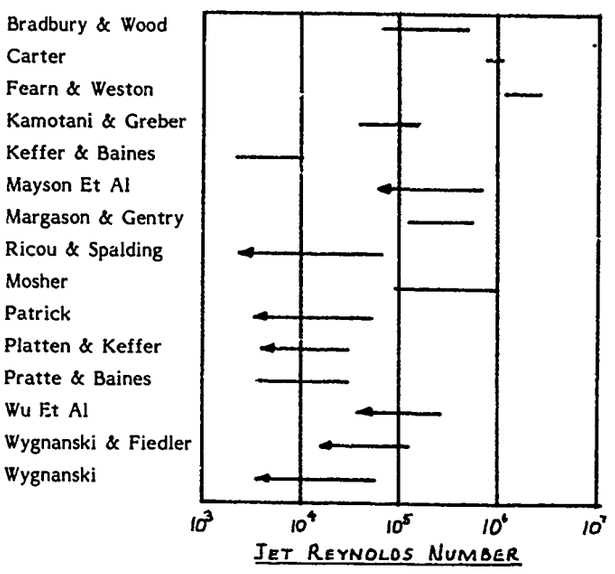

TABLE 2. (2)

INDEPENDENT VARIABLES	GEOMETRIC	NOZZLE	
		MODEL	
	FLUID DYNAMIC	JET FLUID	
		CROSS FLOW FLUID	
FLOW FIELD EFFECTS	ENTRAINMENT	(Directly (measured (or (implied (by	(Potential Core length
	BLOCKAGE		(Jet Trajectory
			(Jet Decay rate
SURFACE EFFECTS	('Pressure Distributions (Interference forces (Interference Moments (Reingestion (Surface erosion (Wind tunnel test limits		

TABLE 3 Empirical equations for the trajectory of a jet in crossflow (Ref.1)

AUTHOR	EQUATION	JET DIAMETER M M	RANGE OF APPLICATION λ	RANGE OF APPLICATION INTERSECTION ANGLE α
Callaghan & Ruggeri	$\frac{x}{d} = 0.118 \frac{1}{\lambda^2} \left(\frac{\rho j}{\rho \infty}\right)^{-1} \left(\frac{Z}{d}\right)^{2.3}$	12–27	2 00–7.14	90°
Ivanov	$\frac{x}{d} = \frac{1}{\lambda} 2.6 \left(\frac{Z}{d}\right)^3 + \frac{Z}{d} \cot \alpha$	—	1.41–33 3	60°–120°
Margason	$\frac{x}{d} = 0.25 \frac{1}{\lambda^2} \left(\frac{Z}{d}\right)^3 \operatorname{cosec}^2 \alpha + \frac{Z}{d} \cot \alpha$	25	1.17–10	30°–180°
Patnck	$\frac{x}{d} = C. \frac{1}{\lambda^{b/n}} \left(\frac{\rho j}{\rho \infty}\right)^{\frac{b}{2n}} \left(\frac{Z}{d}\right)^{\frac{1}{n}}$	Various	Up to 60	90°
Schetz & Billig	$\frac{x}{d} = \frac{1}{\lambda^2} \frac{\rho j}{\rho \infty} \left(\frac{Z}{d}\right)^{2.3}$	—	—	90°
Shandorov	$\frac{x}{d} = \frac{1}{\lambda^2} \left(\frac{Z}{d}\right)^{2.35} + \frac{Z}{d} \left(1 + \frac{1}{\lambda^2}\right) \cot \alpha$	20	1.41–4 76	45°–90°
Storms	$\frac{x}{d} = 0.195 \frac{1}{\lambda^2} \left(\frac{Z}{d}\right)^3$	14	4 00–10	90°
Williams & Wood	$\frac{x}{d} = 2.3 \frac{1}{\lambda^2} \left(\frac{\rho j}{\rho \infty}\right)^{1.5} \left(\frac{Z}{d}\right)^3$	13 25	4–8	90°
Wooler	$\frac{x}{d} = 2.645 \frac{1}{\lambda^{2.3}} \left(\frac{\rho j}{\rho \infty}\right)^{1.25} \left(\frac{Z}{d}\right)^{2.5}$	13 25	4–8	90°
Wooler	$\frac{x}{d} = 0.19 \lambda^2 \cosh \left\{\frac{Z}{.19\ 2d}\right\} - 1$	13 25	4–8	90°
Chassaing et al	$\frac{2Z}{d} = \left(1.53 + 0.90 \lambda\right) \left(\frac{2\alpha}{\sigma}\right)^{0.385}$	20	24–6 4	90°

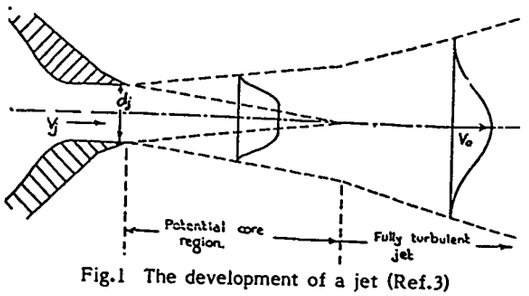

Fig.1 The development of a jet (Ref.3)

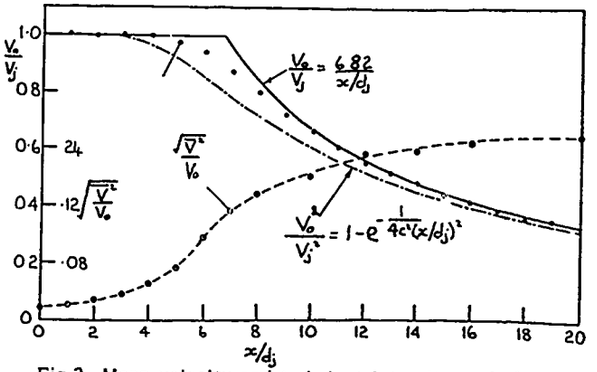

Fig.2 Mean velocity and turbulent intensity variation along the centre line of a jet (Ref.3)

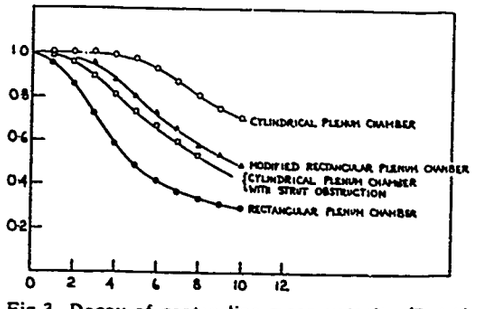

Fig.3 Decay of centre line mean velocity (Ref.3)

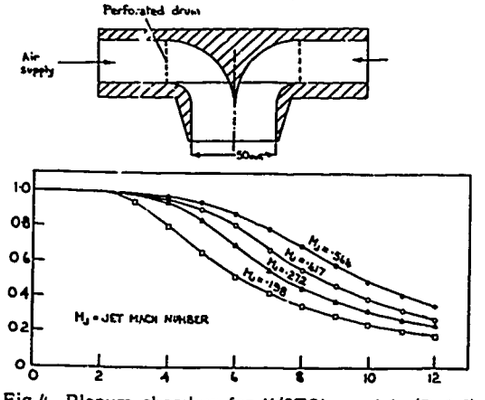

Fig.4 Plenum chamber for V/STOL models (Ref.5)

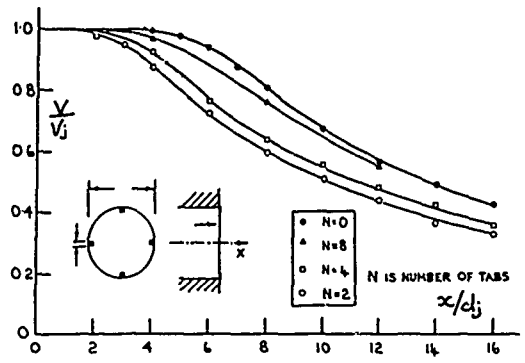

Fig.5 Effect of square tabs on the decay of jet centre line mean velocity (Ref.3)

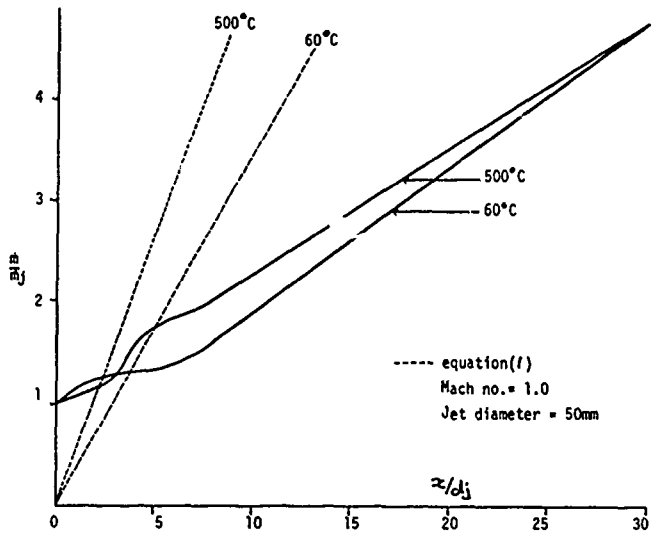

Fig.6 Effect of jet temperature on entrainment in a free jet (Ref.2)

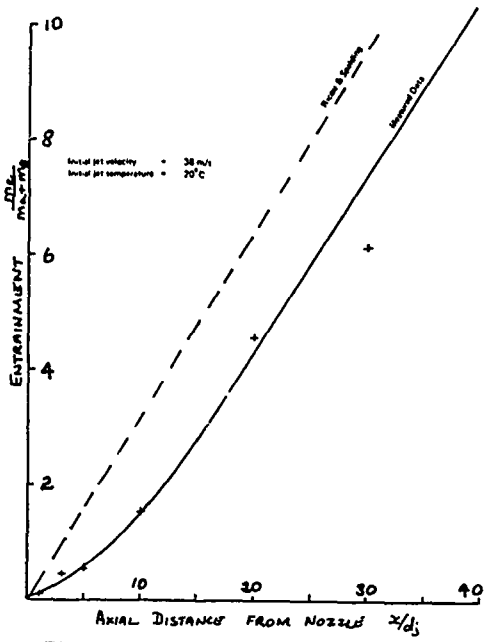

Fig.7 Entrainment into an axisymmetric free jet (Ref. 10)

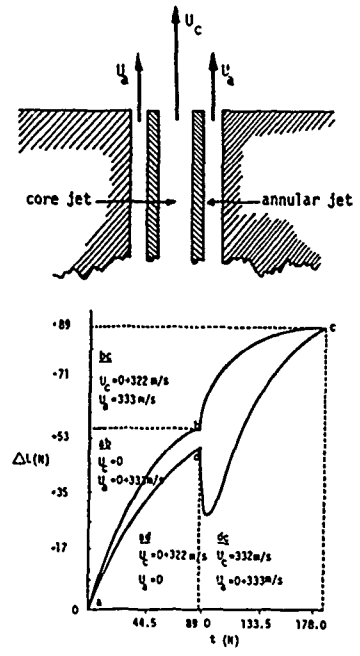

Fig.8 Interference forces induced by a co axial jet (Ref.18)

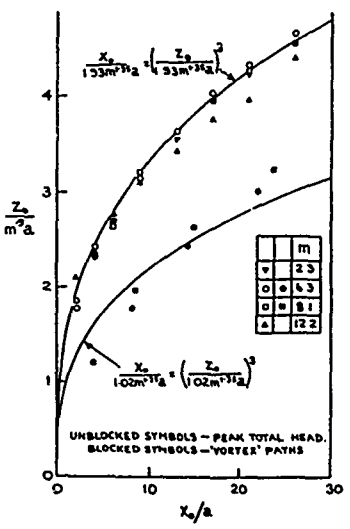

Fig.9 Jet Paths for circular nozzles (Ref.3)

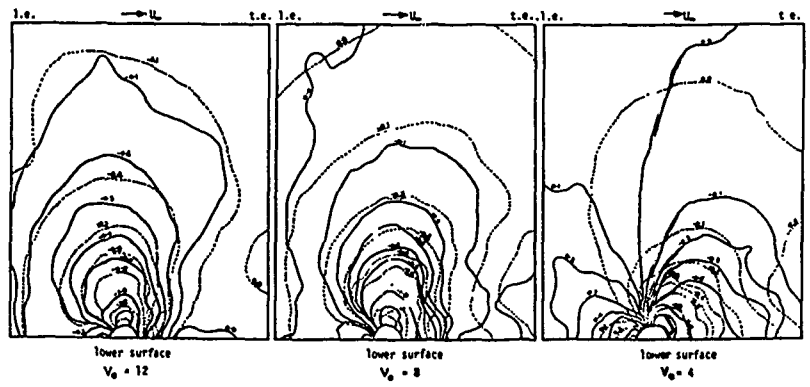

Fig.10 Interference surface pressure contours for a wing and flat plate (Ref.20)

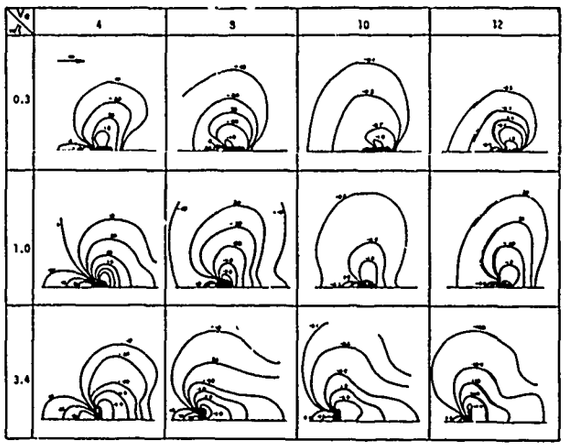

Fig.11 Interference surface pressure contours for a non circular jet (Ref.2)

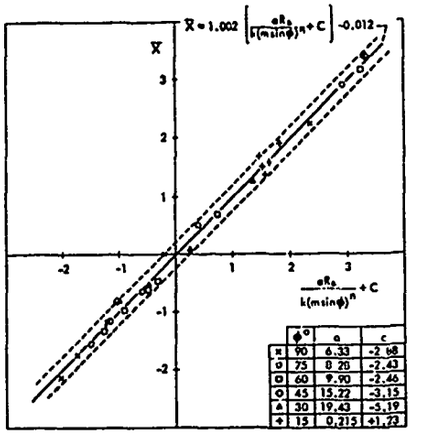

Fig.12 Correlation of centre of pressure with inclination and momentum ratio (Ref.23)

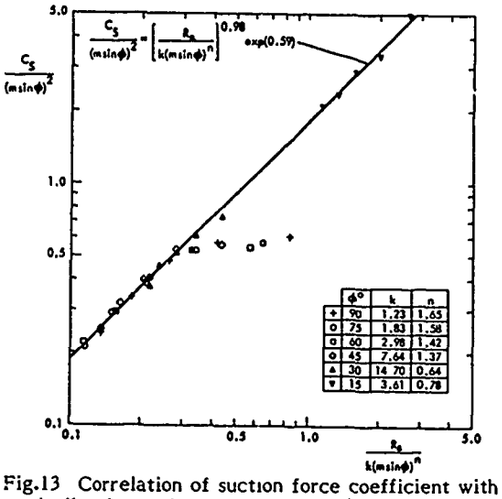

Fig.13 Correlation of suction force coefficient with inclination and momentum ratio (Ref.23)

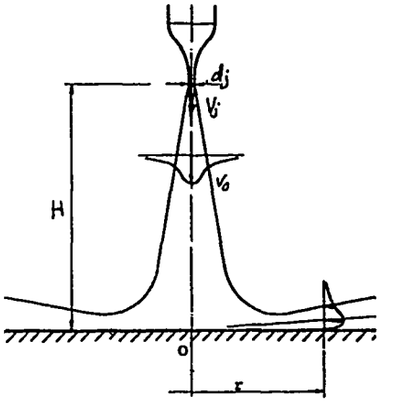

Fig.14 Flow from an impinging jet (Ref.24)

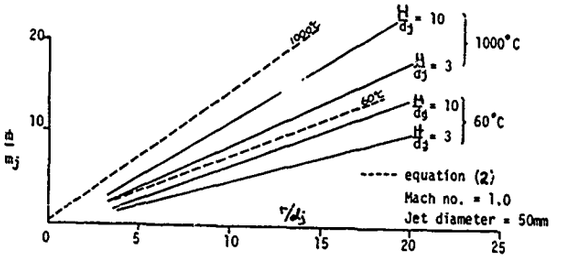

Fig.15 Entrainment into a wall jet (Refs.24,25,8)

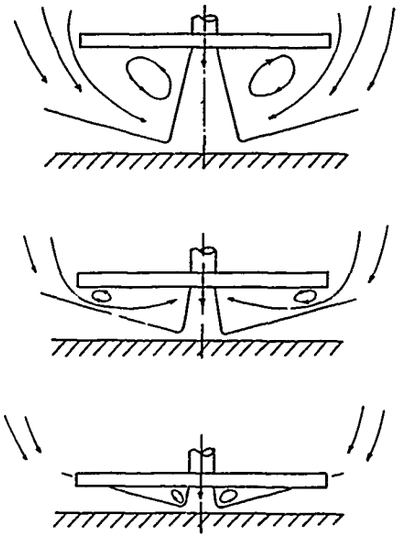

Fig.16 Effect of nozzle height on entrained flow pattern (Ref.27)

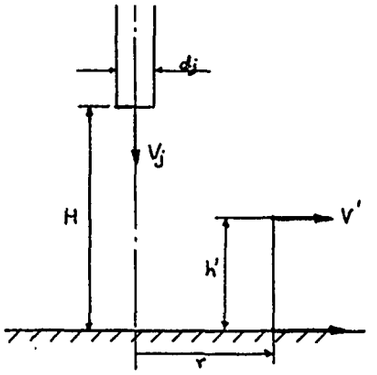

Fig.17 Impinging jet nomenclature (Ref.28)

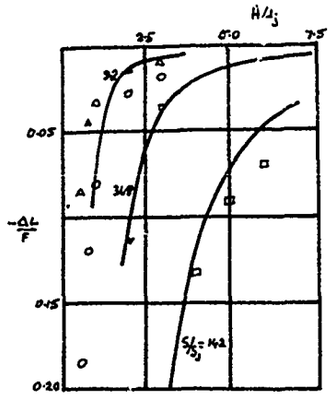

SYMBOL	S/dj
○	9·2
△	9·2
▽	36·8
□	142·0

$$-\frac{\Delta L}{F} = 0.018\left[\frac{(S/d_j)^{1/2}-1}{H/d_j}\right]^{2.3}$$

Fig.18 Lift loss near ground (Ref.28) (entrainment dominant)

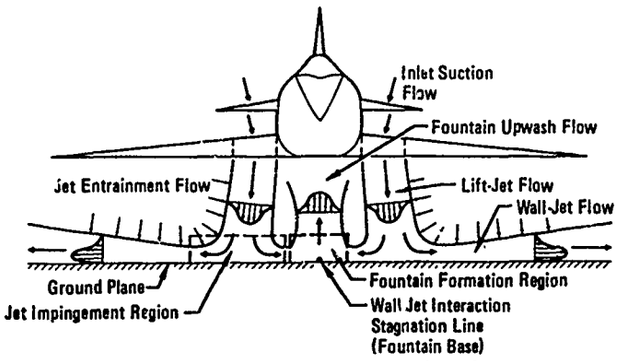

Fig.19 Flowfield about a VTOL aircraft hovering in ground effect (Ref.37)

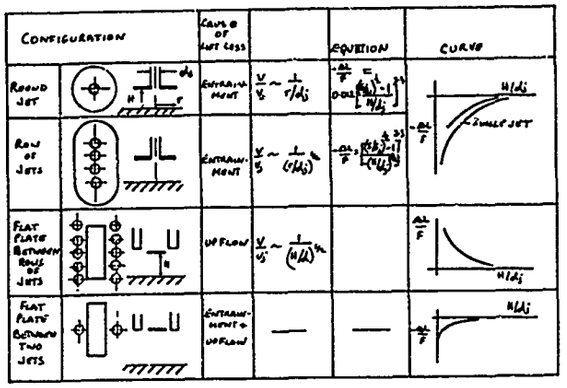

Fig.20 Basic types of ground effects (Ref.28)

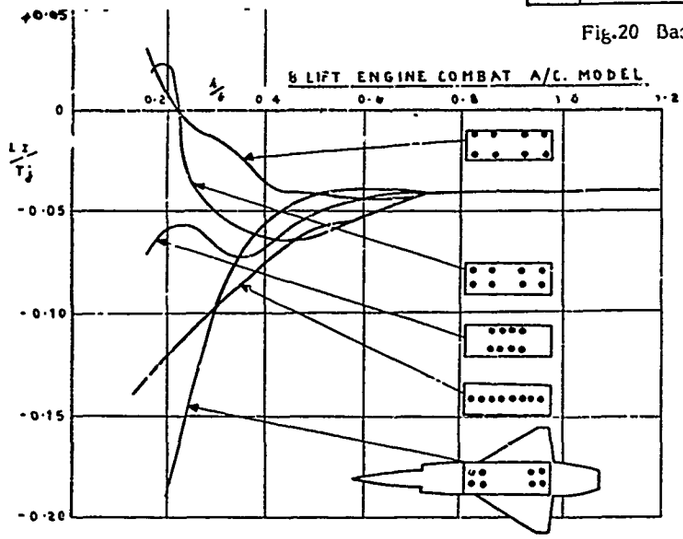

Fig.21 Effect of jet nozzle spacing on hoverlift (Ref.31)

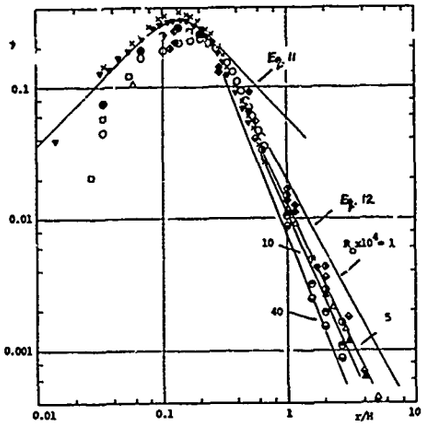

Fig.22 Radial variation of Ψ for the normal jet (Ref.24)

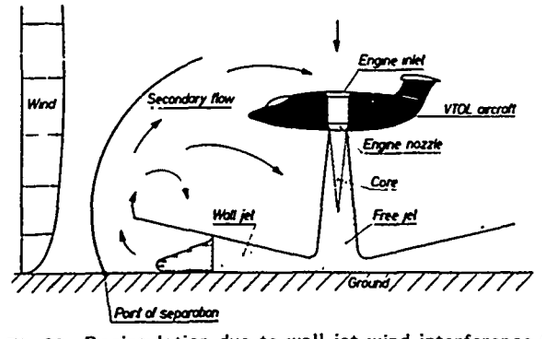

Fig.23 Recirculation due to wall jet wind interference (Ref.8)

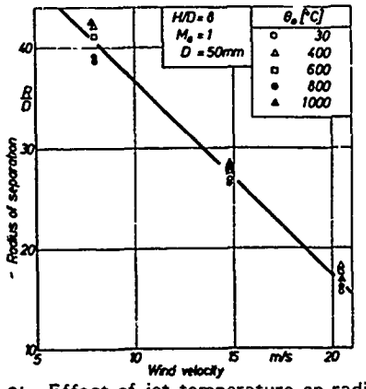

Fig.24 Effect of jet temperature on radius of separation (Ref.8)

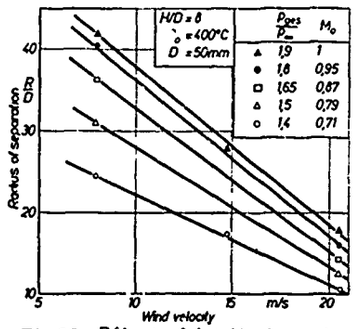

Fig.25 Effect of jet Mach number on radius separation (Ref.8)

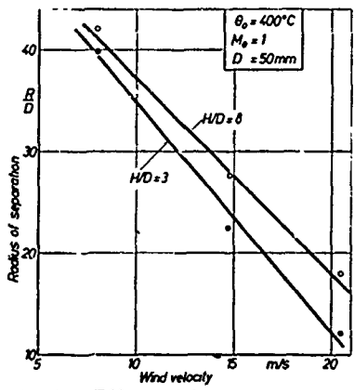

Fig.26 Effect of jet ground height on radius separation (Ref.8)

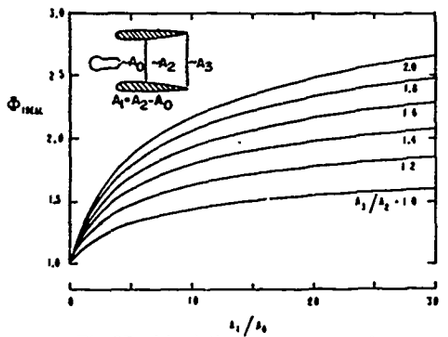

Fig.27 Ideal thrust augmentations for constant area ejectors (Ref.12)

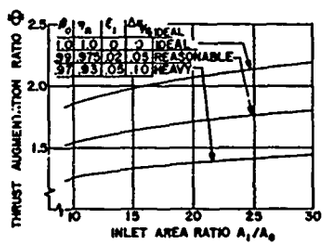

Fig.28 Effect of losses on thrust augmentation ratios (Ref.12)

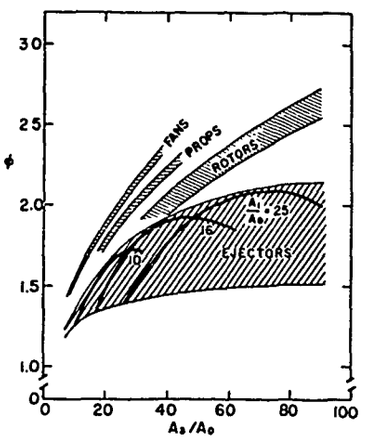

Fig.29 Comparison between ejectors and other devices acting as thrust augmenters (Ref.12)

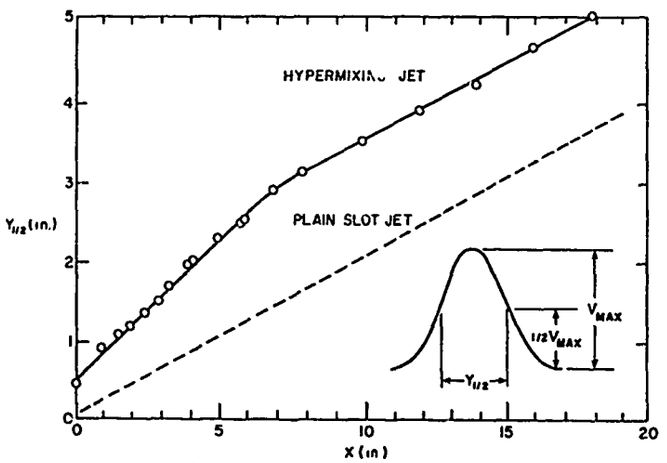

Fig.30 Comparitive spread of plain and hypermixing jets (Ref.12)

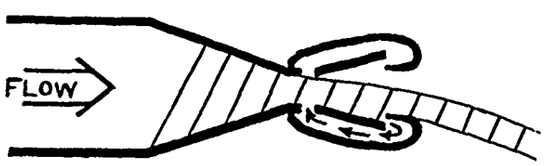

Fig.31 Self acting flapping nozzle (Ref.14)

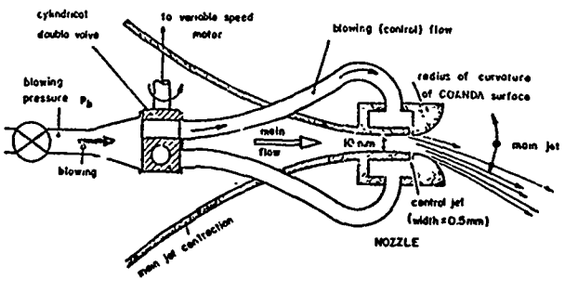

Fig.32 Flapping nozzle (Ref.15)

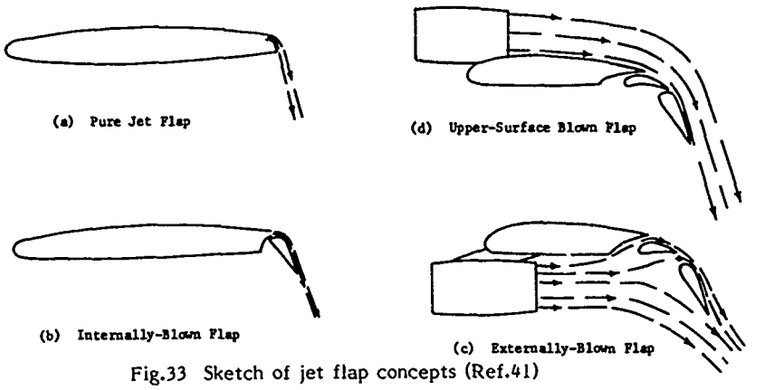

Fig.33 Sketch of jet flap concepts (Ref.41)

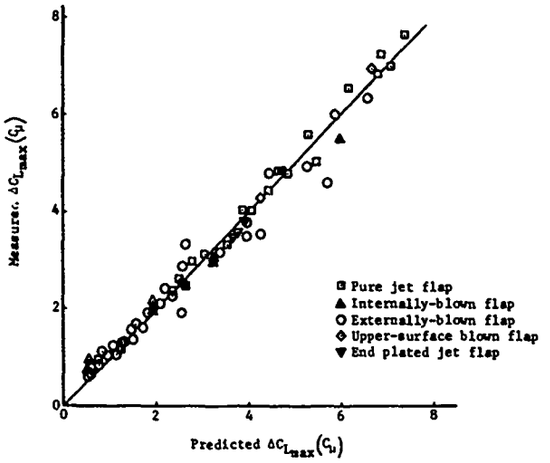

Fig.34 Increment in maximum lift due to blowing (Ref.41)

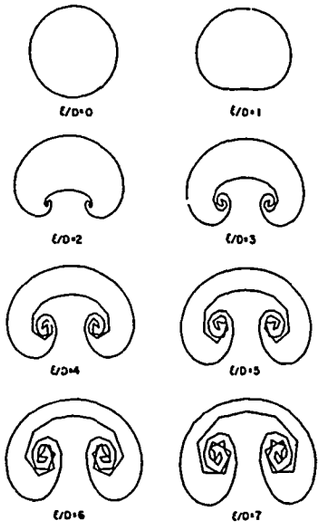

Fig.35 Wake cross sections showing roll up into a pair of vortices (Ref.47)

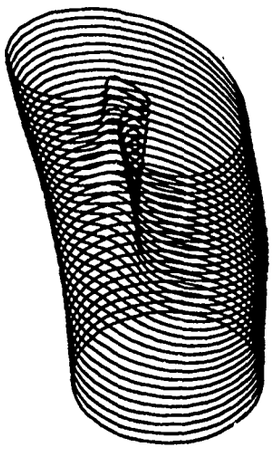

Fig.36 Jet boundary

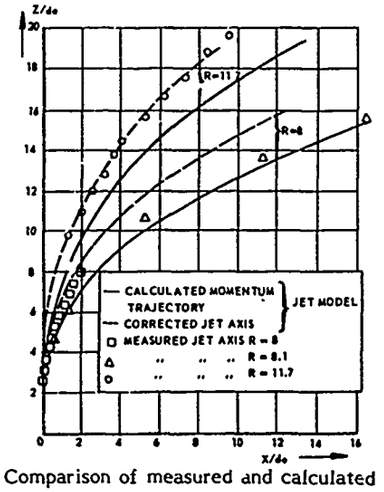

Fig.37 Comparison of measured and calculated jet axes

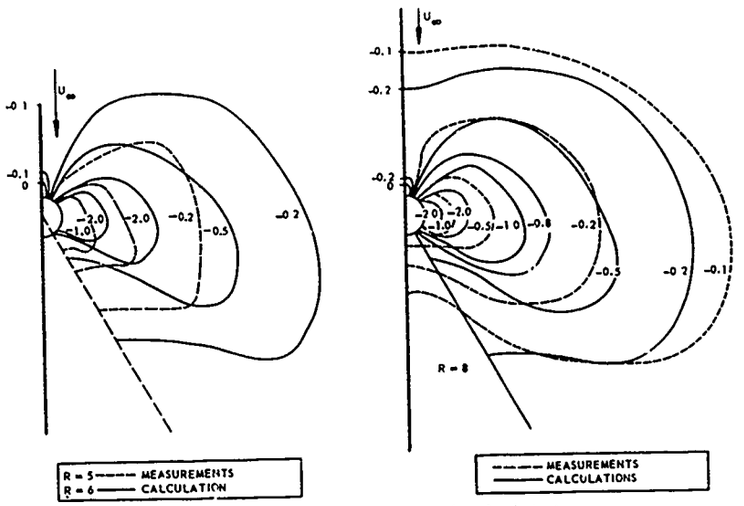

Fig.38 Comparison of measured and calculated pressure distribution on the flat plate

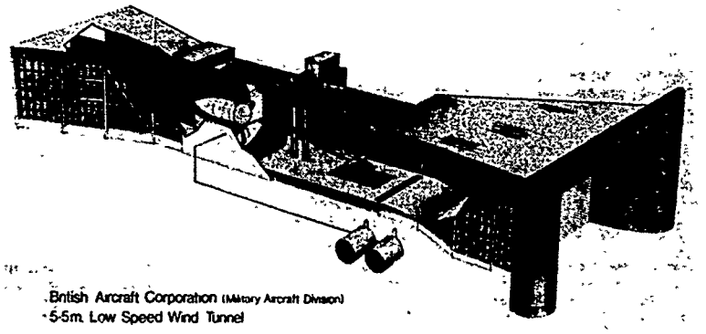

Fig.39 5.5m Low Speed Wind Tunnel (Ref.31)

			L/ϕ	T_0 [°K] turbine inlet	T_1 [°K]	T_2 [°K]	v_1 [m/s]	v_2 [m/s]	m_2/m_1
1	Turboprop		2,5	1200	800	300	500	200	15
2	Turbojet		5	1400	900	—	600	—	—
3	Turbofan		2	1200 –1600	800	300	300 –500	200 –300	5–15
4	Advanced Fan		0,2–0,3	1200 –1600 (1700)	500	300	200 –300	150 –250	20
5	Rotor		—	—	—	300	—	200	—

Fig.40 Properties of various engine exhausts (Ref.51)

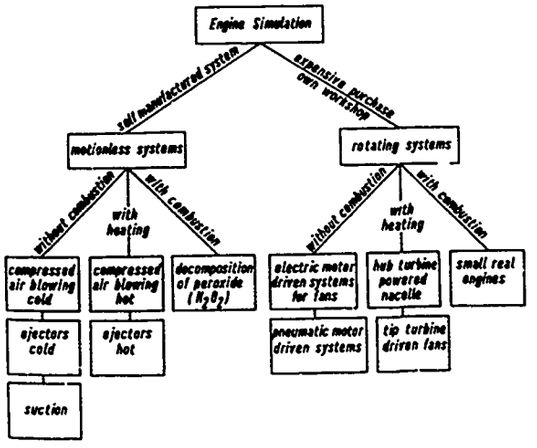

Fig.41 Technique for engine simulation (Ref.41)

Technique	T_o [°K]	T_1 [°K]	T_2	v_1	v_2 [m_A]	$\dot{m}_2/\dot{m}_1$	$\dot{m}_1/\dot{m}_e$	Turbojet	Turbofan	Advanced-fan
Compressed air cold	300	<300	<1	≤1	≤1	1	0	×	×	
Compressed air hot	400 (700)	<1	1	≤1	1	1	0	×	×	
Ejector	300	<300	<1	≤1	≤1	1	≤0,75	×	×	(×)
E-motor driven fan	—	—	1	—	100 (150) Π=1,2	~1	1	×	×	(×)
Hub turbine powered nacelle	<400	~300	1	<1	≤1 Π=1,5	~1	<1	(×)	×	(×)
Tip turbine driven fan	<450	~300	1	<1	≤1 Π=1,2	~1	<1<1		(×)	×
Decomposition of H_2O_2 (peroxide)	—	700÷ 1200	—	~1	—	—	0	×		
Small real engine								×	×	×
Suction								1 – full scale		

Fig.42 Applicability of simulation methods (Ref.41)

Technique	Benefits	Disadvantages
Compressed air cold	simple quick cheap	energy problems for plants pipe disturbances incorrect momentum or velocity no influx
Compressed air hot	adjustable	heat problems for i.e. balances
Ejector systems	influx better energy transformation high drive pressure	not uniform jet profile calibration work influx ≠ exit mass flow
E-motor driven fan	influx = exit mass flow flexible small feeders good jet profile	voluminous limited power low jet pressure ratio
Hub turbine powered nacelle	high jet pressure ratio influx, inner and bypass jets real geometry good jet profile	high costs maintenance problems extensive calibration work
Tip turbine driven fan	moderate jet pressure ratio small axial depth real inner aerodynamic	time consuming development manufactoring problems
Decomposition of of peroxide (H_2O_2)	possible right momentum small pipes	only for small models expensive no influx stream tube
Small real engines	possible real inlet and jet parameters	for large wind tunnels little experience in testing work no engines available which match full scale engines

Fig. 43 Comparison of simulation techniques (Ref.41)

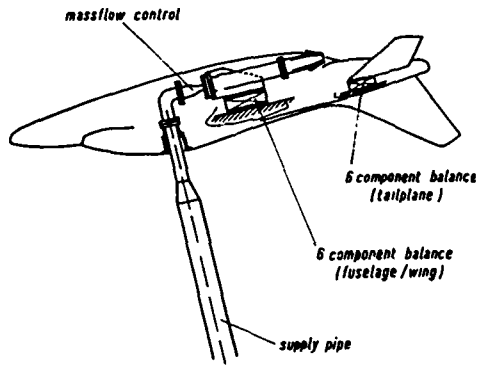

Fig.44 Compressed air blowing techniques

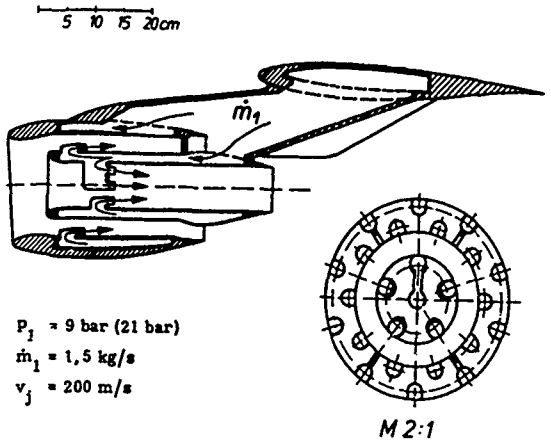

Fig.45 Ejector engine (Ref.55)

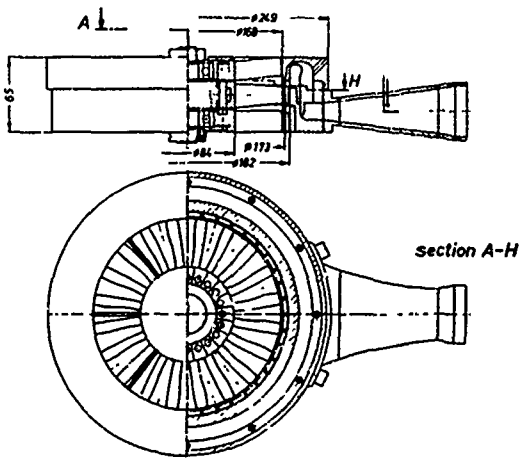

Fig.46 Tip turbine driven fan

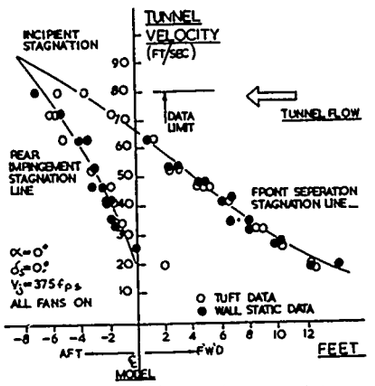

Fig.47 Typical experimental data to establish values of Vis (Ref.55)

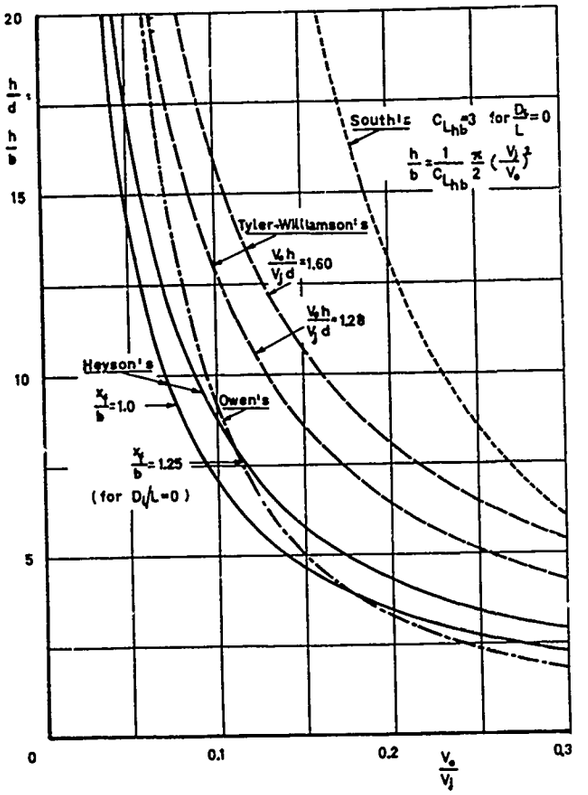

Fig.48 Wind tunnel flow breakdown limits (Ref.53)

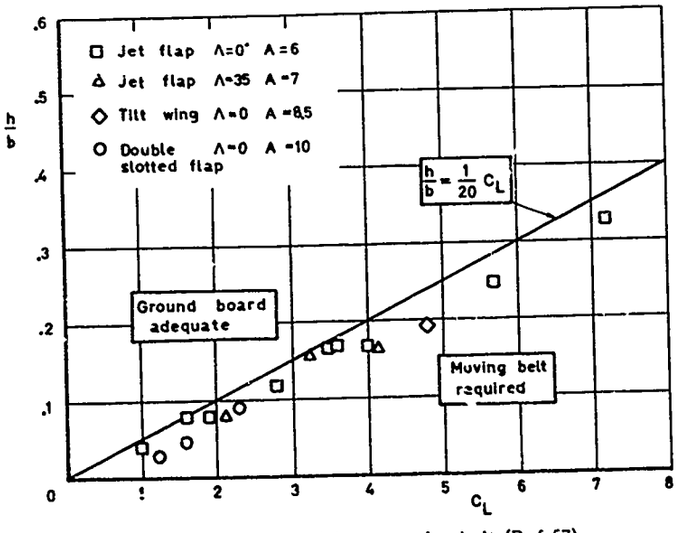

Fig.49 Conditions requiring a moving belt (Ref.57)

THE INFLUENCE OF V/STOL ON WING DESIGN AND TAILPLANE DESIGN

by

C.L.Bore
Head of Research
British Aerospace PLC: Kingston
Richmond Road
Kingston-upon-Thames, Surrey KT2 5QS, UK.

INTRODUCTION

At first glance, one might be excused for supposing that the influence of V/STOL on wing designs may be small. After all, a wing tends to be designed mainly by its cruise and manoeuvre requirements, does it not? However, I will show that the requirements of V/STOL can have a very strong influence on the wing design, and in turn the wing design has a strong influence on the performance of the aircraft.

The main points will be illustrated by following the development of wings of the Harrier family (i.e. Kestrel, Harrier, AV8B/Harrier GR5). If you will have patience to follow a little history, you will find many lessons of V/STOL wing design illuminated.

I will also add a few points about the special aerodynamic features of tailplane design for V/STOL.

THE EARLY WING REQUIREMENTS

Not long after the P.1127 prototypes flew, in 1961, we began to realise that the prototype wings (Fig. 1) were far from ideal for high speed manoeouvring. In fact, there could be boundary layer separations near the wing tips at high subsonic speeds, even at zero lift coefficient. The wing tip chord was small and led to high local suctions, especially when the ailerons were deflected, and interference from the undercarriage pods protruding forward of the leading edge caused separations in a triangle from the tip leading edge. By extending the leading edge near the tips, and cutting back the front of the tip pods so they did not protrude, the flow was improved, but the tip chord was still too small.

However, there was an Air Ministry Operational Requirement (O.R.) for a more powerful aircraft, and by 1962 we were designing a new wing which would be better for vigorous manoeuvring at high subsonic speeds. This development became the Kestrel (Fig. 1).

THE WING OF THE KESTREL (XV6A)

At that time investigations started into two of the crucial questions of V/STOL aerodynamics:

1. "How should one specify the optimum combination of qualities for the wing of a V/STOL aircraft?" and

2. "Given a specification, how may one proceed towards the shape and size of that optimum wing?'

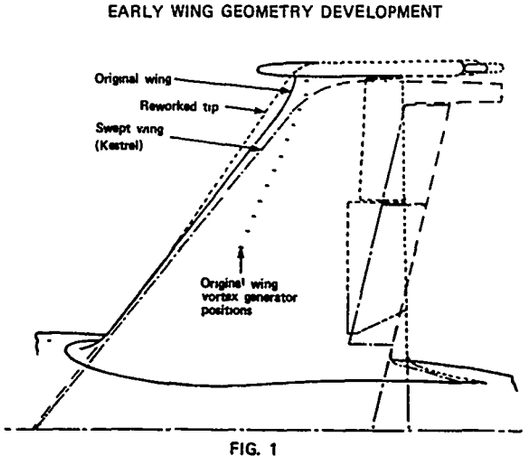

FIG. 1

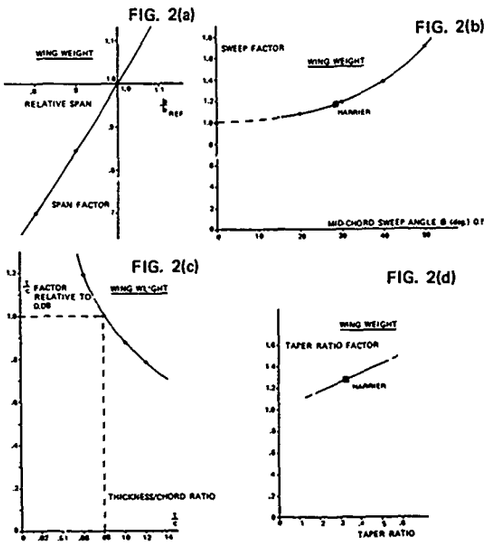

HOW TO SPECIFY AN OPTIMUM WING?

This question can only be answered in relation to the operation requirement (O.R.). In our case, the O.R. called for a low altitude armour-busting aircraft, with a maximum capability of 8g, and not less than 6g at a speed of 400 knots. The primary operating zone was below 10,000 feet (and generally in the lowest 100 feet or so). Good payload and range were required from vertical take-off.

From these requirements it was easy to conclude that our starting point should be: "a wing providing 6g at 400 knots which maximises the payload and range combination". Since the load of stores and fuel from VTO is the difference between VTO thrust and the dry weight, and wing drag was a small fraction of the whole, it followed that our optimum wing would be: "the lightest wing that provided the required manoeuvrability".

HOW TO DESIGN AN OPTIMUM WING?

To get anywhere near answering this question properly involved quite a lot of work, although there were some simple general principles.

Firstly we had an important benefit (a "negative penalty", if you like) stemming directly from the fact of having a vectored thrust V/STOL aircraft. With ample thrust available, take-off acceleration was high. With the ability to vector the entire gross thrust at will, even wing-borne landings at reduced throttle setting did not require all the lift to be provided by the wing and flap system. Thus the size of the wing could be determined by the manoeuvring requirements alone. Secondly, it was obvious that a small wing would weigh less than a big one, so clearly it must be "a good thing" to develop a wing with exceptionally high manoeuvring lift coefficients.

Other guidelines were suggested by the broad form of the wing structure weight charts (Fig. 2). These indicated that the wing weight could be reduced most sensitively by increasing the root thickness and decreasing the span. Since the wing had to contain a lot of fuel, it was tempting to opt for large root thickness and chord (especially as a quarter of our planform area is buried in the fuselage), but this should not be over-done, because if the planform extends past the nozzles too much, the V/STOL suckdown forces would increase. Furthermore an unduly thick wing root may lead to supersonic flow on the underside of the wing root, causing excess drag and lift loss, as discussed later (Fig. 10).

HIGH MANOEUVRING LIFT COEFFICIENT

What shapes of wing achieve the highest lift coefficients? That was a very good question (as the politicians say), but there was no existing answer. So we got hold of every piece of data on maximum lift of swept wings that we could find - including very valuable reports from fullscale tests in the NASA Ames 80 foot by 40 foot wind tunnel. We plotted those data against all sorts of geometrical variables until we found some that made sense. It was quite a tough piece of research (Ref. 1) but the conclusions did simplify the overall understanding substantially.

Basically we showed that for simple swept wings with thicknesses below 14%, the aerofoil section shape effects could be characterised in terms of the shape of the leading edge in planes normal to the leading edge. Roughly, the sectional effects depended mainly on the radius of the section profile normal to the leading edge (see Fig. 3).

The planform shape effects turned out rather unexpectedly, for we found that the limiting lift coefficients depended strongly on aspect ratio as well as leading edge sweep, as shown by the charts for the maximum usable C_L (Fig. 4). From clues such as these of Reference 1, it seemed that for an aspect ratio near 3 (which was the region we wanted) a leading edge sweep of about 40 degrees was near optimum. If we went to lower aspect ratio and high sweep, we would encounter higher lift dependent drag, and we did not want that.

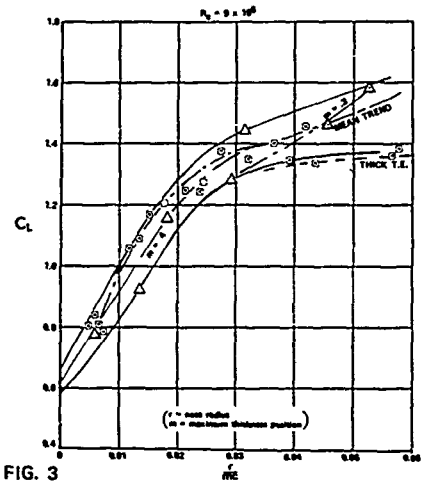

FIG. 3

FIG. 4a
SWEEP CORRECTION FACTOR: KINK

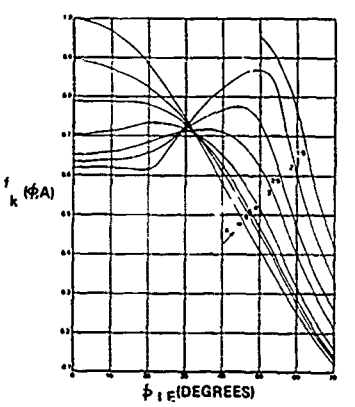

FIG. 4b
SWEEP CORRECTION FACTOR: USABLE

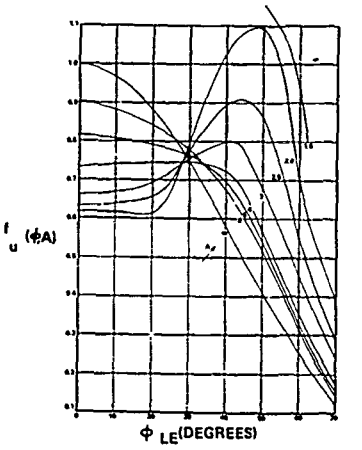

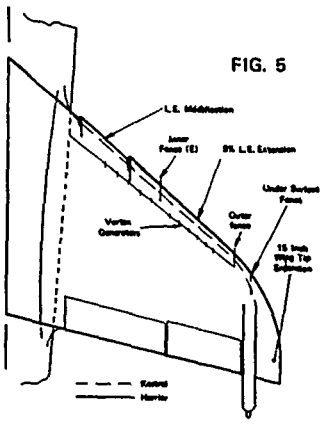

FIG. 5

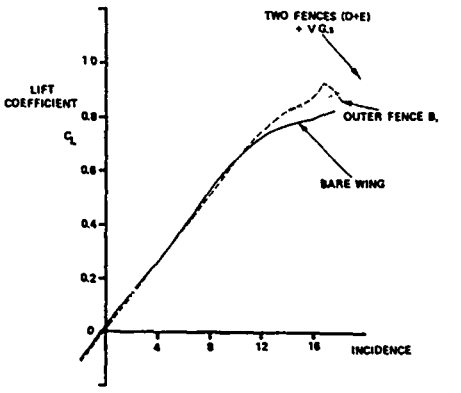

FIG 6 GETTING MORE USABLE LIFT

We knew that the curved streamwise tip of the Hunter wing worked well, so I settled upon the planform for the Kestrel, as shown in Figure 1. For the aerofoil sections, a colleague set about our first attempts at designing the supercritical sections with large leading edge radius. These used his inverse Weber computations in an attempt to incorporate Herbert Pearcey's "peaky" aerofoil characteristics into our three-dimensional wing. Although I was enthusiastic about incorporating supercritical aerofoils into the Kestrel, I personally doubted that the methods used would succeed, and argued that the "uniform isobars" philosophy would lead to some form of violent stall troubles. However, I was over-ruled.

When the Kestrel flew (early 1964) we found that over much of its speed range its wing was a great improvement over the prototype, but there was a range of Mach number centred on 0.88 over which the pilots intensely disliked its tendency to suddenly rock its wings, by up to 25 degrees. This wing rocking occurred at incidences where light buffet would be expected, but came without buffet warning. We found it was due to boundary layer separation (or local stalling) over substantial areas of the outer wing. We found that vortex generators improved some of the P.1127 and Kestrel wings, but not all, so they must have been astride the boundary of effectiveness.

THE P.1154 WING

Since the middle of 1961 we had been working hard on the NATO Basic Military Requirement NBM3, which called for a supersonic V/STOL aircraft, and our design submission of January 1962 was adjudged the technical winner of what was at that time the biggest design competition ever.

I chose a similar planform to that of the Kestrel, but decided to take a quite different route towards supercritical aerofoil sections, and deliberately chose to design for reducing peak suctions coming inboard across the wing, to avoid the sudden stalling of large areas of wing that I expected for the Kestrel design.

After consulting Herbert Pearcey (of the National Physical Laboratory) about his supercritical aerofoils, I concluded that they would be better with much larger leading edge radii, so (with Pearcey's encouragement) I took a set of NPL (STAC) supercritical aerofoils and grafted onto them enlarged nose regions, with radii around 0.8% chord instead of about 0.3% on the originals. NPL tests showed that they worked better than the originals, but of course they had various combinations of best behaviour, in terms of lift coefficient, Mach number and drag rise. There was not enough time to develop aerofoils for full chord supercritical flow, but for our subsonic manoeuvres we only needed the supercritical flow to 50% chord, so we adopted a judicious mix of our aerofoils (applied normal to all planform generators) to define the P.1154 wing.

Having devised the leading edge shape for the P.1154 wing, I wondered how those shapes would have fitted on the front of the Kestrel wing, so I had tracings of the P.1154 sections overlaid over the sections of the Kestrel. It turned out that they all blended very well into the upper surface shapes of the Kestrel, but the Kestrel noses were excessively bluff, so the P.1154 shapes led to nose profiles that extended 5% further forward than the leading edge of the Kestrel (and of course there had to be some fairing into the fatter underside of the Kestrel sections). Having satisfied myself that my "transplanted aerofoils" approach would have fitted onto the Kestrel, the drawings were rolled up and stored. We were, after all, working hard on the supersonic P.1154!

When the Kestrel wing flew and the high subsonic phenomenon of wing rocking was highlighted, the need to avoid it became the priority. Wind tunnel testing soon showed that the amplitude of the wing rocking forces on the P.1154 design was roughly half of that experienced on the Kestrel. After consideration of various means that might be used to reduce unsteadiness, I concluded that variations of wing twist and camber alone were unlikely to lead to completely vice free manoeuvring at all Mach numbers and lift coefficients, so some form of graded boundary layer control would be needed, such as a graded array of vortex generators.

It was around this time that I was bringing together various ideas into an explicit philosophy for combat wing design. In aiming for fully controllable manoeuvring at all speeds and incidence , we were committed to deliberate design for controlled flight with extensive areas of separated flow, and we would have to develop ways to manage the spread of separation. To achieve this objective we would have to resort to wind tunnel testing to gain insight.

THE HARRIER WING

Suddenly (in February 1965) we were told that the one-third built P.1154 was cancelled, and now we had to develop the Kestrel up to carry most of the P.1154 equipment, without changing anything, and fast! In the end we managed that (but changing about 2 million drawings!) So far as possible, we had to preserve as much as possible of the Kestrel wing.

The starting point was the aerofoil section drawings we had rolled up a few years earlier. We already knew that this promised better leading edge aerofoil characteristics and much reduced wing rock, and furthermore it was felt that vortex generators would have far more effectiveness over boundary layer separations caused by weaker shocks. However, the weight of the new aircraft (later known as the Harrier and AV8A) would be greater than that of the Kestrel, so we would have to squeeze more lift out of the modified wing. The extended leading edge gave us 3% more area, so that was a small contribution.

The pitching stability of the Kestrel was marginal when carrying large stores, and the Harrier would have to carry much bigger loads of external stores. So we needed more stability. By adding an extra 15 inches (380 mm) to each wing tip (Fig. 5) I was able to reap several benefits at once. Firstly the lift was now spread further aft, and the aerodynamic centre was moved aft by the amount needed. Secondly the new wing tip could now be designed with considerably better aerofoil sections normal to the leading edge. Thirdly, the wing tip undercarriage pods might now interfere less with the wing tip airflows, and finally the wing area was slightly enlarged.

Now came the intensive research and development. If we were to succeed in making this minimally modified wing manoeuvre the weight of the Harrier adequately, we would have to get substantially more lift per unit area than had ever been achieved before. With the planform and sections already settled, that left boundary layer control as the remaining feature to be developed. The intention was to develop an array of BLC devices that would so control the extent and rate of spread of separation, that the aircraft would be able to manoeuvre much further up the lift curve (Fig. 6).

The idea behind this was simple but important. If an aircraft is usable to its limits, eventually there may be separated flow over most of the wing, leading to high drag. However, the tolerability of the aircraft behaviour depends on how unsteady or intermittent is the separated flow, and on the way the forces and moments vary with incidence. If the boundary layer could be so controlled that the extent of separation was practically the same on both halves of the wing, then wing drop and wing rock would not occur. If the extent of separation could be made to grow only slowly with incidence, then the lift curve should continue to rise, and buffet levels should increase only gently with incidence.

This is not the place to go into detail about how that was achieved, for it is not specifically V/STOL aerodynamics, and is described in References 2, 3. Let us simply record that eventually an array of graded vortex generators, together with small leading edge fences and wing leading edge sawteeth did succeed in raising usable lift coefficients substantially above contemporary standards, as shown in Figure 7. The Harrier can be manoeuvred to "stick hard back" with full control at all Mach numbers and altitudes, with any stores on, except for one recent extreme design.

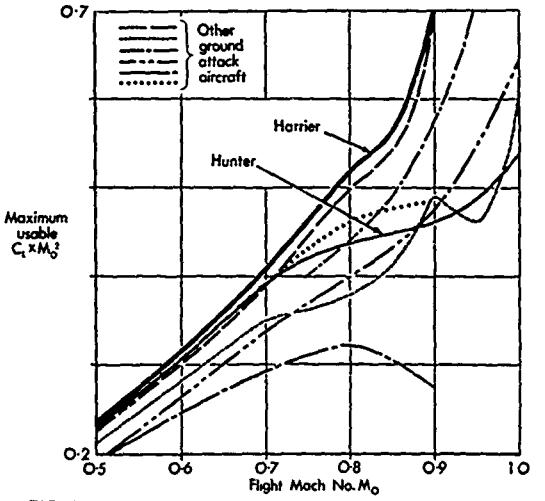

FIG. 7 USABLE MANOEUVRABILITY COEFFICIENTS FOR VARIOUS STRIKE-FIGHTER AIRCRAFT

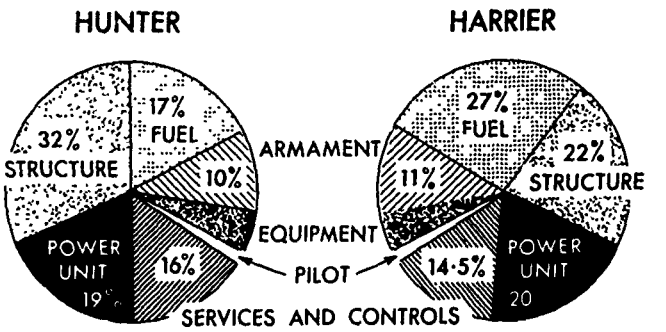

Additional Systems in Harrier, not in Hunter

Engine nozzle actuation	U/VHF Radio & Standby
Reaction Controls	HF/Tac VHF Radio
Water Injection	Equipment cooling system
Nav/Attack system	Air Data Computor
HUD System	Tacan

FIG. 8 TAKE-OFF WEIGHT COMPARISON

EFFECT OF WING DESIGN ON PAYLOAD/RANGE

Now we will examine the import of the work described above. By means of meticulous development, we had achieved a very light wing for the load it had to manoeuvre. The wing of the Harrier weighs about 1,200 pounds, while the wing of our previous fighter - the Hunter - weighed about 1,800 pounds more, to support the same all-up weight of aircraft.

The significance of the comparison with the Hunter is shown in Figure 8, where we see that broadly the fractions of all-up weight taken by engine, services and controls, armament and equipment are all the same.

The two glaring differences are the fraction occupied by structure weight (which is 22% in Harrier compared with 32% in Hunter) and fuel weight (which is 27% in Harrier and 17% in Hunter). Thus the saving in wing weight was translated into much greater fuel capacity and therefore range. In case you suspect that the Hunter was an unrepresentative comparison, see Figure 9, which shows that the average structure weight fraction of six ground attack aircraft was over 30%.

From this you will see why I tend to counter questions about the "essential penalties" of V/STOL with consideration of some of the prizes that can be won, if we work at it thoroughly enough.

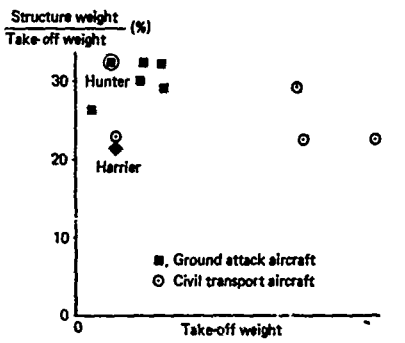

FIG. 9 STRUCTURE WEIGHT COMPARISON

WINGS FOR DEVELOPED HARRIERS

If one designs a wing for a V/STOL aircraft with an engine of (say) 18,000 pounds thrust, then (as we have seen) the process of optimisation drives the area and volume down to the minimum practicable for that size of aircraft. Now suppose that in the course of time the engine thrust is raised to (say) 24,000 pounds. Obviously this offers the opportunity to carry more stores and more fuel, but with the original size of wing, we soon find that there is no space to put these. We will need more pylons and more fuel volume, so clearly these requirements dictate that the minimum size of wing must increase in step with the engine thrust, just as happened on both the British and U.S. "Big Wing" developments from the Harrier.

On both sides of the Atlantic, of course, improved methods of aerodynamic computation have permitted us to adopt still thicker wings for given drag, while advances in structural design reduce further the weight penalties of bigger wings. Nowadays too, we may choose to fit an enormous lifting vortex generator (called a LEX) in place of several smaller VGs. If requirements change to emphasise STO instead of VTO, then the contribution of wing and flap to total lift at take-off can no longer be neglected, but still the desirability and practicability of low weight wings remains. Furthermore, the philosophy of designing for vice-free controllable manoeuvring at all conditions (including substantial separations) retains its force. So attached flow computations are not yet a complete guide to the aerodynamics!

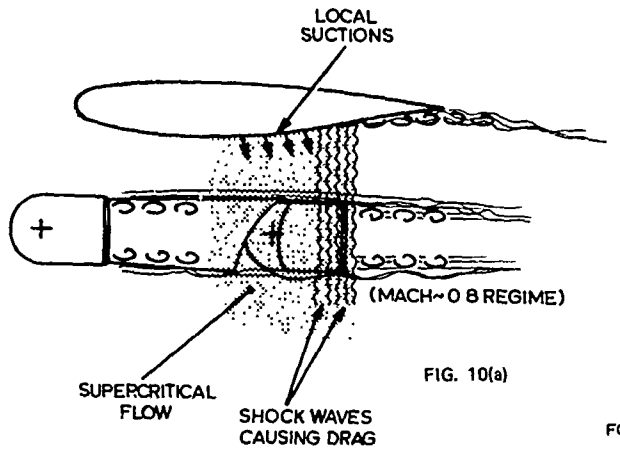

FIG. 10(a)

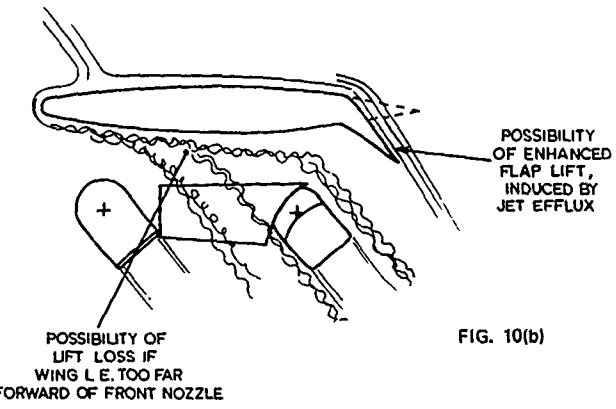

FIG. 10(b)

WHY STOP HERE?

Basically we would like more payload manoeuvring capability per unit of weight, so why not keep going along the routes described? Let us consider some more of the constraints. Figure 10(a) illustrates one constraint against thickening the wing roots too much. If the underside of the wing is allowed to become too convex close to the front nozzles, the sonic flow from the front nozzles may induce the surrounding airflow to become supersonic in the region of the wing root/fuselage/nozzle fairing junction. This would lead to substantial drag penalties and some loss of lift.

To avoid this the shaping of the entire junction may need to be revised, or the front nozzle should be lowered, or some other way of reducing weight should be found - such as distributing the load spanwise.

Figure 10(b) illustrates two considerations from the vectored thrust regime. Both jet effluxes tend to induce inflow from the surrounding air, which gets entrained and drawn downstream. If the leading edge of the wing overhangs the front nozzle too far forward, then the downflow may result in lift loss during vectored thrust flight. Lowering the front nozzle may help. Lift loss is less serious from the rear jets, especially if the flaps are lowered. In some circumstances, the rear efflux passing close to the trailing edge of the flaps may induce lower pressure just above the trailing edge, and thus secure additional flap lift. Naturally this is of more benefit in STOL.

GENERAL CONCLUSIONS

We have seen that one of the most powerful influences upon the payload/range of V/STOL aircraft is exerted by reducing the weight of the wing. The process of designing a lightwight wing involves meticulous effort to achieve exceptionally high manoeuvring lift coefficients, combined with due attention to the geometrical and structural interactions. There are constraints all round, such as the need to avoid undue interference with jet effluxes below the wing roots, and the physical constraint of providing fuel volume and space for low drag store carriage. Any structural complexities which threaten to increase wing weight seriously (such as cut-outs, opening panels for fans or ejectors and so on) are inefficiences which should be entertained only for valuable benefits.

REFERENCES

1. C.L. Bore and A.T. Boyd — Estimation of Maximum Lift of Swept Wings at Low Mach Numbers. J.R.Ae.S. April 1963.

2. C.L. Bore — Harrier Aerodynamics Design: Wing. A/C Eng. December 1969.

3. C.L. Bore — Post Stall Aerodynamics of the Harrier GR1. AGARD-CP-102, Paper 19. April 1972.

TAILPLANE DESIGN

Tailplane design is a good example of the fact that V/STOL generally adds several more criteria to be observed. In our case, there is the whole vectored thrust regime to consider: a regime in which the jet effluxes are especially vigorous relative to the free stream, and they may be at any angle from zero to 100 degrees to the free stream. Even in the conventional flight regime, the presence of four jet effluxes flowing beneath the tailplane leads to changes of trim when the throttle setting is changed (Fig. 1).

Originally, the tailplane of the P.1127 had no anhedral, and its span was conventional. Unfortunately this gave a tendency to pitch up at quite modest lift coefficients (Fig. 2), and gave little contribution to stability during vectored thrust transitions. Note, however, that in low speed vectored thrust flight, the reaction controls contribute strongly to control, so the tailplane is only part of the total control picture.

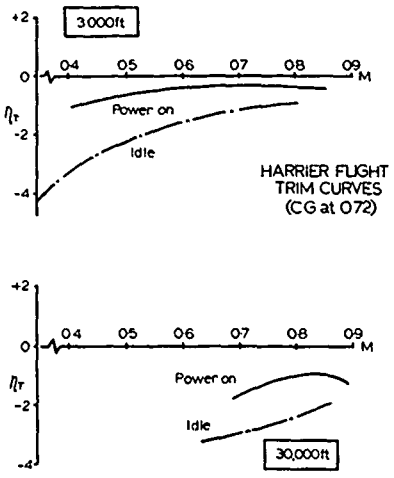

FIG. 1

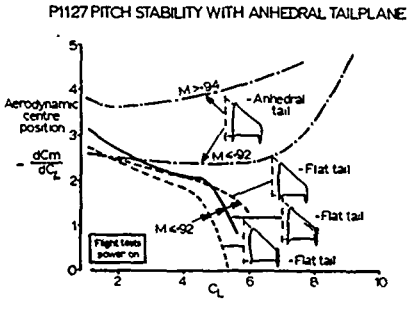

FIG. 2

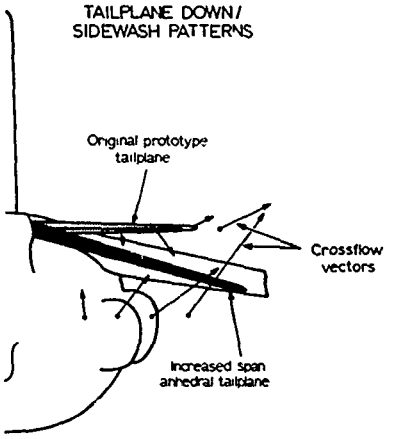

FIG. 3

As we have found many times since, any general ad hoc investigation would have taken a great deal of time and money because of the numerous combinations of configuration and aerodynamic parameters. In this case it was decided to make a thorough survey of flow directions over the whole region where a tailplane might be put. After analysis, it was concluded that most of the flat tailplane was in a field of downwash induced above the jet effluxes (Fig. 3), but there were upwashes and sidewashes further outboard and lower. By imposing anhedral the tailplane could use the vigorous sidewashes to capture a stabilising force contribution. Furthermore, by extending the span of the tailplane the tips were moved into a region of vigorous upwash and sidewash outboard of the jet effluxes.

Checking out the anhedral tail in conventional flight (Fig. 2) it was clear that this gave fairly constant stability up to a lift coefficient approaching 0.8, with increasing pitching stability at higher lift. This was found to be a desirable characteristic.

There are further factors arising from V/STOL layout considerations. For example, in the "conventional" layouts of the Harrier family, the tailplane is subjected to low frequency buffeting from the jets when the engine run up on the ground, and this may be a significant fatigue loading action. Even in conventional flight the tailplane picks up some unsteady air loading from the jets passing beneath it, and this contributes to the fatigue loading of the rear fuselage.

If a radically different aircraft configuration were considered, it would still be wise to note the lesson that flow direction surveys over the whole tail region are very informative, so it would be worthwhile to make such surveys and deduce the best position and dihedral for the tailplane (and may be the best fin cant angles too). Note that these should be done for different throttle settings in conventional flight, and various jet angles in vectored thrust flight.

V/STOL CONCEPTS IN THE UNITED STATES PAST, PRESENT, AND FUTURE

W. P. Nelms and S. B. Anderson
NASA Ames Research Center
Moffett Field, California 94035, U.S.A.

SUMMARY

This lecture summarizes V/STOL aircraft developed in the United States and describes concepts considered for future applications. The discussion is limited to non-helicopter types of vehicles. In particular, past V/STOL aircraft will be reviewed, and some lessons learned from a selected number of concepts will be highlighted. The only current concept described is the AV-8B, which was developed by modifications to the British Harrier. Configurations recently proposed for the future subsonic, multimission aircraft and the future supersonic fighter/attack aircraft will be described. Emphasis in the lecture will be on these supersonic concepts.

1. INTRODUCTION

In the history of aviation development, visions of vertical-takeoff and landing (VTOL) flight preceded visions of fixed-wing operation. Leonardo da Vinci proposed a lift fan VTOL version in 1483 — an idea that would have to wait some 475 years to become reality. Even as the conventional aircraft's appearance and successful development was paced by the requirement for a relatively lightweight power plant, the development of the VTOL concept obviously needed a major breakthrough in the ratio of engine power to weight. VTOL capability has been achieved in the helicopter, but the additional desire for high-speed flight and maneuverability resulted in a continued search for other approaches. The surge to achieve VTOL operation occurred soon after World War II (WW II) when large thrust-to-weight jet and turboprop engines became available. Particularly in the United States, a vast proliferation of VTOL concepts were designed and tested in the period following WW II.

There were many reasons for the failure of some of these concepts to become operational, including a lack of a requirement for VTOL operation, in addition to a need for further technological development. Although a sharp cutback in VTOL flight articles occurred in the U.S. in the late '60s, studies have continued by the Department of Defense (DOD) to weigh the cost effectiveness of various VTOL designs and to consider the impact of the related aeronautical and propulsion disciplines that have improved over the years.

The intent of this lecture paper is to briefly review (in chronological order) some of the past VTOL concepts in the United States (non-rotorcraft) and to summarize the lessons learned, either good or bad. Hopefully, some of these lessons learned will influence present and future concepts developed in the U.S. The prospect of accomplishing this will be left for the reader to ponder, as the paper continues with a description of the present (AV-8B) and proposed concepts.

2. PAST CONCEPTS

Although only a small measure of operational utility has resulted from the large number of VTOL concepts developed and tested in the post-WW II period, valuable information was obtained from these programs which can help guide the design of future vehicles. In contrast to the European approach, which used jet-lift exclusively for the vertical thrust mechanism, a wide variety of lifting principles were examined in the U.S. In part this was due to the differing mission requirements specified by the Air Force, Army, and Navy, and also due to a "flight research" attitude which prevailed on the DOD/NASA ad hoc advisory committees. For this paper, only those vehicles which achieved some form of flight evaluation are discussed; unfortunately, this results in the exclusion of some interesting concepts such as the XFV-12A. The material presented herein is taken from Refs. 1 and 2, which give additional details on the aircraft presented here as well as a description of additional concepts.

2.1 Tail Sitters

In the late 1940s, a U.S. Navy program to permit VTOL operation from small ship platforms spawned several tail-sitter designs; i.e., the vertical attitude takeoff and landing (VATOL) aircraft concepts. Two were turboprops, the Lockheed XFV-1 (Fig. 1) and the Convair XFY-1 (Fig. 2), and the other the jet-powered Ryan X-13. Of the turboprop types, the Convair XFY-1 achieved a more complete VTOL operational evaluation; the Lockheed XFV-1 highly tapered, straight-wing design made the transition to vertical flight only at altitude, using a jury-rigged, landing-gear cradle for conventional takeoff and landings.

The Convair XFY-1, which had a delta wing planform and was powered by an Allison YT40A-14 turboprop, made its first vertical flight in August 1954; six transitions to conventional flight were successfully completed before testing was curtailed because of engine and gear-box reliability problems.

In retrospect, the XFY-1 and the other VATOL concepts had some serious fundamental limitations which were not fully appreciated in the early years of VTOL aircraft testing. Foremost among the deficiencies was the lack of STOL operational capability which could improve the poor payload and range capabilities of these aircraft. The benefits to be gained from STOL capability were not recognized during the early development of these VTOL concepts. Although dispensing with a conventional landing gear improved the empty weight fraction for these VATOL aircraft, some form of gear was required on the vertical and horizontal tail surfaces. Not only were these landing gears limited to relatively low allowable sink rates, but as can be appreciated from the photograph of the Lockheed XFV-1 (Fig. 1), tip-over tendencies were a constant worry in gusty air and on uneven ground, particularly with the propellers turning. Another problem was the pilot skill required to operate these tail-sitter designs in landing approach and touchdown because of (1) the unusual spatial orientation where the pilot looked over his shoulder and down, (2) the sensitivity to atmospheric turbulence, and (3) reduced control power near touchdown. The precision of flightpath control offered by these concepts was,

needless to say, less than desired. In addition, hovering over a given spot and touching down precisely was extremely difficult.

Although vertical takeoff and transition to conventional flight was easily carried out, the transition from conventional flight to landing approach utilized by the Convair XFY-1 was somewhat unorthodox in that a zoom climb was made to achieve a vertical attitude for the descent and to reduce airspeed (altitude gain of about 3,000 ft).

The only jet VATOL, the Ryan X-13 Vertijet, which first flew in May 1956 (Fig. 3), was more successful, completing over 120 flights. It used a high-wing, delta planform and was powered by a Rolls-Royce Avon turbojet. In part because of the concern for operating the turbojet engine close to the ground, the X-13 was flown from an elevated position on a vertical platform. Although it had deficiencies similar to those of the Convair XFY-1 from the standpoint of the lack of STOL capability for increased payload and range, as well as some limitations in precise flightpath control in approach and hookup, the aircraft satisfactorily demonstrated the potential for VATOL operation from a portable landing pad. These tests were carried out in spite of an undesirably large positive dihedral effect (particularly at high angles of attack), and heavy buffet in transitioning from conventional to low-speed flight as the wing operated through the stall angle-of-attack range.

On the positive side, no hot-gas ingestion or aerodynamic suck-down were evident and the high-speed performance potential was not compromised by the VTOL features of these designs.

2.2 Bell Air Test Vehicle and X-14 Aircraft

The Bell Air Test Vehicle (ATV) (Fig. 4) was a proof-of-concept vehicle and the first jet VTOL aircraft to fly in the United States (1953). Using a high wing with a "T" tail layout, and powered by two Fairchild J-44 turbojet engines and a separate Poulouste compressor for reaction-control jets, the ATV was flown from a platform to reduce exhaust ingestion effects. Although it never made the transition to conventional flight, it effectively demonstrated that this VTOL design could indeed be flown at low airspeeds using a simple reaction control system with no stabilization augmentation system (SAS). As a result, work proceeded on the design and development of the Bell X-14 vehicle, which had a much broader flight envelope.

The X-14 (Fig. 5) used Beech Bonanza wings, engine bleed air nozzles at the aircraft extremities for hover control, and Bristol Siddeley Viper turbojet engines with cascade thrust diverters. It first hovered in February 1957 and transitioned in May 1958. This configuration clearly demonstrated the detrimental effects of engine gyroscopic cross-coupling, aerodynamic suck-down, and hot-gas ingestion in hover operations. No STOL performance potential (favorable lift-induced flow) was possible with the type of cascade thrust-deflection system used. Partially vectored thrust caused undesirable random flow which seriously affected precision of low-speed flightpath control. Because of this, the thrust could not be rapidly vectored from forward acceleration to a partial vectored position for STO operation, as is done for the Harrier.

It is of interest to note that in spite of a long, successful, trouble-free, flight operational history (over 25 yr), the cascade-vector principle used on the X-14 has not been used in any subsequent U.S. VTOL designs; however, the Russian experimental YAK-36 ("Free-hand") used a similar VTOL principle.

2.3 Bell XV-3 Tilt Rotor

The XV-3 tilt-rotor aircraft (Fig. 6) transitioned in December 1958, with a two-bladed rotor system. It was powered by a single piston engine in the fuselage. It had a positive aerodynamic ground effect, but could not hover out of ground effect. The XV-3, tested extensively at NASA Ames Research Center, disclosed that the design had good STOL performance capability by virtue of favorable induced flow effects, rapid transition with only small trim changes, and a wide speed and angle-of-attack corridor.

Maximum speed was limited by a pitch and yaw dynamic instability associated with destabilizing side forces on the rotor blade which was forward of the center of gravity. This was aggravated as blade angle was increased for high-speed operation. This instability could have been reduced by stability augmentation or a larger tail volume or both.

In general, the performance and handling qualities of the XV-3 were favorable enough to warrant proceeding to a more advanced (higher-performance) tilt-rotor vehicle (the XV-15, discussed later).

2.4 Ryan VZ3-RY Deflected Slipstream

The VZ3-RY (Fig. 7) was one of the more successful fixed-wing designs employing the deflected slipstream principle for high lift. Powered by a Lycoming T-53-L-1 turboshaft engine, it first flew in December 1958, with large (40% chord) double-slotted flaps and a hot-exhaust nozzle for pitch and yaw control. The VZ3-RY clearly demonstrated good STOL performance; however, hover capability was limited by ineffective turning of the slipstream, recirculation, and random flow disturbances in ground effect (IGE). Improvements in low-speed capability were obtained during tests at NASA Ames Research Center by installing a full-span leading-edge slat. Although this lift improvement allowed hovering out-of-ground-effect (OGE), slipstream recirculation precluded making a true VTOL vehicle of this design. In addition, transition with this concept required precise pilot techniques because of static pitch instability at high C_L, very large pitch trim changes with flap deflection and engine power changes, and poor flightpath control in steep approaches as power was reduced to descend.

2.5 Boeing-Vertol VZ-2 Tilt Wing

The VZ-2 (Fig. 8) high-wing, "T" tail configuration first flew in August 1957, with the first transition in July 1958. It was powered by a Lycoming YT53-L-1 turboshaft engine with cross-shafting between the two propellers. The VZ-2 successfully demonstrated the good STOL performance potential of the tilt-wing concept. Because of low pitch-control power and no SAS to aid the low inherent pitch damping, hover operations had to be restricted to calm air conditions. Tests at NASA Langley Research Center disclosed the need to provide good wing leading-edge stall protection during deceleration or descent when power was reduced. Transition to

wing-supported flight imposed no limitations, lending confidence to proceed to high-performance tilt-wing designs.

2.6 Doak VZ-4 Ducted Fan

The VZ-4 (Fig. 9), a low-wing conventional planform, first flew in February 1958, powered by a Lycoming YT53 turboshaft engine with cross-shafting to tilting ducts at each wing tip. This configuration suffered from low inherent control power about all axes, sensitivity to ground-effect disturbances, large side forces associated with the large ducts, and a large (positive) dihedral effect which restricted operation to calm-air conditions and no crosswinds. No large STOL performance gain was evident with this design. Transition to conventional flight could be made rapidly (17 sec); however, large nose-up trim changes required careful speed and duct-angle programming. The deceleration and/or descent corridor was restricted by duct-lip stall as power was reduced. Although this aircraft was limited in low-speed and hover capability, it indicated the feasibility as well as the inherent problems of the tilt-duct concept which helped the X-22 design which followed and is described later.

2.7 Lockheed XV-4A Augmentor Concept

The XV-4A (Hummingbird) (Fig. 10) made its first conventional flight in July 1962 and first transition in November 1963. The XV-4A was a 7,200-lb, two-seat, twin-engine (JT-12 turbojet) vehicle which used the engine exhaust directed into an augmentor jet ejector system contained in the fuselage to provide increased vertical lift. Jet (bleed-air) reaction nozzles on three axes were used for hover control. Good low- and high-speed performance potential existed for this concept (estimated 530 mph), because the vertical lift capability was completely enclosed in the fuselage and full engine thrust was available for conventional flight. STOL performance was poor, however, because of the large ram drag associated with turning the airflow through the augmentation system and the lack of favorable flow over the wing induced by the augmentor exhaust to increase lift. Hover performance was compromised by inadequate augmentor efficiency, aerodynamic suck-down (approximately 5%), and hot-gas ingestion. The aircraft trim position in hover was nose-up, which increased the possibility of hot-gas ingestion as forward speed was increased. Flow mixing in the augmentor reduced gas temperature from 1,200°F at the engine exit to 300°F at the augmentor exit. An important lesson was learned during transition attempts in which a strong pitch-up was encountered at 60 knots. An unusual operational procedure was used to get through this critical speed range; engine power was reduced when the pitch-up occurred and then added as the aircraft was in the dynamic process of pitching down. This procedure was too difficult and the aircraft (and pilot) were lost during transition in June 1964.

2.8 Ryan XV-5A and XV-5B Fan-in-Wing

The Ryan XV-5 VTOL design (Fig. 11) was a 9,200-lb twin-engine, tri-fan, turbojet-powered research aircraft; it hovered in June 1964 and first transitioned in November 1964. Two fans in the wings and a third in the forward fuselage for pitch control provided vertical lift. This vehicle had many successful flights because of extensive ground and full-scale wind-tunnel test programs that pinpointed potential problem areas before flight. The lift-fan concept proved to be relatively free of mechanical problems. A moderate dihedral effect and low roll-control power limited crosswind operation to 12-15 knots. Although positive aerodynamic lift was inherent in this design (favorable fountain effect), hot-gas ingestion from the exhaust of the tip-turbine fan drive degraded lift-off thrust by as much as 15% until a wheel height of 10 ft was attained. Operational techniques to minimize ground effects included lifting off in a slightly nose-high attitude, keeping the tail to the wind, and gaining height as rapidly as possible. For several reasons STOL performance was extremely poor: (1) large ram drag of the three fans, (2) low horizontal acceleration because of limited turning of exhaust flow (maximum fan-thrust angle was 45°), and (3) low thrust-vector rotation rate. The transition corridor was marginally adequate because of limited forward thrust and the need to abruptly increase angle of attack (about 12°) to gain aerodynamic lift when the wing fan doors were closed. Because of a strong nose-up force with wing fan start-up, a large reduction in angle of attack was required by elevator input. This, together with fan overspeed tendencies, increased conversion difficulties. Low-speed stall characteristics included a potential deep-stall problem. NASA tests of the XV-5B disclosed flightpath control problems during steep (up to 20°) decelerating approaches including the following: (1) power management was compromised by dual height-control methods (lift spoilage or engine speed) (pilot prefers one lever for power management), and (2) there was a need to minimize aerodynamic lift because longitudinal static stability changed adversely as speed decreased.

This configuration has limited high-speed potential because of the relatively thick wing section needed to house the lift fans and vectoring hardware.

Several lessons were learned from operational demonstrations of the XV-5A. One demonstration involved a large pitch trim change in converting from conventional flight. The aircraft was observed to pitch down abruptly from level flight (about 45°) during transition to powered-lift flight. (The pilot ejected just before ground contact but was killed.) The accident was attributed to inadvertent selection of full nose-down stabilizer position at too high an airspeed. Another concern of this design was the susceptibility of the fans to foreign object damage when the vehicle hovered near the ground.

2.9 Ling-Tempco-Vought XC-142 Tilt Wing

The XC-142 tilt-wing (Fig. 12) used four T64-GE-1 engines with cross-shafting to four propellers and a tail propeller for pitch control. The first conventional flight was made in September 1964, the first hover in December 1964, and transition in January 1965. Hover of the XC-142 was satisfactory with no adverse flow upsets, and precise spot positioning was good. This configuration produced no adverse lateral-directional characteristics in sideward flight to 25 knots. In slow forward flight, a long-period (20-sec) oscillation was apparent which could lead to an uncontrollable pitch-up. On one occasion full-forward stick did not arrest the pitch-up, whereupon the pilot reduced engine power, the nose fell through, and the aircraft was extensively damaged in a hard landing. STOL performance was not as good as predicted, and low-speed controllability was compromised IGE by several factors, including (1) severe recirculation of propeller slipstream for wing-tilt angles in the range 40° to 80° (speed range 30 to 60 knots), producing large-amplitude lateral-directional upsets; (2) weak positive, neutral, and negative static longitudinal stability with speed

changes; and (3) low directional control power. The transition corridor was satisfactory, with ample acceleration/deceleration capabilities. Higher drag inherent in the configuration geometry resulted in poor cruise performance.

Many successful demonstration flights were made with the XC-142, some directed at commercial applications; however, the complexity of the design and the deficiencies noted would have made FAA certification difficult. A failure of the drive shaft to the tail propeller (pitch control) in low-speed flight caused a fatal crash which curtailed further development.

2.10 Curtiss Wright X-19A Tilt Prop

The six-passenger X-19A aircraft (Fig. 13) had twin intershafted engines, a tandem high wing, and four tilting, large-chord propellers. These were designed to develop large radial (lift) forces in conventional flight, thereby reducing wing-area requirements and subsequent drag. The first hover flight was made in November 1963. Transition tests progressed to about 120 knots, but the aircraft never completed transition. Poor mechanical control system characteristics, not peculiar to the concept, severely penalized low-speed operation and made precision hover impossible. Upsets caused by random-flow IGE further increased pilot workload in hover. A positive ground effect was observed up to wheel heights of 4 to 5 ft. Low downwash velocities and lack of hot-gas ingestion were favorable features of this design. Control and height coupling was a problem, in part because of sluggish height-control response (engine rpm was varied instead of collective prop pitch). A pilot induced oscillation (PIO) tendency in height control was encountered as a result of these characteristics which were not concept-inherent. A moderately favorable STOL performance could be expected with this configuration as well as good cruise performance because of the clean (low-drag) design. One prototype crashed because of a fatigue failure of a gearbox mounting. This caused the left rear propeller to separate from the aircraft during transition tests. This exemplified an inherent deficiency of this VTOL (lift) arrangement: to safely transmit power to the extremities of the planform, very strong (and fatigue-resistant) structures must be incorporated with an obvious weight penalty.

2.11 Bell X-22A Ducted Fan

This tandem-wing ducted-fan/propeller X-22A aircraft (Fig. 14) was powered by four GE T-58 turboshaft engines in the rear fuselage interconnected to the ducted fans such that in the event of an engine failure the remaining engines would drive all four fans. The first hover flight took place in March 1966, and transition was completed in June 1967. Hover operation OGE in no wind was rated excellent, with no perceptible hot-gas ingestion. A 12% positive thrust increase was generated IGE by the favorable fountain. Airframe shaking and buffeting occurred at wheel heights up to about 15 ft, and cross-wind effects were quite noticeable because of large side forces generated by the ducts. Vertical cross-wind landings required an excessive bank angle to avoid lateral drift. STOL performance was rated good by virtue of the increased duct-lifting forces. High-speed performance was limited by inherent high drag associated with the four large ducts. Transition to conventional flight could be made easily because of a wide transition corridor; however, inherent damping was low. Deceleration and descent at low engine powers caused undesirable duct "buzz" as a result of flow separation on the lower duct lips. Vortex generators appreciably improved this flow-separation problem.

2.12 Bell XV-15 Advanced Tilt Rotor

The Bell XV-15 research aircraft (Fig. 15), a modern version of the XV-3, is powered by two Lycoming LTC 1K-4K engines rated at 1800 shaft hp each. This aircraft first hovered in May 1977. Two interconnected 25-ft-diameter three-bladed rotors are used with a blade twist of 45° from root to tip. Hover characteristics are similar to those of other tandem-rotor helicopter configurations in that wind direction changes rotor span-loading, affecting hover precision. The concept has a large hover envelope (30 knots sideward and 30 knots rearward) with no handling-qualities limitations. There is an unsteadiness when hovering close to the ground which disappears above a wheel height of 6-12 ft. Transition to conventional flight is easily accomplished with this concept because of a wide speed corridor, a large reduction in power required for level flight, and good (0.4 g) acceleration capability. Trim changes are small, and stability and damping are adequate to minimize unwanted flightpath excursions.

In conventional flight, a unique aircraft longitudinal response (which has been called "chugging") occurs in gusty air; it is attributed to gust-induced angle-of-attack changes on the propeller blade. No undesirable limits in stability or damping (which restricted high-speed flight in the XV-3 aircraft) have appeared to speeds of 300 mph. Stalling behavior in conventional flight is mild, with ample warning and no roll-off. In the event of an engine failure, the aircraft can be either landed at low speeds with the propellers windmilling or brought to a hover-type landing in an autorotative mode. One-engine-out hover performance is not possible with the power currently available. Reconversion characteristics permit slow or fast decelerations with adequate descent rates and a wide speed corridor. A variable tilt rate for the rotors would appear to enhance operational flexibility.

This design shows the best potential for combining good hover performance with reasonable cruise efficiency. It remains to be seen if the relatively complex propulsive system can achieve a low-cost maintenance record and high reliability.

2.13 Lessons Learned

An overview of the development of a wide variety of V/STOL concepts has served to identify several problem areas which, when considered collectively, make it easier to understand why no fixed-wing commercial V/STOL design exists today, and why only one type has achieved military operational status.

Foremost among the reasons for lack of acceptance were poor handling qualities, some unexpected and some ignored in the design stage. Deficiencies in handling qualities were serious enough to cause the loss of several aircraft and pilots. The dominating factors were the inadequate control power to trim out the moments associated with power-induced effects, ground-effect disturbances, and changes in power, flap setting and speed. Flightpath control in landing approach was less than desired, particularly for the VATOLs and tilt-wing vehicles with power reduced for steep descents.

The need for some degree of SAS for all lift concepts in hover and low-speed flight was apparent for safely carrying out even simple operational tasks, particularly in turbulence. For many types, VFR operation was marginal and IFR capability impossible because of low inherent stability and damping.

Marginal performance restricted operational evaluations for many V/STOL concepts. Some vehicles exhibited marginal performance in transition to conventional flight. The need for good STOL performance, a virtue not shared by many of the vehicles, was not appreciated at the onset. V/STOL aircraft that effectively utilize propulsion-induced flow to augment aerodynamic lift have the best chance to be truly competitive. Several of the aircraft lacked good low- and high-speed compatibility in that the features that provided VTOL capability severely compromised high-speed performance.

Most of the aircraft suffered in several ways from ground effects. Reingestion of engine exhaust lowered takeoff thrust, and exhaust flow effects resulted in aerodynamic suck-down for most jet-powered concepts. Ground erosion was a major problem for all turbojet operations. Noise from the turbojet engines was a major deficiency for commercial operation. Recirculation of the propeller slipstream resulted in performance degradation and stability and control problems for tilt-wing types. The significance of these ground-effect problems was not appreciated at the aircraft design stage and there is a continued need for better prediction techniques.

3. PRESENT CONCEPT

The only V/STOL fighter aircraft currently in service in the United States (Marine Corps) is the AV-8A Harrier developed by British Aerospace. This aircraft is described in another lecture in this series, so it will not receive attention here. Rather, the higher-performance AV-8B Harrier II, developed by McDonnell Douglas and the major subcontractor, British Aerospace, will be reviewed. Since the concept is well known, the discussion will be brief, focusing primarily on the differences between the AV-8A and AV-8B. At present, four full-scale development AV-8B aircraft are flying, and production is under way for the first squadron of AV-8Bs, scheduled to be operational by 1985.

Figures 16 and 17 show the AV-8B aircraft in hover. Three views are given in Fig. 18. The propulsion system is a single 21,500-lb-thrust, Rolls-Royce Pegasus 11 turbofan engine with four rotating exhaust nozzles. These rotating nozzles direct thrust vertically for VTOL or at intermediate angles for STOL operation. In cruise flight, thrust is directed to the rear, and thrust vectoring can be used to improve maneuverability throughout the flight envelope. Aircraft attitude control during V/STOL and hover is accomplished by reaction controls located at the wing tips, the nose, and the tail. A cannon is available for air-to-ground or air-to-air attack Seven store stations are available for a variety of bombs, flare launchers, rocket pods, AIM-9 missiles, guided weapons, and/or external fuel.

A number of changes were made to the AV-8A design to develop the AV-8B Harrier II. These are summarized in Fig. 19 together with a drawing showing the interior arrangement of the aircraft. A number of advanced technologies have been incorporated into the AV-8B, and these are summarized in Fig. 20. Of note is the new wing having a supercritical airfoil for improved lift and cruise characteristics, plus greater fuel capacity. Graphite-epoxy/composite materials are used for the wing, ailerons, flaps, horizontal stabilator, rudder, and outrigger fairings. Redesigned inlets and fuselage-mounted lift-improvement devices enable greater lift for vertical and short takeoff and for more efficient cruise. A raised cockpit has been incorporated to improve visibility. A positive-circulation, inboard flap is used to increase STOL capability and a wing root leading-edge extension to improve maneuverability.

4. FUTURE CONCEPTS

The past and present V/STOL aircraft which have been described are characterized by actual hardware. As for the future concepts, the descriptions will be based on extensive studies conducted by the U.S. Government and industry. In some cases, the concepts described are several years old and many not necessarily represent the current thinking of the organization involved. However, the concepts represent the possible applications of various propulsive lift systems and are therefore appropriate to include in this paper.

Two classes of future vehicles will be considered. The first is the subsonic, multimission aircraft, sometimes referred to as "Type A," but herein referred to as the medium-speed concept. The second is the supersonic fighter/attack aircraft with twin or single cruise engines. The fighter aircraft will be given the major attention in the paper.

4.1 Medium-Speed Concepts

During the past several years, the subsonic, multimission V/STOL aircraft has received considerable attention in the United States, primarily as a result of the Navy's desire to develop a versatile aircraft to perform a number of critical missions from either large or small surface vessels. These missions include ASW, AEW, COD, Tanker, SAR, Marine Assault, and Missileer. More recently, a V/STOL aircraft of this type is of interest to perform other specialized missions, such as rapid deployment of forces and heavy lift logistic transport.

Numerous V/STOL aircraft concepts to fulfill these roles have been studied by the U.S. Government and industry. These concepts have included a number of approaches to the propulsive lift system. The concepts described are not all-inclusive, but are intended to serve as examples of the application of the various propulsive lift approaches. It should be noted that the concepts described represent the thinking of the contractor involved at the time of the study and may not, in all cases, be the currently preferred concept.

4.1.1 Boeing

In the recent past, Boeing studied several approaches to the medium-speed concept. Two of these are briefly described here.

One concept features two tilting nacelles and a forward lift fan. An artist's rendering of this concept is shown in Fig. 21. The two tilt-fan engines, with a pressure ratio of approximately 1.3, are used for both hover and cruise flight. The nose-mounted lift fan is used for hover and transition only. The tilt engines and nose fan are interconnected by a mechanical system. Pitch and roll control in hover are provided by differential collective fan blade pitch, and yaw control is provided by movable vanes in the fan efflux.

Another concept studied by Boeing features a blown flap system, (Fig. 22). Two fixed-fan engines (pressure ratio of about 1.15) are mounted on the wings. The exhaust is directed below the wing, and in hover is directed downward by triple slotted trailing edge flaps. Also in hover half of the fan exhaust is directed downward in front of the wing through "chin" nozzle ports (Fig. 22). In hover, roll control is achieved by differential fan blade pitch, pitch control by angular change in the trailing-edge flaps and the chin exhaust vanes, and yaw control by differential motion of the flaps and vanes.

4.1.2 General Dynamics

A medium-speed concept studied by General Dynamics, Fort Worth Division, features a powered lift system referred to as ABLE (Advanced Blown Lift Enhancement). The heart of this system is a "lifting nacelle" integrated into the wing that vectors the thrust of turbofan engines by using a series of movable flaps to make up the nozzle as illustrated in Fig. 23. One flap forms the upper surface of the two-dimensional nozzle, and two flaps form the lower surface. The upper flap has two slots. The upper forward slot forms the high-aspect-ratio nozzle for the turbine engine exhaust, and the upper aft slot is a boundary layer control slot. The intent is to energize the external boundary layer and thus maintain attached airflow over the "lifting nacelles" to produce significant gains in STOL and transition performance and in aircraft controllability in these modes of flight. In forward flight, the flaps are arranged as shown on the left in Fig. 23, and in transition flight the flaps are deflected into intermediate positions as in the center of the figure. In hover flight (right in Fig. 23) the lower aft flap becomes a part of the aft wall of a vertical-thrust nozzle. The lower forward flap becomes the forward wall of the nozzle and provides a generous radius of the inside of the turn to reduce separation.

This propulsive lift system has been used in a configuration (A-311) illustrated by the model in Fig. 24. A three-view sketch is shown in Fig. 25, and the means of providing folding capability for a Navy configuration is illustrated in Fig. 26. Reference 3 gives a more complete description of this concept.

Four turbofan engines are used in the lifting nacelles of configuration A-311. The fans are cross-shafted together using bevel gears in the fan nose bullets for engine-out considerations. Two load compressors are mounted between the inboard engines and the fuselage and are driven directly from the cross shaft. These compressors provide compressed air to the pitch trim/control system in the aft fuselage. This compressed air drives two air turbines which in turn drive two fans. The fan exhaust passes through dual nozzles which can be aimed up or down using a movable deflection system. Roll control in hover is achieved by biasing the thrust of the main engines either left or right through the cross shaft. Yaw control in hover is achieved by differentially deflecting the main engine nozzle flaps fore and aft on opposite sides of the aircraft.

4.1.3 Grumman

A medium-speed concept studied extensively by Grumman features a tilt-nacelle arrangement for propulsive lift. This concept (Design 698) is shown in Fig. 27, which depicts the various modes of flight from hover, to transition, to cruise. In this concept, all V/STOL related equipment have been located within the engine nacelles. Some of the features of the concept are noted in Fig. 28. Grumman has been working on the 698 concept since about 1976, and they have accumulated over 6000 hr in wind tunnels and on simulators. References 4-15 describe these study and test activities.

Design 698 is a twin tilt-nacelle configuration controlled in vertical flight through horizontal and vertical vanes located in the turbofan exhaust flow, supported by booms attached to each nacelle. In conventional flight, control is provided by spoilers, an all-movable horizontal stabilizer, and a rudder. The large-scale model of the 698 undergoing tests at NASA Ames uses two General Electric TF34-100 turbofan engines, which are proposed also for the demonstrator aircraft.

As shown in Fig. 29, the control vane assembly behind each engine rotates with the nacelle and thereby maintains its position in the engine's exhaust flow. Each vane assembly consists of one horizontal vane crossed by a pair of vertical vanes. The horizontal vane of each assembly is outfitted with a 30% chord antibalancing flap that is geared to move in opposition to the vane's deflection with a 1:1 ratio. The vertical vanes are positioned to remain clear of the hottest region of the engine exhaust flow.

During vertical flight, the pitch of Design 698 is controlled by symmetrical deflection of the horizontal vanes on the two control vane assemblies. Yaw is controlled by differential deflection of the two horizontal vanes as depicted in Fig. 30. Deflection of the vertical vanes and differential operation of variable inlet guide vanes in front of the two engines work together to provide roll control (Fig. 31). Differential operation of the variable inlet guide vanes amounts to differential thrust control of the two engines. Collective variation of thrust is used to control height during vertical flight.

4.1.4 Lockheed

Lockheed has conducted studies of medium-speed V/STOL concepts for the past several years (Refs. 16-20). In their current approach, a split-fan, fixed-nacelle concept is employed for propulsive lift and aircraft control/trim during vertical/transition operation. This propulsion concept is shown schematically in Figs. 32 and 33, and is described in detail in Ref. 17. The nacelle internal arrangement is shown in Fig. 32, and an example of the control concept is illustrated in Fig. 33. A cross duct and associated nacelle plenums provide cross-flow capability from one nacelle to the other. Figure 32 shows twin engines installed in nacelles below and integral with the wing. Each nacelle has two exhaust nozzles, a thrust-vectoring nozzle located aft of the aircraft center of gravity and a fixed-position nozzle located forward of the aircraft center of gravity, each having variable exit area. Airflow to the forward nozzles is supplied from a plenum located circumferentially around the fan duct aft of the fan exit.

During ground acceleration and cruise operation, the entire engine fan and core flows are mixed and exhausted horizontally through the aft nozzle. During vertical operation the engine core air and a portion of the fan air exhausts vertically through the aft nozzle. The remainder of the fan air is exhausted through the forward nozzle. The modulated split of fan air between the fore and aft nozzles is that required to maintain pitch trim.

During vertical flight, pitch control can be provided by the nacelle fore and aft nozzles or by using fan bleed air from the cross duct to an aft fuselage-mounted nozzle (Fig. 33). Yaw control is provided by differential vectoring of the nacelle aft thrust deflectors. In addition to these examples, Lockheed has studied a number of options for control of the split-fan concept during vertical flight (Ref. 17). These options include nacelle fan air transfer, fan bleed reaction control, compressor bleed reaction control, and combinations of these. The system selected will depend to a large degree on the range/payload mix for the mission under consideration.

Lockheed has developed a number of configurations featuring the split-fan propulsive-lift concept. These configurations are either twin- or four-engine designs. On a four-engine configuration, sufficient crossflow can be provided during an engine failure to maintain adequate lift, trim, and control for a safe vertical landing at reduced gross weight. On a twin-engine design, the crossflow should allow a wings-level attitude for crew ejection during a single-engine failure. Figure 34 shows three views of a twin-engine design using F101 engines with cross-duct coupling. A similar but somewhat smaller aircraft has been configured using two TF34 engines. Three views of a four-engine design using TF34 engines is shown in Fig. 35. In their studies, Lockheed conducted an assessment of cross-shafting versus cross-ducting as a means of coupling multiengine concepts. The cross-ducting approach resulted in an appreciably higher useful load capability (Ref. 16).

4.1.5 McDonnell Douglas

Over the past 10 yr or so, the McDonnell Aircraft Company (MCAIR) has conducted studies of medium-speed V/STOL utility aircraft. Candidate concepts included gas and mechanically coupled lift-fan aircraft. A number of these concepts were wind-tunnel-tested. Parallel to this lift-fan activity, MCAIR conducted the AV-8B program and gained valuable experience in the design of vectored thrust concepts. This experience was recently (1980) applied to the design of another medium-speed concept featuring a "two-poster" propulsive lift system. All of these concepts are briefly described in the following paragraphs.

The first concept, proposed in 1973 for Navy consideration, was a gas driven aircraft (Model 260) utilizing a three-fan, lift plus lift/cruise propulsion system. Figure 36 is an artist's rendering of the MCAIR gas-driven version of the 260 design. The propulsion and vertical-flight-control system are illustrated in Fig. 37. In this system, pitch and roll control are accomplished via energy transfer between the fan assemblies, and yaw control is achieved through differential thrust vectoring. Thrust vectoring of the lift/cruise engines is provided by means of a MCAIR-developed vented "D" nozzle (Ref. 21). Figure 38 illustrates the characteristics of this nozzle in both the cruise and VTOL modes. The nozzle consists of movable deflector hoods and a split yaw vane/closure door assembly attached to a single support beam centrally located on the bottom of the nozzle structure. In the cruise mode, the yaw vane doors are closed to form a flat bottom duct and a "D" shaped exit area (Fig. 38). For transition to vertical flight, the closure doors are each rotated 90° to form a single split-yaw vane. Longitudinal thrust vectoring is then accomplished by rotation of the deflector hood elements. Lateral vectoring is obtained by deflection of the split-yaw vane.

The "D" nozzle utilizes a concept referred to as "venting." This is accomplished by removing the inside wall of the elbow turn of a conventional deflector nozzle design, which has been shown to improve the 90° vectoring performance (Ref. 22). The performance characteristics of the "D" vented nozzle was demonstrated in a NASA Ames/MCAIR test program (1981) using a TF34 engine. The results are discussed in Refs. 22 and 23.

In 1977 MCAIR proposed a mechanically driven version of the Model 260 to the Navy. This concept is shown in Fig. 39. The baseline aircraft featured a low wing, three engines, and a mechanically driven three-fan arrangement. This propulsion and vertical-flight-control concept is illustrated in Fig. 40. The third engine, mounted forward of the vertical fin, is used only during V/STOL operation. All jet-borne aircraft control is provided by differential operation and deflection of the propulsion system, eliminating the need for a separate reaction-control system. All three fans and turboshaft engines are identical, minimizing development and maintenance costs. Lift/cruise thrust from each of the direct-drive, wing-mounted fan/engine assemblies is provided via the "D" vented nozzle.

In 1980 MCAIR initiated definition of a twin-engine vectored-thrust concept with a simpler propulsion system than the three-fan Model 260 concept. This concept is designated Model 276 and is depicted by the artist's rendering in Fig. 41 and discussed in Ref. 24. The Model 276 is a high wing design with two shoulder mounted high by-pass turbofan engines. As shown in Fig. 42, attitude control in powered-lift flight is provided by an engine-bleed reaction-control system in pitch, differential thrust modulation in roll, and differential thrust vectoring in yaw. Power transfer between engines by means of cross shafting permits a wide range of thrust modulation for roll control, including engine-out balance capability. A technology demonstrator of this concept using two "D" vented nozzles and TF34 engines has been defined. Mission performance characteristics of the Model 276 aircraft are discussed in Ref. 24.

4.1.6 Rockwell

During ' · studies of "Type A" aircraft, one of the concepts developed by Rockwell is a design that employs lift-augmenting ejectors for the propulsive lift system. The ejectors are located spanwise in the wing as shown in the artist's concept in Fig. 43. This figure shows the full-span ejectors open in the hover operating mode. The ejectors are powered during vertical flight by the flow from the two turbofan propulsion systems at the wing roots. Integrating the ejectors into the wing as Rockwell has done in this concept provides good transition and STOL performance, since the exhaust flows from the ejectors act as a jet flap to increase the circulation lift of the wing.

Rockwell has considered two variations in the propulsion system for this concept. Depending on the design requirements, each nacelle contains either a single core with a fan or two core engines driving a single fan.

The latter propulsion arrangement allows the loss of a core engine without loss of the aircraft. This is based on the philosophy that the major portion of engine failures are core related rather than associated with the fan.

Figure 44 gives three views of the Rockwell ejector-in-wing concept. An interesting feature of the design is the twin booms which support the vertical tails, the horizontal tail, and the aft reaction control system (RCS) pitch pipes. Also visible in the figure are the twin ducts for the two core engines in each nacelle located below the fan inlet.

For pitch control during hover, Rockwell uses forward and aft pitch pipes. Roll control can be provided by wing-tip RCS or by differential lift from the ejectors. Yaw control is achieved by directing the flow from one ejector aft and the other forward. During up-and-away flight, aileron-type controls are used, as are rudders on the vertical tails and an elevator on the horizontal tail.

4.1.7 Vought

For the past several years, Vought has studied a medium-speed concept (V-530) that features a tandem-fan propulsion system (Refs. 25 and 26). Figure 45 is an artist's rendering of an early V-530 configuration which emerged from studies in support of the Navy's "Type A" subsonic multimission V/STOL notional requirements. The aircraft is a high wing monoplane with moderate-aspect-ratio wing and winglets, and with two shoulder-mounted engine nacelles. The V/STOL propulsion system is essentially self-contained in the two nacelles. Each nacelle contains a core engine, two fixed-pitch fans with variable-inlet guide vanes, and associated inlets and nozzles.

Figure 46 illustrates the tandem-fan propulsion concept. Two fans on a common shaft are located ahead of, and are directly driven by, a turboshaft engine. Small fan diameters resulting from the use of two fans in each nacelle permit direct drive by the core engine with no reduction gear between engine and fans. Also, the tandem placement of these relatively small fans results in a smaller nacelle diameter and therefore reduced drag. Each fan has its own inlet and nozzle, and flow through the two fans is maintained separately at all times. The forward inlet supplies air to the front fan, which has a nozzle that can be vectored from a vertical position for hover, to an intermediate position for transition, and to an aft position for cruise (Fig. 46). The upper inlet feeds both the aft fan and the core engine (which is supercharged by the aft fan). The core and aft fan flows are mixed and discharged through the aft nozzle. This nozzle is also vectorable for VTOL and up-and-away flight.

Figure 47 illustrates the propulsion system arrangement in the two nacelles and the cross shafting between the two nacelles. A common fan size is used in all four fan applications. Power is transferred from the gas turbine in one nacelle through the cross shaft to the fans in the opposite nacelle to maintain thrust symmetry during single-engine operation or to provide asymmetric thrust for lateral control during hover. Variable-inlet guide vanes on each fan provide thrust modulation for pitch and roll control (Fig. 48). Differential deflection of the left and right nacelle nozzles provides yaw control.

The forward two-dimensional nozzle uses a two-piece deflector for vectoring thrust (Fig. 46). Variation of nozzle area in cruise is achieved with a small flap mounted on the nacelle surface. The aft two-dimensional nozzle vectors mixed flow from the core engine and aft fan. The nozzle deflector is hinged along the lower portion of the nacelle and rotates downward for vertical flight. A rotating lower flap is used to achieve the nozzle areas required for cruise.

Vought has conducted a number of tests of the tandem-fan configuration and propulsion system components over the past several years. These have included a series of inlet tests with NASA Lewis Research Center, front and rear nozzle tests, powered model tests to evaluate ground effects, and low-speed wind-tunnel tests. References 25-33 describe some of these activities.

4.2 Supersonic Fighter Concepts

The V/STOL and short takeoff and vertical landing (STOVL) fighter concepts described in this section were developed in two research programs jointly sponsored by NASA Ames Research Center, the Navy, and the industry. The Navy organizations that participated were the David Taylor Naval Ship Research and Development Center and the Naval Air Systems Command. The first research program considered twin-cruise-engine concepts and the second considered single-cruise-engine designs. Although many concepts have been proposed over the years, it is felt that those considered in these two programs represent a reasonable cross section of the current thinking in the United States.

The key ingredient in the research programs was a contracted effort with the following objectives:

1. Identify and analyze a wide variety of high-performance V/STOL concepts that have potential utility to fulfill the Navy fighter/attack role.

2. Estimate the aerodynamic characteristics of the configurations and assess the aerodynamic uncertainties requiring additional research.

3. Define a wind-tunnel program, including model design and construction, to explore these uncertainties and provide an initial high-quality aerodynamic data base for Navy, NASA, and industry use.

The information obtained in the first of these objectives will be emphasized in this paper.

The statement of work for this contractor study was jointly prepared by the Navy and NASA Ames to emphasize aerodynamic technology development of V/STOL fighter/attack aircraft. These guidelines were not intended necessarily to reflect specific future naval aircraft performance or operational requirements. Rather, the intent was to provide a limited set of guidelines sufficient to allow the contractors to perform a conceptual aircraft analysis based upon their definition of a mission and payload. The following is a brief description of the guidelines furnished in the statement of work:

1. The conceptual aircraft analysis is for a high-performance V/STOL concept with potential to fulfill the Navy's fighter/attack role after 1995.

2. The aircraft shall have supersonic dash capability with a sustained Mach number capability of at least 1.6.

3. The aircraft shall be operational from land and from ships smaller than CVs without catapults and arresting gear. Good short takeoff (STO) capability is a requirement.

4. To assure high maneuver performance, the aircraft shall have a sustained load factor (N_{Z_S}) of at least 6.2 at Mach number 0.6, at an altitude of 3048 m (10,000 ft) and at 88% VTOL gross weight.

5. The aircraft shall have a specific excess power at 1 G ($P_{S_{1G}}$) of 274 m/sec (900 ft/sec) at Mach number 0.9, at an altitude of 3048 m (10,000 ft) and at 88% VTOL gross weight.

6. The following aircraft weights are to be used as a guide:

   Twin engine: VTOL gross weight = 9072 to 15,876 kg (20,000 to 35,000 lb); STO sea-based gross weight = VTOL gross weight plus approximately 5,436 kg (10,000 lb).

   Single engine: VTOL gross weight = 6,800 to 13,000 kg (15,000 to 30,000 lb); STO sea-based gross weight = VTOL gross weight plus approximately 3,630 to 4,540 kg (8,000 to 10,000 lb).

The following sections describe the twin- and single-engine fighter concepts studied in the contract efforts. The concepts will be described under headings relating to the contractor involved.

4.2.1 Twin-Engine Concepts

Four contractors proposed twin-engine designs that are described in this section. The contractors were: General Dynamics, Fort Worth Division, Fort Worth, Texas; Grumman Aerospace Corporation, Bethpage, New York; Northrop Corporation, Aircraft Group, Hawthorne, California; and Vought Corporation, Dallas, Texas.

Three horizontal-attitude takeoff and landing (HATOL) and two VATOL concepts are described. Northrop proposed two concepts, a HATOL and a VATOL design.

Typical mission profiles used by the contractors for aircraft sizing are outlined in Fig. 49. These are only examples as the contractors had some variations in such things as payload, combat time, and best cruise altitude and velocity (BCAV). All concepts are single-place aircraft with two cruise engines. Each configuration is briefly described in the following sections, and a complete description of the concepts and the wind-tunnel test activities is given in Refs. 34-50.

4.2.1.1 General Dynamics

The configuration proposed by General Dynamics (Refs. 34 and 35) is a wing-canard HATOL concept that has Alperin jet-diffuser ejectors as its vertical lift system. The design also features a vectored-engine-over (VEO) wing-integrated airframe/propulsion system to achieve good transonic maneuvering and STOL performance. In this design, the full engine flow is directed over the wing aft surface to augment the aerodynamic lift through a jet flap effect. At low speeds, this is combined with spanwise blowing, which utilizes a portion of the engine exhaust at high angles of attack to produce leading-edge vortex augmentation. Figure 50 shows three views of the concept, and Fig. 51 presents isometric sketches of the configuration, showing the four ejector-diffuser bays closed for up-and-away forward flight and open for vertical flight.

Two Pratt and Whitney augmented-turbofan study engines are used. The ejector diffusers are located between the fuselage and nacelles in the thick root section of the wings (Fig. 51). For vertical takeoff and landing, the engine flow is diverted to the four ejector bays, where it is injected in both primary and diffuser nozzles. Pitch control during vertical flight is accomplished by thrust modulation of the forward and aft ejectors; yaw control is achieved by vectoring the ejector flow. Wing-tip reaction controls are used for roll control. The ejector-diffuser nozzles and doors fold into the wing, nacelle, and fuselage to form a smooth configuration for up-and-away flight (Fig. 51). An augmentation ratio of 1.70 (defined as the ratio of total lift to isentropic thrust of the engines) is predicted for this concept at liftoff. A major advantage of the ejector-diffuser lift system, of course, is its relatively cool footprint, which could be an important factor for shipboard operation.

The VEO-wing feature has been studied by General Dynamics both in-house and under several Air Force contracts. The engine flow exits above the wing surface (Fig. 50) through a two-dimensional convergent-divergent exhaust nozzle operating in conjunction with the wing flap to provide vectored thrust for pitch control during transition, improved STOL performance, and maneuver enhancement.

The configuration has a high-mounted variable-incidence canard, a low-mounted wing with trailing-edge elevons/flaperons, and a single all-movable vertical tail. The air-induction system features two axisymmetric inlets with aerodynamically operated blow-in doors for adequate flow during takeoff/landing and low-speed flight.

For this study, General Dynamics sized the aircraft to a deck launch intercept (DLI) mission similar to that in Fig. 49. The weapons consist of two advanced short-range air-to-air missiles, two advanced medium-range air-to-air missiles, and one 30-mm gun with 300 rounds of ammunition. To perform this mission and meet the statement-of-work maneuver guidelines, the aircraft has a VTO gross weight of 15,870 kg (34,987 lb), a length of 16.3 m (53.3 ft), and a wing-span of 11.4 m (37.3 ft). Some of the more important vehicle characteristics are summarized in Table 1.

To serve as a comparative design, General Dynamics conducted a parallel in-house design study of the present concept with a General Electric remote augmented lift system (RALS) instead of the ejector-diffuser vertical lift system. In the RALS propulsion system, the fan air is collected and routed forward to a burner/nozzle arrangement to provide propulsive lift. Figure 52 is a schematic of the RALS propulsion concept. The General Dynamic RALS concept, shown in Fig. 53, uses the same wing/canard arrangement, the same spanwise blowing feature, and the same podded engines, except that the nacelles are more closely spaced than on the ejector-diffuser configuration. The VEO-wing nozzle in this case has provision for full 90° thrust deflection for vertical flight. A vectorable, two-burner, forward lift system is employed which uses fan air from the variable-cycle engines. Sized to the same mission and payload, the RALS concept has a VTO gross weight of 14,810 kg (32,650 lb), or approximately 1,043 kg (2,300 lb) less than the ejector configuration.

4.2.1.2 Grumman

The second HATOL configuration is a lift plus lift/cruise concept proposed by Grumman (Refs. 34 and 36). The configuration, shown in Figs. 54 and 55, is a wing-canard design that employs a General Electric RALS. Grumman modified an earlier V/STOL fighter design (Model 623) by incorporating a canard and a new wing to meet the maneuver requirements in the present statement of work. Two General Electric variable-cycle augmented-turbofan study engines are used with General Electric augmented deflector exhaust nozzles (ADEN) (Fig. 56). The RALS forward lift element is a dual burner/nozzle design. To minimize the size of this forward lift system, the ADEN nozzles are mounted at the wing trailing edge as far forward on the configuration as possible. The ADEN nozzles not only provide vertical lift for takeoff and landing, but also have in-flight thrust vectoring to enhance maneuvering (Fig. 56).

As shown in Fig. 54, the configuration features a high-mounted, variable-incidence canard with leading and trailing edge flaps, an advanced variable-camber wing with leading and trailing edge devices, and twin vertical tails. The canard has 5° of dihedral, and the wing has 10° of anhedral. The air induction system consists of side-mounted, fixed-geometry inlets with top-mounted blow-in doors for increased airflow during takeoff/landing and low-speed operation.

In conventional flight, longitudinal control is provided by the incidence of the canard augmented at low speed and high angle of attack by the canard flaps; roll control is provided by asymmetric deflection of the wing trailing edge devices; and directional control is provided by the rudder surfaces. In hover flight, pitch control is provided by flow shifting between the forward and aft nozzles; wing tip reaction controls are used for roll control; and differential lift/cruise nozzle deflections are used for yaw control.

The configuration has been sized to a deck launched intercept (DLI) mission similar to that shown in Fig. 49. The weapons are two AIM-7 missiles, two AIM-9 missiles, and one internally mounted 20-mm gun and ammunition. To perform this mission with a vertical takeoff and to meet the statement-of-work maneuver guidelines, the configuration has a VTO gross weight of 17,112 kg (37,726 lb). The length is 17.3 m (56.5 ft) and the wingspan is 11.5 m (37.8 ft). Some of the other configuration characteristics are summarized in Table 2.

4.2.1.3 Northrop (HATOL)

The third HATOL concept is a lift plus lift/cruise design by Northrop (Refs. 34 and 37). This design is one of two proposed by Northrop. Three views of the concept are shown in Fig. 57; an artist rendering of the aircraft is given in Fig. 58. Northrop is using a General Electric RALS concept in this design with two variable-cycle turbofan engines, ADEN nozzles, and a single forward augmentor lift system with a gimbaled nozzle. The engine has a miniafterburner (1000°F temperature rise) to provide additional thrust during combat. This augmentation is not used for vertical takeoff or landing.

The configuration is a wing-canard design with two vertical tails mounted on twin afterbodies, as shown in Fig. 57. The clipped delta wing has variable camber, using automatically phased leading and trailing edge flaps. The canard is high mounted and all-movable. Side-mounted, two-dimensional inlets are used with topside auxiliary inlet doors for takeoff. The two ADEN nozzles are mounted side by side on the aft fuselage centerline between two wing-mounted afterbodies. These bodies have been shaped and located to provide: (1) a favorable area distribution, (2) twin surfaces for additional lift augmentation from flow entrained by the deflected ADEN nozzles during takeoff, (3) favorable flow on the upper and lower wing surfaces, and (4) space for landing gear, avionics and fuel storage, which in turn provides a means to adjust the center of gravity.

During takeoff and hover, pitch control is provided by thrust modulation of the forward and aft nozzles; roll control by wing-tip reaction controls. Yaw control is derived from lateral deflection of the forward nozzle. For conventional flight, the wing trailing edge elevons are used for pitch and roll control and pitch stabilization. The all-movable vertical tails provide directional control and stabilization. The leading edge flaps and canard surface are scheduled as a function of angle of attack and speed for optimum aerodynamic performance. Thrust vectoring and combined canard/thrust deflection are used for maneuver enhancement.

For this study, a VTO gross weight of 13,608 kg (30,000 lb) has been selected by Northrop as representative of a 1995 VSTOL aircraft designed to perform the Navy fighter/attack mission similar to that of the F-18. To assist in configuration development during the study, an arbitrary fighter escort mission has been used. To meet the statement of work maneuver requirements with a VTOL gross weight of 13,608 kg (30,000 lb), the aircraft (Fig. 57) has a wingspan of 9.9 m (32.6 ft) and a length of 16.0 m (52.5 ft). Some of the configuration characteristics are summarized in Table 3.

When resized to perform a 926-km (500-n. mi.) fighter escort mission, the configuration has a VTO gross weight of 14,424 kg (31,800 lb) and a VTO wing loading of 2.87 kN/m^2 (60 lb/ft^2).

4.2.1.4 Northrop (VATOL)

The second concept studied by Northrop (Refs. 34 and 38) in the present effort is a VATOL concept shown in Fig. 59 and as an artist's rendering in Fig. 60. The configuration is a tailless design that features a wing leading edge extension (LEX) to maintain lift to high angles of attack. Top-mounted inlets are used to provide

a low radar cross section as well as to free the lower surface for efficient weapon/landing gear integration and to ease mating with the alighting gantry.

Both Northrop concepts have a common wing with leading and trailing edge flaps automatically programmed to provide variable camber for optimum aerodynamic performance.

In this VATOL concept, twin Pratt and Whitney variable-geometry, nonafterburning turbojet engines are used with gimbaled axisymmetric nozzles located aft close to the aircraft centerline. The top-mounted air induction system has fixed geometry, two-dimensional inlets with topside auxiliary inlet doors for low-speed operation.

Control in the vertical takeoff and landing mode is provided by the gimbaled nozzles, which can be deflected ±30° in pitch and ±15° in yaw. Wing-tip-mounted reaction controls provide primary roll control; antisymmetric pitch deflection of the nozzles can be used for auxiliary roll control. In conventional flight, pitch and roll control is provided by the trailing edge elevons, and directional control and stabilization are provided by the all-movable vertical tail. Thrust vectoring in combination with the trailing edge flaps is used for maneuver enhancement.

The configuration has conventional landing gear for overload takeoff and landing in the horizontal attitude. A capturing hook mechanism is integrated with the nose gear to engage the launch-and-retrieval platform for VATOL operations.

Several means have been explored to provide a more favorable pilot orientation during takeoff and landing. These means have included a rotating seat similar to the X-13 concept, an articulating capsule, and a system for hinging the entire aircraft nose. The present design employs a tilting cockpit module.

For this study, a VTO gross weight of 13,608 kg (30,000 lb) has been selected by Northrop as representative of a 1995 VSTOL aircraft designed to perform the Navy fighter/attack mission similar to that of the F-18. To assist in configuration development during the study, an arbitrary fighter escort mission has been used. To meet the statement-of-work maneuver requirements with a VTO gross weight of 13,608 kg (30,000 lb), the aircraft has a wingspan of 9.9 m (32.6 ft) and a length of 15.8 m (51.7 ft). Some of the configuration characteristics are summarized in Table 4.

When resized to perform a 926-km (500-n. mi.) fighter escort mission, the configuration has a VTO gross weight of 10,523 kg (23,200 lb) and a VTO wing loading of 2.73 kN/m^2 (57 lb/ft^2).

4.2.1.5 Vought

The final configuration is a VATOL concept proposed by Vought (Refs. 34 and 39). As shown in Figure 61, the design features a fixed, close-coupled, high-mounted canard with trailing edge flaps, a midwing of low aspect ratio, and a single vertical tail with a rudder. The wing has trailing edge flaps that are optimally phased to operate throughout the flight envelope in unison with the canard flap to implement longitudinal and lateral commands. Full-span leading edge flaps are automatically phased to maintain optimal camber for high maneuver performance. Split-flap speedbrakes are located at the inboard wing trailing edge.

Side-mounted, two-dimensional, fixed geometry inlets (Fig. 61) supply air to two Pratt and Whitney advanced technology, mixed flow, augmented turbofan engines. Blow-in doors are provided for low-speed operation. Axisymmetric convergent-divergent nozzles are mounted side by side in the aft fuselage. These nozzles can be gimbaled ±15° in pitch and yaw to provide control during takeoff/landing, hover, transition, and in-flight maneuvering. A reaction-control system in the wing tips provide roll control for vertical takeoff and landing.

Conventional tricycle landing gear is used for short takeoff (STO) and conventional takeoff and landing (CTOL) operation as well as to facilitate deck handling. A capture mechanism is integrated with the nose landing gear to engage the landing platform grate for vertical attitude takeoff and landing. A tilting-seat arrangement is employed to provide the pilot with a comfortable position in the VATOL mode of flight as well as with a conventional seat position for cruise.

The aircraft has been sized to a DLI mission similar to that of Figure 49. The armament consists of two AIM-7 missiles, two AIM-9 missiles, and one 20-mm gun with 400 rounds of ammunition. To perform this mission with a vertical takeoff and to meet the statement-of-work maneuver requirements, the configuration weighs 10,603 kg (23,375 lb) and has a wing span of 8.7 m (28.5 ft) and a length of 13.8 m (45.3 ft). Some of the configuration characteristics are summarized in Table 5. Figure 62 shows the Vought VATOL concept operating in the STO overload condition of 15,139 kg (33,375 lb).

4.2.2 Single-Engine Concepts

Four contractors proposed designs that are described in this section. The contractors are: General Dynamics, Fort Worth Division, Fort Worth, Texas; McDonnell Douglas Corporation, St. Louis, Missouri; Rockwell International, Columbus, Ohio; and Vought Corporation, Dallas, Texas. The concepts are all single-place aircraft with a single cruise engine. Each concept is briefly described in the following sections, and a complete description is given in Refs. 51-60.

4 2.2.1 General Dynamics

The General Dynamics (GD) single-engine fighter concept (Refs. 51-53) combines both vectored thrust and a thrust-augmenting ejector for vertical flight. This propulsive lift system is combined with a delta wing and a tailless design (Configuration E7). The E7 hover configuration is shown in Fig. 63, and the cruise flight mode is depicted in Fig. 54.

The guidelines for the development of this configuration were, first, that it be based on an existing engine or, at most, on a near-term derivative. Second, the aircraft must be capable of STOVL, rather than pure VTOL flight. Observations of AV-8A operations indicate that the Harrier rarely takes off vertically for a

military mission; the overload capability provided by a short deck or ground run is used most often. For naval use, however, the vertical landing provides such significant advantages in deck cycle times that its retention is highly desirable. Finally, the aircraft must be capable of a meaningful naval mission. The latter sets the maximum hover gross weight requirement: (1) 5% reserve fuel, (2) fuel for 20 min of sea level loiter, and (3) retention of expensive weapons (e.g., AIM-7, AIM-9).

An ejector concept was selected as the propulsive lift system for the GD configuration. The ejector system has advantages beyond providing thrust augmentation; for example, it is significant that the ejector exhaust is relatively cool and that its velocity is low. Although burner systems such as the RALS are capable of equally good augmentation, and although lift engines are probably the most compact systems available, the environmental and inlet ingestion problems associated with the hot and high-velocity exhausts of these systems are significant. An ejector system partially avoids these problems.

The propulsive lift system that appeared attractive was the ejector system developed by de Havilland of Canada working with Ames Research Center (Refs. 54-57). This ejector system has more volume than a short-diffuser type, such as the Alperin ejector, but it has a substantial and dependable augmentation ratio that has been measured on a large-scale, engine-driven model at Ames.

However, all ejector systems present some difficulties, one being the ram drag of the entrained air at forward speeds. The data from the original ejector model tested in the Ames 40- by 80-Foot Wind Tunnel suggested that an aircraft using the ejector would be marginal in transitioning from ejector-borne to wing-borne flight. Although it was demonstrated that this could be overcome by vectoring the ejector nozzles aft, an operational aircraft would require controllable vector angles that in turn would require complex actuation systems. One way to avoid this problem is to duct only part of the engine flow to the ejector and to exhaust the remainder to a single, vectorable nozzle. By using fan air to power the ejector, the duct weights are lowered, because of the cooler flow, and the inlet thermal reingestion becomes modest.

In the GD study, three aircraft were considered, a flight demonstrator and two operational aircraft (a threshold and a goal aircraft). The flight demonstrator would be built around an existing engine or a very near-term derivative. The primary purpose of the demonstrator would be to investigate the VL and STO ends of the flight regimes, and therefore afterburners would not be included. However, the demonstrator has been constrained to possess the same airframe as the operational aircraft so that only extrapolations required from the flight demonstrator are propulsional. In the demonstrator, reaction-control-system power is provided by an auxiliary power unit (APU). The threshold operational aircraft is defined as one whose engine thrust may be assumed to be developed in the normal course of engine growth during the next 15 yr or so, but which will require technological advances primarily in the area of reaction control power provided by the engine. The goal operational aircraft requires a more advanced engine in order to provide significantly enhanced hover thrust. Again it is emphasized that all three airframes are identical.

Configuration. In the GD design, fan air is collected in an annular plenum aft of the engine fan stages and is released into a duct that runs along the top of the fuselage (Fig. 65). This air can flow either into an aft nozzle or into the forward ejector nozzles. The ducts are provided with valving to regulate the flow rate of fan air to the ejectors and to an aft nozzle. An afterburner is placed in the duct forward of the aft nozzle. The engine core flow exhausts through a separate, two-dimensional vectorable nozzle (Fig. 65). An afterburner can be located in the core flow duct also. For vertical flight, the core flow is vectored downward, and all fan flow is ducted to the ejectors. For up-and-away flight, the core flow is vectored aft, the ejector doors are closed, and the fan flow exhausts through its aft nozzle. The afterburners are used as required for acceleration and supersonic flight. For STO operations, the core flow is partially vectored and the fan flow is split between the ejector and its aft nozzle as required for balance and acceleration. The three modes of operation of the propulsion system are illustrated in Fig. 66.

Three views of the E7 configuration are shown in Fig. 67, and a dimensional summary is given in Table 6. The forward fuselage, cockpit and canopy, and vertical tail are geometrically identical to those of the F-16A. The wing has an aspect ratio of 1.67 and a leading edge sweep of 60°. The main landing gear is located in the wing; the nose wheel is located in the forward, underside of the inlet. The aircraft is designed to a limit load factor of 7.5 (11.35 ultimate), and approximately a 35% composite material usage is assumed. The avionics weights are estimated on the basis of functional equivalence to that of the F-18.

Propulsion System. Although the demonstrator aircraft in the study uses a General Electric F101/DFE engine, GD has evaluated other engines, including F100 and Pegasus derivatives as part of another study for NASA Ames Research Center. A two-dimensional vectorable nozzle is used for the core flow and an axisymmetric nozzle is used for the fan flow during up-and-away flight. The inlet system has a modified F-16 conformal shape with a normal shock at supersonic speeds. Both the fan stream and core stream are equipped with afterburning capability in the operational aircraft.

The ejectors are of the Ames/de Havilland type, with a diffuser area ratio of 1.6 and throat-area-to-primary-nozzle-area ratio of 25.0. The ejector bays are located longitudinally in the wing root area. In static tests at Ames Research Center, the de Havilland ejector system demonstrated an augmentation ratio of 1.725 (Refs. 54-57). This was degraded to 1.63 for the present studies because of design compromises likely in an actual aircraft. Figure 63 shows the ejector in the open position for hover.

Mission Performance. The primary mission for which the E7 is sized is the naval escort mission (Type Spec. 169) shown in Fig. 68, with the interdiction mission secondary. These missions have been modified to specify a 122-m (400-ft), zero-wind, zero-sink takeoff with vertical landing. The payload consists of two AMRAAM plus two AIM-9L missiles. No gun is used. A summary weight statement of the operational aircraft is given in Table 7.

Point performance parameters are shown in the first column of Table 8 for the goal operational aircraft. The second column shows the performance calculated at 60% of full fuel weight in accordance with TS 169. The E7 configuration meets or exceeds all performance thresholds. The radius for the escort mission is 402 km (217 n. mi.) greater than that required by the specification, and is a direct result of sizing to meet the interdiction mission with internal fuel. The performance values given in the third column are calculated at

88% VTOL gross weight. They have no meaning in a military sense, but are included to provide a measure of performance for comparison with NASA guidelines shown in the last column.

4.2.2.2 McDonnell Douglas

The concept studied by McDonnell Douglas (MCAIR) is a canard/wing design with swiveling nozzles forward and aft of the aircraft center of gravity. The four-poster configuration, MCAIR Model 279-3, is shown in Figs. 69 and 70; Fig. 69 depicts the vertical flight configuration, and the cruise flight mode is shown in Fig. 70. References 51 and 58 give details of this concept.

Configuration. Model 279-3 features a close-coupled canard and side-mounted half-axisymmetric inlets to provide air to a single engine with modulated fan-stream augmentation. Four swiveling nozzles provide thrust vectoring capability for vertical flight as well as for in-flight maneuvering. Fan air flows through the forward nozzles and the engine core flow exits through the aft nozzles. Modulation of the fan stream and engine speed provides the capability of trimming center of gravity travel associated with fuel burnoff and store loading. This modulation can also provide a portion of the pitch maneuvering control or can be used as a backup system. The location of the aft nozzles near the wing trailing edge offers the potential of enhanced circulation, translating into increased maneuverability and STOL performance. Thrust vectoring can increase the sustained load factor of Model 279-3 by 0.2 g and the instantaneous load factor by 2.0 g's at 0.6 Mach number at an altitude of 3,048 m (10,000 ft).

As shown in Fig. 69, the main landing gear of Model 279-3 are located fore and aft on the fuselage in a bicycle fashion with outriggers in pods on the wing.

Three views of the MCAIR concept are shown in Fig. 71, and a dimensional summary is given in Table 9. The wing has an aspect ratio of 3.0, a leading-edge sweep of 45°, and 9° of anhedral. The close-coupled canard is mounted high on the inlet sides and has 0° of dihedral, a leading-edge sweep of 50°, and an aspect ratio of 3.0. The exposed area of the canard is 20% of the wing reference area. The single vertical tail is mounted on the aft fuselage.

The configuration has a vertical takeoff wing loading of 3.34 kN/m^2 (69.7 lb/ft^2) and a tropical-day, vertical-takeoff, thrust-to-weight ratio of 1.15 with full fan-stream burning.

Aerodynamic Surfaces. Pitch control is provided by the all-movable, close-coupled horizontal canard; roll control by the differential ailerons; and directional control by the rudder. The wing leading and trailing edge flaps and also the canard are deflected as a function of angle of attack and Mach number to maximize maneuvering capability. The leading edge flaps also are used supersonically as decamber flaps to reduce drag. The trailing edge flaps, which are plain flaps at small deflections, become single slotted flaps at large deflections, for high-lift operation. These flaps, which are close to the aft nozzle, increase the STOL lift. The location of the forward nozzle under the wing, rather than at the leading edge, also improves lift during STOL.

The wing planform selection is based on a compromise between subsonic and supersonic performance. Subsonic emphasis is on high sustained maneuverability requiring low drag due to lift. Supersonic emphasis is on lower-lift-coefficient maneuvering conditions during which the minimum drag coefficient C_{D_0} is equally important. The wing airfoil camber increases outboard on the wing. There is no twist at the wing-fuselage juncture, but there is leading-edge-down twist at the wing tip.

Control System. The Model 279-3 has a digital fly-by-wire control system, which is necessary to augment the subsonic longitudinal instability. This active control system also makes possible (1) engine/fan-stream augmentation/reaction-control-system integration, (2) augmented thrust-vectoring control, and (3) coupled flight/propulsion control.

A three-axis reaction control system (RCS), operating on engine bleed air, provides control moments independent of dynamic pressure. During VTOL operation it provides the complete maneuvering control. The pitch RCS is located in the aft fuselage and the forward lower mold line of the inlet, just forward of the nose gear. The lateral RCS thrusts both up and down in opposite wing tips. The directional RCS, thrusting laterally in either direction, is located in the aft tip of the fuselage.

During VTOL operation the thrust center is positioned by varying the engine speed and the fan-stream augmentation, using the flight controller. Decreasing the forward nozzle thrust moves the thrust center aft, with the level of thrust maintained by increasing the engine speed. This provides the static trim during VTOL; transient control is provided by the pitch RCS.

Additional control is provided by the engine nozzle thrust-vectoring control (TVC). The fore and aft nozzles are symmetrically deflected a small amount for rapid load-factor changes, with rapid turns plus deceleration followed by acceleration. Differential deflection of the fore and aft nozzles is used for STOL control to augment the canard deflection in controlling the high-lift flap pitching moment.

Propulsion System. A single, advanced Pratt and Whitney thrust-vectoring engine (STF 561-C2) with fan-stream augmentation serves as the propulsion system. It has a twin-spool turbofan gas generator utilizing a two-stage fan and a five-stage low-aspect-ratio high-through-flow axial compressor with a single-stage, high-pressure turbine and a two-stage, low-pressure turbine. The bypass ratio is 1.16, the overall pressure ratio is 25.0, and the fan pressure ratio is 3.50. Table 10 gives additional propulsion system characteristics.

The forward, side-mounted nozzles incorporate fan-stream burning augmentors. There is no engine-core augmentation associated with the aft nozzles. The half-axisymmetric, side-mounted inlets have fixed 16.5° half-conical spikes.

Structure. Composites are used extensively in the Model 279-3. The structural weight consists of 41% graphite epoxy, 21% aluminum, 13% titanium, 8% steel, and 17% other materials. Graphite epoxy is distributed as follows: wing 50%, canard 52%, vertical tail 65%, fuselage 46%, and the engine section 55%.

Mission Performance. MCAIR sized the configuration to the vertical-takeoff, supersonic, DLI mission defined in Fig. 72. Weapons and ammunition are retained throughout the mission. To accomplish this mission and remain within the guideline vertical takeoff gross weight of 13,606 kg (30,000 lb), the aircraft has a mission radius of 191 km (103 n. mi.) and a vertical takeoff gross weight of 13,535 kg (29,840 lb). With full internal fuel [gross weight = 14,161 kg (31,220 lb)] and a rolling takeoff of less than 15 m (50 ft), the radius of the DLI mission is increased to 296 km (160 n. mi.) A weight summary for the vertical takeoff supersonic DLI mission is given in Table 11.

Performance of the Model 279-3 and NASA guideline performance are shown in Table 12. As indicated, all performance requirements are met or exceeded.

The STO characteristics of the Model 279-3 with full internal fuel have been determined by MCAIR for both a flat deck and a 12° ski jump. For a 122-m (400-ft) flat-deck run with zero wind over the deck, the Model 279-3 has an STO gross weight of 18,960 kg (41,800 lb) as shown in Table 12. With this same takeoff run, the STO weight is increased 17%, to 22,135 kg (48,800 lb) using the ski jump.

4.2.2.3 Rockwell International

The single-engine V/STOL fighter concept studied by Rockwell (Refs. 51 and 59), employs thrust-augmenting ejectors for the vertical lift system. This propulsive lift concept is used in two tailless designs by Rockwell. The baseline configuration has a double-delta wing planform. The alternative configuration has a straight leading edge, clipped delta wing. The baseline design will be described first.

Baseline Configuration. The baseline configuration is a tailless design with a double-delta clipped wing, a top-mounted inlet system, fore and aft thrust-augmenting ejectors, and twin vertical tails mounted on the aft fuselage (Fig. 73).

Rockwell selected the ejector concept for the propulsive lift system because of its low velocity and low-temperature footprint compared with that of a direct-lift, deflected-thrust, or RALS concept. In the Rockwell system, all of the mixed gas efflux (intermediate power) is diverted to the lifting system for vertical flight. The lifting system is composed of fore and aft rectangular thrust-augmenting ejectors with end plates arranged in a spanwise direction in each wing panel (Fig. 73). Each ejector unit consists of a pair of opposing Coanda flaps with end plates and a fully deflectable centerbody (0° to 90°). Engine air is injected along the shoulder of each flap and through the centerbody. The centerbody stows to form the upper mold line of the wing and the forward Coanda flap retracts to form the lower mold line. For cruise flight, the thrust diverter (upstream of the afterburner) is opened, allowing the engine efflux to flow through the conventional nozzle. The sketches in Fig. 74 show the operation of the ejector system in various flight modes.

The long-chord, low-aspect-ratio wing contains the fore and aft ejectors in an aerodynamically thin surface. Together with the highly swept leading edges, this delta shape should provide low wave drag. The highly swept leading edges should also allow moderate leading edge radii to provide leading edge suction at subsonic and supersonic speeds. Wing-trailing-edge elevons combined with moderate airframe instability provide increasing camber to trim increasing lift. The long wing chord also shields the top inlet from body crossflow.

Three views of the baseline configuration are shown in Fig. 75, and lifting surface dimensional parameters are given in Table 13. The wing has an aspect ratio of 1.83 and the leading edge sweeps are 48.1° inboard and 64.1° outboard. The wing thickness-to-chord ratio varies from about 0.037 inboard to 0.034 outboard. Twin vertical tails with a leading edge sweep of 53.1° are mounted on the aft fuselage.

As shown in Fig. 75, the landing gear is a bicycle arrangement with the main fore and aft gear in the fuselage. Outrigger gear are stowed in the end plates for the aft ejector.

The baseline configuration has a wing loading of about 2.11 kN/m^2 (44 lb/ft^2) at vertical takeoff gross weight. For this same weight, the maximum afterburning thrust-to-weight ratio is 1.41 (uninstalled, sea-level-static, standard day).

Control. Control in the vertical flight mode is provided by differentially varying the fore and aft and left and right ejector lift magnitude and direction. The ejector lift magnitude is reduced by moving the trailing edges of the Coanda flaps closer together. This system is supplemented by a pitch-reaction-control system for rapid pitch-control inputs.

Control and stability augmentation in conventional flight are provided by wing-trailing-edge elevons and rudders. The control power and airframe instability are designed to permit operation at angles of attack from 0 to 90°. Additional control power and further reduced trim drag can be provided by an all-movable canard on the lower shoulder of the forward fuselage.

Forward flight is achieved by retracting all flaps in a conventional manner. Control during the transition from vertical to conventional flight is accomplished by gradually changing from thrust-magnitude and direction control to elevon-type control (i.e., both Coanda flaps in an augmentor segment move in the same direction) as the augmentor flaps are retracted through 60° deflection. The yaw control reverts from a differential aft augmentor thrust-vector control to differential thrust-magnitude control, and finally to rudder control.

Propulsion System. A single, advanced Pratt and Whitney augmented turbofan parametric engine serves as the propulsion system. The bypass ratio is 0.54, the overall pressure ratio is 30.0, and the fan pressure ratio is 3.60. Table 14 gives additional engine characteristics.

The intermediate-power-to-vertical-takeoff gross weight ratio is 0.86. The ejector system augments the engine intermediate-power gross isentropic thrust about 50% for vertical takeoff and landing.

The top-mounted inlet system has a simple fixed-ramp and is designed for operation to a maximum speed of Mach 2.0. An auxiliary inlet is provided to supply additional air to the engine for vertical takeoff and landing and for conversion flight operations.

Structure. The wing structure features a large central torque box plus a "back porch." The back porch is the surface between the aft augmentor and the flap (Fig. 75). The central torque box and back porch act in differential bending to provide a strong, stiff support for the wing outer panel. Composites are used throughout to minimize weight. The augmentor ducts utilize titanium aluminides, or fiber- or filament-reinforced titanium composites to accommodate the 642°C (1188°F) mixed gas temperature.

Mission Performance. The baseline aircraft was sized for a 278-km (150-n. mi.) radius vertical-takeoff, DLI mission and for 556-km (300-n. mi.) radius short-takeoff DLI mission. The DLI mission is defined in Fig. 76. Two AIAAM missiles are carried on the VTO mission and four are carried on the STO mission. No gun is carried, and the missiles are excluded from the performance calculations. In order to meet these missions and the guideline performance, the VTO gross weight is 10,866 kg (24,000 lb), and the STO gross weight is 13,336 kg (29,400 lb). Short takeoff distance is less than 122 m (400 ft). At 88% of the VTO gross weight, the aircraft has a sustained load factor of 6.9 g at Mach 0.6 at an altitude of 3,048 m (10,000 ft). At Mach 0.9 at an altitude of 3,048 m (10,000 ft) the $P_{S_{1G}}$ is 357 m/sec (1,170 ft/sec). The maximum speed capability is in excess of M = 2.0. These performance characteristics are compared with the study guidelines in Table 15. A summary of the baseline configuration weights is given in Table 16.

Alternative Configuration. The alternative configuration has a straight leading edge, clipped delta wing, with the same top-mounted inlet, but with the forward augmentor oriented in a chordwise, rather than spanwise, direction (Fig. 77). This configuration provides the same conventional flight benefits as the baseline configuration and possesses the same key features. The major differences are the flexibility available for wing planform design, the larger central wing structural torque box, and the increased capability for overload external-store stations on the wing.

The aft spanwise augmentor is identical in concept and is very similar in size and shape to the baseline configuration. The forward chordwise augmentor uses the side of the fuselage for its inboard Coanda flap and a movable outboard Coanda flap to provide thrust-magnitude control and to fair out the wing root lower mold line in conventional flight. A series of spanwise-oriented centerbodies swivel from 90° in vertical flight to 0° (stowed) in conventional flight as the aircraft transitions. In conventional flight the stowed centerbodies form the upper mold line of the wing root.

Three views of the aircraft are shown in Fig. 78. Key lifting-surface dimensional parameters are presented in Table 17. The alternative wing has a straight leading edge of 60° sweep and a constant thickness-to-chord ratio of 0.038. The aspect ratio and wing reference area are essentially equal to those of the baseline configuration; the vertical tails are identical in both configurations.

The alternative configuration engine, avionics, weapons, and performance characteristics are essentially the same as those of the baseline configuration. A weight summary of the alternative configuration is given in Table 18.

4.2.2.4 Vought

The Vought single-engine V/STOL fighter, TF120, is a wing/canard design featuring Vought's series-flow, tandem-fan propulsion concept. The tandem fan is a dual-mode, variable-cycle engine which will be described later. Figure 79 shows an early version of the configuration and Fig. 80 is a later version in which the canard has been mounted on the wing strakes. References 51 and 60 give details of this concept.

Configuration. Figure 81 shows three views of the Vought TF120 concept. The TF120 is a canard/delta-wing configuration featuring extensive wing-body blending in both planform and cross section. Canard control surfaces are located on the wing strakes. Small booms extend aft from the wing to support twin outboard vertical fins and ventrals. Both the fins and ventrals are canted inboard and both are all-movable surfaces. Two small, variable-incidence control fins mounted on the lower corners of the inlets pivot from vertical to horizontal depending on the flight regime.

The side-mounted inlets provide airflow to a single turbofan engine. A nozzle similar to the General Electric ADEN is mounted aft and vectors the thrust from 0° to greater than 90°. The landing gear is a conventional tricycle design. The main wheels fold inboard and slightly forward into the blended-body section at approximately the intersection of the strake and wing leading edge. The nose wheel retracts forward into the nose just ahead of the cockpit.

Four AMRAAM missiles are mounted on the lower blended fuselage inboard of the wing root. A 20-mm Gatling gun and 400-round ammunition drum are also located in the blended wing root area on the left side of the aircraft.

Table 19 gives a summary of the geometry of the various aircraft surfaces. The wing has an aspect ratio of 2.24, a leading-edge sweep of 50°, and a thickness-to-chord ratio of 0.06 at the root and 0.05 at the tip. The canard has a leading-edge sweep of 55° and a dihedral of 10°. The total canard exposed area is about 12% of the theoretical wing area. The twin vertical tails have a leading edge sweep of 45°. Ventral fins on the forward, lower inlet surface have a total exposed area that is about 2% that of the wing theoretical area.

Based on the maximum vertical takeoff gross weight, the TF120 has a vertical takeoff wing loading of 3.47 kN/m^2 (72.4 lb/ft^2) and a vertical thrust-to-weight ratio of 1.16. For this same gross weight and the maximum augmented thrust for the high-speed flight mode (series flow), the thrust-to-weight ratio is 1.73.

Control. The TF120 is a control-configured vehicle with movable surfaces that can be optimally phased throughout the operating envelope. In addition to providing direct lift and direct side force, this system can cope with battle damage or random failures with fewer channels of redundancy than usually postulated for fly-by-wire systems because of the multiplicity of controls.

The ventral fins below the inlets are unit control surfaces with two axes of travel. In addition to pivoting to generate normal forces, these surfaces can be adjusted to any dihedral angle between -15° to -75° In the down position they help generate direct side forces and aid in directional control. At supersonic speeds they fold out to reduce the rearward shift in aerodynamic center and augment longitudinal and lateral control. At a -45° setting the fins can be used as two-axis controls for gust alleviation and precision target tracking. The aft vertical fins and ventral fins are mechanically independent, all-moving controls. Therefore, a total of six control surfaces are available to generate side forces. The four ventrals provide control effectiveness into the post-stall regime to enhance combat agility.

Force controls available for longitudinal and lateral control are wing-trailing-edge flaps (elevons), canards, and the inlet ventral fins. A trailing edge flap attached to the ADEN provides longitudinal trim and high-speed, thrust-vectoring capability.

With the control surface group under integrated software control, it is possible to compensate for wide-ranging flight conditions, control nonlinearities, and component failures to achieve a high level of system performance. However, a high-quality aerodynamic database will be required to realize this potential.

During vertical takeoff and landing and during hover flight, the series-flow tandem-fan concept achieves longitudinal control by differential modulation of the fore and aft thrust. This is accomplished using variable inlet guide vanes (VIGV) for both the forward and aft fans. VIGV thrust modulation delivers rapid pitch-attitude response. Vanes in both exhaust streams provide yaw control in hover. Roll control is accomplished by a demand bleed-reaction jet system. A roll-control valve and an upward and a downward ejector are located in each wing tip. The flow to the reaction-control jets is ducted through piping in the wing leading edges.

Propulsion System. The propulsion system for the TF120 is the series-flow tandem-fan, variable-cycle engine. The system is composed of shaft-coupled forward and aft fan units driven by a turbofan engine, as shown in Fig. 82. Both fans have VIGV for thrust modulation in the parallel-flow mode (vertical operation) and for fan-matching in the series-flow mode (high-speed operation). The flow-diverter valve, a moderate temperature burner for the forward fan, the forward fan ventral nozzle, and the rear fan inlet are located between the two fan units.

In high-speed flight, the propulsion cycle is a conventional afterburning turbofan. For vertical operation, the front fan flow is separated from the aft-fan/core-engine flow by simultaneously closing the duct splitter valve and opening the front fan exhaust nozzle and aft fan inlet. A unique "venetian blind" splitter valve acts as a variable-porosity wall to minimize flow distortion during mode transition.

The forward fan uses low-temperature duct burning during vertical operation. The VIGVs provide the rapid and precise thrust modulation needed for hover control.

The side inlets are fixed-geometry, vertical-ramp, bifurcated duct design with blow-in doors for improved VTO performance. The aft vertical mode inlet is a flush design located on the upper fuselage.

The forward nozzle is a parallel-flow, tandem-fan V/STOL nozzle; it has a low-temperature burner incorporated into the system to augment thrust during VTO. An ADEN-type nozzle is used to vector the aft flow stream. Full afterburning of the aft flow stream is possible anywhere in the flight envelope, but is not required in the hover mode. The exhaust footprint is comparable to that of the Harrier.

Table 20 gives the tandem-fan baseline cycle characteristics for both the parallel-flow mode (vertical operation) and the series-flow mode (high-speed operation). In the vertical-flight mode, the thrust split is 67% fore and 33% aft. The fan pressure ratios in the VTOL mode are 2.2 fore and 1.75 aft, and in the series-flow (high-speed) mode the ratio is 3.44. The overall pressure ratio is 17.5 in the VTOL mode and 25.2 in the high-speed mode.

Mission Performance. Vought determined the performance of the TF120 on three hypothetical design missions: A supersonic intercept (SI), a fighter escort (FE), and an interdiction (INX) (Fig. 83). The first two are vertical takeoff missions and the third requires a short takeoff. The payload for the SI mission is four AMRAAMs and a 20-mm gun. The payload for the FE mission (which requires the two 370-gal fuel tanks) is four AMRAAMs, two short-range missiles, and a gun. On the INX mission, which requires two 370-gal fuel tanks, the payload is two short-range missiles and four bombs. On all three missions, all missiles and ammunition are retained. The results of the mission studies are summarized in Table 21. The SI radius is 370 km (200 n. mi.) for a Mach 1.6 dash. Increasing the dash speed to Mach 2.0 reduces the radius to 258 km (139 n. mi.). With external fuel and an SIO weight of 15,720 kg (34,664 lb), the interdiction mission radius is 960 km (519 n. mi.). Table 22 gives a weight summary for the SI mission.

A summary comparing the TF120 performance to the NASA guidelines is given in Table 23, which shows performance for maximum afterburning power setting as well as the maximum Mach number and altitude for intermediate power setting. At Mach 0.6 at an altitude of 3,048 m (10,000 ft), the TF120 has a sustained load factor of 6.62. The aircraft has a $P_{S_{1G}}$ of 526 m/sec (1725 ft/sec) at Mach 0.9 and an altitude of 3,048 m (10,000 ft). The TF120 has a maximum Mach number of 2.4 at maximum power and also has supersonic capability (M = 1.42) at intermediate power.

5. CONCLUDING REMARKS

This lecture has summarized V/STOL concepts in the United States, including some from the past and some that may come in the future. Of the multitude of concepts that were studied in the past, only about 15 or so that reached some form of flight evaluation have been described. Nearly all of these concepts suffered from some weaknesses or problems. These problems included such things as (1) poor handling qualities, (2) the lack of a SAS for hover and low-speed flight, (3) marginal aircraft performance envelopes which restricted operational evaluations, (4) little or no STO capability, (5) low payload/range performance, (6) compromised high-speed performance due to features that provide VTOL capability, and (7) reingestion of hot gases. The lessons

learned from these past concepts need not be repeated, as the past efforts have provided a valuable database for present and future designs.

Design changes to a successful V/STOL aircraft, the British AV-8A Harrier, have resulted in an improved concept, the AV-8B Harrier II. This is the only current concept considered in the paper. A number of subsonic, multimission concepts proposed by U.S. industry indicate that there are still many approaches to V/STOL that have not been flight-demonstrated. A major portion of the paper has been devoted to the future V/STOL fighter, which also has not been flight-tested in the U.S. A number of different propulsive lift concepts proposed for these fighter designs have been described along with the configuration geometry, control concepts, and the mission performance. Many of these concepts appear to have benefited from the lessons of earlier efforts and have reasonable range/payload, control power, and STOL overload capability. In one case, a third generation of a successful concept, the Harrier, is under consideration as a supersonic V/STOL fighter. From this chronology we might say that the concept of V/STOL aircraft has survived its "birth pains" and is about to enter the growth stage.

6. REFERENCES

1. Anderson, S. B., "Historical Overview of S/TOL Aircraft Technology," NASA TM-81280, March 1981.

2. Anderson, S. B., "An Overview of V/STOL Aircraft Development," AIAA Paper 83-2491, Presented at AIAA Aircraft Design, Systems and Technology Meeting, Fort Worth, Texas, October 17-19, 1983.

3. Bradfield, G. W., "Design Features of a Sea Based Multipurpose V/STOL, STOVL and STOL Aircraft in a Support Role for the U.S. Navy." AIAA Paper 81-2650, AIAA/NASA Ames VSTOL Conference, Palo Alto, California, December 7-9, 1981.

4. Kalemaris, S., and Buchmann, W. G., "Aero-Propulsion Development of a Twin-Fan V/STOL Aircraft." AIAA Paper 77-595, June 1977.

5. Potonides, H. C., "Development of an Inlet for a Tilt Nacelle Subsonic V/STOL Aircraft." ASME-Gr-121, April 1979.

6. Potonides, H. C., Cea, R. A., and Nelson, T. F., "Design and Experimental Studies of a Type A V/STOL Inlet." AIAA Paper 78-956R, July 1978.

7. Burley, R. R., "Effect of Lip and Centerbody Geometry on Aerodynamic Performance of Inlets for Tilt Nacelle VTOL Aircraft." AIAA Paper 79-0381, 1979.

8. Johns, A. L., Williams, R. C., and Potonides, H. C., "Performance of a V/STOL Tilt Nacelle Inlet with Blowing Boundary Layer Control." AIAA Paper 79-1163, June 1979.

9. Kress, R. W., "An Affordable Means of Increasing Sea-Based Air Power." SAE Paper 801241, October 1980.

10. Falarski, M. D., Dudley, M. R., Buchmann, W. G., and Pisano, A., "Aerodynamic Characteristics of a Large-Scale Twin Tilt-Nacelle V/STOL Model." AIAA Paper 81-0150, January 1981.

11. Perera, M., "Hover and Transition Flight Performance of a Twin Tilt-Nacelle V/STOL Configuration." AIAA Paper 83-1824, July 1983.

12. Lehman, C. L., and Crafa, V. J., "Nacelle Design for Grumman Design 698." SAE Paper 831492, October 1983.

13. Wilson, S. B. III, Donley, S., Valckenaere, W., Buchmann, W. G., and Blake M., "Handling Characteristics of a Simulated Twin-Tilt Nacelle V/STOL Aircraft." SAE Paper 831549, October 1983.

14. Kalemaris, S. G., "V/STOL for Sea Control." AIAA Paper 83-2436, October 1983.

15. Kohn, J. S., "Aerodynamics, Propulsion and Longitudinal Control Requirements for a Tilt-Nacelle V/STOL with Control Vanes Submerged in the Nacelle Slipstream." AIAA Paper 83-2513, October 1983.

16. Waller, J. D., and Yackle, A. R., "A Split Fan Concept for a Medium Speed V/STOL." SAE Technical Paper 831548, October 1983.

17. Glasgow, E. R., Beck, W. E., and Carlson, J. G., "Cross-Ducted Propulsion Systems for Medium-Speed V/STOL Applications." SAE Technical Paper 831493, October 1983.

18. Glasgow, E. R., and Skarshaug, R. E., "Type A V/STOL Propulsion System Development." AIAA Paper 79-1287R, October 1980.

19. Glasgow, E. R., Beck, W. E., and Woollett, R. R., "Zero-Length Slotted-Lip Inlet for Subsonic Military Aircraft." AIAA Paper 80-1245R, February 1982.

20. Priestley, R. T., Sr., and Yackle, A. R., "V/STOL, STOL, CTOL Comparisons." SAWE Paper 1499, May 1982.

21. Rosenberg, E. W., and Esker, D. W., "Development of the "D" Vented Thrust Deflecting Nozzle." AIAA Paper 80-1856, August 1980.

22. Rosenberg, E. W., and Christiansen, R. S., "Ground Test of a Large Scale "D" Vented Thrust Deflecting Nozzle." AIAA Paper 81-2630, December 1981.

23. Rosenberg, E. W., "Test and Analysis of a Vented "D" Thrust Deflecting Nozzle on a Turbofan Engine," NASA CR 166279, March 1982.

24. Adelt, W. H., "Type A V/STOL: One Aircraft for All Support Missions?" AIAA Paper 81-2661R, J. of Aircraft, Vol. 20, No. 6, June 1983.

25. Beatty, T. D., and Riccius, M. V., "Vought Ground Effects and Transition Tests of a Tandem Fan Medium Speed V/STOL Configuration." SAE Paper 831547, October 1983.

26. Clingingsmith, T. W., "Medium Speed V/STOL Propulsion Installation Losses — Comparison of Prediction and Model Test Data." SAE Paper 831494, October 1983.

27. Rhoades, W. W., and Ybarra, A. H., "Low Speed Test of the Aft Inlet Designed for a Tandem Fan V/STOL Nacelle." NASA CR-159752, February 1980.

28. Ybarra, A. H., "Additional Testing of the Inlets Designed for Tandem Fan V/STOL Nacelles." NASA CR-165310, June 1981.

29. Williams, R. C., and Ybarra, A. H., "Low Speed Testing of the Inlets Designed for Tandem Fan V/STOL Nacelles." NASA TM 82728 (AIAA 81-2627), December 1981.

30. Limage, C. R., "Development of Low Pressure Ratio Vectoring Nozzles for V/STOL Aircraft." SAE Paper 770988, November 1977.

31. Burstadt, P. L., and Johns, A. L., "Experimental Results of a Deflected Thrust V/STOL Nozzle Research Program." AIAA Paper 83-0170, January 1983.

32. Pennington, D. F., "Tandem Fan Model — Front Fan Nozzle Test Applicable to a Type A V/STOL Aircraft." NASA CR-168024, July 1983.

33. Louthan, J. D., "The Impact of Propulsion Performance Parameters on V/STOL Design and Sizing." AIAA Paper 80-1875, August 1980.

34. Nelms, W. P., "Studies of Aerodynamic Technology for VSTOL Fighter/Attack Aircraft." AIAA Paper 78-1511, August 1978.

35. Lummus, J. R., "Study of Aerodynamic Technology for VSTOL Fighter/Attack Aircraft." NASA CR-152128, 1978.

36. Burhans, W. R., Crafa, V. J., Dannenhoffer, N. F., Dellamura, F. A., and Krepski, R. E., "Study of Aerodynamic Technology for VSTOL Fighter/Attack Aircraft." NASA CR-152129, 1978.

37. Brown, S. H., "Study of Aerodynamic Technology for VSTOL Fighter/Attack Aircraft — Horizontal Attitude Concept." NASA CR-152130, 1978.

38. Gerhardt, H. A., and Chen, W. S., "Study of Aerodynamic Technology for VSTOL Fighter/Attack Aircraft — Vertical Attitude Concept." NASA CR-152131, 1978.

39. Driggers, H. H., "Study of Aerodynamic Technology for VSTOL Fighter/Attack Aircraft." NASA CR-152132, 1978.

40. Nelms, W. P., and Durston, D. A., "Preliminary Aerodynamic Characteristics of Several Advanced VSTOL Fighter/Attack Aircraft Concepts." SAE Paper 801178, October 1980.

41. Nelms, W. P., Durston, D. A., and Lummus, J. R., "Experimental Aerodynamics Characteristics of Two VSTOL Fighter/Attack Aircraft Configurations at Mach Numbers from 0.4 to 1.4." NASA TM-81234, December 1980.

42. Lummus, J. R., Joyce, G. T., and O'Malley, C. D., "Analysis of Wind Tunnel Tests Results for a 9.39-Percent Scale Model of a VSTOL Fighter/Attack Aircraft." NASA CR-152391, Vols. 1-4, January 1981.

43. Lummus, J. R., "Aerodynamic Characteristics of a VSTOL Fighter Configuration." AIAA Paper 81-1292, 1981.

44. Nelms, W. P., Durston, D. A., and Lummus, J. R., "Experimental Aerodynamic Characteristics of Two VSTOL Fighter/Attack Aircraft Configurations at Mach Numbers from 1.6 to 2.0." NASA TM-81286, May 1981.

45. Durston, D. A., and Smith, S. C., "Lift Enhancing Surfaces on Several Advanced VSTOL Fighter/Attack Concepts." AIAA Paper 81-1675, August 1981.

46. Moore, W. A., "Wind Tunnel Data Analysis of the Northrop Horizontal Attitude VSTOL Fighter Configuration for Mach Numbers from 0.4 to 1.4." NASA CR-166277, 1982.

47. Moore, W. A., "Wind Tunnel Data Analysis of the Northrop Vertical Attitude VSTOL Fighter Configuration for Mach Numbers from 0.4 to 1.4." NASA CR-166278, 1982.

48 Durston, D. A., and Smeltzer, D. B., "Inlet and Airframe Compatibility for a VSTOL Fighter/Attack Aircraft With Top-Mounted Inlets." ICAS Paper 82-4.2.2, August 1982.

49. Durston, D. A., and Smeltzer, D. B., "Inlet and Airframe Compatibility for a V/STOL Fighter/Attack Aircraft With Top-Mounted Inlets." NASA TM-84252, June 1982.

50. Durston, D. A., and Schreiner, J. A., "High Angle of Attack Aerodynamics of a Strake-Canard-Wing V/STOL Fighter Configuration." AIAA Paper 83-2510, October 1983.

51. Nelms, W. P., and Durston, D. A., "Concept Definition and Aerodynamic Technology Studies for Single Engine VSTOL Fighter/Attack Aircraft." AIAA Paper 81-2647, December 1981.

52. Foley, W. H., Sheridan, A. E., and Smith, C. W., "Study of Aerodynamic Technology for Single-Cruise-Engine VSTOL Fighter/Attack Aircraft." NASA CR-166268, 1982.

53. Foley, W. H., "An Integrated Aerodynamic/Propulsive Design for a STOVL Fighter/Attack Aircraft." ICAS-82-1.6.2, 1982.

54. Garland, D. B., "Static Tests of the J-97 Powered, External Augmentor V/STOL Wind Tunnel Model." de Havilland Report DHC-DND 77-4, February 1978.

55. Garland, D. B., "Phase 1 Wind Tunnel Tests of the J-97 Powered, External Augmentor V/STOL Model." de Havilland Report DHC-DND 79-4, September 1979.

56. Garland, D. B., and Harris, J. L., "Phase 2 and 3 Wind Tunnel Tests of the J-97 Powered, External Augmentor V/STOL Model." de Havilland Report DHC-DND 80-1, March 1980.

57. Gilbertson, F. L., and Garland, D. B., "Static Tests of the J-97 Powered External Augmentor V/STOL Model at the Ames Research Center." de Havilland Report DHC-DND 80-2 (Draft Copy, 1980).

58. Hess, J. R., and Bear, R. L., "Study of Aerodynamic Technology for Single-Cruise-Engine VSTOL Fighter/Attack Aircraft." NASA CR-166269, 1982.

59. Mark, L., "Study of Aerodynamic Technology for Single-Cruise-Engine VSTOL Fighter/Attack Aircraft." NASA CR-166270, 1982.

60. Driggers, H. H., "Study of Aerodynamic Technology for Single-Cruise-Engine VSTOL Fighter/Attack Aircraft." NASA CR-166271, 1982.

7. ACKNOWLEDGEMENTS

The authors wish to acknowledge the inputs to this lecture provided by the many members of the U.S. industry, particularly those contributing to the "Medium-Speed Concept" section/

TABLE 1. GENERAL DYNAMICS HATOL CONFIGURATION CHARACTERISTICS

Wing	
Area	35.7 m (384 ft²)
Aspect ratio	3.62
Taper ratio	0.19
Root chord	5.28 m (17.31 ft)
Tip chord	1.00 m (3.29 ft)
t/c (root/tip)	0.04/0.04
Leading-edge sweep	40°
Canard	
Area (exposed)	7.14 m (76.9 ft²)
Aspect ratio	2.16
Taper ratio	0.37
Root chord	2.65 m (8.71 ft)
Tip chord	0.98 m (3.22 ft)
t/c (root/tip)	0.05/0.03
Leading-edge sweep	45°
Vertical tail	
Area	4.41 m² (47.5 ft²)
Aspect ratio	1.27
Taper ratio	0.43
Root chord	2.61 m (8.55 ft)
Tip chord	1.12 m (3.68 ft)
t/c (root/tip)	0.053/0.04
Leading-edge sweep	47.5°

Weight summary (DLI mission)

	kg	lb
Structure	5138	(11327)
Propulsion	3876	(8545)
Fixed equipment	1601	(3530)
Payload	865	(1907)
Fuel	4390	(9678)
VTO gross weight	15870	(34987)

General (DLI mission)

W/S (VTO gross weight)
4.36 kN/m² (91 lb/ft²)

T/W (SLS, uninstalled, max A/B)
1.30

TABLE 2. GRUMMAN HATOL CONFIGURATION CHARACTERISTICS

Wing	
Area	35.3 m (380 ft²)
Aspect ratio	3.75
Taper ratio	0.30
Root chord	4.72 m (15.5 ft)
Tip chord	1.41 m (4.64 ft)
t/c (root/tip)	0.06/0.06
Leading-edge sweep	35°
Canard	
Area (exposed)	7.90 m² (85 ft²)
Aspect ratio	1.56
Taper ratio	0.37
Root chord	2.32 m (7.61 ft)
Tip chord	0.86 m (2.82 ft)
t/c (root/tip)	0.06/0.06
Leading-edge sweep	37.5°
Vertical tail (per panel)	
Area	3.90 m² (42 ft²)
Aspect ratio	1.37
Taper ratio	0.37
Root chord	2.48 m (8.13 ft)
Tip chord	0.91 m (3.00 ft)
t/c (root/tip)	0.05/0.05
Leading-edge sweep	47.5°

Weight summary (DLI mission)

	kg	lb
Structure	5047	(11126)
Propulsion	3617	(7974)
Fixed equipment	2339	(5156)
Payload	1204	(2654)
Fuel	4906	(10816)
VTO gross weight	17113	(37726)

General (DLI mission)

W/S (VTO gross weight)
4.74 kN/m² (99 lb/ft²)

T/W (SLS, uninstalled, max A/B)
1.47

TABLE 3. NORTHROP HATOL CONFIGURATION CHARACTERISTICS

Wing	
Area	46.5 m (500 ft²)
Aspect ratio	2.12
Taper ratio	0.18
Root chord	7.92 m (26 0 ft)
Tip chord	1.43 m (4.68 ft)
t/c (root/tip)	0.04/0.04
Leading-edge sweep	50°

Canard	
Area (exposed)	4.23 m² (45.5 ft²)
Aspect ratio	1.53
Taper ratio	0.27
Root chord	2.62 m (8.58 ft)
Tip chord	0.71 m (2.33 ft)
t/c (root/tip)	0.04/0.04
Leading-edge sweep	60°

Vertical tail (per panel)	
Area	2.42 m² (26.0 ft²)
Aspect ratio	1.31
Taper ratio	0.31
Root chord	2.08 m (6.83 ft)
Tip chord	0.63 m (2.08 ft)
t/c (root/tip)	0.04/0.04
Leading-edge sweep	42.5°

General (DLI mission)
VTO gross weight 13,608 kg (30,000 lb)
W/S (VTO gross weight) 2.87 kN/m² (60 lb/ft²)
T/W (SLS, installed, intermediate power) 1.20

TABLE 4. NORTHROP VATOL CONFIGURATION CHARACTERISTICS

Wing	
Area	46.5 m² (500 ft²)
Aspect ratio	2.12
Taper ratio	0.18
Root chord	7.92 m (26.0 ft)
Tip chord	1.43 m (4.68 ft)
t/c (root/tip)	0.04/0.04
Leading-edge sweep	50°

Vertical tail	
Area	2.51 m² (27.0 ft²)
Aspect ratio	1.10
Taper ratio	0.34
Root chord	2.26 m (7.42 ft)
Tip chord	0.76 m (2.50 ft)
t/c (root/tip)	0.04/0.04
Leading-edge sweep	50°

General (DLI mission)
VTO gross weight 13,608 kg (30,000 lb)
W/S (VTO gross weight) 2.87 kN/m² (60 lb/ft²)
T/W (SLS, uninstalled, intermediate power) 1.29

TABLE 5. VOUGHT VATOL CONFIGURATION CHARACTERISTICS

Wing	
Area	32.9 m² (354 ft²)
Aspect ratio	2.30
Taper ratio	0.15
Root chord	6.61 m (21.7 ft)
Tip chord	0.99 m (3.25 ft)
t/c (root/tip)	0.05/0.05
Leading-edge sweep	50°

Canard	
Area (exposed)	4.89 m² (52.6 ft²)
Aspect ratio	0.80
Taper ratio	0.25
Root chord	2.80 m (9.17 ft)
Tip chord	0.70 m (2.29 ft)
t/c (root/tip)	0.05/0.04
Leading-edge sweep	60°

Vertical tail	
Area	5.57 m² (60.0 ft²)
Aspect ratio	1.00
Taper ratio	0.30
Root chord	3.63 m (11.92 ft)
Tip chord	1.09 m (3.58 ft)
t/c (root/tip)	0.05/0.04
Leading-edge sweep	53°

Weight summary (DLI mission)

	kg	lb
Structure	2328	(5133)
Propulsion	1985	(4375)
Fixed equipment	1461	(3221)
Payload	1101	(2427)
Fuel	3728	(8219)
VTO gross weight	10603	(23375)

General (DLI mission)
W/S (VTO gross weight) 3.16 kN/m² (66 lb/ft²)
T/W (SLS, uninstalled, max A/B) 1.45

TABLE 6. GENERAL DYNAMICS E7 CONFIGURATION DIMENSIONAL DATA

Parameter	Wing	Vertical tail
Reference area, m^2 (ft^2)	58.58 (630.6)	5.09 (54.8)
Aspect ratio	1.665	1.294
Taper ratio	0.115	0.437
Span, m (ft)	9.88 (32.40)	2.57 (8.42)
Root chord, m (ft)	10.64 (34.90)	2.77 (9.10)
Tip chord, m (ft)	1.22 (4.00)	1.21 (3.96)
MAC, m (ft)	7.18 (23.56)	
Leading-edge sweep, deg	60	47.5
Trailing-edge sweep, deg	-10	
t/c root	0.04	0.053
t/c tip	0.04	0.030
Airfoil	NACA 64A004	Biconvex

TABLE 7. GENERAL DYNAMICS E7 CONFIGURATION WEIGHT SUMMARY

Item	Weight, kg (lb)
Structure	3848 (8494)
Propulsion	2573 (5672)
Systems and Equipment	1813 (3996)
Weight empty	8239 (18162)
Operational weight	8612 (18986)
Payload*	449 (990)
Zero fuel weight	9061 (19976)
Fuel	5578 (12297)
Takeoff gross weight	14640 (32273)

*Two AIM-9L and two AMRAAM.

TABLE 8. GENERAL DYNAMICS CONFIGURATION E7 POINT PERFORMANCE

	Note 1	Note 2	Note 3
Point performance weight	11461 (25267)	12402 (27341)	8722 (19228)
Escort mission			
Fuel, kg (lb)	4380 (9657)	5568 (12275)	
TOGW, kg (lb)	13667 (30130)	14629 (32251)	
Radius, km (NM)	741 (400)	1143 (617)	
Interdiction mission			
Fuel, kg (lb)		5568 (12275)	
TOGW, kg (lb)		16112 (35522)	
Radius, km (NM)		1020 (551)	
Maximum Mach			
35 KFT, maximum thrust	1.73	1.73	1.73
10 KFT, int. thrust	1.02	1.02	1.02
Turn load factor			6.9
M 0.60, 10 KFT			7.6
M 0.65, 10 KFT	5.5	5.3	
P_S @ 1 g, M 0.9, 10 KFT, m/sec (ft/sec)	237 (777)	228 (747)	323 (1059)

Notes: (1) Pt. perf. @ 60% escort fuel weight.
(2) Pt. perf. @ 60% full fuel weight.
(3) Pt. perf. @ 88% VTOL weight.

TABLE 9. MCAIR CONFIGURATION DIMENSIONAL DATA

Parameter	Wing	Canard (exposed)	Vertical tail
Reference area, m^2 (ft^2)	39.80 (428.4)	7.95 (85.6)	6.04 (65.0)
Aspect ratio	3.0	3.0	1.2
Taper ratio	0.25	0.25	0.35
Span, m (ft)	10.92 (35.84)	4.88 (16.02)	2.69 (8.83)
Semispan, m (in.)	5.46 (215.04)	2.44 (96.14)	2.69 (105.98)
Root chord, m (in.)	5.83 (229.44)	2.61 (102.59)	3.32 (130.64)
Tip chord, m (in.)	1.46 (57.36)	0.65 (25.64)	1.16 (45.80)
Mean aero. chord, m (in.)	4.08 (160.52)	1.82 (71.81)	2.42 (95.14)
Leading-edge sweep, deg	45	50	45
Incidence, deg	0 at fuselage	0	0
Dihedral, deg	-9	0	-
Twist, deg	-4 at tip	0	-
Airfoil, root	64AX06MOD	64A005	64A005
Airfoil, tip	64AX04MOD	64A003	64A003

TABLE 10. MCAIR CONFIGURATION PROPULSION SYSTEM CHARACTERISTICS

Engine: P&WA STF-561-C2

F_N total: 152,638 N (34,316 lb) installed (F_N VTO at 90°F, T/W = 1.15)

Thrust split: fwd 61%, aft 39%

Inlet: Fixed half conical spike, 16.5° cone

AC = 1.13 m^2 (12.17 ft^2)

BPR = 1.16, FPR = 3.50, OPR = 25.0

Maximum air flow: 167 kg/sec (369 lb/sec)

CET_{MAX} = 1760°C (3200°F), $T_{PCB_{VTO}}$ = 1866°C (3390°F)

$T_{PCB_{MAX}}$ = 1949°C (3540°F) at M = 2.0 and 7,620 m (25,000 ft)

TABLE 11. MCAIR CONFIGURATION WEIGHT SUMMARY

Item	Weight, kg (lb)
Structure	4351 (9592)
Propulsion	2003 (4415)
Fixed equipment	2186 (4820)
Weight empty	8540 (18827)
Operating weight empty	8985 (19808)
Payload*	665 (1466)
VTO usable fuel	3885 (8566)
STO usable fuel	4513 (9950)
VTO gross weight*	13535 (29840)
STO gross weight*	14161 (31220)

*Includes two AMRAAM and two AIM-9 missiles and 25-mm gun with 400 rounds of ammunition.

TABLE 12. MCAIR CONFIGURATION PERFORMANCE SUMMARY

Item	NASA guideline	Model 279-3
Sustained load factor at Mach 0.6, 3,048 m (10,000 ft), 88% VTOGW	6.2	6.2
PS_{1G} at Mach 0.9, 3,048 m (10,000 ft), 88% VTOGW, m/sec (ft/sec)	274 (900)	317 (1,040)
DLI mission radius, VTOGW = 13,535 kg (29,840 lb), km (n. mi.)	---	191 (103)
Sustained Mach number	1.6	2.0
STO sea-based gross weight, kg (lb)	17,164-18,071 (37,840-39,840)	16,960* (41,800)*

Note: Two AMRAAM, two AIM-9, and 25-mm gun with 400 rounds of ammunition.
*Flat deck run of 122 m (400 ft) at 0-knot wind over deck (WOD) or 61 m (200 ft) at 20-knots WOD.

TABLE 13. ROCKWELL BASELINE CONFIGURATION DIMENSIONAL DATA

Wing (total)	
Area, m^2 (ft^2)	50.26 (541.0)
Aspect ratio	1.8
Span, m (ft)	9.60 (31.5)
Root chord, m (ft)	8.36 (27.43)
Tip chord, m (ft)	0.98 (3.2)
MAC, m (ft)	6.14 (20.13)
Leading-edge sweep, inboard, deg	48.0
Leading-edge sweep, outboard, deg	64.0
Airfoil	65-005 MOD
t/c, inboard	0.038
t/c, outboard	0.034
Vertical (per panel)	
Area, m^2 (ft^2)	3.40 (36.7)
Aspect ratio	1.41
Root chord, m (ft)	2.35 (7.68)
Tip chord, m (ft)	0.78 (2.55)
Taper ratio	0.33
Leading-edge sweep, deg	41.6
MAC, m (ft)	1.69 (5.54)
Span, m (ft)	2.20 (7.2)
Cant angle, deg	30
Airfoil	NASA 65-00

TABLE 14. ROCKWELL CONFIGURATION ENGINE CHARACTERISTICS

Thrust (sea level, standard day, uninstalled)	
Max A/B, N (lb)	150,699 (33,880)
Intermediate, N (lb)	91,629 (20,600)
Bypass ratio (BPR)	0.51
Fan pressure ratio (FPR)	3.6
Overall pressure ratio (OPR)	30.0
Combustor exit temperature, °C (°F)	1,538 (2,800)

TABLE 15. ROCKWELL BASELINE CONFIGURATION PERFORMANCE SUMMARY

Item	NASA guideline	Rockwell baseline configuration
Sustained load factor at Mach 0.6, 3,048 m (10,000 ft), 88% VTOGW	6.2	6.3
$P_{S_{1G}}$ at Mach 0.9, 3,048 m (10,000 ft), 88% VTOGW, m/sec (ft/sec)	274 (900)	357 (1,170)
DLI mission radius, VTOGW = 10,886 kg (24,000 lb), km (n. mi.)	---	278 (150)
Sustained Mach number	1.6	1.9

TABLE 16. ROCKWELL BASELINE CONFIGURATION WEIGHT SUMMARY

Item	Weight, kg (lb)
Structure	4143 (9133)
Propulsion	2437 (5373)
Fixed equipment	1462 (3223)
Weight empty	8042 (17729)
Operating weight empty	8248 (18184)
Payload	544 (1200)
Fuel	2559 (5641)
VTO gross weight	11351 (25025)

TABLE 17. ROCKWELL ALTERNATIVE CONFIGURATION DIMENSIONAL DATA

Wing (total)	
Area, m^2 (ft^2)	50.96 (548.5)
Aspect ratio	1.809
Span, m (ft)	9.60 (31.5)
Root chord, m (ft)	9.46 (31.03)
Tip chord, m (ft)	1.16 (3.79)
Taper ratio	0.122
MAC, m (ft)	6.39 (20.96)
Leading-edge sweep, deg	60
Airfoil	65-005 MOD
t/c, inboard	0.038
t/c, outboard	0.034
Vertical (per panel)	
Area, m^2 (ft^2)	3.40 (36.7)
Aspect ratio	1.41
Root chord, m (ft)	2.35 (7.68)
Tip chord, m (ft)	0.78 (2.55)
Taper ratio	0.33
Leading-edge sweep	41.6
MAC, m (ft)	1.69 (5.54)
Span, m (ft)	2.20 (7.2)
Cant angle, deg	30
Airfoil	NASA 65-00

TABLE 18. ROCKWELL ALTERNATIVE CONFIGURATION WEIGHT SUMMARY

Item	Weight, kg (lb)
Structure	3916 (8633)
Propulsion	2475 (5456)
Fixed equipment	1454 (3206)
Weight empty	7845 (17295)
Operating weight empty	8052 (17750)
Payload	544 (1200)
Fuel	2427 (5350)
VTO gross weight	11023 (24300)

TABLE 19. VOUGHT CONFIGURATION DIMENSIONAL DATA

	Wing (total)	Canard (each)	Vertical fin (each)	Aft ventral (each)	Forward ventral (each)
Area, m^2 (ft^2)	32.52 (350.0)	1.93 (20.8)	2.43 (26.2)	0.79 (8.5)	0.33 (3.6)
Aspect ratio	2.24	1.20	1.30	0.58	1.12
Taper ratio	0.15	0.28	0.35	0.0	0.30
Span, m (ft)	8.53 (28.00)	1.52 (5.00)	1.77 (5.84)	0.67 (2.21)	0.61 (2.00)
Root chord, m (ft)	6.63 (21.74)	1.98 (6.51)	2.03 (6.65)	2.03 (6.67)	0.84 (2.75)
Tip chord, m (ft)	0.99 (3.26)	0.55 (1.82)	0.71 (2.33)	0.0 (0.0)	0.25 (0.83)
Mean geometric chord, m (ft)	4.50 (14.78)	1.40 (4.60)	1.47 (4.84)	1.55 (5.10)	0.59 (1.97)
Leading edge sweep, deg	50.0	55.0	45.0	45.0	45.0
t/c, root/tip	0.06/0.05	0.04	0.04	0.03	0.04
Airfoil, root/tip	65A006/65A005	65A004	65A004	65A003	65A004
Dihedral, deg	0	10	---	---	-15 to -75
Fin cant, deg	---	---	15	15	---
Definition	Idealized no strake or trailing-edge extension	Root chord at strake	From wing reference plane	From wing reference plane	Exposed area

TABLE 20. VOUGHT TANDEM-FAN BASELINE CYCLE CHARACTERISTICS

	Parallel flow (VTOL)	Series flow (high speed)
Fan pressure ratio	2.2/1.75	3.44
Bypass ratio	3.43	1.00
Compressor PR	10.0	7.33
Overall PR	17.5	25.2
Combustor temperature, °C (°F)	1,538 (2,800)	1,479 (2,695)
Exhaust temperature, °C (°F)	510/510 (950/950)	1,871 (3,400)
Thrust, augmented, N (lb)	130,264 (29,286)	195,023 (43,845)
SFC, augmented	0.977	2.024
Thrust, unaugmented, N (lb)	111,200 (25,000)	117,810 (26,486)
SFC	0.541	0.665
Corrected airflow, kg/sec (lb/sec)	196/115 (433/254)	196 (433)
Core corrected airflow, kg/sec (lb/sec)	44 (97)	35 (78)
Actual airflow, kg/sec (lb/sec)	181/106 (400/234)	187 (412)
Core actual airflow, kg/sec (lb/sec)	65 (143)	93 (206)

TABLE 21. VOUGHT TF120 MISSION CAPABILITY

Parameter	Internal fuel	Plus two 370-gal tanks
VTO weight, kg (lb)	11312 (24940)	
STO weight, kg (lb)		15723 (34664)
Fuel, kg (lb)	3846 (8480)	6129 (13512)
Supersonic intercept radius		
M = 1.6, 15240 m (50000 ft), km (n. mi.)	371 (200)	
M = 2.0, 18288 m (60000 ft), km (n. mi.)	258 (139)	
Fighter escort radius, n. mi.	1003 (541)	1553 (838)
Interdiction radius, n. mi.		962 (519)

TABLE 22. VOUGHT TF 120 WEIGHT SUMMARY

Item	Weight, kg (lb)
Structure	2442 (5384)
Propulsion	2553 (5629)
Fixed equipment	1469 (3240)
Weight empty	6464 (14253)
Operating weight empty	6711 (14798)
Payload*	754 (1662)
Usable fuel	3846 (8480)
VTO gross weight	11310 (24940)

*Four AMRAAM and 20-mm gun with 400 rounds of ammunition.

TABLE 23. VOUGHT TF120 PERFORMANCE SUMMARY

Item	NASA guideline	Vought TF120	
		Max A/B	Intermediate
Sustained load factor at Mach 0.6, 3,048 m (10,000 ft), 83% VTOGW	6.2	6.62	
$P_{S_{1G}}$ at Mach 0.9, 3,048 m (10,000 ft), 88% VTOGW, m/sec (ft/sec)	274 (900)	526 (1,725)	
Acceleration from M = 0.8 to M = 1.6 at 10,973 m (36,000 ft), sec	---	34	
Maximum Mach number at 10,973 m (36,000 ft)	1.6	2.40	1.42
Ceiling, m (ft)	---	20,379 (66,860)	16,331 (53,580)

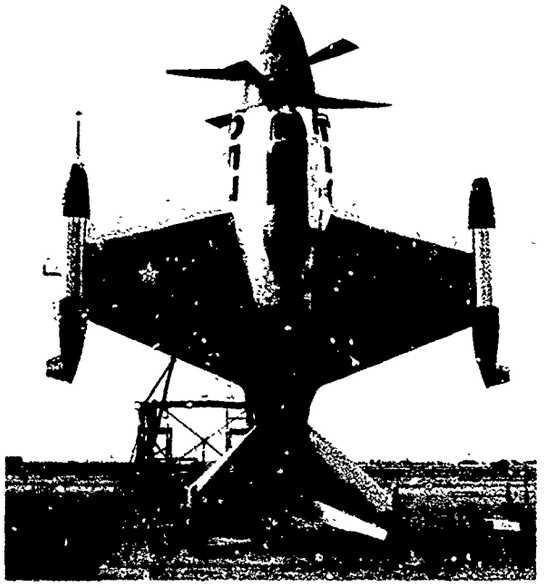

Figure 1. Lockheed XFV-1.

Figure 2. Convair XFY-1 Pogo.

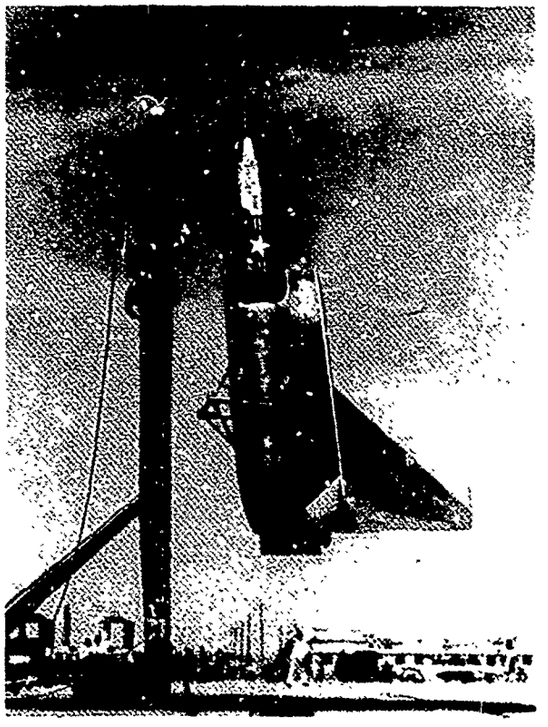

Figure 3. Ryan X-13 Vertijet.

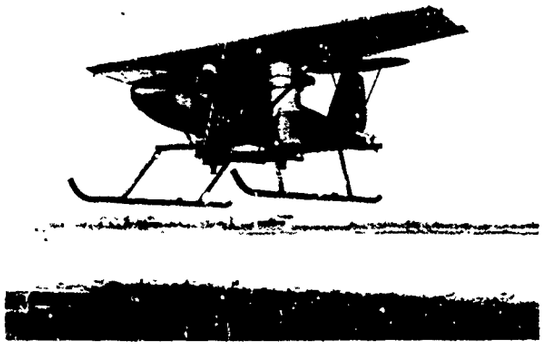

Figure 4. Bell Air Test Vehicle (ATV).

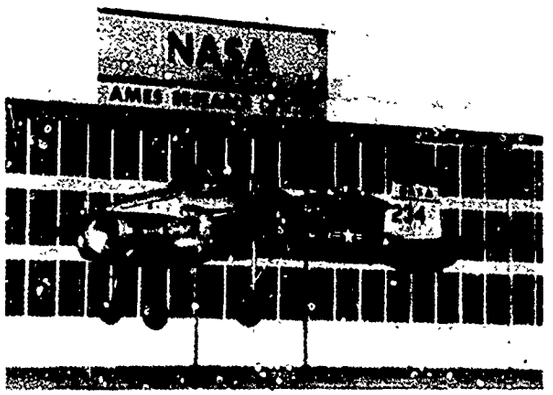

Figure 5. Bell X-14.

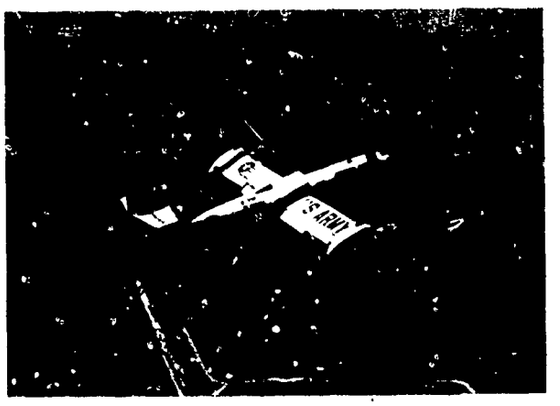

Figure 6. Bell XV-3 Tilt Rotor.

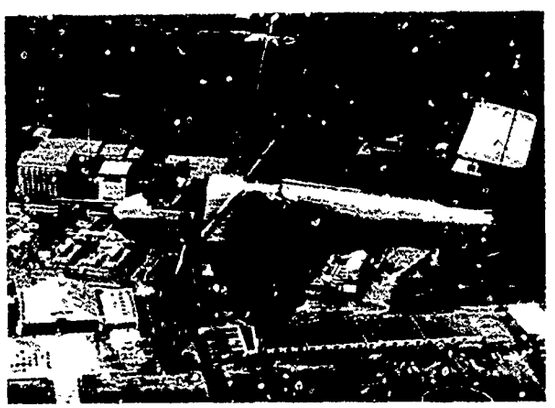

Figure 7. Ryan VZ3-RY.

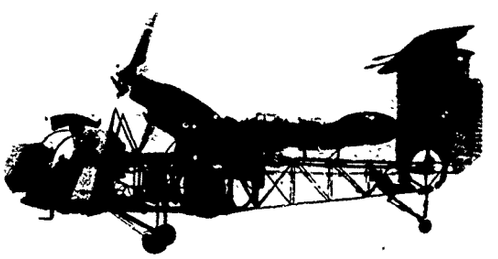

Figure 8. Boeing-Vertol VZ-2.

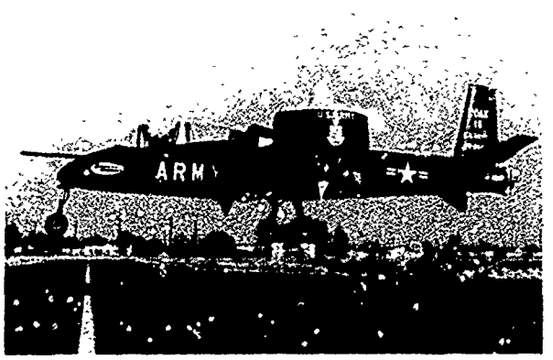

Figure 9. Doak VZ-4 Ducted Fan.

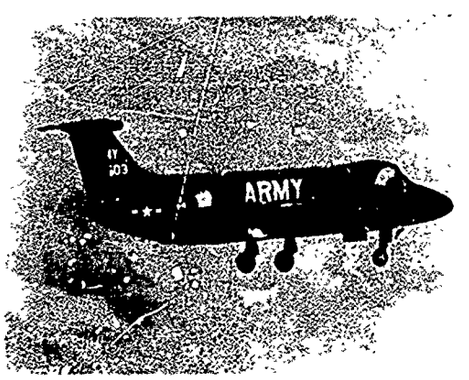

Figure 10. Lockheed XV-4A Hummingbird.

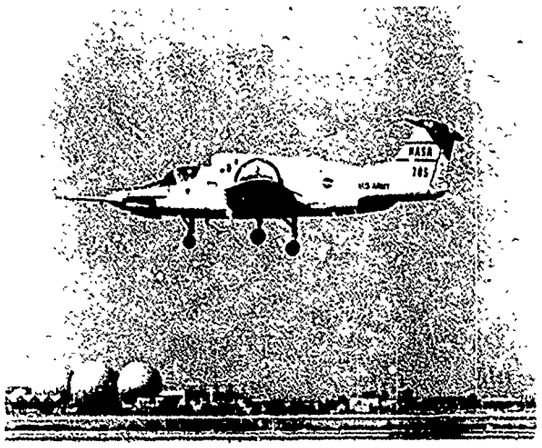

Figure 11. Ryan XV-5B.

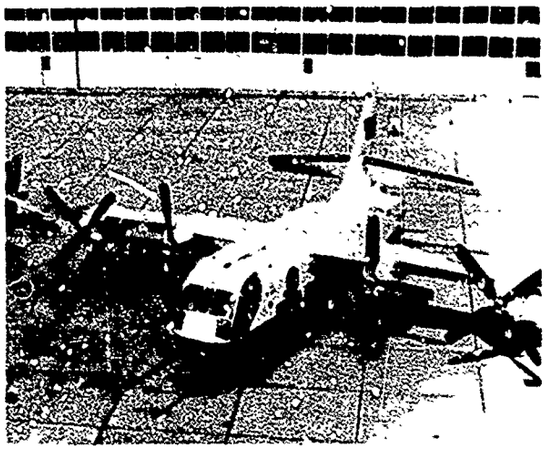

Figure 12. LTV XC-142 Tilt Wing.

Figure 13. Curtiss Wright X-19A Tilt Prop.

Figure 14. Bell X-22A Ducted Fan.

Figure 15. Bell XV-15 Tilt Rotor.

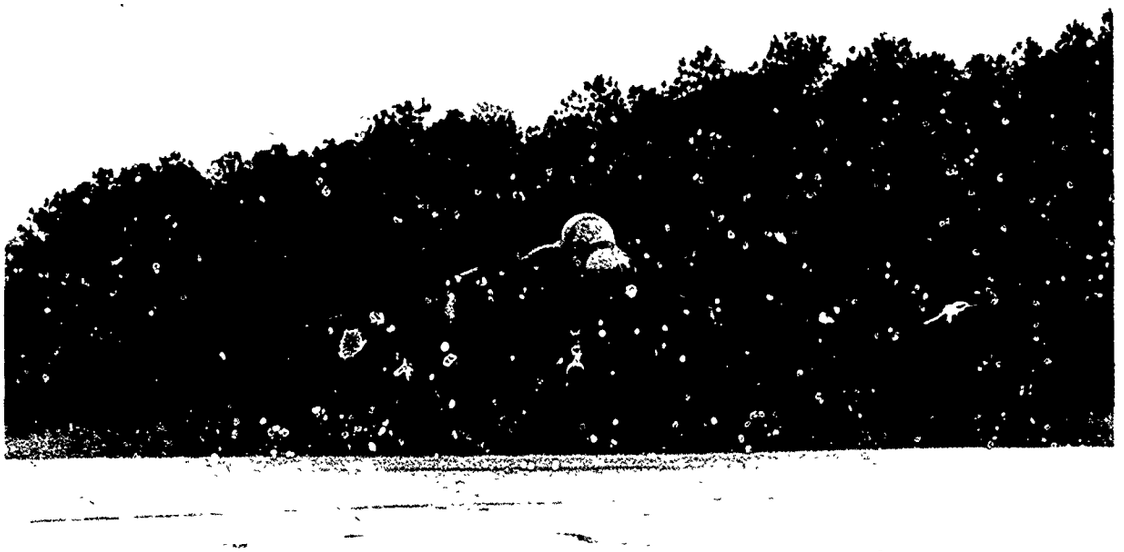

Figure 16. AV-8B Harrier II.

Figure 17. AV-8B Harrier II.

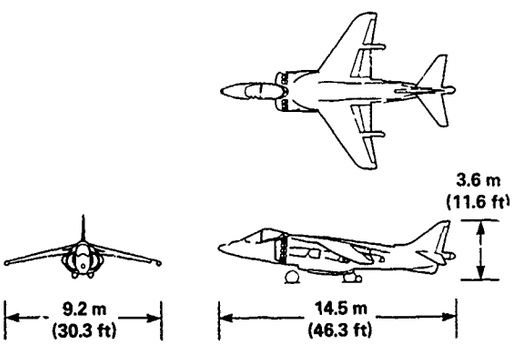

Figure 18. AV-8B Harrier II.

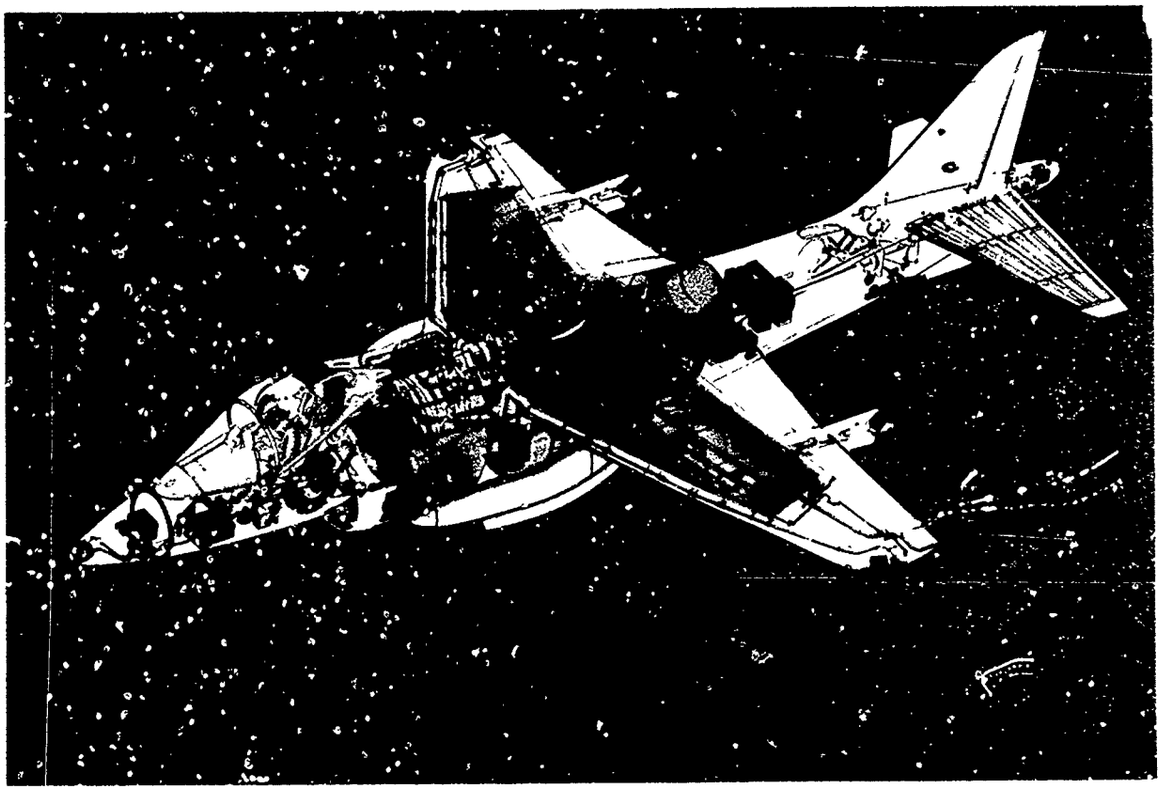

Figure 19. Changes to the AV-8A to develop the AV-8B Harrier II.

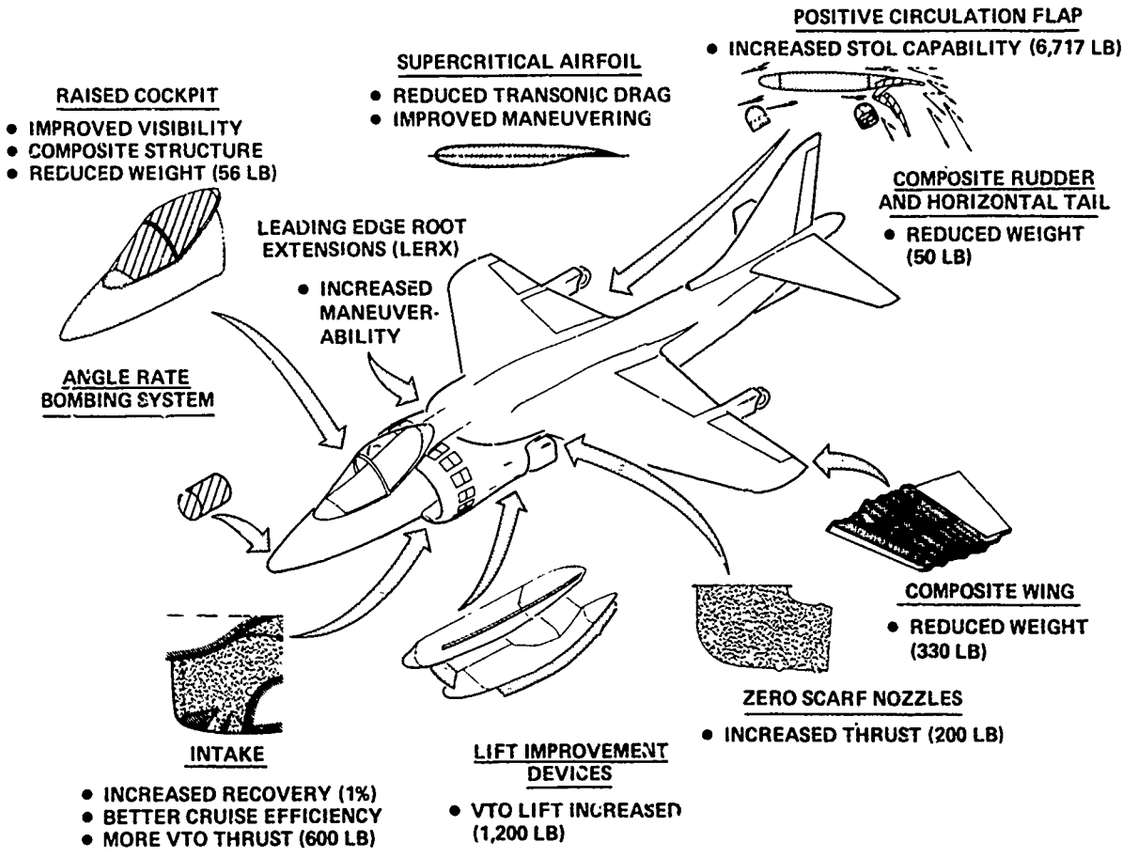

Figure 20. Advanced technologies incorporated into the AV-8B.

Figure 21. Boeing tilt-nacelle medium-speed concept.

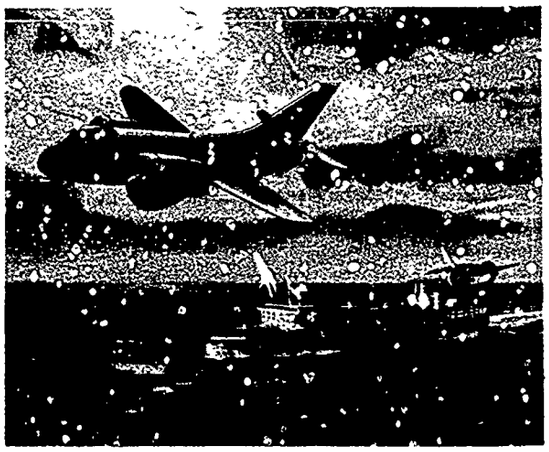

Figure 22. Boeing blown-flap medium-speed concept.

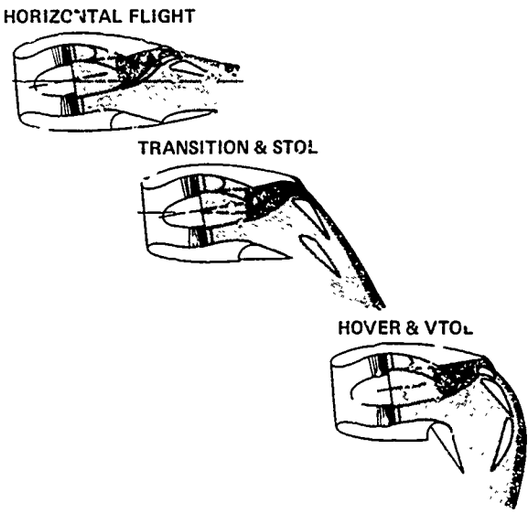

Figure 23. General Dynamics ABLE medium-speed propulsive-lift concept.

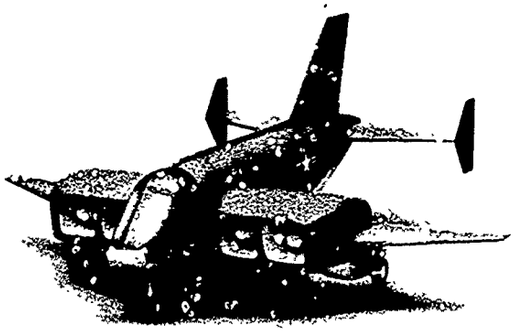

Figure 24. General Dynamics medium-speed concept.

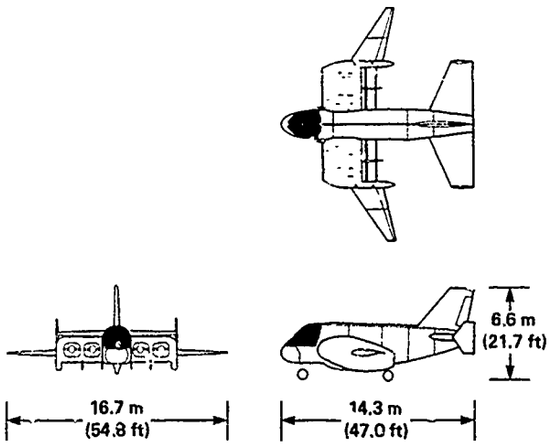

Figure 25. Three views of the General Dynamics medium-speed concept.

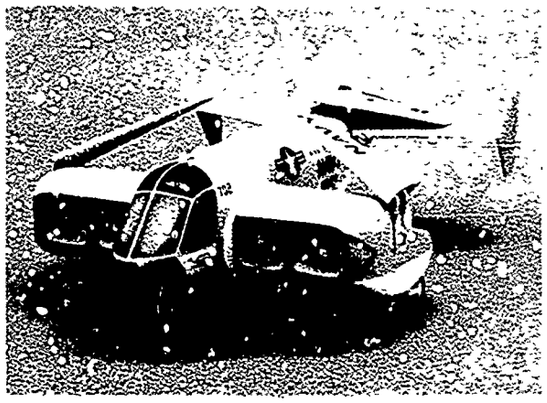

Figure 26. Folding capability of the General Dynamics medium-speed concept.

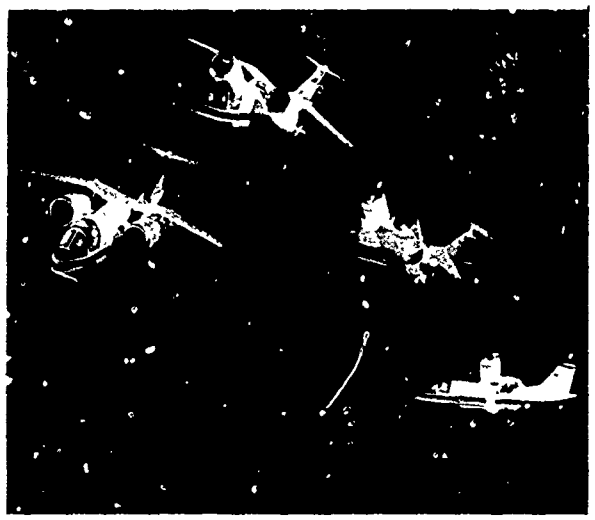

Figure 27. Grumman tilt-nacelle medium-speed concept (Design 698).

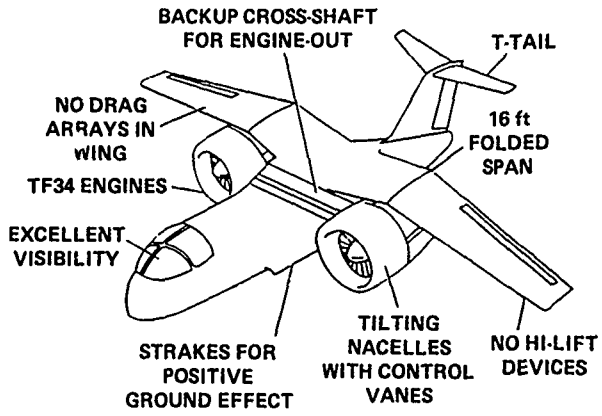

Figure 28. Features of Grumman Design 698.

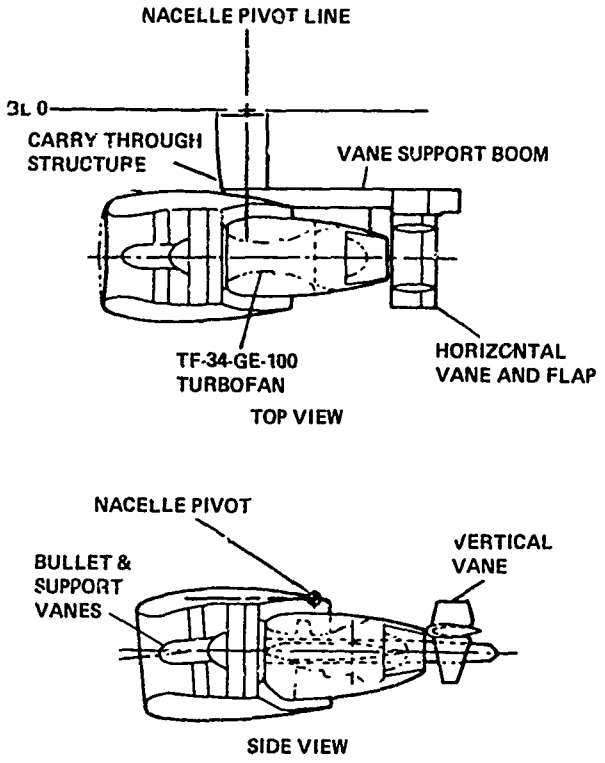

Figure 29. Design 698 tilting nacelle.

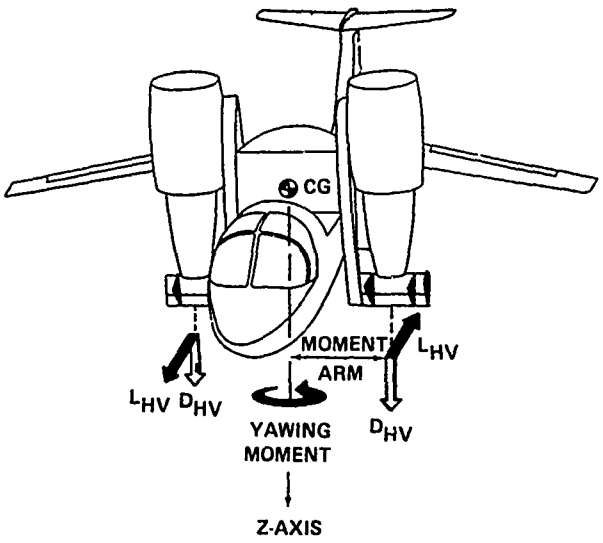

Figure 30. Differential horizontal vane deflection for yaw.

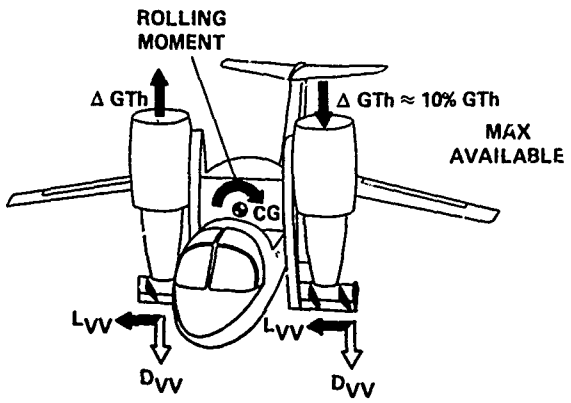

Figure 31. Vertical vane deflection and differential thrust for roll.

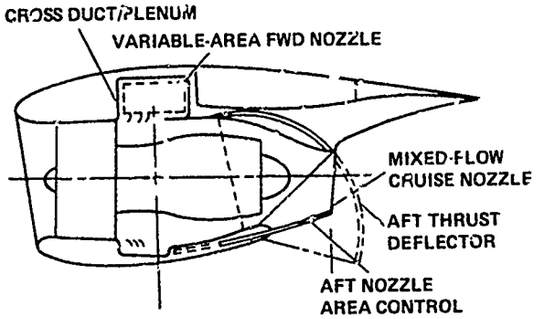

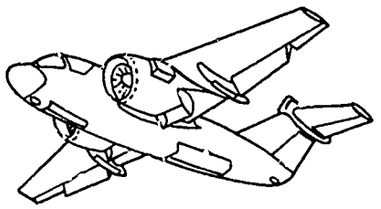

Figure 32. Lockheed split-fan propulsive-lift concept.

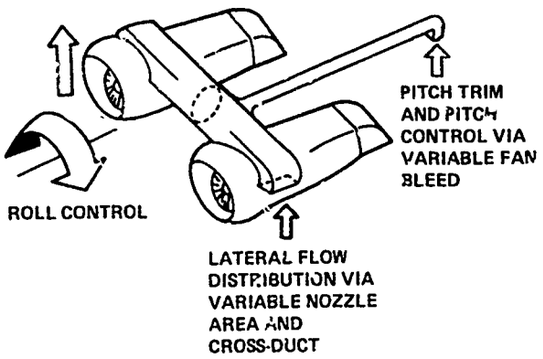

Figure 33. Lockheed split-fan hover-control concept.

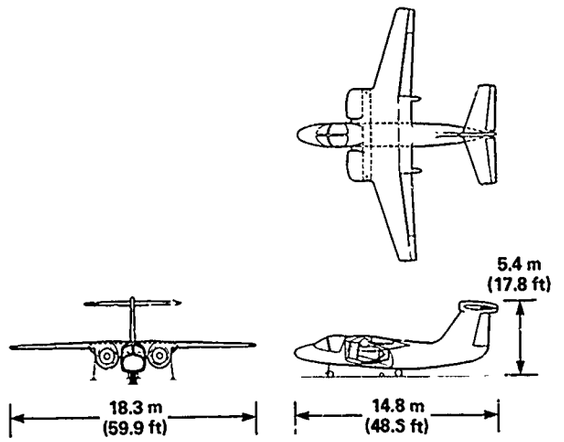

Figure 34. Lockheed twin engine, split-fan, medium-speed concept.

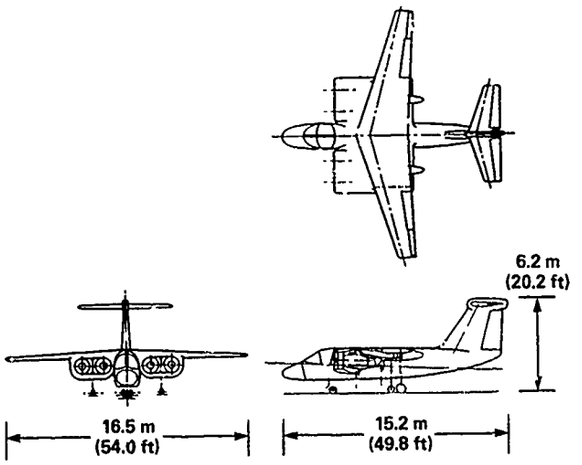

Figure 35. Lockheed four engine, split-fan, medium-speed concept.

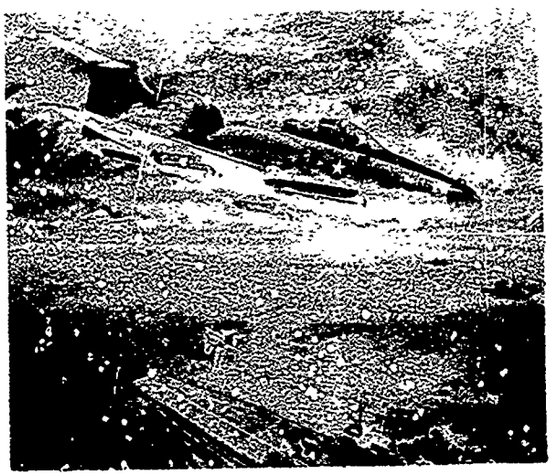

Figure 36. MCAIR gas-driven fan Model 260 medium-speed concept.

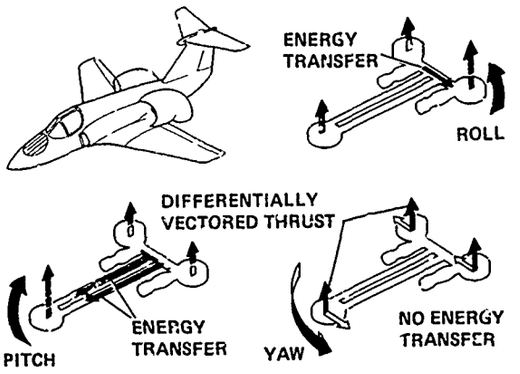

Figure 37. Gas-driven Model 260 propulsion/control system.

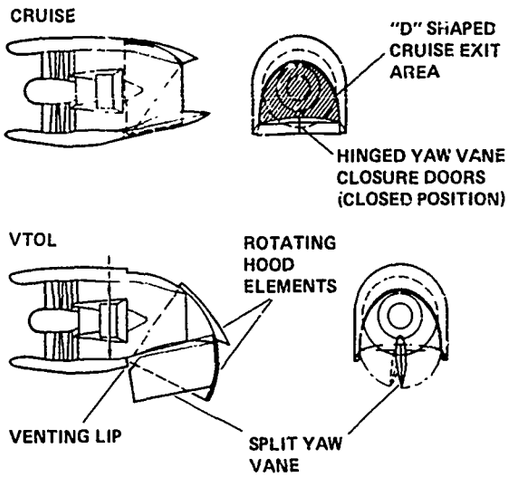

Figure 38. Vented "D" nozzle characteristics.

Figure 39. MCAIR mechanically driven three-fan Model 260 medium-speed concept.

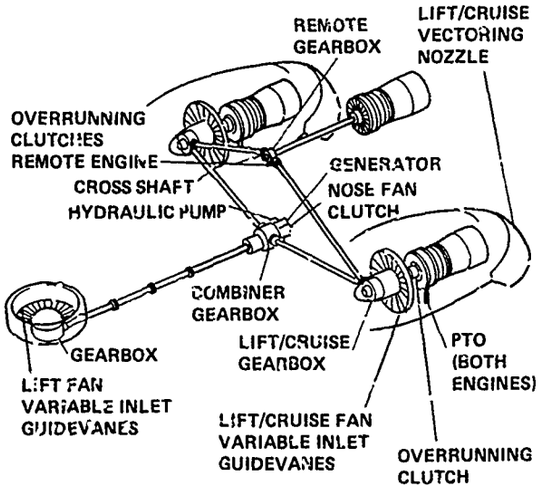

Figure 40. Mechanically driven Model 260 propulsion/control system.

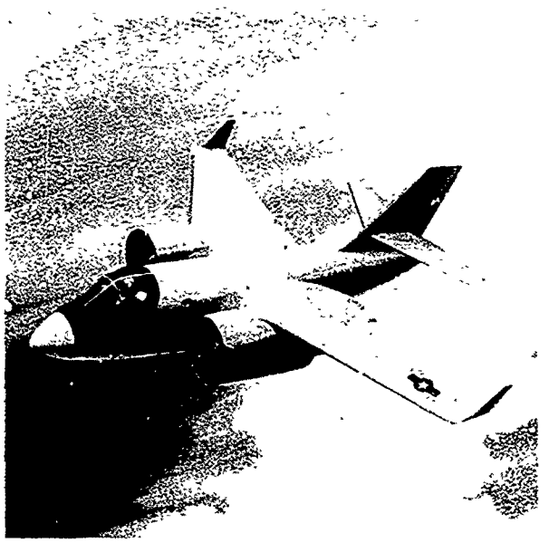

Figure 41. MCAIR vectored-thrust Model 276 medium-speed concept.

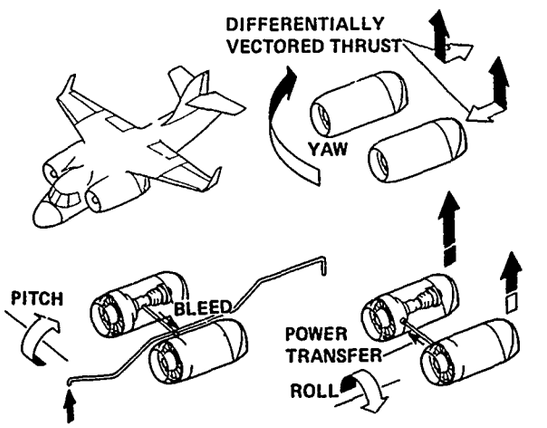

Figure 42. Vectored-thrust Model 276 propulsion/control system.

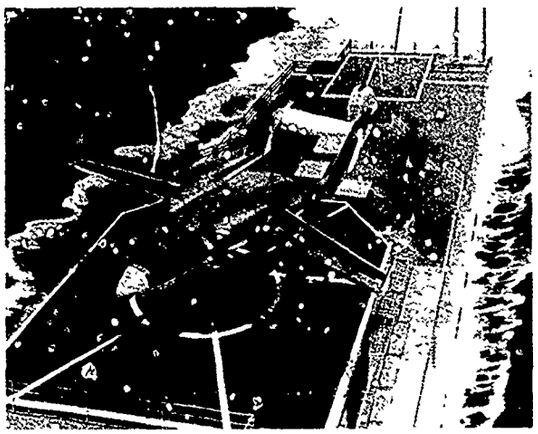

Figure 43. Rockwell ejector-in-wing medium-speed concept.

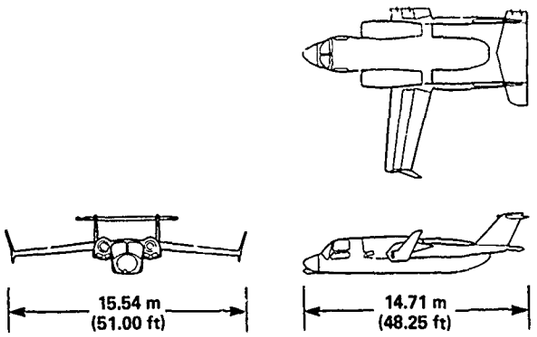

Figure 44. Three views of Rockwell ejector-in-wing medium-speed concept.

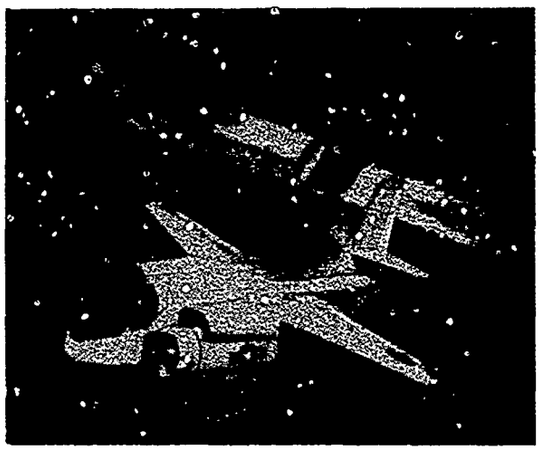

Figure 45. Vought tandem-fan medium-speed concept (V-530).

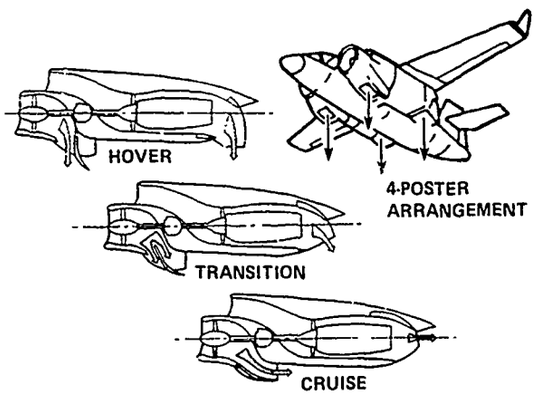

Figure 46. Vought tandem-fan propulsion concept.

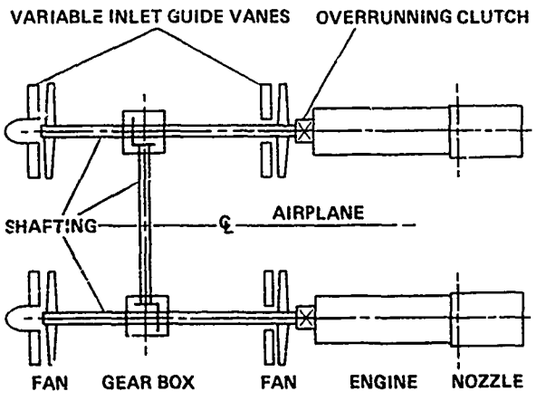

Figure 47. Vought tandem-fan drive system arrangement.

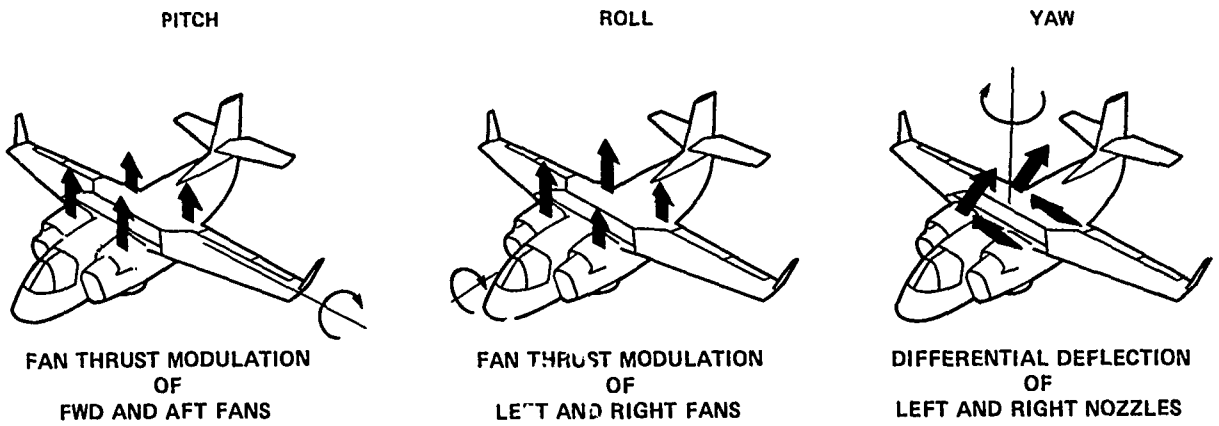

Figure 48. Vought tandem-fan hover-control concepts.

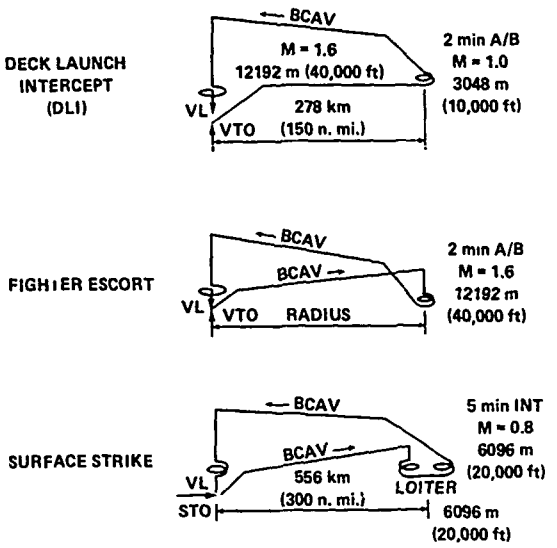

Figure 49. Example mission profiles for twin-engine VSTOL fighter/attack aircraft.

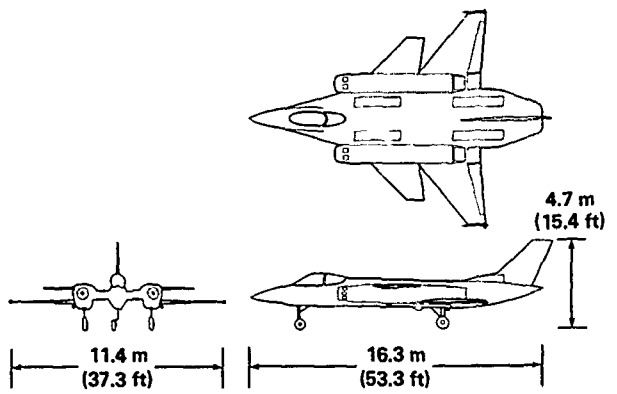

Figure 50. General Dynamics HATOL ejector-diffuser concept.

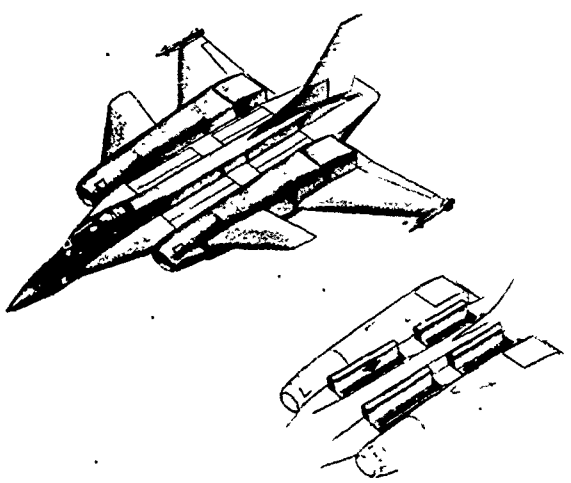

Figure 51. Ejector-diffuser bays open and closed on the General Dynamics concept.

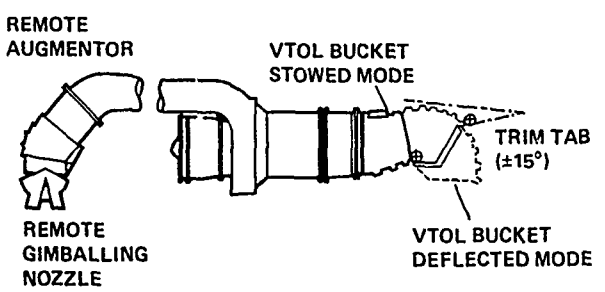

Figure 52. Remote Augmented Lift System (RALS).

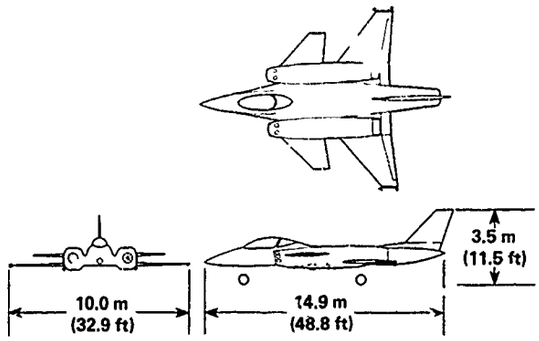

Figure 53. General Dynamics HATOL RALS concept.

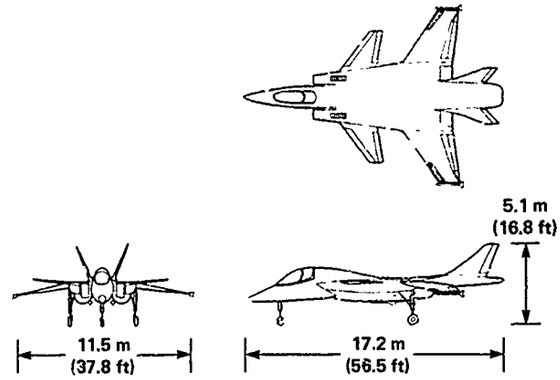

Figure 54. Grumman HATOL concept.

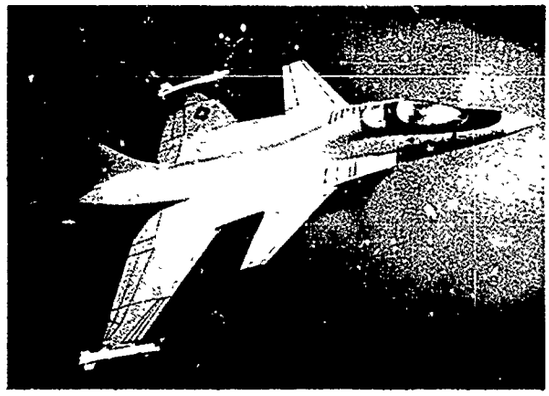

Figure 55. Grumman HATOL concept.

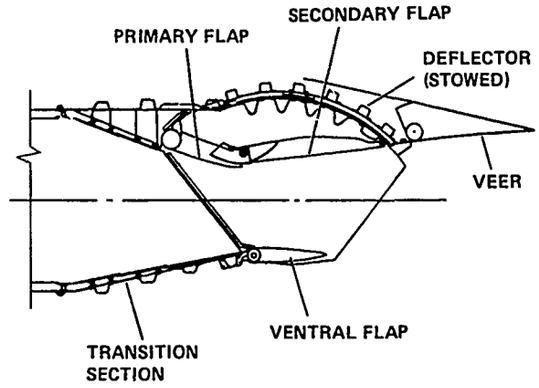

Figure 56. Schematic of ADEN.

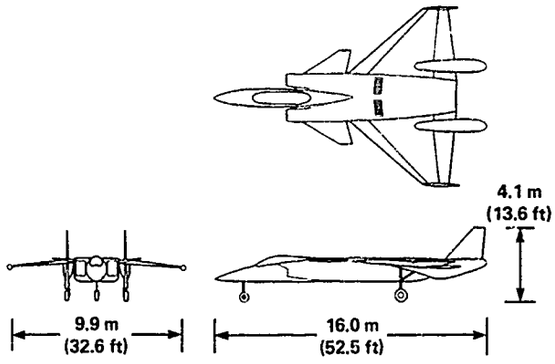

Figure 57. Northrop HATOL concept.

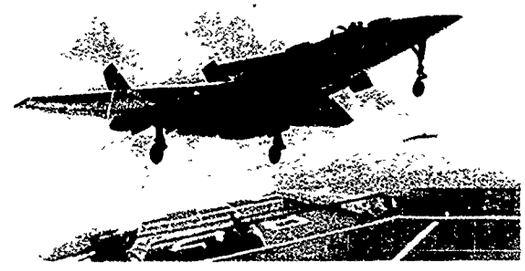

Figure 58. Artist rendering of the Northrop HATOL concept.

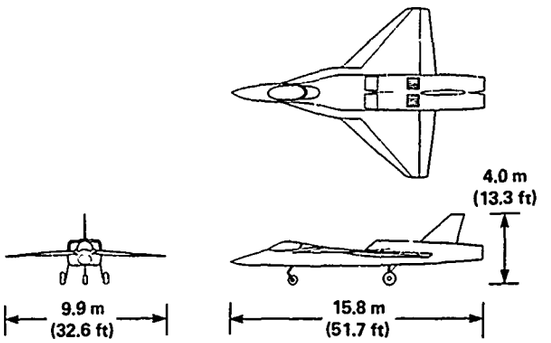

Figure 59. Northrop VATOL concept.

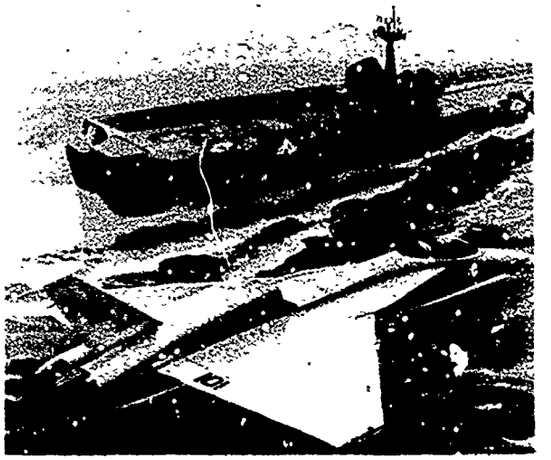

Figure 60. Artist rendering of the Northrop VATOL concept.

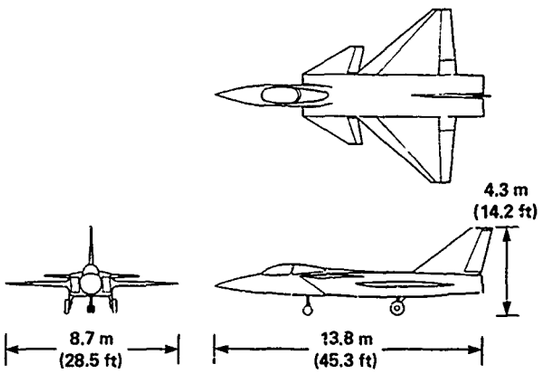

Figure 61. Vought VATOL concept.

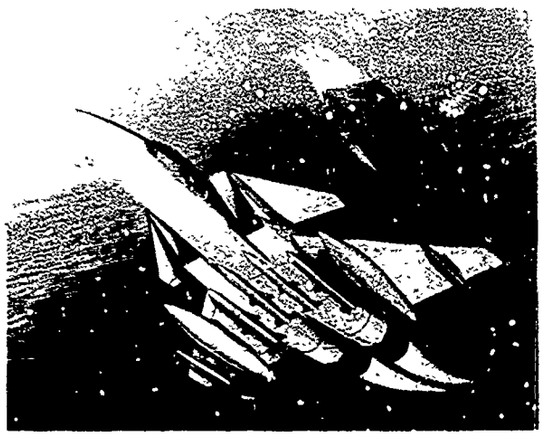

Figure 62. Artist rendering of the Vought VATOL concept in a STOVL configuration.

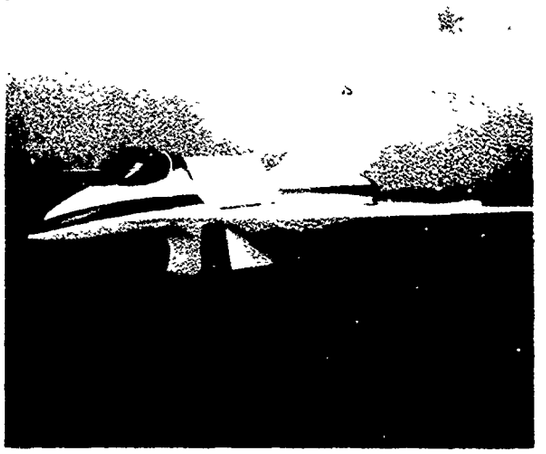

Figure 63. General Dynamics E7 configuration in hover flight.

Figure 64. General Dynamics E7 configuration in cruise flight

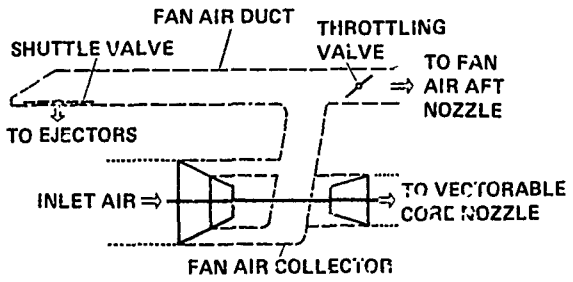

Figure 65. General Dynamics E7 configuration propulsive system schematic.

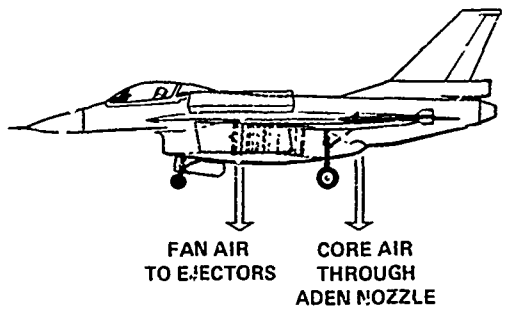

(a) Hover configuration.

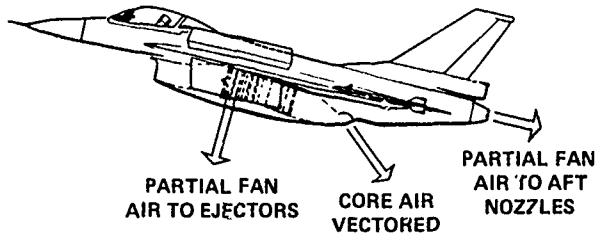

(b) STO and transition configuration.

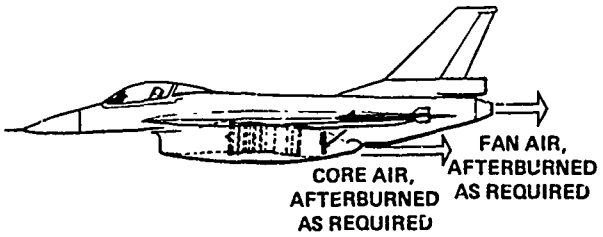

(c) Up-and-away configuration.

Figure 66. Three modes of operation of E7 propulsion system.

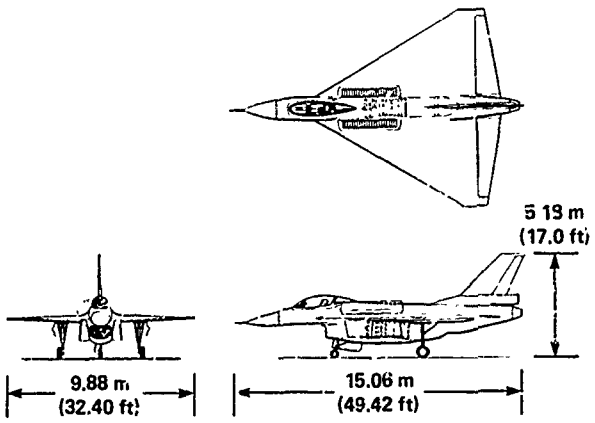

Figure 67. General Dynamics E7 configuration.

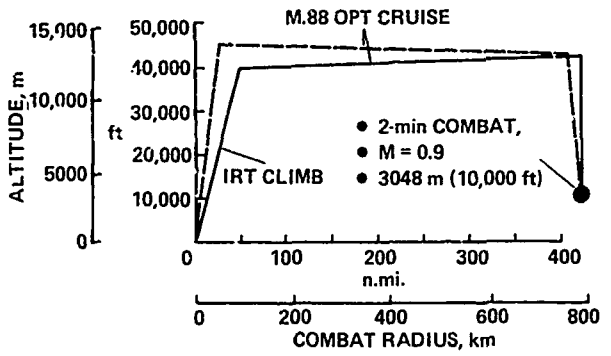

Figure 68. Naval escort mission used in the General Dynamics studies.

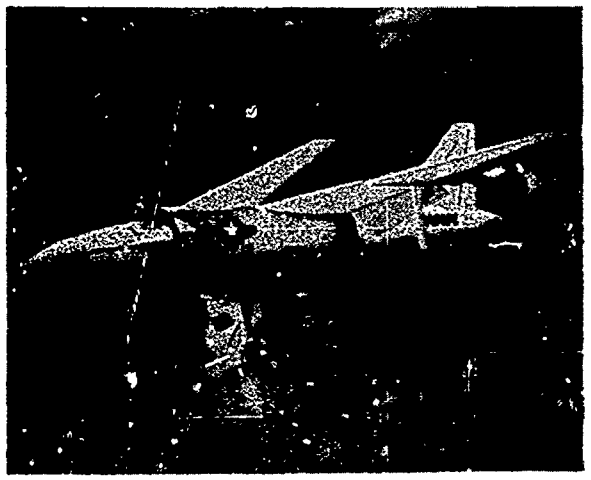

Figure 69. MCAIR configuration in hover flight.

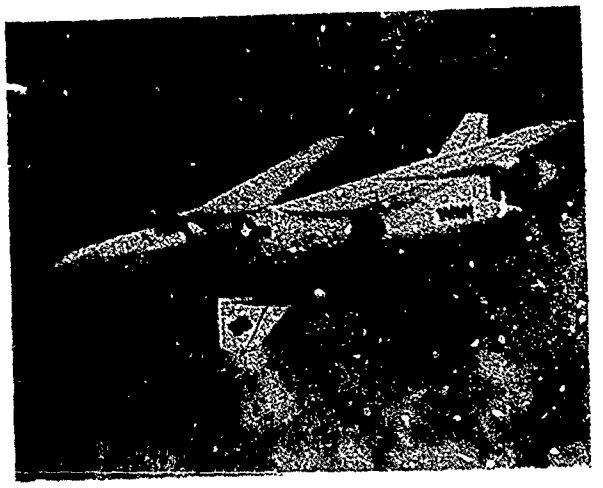

Figure 70. MCAIR configuration in cruise flight.

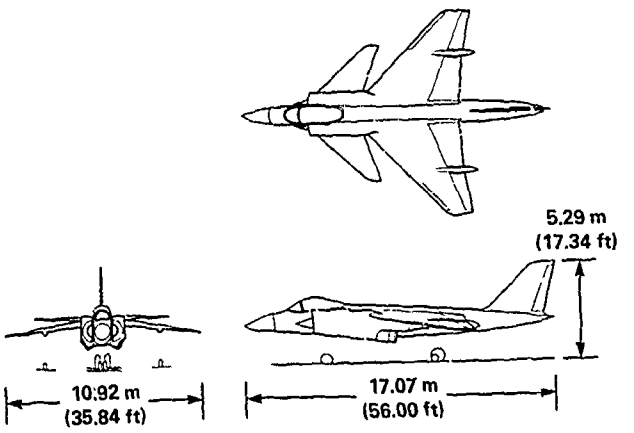

Figure 71. MCAIR 279-3 configuration.

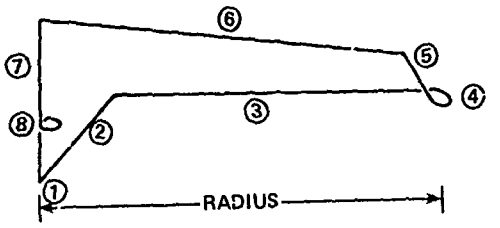

STORE LOADING: (2) SRM + (2) AMRAAM	
① WARM-UP, VTO, ACCELERATION	2 min, IRT; 0.5 min MAXIMUM POWER
② CLIMB	TO DASH CONDITION: MAXIMUM POWER
③ DASH	MACH 1.6 @ 12,192 m (40,000 ft)
④ COMBAT	2 min, MAXIMUM POWER AT DASH CONDITION
⑤ DECELERATE-CLIMB	TO BCAV
⑥ CRUISE	BCAV
⑦ DESCENT	TO SEA LEVEL NO FUEL OR DISTANCE CREDIT
⑧ LANDING ALLOWANCE	
LOITER	10 min, AT SEA LEVEL, MINIMUM FUEL
LANDING	45 sec AT LANDING POWER
RESERVE	5% TOTAL FUEL

SERVICE TOLERANCE
5% FUEL FLOW

Figure 72. Vertical-takeoff supersonic deck-launched intercept (DLI) mission used in the MCAIR studies.

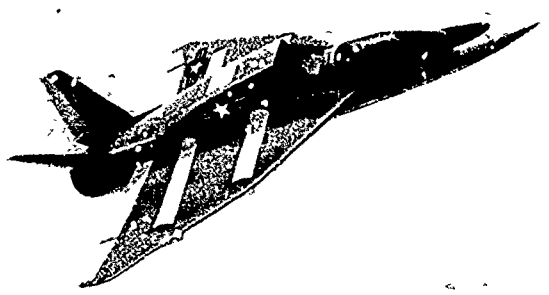

Figure 73. Rockwell baseline configuration in cruise flight.

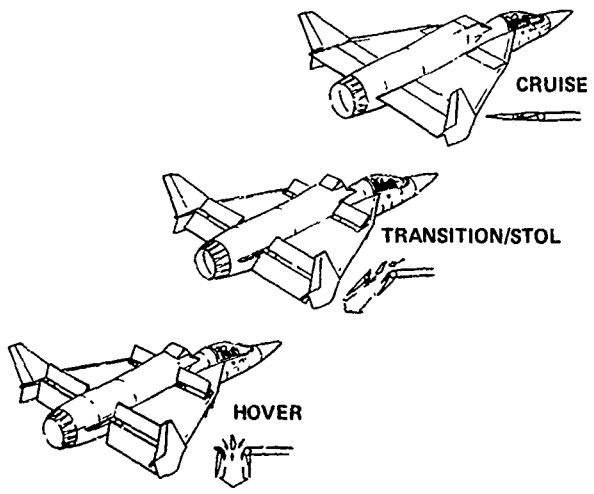

Figure 74. Rockwell configuration in various flight modes.

Figure 75. Rockwell baseline configuration.

MISSION PROFILE

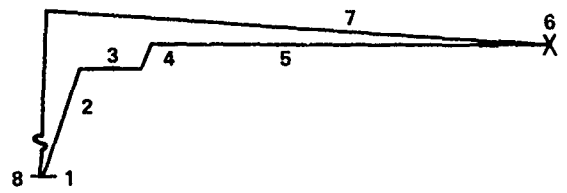

1. WARMUP TAKEOFF AND ACCEL. TO CLIMB SPEED 4 min IDLE PLUS 1.25 min INTERMEDIATE
2. CLIMB TO 12,192 m (40,000 ft) MAX A/B
3. ACCEL. TO 1.6 MACH NUMBER @ 12,192 m (40,000 ft)
4. CLIMB @ 1.6 MACH TO 15,240 m (50,000 ft)
5. CRUISE @ 1.6 MACH @ 15,240 m (50,000 ft)
6. COMBAT 2 min @ 1.6 MACH @ MAX A/B
7. CRUISE BACK TO BASE @ BEST CRUISE ALTITUDE AND VELOCITY (BCAV)
8. LANDING RESERVE (5% INITIAL FUEL + 10 min LOITER AT SEA LEVEL)

Figure 76. Deck-launched intercept (DLI) mission used in the Rockwell studies.

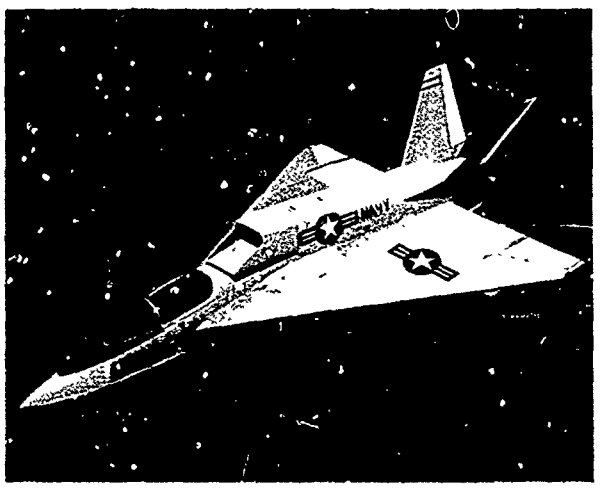

Figure 77. Rockwell alternative configuration in cruise flight.

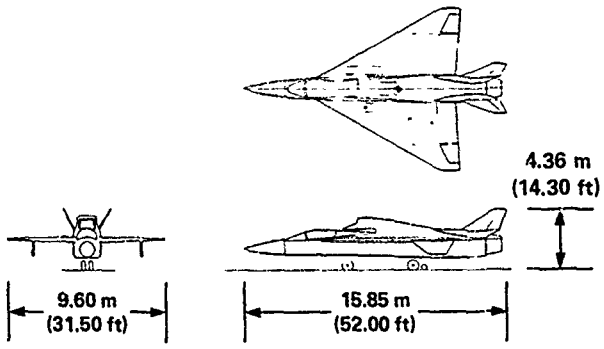

Figure 78. Rockwell alternative configuration.

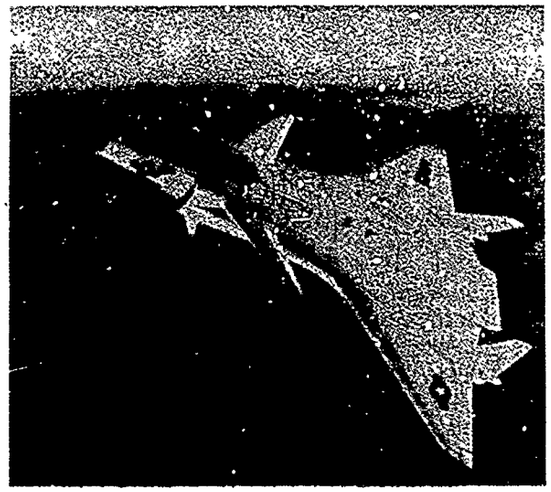

Figure 79. Early Vought configuration in cruise flight.

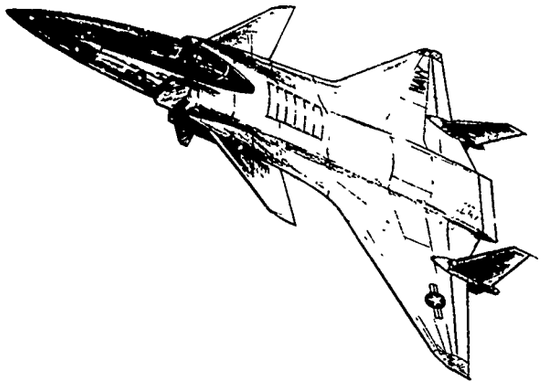

Figure 80. Vought configuration in cruise flight.

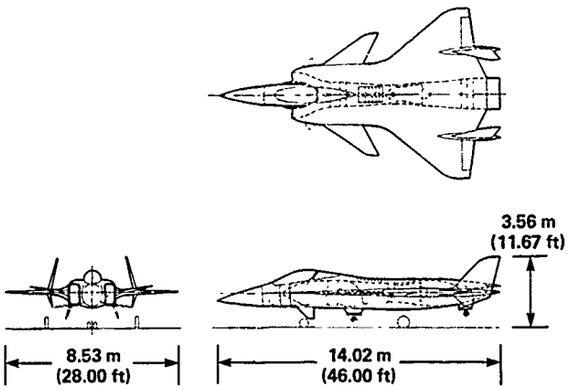

Figure 81. Vought configuration.

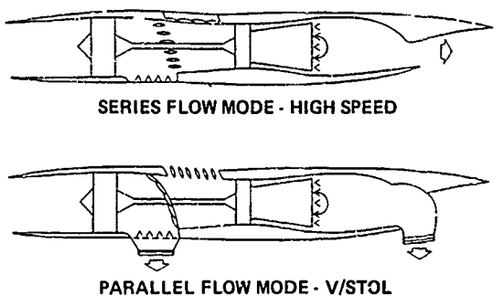

Figure 82. Schematic of Vought tandem-fan concept.

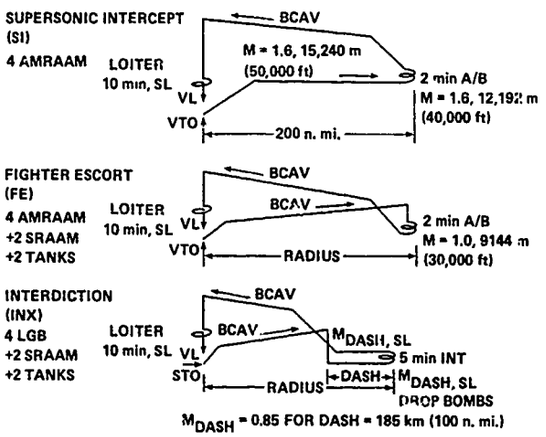

Figure 83. Vought notional design missions.

LAYOUT CONSIDERATIONS AND TYPES OF VSTOL AIRCRAFT

J. FLETCHER
HEAD OF ADVANCED PROJECTS DEPARTMENT
BRITISH AEROSPACE PLC
AIRCRAFT GROUP
WARTON DIVISION

1. Introduction

Since the Rolls Royce "Thrust Measuring Rig" first flew in 1954 various vertical take off and landing aircraft have gone through an extraordinarily varied, and sometimes painful, period of experiment (Fig. 1). During this 30 year period a surprising number of projects have reached the prototype stage and most have flown with varying amounts of success. Of these, only the Harrier has achieved maturity and together with the Russian "Forger", these two vehicles share the distinction of being the sole VTOL representatives in regular squadron service. It will not escape notice that neither of these vehicles are truly supersonic. As will emerge later in this discussion, the imposition of supersonic performance (such as is exemplified in most modern aircraft requirements) upon the already harsh demands of VTOL operation, provides a design challenge of the utmost severity. During the course of this lecture, it is the intention to discuss and illustrate the several aspects of modern VTOL vehicle design that have a major effect on conceptual and configurational issues.

The generic pseudonym "VTOL" will be generally used, unless there is a good reason to distinguish between the various possible modes of operation e.g. STOVL.

2. The Weight Problem

a) The thrust to weight ratio in powered lift conditions is obviously critical and thus the drive to minimise aircraft mass is even more crucial than usual. Fig. 2 shows the mass breakdown of two aircraft, (one VTOL design and one CTOL design), of comparable role and performance. In the case of the VTOL aircraft, 3 points are notable;

i) the lower than usual structure fraction, which reflects deliberate configurational economies and persistent development effort.

ii) the higher than usual powerplant fraction, which reflects the considerably higher installed thrust to weight ratio.

iii) the lower than usual fuel fraction, which reflects the relative lack of volume available for fuel due to a small wing, (not sized for T.O. or landing) larger engine and limitations on fuel tank positions resulting from the central engine location.

It is interesting to observe some of the measures adopted on Harrier in order to address the weight problem. For example, a one-piece wing and a simple short fuselage with minimal cut-outs. Such weight economy was considered mandatory in the early 1960's, sometimes at the expense of role equipment, ease of engine removal, and the like. However, with the advent of more modern design technology it may be felt that the structural weight problem of a VTOL aircraft is considerably ameliorated. Unfortunately, present and future requirements demand an increasing amount of role equipment to improve operational effectiveness, and an increasing attention to the practical features that affect unit cost and operating costs. Added to these are the general demands for higher performance. Consequently, scrupulous attention to every detail of weight saving will still be demanded.

b) An important consideration with regard to VTOL aircraft concerns fuel weight. Service requirements generally specify one or more mission profiles. Hence, one has also to consider very critically the aircraft drag and engine sfc. These naturally reflect the particular configurations and engine size and cycle chosen to effect VTOL operation. For example, the high installed thrust demanded by VTOL will mean that an engine arrangement designed to provide both lift and forward flight will be well throttled back in an economic cruise condition. This implies that it is operating on a very unfavourable portion of the sfc loop, which leads to higher than usual fuel flows. Such VTOL fuel weight penalties have been at least partially offset in recent years by the increasing T/W ratios implied by the demands for high mobility and agility. Clearly the use of engine reheat, if available, has a bearing on the comparison as it may provide a better matched engine if used in forward flight and not in powered lift conditions. Even this possibility has to be carefully weighed against the excessive demands of sustained reheat operation.

c) Another interesting aspect of the VTOL weight issue, concerns the type and forms of propulsion system. In the early days of VTOL there was much debate concerning the use of lightweight engines specifically designed for lift. It was often shown, as in Fig. 3, that there was an optimum ratio of dedicated lift engine weight to total propulsion weight. The minimum weight installation varied with the requisite mission profile. It is noticeable that for the close air support mission the minimum weight solution occurs with lift engines providing 50-60% of the total installed thrust. Note that this was a minimum weight solution. Minimum cost would have provided a different answer! Over the intervening years several factors have been brought to bear that have changed this initial conclusion. The current view of close air support aircraft is that they should have much more agility, in order to be able to offer a highly competitive self-defence capability. This infers

that the design will be closer to the low level air superiority mission shown in Fig. 3, with the result that the optimum solution moves closer to 0% dedicated engine thrust. This is also shown to be a good solution for the high level intercept mission, thus implying that the integrated lift and cruise engine designs will satisfy a wide range of requirements.

It is of interest too, to chart the weight trends, on the same basis, of the several VTOL projects that have reached the flight demonstrator stage or have received a fair amount of design detail (Fig. 4). Note also some of the typical 'trade-offs' available to the designer, should he wish to make weight economies.

Other factors that have moved against the use of lift engines, are;

i) the high installational complexity.

ii) the relative improvement in "propulsion" engine T/W (lift engine developments in the 1960's tended to spin off onto all engine development).

iii) the increasing awareness of the importance of life cycle costs (forced by increasing labour costs) and mission availability. A multiplicity of engines clearly does not enhance either of these factors.

On overall balance, therefore, the use of lift engines has passed from favour and integrated engine solutions i.e. ones where the engine(s) provides elements of both lift and forward propulsion, are now believed to be much more viable.

Clearly, there are many more aspects of the VTOL weight question for example, the ground environment issues such as engine efflux re-ingestion which may have a bearing on the choice of powerplant. These aspects however will be dealt with later.

d) Hot gas reingestion and ground erosion are both topics that have a serious effect on several aspects of VTOL aircraft design. In this instance they exert an indirect influence on TOW, via their impact on the choice of engine cycle.

Hot Gas Reingestion (HGR) is primarily dependent upon airframe, intake and nozzle(s) configuration. However it is also influenced by engine exhaust temperatures and pressures. Engine thermodynamic cycles, normally determined by flight and mission performance considerations, may well have to be biassed with HGR and ground erosion in mind.

The consequence of hot gas reingestion will depend upon the mass and temperature distribution of the flow entering the intake and the tolerance of the engine. The resultant thrust loss and engine handling will reflect the chosen engine cycle together with the engine design assumptions with regard to fan and compressor surge margins.

Regrettably, modern engines with their comparatively highly loaded stages would appear more susceptible to surge than, say, the Pegasus engine.

Ground erosion is also a function of the temperature and pressure of the engine efflux and different surfaces react differently to the two parameters. The usual mechanism of failure involves a combination, in some degree, of temperature effects causing drying and/or differential expansion with any local failures sustained then being exacerbated by the jet pressure. It thus follows that the more benign the "footprint", the less likelihood there is of erosion damage to a given surface. The optimum design trade off will depend upon the operational demands, the efflux conditions and the landing surface properties. In turn, then, this may influence the choice of engine cycle, and hence the aircraft size and weight.

Generally, improving technology will lead to higher fan pressure ratios (FPR's) and stator outlet temperatures (SOT's) in the search for a smaller, lighter and more fuel efficient engine. Hence, inhibiting the jet efflux conditions implies some weight penalty.

3. Thrust Requirements for Vertical Manoeuvres

A proper excess of available thrust over aircraft weight is essential for VTOL. The amount required depends on:-

i) lift interference (L_I)

ii) hot gas ingestion (HGI)

iii) aircraft trim and control

iv) height control $\left(\frac{dh}{dt}\right)$

Of these i) and ii) are functions of aircraft/nozzle layout and are influenced by ground proximity and forward speed. In free air (out of ground effect) lift interference is dominated by the relative positions of the jet(s), the intake(s) and the airframe configuration. The most adverse case is probably for jets and intakes to be positioned on the centre of a large wing (e.g. SC1, Mirage III V) and such cases tend to become increasingly worse as speed increases from the hover condition to forward flight. Other lectures will cover this aspect in greater detail. Sufficient

to say here, that the implied thrust loss at hover conditions could typically be in the range 3-4%.

In ground effects however, much can be done by detailed geometric tailoring usually referred to as CADS (Cushion Augmentation Devices), LIDS (Lift Improvement Devices) and DAMS (acting as dams to the jet exhaust) to achieve acceptable characteristics, both with regard to lift interference and HGI.

iii) and iv) depend very much on the particular operational and design concept adopted. For example, can fore and aft nozzles be used to advantage in a trimming capacity, or will engine compressor bleed be necessary? Is hover only required at landing weights, or some other higher weight?

There is a fundamental difference between design for a vertical take-off and a vertical landing (Fig. 5). Firstly the take-off is more likely to be at a higher aircraft mass and will generally require higher height control margins to ensure safe take-off in the most severe conditions e.g. where HGI is likely to be encountered. It is assumed that the thrust margins of Fig. 5 are estimated for the required atmospheric and airfield conditions (e.g. ISA + 15^{0}C, 2000 ft). It is generally accepted that if the aircraft can sustain a free air hover it can perform a vertical landing. However with adverse combinations of lift interference, hot gas ingestion and engine rating characteristics, a larger thrust margin might become necessary.

A requirement for vertical take-off will generally prove the driver for engine size whereas flight requirements frequently exceed the vertical landing requirements. This has obvious implications on the choice of propulsion cycle and aircraft layout.

In considering the possibilities of ultra-short take-off and landing, as distinct from VTOL, it will be noted that with the thrust/weight ratio and wing loading typical of many modern combat aircraft, short take-off is automatically assured. However, the freedom to vector the jet exhaust can reduce take-off distances further, to some extent, but more importantly it provides lower take-off speeds and improved climb-out profiles. Short powered-lift landings are more difficult to accommodate. They require large jet deflection angles and depend as much on transient factors, such as engine run down times, as on any other factor.

Engine Rating Considerations

Modern engines are generally rated on $N/(T_1)^{0.5}$ and SOT as shown (Fig. 6). Extraction of

air for control purposes has two effects; increasing SOT and reducing thrust - some of which may be recovered, depending on the engine control system design.

The engine manufacturer may well allow a higher SOT for a short time i.e. sufficient to effect transitions, to offset the effect of air bleed of a given datum value. The 'datum' value has to be based on a judgement as to the high probability of a sustained demand (which may be a combination of demands for individual control axes) during a transition. Higher levels of bleed (probably 2 to 3 times the datum value) can be provided but are expensive in terms of overall thrust as the engine becomes SOT limited and are to be regarded as extremes of control demand, which are only to be sustained for very brief periods - probably at the cost of a normally excessive SOT, or, thrust-over-weight deficiency.

4. Aerodynamic and Propulsion Implications

a) Propulsive concepts

There are numerous propulsion concepts that can be postulated, some of the main examples being illustrated in Fig. 7. Four candidates have emerged as showing merit for various reasons. The four concepts (Figs 8 to 12) are,

i) vectored thrust (which may be 2, 3 or 4 poster)

ii) the tandem fan

iii) the remote augmentor lift system (RALS) - see ref. 1 for example, and,

iv) the ejector augmentor

Some of the configurational constraints of these particular concepts, especially aircraft length, nozzle disposition and intake location may be inferred from Fig. 13 and major advantages are outlined in Table 1.

The layout and aerodynamic characteristics of the airframe will clearly be affected by the choice of propulsion system. This latter will, in turn, be heavily influenced by the performance requirements, since each of the proposed propulsion concepts appears best matched to a particular flight regime, which is not necessarily the same for all the systems. Thus a situation emerges where, irrespective of other considerations, the demanded mission and performance requirements may well favour a particular propulsion system. Further than this, in some cases there may also be a preferred airframe configuration. Thus a conclusion is reached whereby some design solutions (airframe and propulsion) are seen to be inherently matched to certain specific performance regimes and not to others.

An example of this interactive process is the installation of a 2 poster engine with nozzles close to the wing trailing edge, to maximise jet induced benefits. The nozzle location dictates the CG position and then the chosen stability/instability margin determines the aerodynamic centre. Almost the only available configurational solution is a relatively high aspect ratio, sharply swept, wing allied to an aft tail; see Fig. 14. This would not, for instance, be thought a layout best suited to high supersonic cruise.

It is interesting to note at this juncture that, as the volumes shown in Fig. 15 intimate, some of these engine installations are very bulky and make low supersonic drag more difficult to achieve. This was one consideration behind the continued study of the vectored thrust principle, both in its vectored nozzle and tilt nacelle forms. However, it will be readily appreciated that the resultant area distributions will be quite different, one to another, and this is more important to supersonic performance than sheer bulk.

Another important variable to consider when studying the various propulsion concepts is the ratio of forward propulsive thrust to the available lifting thrust. In so doing one can attempt to get the best match between the flight performance requirements and the VTOL powered lifting requirements. Fig. 16 illustrates some examples of this. Clearly the use of thrust augmentation (PCB or reheat) has an important influence on this picture.

The requirements of vertical operation on the one hand and high supersonic manoeuvre on the other, are very disparate. Low jet temperature, low pressure, low velocity and high mass flow for good ground footprint and good Froude efficiency (hence fuel economy) are required for the former while high specific thrust for good flight performance is required for the latter.

It is interesting to observe that when a truly variable cycle engine can confidently be contemplated, then it is for VTOL that it will find a willing beneficiary. It is equally interesting to observe that the tandem fan, the ejector augmentor, lift + lift/cruise and the use of RALS are all, to some extent, simple attempts at cycle variability.

It will be noticed that the situation is also influenced by the design levels of stability, which will reflect the flight control system design. With modern fly-by-wire technology, the tendency is to design for certain levels of instability - as shown in Fig. 14.

b) Intakes

The usual dilemma facing the intake designer is exacerbated by the demands of VTOL and this topic will be dealt with in more detail by a later contributor. The major effect of VTOL is to considerably extend the operating speed range, with greater importance being attached to the provision of high quality air to the engine at zero forward speed. The effect of poor intake performance, both in terms of pressure loss and distortion, will be especially noticeable at vertical take off, hover and vertical landing. Intake total pressure loss leads to a reduction in gross thrust; typically a 1% loss of dynamic pressure can lead to a 1-1.5% loss of gross thrust dependng upon cycle pressure ratio. A 1.5% loss of gross thrust in VTOL conditions is clearly equivalent to a 1.5% increase in weight. Local distortion of pressure (and temperature) can lead to serious engine handling and/or operating limitations. These requirements have to be accommodated in addition to the usual constraints imposed by cruise, high speed and manoeuvring flight, where it is also necessary to minimise spillage drag.

A basic conceptual difference arises between fixed inlets, as employed in the more traditional solution such as Harrier, and rotating inlets such as occur on tilt nacelle configurations shown by VJ101 (Fig. 17) and the wind tunnel nacelle model for Fig. 18.

Wind tunnel model experience with the nacelle indicated that a relatively short, straight duct behind a pitot intake equipped with auxiliary doors can be designed to operate very satisfactorily over a wide range of speed and nacelle incidence. The static performance (with the nacelle near-vertical), was also shown to be encouraging, see Fig. 19 . It was ascertained that this arrangement would also provide satisfactory distortion recovery performance at very low forward speeds. Further confirmation of the tilt nacelle arrangement stems from the experience of VJ101 with a similar rotating nacelle, albeit equipped in this case with a translating cowl for powered lift operation.

The geometric location of such intakes, with the nacelle vertical has advantages with regard to the minimisation of HGI and foreign body reingestion (FOD), though the model test data indicated residual problems might exist under certain head wind conditions. The test program did not include any configuration optimisation other than the manipulation of the wall jet by varying nacelle toe-out.

The intake position on Harrier type configurations is constrained in a fore and aft sense. The most forward station may well be dictated by pilot vision. The most rearward position is governed by the proximity to the engine face position, which is itself controlled by the paramount need to have the centre of vertical thrust at the CG location. This leads to a short and sharply offset S-duct which needs very special care so as to avoid undue loss and distortion, especially for supersonic applications. Clearly the propulsion concept has a major bearing on the power plant position, and thus, the intake configuration (Fig. 13).

In general, the intake design is a fine compromise between several conflicting requirements which include, HGI, FOD, intake performance, duct performance, pilot vision, spillage drag and the supersonic area distribution. More recently, the radar signature of inlet and engine face have assumed major importance. This adds yet another parameter for the consideration of the inlet designer.

c) Nozzles

Nozzles also fall into two categories broadly corresponding to the two cases for intakes. We have fully vectoring nozzles i.e. through approximately 90^0, and nozzles with zero, or limited deflection. The latter nozzle can be similar to a conventional installation in performance terms and may incorporate a conventional reheat and variable nozzle system.

A vectoring nozzle whilst potentially advantageous in configurational terms, will incur an additional internal performance loss. This loss depends on the duct and nozzle design, with particular importance attaching to duct contraction ratio and total flow deflection angle. The latter's influence is indicated in Figs 20 and 21. This angle may be minimised by the use of "droop" and "trail" as illustrated on the figure. The use of droop is limited by the need to minimise nose up pitching moments due to any resulting thrust line offset. Trail is likely to be constrained by its influence upon vertical thrust position, which in turn, will impinge on aircraft CG position and engine intake location. Nozzle pressure ratio obviously has an effect on these relationships and Fig. 21 shows this using the 180^0 flow turning case as the datum.

Traditionally, exhaust nozzles, being pressure vessels, have been axisymmetric in an effort to minimise weight. It would also appear, based on past experience, that variable geometry nozzles are lighter and cheaper when made axisymmetric. Latterly however, various influences such as stealth, aerodynamic induced effects, focussing of wall jet momentum, etc., have been recognised which provide a new impetus to the study of non-axisymmetric (or 2-dimensional) nozzles.

Whilst variable geometry 2-D nozzles see Fig. 22 have yet to see widespread acceptance, the study and development of such devices in the USA may well prompt more interest.

Nozzle design has an important influence on aircraft drag. A rotating nacelle solution, for example, will have much the same influence as a conventional engine installation. Vectoring, fuselage side, nozzles present special considerations which have received much study on the Harrier. Considerable skill and ingenuity is needed to minimise the consequences of the nozzle elbows on area distribution, interference and excrescence drag in particular.

RALS, lift and lift/cruise, tandem fan and ejector solutions all have their own nozzle installation peculiarities. In general these are internal flow diversion solutions, which are substantially comparable to conventional aircraft, when in the forward flight mode. In the lift mode they are likely to incorporate one or more nozzles with a limited vectoring capacity, and this has to be taken into account when predicting transition flight characteristics and performance (Fig. 23).

d) Jet Effects

The propulsive jet will create its own flow field and the integration of this with the flow field due to the rest of the airframe can be crucial. With some VTOL concepts (not all), the jet has a unique position with regard to the airframe, even in normal flight modes. Special situations for study may arise, therefore, on VTOL vehicles.

Lift

It is well established that any external influence tending to increase circulation round a wing will lead to increased lift, and vice versa. A jet located above the trailing edge (TE) appears most favourable, with a lower surface TE position being almost as good. The induced effects may be maximised by vectoring the jet at the trailing edge in conjunction with the wing LE and TE devices. Equally, the worst location for the jet occurs when under the wing LE, although the exact trade-off between lift loss and jet position, in this case, is not well established.

Drag

In addition to increasing local lift, a favourable jet flow field can also lead to reduced drag. Whilst the lift effects can be explained in terms of circulation, it is not clear whether the drag reduction is fundamental e.g. stimulation of a thick boundary layer, or at least in part, simply due to the beneficial effects on local flow deficiencies which may have arisen from inadequate design. Fig. 24 illustrates the jet effect on the lift/drag characteristics of a 2-poster trailing edge installation.

The jet-induced effects can be quite powerful, especially during low speed manoeuvre and, when allied to the potential capacity to deflect the gross thrust in flight, can provide handsome advantages in air to air combat.

Structural Environment

Another consequence of a jet in close proximity to significant parts of the airframe (which is likely with many VTOL concepts) arises from its thermal/acoustic signature. In the case of nozzles mounted alongside the fuselage, the airframe is subjected to both high temperature and intense noise. It is necessary to apply appropriate constructional techniques and to use the correct materials if adequate service life is to be obtained. Certain equipment contained within the structure e.g. avionics, may require special treatment. As mentioned previously, current thermodynamic cycle trends may well exacerbate these effects.

The other alternative, of course, is to minimise such effects by deleting the normal afterbody and empennage arrangement and replacing these with a twin-boom arrangement. The pros and cons of these alternatives is a subject which is currently exercising the talents of many designers.

Ground Environment

The ground environment is largely dependent upon the engine cycle, since this will dictate gas temperatures (Fig. 16), pressures and hence velocities. In jet borne flight one important influence occurs from the wall jet development on the ground. This in turn is influenced by the number of jets, their shape, orientation and position. The flow from each nozzle hits the ground and dissipates radially in a wall jet. Where two such wall jets meet, some horizontal momentum is destroyed and a vertical, upwards moving 'fountain' is created see Fig. 25. This formation can have three important consequences,

(a) if close to the intake it can lead to HGI

(b) it can be 'captured' by the aforementioned CADS and DAMS devices (Fig. 26) and used to generate lift, (so offsetting any incidental lift losses) and

(c) as it is a form of wall jet manipulation, it may be used to channel unwanted gases in advantageous directions, i.e. away from the intakes. In this case, good design can be employed to optimise the effect, e.g. a three jet layout, one cool front jet and two rear jets will minimise the forward movement of hot moving gas flow; which is otherwise difficult to deal with. Although HGI may not occur through this kind of "near-field" gas movement, a headwind will cause the forward wall jet to roll up, which, unless preventative techniques are employed, will eventually be inhaled by the intake.

An alternative mechanism, which has received some investigation, is to exploit the properties of non-axisymmetric nozzles, since they exhibit some directional focussing of the wall jet (see Fig. 27). Appropriate orientation of the nozzles will then minimise the amount of gas likely to find its way into the intake. This appears to be especially effective for a "2-poster" configuration.

The wall jet can cause problems in other ways, via its entrained flow field. Typically, any asymmetry in the distribution of static pressure over the airframe will cause uncommanded moments. For instance a vertical landing with bank on may cause the lower wing to be sucked down harder than the upper wing, so calling for a corrective control reaction. Similarly, landing at incidence, as for example, due to undercarriage geometry, can cause pitch up, due to the wall jet flow under the rear fuselage.

A factor that is often overlooked at the project stage is the consequence of a highly energetic jet (and hence wall jet when in ground effect) on ground personnel and any ground support equipment required to service the aeroplane. Fig. 28 represents a quite simple estimate of the wall jet flow field some 8m from the centre of a single vertical jet of approx 100 Kn thrust. Clearly, such conditions close to the ground need special consideration with regard to neighbouring personnel or equipment. A serious noise hazard is also likely to accompany jets in this category and will also require some special consideration. It may well be that the chosen engine cycle for VTOL phases of flight will need to be constrained. Hence the remarks, made earlier, regarding the desirability of variable cycle engine concepts.

In practice, as exemplified by much Harrier operational experience, these effects are minimised by ensuring that periods of powered flight in close ground proximity are kept to the absolute minimum.

e) Thrust Split Considerations

For reasons of longitudinal balance in powered lift conditions, the split of thrust between front and rear nozzles (where appropriate) has to be carefully considered.

For an unmixed engine (separate fan and core flow) the front and rear thrusts will depend upon the choice of engine cycle, a design parameter also likely to be heavily influenced by the required in-flight performance. Further, the possible desire to integrate rear nozzles with the wing trailing edge (in order to maximise the beneficial induced effects) will dictate the position of the front nozzles for a given CG position. It is important to secure a configuration in which any lift losses due to the location of these front balancing nozzles, in minimised. Structure and layout considerations may restrict the freedom and choice for the front nozzle position.

The compromise is finally compounded by the choice of wing planform, since this dictates the location of the wing leading and trailing edge, relative to the nozzles. Desired wing to nozzle relationships obviously constitute a constraint on the overall aircraft configuration. A further complication arises from the fact that the ratio of front to rear thrust split, and hence the aircraft balance in pitch, will change with throttle setting. This effect is seen on the Harrier as shown in Fig 29, where the thrust centre moves aft with increase of thrust and thus, neatly matches (approximately) the aft movement of the c.g. as fuel is added to the empty aircraft.

The situation is slightly eased for mixed engines, since theoretically, the thrust split may be tailored independently of the engine cycle. However, this implies the need for some form of flow ducting and nozzle area control; complications that have usually only been considered acceptable when associated with extra lifting means e.g. RALS or ejectors.

The choice of a RALS propulsion system also appears to introduce a further degree of freedom, in that there is a limited freedom for front (RALS) nozzle location and the temperature of the balancing jet is variable; the latter may thus be used to modulate the balancing thrust.

Similarly, the use of ejectors would provide a means of tailoring the thrust split, by variation in primary flow distribution and in augmentation ratio. In practice, there is likely to be some constraint on the latter mechanism due to the sheer size of high area ratio (and hence high augmentation ratio) ejectors, which will limit their installational possibilities.

The thrust split available from a tandem fan unit (which is an unmixed engine, in its VTOL or "parallel", mode of operation) may be manipulated by the choice of the fan pressure ratio split. This choice, however, may be limited to a narrow range of values in order to secure satisfactory engine matching in the different modes. The position of the fan efflux nozzle may also be moved to some extent in order to achieve aircraft balance though this is not strictly a variation in thrust split.

The desire to achieve a good relationship between nozzles and airframe (in particular, the wing) has implications, not only with regard to the propulsion concept; it also has significance with regard to the choice between canard and aft tail layouts. In order to respect a desired relationship between CG and aero centre for normal flight and to secure thrust balance in jet borne flight the relative locations of wing and jets will be closely prescribed. The freedom to manipulate the aero centre by means of wing planform is limited since the wing design is largely dictated by the required flight performance. Thus the foreplane/tailplane represents a powerful means of tailoring the a.c. position and thus, the overall thrust centre, see Fig. 14 again.

Having discussed some of the various propulsion concepts, their interactive effects with airframe configuration through considerations related to intake positioning, to nozzle/airframe location, to vertical balance requirements (including the thrust split implications), to ground environment issues, it is appropriate to contemplate some of the resultant configuration possibilities. Figs 30 to 34 illustrate respectively a 2-poster vectored thrust, a 2-poster tilt nacelle, a tandem fan example, a RALS example and one employing ejector augmentors.

f) Transition Flight

When we refer to the requirement for the thrust line to pass through the centre of gravity we instinctively think of the case with the jets at 90^{0} deflection. At other conditions however there may well be an offset between the total thrust vector and the c.g. position. This can arise, for example, in those cases, where it is not possible to provide full 90^{0} vectoring on all the exhaust nozzles (this might be true in the case of an ejector augmentor). It also tends to occur when large values of "droop" are used on the previously discussed vectored nozzle arrangements. Inevitably, these thrust offsets give rise to pitching moments (usually nose-up) which can be difficult to handle at transition speeds. The nett result of this situation is to limit the amount of thrust that can be applied, and the movement of the thrust vector away from the 90^{0} position. This means, of course, a poor acceleration performance in the transition from hover to forward flight.

This is not a problem on the decelerating transition due to the reduced thrust levels used and to the fact that there is no obvious requirement to apply high thrust levels at angles well away from the vertical.

The transition manoeuvre (powered lift to wing-lift, and vice versa) is fundamentally dependent upon several factors one of which, the thrust offset, is noted above. Excessive pitching moments, whether due to variation of thrust offset or aerodynamic induced effects, are embarrassing at low forward speeds during the transition due to the lack of control power available. At high speeds, although the aircraft may be trimmed, any resulting trim drag may be undesirable. Thus it is imperative to minimise the offset between the CG and the gross thrust vector, including induced effects, over the full range of thrust vector angles. It is also important to note that this latter design rule applies to the total effective thrust vector. By implication, this means that all thrust (or jet) induced effects have also got to be taken into account. E.g. a jet-induced increase of wing lift might further contribute to nose-up pitching.

Clearly, the more horizontal component of thrust that can be applied (whether limited by the mechanical vectoring arrangements, or by trim considerations) the better the forward acceleration. In general, this is most efficiently arranged by complete (>90°) vectoring of the total gross thrust. The alternative solution, which is to separate lift and propulsion contributions, in general, requires a greater installed thrust to achieve a given transition profile, or a reduced transition performance. Fig. 35 will help to explain this hypothesis. Fig. 23 illustrates a typical case of limited thrust vectoring.

The effect of ram drag is to reduce the horizontal component of nett thrust minus drag available for acceleration to flight speed. It is perhaps paradoxical that while the high specific thrust sought for good supersonic performance implies low ram drag during transition, it also results in poor propulsive efficiency in the lift mode and at low forward speeds, and provides a very hostile exhaust environment on the ground. The corollary is that concepts aimed at a benign footprint will suffer a high ram drag. One extreme in this situation is the ejector solution designed for a benign footprint, where it is quite theoretically feasible to fail to achieve complete transition because of high ram drag together with the difficulty of vectoring the thrust output from ejector devices. These considerations may set practical limits to the amount of mass-flow, and thus the area ratios and thrust augmentation, that can be usefully applied to ejector powered VTOL vehicles.

One other area of transition performance that requires attention is the ability to accurately control the vehicle throughout the manoeuvre. This problem is likely to be more acute during the decelerating transition, where the landing pad represents a finite and mandatory final destination, often of very limited size. In general, the decelerating transition requires a descending flight path. This determines a minimum demand for a rearward thrust component a) to counteract the flight path weight component and b) to give the pilot some margin for deceleration control, while still satisfying the normal to flight path (lift minus weight) thrust demand. This usually implies some forward nozzle vector angle in a thrust vectoring arrangement i.e. a vector range of more than 90°. In tilt-wing propellor and tilt wing/duct configurations, it has been known to be a source of difficulty because of the buffet problem that can be incurred with large flying surfaces at high angles of attack at forward transition speeds.

g) Stability and Control

The S & C demands may conveniently be divided into 2 regimes, (i) normal flight and (ii) jet borne flight. The normal flight condition, with some slight qualification, will tend to reflect the vast body of knowledge accumulated on conventional aircraft and would not be expected to generate any unanticipated problems. The reservations would be confined to any situations where the dictates of VTOL intrude on otherwise conventional configurations. Perhaps a very good illustration is one effect of the use of vectoring fuselage mounted nozzles on P1127 and Kestrel. The local flowfield from the rearward facing jets in conventional flight caused extensive modification of the usual wing downwash field at the tailplane location. This resulted in unexpected variations in the aircraft stability, primarily giving a reduction in pitch control at high incidence. This was overcome by variations of the rear nozzle design and tailplane configuration (anhedral and span) such that it became immersed in a more favourable flowfield. The development of this situation is shown in Figs 36 and 37.

The jet-borne case is potentially more difficult due to the wide spectrum of possible aerodynamic interactions. Some of the more serious of these have become obvious through practical experience. The general problem can be exemplified by possibly the most extreme arrangement, i.e. SC1 or Mirage IIIV, where the inlet and exhaust occur near the centre of area of the planform. The inlet and exhaust both give rise to their own local flow fields which interact with that of the airframe and generate a significant pressure distribution over the vehicle. If this pressure distribution becomes distorted, or asymmetric, due say to changes of headwind or sideslip, the effects tend to produce exaggerated disturbing moments. Typically these might be a large nose up pitching moment when in transition flight and large "anhedral" rolling moments should sideslip be allowed to develop. The situation is often exacerbated by the presence and influence of the ground plane.

These effects are clearly very dependent on intake and jet exhaust location, but are present to a greater or lesser extent, on most VTOL configurations. The phenomena can only be studied (and then sometimes only to a limited extent, due to the constraints of practical modelling) by a sophisticated 'powered' wind tunnel model.

The usual form of control at sub aerodynamic speeds is by employing some type of reaction control system. The best known form is the "puff pipe", employing high pressure air bled from the compressor which is ducted to variable area nozzles at the aircraft extremities (Fig. 38). This has some advantages in that its relatively high pressure minimises pipe sizes whilst not being excessively hot (say 250°C). However this might cause anxiety with regard to battle damage. Nevertheless it is a simple, robust system and has been well-proven by many hours of Harrier experience. Many hours of test bed proving and development have minimised the effect of the compressor bleed on engine performance.

Some projects (e.g. VJ101) have used engine thrust modulation to provide roll control, differential deflection for yaw and either thrust modulation (with lift engines) or symmetric thrust deflection, for pitch control. The use of thrust modulation with a reheat fuel control system has been shown to give excellent response. The use of "dry" unreheated thrust depends greatly on engine size and control system design (the original RB108 lift engines were shown to have excellent response). With modern digital control systems it is believed that engine thrust response will be much improved. Such systems imply some degree of integration between engine and flight control systems.

The use of integrated flight and engine control systems makes control modes such as those outlined above perfectly feasible, though extensive simulation and accurate modelling will be necessary to refine and prove the system prior to flight.

Modern FCS technology can also provide perfectly tailored handling qualities in the otherwise difficult phases of flight where aerodynamic non-linearities, significant jet induced interactions and high work load (i.e. instrument landing conditions) can all coincide. This aspect has been extensively investigated at BAe Warton and a system and control/handling philosophy was evolved that has proven gratifyingly effective. An integrated flight control system of the type envisaged is a natural and challenging follow-on from the current work being done on the various fly-by-wire programmes e.g. FBW Jaguar, also at Warton.

Finally, it is tempting to believe that in the hover, VTOL aircraft are particularly susceptible to gusts, but with current aircraft densities, it needs a very vigorous gust to cause any significant disturbance. The problems are usually to be faced at intermediate transition speeds because of the relative strengths of the aerodynamic effect of gusts and the relative powers of aerodynamic and reaction control systems. Fig. 39 will help to explain this paradox.

h) VIFF

As mentioned in section 4(d) above the use of jet induced effects can greatly improve combat performance, especially if the jet vector is tailored to suit. Benefit accrues of course from the direct thrust components of vectoring. To maximise the total result it is necessary to provide an optimised schedule for jet deflection and high lift device settings against Mach No., incidence and, if possible, throttle setting. Both simulated and actual combat experiments have corroborated the virtues, though any conclusions should be tempered by consideration of the possible influence of more capable weapons and the development of appropriate counter tactics. Nevertheless the facility does contribute a powerful extra dimension to aerial combat.

Clearly the resultant effects on aircraft trim need special design consideration. However with the advent of sophisticated digital control systems noted in the previous section, such effects probably become a manageable proposition.

j) Undercarriage Design

The undercarriage poses a special problem on VTOL aircraft. If a vehicle is only intended to operate in a truly vertical sense, then perhaps the inevitable compromise eases, but the intrinsic benefits of employing VTOL aircraft in a short take off or landing mode are so marked that both conventional or semi-conventional operation are extremely advantageous. The bicycle and out-rigger units employed on Harrier are well known. This was an extremely light-weight solution adopted on the early prototypes. However more conventional tricycle gears have been proposed on vectored thrust layouts and they offer the facility to rotate the aircraft for take-off, which can obviously benefit the ultra-short take-off performance capabilities.

A particularly tricky problem with VTOL undercarriage design is correct placement of the main wheels. A conventional gear can usually be accommodated such that the c.g. is within a line, say, 10^{0} forward of the main wheel pivot. Inertia forces in a conventional landing then guarantee positive and instant de-rotation. The problem however is rather different during vertical landing. For example the aircraft might land in a nose-up attitude (to accommodate local terrain variations for instance). If this is compounded with a rearwards movement of the aircraft, a nose-up pitch at touchdown is inevitable which can easily produce an overturning moment. Slightly more c.g. to wheel pivot overhang is thus advisable on VTOL machines. This can be achieved with a two-position undercarriage leg. The Short SC1 was an example of such an arrangement.

Finally it is also important to position any undercarriage component outside the arc swept by high temperature jets to avoid the likelihood of damage.

k) Weapons Carriage

External stores are generally carried under wing, under-fuselage or both. The under-wing position provides great flexibility in terms of numbers of locations and types of weapons. This solution suffers the disadvantage of disturbing the flow field around the wing. Fuselage stores mounting avoids this problem and when weapons are semi-submerged the drag is significantly reduced, especially for supersonic operation. In the quest for a large payload, many aircraft use a combination of wing and fuselage mounting.

For VSTOL aircraft the carriage of stores will depend to some degree upon the propulsion system. For instance wing mounted ejectors may prohibit the carriage of wing stores and fuselage mounted lift engines will inhibit fuselage carriage.

Furthermore, the environment will influence the usable stores locations and this will be dependent upon engine cycle and aircraft configuration. The use of CADS and DAMS will concentrate the efflux fountain on the lower fuselage and will physically impede stores carriage, perhaps forcing the use of wing pylons or unconventional locations, such as the upper-fuselage or wing stations.

Finally, VTOL aircraft are particularly sensitive to the problem of c.g. variation (again this is shown in Fig. 29). The possibility of a 'hang up', i.e. a weapon failing to release, is likely to be a limiting case.

Thus the choice of locations for weapons carriage on a VTOL machine is the result of an amalgam of temperature, buffet, noise, access and drag, with the usual implications of store carriage on aircraft stability and wing efficiency.

5. Summary and Conclusions

In summary, the problems of design for VTOL, especially when compounded by the requirements of supersonic flight, have proven difficult to overcome. As far as is known, a successful supersonic VSTOL aircraft has yet to appear. A few designs have achieved both vertical operation and supersonic speed but all appeared unsatisfactory for various reasons. This, of course, is not to say such a goal is unachievable and work continues to this end.

The major difficulty for VTOL desgn would appear to concern the choice of a suitable powerplant and engine cycle together with their amalgamation into a suitable airframe. In particular, it is required to marry together a wing design appropriate to the design mission the total aircraft aero centre, the vehicles centre of gravity, the nozzles and gross thrust vector, all in favourable confluence. Havng achieved all this, a practical service aircraft will demand adequate and satisfactory stores locations.

The demand for high installed T/W for reasons of enhanced flight performance and agility has meant that an integrated powerplant is probably the best design solution.

In addition, several simple design rules have been illustrated. Examples are: the need to determine and control total thrust vectors; the desirability of full vectoring of the total thrust; the desirability of exploiting to the full the potential for favourable jet induced effects.

Finally, as in most facets of engineering, in the final analysis it is wise to avoid the seduction of complex designs; all else being equal. The simplest solution will likely be the most satisfactory. As usual, our American colleagues have coined a very apposite acronym - 'KISS'; keep it simple - stupid!

6. References

1. AIAA ref. 80-1853 The Effects of Turbine Inlet Temperature and Engine Complexity on VCE/RALS Powered Supersonic V/STOL Aircraft by W.S. Willis.

7. Acknowledgements

The author wishes to thank his many colleagues in British Aerospace and Rolls Royce for their help and advice in the writing and preparation of this paper. In particular, he should mention David Humpherson, Geoff Stott and Ron Williams (Kingston Division) for a lot of sizeable contributions; and finally Edna, who typed the whole thing without complaint.

TABLE 1

POWERPLANT	ADVANTAGE	DISADVANTAGE
Vectored Thrust	Proven, compact mechanically simple, beneficial induced effects possible. Potential use of PCB or reheat for flight boost.	Thermal/acoustic structural environment. Relatively large cross section. Lift losses possible with the use of front jets. Very short, sometimes curved, inlet duct.
Tandem Fan	Engine cycle variation. Potentially, ground environment as per Harrier. Better matching with in flight performance. Some easing of balancing problems.	Physically longer and heavier engine installation. Need for secondary intake and complex diverter arrangement. Demonstration required.
RALS	Good match for flight performance. Some easing of balancing problem Potentially noisy. Potentially good afterbody arrangement with reheat available.	Complexity, weight, volume, cost. Need for diverter valve. Some demonstration required.
Ejector	Good "footprint", though primary nozzles are likely to be noisy. Effectively variable cycle - good matching with in flight performance.	Complexity, weight, volume, cost, Probable need for a diverter valve. Extensive R & D and demonstration required.

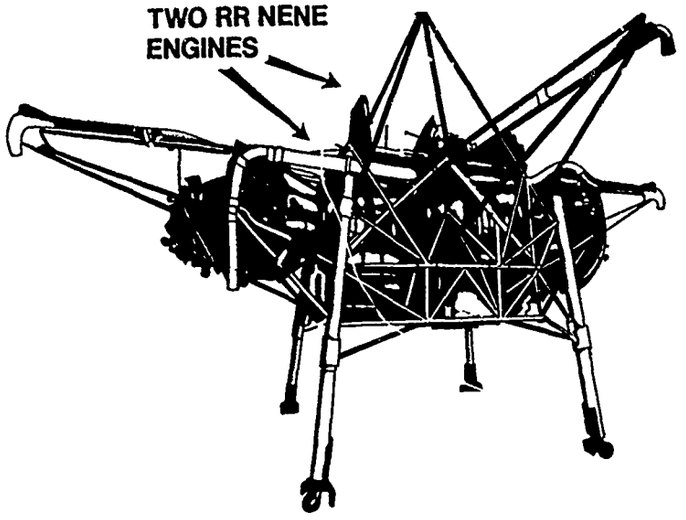

ROLLS-ROYCE BEDSTEAD

SHORT SC.1

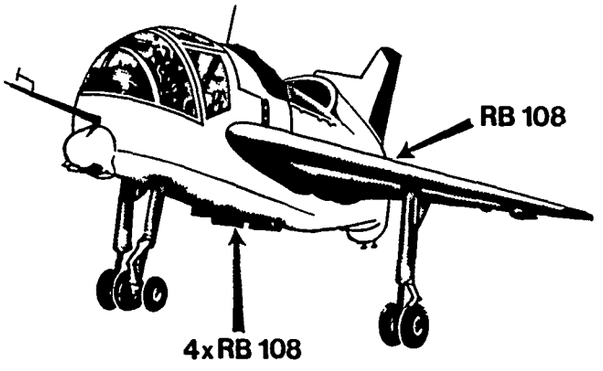

FIG.1 **JET LIFT EXPERIMENTS**

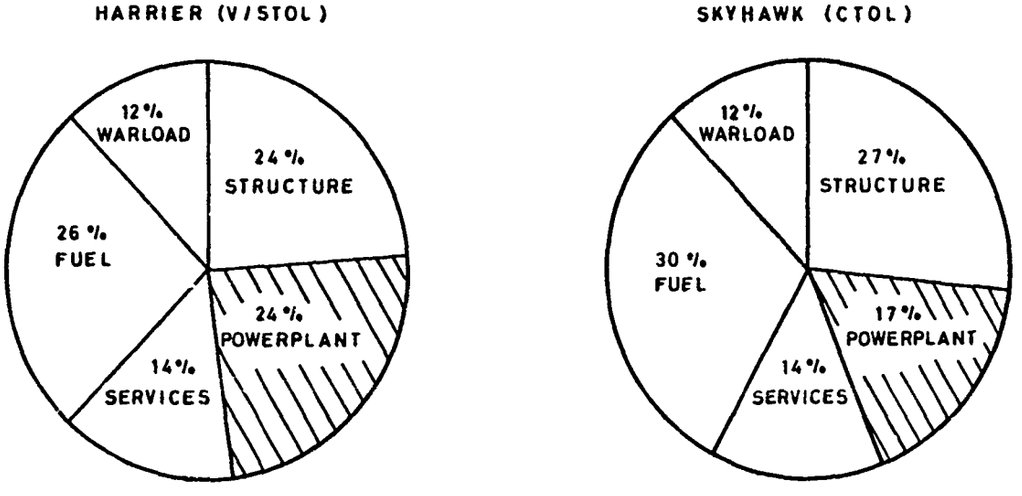

FIG.2 COMPARISON OF MASS BREAKDOWN

FIG. 3 EFFECT OF MISSION ON TOW AND INSTALLED LIFT ENGINE THRUST

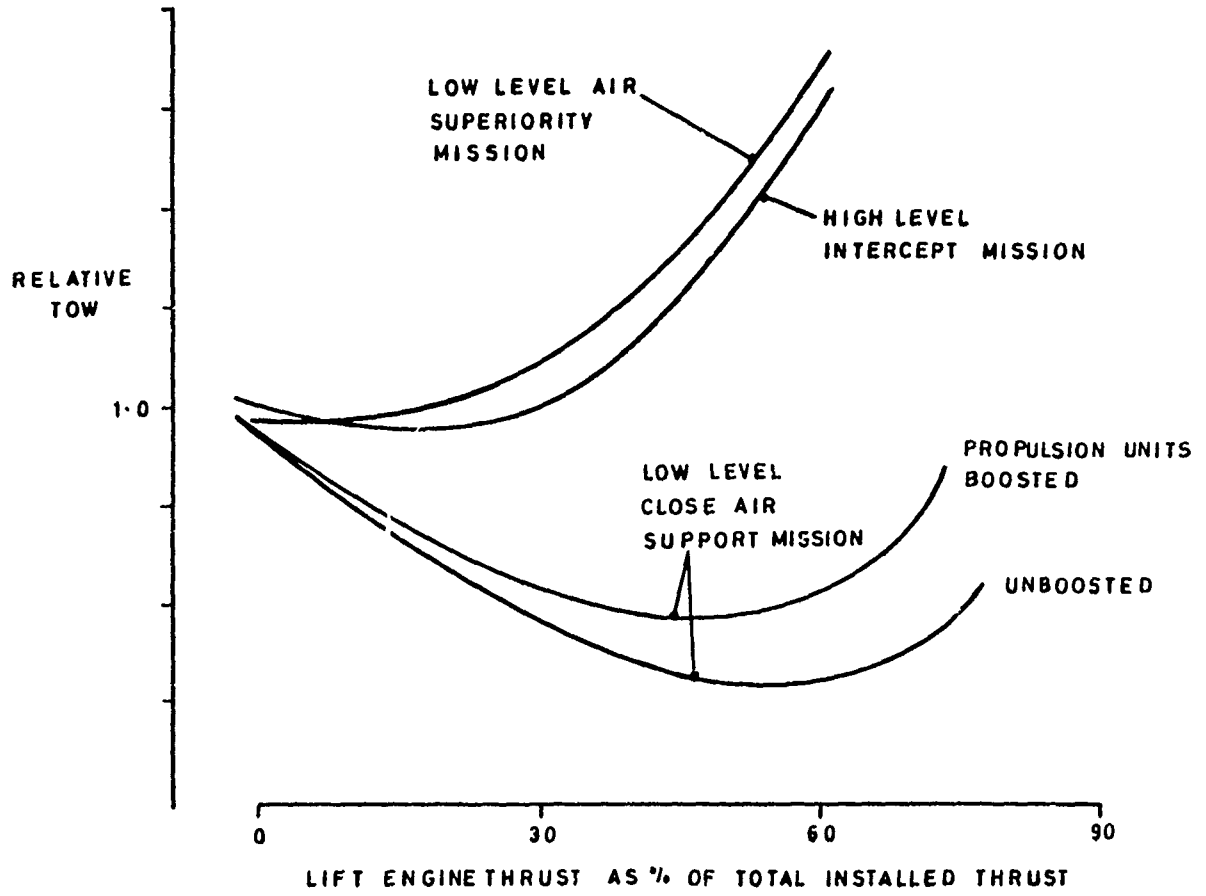

FIG. 4 EARLY V/STOL DESIGN OPTIONS

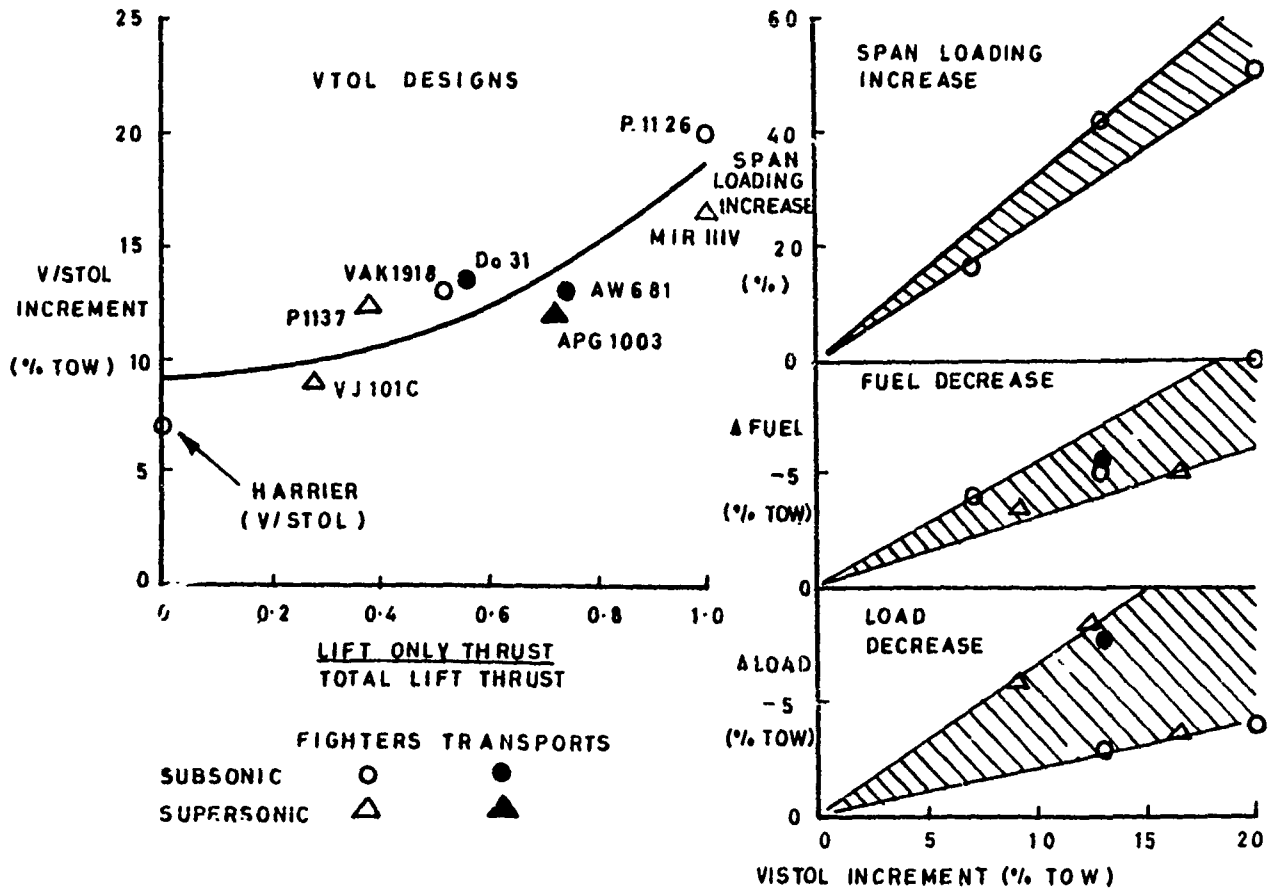

FIG. 5 THRUST REQUIREMENTS FOR VERTICAL MANOEUVRES.

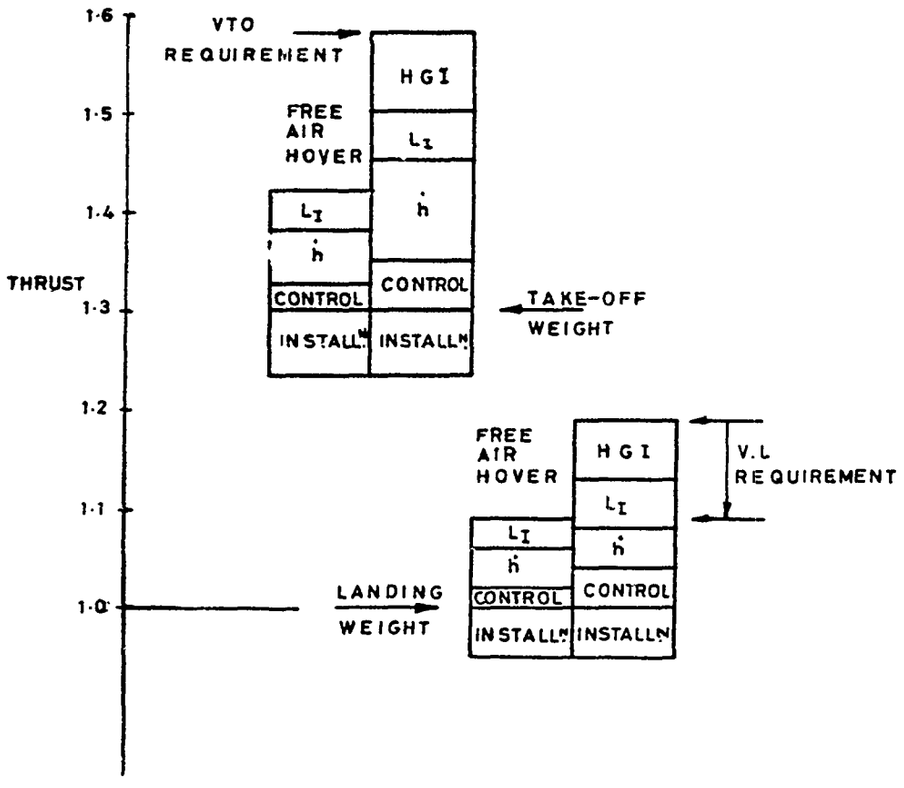

FIG. 6 ENGINE RATING CONSIDERATIONS

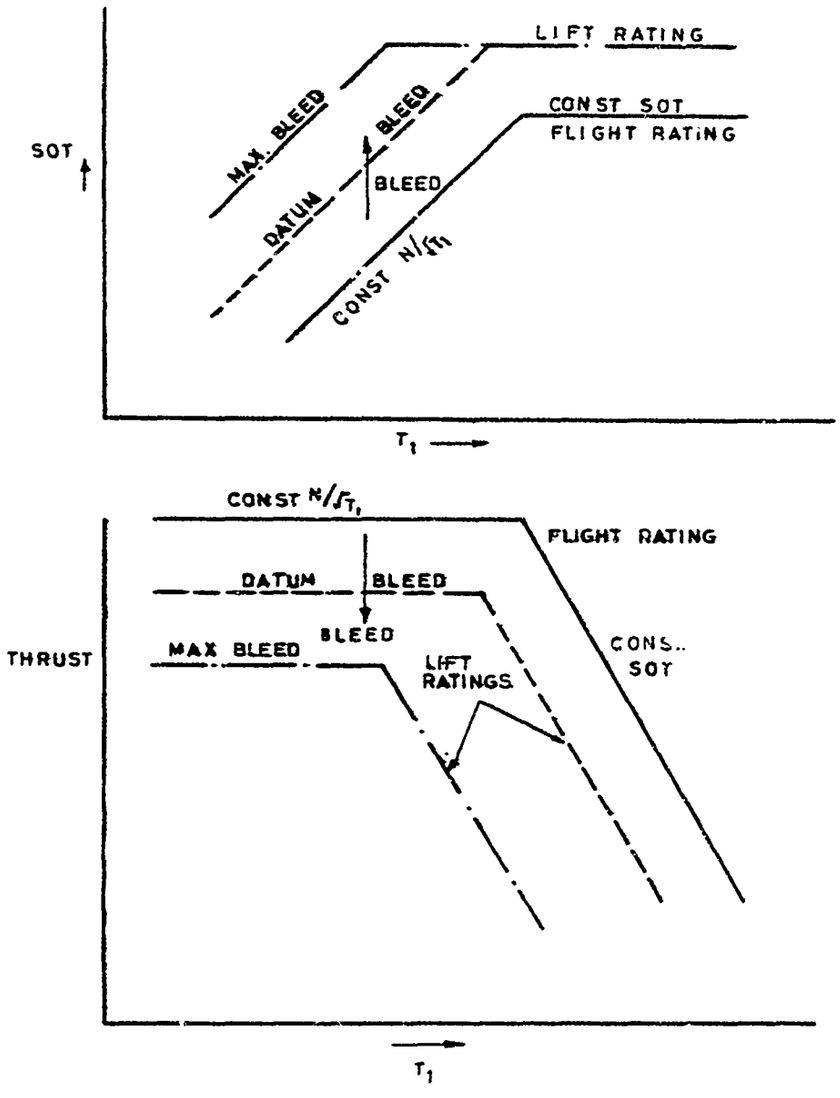

FIG. 7

V/STOL PROPULSION CONCEPTS

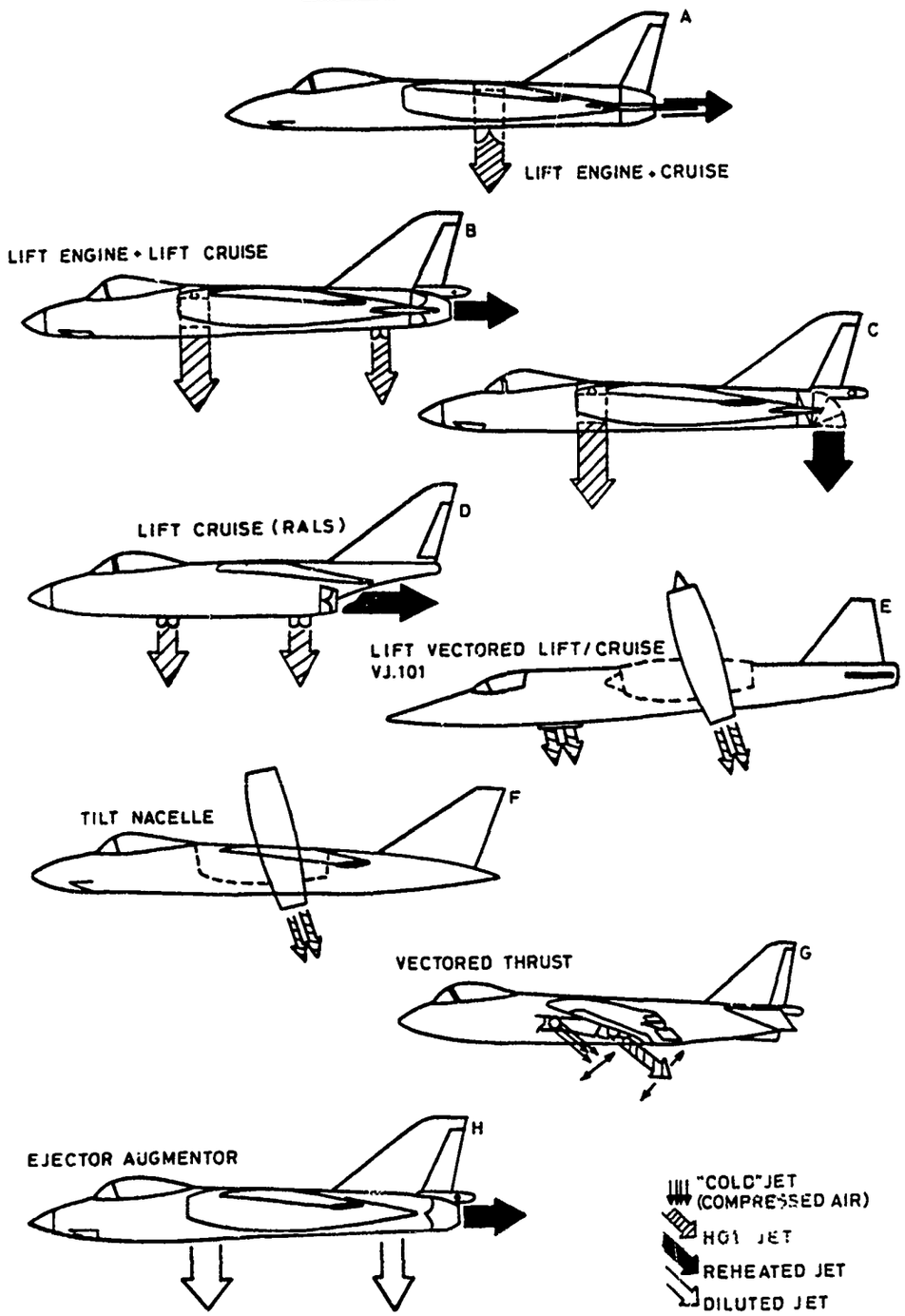

FIG. 8 TWO POSTER POWERPLANT

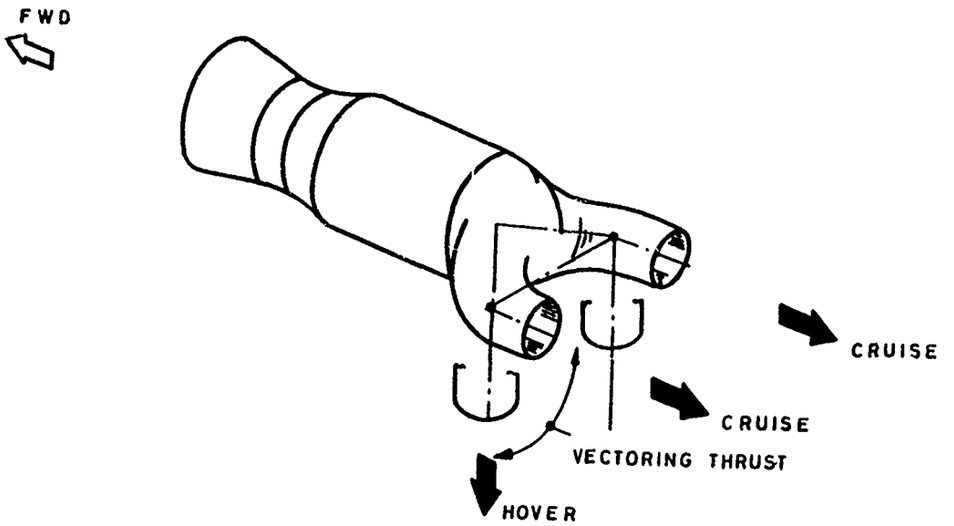

FIG. 9 FOUR-POSTER POWERPLANT

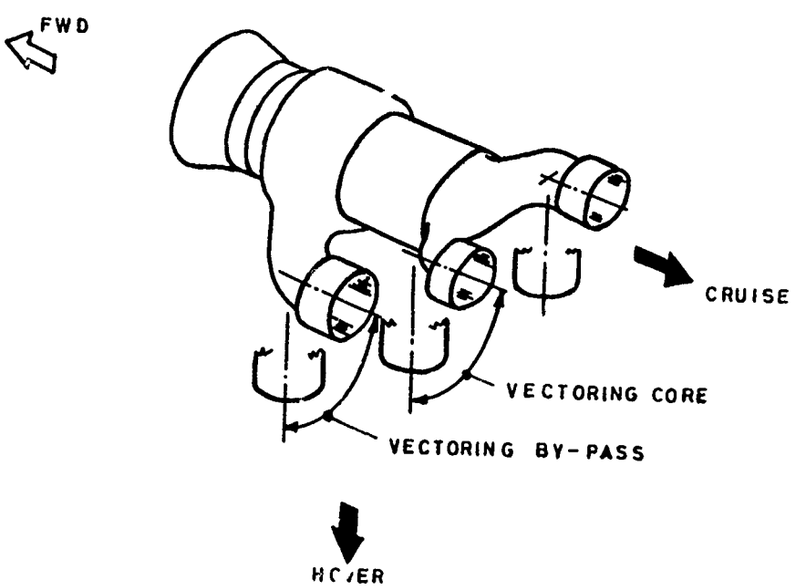

FIG. 10 TANDEM FAN POWERPLANT

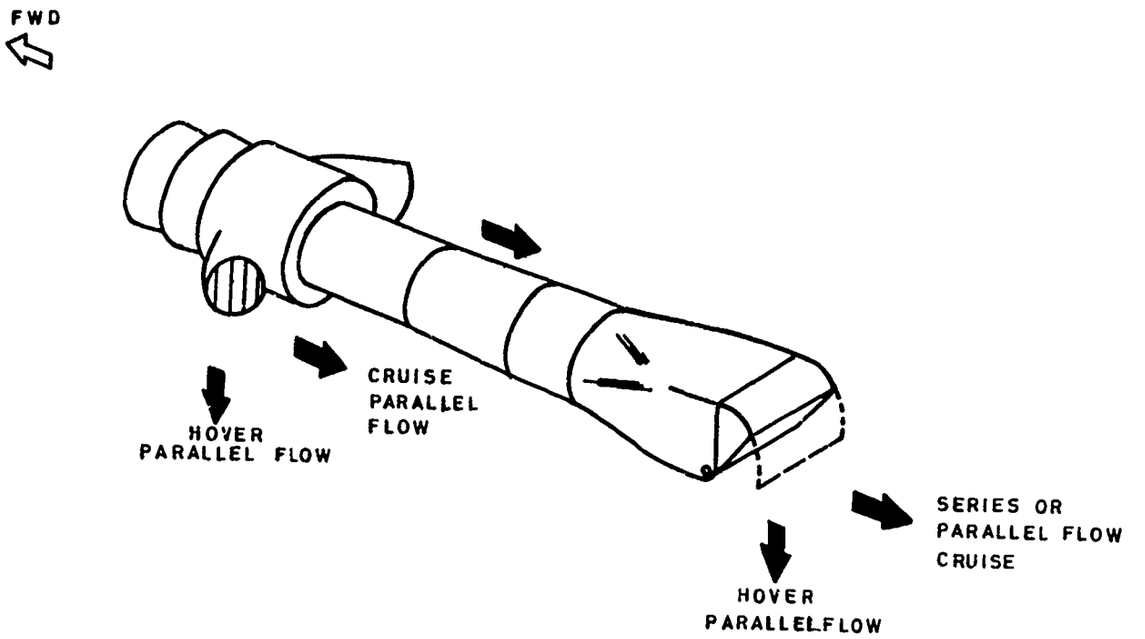

FIG. 11 RALS POWERPLANT

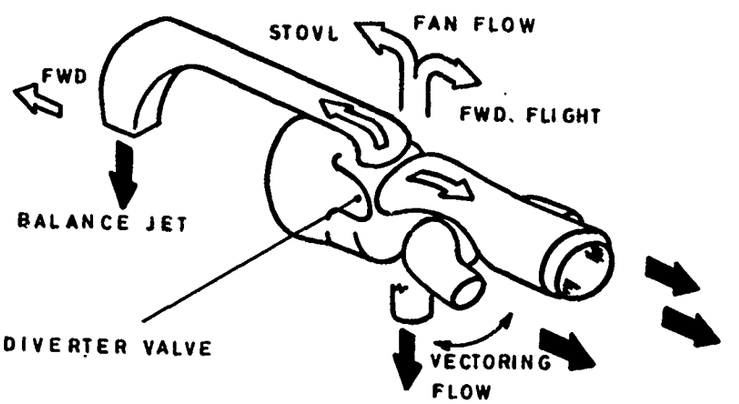

AUGMENTOR EJECTORS POWERPLANT FIG.12

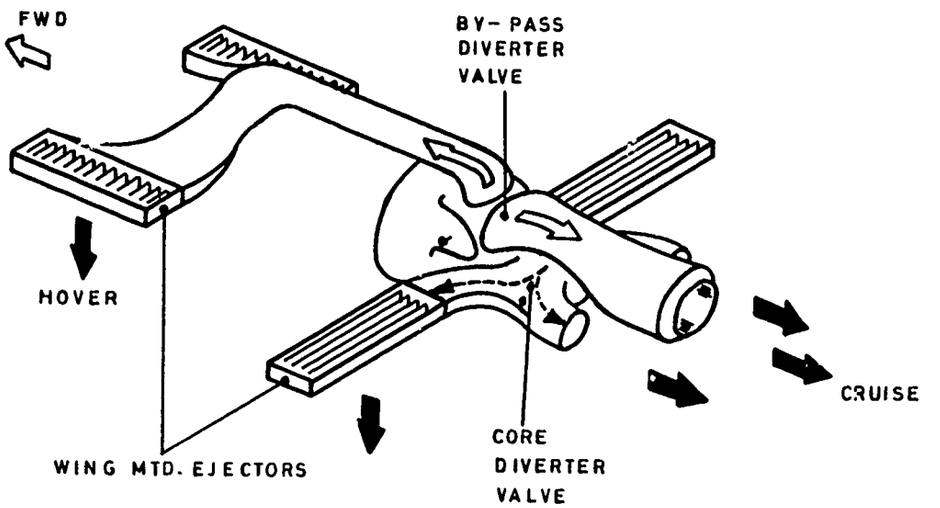

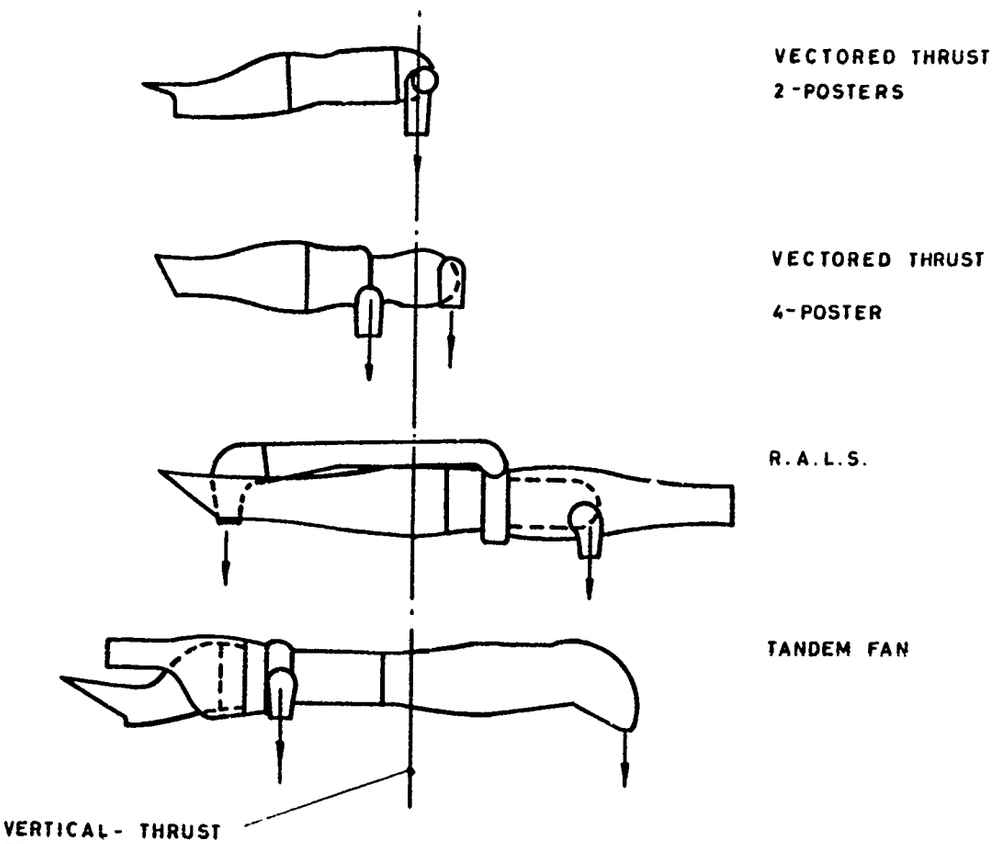

CONFIGURATION CONSTRAINTS FIG.13

FIG. 14

INDICATIVE CONFIGURATION COMPARISON

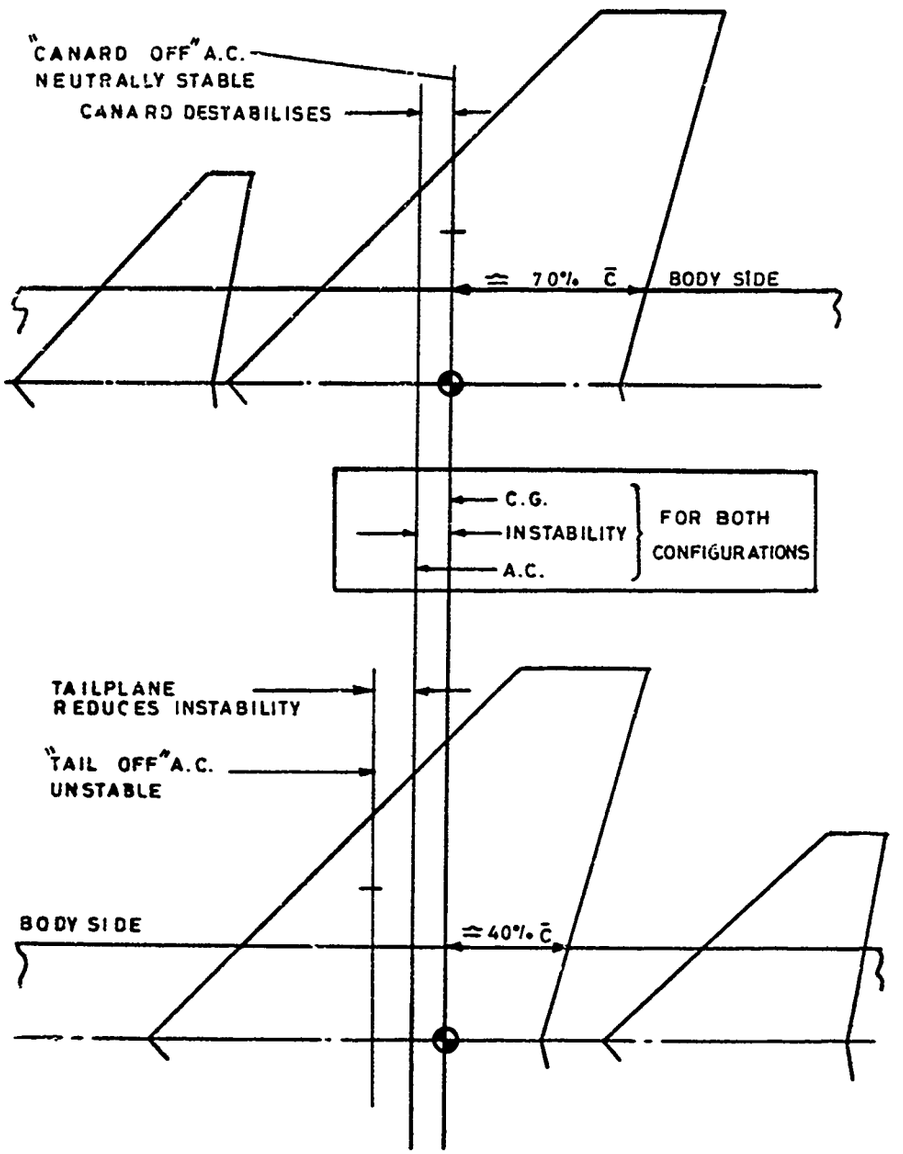

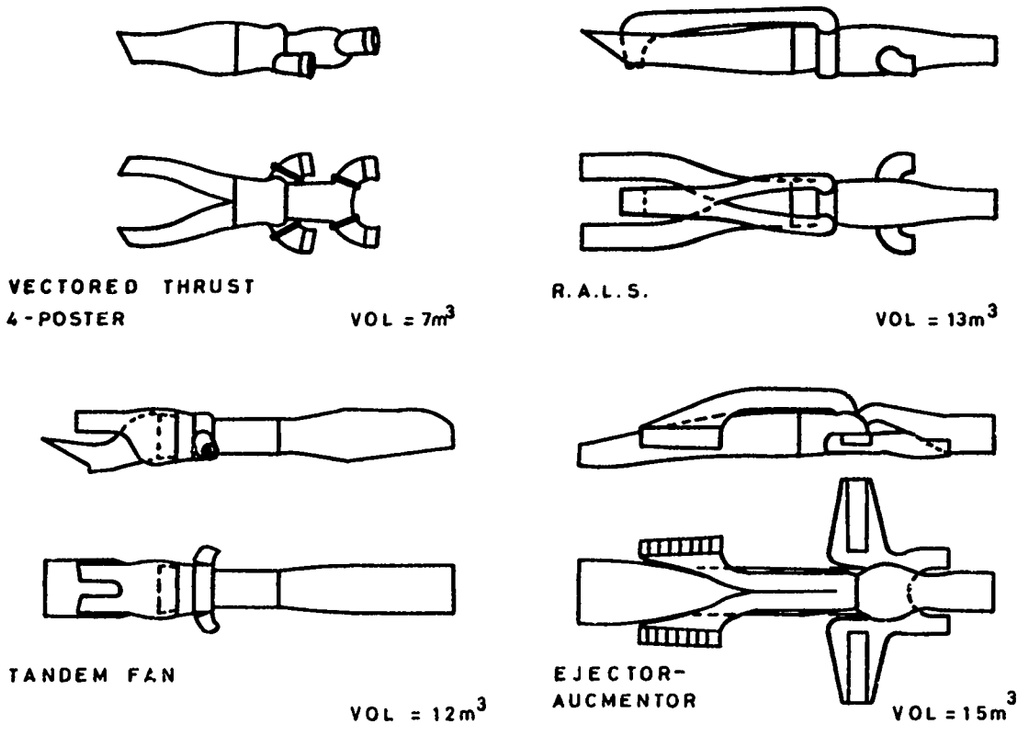

POWER - PLANT VOLUME

(ALL SCALED TO 140 KNS VERTICAL THRUST)

FIG. 15

FIG. 16

EXHAUST GAS TEMPERATURES FOR
POWERED LIFT SUPERSONIC AIRCRAFT

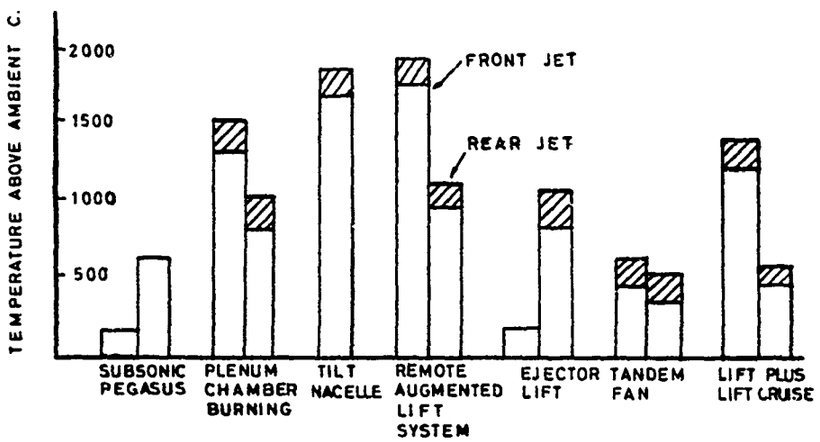

RATIO OF FORWARD THRUST TO LIFT THRUST
FOR VARIOUS SUPERSONIC PROPULSION SYSTEMS

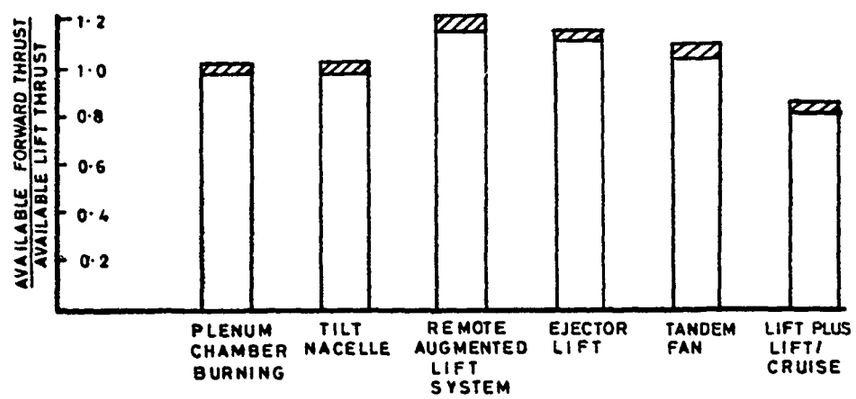

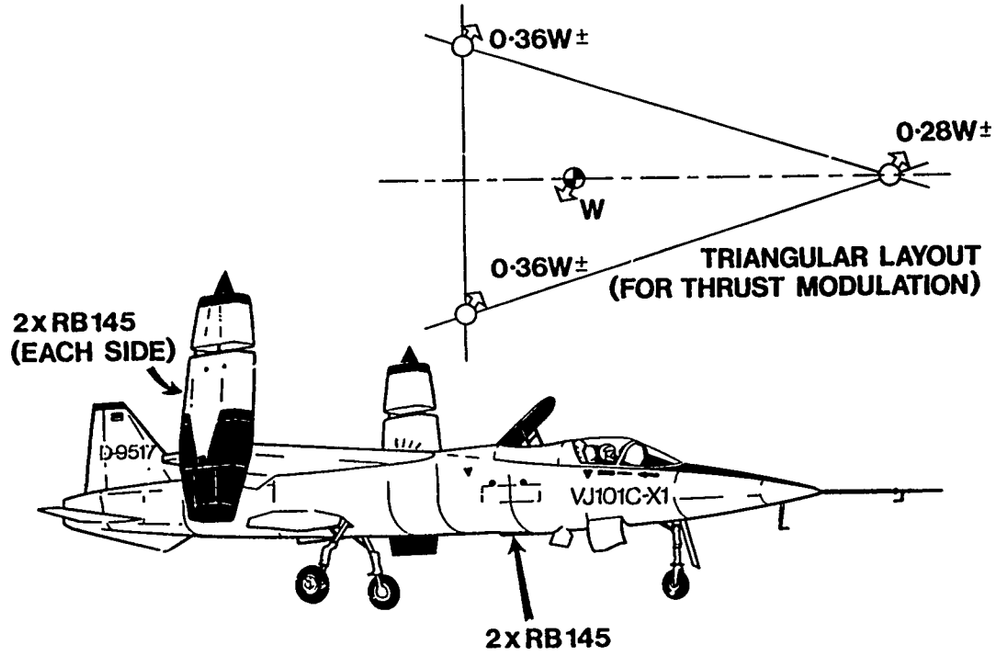

FIG. 17

EWR VJ101C SUPERSONIC FIGHTER

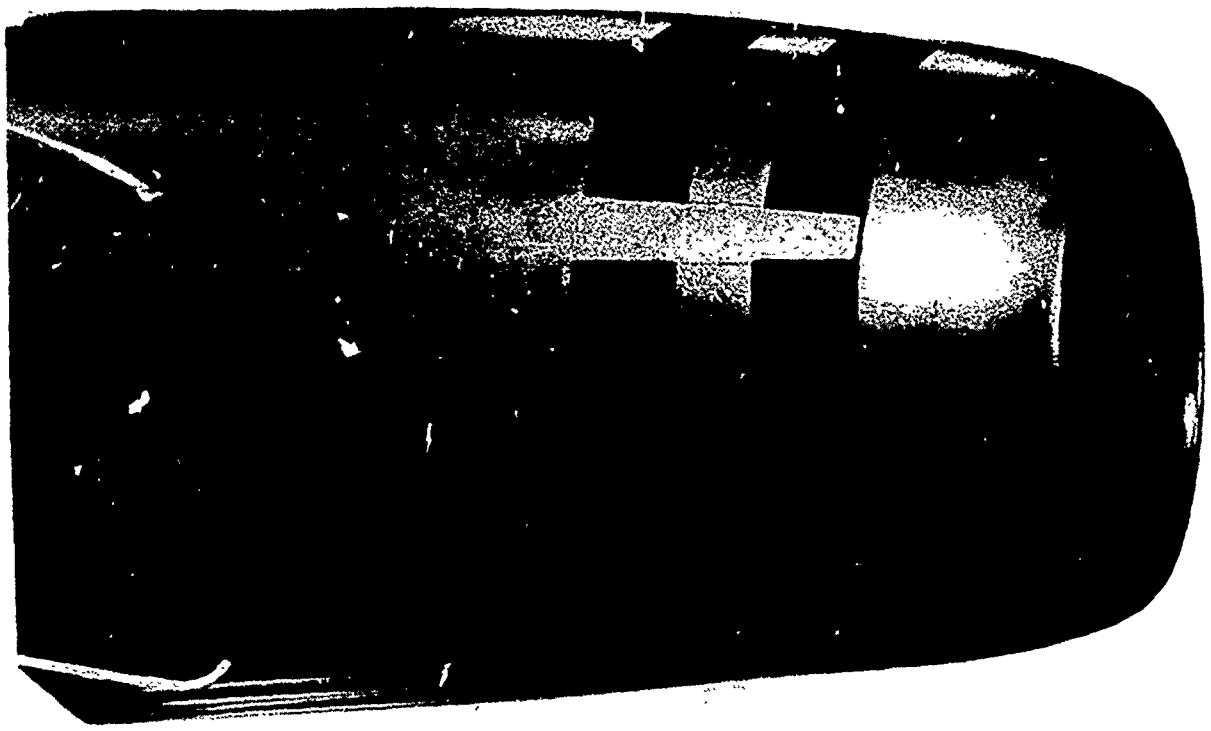

WIND TUNNEL MODEL OF U.S.T.O.L PROJECT PITOT AIR INTAKE FIG.18

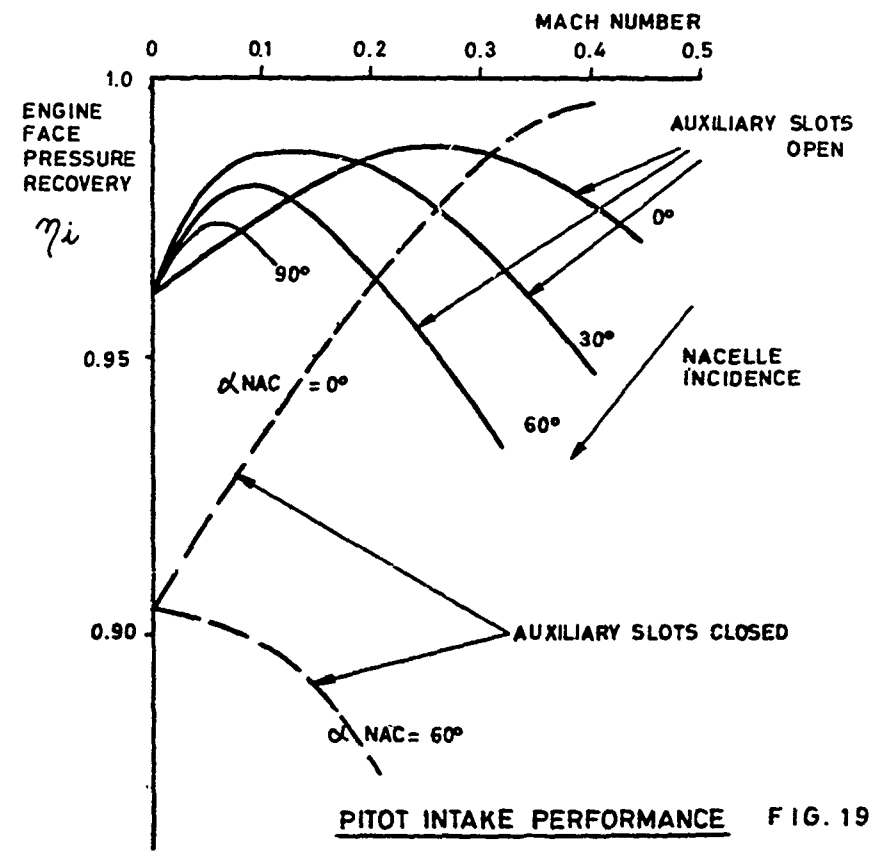

PITOT INTAKE PERFORMANCE FIG. 19

FIG 20 VECTORED THRUST COMBAT AIRCRAFT
EFFECT OF DUCT BEND ANGLE

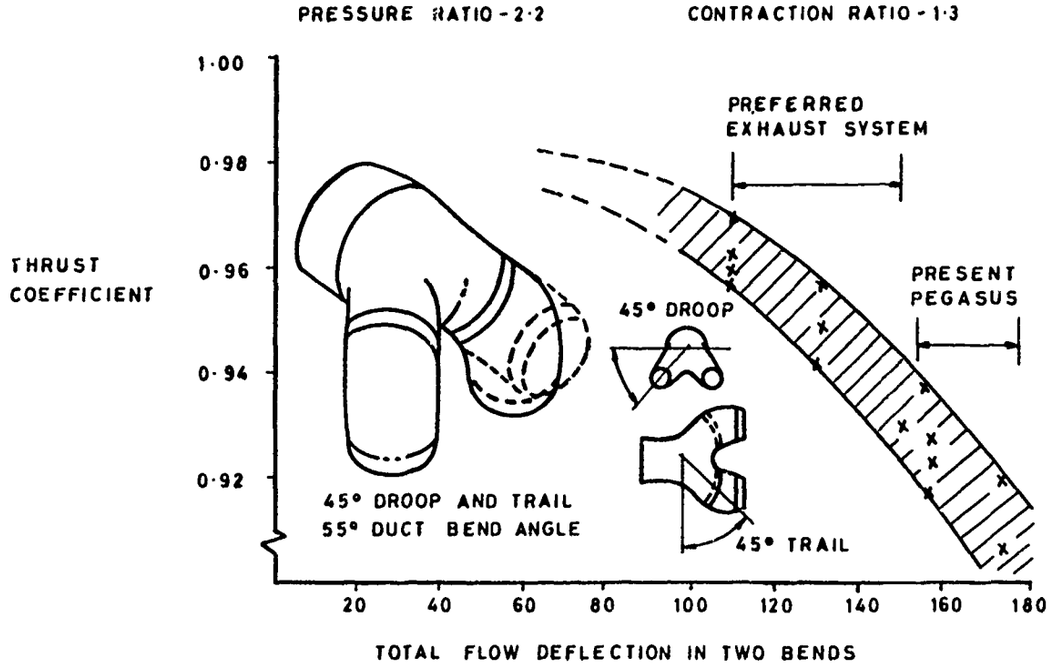

FIG. 21 FRONT NOZZLES

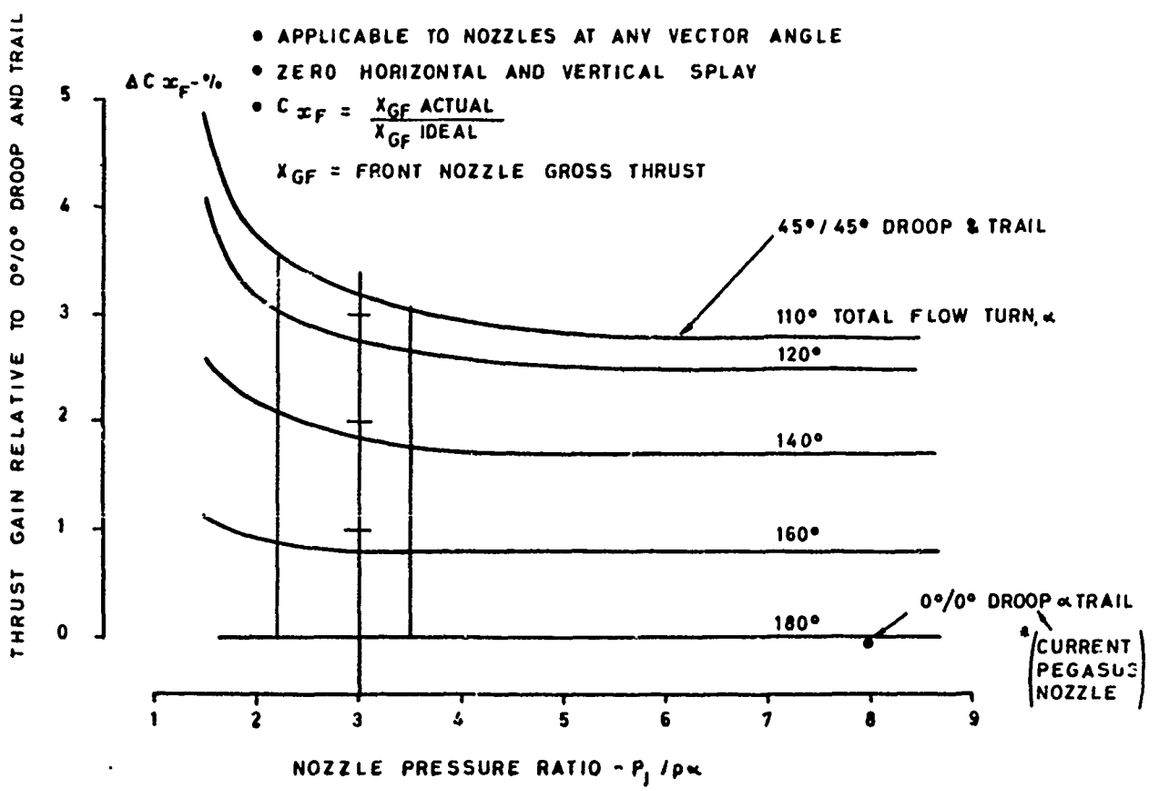

FIG. 22 TWO DIMENSIONAL NOZZLE

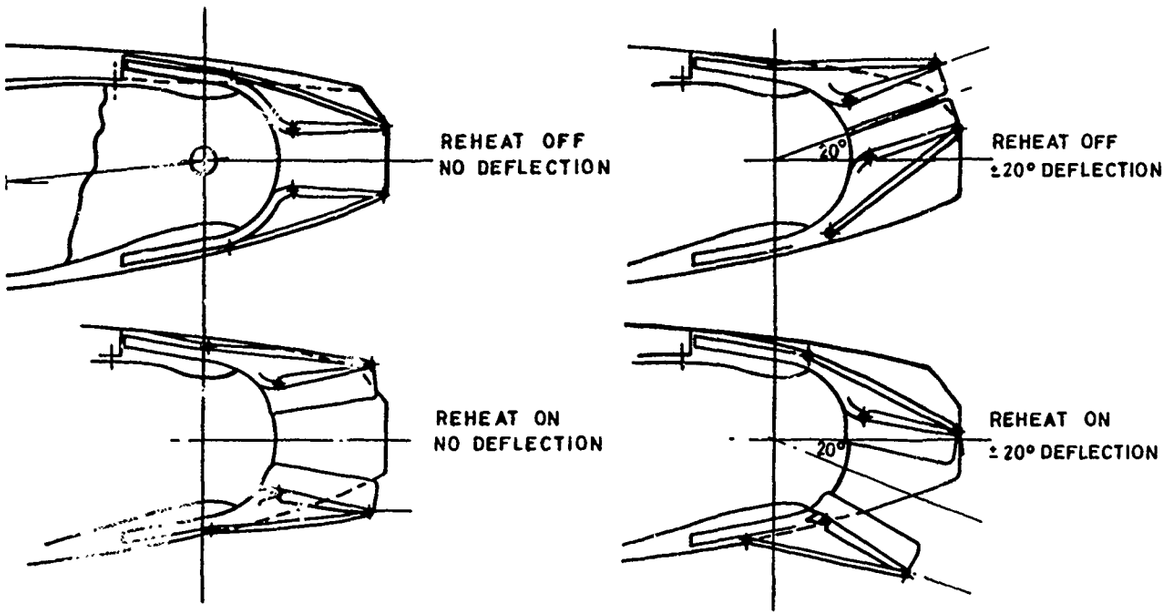

FIG. 23 VECTORING CAPABILITY OF FRONT AND REAR NOZZLES

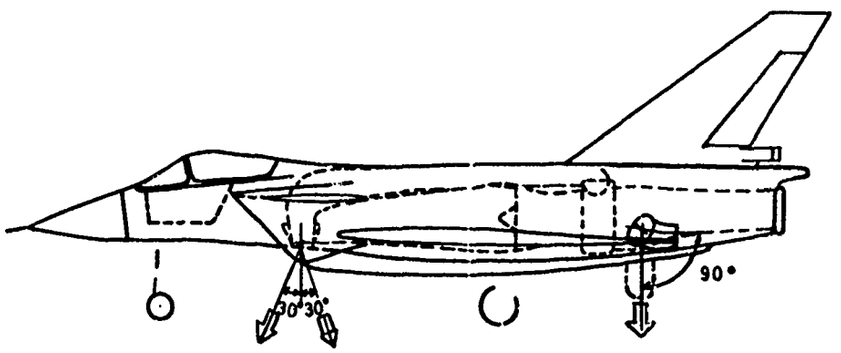

FIG. 24

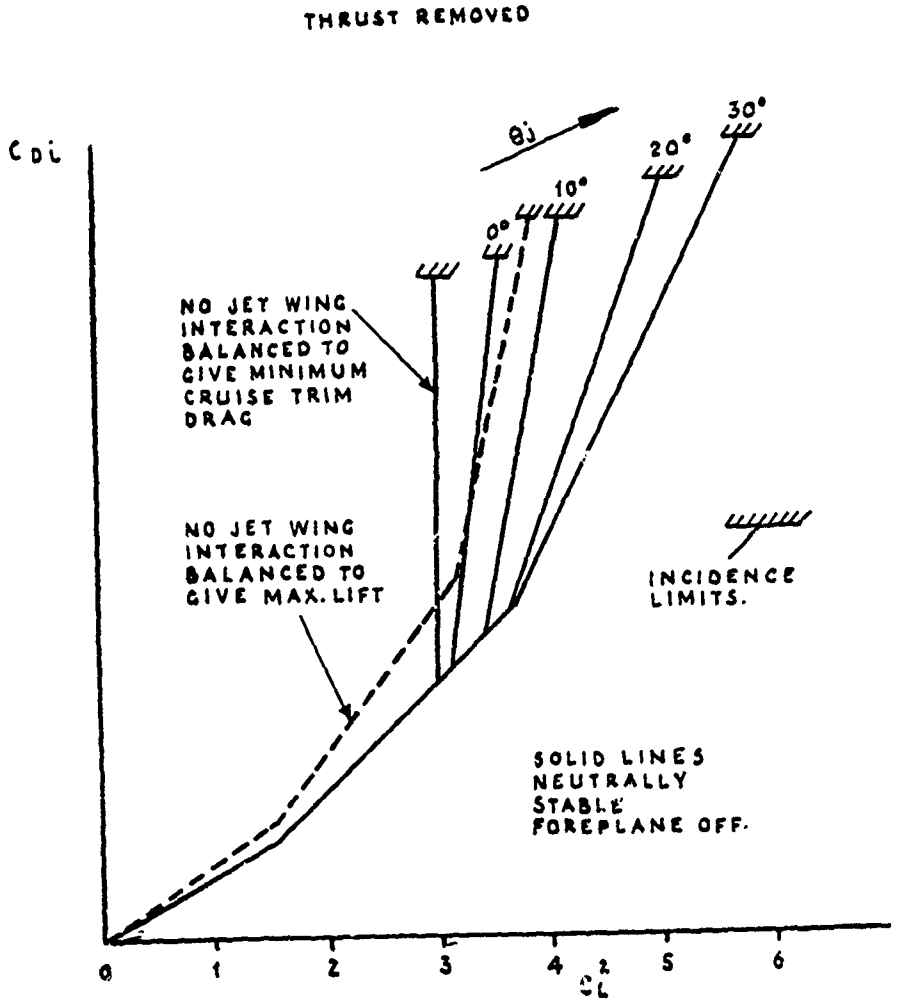

PREDICTED TRIMMED INDUCED DRAG POLAR

WITH JET ENHANCEMENT

FIG. 25 FLOW PATTERNS DURING VTO

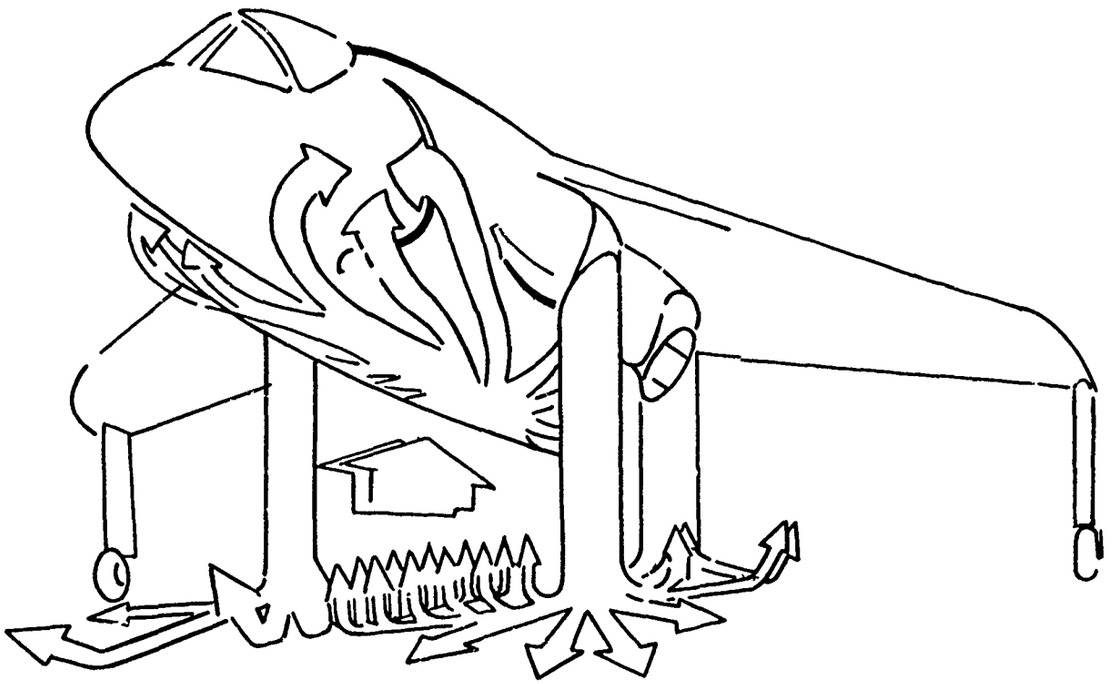

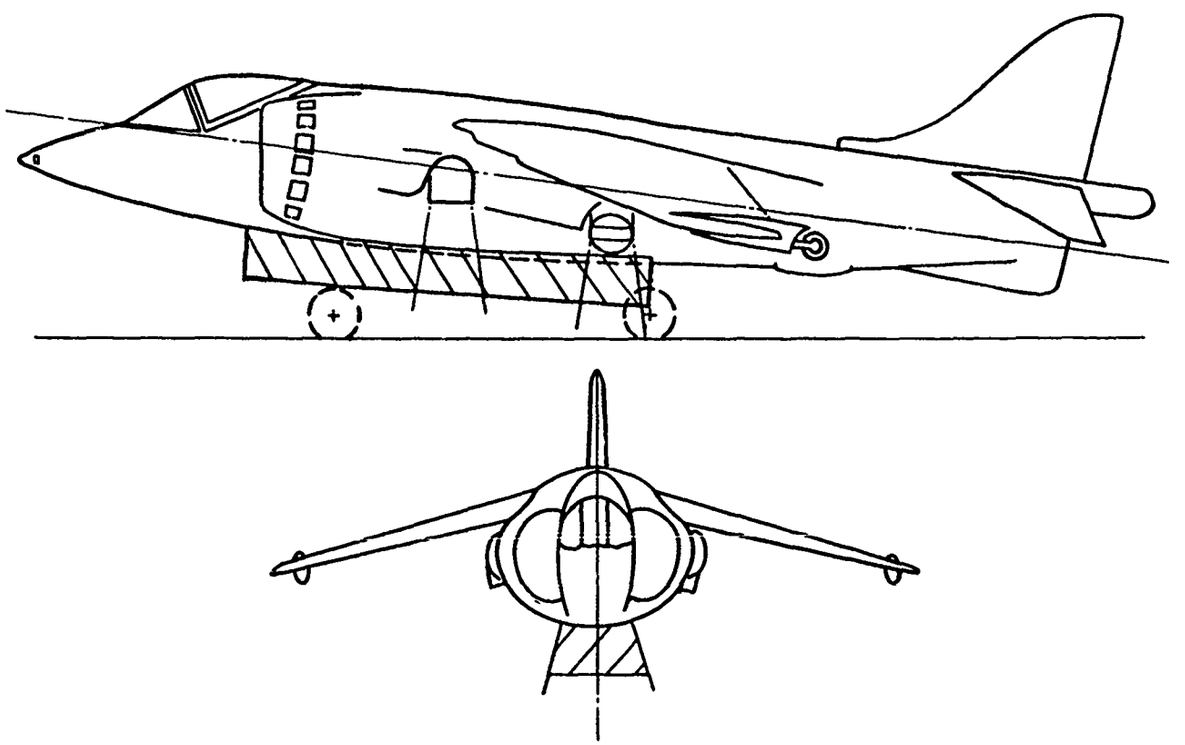

FIG. 26 ILLUSTRATION OF POSSIBLE CADS CONFIGURATION

CONDITIONS IN THE WALL JET AT 25FT. RADIUS FROM THE CENTRE OF THE A/C

FIG. 28

TYPICAL PEAK DYNAMIC PRESSURE

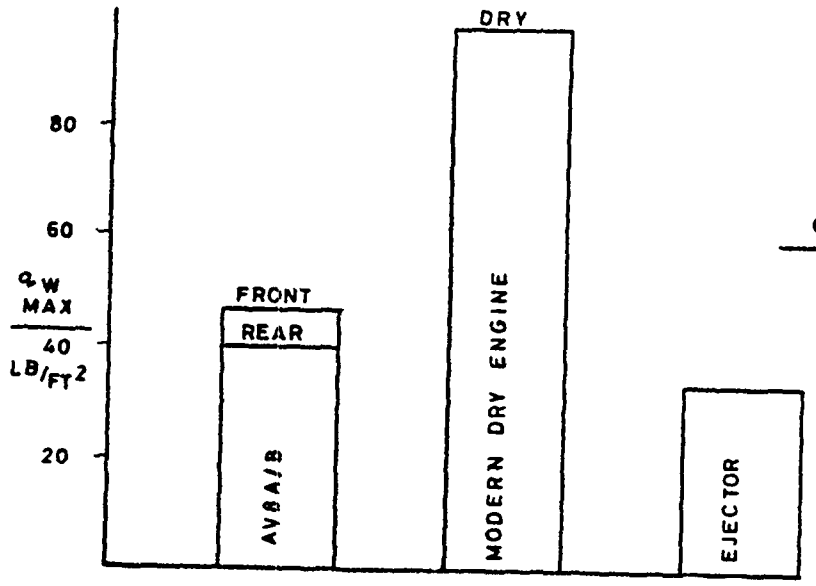

TYPICAL PEAK TOTAL TEMPERATURE

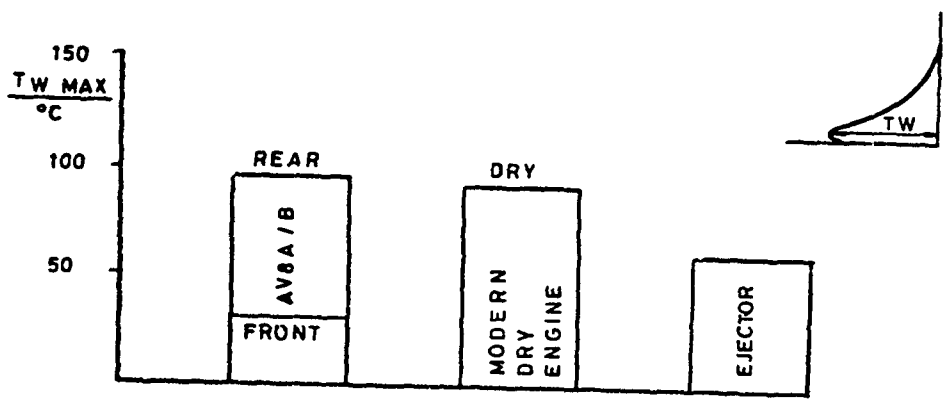

WALLJET MOMENTUM FLUX VECTOR BOUNDARIES

FIG. 27

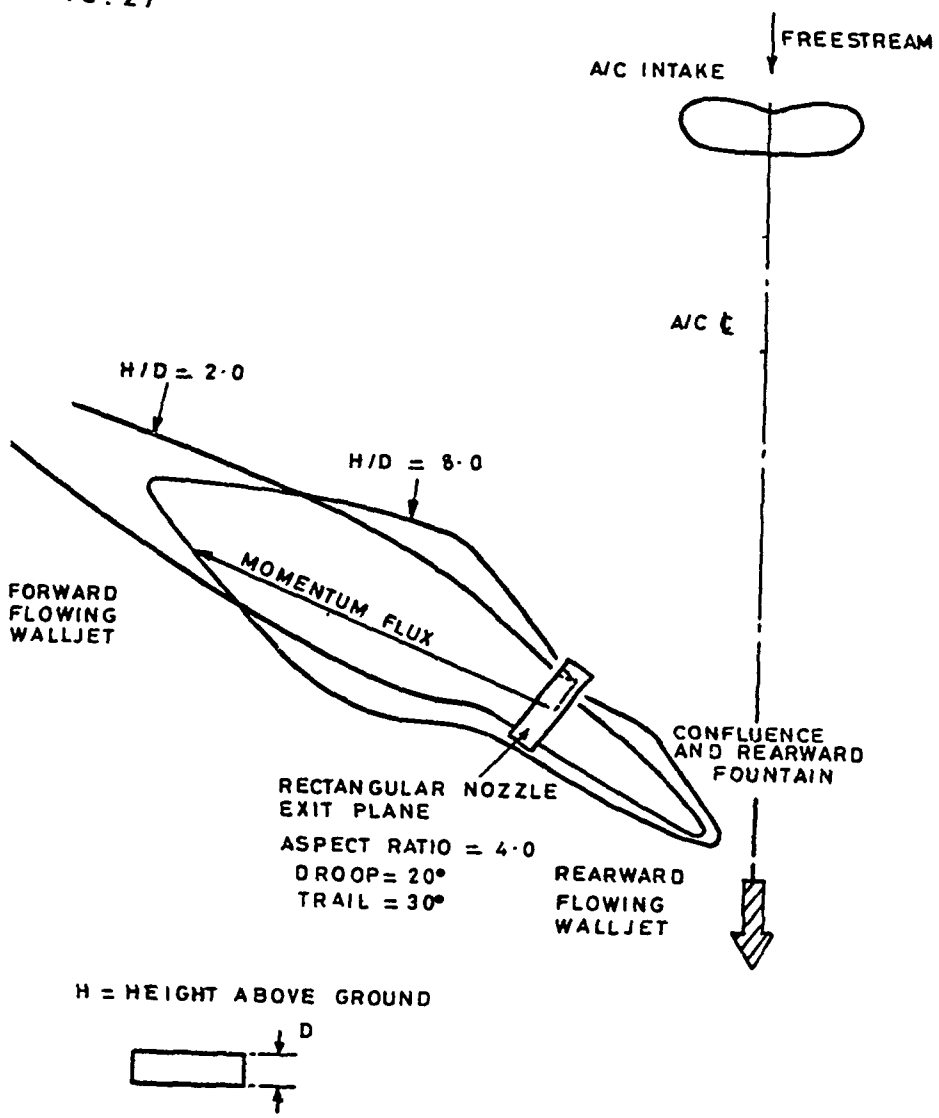

FIG. 29 C OF G ENVELOPE

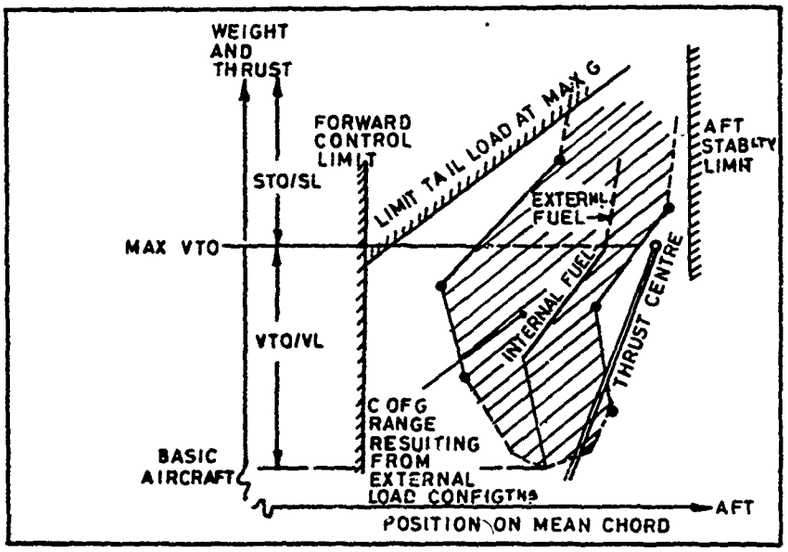

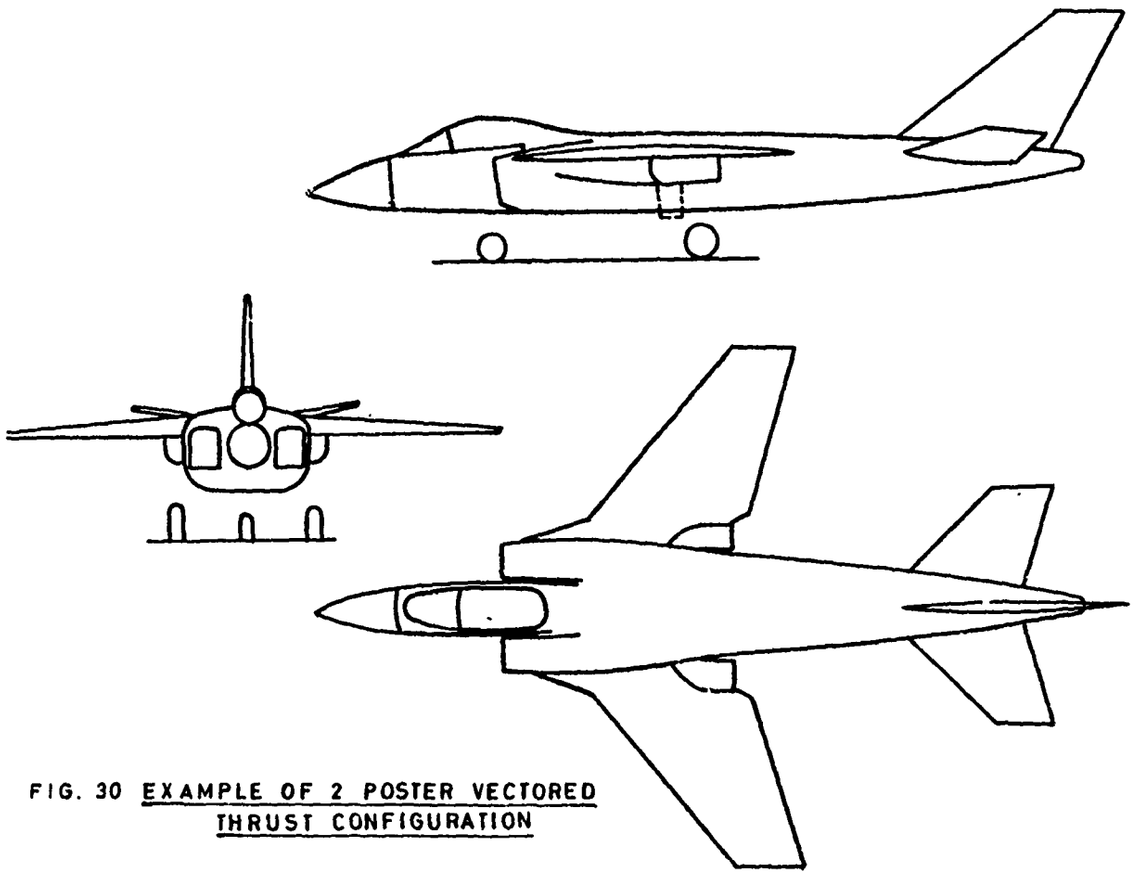

FIG. 30 EXAMPLE OF 2 POSTER VECTORED THRUST CONFIGURATION

FIG. 31

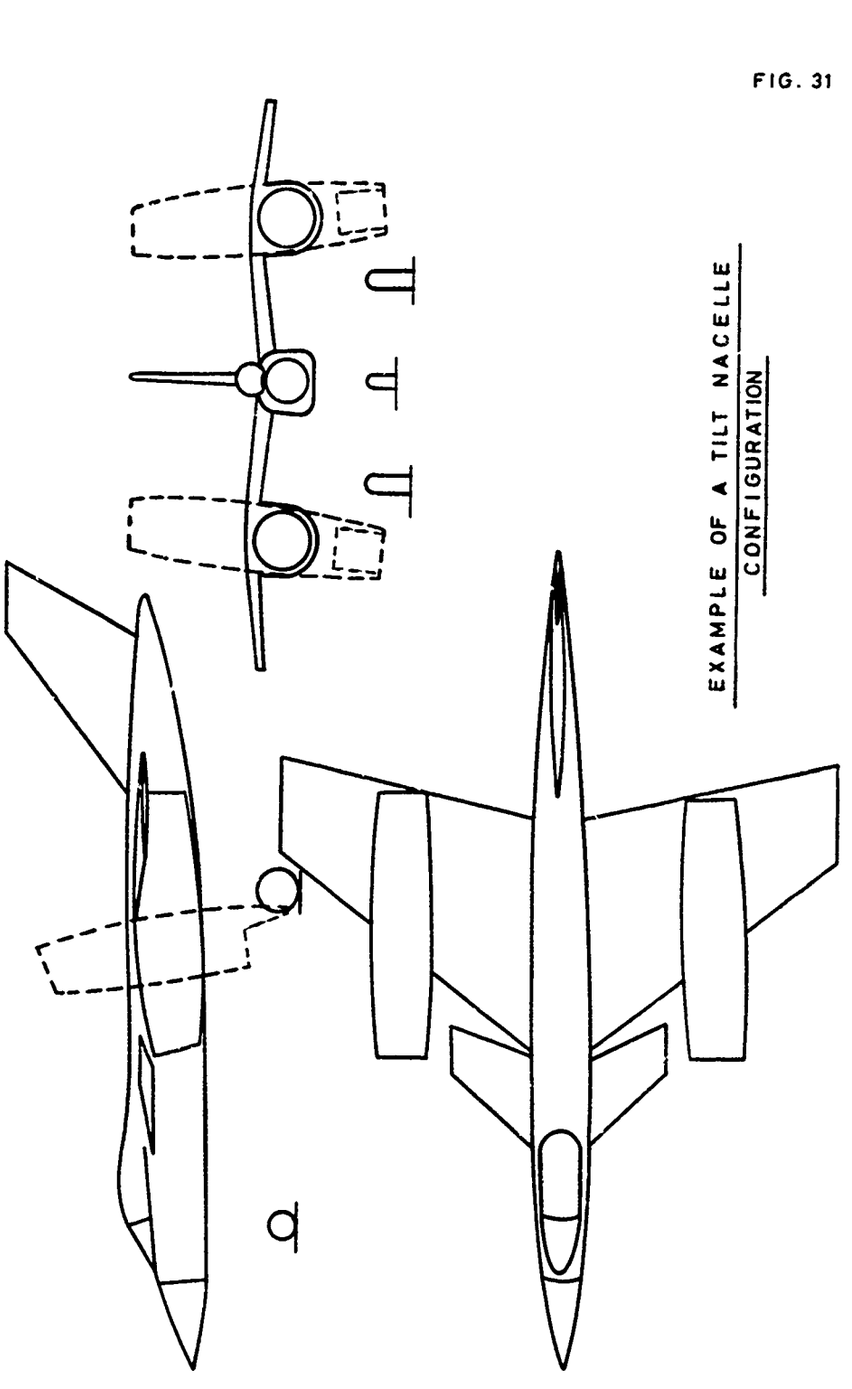

EXAMPLE OF A TILT NACELLE CONFIGURATION

FIG. 32

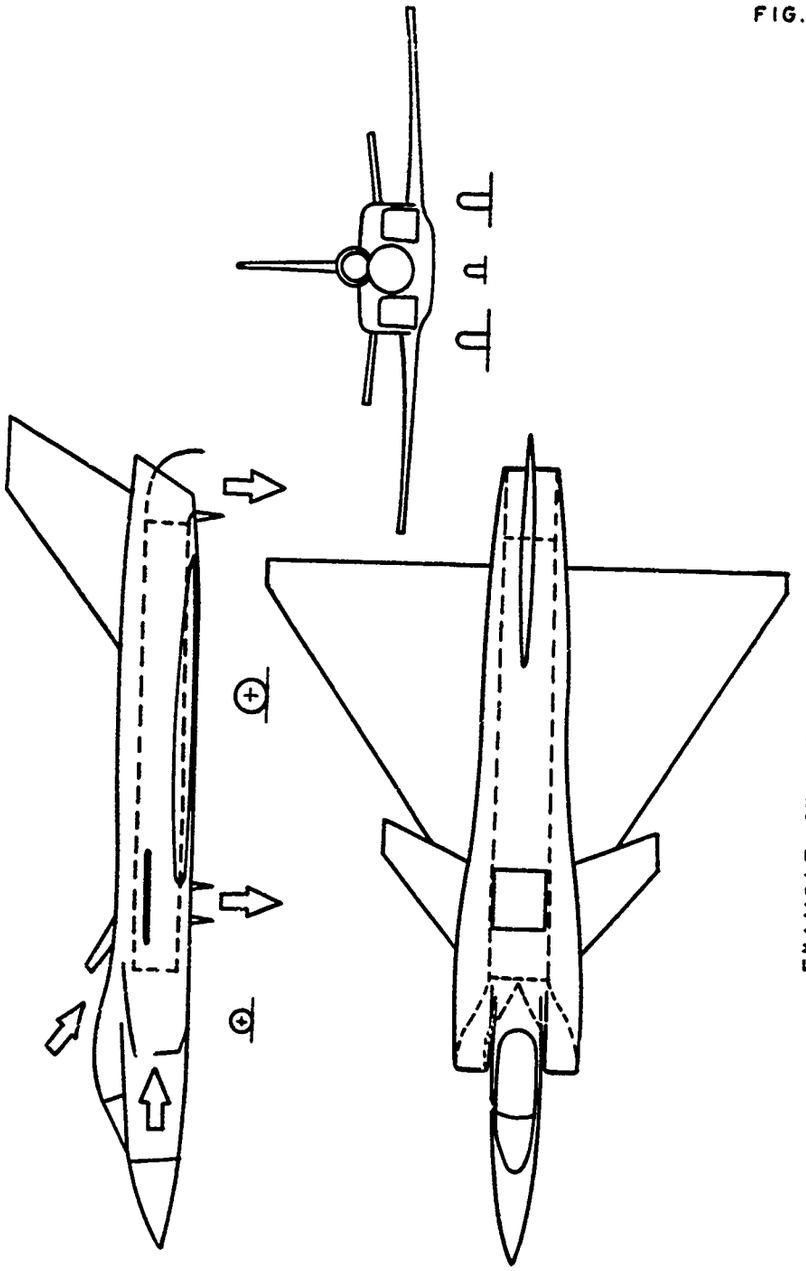

EXAMPLE OF A TANDEM FAN CONFIGURATION

FIG: 33

EXAMPLE OF R.A.L.S. CONFIGURATION

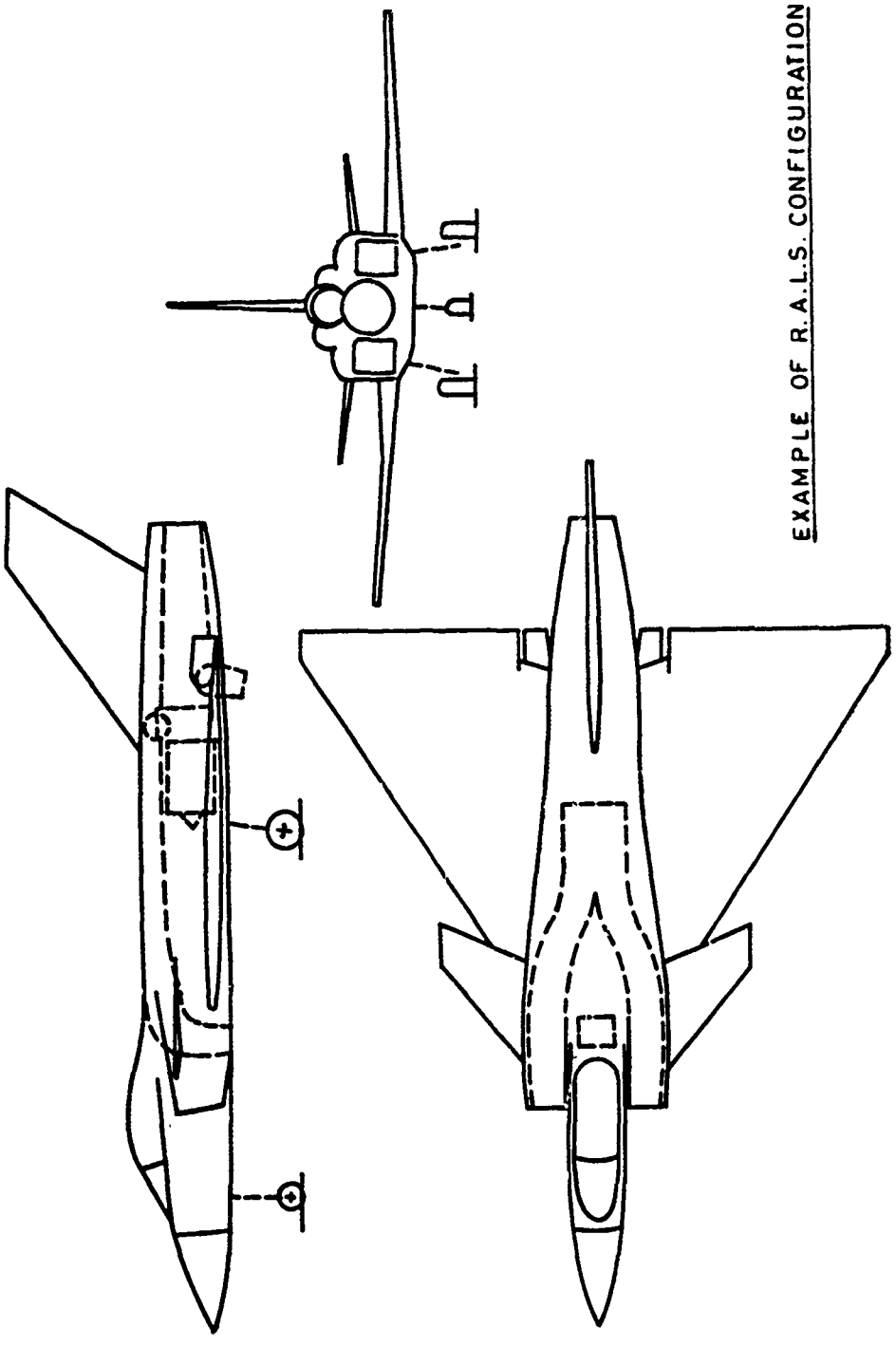

FIG. 34

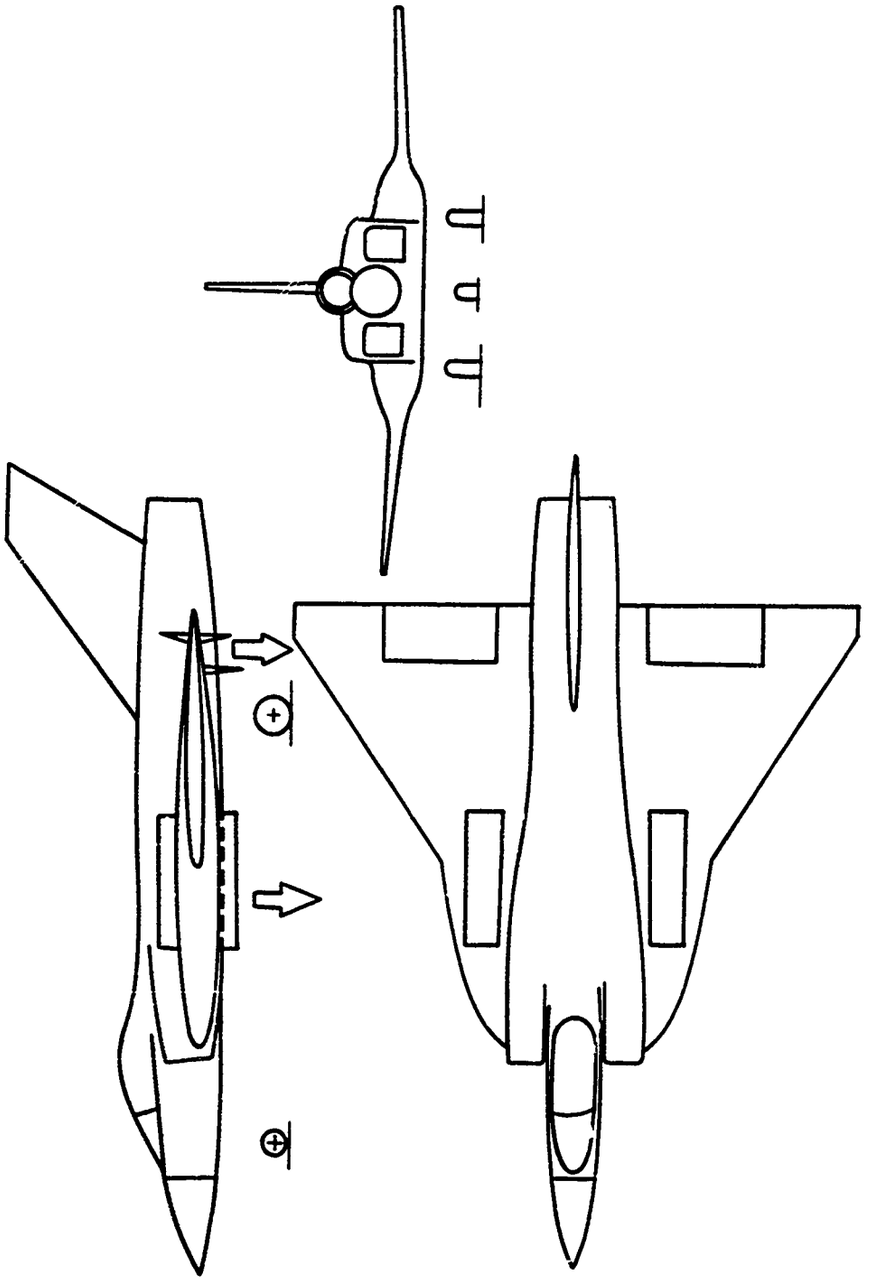

EXAMPLE OF EJECTOR AUGMENTOR CONFIGURATION

FIG. 35

ADVANTAGES OF GROSS THRUST VECTORING

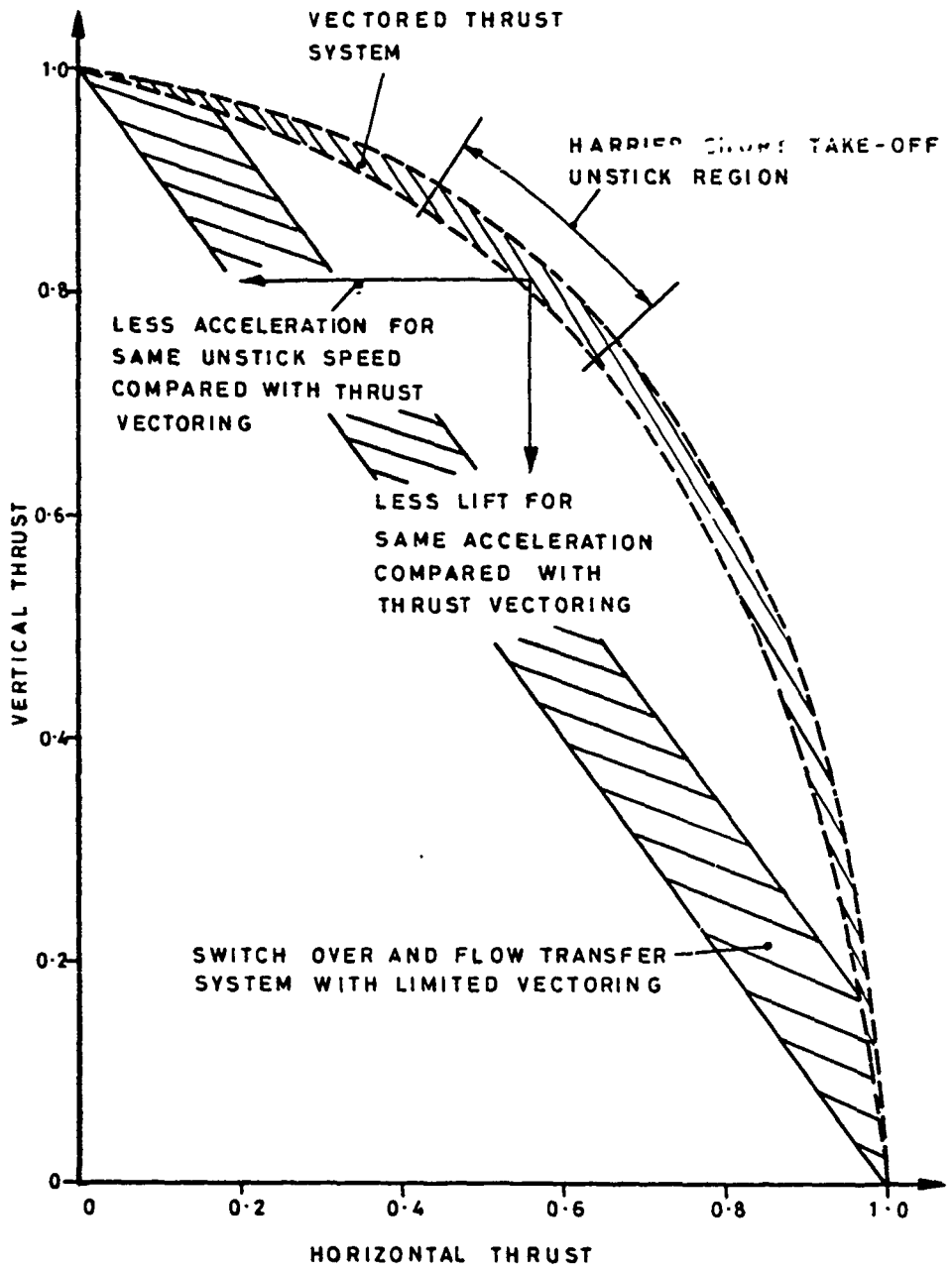

FIG. 36 **KESTREL (1964) CHANGES MADE TO IMPROVE LONGITUDINAL STABILITY AND CONTROL**

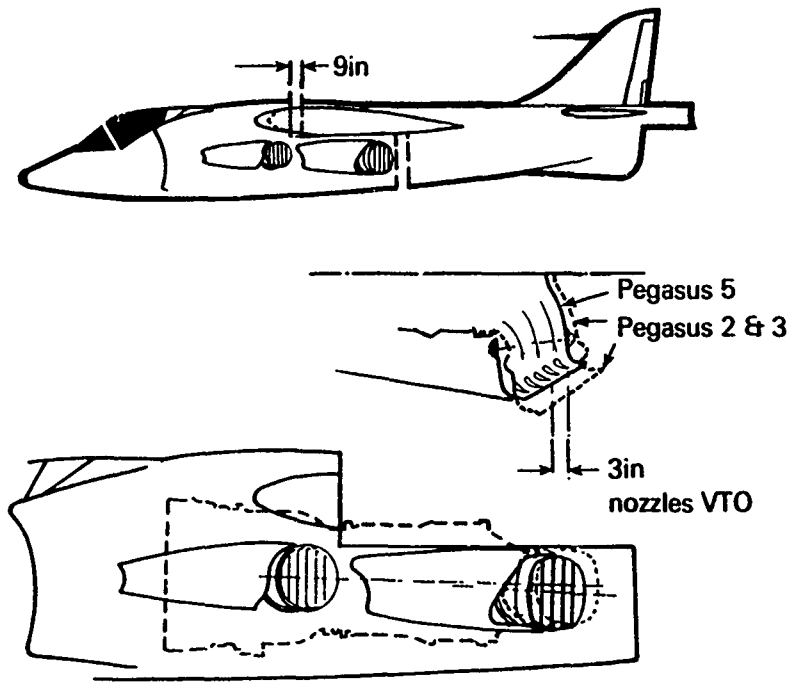

FIG. 37

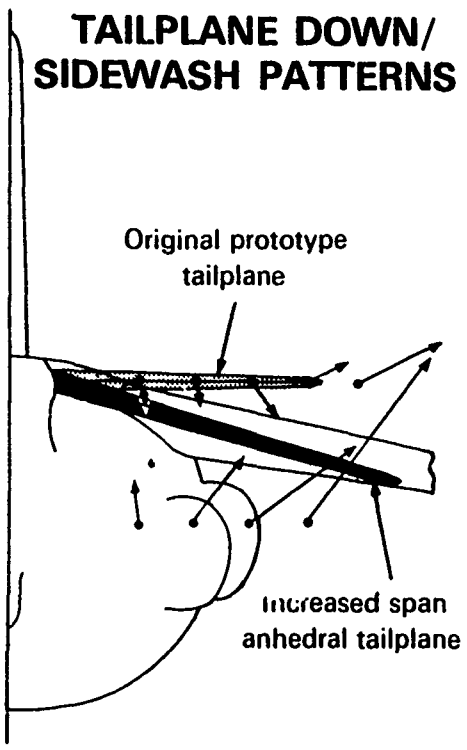

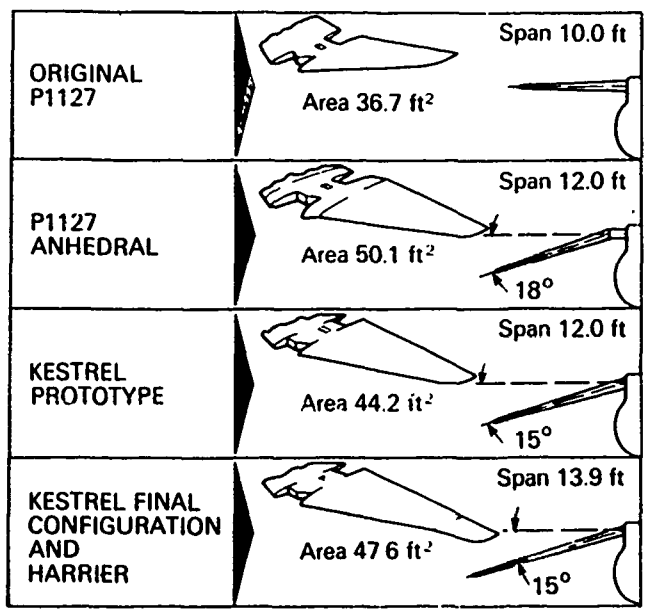

FIG. 38

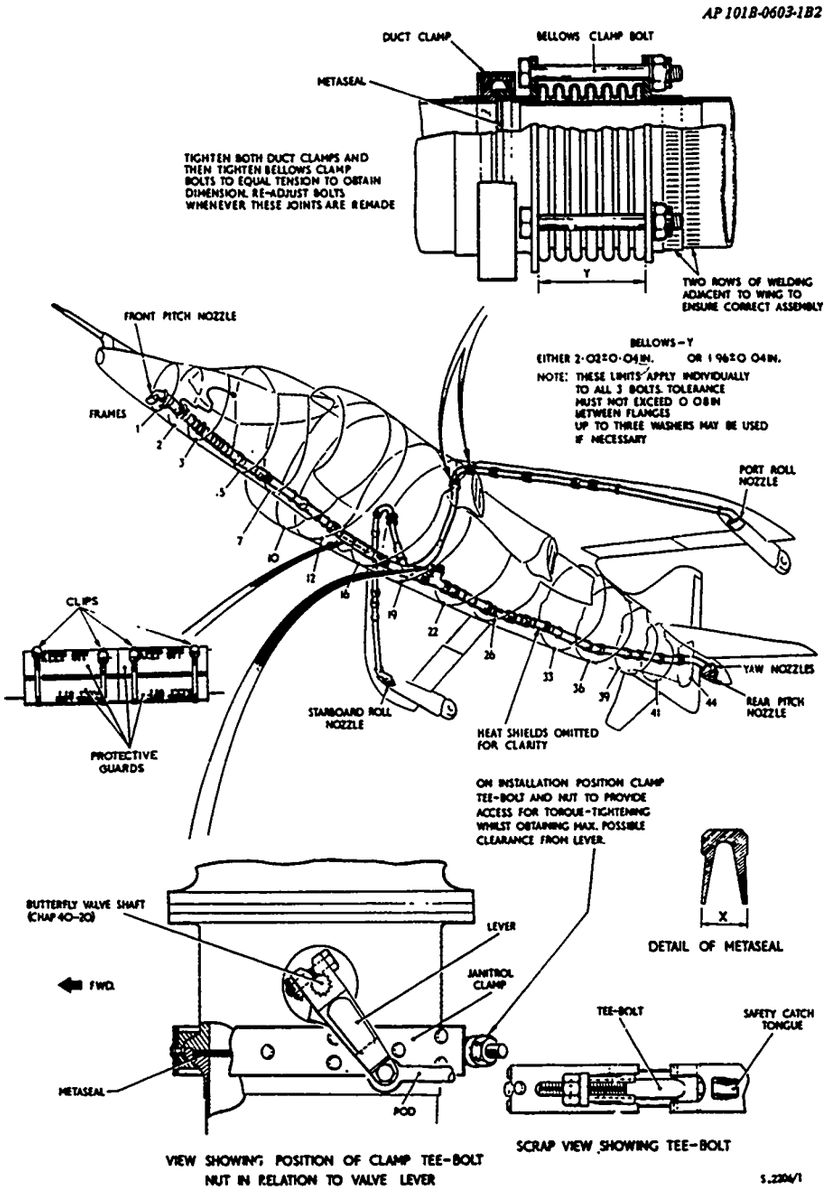

Reaction control nozzles and ducts – general arrangement

▶ *Mod 1463 incorporated* ◀

FIG. 39

POTENTIAL CONTROL PROBLEM DURING TRANSITION

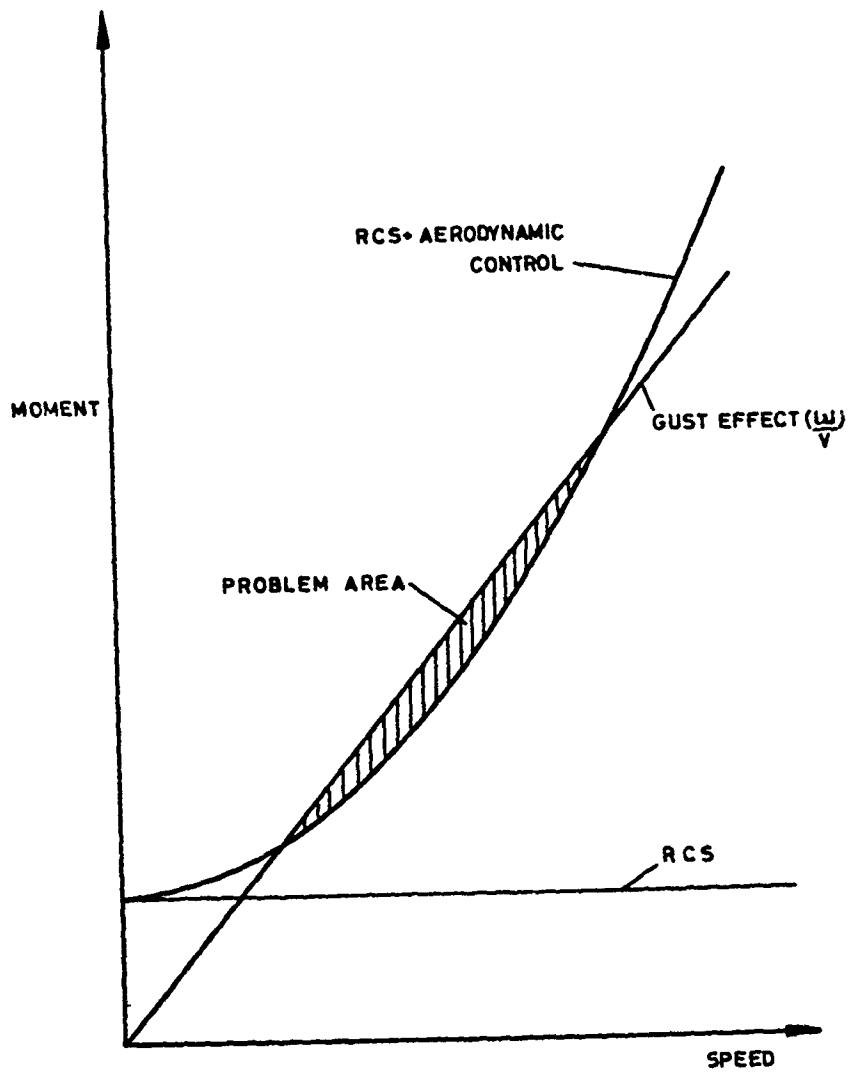

V/STOL PROPULSION SYSTEM AERODYNAMICS

By

W J Lewis
Assistant Chief Engineer
Rolls-Royce Limited
PO Box 3, Filton
Bristol BS12 7QE
England

SUMMARY

Different V/STOL propulsion system concepts are briefly described. Highlighted are those features of the systems which present the aerodynamicist with either more severe problems or different problems from those present on CTOL engines. After illustrating some of the demands V/STOL makes on the engine cycle choice and some of the compromises necessary, the individual parts of the propulsion system are considered in turn. Because of the enormous scope of the subject, attention has been limited to aspects which are common to a number of the different propulsion systems.

SYMBOLS

A	Area
g	Gravitational acceleration
P	Stagnation pressure
p	Static pressure
T	Stagnation temperature
u	Blade speed
V	Gas flow velocity
W	Gas flow
X	Thrust
γ	Ratio of specific heats
λ	Bypass ratio
η	Efficiency
ρ	Density
Θ	Angle
χ	% of compressor flow diverted to reaction controls

SUBSCRIPTS

a	Axial directio
B	HP compressor delivery
c	Engine core
F	Front nozzle
I	Intake duct
J	Jet or nozzles
L	Intake lip
o	Free stream
R	Rear nozzle
α	Ambient
ENG	Total engine
EX	Turbine exit
IN	Turbine inlet
ΔP or ΔH	Total head loss
$q = \frac{1}{2} \rho V^2$	Dynamic head
$Cp = \frac{p-p_\alpha}{\frac{1}{2} \rho V^2}$	Pressure coefficient

V/STOL PROPULSION SYSTEM AERODYNAMICS

Over the years since jet lift was first considered as a means of achieving V/STOL, a wide diversity of different propulsion systems have been studied. These different systems can be grouped in a number of different ways and present the aerodynamicist with a wide range of different problems. However, they all have one common feature, at low speeds when the systems are providing lift the engine airflow has to be deflected through at least one right angle, either as it enters the air intake, as it leaves the engine through the exhaust nozzle or internally in the engine.

The difficulties of ducting relatively high speed subsonic flows around bends were well known before the jet engine appeared and have been studied in depth. Figures 1 and 2 illustrate the pressure losses and flow distortions due to bends. Figure 3 shows the thrust loss due to the bend pressure loss as a function of the flow Mach number in the bend and the nozzle total:ambient pressure ratio. It might therefore appear that the optimum V/STOL propulsion system is the one with the minimum number of bends, which has those bends remote from the rotating turbo-machinery to avoid the adverse effects of non-uniform flows and pressure fields and which has the highest possible nozzle pressure ratio. However this is not so for a number of reasons, not least of which are the need for system simplicity, low weight and volume, and aircraft balance.

Figure 1

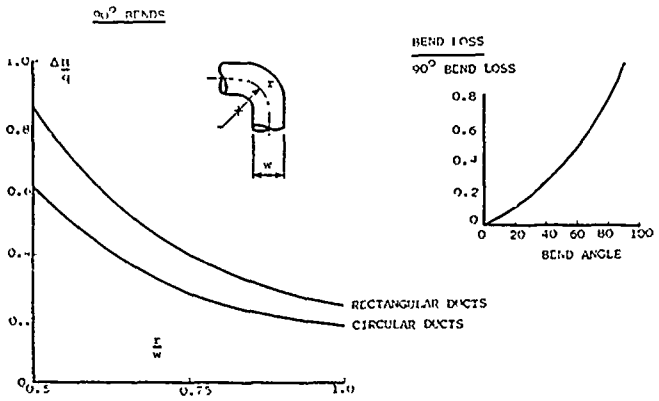

PRESSURE LOSSES IN SINGLE BENDS

Figure 2

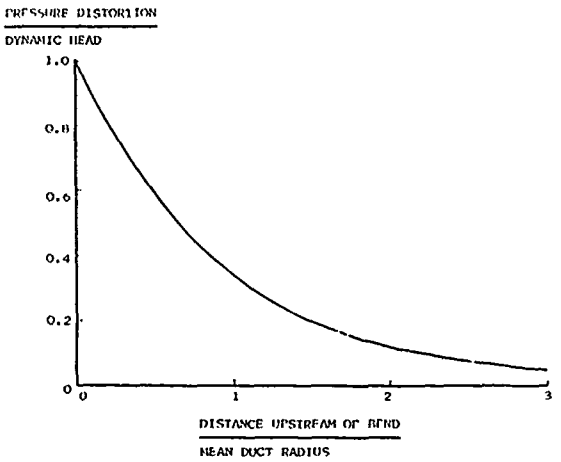

PREDICTED STATIC PRESSURE DISTORTION DUE TO BENDS

Figure 3

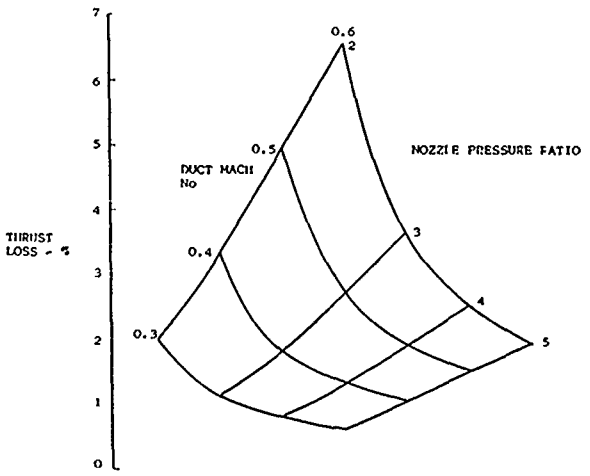

THRUST LOSS DUE TO A SINGLE BEND

One other feature, not found in all the different V/STOL propulsion systems, but which can be advantageous, is the ability to achieve 'total' thrust vectoring. This is defined as directing all the elements of the thrust of the engine in the required direction. In some systems there are two or more jets acting in different directions having a resultant which acts in the required direction. This occurs where at least one of the individual jets cannot be varied through the full range of angles between the lift and wing borne flight positions. Compared to these latter systems, which demand a controlled modulation of thrust or transfer of flow from one exhaust nozzle to another to maintain aircraft trim, total thrust vectoring offers considerable advantages (Figure 4) in terms of acceleration thrust during the transition from hover or for an STO from the unstick speed to wing borne flight. Alternatively, in the case of an STO, if the acceleration thrust is maintained for the purpose of achieving a short transition time, the amount of lift thrust can be increased at the unstick speed with total thrust vectoring, allowing a greater weight to be lifted from a given ground roll.

Figure 4

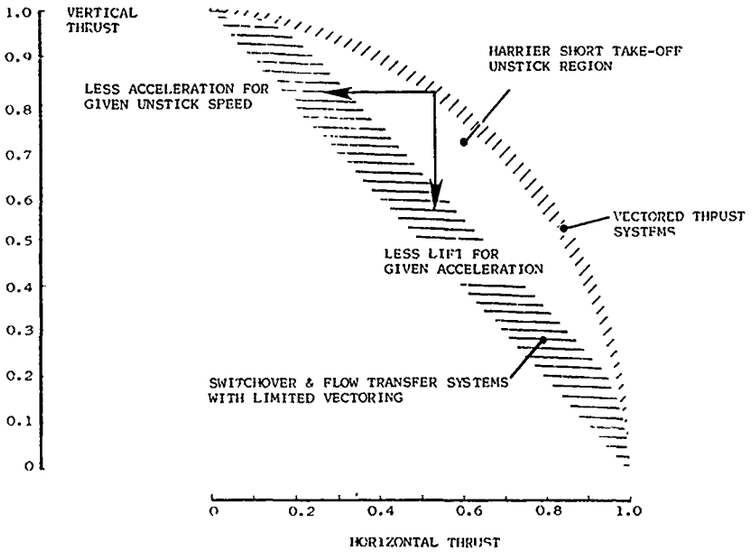

ADVANTAGE OF TOTAL THRUST VECTORING

Features of the Different Propulsion Systems

The vectored thrust engine, an example of which is the Pegasus in the Harrier/AV8 aircraft, can be adapted for supersonic V/STOL aircraft by means of thrust augmentation which incidentally can also be used for take-off and landing to increase the useful load that can be carried. The method of augmentation is to burn fuel in the plenum chamber supplying the bypass flow to the vectoring front nozzles (Figure 5). This plenum chamber burning (PCB) is preferred because it keeps the thrust centre well forward when the nozzles are vertical and because the bypass air is at a low temperature, PCB permits a higher thrust boost compared to afterburning in the core flow for a given exhaust gas temperature.

For both the subsonic combat aircraft, like the Harrier, and their future supersonic brethren, the thermodynamic cycle of the basic engine is likely to be the same. It will be dictated by the need to:

- keep the thrust centre as far forward, relative to the engine centre of gravity (cg), as possible. The engine may weigh as much as 30% of the empty weight of the aircraft so the engine position will have a considerable impact on the position of the cg of the aircraft and one of the difficulties of this type of propulsion system is to get sufficient front thrust to allow the engine to be placed as far back in the aircraft as possible and thus ease the aircraft balance.
- keep the overall cross section of the engine small. The need to align thrust centre and aircraft cg implies that the wing lift and hence the wing has to be over the engine so that the frontal area of the wing is added to the engine cross section leading to a large aircraft frontal area.

The demands on the aerodynamicist are therefore:

- to design for high flow Mach numbers and low hub:tip ratios through the engine thereby keeping the diameter as small as possible.
- to keep the fan length short so that the engine cg is not too far forward. The fan weighs between 20% and 25% of the basic engine weight and so has a significant impact on the engine cg.
- to design efficient exhaust systems with the minimum rearward displacement to keep the thrust centre well forward.
- to make the turbomachinery operate efficiently in non-uniform static pressure flow fields caused by intake and exhaust system bends as well as with non-uniform inlet total pressure and temperatures.

Figure 5

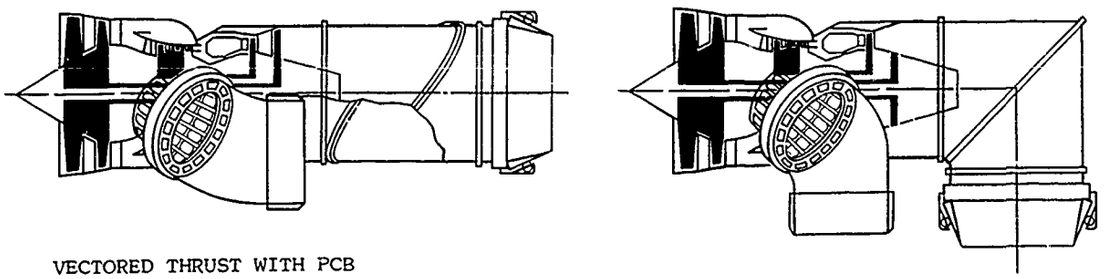

VECTORED THRUST WITH PCB

The tilt nacelle propulsion concept (Figure 6) is another 'total' thrust vectoring system which may also be used both for subsonic and supersonic aircraft; in the latter case the engine thrust would be augmented by means of a reheat system. It must be pointed out, however, that the power requirements to vector the thrust rapidly, will be much higher than for nozzle vectoring as on the Pegasus type of engine due to the much greater inertia of the engine nacelle. There is a need for the engines to be as short as possible tc achieve adequate ground clearance for the nozzle and minimise pitching moments due to the intake momentum drag acting a large distance above the cg with the nacelles tilted. However, there is really only one different demand on the aerodynamicist compared to the work required for a CTOL aircraft. Both the tilt nacelle aircraft currently projected use engine jet deflection to provide control at low airspeeds. The deflection system is downstream of the nozzle exit plane and therefore presents the problem of designing a deflector which operates efficiently in a gas stream at transonic or supersonic velocities and which does not introduce severe losses in normal cruise flight.

It has also been proposed in the past, that dedicated lift engines be installed in stowable, tilting nacelles, thereby giving thrust vectoring, rather than fixing the engines in the aircraft fuselage. This has been the more popular method of treating the lift plus lift/cruise engine propulsion system, (Figure 7). The choice between fuselage installed or stowable lift engines is not much influenced by aerodynamic considerations, the factors influencing the decision are structural heating and control, although the intake design problems are different. The stowable engine, provided that it can be suitably positioned on the airframe is capable of full vectoring so the air intake, which has to be short, may have to operate over a wide range of incidence. The fixed lift engine also has a short air intake but it always has to operate at about 90° incidence. Some vectoring of the exhaust flow of the fixed engine is desirable. Because the lift engines use valuable volume the pressure is on the designer to make them as small (and as light) as possible. This again forces the turbomachinery aerodynamicist towards high aspect ratio blading to keep length down and high flow Mach numbers and low hub:tip ratios to keep the diameter down. The aerodynamicist's problems are somewhat simplified because the flight conditions and operating range of lift engines are limited so reducing the need to design for high efficiency over a wide range of conditions and for a wide Reynolds number range. An advantage of the lift plus lift/cruise system is that the lift/cruise engine may be a conventional mixed flow turbofan, with or without an afterburner, but with the addition of a vectoring nozzle. A notable exception to this, however, was the vectored thrust RE193 engine in the VAK 191B. However, the use of a mixed flow turbofan engine reduces the aerodynamic problems - the design and installation of the vectoring nozzle and the supply of flow for the reaction control system are the only two features which are additional to those on a CTOL engine.

Figure 6

TILT NACELLE

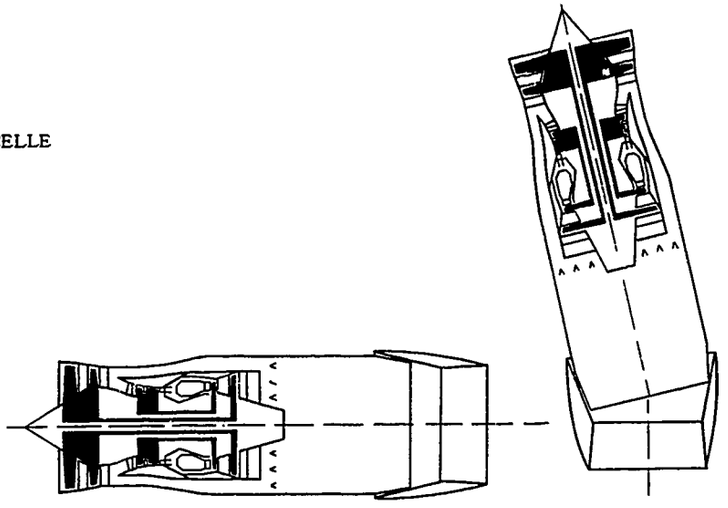

Figure 7

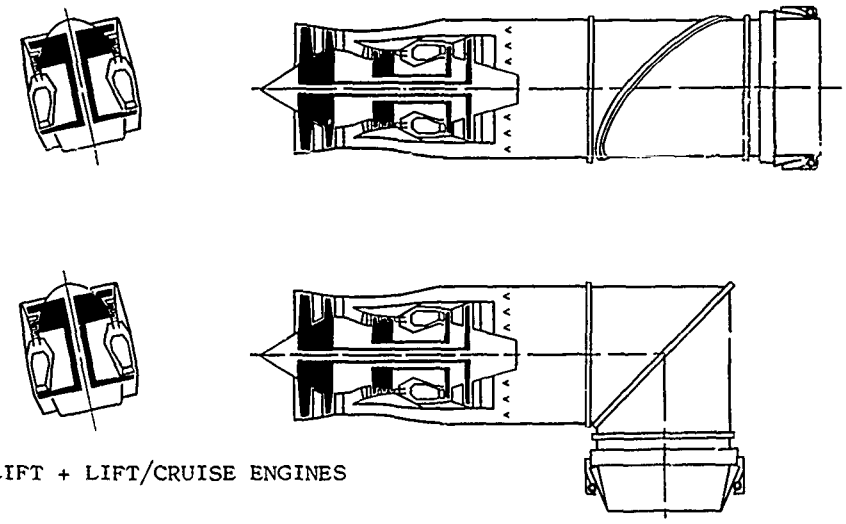

LIFT + LIFT/CRUISE ENGINES

The three remaining propulsion concepts to be considered all rely on some form of mode change to convert from the wing borne to the jet lift configuration. These three systems are the ejector lift, remote augmented lift (RALS) and tandem fan systems. In the case of the first two of these (Figures 8 and 9) the engine in the wing borne flight mode may be a mixed flow reheated turbofan or a cold duct burning separate flow turbofan. For jet lift, in both cases the bypass flow is ducted forward in the fuselage and then exhausted downwards and its thrust augmented (either by mass flow or heat addition). Since this lift thrust component can be well forward of the engine the engine itself can be situated to the rear of the fuselage. Some form of valve system is necessary to direct the bypass to the appropriate nozzle system so the aerodynamic problems that apply to these propulsion systems are those associated with the diverter valve, the ducting system to the front lift jet system, the engine vectoring nozzle and reaction control bleed flows. The diverter valve system must operate in such a manner that the fan working line is maintained which in the case of a mixed engine may also demand a variable area mixer. The axial position of the valve system and hence the bypass air offtake relative to the fan will determine the magnitude of the non-uniform back pressure on the fan.

Figure 8

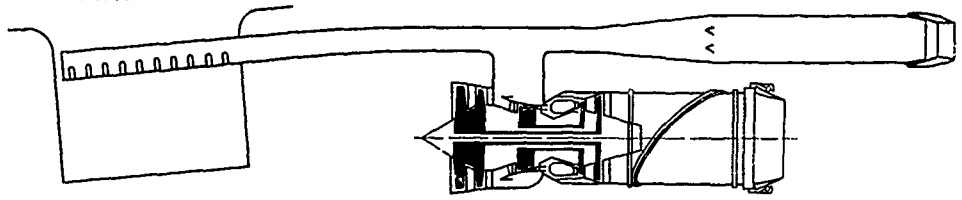

EJECTOR LIFT

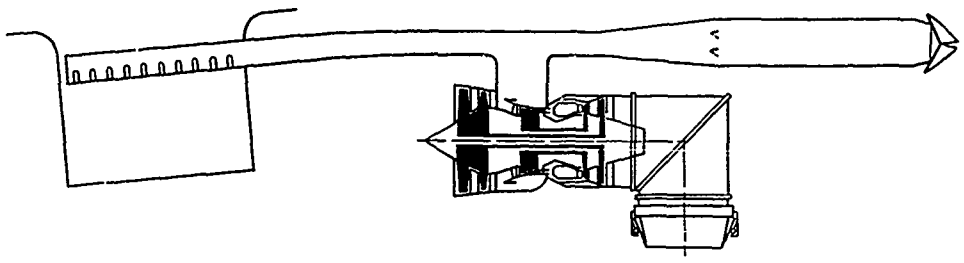

Figure 9

REMOTE AUGMENTED LIFT SYSTEM (RALS)

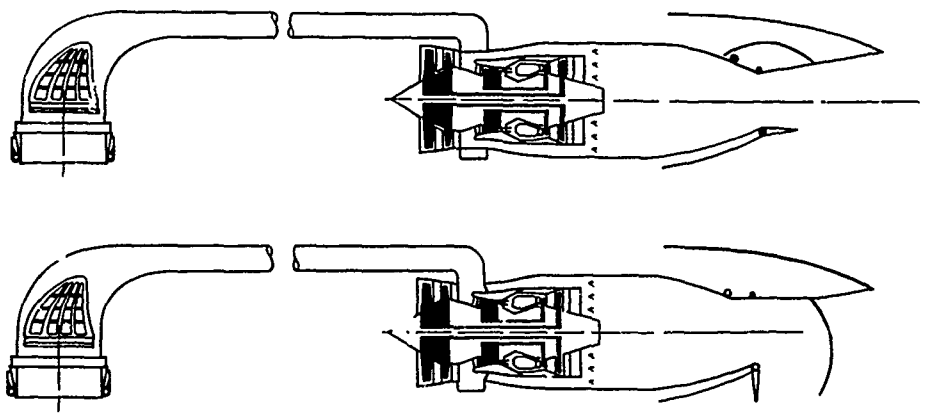

The third system mentioned above, the tandem fan, has been proposed as a non vectoring system where the mode change valve is used to maintain the correct proportions of lift thrust, front:rear thrust split and propulsive thrust during transition (Figure 10) or as a fully thrust vectoring system where the mode change can take place after the transition to fully wing borne flight (Figure 11). This simplifies and reduces the reliability requirements of the control systems since the safety of the aircraft is not dependent on maintaining the correct thrust relationships during the mode change. In either system, because the changeover valve is between fan stages, a design is required which does not present the rear fan with an excessive temperature and pressure distortion. Other features demanding attention from the aerodynamicist are those associated with the vectored thrust system - to a greater or lesser degree. For example:

- high flow Mach numbers and short length fans
- efficient operation of the turbomachinery in non-uniform static pressure fields caused by the air intake and the exhaust system.

Figure 10

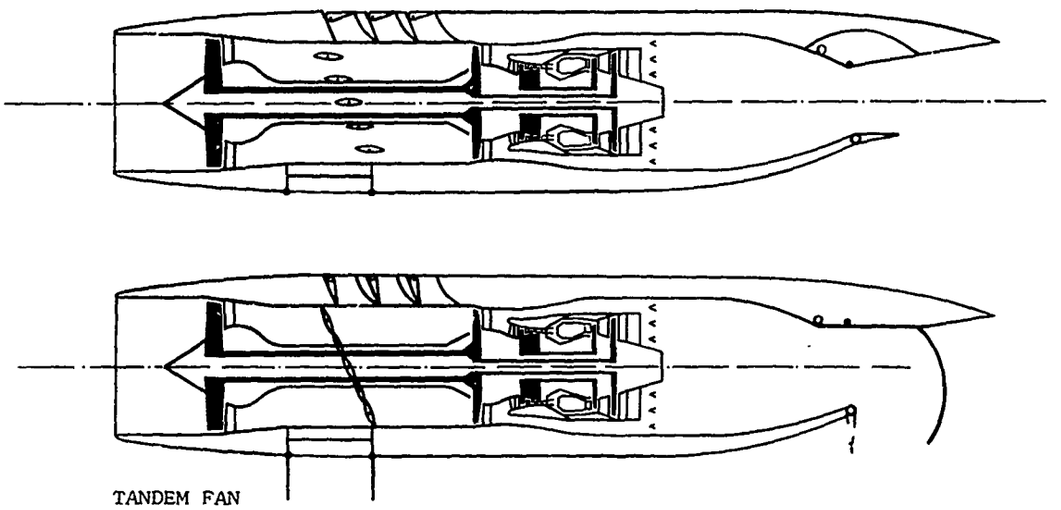

TANDEM FAN

Figure 11

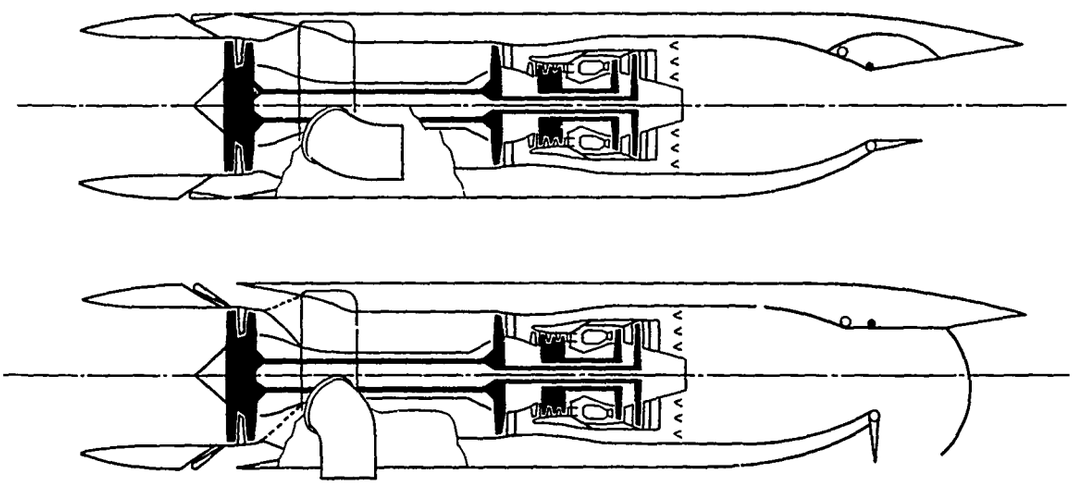

HYBRID FAN

Figure 12 attempts to indicate the areas demanding attention for each of the different propulsion systems, but in order to keep the following sections to a manageable length only those features common to several of the systems will be considered.

Figure 12

	VECTORED THRUST	TILT NACELLE	LIFT ENGINE	EJECTOR LIFT	RALS	HYBRID TANDEM FAN
High Incidence Intakes		•	•			
Auxiliary Inlets	•	•	•	•	•	•
Short Fans	•	•	•			•
Temperature Distortion On Fan	•	•	•	•	•	•
Intake Curvature Effects On Fan	•		•			•
Nozzle Curvature Effects On Fan	•			•	•	•
Engine Matching Through Mode Changes					•	•
Diverter Valves				•	•	•
Small Diameter Combustors	•					
Small Diameter LP Turbine	•					
Nozzle Curvature Effects on LP Turbine	•			•		
Nozzle Discharge Coefficient Effects	•			•		
Nozzle Thrust Centre	•			•	•	•
Nozzle Drag	•			•		•

TECHNICAL FEATURES OF V/STOL POWERPLANTS

Figure 13

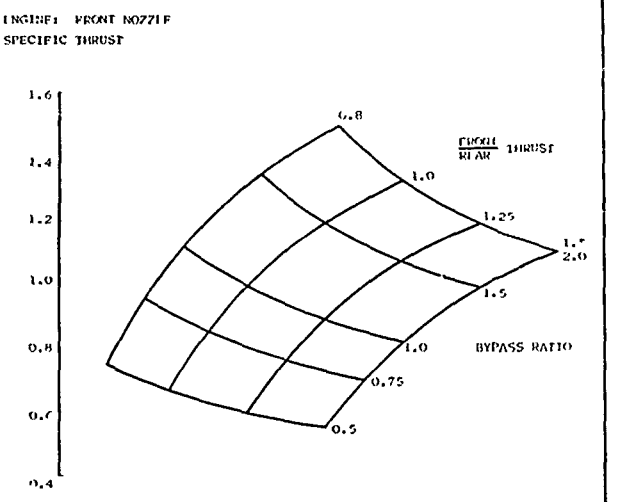

VARIATION OF SPECIFIC THRUST

Engine Considerations

The thermodynamic cycle of the vectored thrust engine is governed by the fan pressure ratio and hence the specific thrust (thrust per unit of airflow) of the front nozzle system. The overall engine specific thrust is then defined solely by the required front:rear nozzle thrust split and the bypass ratio. Figure 13 illustrates the ratio of the total engine specific thrust to the front nozzle specific thrust as a function of both bypass ratio and front:rear thrust split. This curve requires no knowledge whatsoever of the engine thermodynamic cycle and may be derived as follows:

$$\left(\frac{X}{W}\right)_{ENG} = \frac{X_F + X_R}{W_F + W_R} = \frac{1 + \frac{X_R}{X_F}}{1 + \frac{W_R}{W_F}} \quad \frac{X_F}{W_F}$$

$$\text{so } \frac{\left(\frac{X}{W}\right)_{ENG}}{\left(\frac{X}{W}\right)_F} = \frac{\lambda}{1 + \lambda} \left(1 + \frac{X_R}{X_F}\right) \text{ where } \lambda = \frac{W_F}{W_R} \text{ (bypass ratio)} \quad \ldots\ldots\ldots ①$$

It should be mentioned, however, that by the addition of one other contraint, eg jet pipe temperature, the thermodynamic cycle for a given total engine specific thrust is defined for all points on Figure 13.

An aerodynamic limitation to the engine specific thrust may be the amount of flow that can be bled from the HP compressor for use in a reaction control system. If this amount is limited to a certain percentage of the core flow then the variation of the ratio of the total engine:front nozzle specific thrust can again be determined as a function of the front:rear thrust split, eg:

$$\frac{W_B}{W_{ENG}} = \frac{W_B}{Wc} \quad \frac{Wc}{W_{ENG}} = \frac{W_B}{Wc} \quad \frac{1}{1 + \lambda}$$

$$\text{so } \frac{\left(\frac{X}{W}\right)_{ENG}}{\left(\frac{X}{W}\right)_B} \quad \frac{X_B}{X_{ENG}} = \frac{W_B}{Wc} \quad \frac{1}{1 + \lambda} \quad \ldots\ldots\ldots\ldots ②$$

Combining equations 1 and 2 and eliminating λ then gives -

$$\left(\frac{X}{W}\right)_{ENG} = \frac{\left(\frac{X}{W}\right)_B \frac{X_{ENG}}{X_B} \quad \frac{W_B}{Wc}\left(\frac{X}{W}\right)_F\left(1 + \frac{X_R}{X_F}\right)}{\left(\frac{X}{W}\right)_B \frac{X_{ENG}}{X_B} \quad \frac{W_B}{Wc} + \left(\frac{X}{W}\right)_F\left(1 + \frac{X_R}{X_F}\right)}$$

$$= \frac{\left(\frac{X}{W}\right)_B \left(\frac{X}{W}\right)_F \left(1 + \frac{X_R}{X_F}\right)}{\left(\frac{X}{W}\right)_B + \frac{X_B}{X_{ENG}} \quad \frac{Wc}{W_B}\left(\frac{X}{W}\right)_F \left(1 + \frac{X_R}{X_F}\right)}$$

Assuming values for $\left(\frac{X}{W}\right)_F$, $\frac{W_B}{Wc}$, $\left(\frac{X}{W}\right)_B$ and $\frac{X_{ENG}}{X_B}$,

then the variation of the engine specific thrust with front:rear thrust split can be determined. Experience from the Harrier would suggest:

$$\left(\frac{X}{W}\right)_B = 70 \quad \text{and} \quad \frac{X_{ENG}}{X_B} = 15$$

Figure 14 shows the variation of engine specific thrust with thrust split for different values of front nozzle specific thrust and limiting bleed flow. This indicates that for a given front nozzle specific thrust the overall specific thrust of the engine decreases as the front:rear thrust ratio is increased ie as the balance of the aircraft gets easier the engine size has to increase to maintain a given thrust. Although Figure 14 requires no knowledge of the basic engine cycle it must be emphasised that both Figure 13 and Figure 14 imply a range of thermodynamic cycles having different technology levels. No account has been taken of possible technology limitations (such as turbine temperatures). These will set a limit on the specific thrust achievable. Similar curves would be applicable to other separate exhaust flow propulsion systems including RALS and the ejector lift system, as well as to vectored thrust with or without PCB. However, in the case of the two former systems the equations will be more complicated because the thrust augmentation will almost certainly be different in the jet lift case compared to the normal flight case.

Figure 14

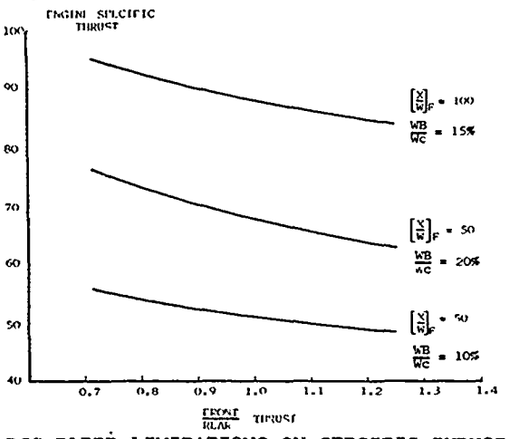

RCS BLEED LIMITATIONS ON SPECIFIC THRUST

Figure 15

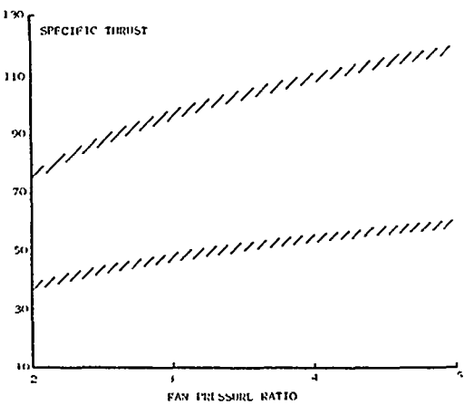

VARIATION OF SPECIFIC THRUST WITH PRESSURE RATIO

It is evident from Figures 13 and 14 that the specific thrust of the front nozzle flow is a determining factor in the specific thrust of the engine and Figure 15 shows how the front nozzle specific thrust varies with fan pressure ratio for unboosted flow and for an augmented flow assuming 100% thrust boost. It will be noted that for the separate flow engine the fan is a critical feature, the overall engine specific thrust will be highest with the highest fan pressure ratio.

The mixed engine such as may be used for RALS and the ejector lift system has a similar characteristic to the separate flow engine, but with one important difference. In order to achieve mixing, near equality of the LP turbine exit and fan exit total pressures is necessary. For a given overall pressure ratio and turbine temperature this mixing constraint gives a unique relationship between fan pressure ratio and bypass ratio (Figure 16) and this combination defines the front:rear thrust split, the duct size required to direct the bypass flow to the front lift system and also the engine specific thrust in the normal flight condition. These parameters are shown in Figures 17, 18 and 19 as a function of the engine fan pressure ratio for a particular overall pressure ratio and turbine temperature. Figure 20 shows the variation of specific thrust with thrust split and indicates the same trend as for the separate flow engine ie the high specific thrust engine is possible with a low front:rear thrust split and vice versa. This curve is for dry power. Figure 19 shows that the variation of specific thrust with fan pressure ratio (bypass:core thrust ratio) is much less than in the case of a separate exhaust flow engine. Therefore the sizing of a mixed engine system in terms of total airflow may not depend on the required thrust split to the same degree as for a separate exhaust flow engine.

Figure 16

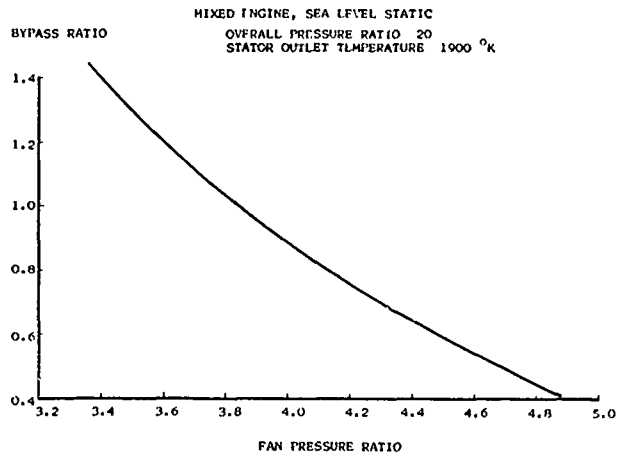

VARIATION OF BYPASS RATIC WITH FAN PRESSURE RATIO (ILLUSTRATION)

Figure 17

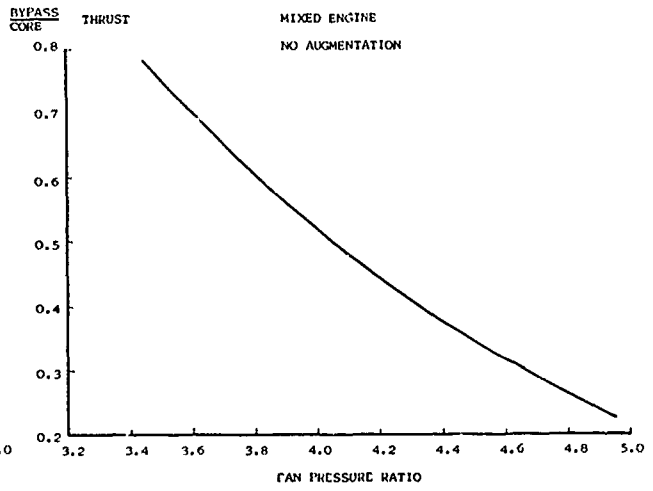

VARIATION OF BYPASS:CORE THRUST SPLIT WITH FAN PRESSURE RATIO

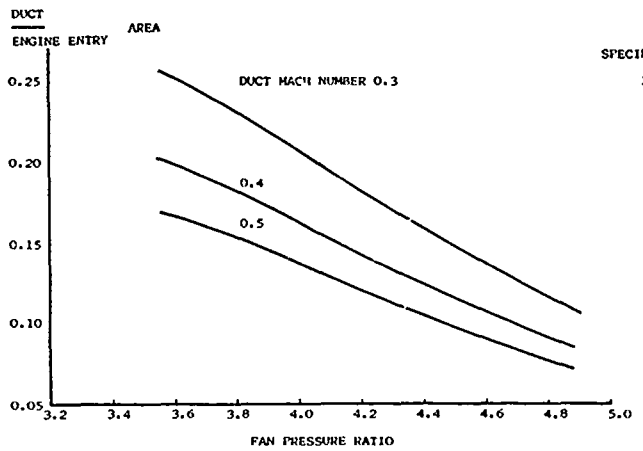

Figure 18

BYPASS AIR DUCT SIZE

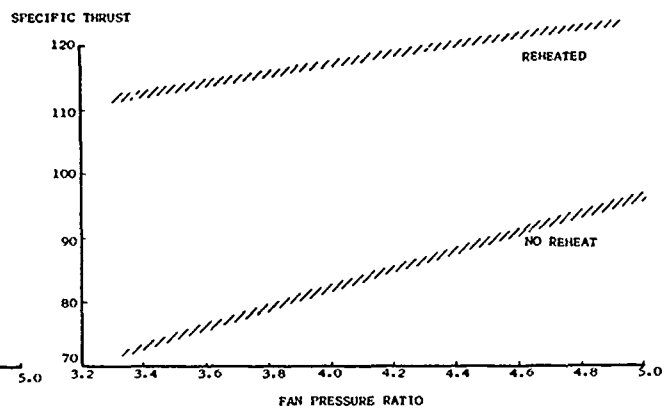

Figure 19

EFFECT OF FAN PRESSURE RATIO ON SPECIFIC THRUST

Fan

It cannot be repeated too often that the fan is one of the most important components of a V/STOL engine. While the design features required are desirable for all engine types and applications the benefits are that much greater for a V/STOL engine. The requirements are:

- high inlet Mach number
- low hub:tip ratio at inlet
- low hub:tip ratio at outlet
- high aspect ratio blading

The first two requirements are to keep the fan diameter as small as possible, the third is to avoid too severe an offset in the duct into the HP compressor (although the entry hub:tip ratio of the HP compressor has an important bearing in this respect), and the last requirement is to keep the fan as short as possible.

The purpose of the fan is to compress the entering airflow and this is achieved by diffusing the flow through each individual blade row by reducing the relative swirl of the flow. To maintain reasonable flow Mach numbers and avoid too high a diffusion rate the annulus area is reduced through the fan from front to rear. The increase in stagnation pressure through the fan is obtained by increasing the blade speed relative to the absolute speed of the approaching flow and a high blade speed will therefore give the highest pressure rise through the system. Figure 21 illustrates how the stage pressure rise varies with the ratio of the inlet velocity to the blade speed. This shows that, as well as a low inlet:blade speed ratio giving a high pressure rise an increase in blade speed for a constant value of inlet velocity to blade speed increases the pressure rise. The magnitude of the pressure rise, when non-dimensionalised by dividing by the square of the blade speed, depends on the deflection and design of the blade and one limitation is the amount of diffusion possible through the blade row.

Figure 20

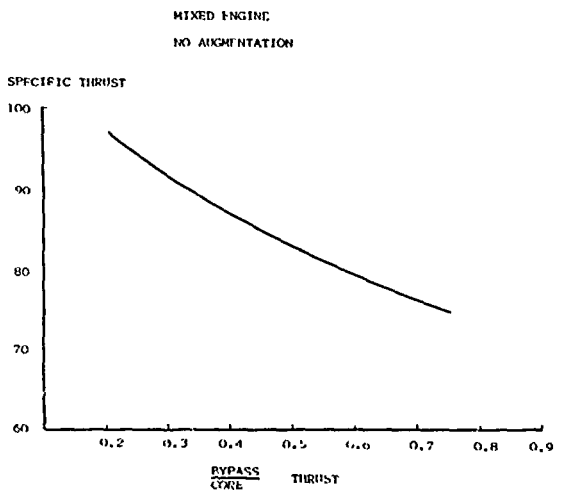

VARIATION OF SPECIFIC THRUST WITH THRUST SPLIT

Figure 21

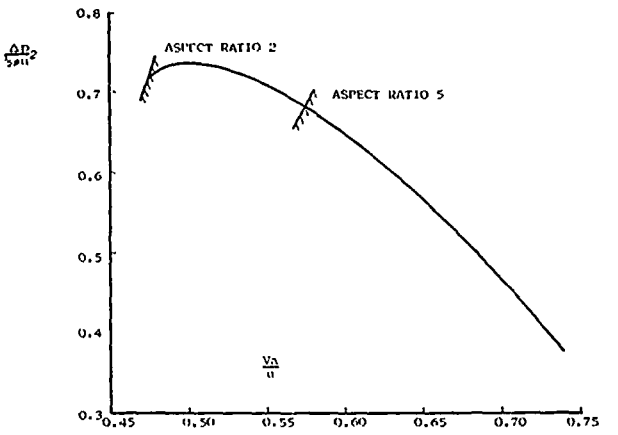

COMPRESSOR MEAN STAGE CHARACTERISTIC

Unfortunately blade speed varies linearly with radius so for a given tip speed a low hub:tip ratio fan implies a low blade speed at the hub. This will demand the highest possible deflections at the hub whilst at the tip little deflection through the rotor blade is required to achieve the same pressure rise. Therefore, the pressure rise of a given blade design with a given tip speed will be limited by the performance at the hub and an increase can only be achieved by an increase in hub:tip ratio. The features which lead to the highest pressure rise per stage are thus the opposite of those which are required for V/STOL engine.

The length of the fan is affected by the severity of the adverse pressure gradients on the hub and casing wells and also by the angular changes to the hub line between the stages. High aspect ratio blading (short fans) must have a higher adverse pressure gradient than low aspect ratio blades and as shown on Figure 21 the cut off due to surge, occurs at lower values of pressure rise as the blade aspect ratio is increased.

Figure 22 shows how the stage lift coefficient at surge varies with the blade passage aspect ratio. This parameter is related to the blade aspect ratio by pitch:chord ratio and stagger angle. If these two parameters are constant the blade aspect ratio is proportional to the passage aspect ratio. Figure 22 shows that reducing the passage aspect ratio from 5 to 2 increases the lift coefficient and hence the stage pressure rise by about 50%.

To quantify these effects Figures 23 and 24 show how, for a given blade tip speed, the pressure ratio of a three stage fan is related to aspect ratio, hub:tip ratio at entry and inlet flow Mach number. The values shown on these figures assume uniform inlet and outlet flows.

The adverse pressure gradients through the compression system can be reduced by reducing the annulus area through the fan and increasing the Mach number of the flow at outlet. This has an adverse effect on the pressure losses in the ducting downstream and is particularly important on an engine like the Pegasus where the front nozzles are very close to the fan and there is no room for efficient diffusion of the flow upstream of the bends leading to the nozzles. It also makes the design of the swan neck duct into the HP compressor more difficult as diffusion may have to take place through the duct to achieve the correct Mach number at entry to the HP compressor.

Figure 22

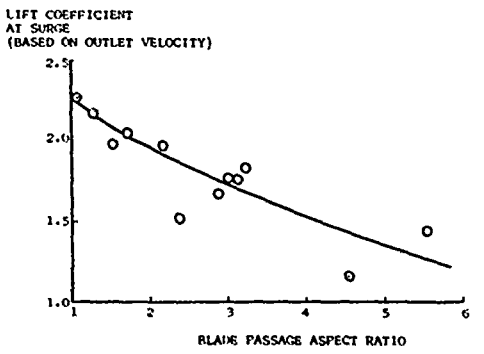

TREND OF SURGE LIFT COEFFICIENT WITH ASPECT RATIO

Figure 23

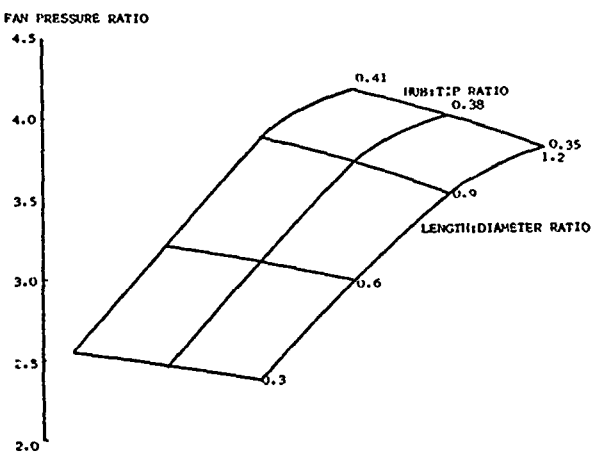

VARIATION OF FAN PRESSURE RATIO WITH GEOMETRY

CONSTANT TIP SPEED, SURGE MARGIN AND INLET MACH NUMBER

Figure 24

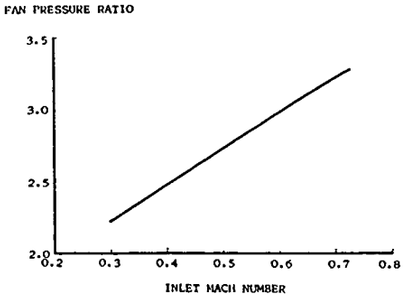

EFFECT OF INLET MACH NUMBER ON FAN PRESSURE RATIO FIXED GEOMETRY, TIP-SPEED AND SURGE MARGIN

Figure 25

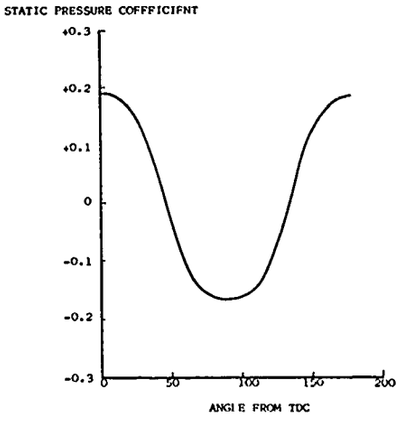

PRESSURE DISTRIBUTION AT PEGASUS FAN OUTLET

Increasing the contraction through the fan is also likely to reduce the part load surge margin and may lead to a need for variable geometry with the associated complications and weight penalty at lower fan pressure ratios than would otherwise be the case.

A non-uniform outlet pressure distribution will occur if there is asymmetric duct curvature close to the fan outlet plane. An outlet port such as required for a vectoring front nozzle system, for ducting the bypass flow away to a RALS burner or to an ejector system will introduce a circumferential static pressure distortion upstream. The magnitude of this distortion at the fan exit will depend on its distance upstream of the offtake. The measured variation at the fan exit plane on the Pegasus engine is shown on Figure 25. This distortion leads to a variation in the operating point of the last fan stage and consequently gives a variation in the pressure rise of this stage. Figure 26 shows the pressure ratio for the three stages of a Pegasus fan measured on the vertical and horizontal centre-lines where the outlet static pressure is above and below the mean value respectively.

HP Compressor Bleed for Reaction Controls

The amount of flow required for reaction controls as a percentage of the HP compressor delivery airflow depends on the magnitude of the ratio of the lift thrust to engine core airflow and on the uses for which the bleed flow is required, ie pitch trim and control and yaw and roll control or only some of these functions. Compared to the Pegasus engine in the Harrier the lift thrust of an advanced engine with augmentation may be at least twice that of the Pegasus with roughly the same core flow. In crude terms this implies an aircraft weight twice that of the Harrier which will require twice as much bleed flow for the reaction controls. Selection of bleed flow will change the operating point on the compressor characteristic apart from any overtemperaturing or thrust losses and care is required to ensure that operation can be maintained with adequate surge margin with no bleed whilst avoiding flutter when the bleed is flowing. Figure 27 is a sample characteristic of an HP compressor with the operating lines bleed on and bleed off illustrated.

Figure 26

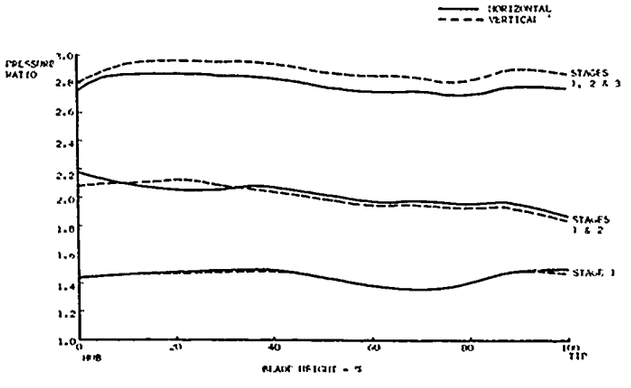

PEGASUS LP COMPRESSOR EFFECT OF EXIT DISTORTION

Figure 27

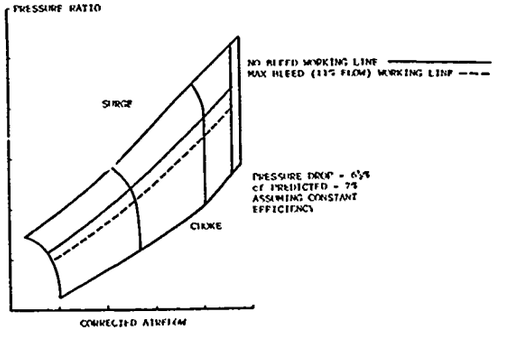

PEGASUS HP COMPRESSOR WORKING LINES

The flutter boundaries for a HP compressor are shown on Figure 28. The boundary of concern when the bleed is on is that of choked flutter. As the bleed flow is extracted the working line will drop due to the increased outlet area for the compressor delivery flow and the Mach number at exit will increase. Flutter may occur before the outlet stator throat flow is choked but if it does not it cannot occur with further increases in exit Mach number. Thus, in crude terms a choked throat flow in the outlet stator corresponds to the highest exit Mach number that may be tolerated so that a compressor with low outlet Mach numbers and little diffusion through the exit guide vane is desirable for large bleed flows. To a first approximation the variation in compressor outlet Mach number with bleed flow can be estimated and then, assuming a given amount of diffusion through the outlet guide vane, the limiting design outlet Mach number determined. One procedure for this estimation is to assume both the HP turbine entry and the final nozzle are choked, then ignoring Cp effects:

$$\sqrt{\frac{T_{EX}}{T_{IN}}} \cdot \frac{P_{IN}}{P_{EX}} = \text{CONSTANT}$$

so $\frac{T_{EX}}{T_{IN}}$ is constant because $\frac{T_{EX}}{T_{IN}} = \left(\frac{P_{EX}}{P_{IN}}\right)^{\frac{\gamma-1}{\gamma}}$

Thus $1 - \frac{T_{EX}}{T_{IN}} = \frac{\Delta T}{T_{IN}} = \text{constant} \ldots\ldots\ldots$ ③

If engine rpm is maintained as bleed flow is changed (to maintain engine thrust) then it may be assumed that the compressor temperature rise is independent of the bleed flow amount so the turbine work will also be independent of the bleed amount. As the bleed flow is increased there is less airflow through the turbine so to maintain the turbine work the temperature drop must increase

$$(W\Delta T)_{\text{NO BLEED}} = (W\Delta T)_{\text{BLEED ON}} \quad \text{so} \quad \Delta T_{\text{BLEED ON}} = \frac{\Delta T_{\text{NO BLEED}}}{1-X}$$

where x is the percentage of turbine flow diverted to the reaction controls. Therefore, the turbine inlet temperature is increased by the same factor of:

$\frac{1}{1-X}$ (from 3) and since the non-dimensional flow function:

$\frac{W\sqrt{T}}{P}$ is constant (the turbine inlet nozzles are choked) then:

$$\frac{P_{\text{BLEED ON}}}{P_{\text{NO BLEED}}} = \frac{(W\sqrt{T})_{\text{BLEED ON}}}{(W\sqrt{T})_{\text{NO BLEED}}} = \frac{1-X}{\sqrt{1-X}} = \sqrt{1-X}$$

So, assuming the compressor characteristic is vertical ie changes in back pressure do not change the airflow, and noting in this case that the compressor temperature rise is assumed constant, the compressor outlet flow function will increase solely because of the reduction in the delivery pressure by the factor $\sqrt{(1-X)}$. This is the most optimistic situation. Alternatively, it may be assumed that the compressor efficiency is constant so that as the delivery pressure is reduced with the increase of bleed flow the compressor temperature rise is also reduced. This will reduce the turbine work requirement and hence the turbine inlet temperature thus increasing the effective nozzle area for the compressor outlet flow. This represents the other extreme from assuming a constant compressor temperature rise. No simple expression can be derived and the pressure drop is a function of the HP compressor pressure ratio. However, for a pressure ratio of 6:1 the pressure drop due to bleed is approximately three quarters of the bleed flow demand compared to roughly one half when the compressor temperature rise is assumed constant.

COMPRESSOR MAP SHOWING BOUNDARIES FOR FOUR TYPES OF FLUTTER

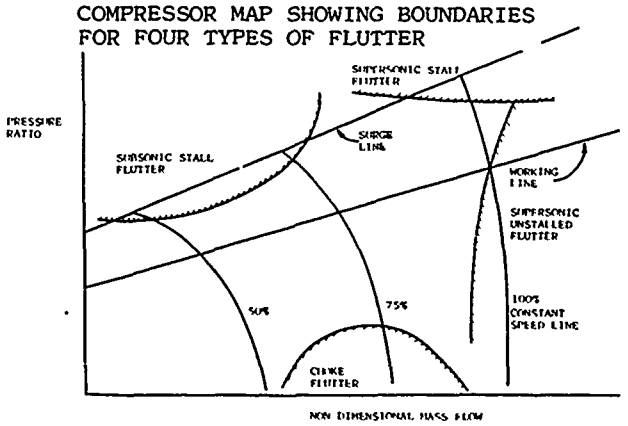

Figure 28

EFFECT OF HP COMPRESSOR DELIVERY BLEED ON STATOR THROAT AND OUTLET MACH NUMBER

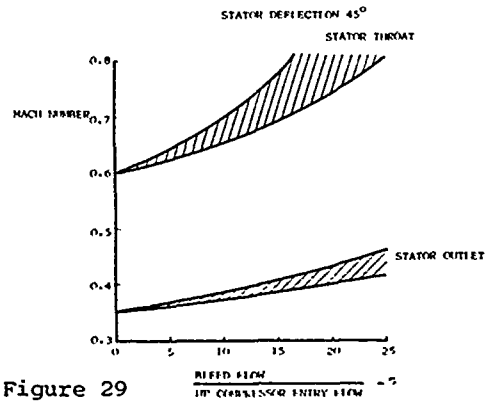

Figure 29

Figure 29 shows the variation in stator outlet and throat Mach numbers with bleed flow derived by the above methods and with the assumptions shown on the figure. With similar assumptions regarding the diffusion through the outlet guide vanes, Figure 30 shows how the design cutlet Mach number needs to change with bleed flow requirement. Although this shows that relatively large flows may be bled without requiring unreasonably low compressor design outlet Mach numbers, it must be remembered that the increase in Mach number with bleed leads to higher combustion chamber entry diffuser losses and may effect the aerodynamic flows in the combustion chamber.

The position and detailed design of the bleed manifold itself also has an effect on the combustion chamber flow conditions and the outlet temperature distribution. Figures 31, 32, 33 and 34 are diagrams of a number of different bleed manifold porting arrangements tried on the Pegasus. Results of the combustion chamber outlet temperature distribution measurements for these arrangements are shown on Figure 36. This shows how the temperature distribution is sensitive to the particular manifold arrangement for no bleed flow and it also shows the variation with bleed flow. For comparison the results of measurements made on a civil high bypass ratio turbofan (bled to an unusually high degree) with a different bleed arrangement (Figure 35) are also shown.

Figure 30

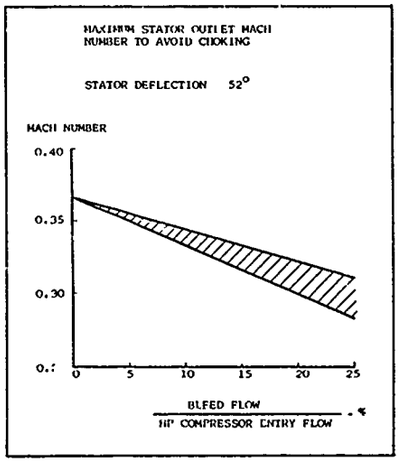

HP COMPRESSOR DELIVERY BLEED EFFECTS

Figure 31

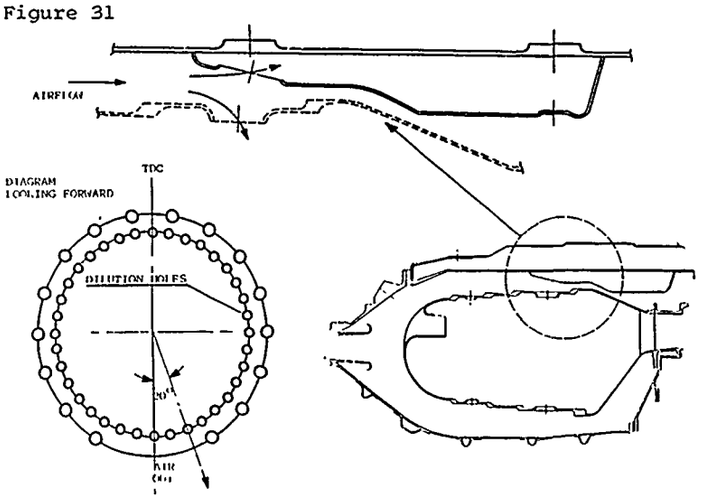

PEGASUS BLEED PORT ARRARGEMENT CONFIGURATION 1

Figure 32

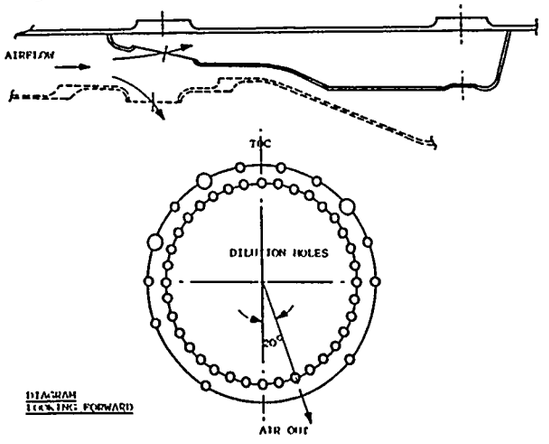

PEGASUS BLEED PORT ARRANGEMENT CONFIGURATION 2

Figure 33

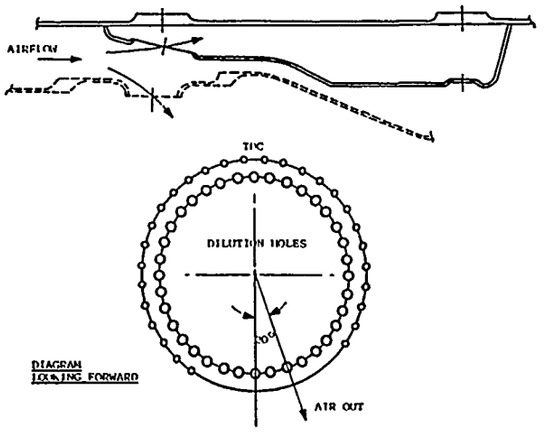

PEGASUS BLEED PORT ARRANGEMENT CONFIGURATION 3

LP Turbine

On vectored thrust engines in particular, the need to keep frontal area as small as possible requires a small diameter HP compressor system (since the plenum chamber leading to the front nozzles is around this component) which in turn leads to a small diameter combustor, HP turbine and LP turbine. The main aerodynamics problems are introduced with the need to keep the LP turbine diameter small. This means a low hub:tip ratio and a low mean blade speed requiring high loading to avoid the penalty of additional stages. Figure 37 shows the effect of loading on efficiency. Noted on this curve is the Pegasus LP turbine which falls some way short of the band covering the majority of the data. This shortfall is caused by the high outlet Mach number on the Pegasus turbine, also due to the need to keep the outlet diameter as small as possible and also by the non-uniform outlet static pressure caused by the bifurcated exhaust system.

Figure 34

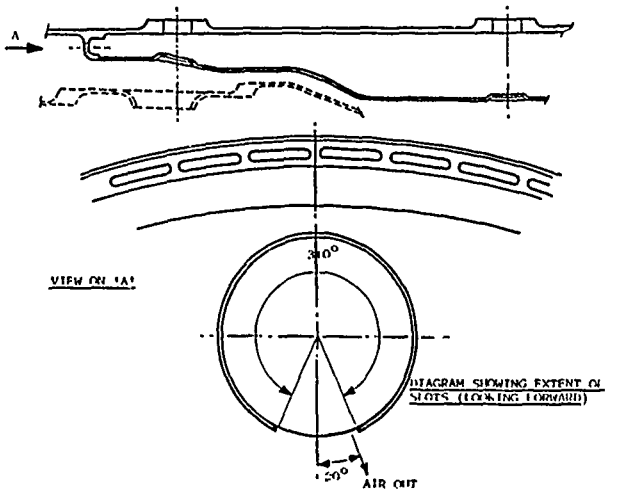

PEGASUS BLEED PORT ARRANGEMENT
CONFIGURATION 4

Figure 35

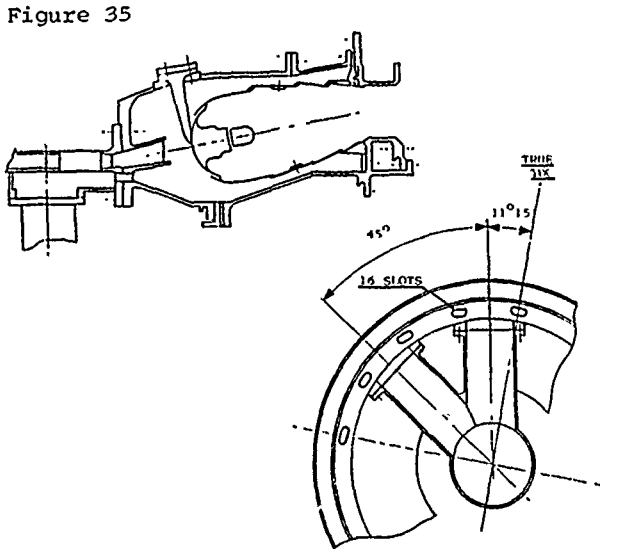

RB401 BLEED SYSTEM
CONFIGURATION 5

Figure 36

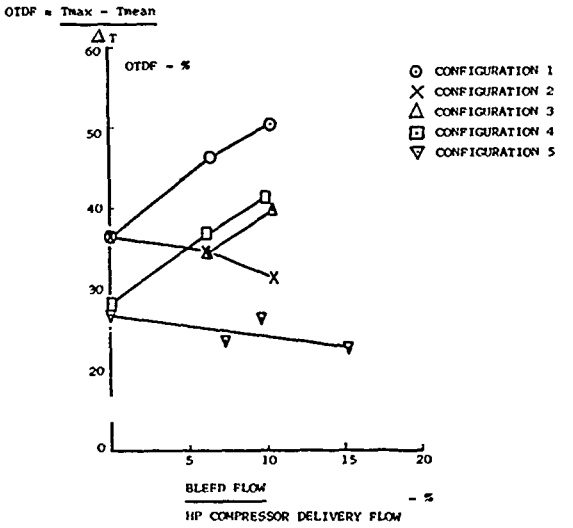

EFFECT OF BLEED FLOW ON COMBUSTION CHAMBER OTDF

Figure 37

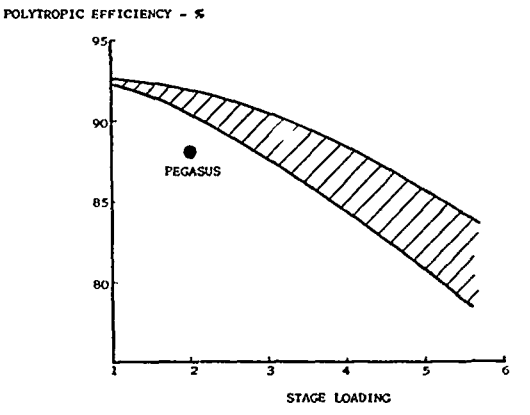

LP TURBINE EFFICIENCY

The critical region in the turbine is the hub and a high loading may imply diffusion through the rotor blade and negative work (the flow is being compressed) which if too severe will lead to separation. Figure 38 shows how the exit Mach number changes with stage duty and overall diameter (hub:tip ratio). Eventually, an additional stage with the related cooling, cost and weight penalties will be necessary.

There is little evidence available on the effect of a non-uniform back pressure on the turbine aerodynamics. One effect that could be directly measured on the Pegasus engine was the reduction in efficiency caused by the need to fit wire lacing to the rotor blade to reduce vibration although tip shrouds would achieve the same objective without an efficiency loss. Some test work has been carried out on the Pegasus engine with the standard exhaust system and a 'straight through' exhaust system which removes the pressure non-uniformities. In this case the measured change of performance is due to the change in the exhaust system thrust efficiency as well as to changes in the turbine efficiency.

Figure 39 (taken from the test report) shows the changes in both the turbine efficiency and in the overall thrust efficiency of the engine exhaust system. It will be noted that a small improvement in turbine efficiency (of the order of 1%) is achieved with the 'straight through' system. By far the bigger gain occurs from the change in the thrust efficiency.

Figure 38

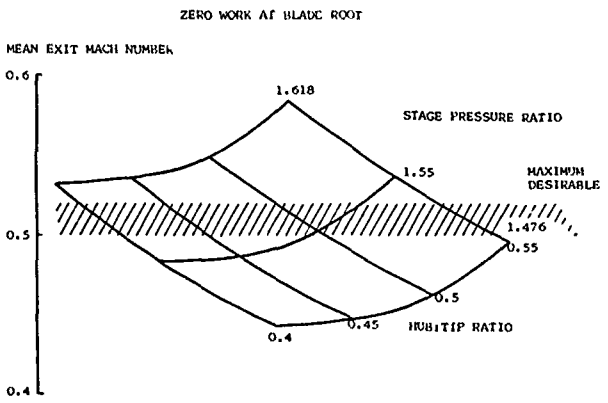

PEGASUS LP TURBINE FINAL STAGE

Figure 39

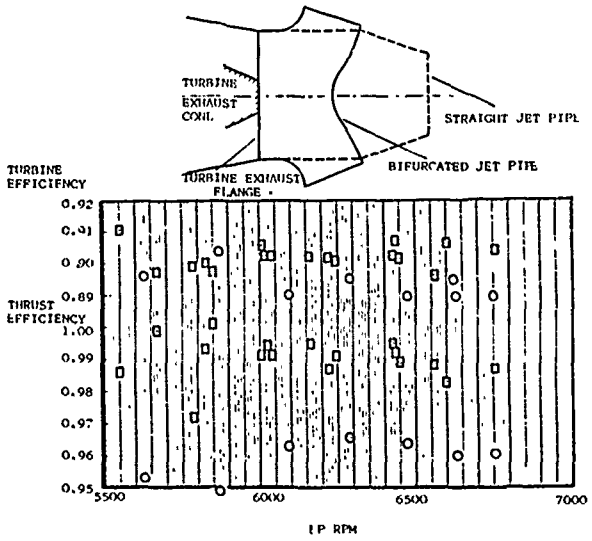

PEGASUS Mk 101 EXHAUST LOSS TESTS

Exhaust System

The four main elements to be considered in the design and specification of the exhaust system for a V/STOL powerplant are:

- performance, which is not only directly affected by the thrust efficiency of the final nozzle but by the pressure losses incurred by directing the exhaust gas through the required angle to achieve the appropriate thrust direction.
- effective flow area, which may change with the thrust direction on a nominally constant area geometry.
- thrust line. This must be considered as the sum of two parts, the direction of the thrust which may not coincide with the geometric deflection of the nozzle, depending on the particular nozzle geometry and the position of the line of action of the thrust which will probably not be at the centre of area of the nozzle outlet section.
- non-uniform back pressure effects on the engine rotating machinery (fan and turbine) due to directing the flow away from the engine centreline. The effect of this on the engine has been covered earlier.

To maximise the thrust efficiency of the exhaust system it is imperative to reduce the bend losses to a minimum. One method of doing this is to reduce the bend angles and Figure 40 shows how the overall exhaust system thrust efficiency (ie from the fan or LP turbine exit to atmosphere) varies with the total turning in the system - as would be expected, as the amount of turning increases the thrust efficiency decreases. With a horizontal engine attitude the minimum bend angle is 90^{o} but for the 'elbow' vectoring nozzles on the Pegasus this value is impossible to achieve although by drooping and trailing the nozzle bearings (Figure 41) the total turning can be reduced to about 110^{o} which gives a large increase in thrust performance compared to the existing system. The thrust performance also depends on the Mach number through the system but for practical purposes this is fixed by the outlet Mach number from the fan or the LP turbine and little benefit is derived from diffusing to a lower Mach number. This is because of the need to keep the axial length of the system as short as possible so that the diffusion has to be carried out around the initial bends. Normally benefits can only be obtained if the diffusion is carried out sufficiently far upstream of the bend as may be the case with a vectoring nozzle downstream of a reheat system. It might be expected that the bend radius ratio is an important feature affecting performance but because of the need to keep the thrust line as far forward as possible, this parameter does not appear to have been studied in depth. Figure 42 shows the variation of thrust efficiency for a single vectoring nozzle with differing effective radius ratios made up by a combination of a large radius and sharp bends. Also shown is the variation of nozzle discharge coefficient.

It has been found that the shape of the thrust efficiency curve as a function of the system pressure ratio can be reproduced by assuming that the thrust loss is composed of two components, that due to a total pressure loss which is assumed to be created by the initial diffusion and the bends and the loss due to the nozzle itself. Figure 43 shows a comparison between the predicted and measured thrust efficiencies for two geometries. Although reasonable agreement can be demonstrated, in several cases an interference effect is present which increases the pressure loss so that it is greater than would be predicted from bend loss data.

The effective flow area of the nozzle (its discharge coefficient) should remain constant over the full range of angles to avoid internal rematching of the engine during thrust vectoring. For single nozzle vectoring systems the increasing pressure loss with increasing bend angle implies a lower discharge coefficient vectored compared to non-vectored (Figure 42). One of the demands on the nozzle designer may be to devise a system which adjusts the geometric exit area to maintain a constant effective area as the nozzle is vectored. This problem does not arise to the same extent in the case of 'elbow' nozzles. As will be noted from Figure 44 the discharge coefficients differ much less between the horizontal and vertical positions than for the single vectoring nozzle. The similar levels of both thrust and discharge coefficients imply roughly similar total pressure losses in both nozzle positions.

Figure 40

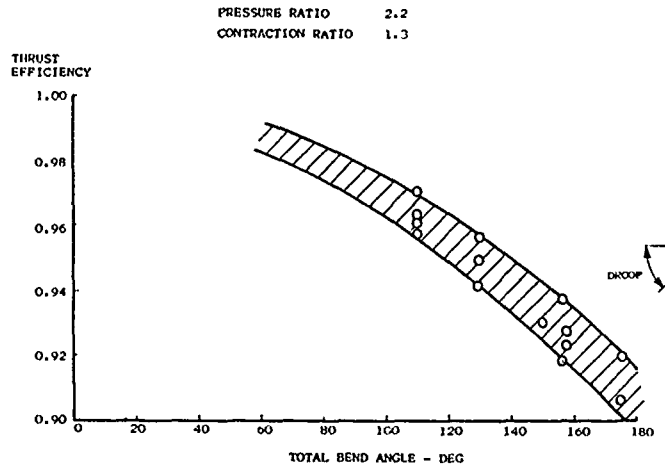

EFFECT OF TURNING ON THRUST EFFICIENCY

Figure 41

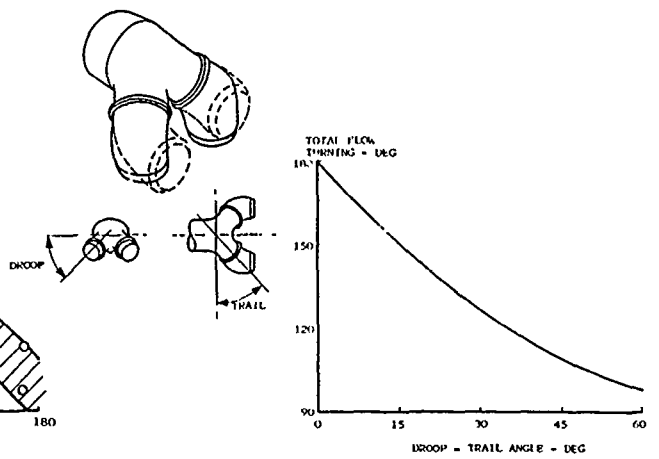

'DROOP' AND 'TRAIL' FOR ELBOW NOZZLES
REDUCTION OF FLOW TURNING
NO HORIZONTAL OR VERTICAL SPLAY

While failure to achieve the exact amount of turning of the thrust during vectoring may not be critical, since a certain amount of geometric under or overturning may be used to correct any errors, the position of the thrust line when the nozzle is vertical is of much greater importance. The momentum of the flow through the engine in the axial direction generally causes the thrust line to be rearwards of the centre of area of the nozzle throat section. An error in determining the true position of this thrust line directly affects the aircraft balance in the jet lift condition and will demand a correction from the reaction control system with the associated thrust loss. There are surprisingly little data available on the subject of thrust line position, partly because, in the past thrust measuring rigs have not been designed to measure it. However, Figure 45 shows that the thrust line may be rearwards of the nozzle centreline by as much as 15% of the width of the nozzle.

Figure 42

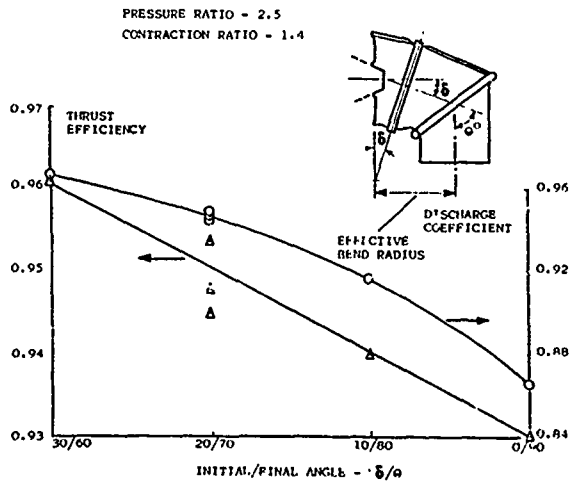

PERFORMANCE OF SINGLE, AXISYMMETRIC VECTORING NOZZLE

Figure 43

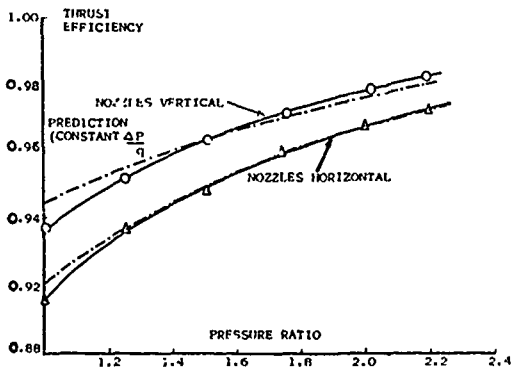

COMPARISON OF PREDICTED AND MEASURED THRUST PERFORMANCE
PEGASUS TYPE REAR NOZZLES

Figure 44

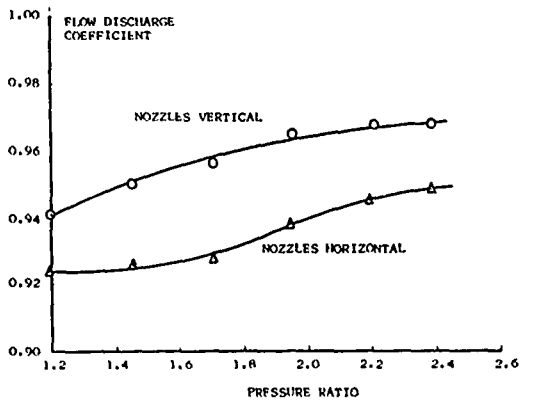

VARIATION OF NOZZLE DISCHARGE COEFFICIENT PEGASUS TYPE REAR NOZZLES

Figure 45

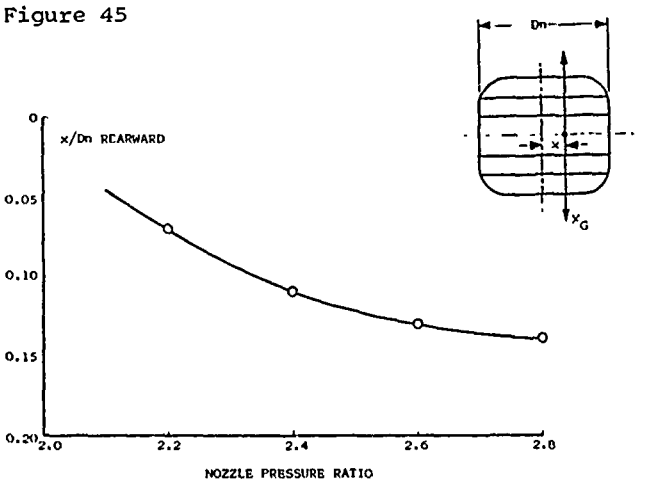

PEGASUS 6 THRUST CENTRE MODEL POSITION OF CENTRE OF THRUST FOR REAR NOZZLE PAIR

So far, only internal nozzle flow effects have been discussed. When the installed performance with external flow is considered the main interest is with side nozzles, particularly variable area nozzles for a vectored thrust engine with PCB. Unfortunately, few answers exist to numerous questions, two of which are:

- two dimensional or axisymmetric nozzles
- separated or attached jet flow

The aerodynamicist cannot isolate himself when trying to resolve these questions. A two dimensional nozzle may integrate better with the fuselage and reduce the total cross sectional area slightly but it will be much more difficult to keep the jet flow away from the fuselage surface should it be thought necessary so to do to avoid structural overheating. While it may be easier to keep an axisymmetric jet away from the fuselage surface, the need to provide a variable throat area will introduce base area when operating at low PCB temperatures or in the non-augmented condition.

The only method to maintain a separated jet flow is to inject additional airflow into the space between the jet boundary and the fuselage. To avoid drag penalties this airflow needs to be at or close to free stream total pressure which in turn demands a clean entry into the base region of the nozzle/fuselage combination over and past the nozzle duct and bearing. Figure 46 illustrates one method of achieving this and includes some results obtained in a wind tunnel using hot jets.

Engine/Intake Compatibility

The major differences between V/STOL engines and CTOL engines on the subject of compatibility are:

- total pressure distortion may be more intense and more localised because the intake duct length on a V/STOL installation will tend to be shorter allowing less mixing of lip separations.
- there will be much greater levels of intake temperature distortion caused by hot gas reingestion when operating in ground effect with the exhaust nozzles vertical.
- the short intake length may lead to rapid duct curvature close to the engine entry plane which will introduce a non-uniform static pressure across the engine face.

While the first two of the above include both steady state and time dependent distortions the last is only a steady state effect. In all cases the distortion is really a change in the velocity and the direction (particularly when swirl is present) of the flow approaching the rotor. Pressure and temperature distortion indices are used mainly for convenience since these quantities can be measured more easily than velocity.

Flow distortion may change the compressor characteristic and in particular it may reduce the surge margin ie the margin between the operating line and the surge line of the compressor. Although the most sensible method of defining surge margin would appear to be at a constant rotational speed there are a number of different definitions. The methodology adopted by the SAE is to define the surge margin at a constant corrected airflow:

$$\text{surge margin} = \frac{\text{present ratio at surge}}{\text{operating pressure ratio}} - 1$$

The loss of surge margin due to inlet flow distortion may then be related to the reduction in the surge pressure ratio as shown on Figure 47.

Figure 46

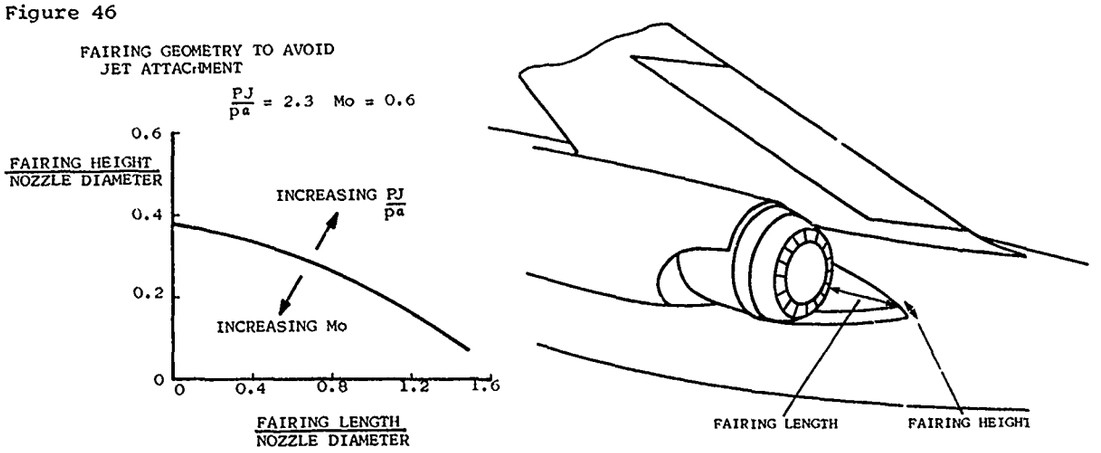

VECTORED THRUST SIDE NOZZLE INSTALLATION

Figure 47

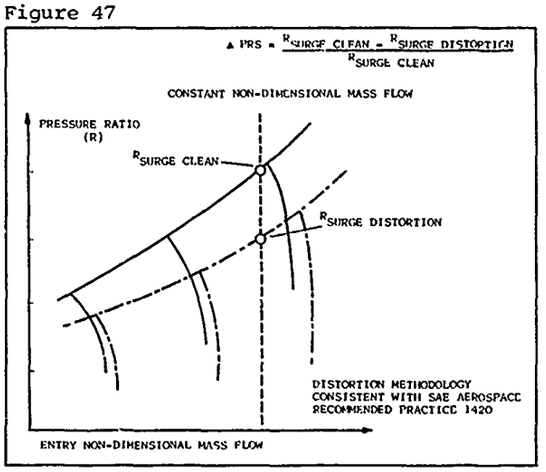

SURGE PRESSURE RATIO LOSS (Δ PRS)

igure 48

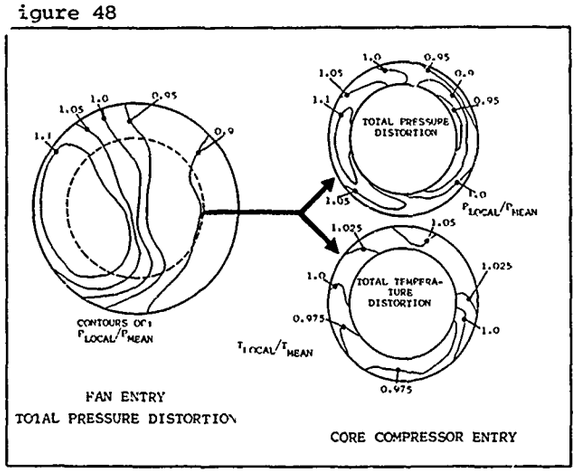

FAN INLET DISTORTION TRANSFER CHARACTERISTICS

One method of predicting the effect of distortion is to use the parallel compressor model. In this case the compressor is assumed to be divided into two parts both exhausting into the same outlet pressure. One part is assumed to receive the airflow in the nominal undisturbed state and the other receives flow at a state corresponding to the mean over the region of the distorted flow. The circumferential extent of the distorted flow which is necessary to reduce surge pressure ratio depends on the particular compressor design. It is affected by the characteristics of the individual stages and depends on whether the distortion is attenuated or magnified through the compressor. Regardless of any change in the surge pressure ratio a pressure distortion at inlet will lead to both pressure and temperature distortions at outlet, (Figure 48), so that a HP compressor may have to accept temperature distortions although the fan may not.

Temperature Distortion

The radial content of any temperature distortion is particularly significant from a performance viewpoint. High temperature flow entering the core will have a much greater impact on engine thrust than if it enters the bypass duct. The following table is an example which shows the effect on thrust of a 10°C intake temperature rise in the total intake airflow, in the core airflow only and in the bypass airflow only. It needs to be emphasised that this is a somewhat artificial comparison since the effect of radial distortion on the compression system is ignored and the total heat content implied by the above numbers is varying. To compare for the same total heat content requires a correction involving the engine bypass ratio, for example if the bypass ratio is unity a mean intake temperature rise of 10°C is equivalent to a 20°C rise in either the core flow or the bypass flow.

Unmixed engine (bypass ratio ~ 1.3) at sea level, static condition

Effect of 10°C temperature rise to airflow

Airflow at increased temperature	Thrust loss %
Total engine	~ 7
Core only	~ 7
Bypass only	~ 1

No direct information showing the effect of radial temperature distortion is available but Figure 49 shows the effect of a radial pressure distortion can be favourable and it may be speculated that a temperature distortion could show a similar benefit.

The index used to describe steady state circumferential temperature distortions in general is:

$$TC(\Theta) = \frac{T_{max}}{\overline{T}} - 1 \quad \text{where}$$

T max is the highest average temperature in a segment with a critical angle Θ and $\overline{T}$ is the mean total temperature. This distortion index may be defined for a number of different regions ie at entry to the whole fan, at entry to the fan but in the annulus supplying the core flow only and at the entry to the HP compressor. In addition the critical angle may vary from engine to engine and a correlation of the loss of surge pressure ratio as a function of TC (Θ) is shown on Figure 50 for a number of different engines where Θ varies from 60° to 180°.

A likely phenomenon is a combination of both temperature and pressure distortion where, for example, the temperature rise due to hot gas reingestion may be superimposed on the pressure distortion due to the intake. Figure 51 shows the effect of a superimposed pressure and temperature distortion on the surge pressure ratio loss of an HP compressor. The maximum temperature and minimum pressure were superimposed and it will be noted that the effect is additive. It is possible to predict the effect of combined pressure and temperature distortions using the parallel compressor model and Figure 52 is a comparison of the measured loss in surge pressure ratio with the calculated loss using this approach.

Figure 49

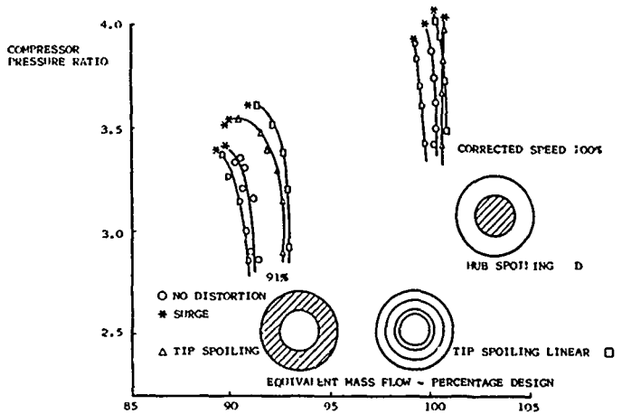

RADIAL DISTORTION EFFECTS

Figure 50

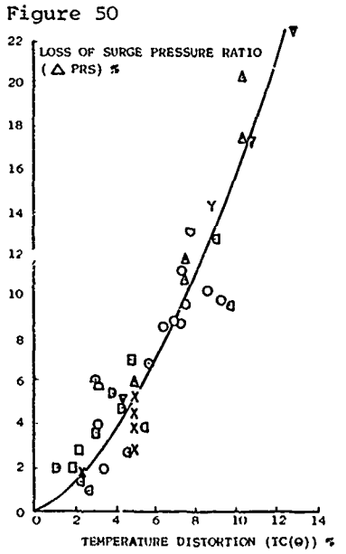

LOSS OF SURGE PRESSURE RATIO

Figure 51

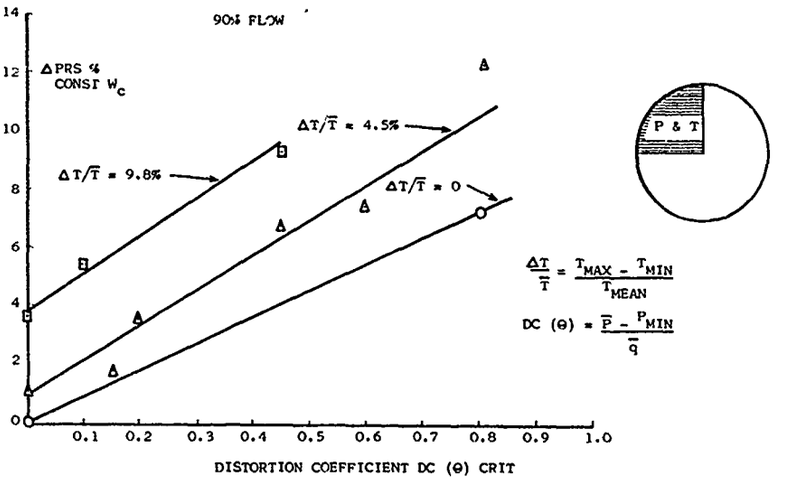

SUPERIMPOSED PRESSURE & TEMPERATURE DISTORTION

Static Pressure Distortion

As mentioned previously, the intakes for V/STOL propulsion systems tend to be much shorter than those for CTOL engines, particularly in the case of the vectored thrust type of lift engine. These short intakes imply high duct or flow curvature adjacent to the engine entry plane which, even if there is no total pressure distortion, will lead to a variation of static pressure to maintain radial equilibrium. Figure 53 is an example of the static pressure distortion and hence velocity due to the Harrier air intake. The distortion can be reduced, if there is sufficient room by either introducing a cylindrical section of duct between the bend and the engine face or by reducing the bend curvature and Figure 54 shows both how the distortion is predicted to vary with length and the results of measurements on intake duct models.

Full scale engine tests have also been carried out with a short highly curved bifurcated intake and a number of parallel extension pieces fitted between the intake and the engine. The results of these tests are summarised on Figure 55 which shows that large increases in thrust are possible with relatively small lengths of duct extension, particularly if the engine is operating at its limiting temperature.

Figure 52

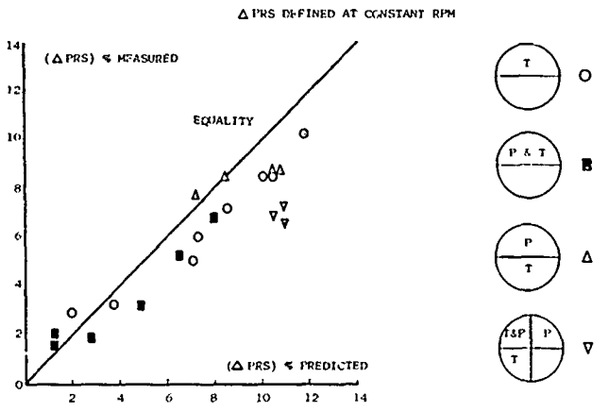

COMBINED TEMPERATURE AND PRESSURE DISTORTION

Figure 53

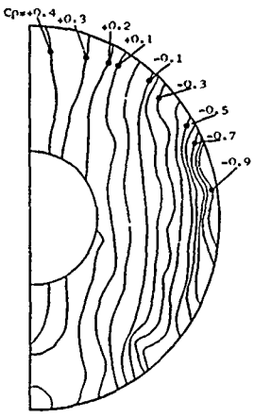

SHORT, HIGHLY CURVED INTAKE VARIATION OF STATIC PRESSURE AT ENGINE FACE

Figure 54

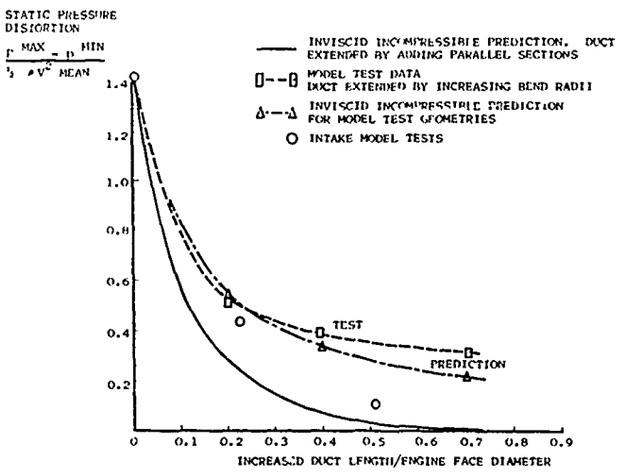

SHORT, HIGHLY CURVED INTAKE STATIC PRESSURE DISTORTION EFFECT OF INCREASING DUCT LENGTH

Figure 55

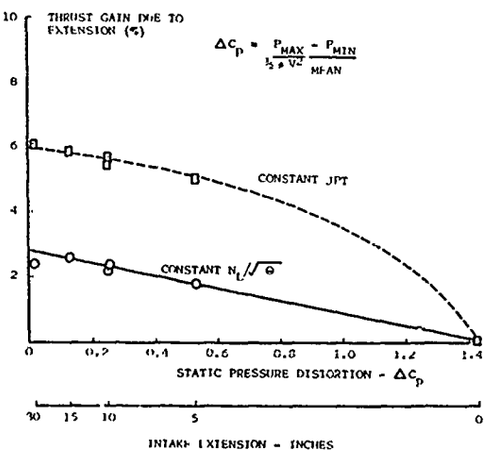

SHORT, HIGHLY CURVED INTAKE EFFECT ON ENGINE THRUST BY REDUCING STATIC PRESSURE DISTORTION

Air Intake

In general the air intake requirements for V/STOL powerplants will be similar to those for CTOL engines with two major differences, viz:

- the necessity for high total pressure recovery down to zero forward speed. This is because it is essential that the engine be provided with the best quality airflow during jet borne operation and a high recovery not only ensures the availability of the maximum thrust and hence the minimum engine size but is a guarantee of low total pressure distortion.

- in some cases the ability to operate efficiently at high angles of incidence (up to 90^{o}) at low flight speeds. This requirement applies to both tilt nacelle systems and to lift engines which are fixed in the fuselage.

The pressure recovery at zero forward speeds for a fixed intake geometry is primarily a function of the lip contraction ratio (defined as the ratio of the highlight to throat areas). This area is required to support the suction pressures that balance the momentum of the intake airflow. In incompressible flow:

$$(\bar{p}_L - p_\alpha)\, A_L + \frac{WV}{g} + (p_1 - p_\alpha)\, A_1 = 0$$

so $\bar{C}p_L\, A_L + 2A_1 - A_1 = 0$ since for no total pressure loss

$p_\alpha = P_1$ so $p_1 - p_\alpha = -q_1$

so $\bar{C}p_L = -\frac{A_1}{A_L} = -\frac{1}{CR - 1}$ when CR is the lip contraction ratio.

In practice there is a minimum value of lip area (contraction ratio) for which no intake total pressure loss is possible, since low values of contraction ratio imply a high negative value of Cp leading to flow separation due to the adverse pressure gradient in recompressing to the duct static pressure. The variation of total pressure recovery with lip contraction ratio is shown on Figure 56 for axisymmetric pitot intakes with a throat Mach number of 0.6. Deviations from this ideal shape will require an increase in contraction ratio to achieve zero total pressure loss. A combination of the lip/fuselage junction and duct curvature as on the Harrier is unable to provide this ideal pressure recovery even with a contraction ratio of over 1.3:1. The other extreme is when the lip is sharp, as may be required for a supersonic intake. In this case, assuming no lip force whatsoever the total pressure loss can be determined as follows:

$$\frac{WV}{g} + \left[(p_1 - P_1) + (P_1 - p_\alpha)\right] A_1 = 0 \qquad \text{so } 1 + \frac{P_1 - p_\alpha}{q_1} = 0 \qquad \text{ie } \frac{\Delta H}{q_1} = 1$$

A large contraction ratio may be undesirable for other reasons. On a subsonic aircraft the spillage drag in cruising flight can be minimised by providing sufficient external cowl surface area to support suction pressures capable of cancelling the force on the pre-entry streamtube. However, the greater the highlight area the greater the cowl area required (Figure 57). Similarly, at supersonic speeds a blunt lip also creates a high drag (Figure 58). Consequently, some way of maintaining high pressure recovery at zero forward speeds without incurring high drag in cruising flight is necessary and Figure 59 shows some of the many ideas proposed. The majority of these is some form of auxiliary inlet. It must be stated here that the use of an auxiliary inlet does not suppress a lip separation on a low contraction ratio inlet. The function of the auxiliary inlet is to reduce the flow Mach number past the main inlet lip and hence reduce the total pressure loss by reducing the dynamic head. The total pressure loss at the engine entry plane will be further reduced if the auxiliary system can be designed with sufficient contraction ratio to avoid losses so that the flow entering the main intake is mixed with the auxiliary flow which is then at a higher total pressure.

Figure 56

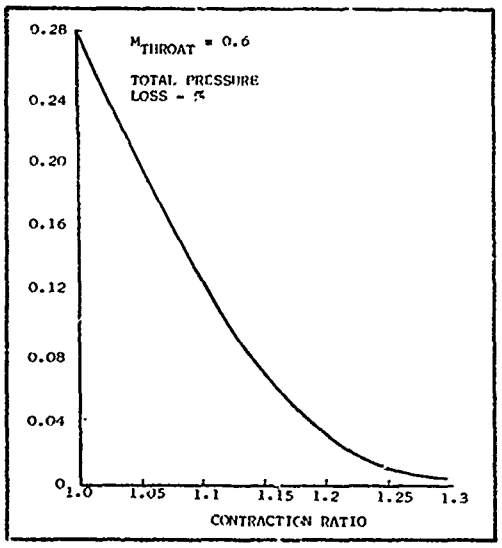

AXISYMMETRIC AIR INTAKES
GROUND RUNNING TOTAL PRESSURE LOSS

Figure 57

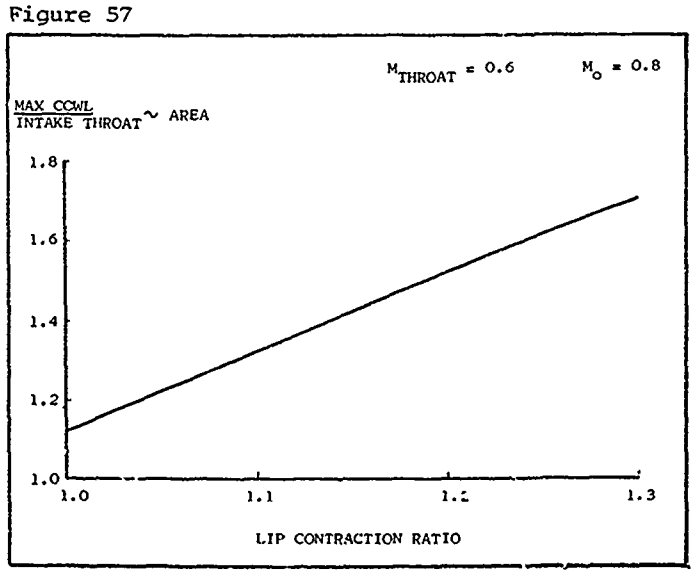

COWL AREA FOR NO SPILLAGE DRAG

Figure 58

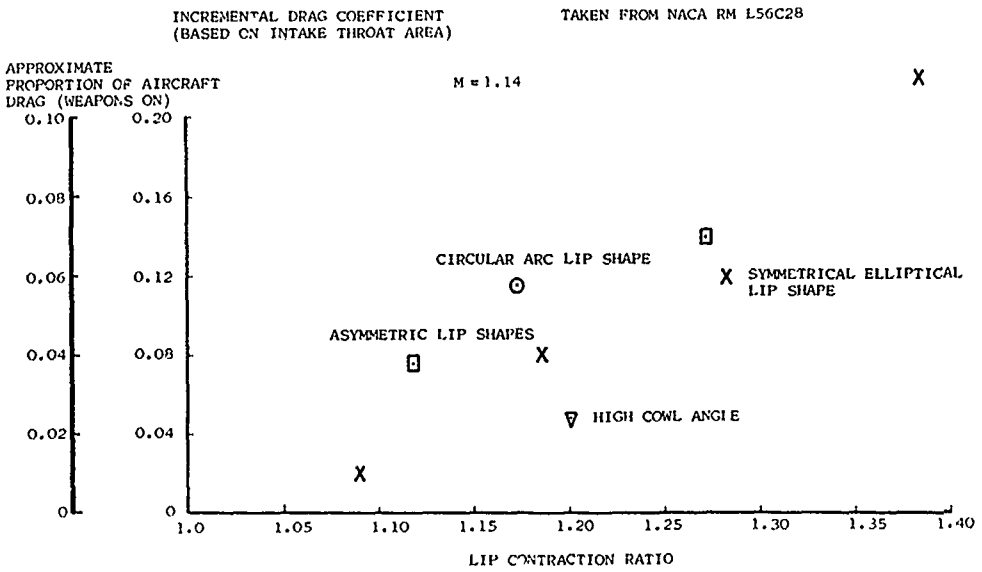

EFFECT OF LIP BLUNTNESS ON SUPERSONIC DRAG

Figure 59

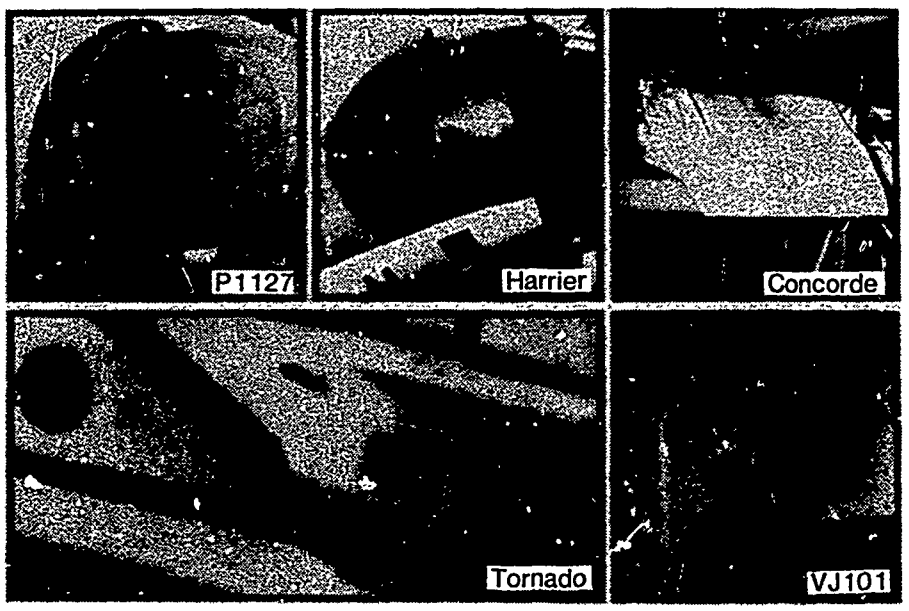

ALTERNATIVE LOW DRAG/HIGH PRESSURE RECOVERY INTAKES

The tilt nacelle system requires intakes which operate efficiently at high angles of incidence during the initial stages of both accelerating and decellerating aircraft transition and the fuselage installed fixed lift engine may be treated as a special case of the tilt nacelle intake problem in so far as the intake is at a fixed angle of incidence. An additional problem occuring with the lift engine intake, however, is that the engine has to be started at relatively high forward speeds at the commencement of a decellerating transition.

The conditions (angle of incidence and mass flow ratio) that the tilt nacelle intake system has to operate under depends on the particular aircraft and the decellerating transition requirements. The most severe problem is likely to occur at the start of the transition in which case high nacelle incidence is desirable to reduce the propulsive force as much as possible and engine thrust must be low to avoid too much lift. As aircraft speed reduces the engine thrust must increase, increasing mass flow ratio and improving the intake flow conditions. A great deal of work has been carried out to study the intake performance in these conditions for subsonic aircraft mainly as a result of the interest shown in tilt nacelle systems for multi-mission V/STOL naval aircraft. This work has shown that high pressure recovery and low distortion can be achieved in a sufficiently wide corridor of operating conditions (Figure 60) to permit satisfactory decellerating transitions to be performed without risk of engine surge or severe thrust losses. An intake designed for supersonic speeds will need an auxiliary inlet to achieve satisfactory flow conditions at the engine entry plane during the landing transition and Figure 61 shows the variation in pressure loss with inlet velocity ratio for such an intake. Figure 62 shows the operating range during actual landing transitions with such a tilt nacelle system compared with the measured engine surge boundary.

Figure 60

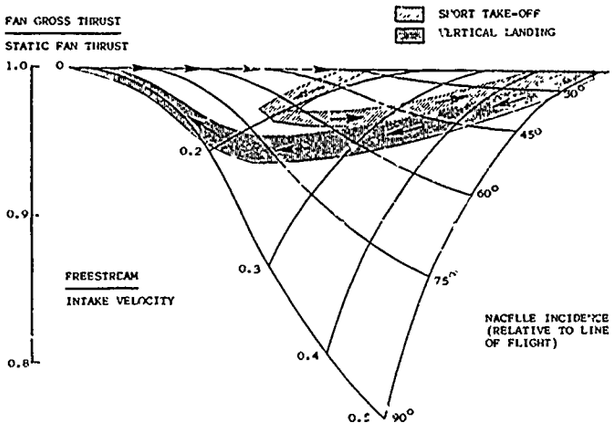

SUBSONIC TILT NACELLE
INTAKE PERFORMANCE AT LOW SPEEDS

Figure 61

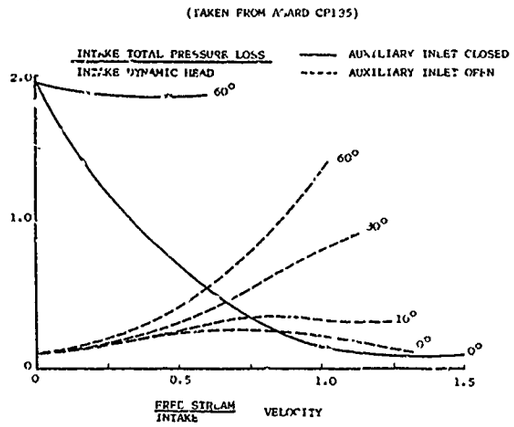

PRESSURE LOSS FOR SHARP LIP TILT
NACELLE INTAKE

Much development work on lift engine intakes has been carried out mainly to solve the problem of obtaining satisfactory flow conditions for engine start-up at the start of a decellerating transition. In this regime the inlet mass flow ratio is low and the intake behaves as a static pressure tapping with a recirculating flow within the duct. Figure 63 shows the variation of pressure loss as a function of mass flow ratio for a single life engine intake operating in a 90° cross flow. In order to improve the pressure recovery at low mass flow ratios a number of different approaches have been tried and reached various stages of development. The system used on the VAK 191B and the VJ 101 where the inlet doors can be raised to form a scoop for low mass flow operation and then spring loaded shutters in the surface of the door can open for operation at high mass flow ratios are also shown on Figure 63. Another approach has been to use high pressure blowing on the windward area of the lip to suppress flow separation. Figure 64 shows the effect of this on total pressure recovery and flow distortion.

Concluding Remarks

It is hoped that the foregoing illustrates some of the factors to be considered by the aerodynamicist in the design of V/STOL propulsion systems. As will have been noted in many instances some compromise is necessary purely in an aerodynamic sense. However, the aerodynamicist cannot work in isolation, there are many other considerations - eg weight, volume and mechanical design - which will not only demand many more compromises but also the need for close working with other specialist areas. Close cooperation with the airframe manufacturer is also essential to develop the best installation for the propulsion system.

Figure 62

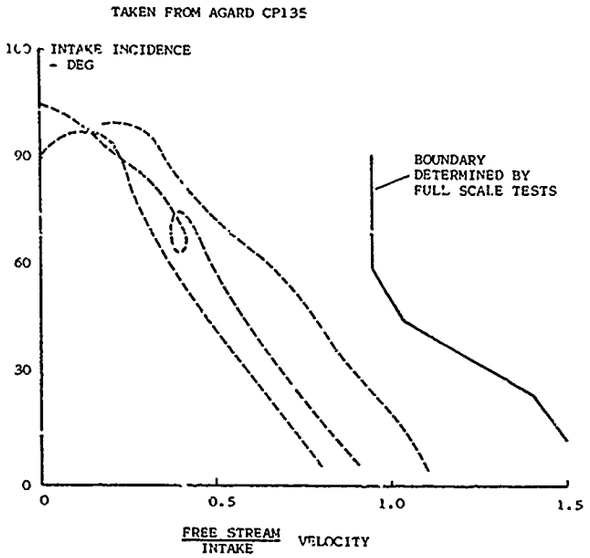

TILT NACELLE LANDING TRANSITIONS

Figure 63

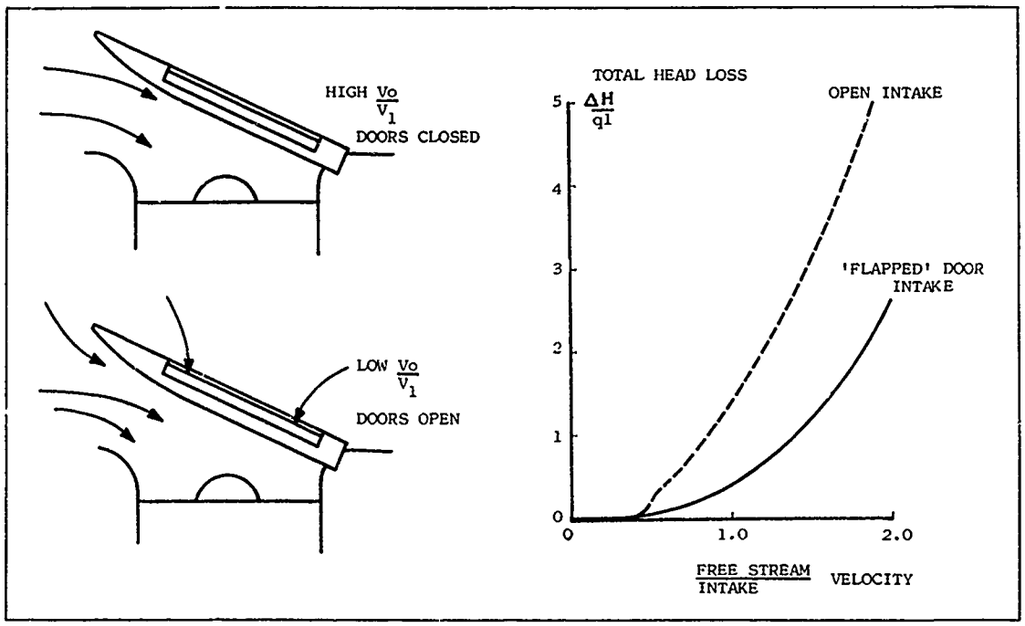

LIFT ENGINE INTAKE PERFORMANCE

Figure 64

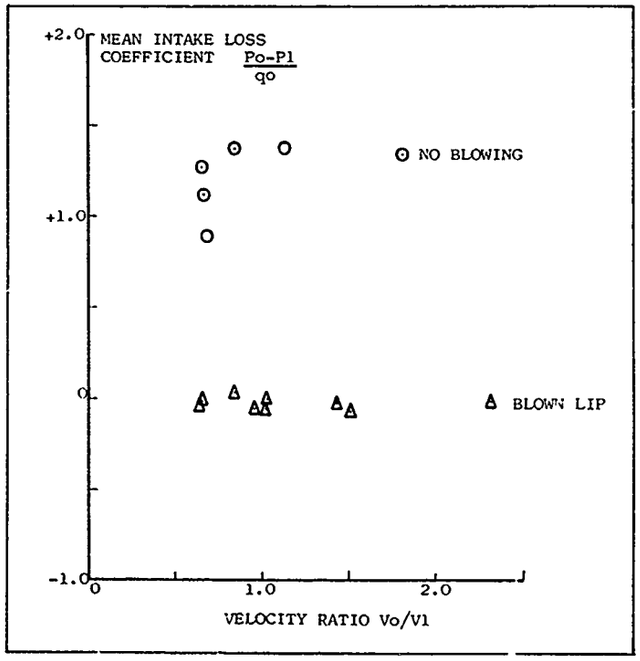

EFFECT OF LIP BLOWING ON LIFT ENGINE INTAKE LOSS

JET FLOWFIELDS*

by

+Donald R.Kotansky
McDonnell Aircraft Company
McDonnell Douglas Corporation
P.O. Box 516
St. Louis, MO 63066
USA

SUMMARY

The design and development of high performance military V/STOL aircraft requires an efficient blend of new airframe and propulsion lift system technology with advanced CTOL high speed aircraft characteristics. Although the design process is driven by requirements throughout the aircraft flight envelope, the takeoff, landing, and transitional operations present the configuration analyst with a unique set of design requirements whether VTOL or STOL operations are desired. Although the aerodynamics of "up-and-away" flight are relatively well understood, having been the subject of theoretical and applied aerodynamics for more than 75 years, the aerodynamics of V/STOL operations, especially in ground effect, have received far less attention even though the aero/fluid mechanics of the flowfields encountered are extremely complicated.

This lecture will attempt to describe the unique aero/fluid mechanics of V/STOL jet flowfields both in and out of ground effect and how they influence and may be accommodated in the aircraft design process. Key topics to be addressed include the following:

- o Jet development in static and cross-flow conditions, jet impingement (round jets/rectangular jets including nozzle pressure ratio and temperature effects),
- o Multiple jet impingement and fountain upwash formation and development (ground surface flows, stagnation lines, fountain characteristics),
- o Fountain impingement on the airframe,
- o Jet induced effects on the airframe in and out of ground effect including trim and stability considerations,
- o Effects of forward (STOL) and cross-wind velocities, and
- o Exhaust gas ingestion (VTOL, STOL).

Discussion of the above items will include their influence on vehicle design and system performance and their quantification and prediction via the following:

- o Theoretical and empirical predictions, and
- o Small and large scale wind tunnel tests.

Aero/propulsion devices to be discussed include V/STOL multiple jet lift systems (low and high pressure ratio) and STOL thrust vectoring/reversing nozzles.

Ground Effect:

An engineering methodology based on an empirical data base and analytical fluid dynamic models has been developed for the prediction of propulsive lift system induced aerodynamic effects for multiple lift jet VTOL aircraft operating in the hover mode in and out of ground effect. The methodology takes into account the effects of aircraft geometry, aircraft orientation (pitch, roll) as well as height above ground. Lift jet vector and splay directions with respect to the airframe, lift jet exit flow conditions, and both axisymmetric and rectangular nozzle exit geometry are also accommodated. The methodology has been embodied in a McDonnell Aircraft Company (MCAIR) computer code which accommodates configurations with up to six lift jets.

In ground effect, the prediction methodology proceeds logically from the aircraft lift jet exits through the free jets, jet impingement points, wall jets, fountain bases (stagnation lines) and fountain upwash flow and impact on the airframe undersurface. The induced suckdown flows are computed from the potential flowfield induced by the turbulent entrainment of both the free jets and wall jets in ground effect and from the free jets alone out of ground effect. Key elements of this methodology are emphasized in this paper including geometric considerations, computation of stagnation lines, fountain upwash formation and development, and fountain impingement on the airframe undersurface. Modifications to the basic modelling approach are presented for single impinging jets in uniform cross-flow.

*Portions of the information presented in this lecture were derived from studies supported by the Naval Air Development Center (Contracts N62269-76-C-0086 and N62269-81-C-0717), the Office of Naval Research (Contract N00014-79-C-0130), the NASA Ames Research Center (Contracts NAS2-9646, NAS2-10184 and NAS2-11161) and McDonnell Aircraft Company Independent Research and Development Resources.

+Branch Chief - Technology, Aerodynamics

Transition:

A numerical procedure has been developed for the analysis of aerodynamic forces and moments on V/STOL aircraft operating in the transition regime between hover and conventional forward flight. The procedure specifically treats the jet induced effects on the airframe. The overall methodology employs previously existing computer programs for the calculation of the jet properties and inviscid parameters. The trajectories, cross sectional area variation, and mass entrainment rates of the jets are calculated by available methods such as the Adler-Baron Jet-in-Cross-Flow Program. The inviscid effects of the interaction between the jets and airframe on the aerodynamic properties are determined by use of the MCAIR 3-D Subsonic Potential Flow Program, a surface panel method.

This lecture is divided into three parts consisting of:

I Hover In and Out of Ground Effect,
II Cross-Flow in Ground Effect, and
III Uniform Cross-Flow Out of Ground Effect (Flight Transitional Flow Fields).

NOMENCLATURE

A	Area
AR	Aspect ratio
C	Constant
C_p	Pressure coefficient
D	Jet exit diameter (circular nozzle), nozzle exit width (rectangular nozzle)
D_e	Equivalent circular jet exit diameter
F	Force
$f(\phi)$	Radial momentum flux distribution about jet impingement point (normalized)
H	Nozzle exit height above ground plane measured perpendicular to ground plane
H'	Height above ground of fuselage surface directly below aircraft Center of Gravity (C.G.)
h	Local wall jet height h = h(R)
L	Nozzle exit length (rectangular nozzle), lift
LID	Lift improvement device
$\dot{m}$	Mass flow
$\dot{M}$	Momentum flux
N,n	Normal distance above ground plane in wall jet, number of jets
NPR	Nozzle pressure ratio
NTR	Nozzle temperature ratio
q	Dynamic pressure, $1/2\rho V^2$ or $1/2\rho U^2$
R	Radial distance (usually from jet impingement point)
S	Nozzle exit centerline spacing
S'	Distance between jet impingement points on ground plane
$R_{V/2}$, $S_{V/2}$	Velocity profile width at point in profile where V = Vmax/2
U	Wall jet velocity
V	Jet, fountain velocity
V_c	Mean flow velocity (cross-flow)
X,Y,Z	Cartesian coordinates with Z normal to the ground plane
Z_{jc}	Jet axial distance measured from nozzle exit
α	Jet impingement angle measured from ground plane, aircraft angle of attack
γ	Momentum normalization correction
θ	Stagnation line slope in ground plane, jet impingement angle measured from ground plane in roll

δ	Nozzle vector angle
κ	Fountain sidewash angle measured from the ground plane
λ_{fI}	Fountain upwash momentum flux transfer coefficient
$\lambda_{\dot{M}}$	Momentum flux magnitude recovery (conservation) factor
ρ	Density
σ	Constant
ϕ	Azimuthal angle in ground plane, $\phi = 0°$ in direction of the horizontal component of free jet mean velocity in oblique impingement situations
ϕ'	Computational polar angle measured in the ground plane about a jet impingement point referenced to the line joining two jet impingement points
ψ	$\sqrt{q_c/q_{je}}$
ω	Fountain upwash inclination measured from the ground plane

Subscripts

1,2	Jet designation	max	Maximum
c	Cross-flow	min	Minimum
F,f	Fountain, final	N	Normal
fI	Fountain impingement	o	Initial
j	Jet	R	Radial
jc	Jet-in-cross-flow	s	Suckdown
je	Jet exit	TH	Theoretical
L	Lower	wj	Wall jet

INTRODUCTION

The design of successful high performance military VTOL aircraft requires a critical blend of new airframe and propulsive lift system technology with tried and proven CTOL high speed aircraft characteristics. The VTOL aircraft configuration analyst is beset with a myriad of performance requirements, airframe configuration variables and propulsive lift system options; yet there is a dearth of comprehensive vehicle performance prediction methods to aid in the identification of promising vehicle configurations. This, in combination with the many physical variables involved, can result in a largely subjective and empirical approach to vehicle configuration definition based on past experience. The unique operational requirements of VTOL aircraft that are responsible for this complex design dilemma are, of course, the vertical and transition flight requirements. These flight modes necessitate a knowledge of forces and moments on the vehicle which are unfamiliar to the CTOL aircraft designer. These flowfield effects are characteristically dependent on the selected propulsive lift system and its physical integration into the airframe due to the interactive nature of the lift jet induced aerodynamics with the airframe. These jet induced flowfield interactions occur in the transition and in the hover or vertical flight modes both in and out of ground effect. A purpose of this lecture is to provide insight and a quantitative basis for the modelling and prediction of jet and multiple jet induced flowfields and the resulting aerodynamic forces and moments on the airframe in and out of ground effect. A propulsion system designed without taking into account the induced forces may not provide sufficient thrust for an adequately controlled takeoff without a reduction in payload. In addition to these induced net loads, situations are encountered where unfavorable moments are produced on the airframe, resulting in significant stability and control considerations. Until accurate, general purpose flowfield prediction techniques become available for these complicated viscous flowfields, dependence on wind tunnel testing for design and performance verification will be relatively high.

I. HOVER IN AND OUT OF GROUND EFFECT

The induced forces (and moments) in and out of ground effect usually result from one of two reasonably well understood flow phenomena. These are jet entrainment and the formation of jet flow fountains. Jet entrainment causes otherwise static air to be set into motion, resulting in locally reduced static pressures on nearby airframe undersurfaces thus introducing negative aerodynamic loads. The jet entrainment effect occurs both in and out of regions influenced by the presence of the ground but is frequently accentuated as the distance between the nozzle exit and the ground is reduced. This is attributable to the proximity of the additional entrainment resulting from the ground wall jets. The flowfield about a VTOL aircraft hovering in ground effect is shown schematically in Figure 1.

The formation of jet flow fountains requires the impingement of the jets on the ground or shipboard landing pad and, therefore, is peculiar to operation close to the ground. The formation of fountains is configuration dependent in that multiple jets are required, and the jet impingement points, relative strengths of the jets, and jet impingement angles strongly influence the characteristics of the fountain.

The upward convection of jet flow in the fountains usually results in a positive aerodynamic lift, caused by the positive pressurization of airframe undersurfaces containing and deflecting the fountain upwash flow. Because of the upward convection of the lift jet flow in the fountains, a degradation of propulsion system performance may result from exhaust gas ingestion intc the aircraft inlets. In this respect, fountains can be detrimental to VTOL aircraft performance in proximity to the ground. Significant VTOL hover flowfield interactions and their resulting effects on vehicle performance in ground effect are summarized in Figure 2.

The following sections of this part of the lecture will outline the empirically based methodology developed by the McDonnell Aircraft Company (MCAIR) for the modelling and prediction of multiple jet VTOL aircraft flowfields in ground effect. This methodology was developed during the period from 1975 through 1983. The reader will be referred to appropriate published references for detailed mathematical developments and thorough documentation of experimental data. Key elements in the development of the methodology are emphasized in this lecture.

GEOMETRIC CONSIDERATIONS

The viscous (turbulent) flowfield between a multiple jet VTOL aircraft and the ground is strongly dependent on many geometric factors related to the geometry of the airframe, integration of the propulsive lift system including the geometry of the nozzle exits, and the spatial relationship of the airframe to the ground plane. The significant jet mean flow geometry and overall flowfield geometry includes:

- o Lift jet system arrangement including the number of jets, jet exit spacings and jet exit orientation with respect to the aircraft axes (including longitudinal "vector" and lateral "splay" angles),
- o Nozzle exit shapes and mean velocity distributions at the nozzle exits, and
- o Aircraft surface geometry, aircraft spatial orientation and height above ground.

Most of the above geometric variables were taken into account in the initial development of a ground flow field prediction methodology by MCAIR, Reference 1. This work was based on the fundamental free jet flow development and impingement characteristics of round jets which, for the most part, were available in the published literature. Specifically, the free jet entrainment data of Kleis and Foss, Reference 2, and the geometric and kinematic properties of free and impinging round jets established by Donaldson and Snedeker, Reference 3, were used extensively. The data of Donaldson and Snedeker were also used to determine analytical expressions for wall jet entrainment. These have since been modified through empirical corrections based on hot film anemometer measurements made at MCAIR.

A key element in the modelling of the ground surface flow field below a hovering VTOL aircraft is the azimuthal distribution of radial momentum flux about the individual jet impingement points on the ground plane. This distribution is strongly dependent on the exit shape of the jet nozzle (for low values of H/D) and the local impingement angle of the jet on the ground plane. The data of Donaldson and Snedeker shown in Figure 3 indicate that for a round turbulent jet this distribution is sensitive to the local jet impingement angle and relatively insensitive to the ratio of height above ground to nozzle exit diameter (H/D). These distributions of momentum flux together with the magnitudes of the total momentum fluxes emanating from the aircraft nozzle exits establish the location and (momentum) strength of the fountains in the flow field below the aircraft. MCAIR measurements of the azimuthal distribution of radial momentum flux for a single impinging round jet indicate that the data of Donaldson and Snedeker (as shown in Figure 3) exhibit excessive momentum flux in the region $0 \leq \phi \leq 45°$, Reference 4. This is illustrated in Figure 4.

Another significant geometric consideration is the number and arrangement of the propulsive lift jets in the aircraft lift system. Figure 5 shows a generic idealized multiple lift jet arrangement of equal thrust jets spaced symmetrically about a hypothetical center of gravity. The octagonal central area circumscribed by the lines connecting the eight lift jet centerlines represents an idealized "inner region". All area outside of this region extending to infinity constitutes the idealized "outer region". The interaction lines of the wall jets resulting from the ground impingement of the lift jet pairs are shown as the dashed lines in Figure 5. These lines indicate the ideal locations of the wall jet stagnation lines which form in both the inner and outer regions. A stagnation line pattern as shown in Figure 5 would result from the ideal vertical impingement of round jets producing a $f(\phi) = 1$ distribution of wall jet radial momentum flux (see Figure 3). Figure 6 shows the maximum available fountain force as a function of the number of lift jets in an idealized multiple lift jet system of this type. The lower curve in Figure 6 shows the maximum fountain force F_F available from the inner region only,

$$F_F(\text{inner region}) = \left(\frac{1}{2} - \frac{1}{N}\right) F_T \qquad (1)$$

where F_T is the total lift system thrust and N is the number of jets in the idealized lift system.

It should be noted that a two jet lift system has no inner region, by definition, and, therefore, all fountain force obtained from a two jet fountain is outer region force. The result shown in equation (1) is predicated on the assumption that all lift jet momentum flux that enters a volume below the aircraft whose planform is the inner region eventually is turned to vertical and imparts this vertical momentum to the airframe. The upper curve in Figure 6 indicates the total available ideal fountain force including contributions from both the inner and outer regions. The lift jet momentum flux entering the outer region volume is assumed to impinge on the airframe with an ideal sidewash angle of incidence resulting from the turning of the flow in an upward direction at the stagnation lines. Performing an integration of the vertical component of the outer region momentum flux and adding the result to the force from the inner region,

$$F_F(\text{outer region + inner region}) = \left(\frac{1}{2} - \frac{1}{N} + \frac{1}{\pi}\right)F_T \qquad (2)$$

The potential benefits to be gained from additional fountain force resulting from the use of increasing numbers of jets up to six or even eight is obvious, but it must be realized that actual fountain forces produced on the airframe undersurface are much less than the ideal values shown in Figure 6 by a factor of one third to one quarter based on the ideal inner plus outer region values. (The reasons for this are discussed later in this lecture.) Limited data on experimentally measured values of fountain force are shown in Figure 6 for two and four jet configurations. These data were recorded on special experimental configurations for which jet entrainment induced suckdown effects were minimal.

Recent interest in certain VTOL and STOL propulsive lift systems, such as thrust augmenting ejector systems and other concepts employing non- circular nozzles, has revealed a need for the understanding of the basic free jet and jet impingement characteristics of jets emanating from rectangular exit area nozzles. Consequently, two experimental programs, References 5 and 6, were undertaken to investigate the wall jet characteristics produced by the impingement on a ground plane of jets emanating from low and high aspect ratio rectangular exit area nozzles. The primary purpose of these studies was to experimentally determine the azimuthal distributions of wall jet radial momentum flux about the impingement points of these jets for rectangular nozzles with exit area aspect ratios (L/D) of one, two, three, four, six and eight for both vertical and oblique impingement.

The high aspect ratio rectangular nozzle data ($4 \leq L/D \leq 8$) obtained in the first investigation (for low nozzle pressure ratios only) (Reference 5) indicated that, unlike axisymmetric jets, the wall jet radial momentum flux distributions for vertical impingement are highly directional, even for the aspect ratio four (L/D = 4) nozzle at heights above ground as great as sixteen nozzle widths. Consequently, the second study (Reference 6) was undertaken to extend the data base to include rectangular nozzles with exit area aspect ratios of one, two and three. Wall jet radial momentum flux distributions were obtained for the three low aspect ratio nozzles as a function of jet impingement angle, nozzle exit height above ground and nozzle pressure ratio which included choked and under-expanded nozzle exit flow conditions. The ground flow field computer program, aircraft/ground/stagnation line/fountain (AGSF), originally developed by MCAIR for round jets was updated to include the impingement data obtained for both the high and low aspect ratio rectangular nozzles.

Figure 7 presents a qualitative view of the wall jet radial momentum flux distributions associated with impinging jets issuing from both axisymmetric and rectangular nozzles. The axisymmetric nozzle produces a uniform distribution in vertical impingement $f(\phi)$ = const. ($\alpha_j = 90°$). In oblique impingement, a peak occurs in the distribution in the $\phi = 0°$ direction with the relative magnitude of the peak increasing with decreasing impingement angle. The rectangular nozzles in vertical impingement, on the other hand, produce a prominent peak of the momentum flux distribution in a direction perpendicular to the long sides of the nozzle exit, as indicated in Figure 7 by the L/D = 4 nozzle at $\alpha_j = 90°$. The primary effect of oblique impingement of the rectangular nozzle in pitch (rotation about the nozzle exit minor axis) is to shift the peak to an azimuthal location approximately coincident with the magnitude of the impingement angle. The L/D = 1 (square) nozzle at low pressure ratios exhibits characteristics similar to that of the axisymmetric nozzle. At high pressure ratios, however, the square nozzle exhibits characteristics common to both axisymmetric and rectangular nozzles with a primary peak occurring at $\phi = 0°$, as with axisymmetric nozzles, and a secondary peak occurring at an azimuthal angle approximately coincident with the jet impingement angle, as exhibited by rectangular nozzles. The data from these investigations is summarized in Reference 7.

These experimental test programs were designed to provide data for the determination of basic and integrated fluid flow properties associated with the impingement of turbulent jets issuing from rectangular exit area nozzles over a meaningful range of pertinent parameters relevant to the operation of V/STOL aircraft in the hover mode in ground effect. Free jet surveys were performed for each of the nozzles to investigate the quality of the flow issuing from the nozzles and to verify exit flow symmetry. The desired wall jet radial momentum flux distributions were determined by numerical integration of the wall jet velocity profiles which were obtained by surveying the turbulent wall jets at azimuthal locations about the periphery of the jet impingement region. The wall jet surveys were performed by traversing a dual sensor "cross-flow" hot film anemometer probe through a 0.508 cm (0.200 in) hole in the ground board in a direction perpendicular to the ground board surface, thus allowing the determination of wall jet flow angularity in a plane parallel to the ground plane as well as mean flow velocities.

For vertical impingement, the wall jets were surveyed through an azimuthal sector including at least one quarter of the jet impingement region since two planes of flow symmetry existed. For oblique impingement, i.e., rotation of the rectangular nozzle about the nozzle exit minor axis of symmetry (pitch) or rotation about the nozzle exit major axis of symmetry (roll), the wall jets were surveyed about one half of the jet impingement region since only one plane of flow symmetry existed. The wall jet surveys were made in 15° increments of azimuth (ϕ) about the impingement region. For oblique impingement, however, additional surveys were performed in 5° increments of azimuth about the region corresponding to the wall jet radial momentum flux distribution peak. Figure 8 defines the rectangular nozzle test geometry and nomenclature. The rectangular nozzle exit width, D, was a fixed dimension of 2.0 cm (.797 in) for all nozzle configurations.

The Reynolds number effects on the wall jet velocity profiles resulting from vertical jet impingement were evaluated for the rectangular nozzles. The characteristic shapes of the normalized wall jet velocity profiles were determined for a set of constant test parameters while the Reynolds number (established by nozzle pressure ratio) was varied. Three Reynolds numbers, R_{e_D} were investigated for each nozzle. For the low aspect ratio nozzles, Reynolds numbers of 220,000, 547,000 and 722,000 were investigated, corresponding to nozzle pressure ratios (NPR) of 1.15, 1.89 and 2.50. For the high aspect ratio nozzles, which were restricted to low nozzle pressure ratio testing, Reynolds numbers of 146,000, 205,000 and 275,000 were investigated corresponding to nozzle pressure ratios of 1.07, 1.15 and 1.28. Figure 9 presents a typical set of velocity profiles obtained for the L/D = 3 nozzle at H/D = 8.0, R/D = 14.0 and

for an azimuthal angle of $\phi = 90°$, where $\phi = 90°$ corresponds to the direction perpendicular to the nozzle exit major axis. Based on data of this type, it was concluded that the normalized wall jet velocity profiles are similar and, therefore, no significant Reynolds number effects are indicated. In addition, it should be noted that for Reynolds numbers of 547,000 and 722,000 (NPR = 1.89, 2.50) the exit flow is compressible. Thus, Figure 9 also suggests the absence of upstream compressibility effects on the local wall jet flow. The effect of nozzle aspect ratio on the local wall jet flow is also negligible, as shown in Figure 10 for $\phi = 90°$ at a radial distance of 14.0 nozzle exit widths (R/D = 14.0) from the jet impingement point.

The azimuthal distributions of wall jet radial momentum flux were determined for each of the six single nozzle configurations and are presented in Figures 11-13 for the aspect ratio one, two and six nozzles in vertical impingement. The dependent variable for each curve is the integral of the wall jet velocity squared, multiplied by the radial distance, R, from the jet impingement point to the point of measurement and is representative of the magnitude of the wall jet radial momentum flux. The radial distance, R, is included in the dependent variable to account for the increase in area with radial distance and, therefore, allows comparison of data recorded at different radial stations. The wall jet radial momentum flux was measured over one quarter of the periphery of the impingement region from $\phi = 0°$, corresponding to a direction perpendicular to the nozzle minor axis, to $\phi = 90°$ which corresponds to a direction perpendicular to the nozzle exit major axis. Each figure presents data recorded at two radial stations (R/D = 14.0, 29.0) with nozzle pressure ratio (NPR) as a parameter.

For the aspect ratio 1 (square) nozzle, the momentum flux distributions, shown in Figure 11, exhibit peaks in directions perpendicular to the side walls of the nozzles ($\phi = 0°$, $\phi = 90°$). The peaks are strongest at H/D = 2, weaker at H/D = 8 and practically non-existent at H/D = 16 where the jet appears to impinge in a manner similar to that of an axisymmetric jet. Some azimuthal asymmetry in the wall jet flow was indicated, particularly for the highest nozzle pressure ratio at a nozzle height of H/D = 2 by a stronger flux of momentum in the $\phi = 90°$ direction than in the $\phi = 0°$ direction (Figure 11a). The reduction in wall jet radial momentum flux magnitude with increasing R/D results from skin friction on the ground plane.

The momentum flux distributions for the higher aspect ratio nozzles ($2 \leq L/D \leq 8$) all exhibit similar characteristics at low nozzle pressure ratios with a peak at $\phi = 90°$ (perpendicular to the nozzle exit major axis) as exemplified by the aspect ratio two and aspect ratio six nozzle results shown in Figures 12 and 13. However, at NPR = 2.50, although the aspect ratio two and three nozzles displayed the characteristic peak at $\phi = 90°$ for H/D = 2; at H/D = 8 the momentum flux distribution peak became broader and shifted to approximately $\phi = 60°$; and at H/D = 16, the peak shifted to approximately $\phi = 45°$. A minor peak is exhibited at $\phi = 0°$ (perpendicular to the nozzle exit minor axis) for the higher pressure ratios at H/D = 2, but vanishes at H/D = 8. A comparison of the data indicates a dependence of momentum flux peak strength on nozzle aspect ratio by an increase in peak relative magnitude with increased L/D.

For oblique impingement in pitch, the momentum flux distributions for the L/D = 1 nozzle (shown in Figure 14) display a prominent peak at $\phi = 0°$ as found for an axisymmetric nozzle in oblique impingement. At a nozzle pressure ratio of 1.15, the momentum flux gradually decreases with increasing azimuth angle. At the higher nozzle pressure ratios, however, a smaller peak is exhibited at $\phi = 180°$ and, at the lowest height surveyed a third intermediate peak, or developing peak, appears at an azimuthal angle approximately coincident with the magnitude of the impingement angle, α_j. Although the data are not shown here, this effect was much more pronounced at an impingement angle of 75°. The occurrence of a peak in momentum flux at an azimuthal angle approximately coincident with the magnitude of the impingement angle is characteristic of rectangular nozzles (L/D > 1) as exhibited by the L/D = 2 nozzle and the L/D = 6 nozzle in Figures 15 and 16 respectively. Thus, at high pressure ratios and low nozzle heights, the L/D = 1 (square) nozzle displays characteristics common to both axisymmetric and rectangular (L/D > 1) nozzles. The data in Figure 15 for the aspect ratio two nozzle indicate a broadening and a shift of the location of the momentum flux peak toward $\phi = 0°$ at the higher H/Ds for a nozzle pressure ratio of 2.50. Similar behavior was observed for the aspect ratio three nozzle.

Because of the symmetry of the L/D = 1 (square) nozzle, the momentum flux distributions determined for oblique impingement in pitch apply equally well for oblique impingement in roll. For the rectangular nozzles (L/D > 1) in roll, the data indicate a prominent peak at $\phi = 0°$ and a lesser peak at $\phi = 180°$. These trends are illustrated in Figures 17 and 18 for the aspect ratio two and aspect ratio six nozzles, respectively. The flux of momentum in the $\phi = 0°$ direction increases with increasing nozzle aspect ratio L/D, and decreasing impingement angle, θ_j. At the greater nozzle heights and a nozzle pressure ratio of 2.50, however, there was considerable broadening of the momentum flux peak from $\phi = 0°$ to $\phi = 30°$ for the L/D = 2 and L/D = 3 nozzles.

COMPUTATION OF STAGNATION LINES AND FOUNTAIN UPWASH INCLINATION

In Reference 1 an analytical model was developed for the computation of wall jet stagnation lines formed between any pair of impinging jets for completely arbitrary conditions. Required input for these computations is simply the jet thrust scaled azimuthal distributions of radial momentum flux. This model is termed the "Momentum Flux Method".

The Momentum Flux Method established the location of the stagnation line between two jet impingement points by balancing the total momentum flux in the wall jets in a direction locally normal to the stagnation line in the ground plane. As a result of the requirement of a total momentum flux balance (normal to the stagnation line), the upward direction of the fountain in a vertical plane normal to stagnation line must itself be vertical, although a non-vertical sidewash component is allowed.

Green, Reference 8, modified the criterion for determination of the location of the stagnation line by requiring a balance of wall jet momentum flux per unit area of the wall jet at the stagnation line. The balance of momentum flux per unit area is also imposed in a direction normal to the stagnation line in the ground plane. Imposition of this criterion results in an imbalance of total wall jet momentum flux at the stagnation line in a direction normal to the stagnation line in the ground plane and, consequently, allows a non-vertical trajectory of the fountain upwash flow in a vertical plane normal to the stagnation line. This model for the determination of the stagnation line location is denoted as the "Momentum Flux Density Method". The basic equations for the "Momentum Flux Method" (MFM) and the "Momentum Flux Density Method (MFDM) models are compared in Table 1 (see Figure 19 for nomenclature definition).

The momentum balance for the determination of the local stagnation line slope is applied to the elemental control volume in the ground plane as shown in Figure 20. The conservation of momentum normal to the stagnation line for the control volume in the absence of any pressure and viscous forces is the following:

$$\iint_{C.S.} \vec{U}_{N_\ell} \, (\rho \, \vec{U} \cdot d\vec{A}) = 0 \tag{3}$$

Sides 1 and 2 of the control volume ar chosen normal to the radial velocity vectors, $\vec{U}_{R1}$ and $\vec{U}_{R2}$, emanating from the individual jet impingement points. Assuming no loss in wall jet radial momentum with geometric local radius R for each wall jet based on the experimental results of References 3 and 7, the momentum flux for each circumferential sector is:

$$\int_0^\infty \rho U_R{}^2 \, R \, \partial\phi' \, d \, N = \Upsilon \, f(\phi) \, \dot{M}_j \, \frac{\partial\phi'}{2\pi} \tag{4}$$

where N is the distance normal to the ground plane. Applying Equation (3) to the control volume (Figure 20), and using the fact that no flow occurs through control volume sides 3 and 4, the following result is obtained:

$$\int_0^\infty \rho U_{R1}{}^2 \, R_1 \sin(\theta - \phi_1') \, \partial\phi_1' \, dN = \int_0^\infty \rho U_{R2}{}^2 \, R_2 \sin(\phi_2' - \theta) \, \partial\phi_2' \, dN \tag{5}$$

where the angles are defined in Figure 19.

Substituting Equation (4) into the above result, the following is obtained:

$$\Upsilon_1 \, f_1(\phi_1) \, \dot{M}_{j1} \sin(\theta - \phi_1')\partial\phi_1' = \Upsilon_2 \, f_2(\phi_2) \, \dot{M}_{j2} \sin(\phi_2' - \theta)\partial\phi_2'. \tag{6}$$

From the geometry shown in Figure 19, the following is obtained:

$$\partial\phi_1' = \frac{d\ell \sin(\theta - \phi_1')}{R_1} \tag{7a}$$

and

$$\partial\phi_2' = \frac{d\ell \sin(\phi_2' - \theta)}{R_2} \tag{7b}$$

Substituting Equations (7a and b) into Equation (6) there results:

$$\frac{\Upsilon_1 \, f_1(\phi_1) \, \dot{M}_{j1} \sin^2(\theta - \phi_1')}{R_1} = \frac{\Upsilon_2 \, f_2(\phi_2) \, \dot{M}_{j2} \sin^2(\phi_2' - \theta)}{R_2} \tag{8}$$

Solving Equation (8), the MFM result is obtained after some further geometric substitutions are made from the geometry in Figure 19:

$$\tan\theta = \frac{dy}{dx}\bigg|_\ell = \frac{\beta \sin\phi_2'}{1 + \beta\cos\phi_2'} \tag{9}$$

where

$$\beta = \frac{R_1}{S'}\sqrt{\frac{[\Upsilon_2 \, f_2(\phi_2)/\Upsilon_1 \, f_1(\phi_1)]\,(\dot{M}_{j2}/\dot{M}_{j1})}{R_2/R_1}} + \frac{R_2}{S'} \tag{10}$$

The distinction made in the above equations between the angles ϕ and ϕ' is necessitated by the fact that the $\phi' = 0$ direction is parallel to a line joining the jet impingement points, whereas $\phi = 0$ is related to the individual jet impingement geometries. ϕ' and ϕ are related by a simple rotation about the impingement point of the type of data shown in Figure 3.

The stagnation line solution for any jet pair is obtained by a stepwise marching process beginning at the point where the stagnation line crosses the line joining the jet impingement points. At this common point, the radii R_1 and R_2 as shown in Figure 19 are related as follows:

$$\frac{R_2}{R_1} = \frac{\dot{M}_{j2}\,\gamma_2\,\ f_2(\phi_2)}{\dot{M}_{j1}\,\gamma_1\,\ f_1(\phi_1)} \tag{11}$$

This may be obtained from Equation (8) by setting $\phi_1' = 0$ and $\phi_2' = \pi$ in that equation. For vertical jet impingement, Equation (11) simplifies to

$$\frac{R_2}{R_1} = \frac{\dot{M}_{j2}}{\dot{M}_{j1}} \tag{12}$$

The corresponding results for the MFDM may be obtained by dividing the "left hand side" of Equation (6) by $h_1 R_1 \partial\phi_1'$ and the "right hand side" by $h_2 R_2 \partial\phi_2'$ to balance local momentum flux per unit area. This produces

$$\frac{\gamma_1\, f_1\, \dot{M}_{j1} \sin(\theta - \phi_1')}{h_1 R_1} = \frac{\gamma_2\, f_2\, \dot{M}_{j2} \sin(\phi_2' - \theta)}{h_2 R_2} \tag{13}$$

Now if it is assumed additionally that

$$h_1 = \sigma R_1 \text{ and } h_2 = \sigma R_2 \tag{14}$$

substitution of (14) into (13) yields

$$\frac{\gamma_1\, f_1\, \dot{M}_{j1} \sin(\theta - \phi_1')}{R_1^2} = \frac{\gamma_2\, f_2\, \dot{M}_{j2} \sin(\phi_2' - \theta)}{R_2^2} \tag{15}$$

Solution of Equation (15) for $\tan\theta$ yields the following results for the MFDM:

$$\tan\theta = \frac{\beta \sin\phi'_2}{1 + \beta\cos\phi'_2} \tag{16}$$

where

$$\beta = \frac{R_1}{S'}\left[\frac{[\gamma_2\, f_2(\phi_2)\, \dot{M}_{j_2}]/[\gamma_1\, f_1(\phi_1)\, \dot{M}_{j_1}]}{R_2^2/R_1^2}\right] + \frac{R_2}{S'} \tag{17}$$

and, at the line joining the jet impingement points in the ground plane,

$$\frac{R_2}{R_1} = \sqrt{\frac{\dot{M}_{j_2}\, f_2\,(\phi_2)\, \gamma_2}{\dot{M}_{j_1}\, f_1\,(\phi_1)\, \gamma_1}} \tag{18}$$

It should be noted that in addition to the "balance" of local momentum flux per unit area in the wall jets, the assumption inherent in Equation (14) is required to derive the MFDM results from basic principles.

Computations of wall jet stagnation lines using the MFM and the MFDM have been compared with actual stagnation line locations obtained experimentally through flow visualization techniques, and the results were presented, for example, in References 4 and 6. Based on these and other comparisons, the MFDM was found to give a more accurate prediction of wall jet stagnation line location.

A comparison of a stagnation line predicted with the MFDM with the results of surface flow visualization is shown in Figure 21. The computed stagnation line is shown dashed in the figure. In the case shown (from Reference 4) the two jets are impinging vertically; both jets have equal nozzle pressure ratios (NPR = 1.89); but the stronger jet has four times the nozzle exit area of the weaker jet. As shown by these results, the MFDM provides a good prediction of stagnation line location, and this was found to occur for the wide range of jet pair impingement configuration parameters investigated in Reference 4.

In the MFDM, since total wall jet momentum flux (normal to the stagnation line) is not balanced, a relation can be derived for fountain upwash inclination based on the "unbalanced" portion of the interacting wall jet total momentum fluxes. A control volume located on the stagnation line is selected (as before), and the horizontal component of fountain upwash momentum is included in the total momentum balance yielding the following:

$$\frac{\gamma_1 f_1 \dot{M}_{j1}}{2\pi} \sin(\theta - \phi'_1)\, \partial\phi'_1$$

$$- \frac{\gamma_2 f_2 \dot{M}_{j2}}{2\pi} \sin(\phi'_2 - \theta)\, \partial\phi'_2 \qquad (19)$$

$$+ \rho V_f \cos\omega \left[U_{R_1} R_1\, \partial\phi'_1 + U_{R_2} R_2\, \partial\phi'_2 \right] h = 0$$

where V_f is the fountain upwash velocity, ω is the fountain inclination angle and h is the wall jet height. Assuming a total momentum flux magnitude conservation factor $\lambda_{\dot{M}}$ in the fountain formation region:

$$\rho V_f \left[U_{R_1} R_1\, \partial\phi'_1 + U_{R_2} R_2\, \partial\phi'_2 \right] h$$

$$= \lambda_{\dot{M}} \left[\gamma_1 f_1 \dot{M}_{j1} \frac{\partial\phi'_1}{2\pi} + \gamma_2 f_2 \dot{M}_{j2} \frac{\partial\phi'_2}{2\pi} \right] \qquad (20)$$

Substituting Equation (20) into Equation (19) and solving for $\lambda_{\dot{M}} \cos\omega$ the following general result is obtained for any location on the stagnation line:

$$\lambda_{\dot{M}} \cos\omega = \frac{\dfrac{\gamma_2 f_2 \dot{M}_{j2}}{R_2} \sin^2(\phi'_2 - \theta)}{\dfrac{\gamma_2 f_2 \dot{M}_{j2}}{R_2} \sin(\phi'_2 - \theta)} \qquad (21)$$

$$- \frac{\dfrac{\gamma_1 f_1 \dot{M}_{j1}}{R_1} \sin^2(\theta - \phi'_1)}{+ \dfrac{\gamma_1 f_1 \dot{M}_{j1}}{R_1} \sin(\theta - \phi'_1)}$$

For the special case of two round jets impinging vertically, on the line joining the jet impingement points,

$$\lambda_{\dot{M}} \cos\omega = \frac{1 - \sqrt{\dot{M}_{j1}/\dot{M}_{j2}}}{1 + \sqrt{\dot{M}_{j1}/\dot{M}_{j2}}} \qquad (22)$$

Figure 22 demonstrates the relation between ω and the impinging jet pair momentum flux ratio as obtained from Equation (22) with $\lambda_{\dot{M}}$ as a parameter. The validity of this model of fountain upwash flow inclination was investigated and verified with experimental data from the test program described in Reference 4 and is summarized briefly in the paragraphs following.

An analytical model for the fountain sidewash inclination was presented in Reference 1. The result is

$$\tan\kappa = \frac{2}{\cot(\theta - \phi'_1) + \cot(\phi'_2 - \theta)} \qquad (23)$$

where κ is the fountain sidewash inclination angle, and the other symbols are defined in Figure 19.

FOUNTAIN UPWASH FORMATION AND DEVELOPMENT

It has been observed consistently that fountain forces are substantially smaller than even conservatively estimated values based on lift jet thrust and momentum conservation. This is demonstrated quantitatively by the experimental data shown in Figure 6. For this reason, a thorough investigation of the fountain upwash formation and development process was conducted by MCAIR for fountains formed by two impinging round jets for a wide range of parametric test conditions. These results are reported in entirety in Reference 4. An important result of this investigation was the quantification of a fountain upwash formation normal momentum flux recovery coefficient, $\lambda_{\dot{M}N}$.

The fountain upwash normal momentum flux recovery factor ($\lambda_{\dot{M}N}$) is defined as the ratio of the fountain normal momentum flux exiting the fountain formation region to the total wall jet radial momentum flux entering the fountain formation region (see Figure 1). In the subject investigation, the flow throughout the fountain region was incompressible (ρ = constant), and the fountain formation region was assumed to be small so that radial area change effects were negligible ($dR \approx 0$). Thus

$$\lambda_{\dot{M}N} = \frac{\left(\int_{X_o}^{X_f} V_N^2 \, dX\right)_f}{\left(\int_0^{N1} U_R^2 \, dN\right)_{wj(1+2)}} \tag{24}$$

where $\left(\int_{X_o}^{X_f} V_N^2 \, dX\right)_f$ is representative of the fountain normal momentum flux at Z/D = 1.0 and $\left(\int_0^{N1} U_R^2 \, dN\right)_{wj(1+2)}$ is representative of the sum of the local wall jet radial momentum fluxes entering the fountain base produced by the impinging jets in the system. A typical set of wall jet and fountain upwash flow mean velocity surveys for one test condition are shown in Figure 23. The surveys were obtained with a hot film anemometer. Since the local velocity ratios, V_{min}/V_{max}, for the fountain velocity profiles were considerably higher than those determined for the wall jet velocity profiles, the following procedure was established to define the limits of integration and to render consistency to the calculation process.

The upper limits of integration of the wall jet velocity profiles were established for each case by the normal distance, N_1, corresponding to the larger velocity ratio, U_{min}/U_{max}, of the two wall jet velocity profiles. The wall jet velocity and velocity squared profiles for jet 1 and jet 2 were then integrated and summed to yield $\left(\int_0^{N1} U_R \, dN\right)_{wj}$ and $\left(\int_0^{N1} U_R^2 \, dN\right)_{wj}$. Now, since the fountain formation region is assumed to be small, with little exposed jet area available for mass entrainment, conservation of mass was assumed in the fountain formation region to yield

$$\left(\int_{X_o}^{X_f} V_N \, dX\right)_{f_{Z/D=1}} = \left(\int_0^{N1} U_R \, dN\right)_{wj(1+2)} \tag{25}$$

Thus, the initial and final limits of integration (X_o, X_f) for the fountain velocity and velocity squared profiles were determined such that Equation (25) was satisfied.

Figure 24 presents the fountain normal momentum flux recovery factor, $\lambda_{\dot{M}N}$ as a function of the jet exit momentum flux ratio, $\dot{M}_{je_{LOW}}/\dot{M}_{je_{HIGH}}$, for the data of Reference 4. The data indicate a general decrease in the fountain momentum flux recovery with a decrease in the nozzle thrust bias (increased $\dot{M}_{je_{LOW}}/\dot{M}_{je_{HIGH}}$). In addition, a slight increase in $\lambda_{\dot{M}N}$ is shown in the presence of a nozzle exit plane plate over that found without the plate. A polynomial curve-fit (also shown in Figure 24) was determined for the data and is given approximately by the following expression:

$$\lambda_{\dot{M}N} = 1.0 - 1.5\left(\frac{\dot{M}_{je_{LOW}}}{\dot{M}_{je_{HIGH}}}\right) + 1.5\left(\frac{\dot{M}_{je_{LOW}}}{\dot{M}_{je_{HIGH}}}\right)^2 - 0.5\left(\frac{\dot{M}_{je_{LOW}}}{\dot{M}_{je_{HIGH}}}\right)^3 \tag{26}$$

The behavior of the normal momentum flux recovery factor with the jet exit momentum flux ratio is not surprising. The strongest wall jet interaction and associated loss of mean flow energy or momentum occurs with two equal strength impinging jets. As one of the impinging jets becomes weaker (increased thrust bias), the wall jet interaction becomes weaker. For a high thrust bias, the weaker wall jet simply tends to deflect the stronger jet with an attendant reduction in mixing and loss of mean flow energy.

Fountain geometric spreading characteristics and fountain mass flow were determined from the fountain upwash velocity profile data for all of the cases investigated. For the data of Figure 23, the fountain spreading characteristics and mass flow are shown in Figure 25. Fountain spreading characteristics for four jet fountains formed from four round jets oriented in an approximately square array are shown in Figure 26. $R_{V/2}$ is an averaged half velocity radius obtained from hot film anemometer surveys of the fountain upwash at a number of azimuthal positions. The parametric data shown (Cases 10 - 13) represent variations in nozzle pressure ratios for pairs of jets in the array.

Fountain upwash trajectories were also determined for all of the cases investigated in Reference 4. The trajectories were defined as the loci of the maximum velocity points as determined from the fountain upwash velocity profiles. The fountain upwash inclination, ω, was determined as the angle between the ground plane and a straight line connecting the fountain base and the fountain upwash trajectory at Z/D = 3. These fountain upwash inclination data are plotted as a function of the jet exit momentum flux ratio ($\dot{M}_{je_{LOW}}/\dot{M}_{je_{HIGH}}$) in Figure 27. Also shown in the figure are the theoretical values of the fountain inclination, ω_{TH}, based on Equation (22). The data shown in Figure 27 indicate that for a fountain inclination determined at Z/D = 3, a momentum flux recovery factor, $\lambda_{\dot{M}}$, of approximately 0.65 results in a reasonable fit to the experimental data.

FOUNTAIN IMPINGEMENT ON THE AIRFRAME

The establishment of the above ground flow field modelling elements, together with recent improvements made to three-dimensional panel methods for the determination of jet entrainment induced suckdown, leaves only one empirical element remaining to complete the prediction methodology for a wide range of VTOL aircraft configurations. This remaining element is the quantification of the amount of momentum flux transferred to the airframe undersurface from the upwash momentum flux in the fountain. This quantity, λ_{fI}, is termed the fountain upwash momentum flux transfer coefficient. λ_{fI} is dependent on airframe undersurface shape and aircraft height above ground, H/D.

To demonstrate the usefulness of the existing methodology, fountain impingement forces were determined and compared with experimental data for simple bodies and planforms for which λ_{fI} was expected to be approximately unity and for which suckdown forces were expected to be insignificant. Results are shown in Figure 28 and were very encouraging. The deviations between the predictions and the data at H/Ds of 1 and under are, most likely, beyond the validity range of the prediction methodology due to the basic changes in the flow structure beneath a body at these low H/Ds. That is, distinct regions of free jet flow, jet impingement, wall jets, fountain formation, and fountain upwash most likely do not exist at these conditions.

Fountain impingement forces measured on a swept low wing/fuselage combination are shown in Figure 29. The data shown here were produced by the impingement of single and multiple radial jets simulating fountain upwash flows produced by the vertical impingement on a ground plane of two and four round jets all with equal thrust. The normal force data shown has been non-dimensionalized by the total thrust of the simulated jet lift system. In the two jet case, the plane of the radial jet was perpendicular to the aircraft longitudinal axis, and in the simulated four jet case, the radial jet planes were mutually orthogonal and aligned parallel to the aircraft longitudinal and lateral axes. The data in Figure 29 show the variation in net fountain force with longitudinal location of the center of the fountain as the fountain impingement region was moved from the forward fuselage to aft of the wing trailing edge. As would be expected, the maximum fountain force results when the lateral fountain legs impinge on the widest portion of the wing. A noticeable drop in fountain force magnitude occurs when the lateral fountain legs are moved aft of the wing trailing edge. These data also indicate the relative magnitudes of two versus four jet fountains. The maximum points on these curves have been plotted in Figure 6 for comparison with the theoretical maximum fountain force. The indicated increase in fountain force with increasing H/D for the two jet fountain is due to variation of fountain induced suckdown which decreased in this test installation as the aircraft model was raised above the ground. The comparative decrease in fountain force with H/D produced by the four jet fountain is characteristic of fountains with three or more jets which form a central core of upwash flow.

Fountain impingement momentum flux transfer coefficients, λ_{fI}, were determined for three realistic V/STOL aircraft configurations for which laboratory test data in ground effect were available. Fortunately, data were available for a two jet, a three jet and a four jet configuration. λ_{fI} was determined as a function of height above ground by using the methodology presented herein to "back out" λ_{fI} from the measured lift on the aircraft models in ground effect. This was accomplished via the following steps:

1. The suckdown force, F_s, due to the entrainment of both the free jets and the wall jets was calculated using an advanced panel method,

2. The fountain upwash momentum flux incident on the aircraft undersurface, $\dot{M}_{fI}$, was calculated using the ground flowfield methodology presented herein, and

3. λ_{fI} was calculated using the relation

$$\lambda_{fI} \dot{M}_{fI} = \Delta L - F_s \tag{27}$$

where ΔL was obtained from laboratory test measurements on the three aircraft models.

1. SUCKDOWN FORCE CALCULATIONS - To calculate the suckdown force on a V/STOL aircraft hovering in ground effect, the aircraft, lift jet and wall jet surfaces are paneled for use with a surface singularity panel method. Figure 30 presents the paneled representation of the YAV-8B in hover in ground effect. The panel methodology selected for use in this study is a modified version of the PAN AIR surface singularity methodology of Reference 9. The modification permits the specification of non-zero normal velocity boundary conditions on jet surface panels to represent jet entrainment flow. Zero flow normal to the panel surface is prescribed as the boundary condition on aircraft surfaces. The suckdown methodology was verified, and the entrainment models utilized by the AGSF program were investigated prior to applying the methodology to the complete aircraft configurations (Reference 10).

a. Verification of Suckdown Methodology - In order to verify the validity of this approach when applied to aircraft in hover (V_∞=0), a simple test case consisting of an axisymmetric jet issuing from an infinite flat plate into static air was modeled. The pressure distribution on the surface of the plate was calculated using two different, empirically determined, axisymmetric jet mass entrainment models. Figure 31 presents the entrained mass flow distributions determined for a circular jet in five separate previous investigations. The wide disparity in the curves illustrates the uncertainty in the measurement of such data.

The calculated pressure distributions on the surface of the plate were integrated as a function of radial distance along the plate to yield a normal force coefficient (C_N). The variation of integrated normal force with radial distance is illustrated in Figure 32 for the two entrainment models. Also shown in Figure 32 is the normal force on the plate induced by a single circular jet (operating at the same conditions as the test case) determined from the empirical relation derived by Byrne contained in Reference 15. This relationship (shown in Figure 33) represents a correlation of induced lift data obtained experimentally for several V/STOL aircraft models in hover out of ground effect. The normal force curves

of Figure 32 indicate that both entrainment models tend to underpredict the actual jet induced suckdown force. It was concluded from this study that the potential flow representation of jet induced suckdown is valid, but the existing empirical entrainment distributions are too weak and must be corrected to accurately model jet induced forces. As a result of this finding, an experimental test program was conducted using a new technique to indirectly measure axisymmetric free jet entrainment using a hot film anemometer. A procedure for correcting existing entrainment distributions for calculating suckdown forces in hover in ground effect (IGE) is presented in the paragraphs following.

b. Effect of Lift Jet Paneling - The effect of the lift jet paneling geometry was investigated using the paneled model of the YAV-8B aircraft in hover out of ground effect (OGE). Figure 34 illustrates the paneled aircraft with two possible paneled jet models. In one case, the paneling represents the spreading jet geometry calculated by the AGSF program. In the other case, an equivalent cylindrical jet paneling was applied. The entrainment data of Kleis and Foss was utilized for both cases. It was verified that both paneled jet representations generate the same calculated suckdown force on the aircraft, $\frac{\Delta L}{T} = -.006$. This confirms that the simple cylindrical jet paneling is entirely adequate, provided that the jet normal velocity (entrainment) distribution is adjusted to account for the smaller jet perimeter. However, the experimentally measured suckdown force on the YAV-8B in hover OGE is -.020, substantially larger than predicted. This result reemphasizes the result determined using the infinite flat plate model that existing empirical free jet entrainment rates underestimate actual entrainment and require adjustment.

c. Corrected Free Jet Entrainment Velocities - Due to the uncertainty in empirical distributions of free jet entrainment rates (Figure 31), the free jet entrainment velocities utilized to calculate suckdown forces in hover IGE are based on corrected values of the free jet entrainment velocities (V_{fent}) utilized for hover OGE. In this procedure, the suckdown force out of ground effect $\left(\frac{F_s}{T}\right)$ is calculated using the entrainment data of Kleis and Foss. The result is then compared with experimental data (or, if such data is not readily available, with the general curve developed by Byrne [Reference 15], Figure 33) to yield the corrected free jet entrainment velocity, V'_{fent}, as follows:

$$V'_{fent} = \sqrt{\frac{(\Delta L/T)_{exp}}{(F_s/T)_{calc}}}\, V_{fent} \quad \text{(out of ground effect)} \tag{28}$$

d. Evaluation of Wall Jet Entrainment Velocities - As originally calculated by the AGSF program, the wall jet entrainment velocities (V_{went}) varied directly with the radius of the jet impingement region (R_I) and the free jet centerline velocity at impingement (V_{jcI}) and inversely with radius (R). Although this relation provided the correct variation of V_{went} with radial distance, the variation of V_{went} with nozzle height (H/D) was the opposite of that which would be expected. This unreasonable variation was found to result from the fact that R_I increases more rapidly than V_{jcI} decreases with respect to increasing H/D. The expression for V_{jcI} is based upon empirical data and is generally assumed to be accurate. Consequently, V_{went} was redefined, in a manner consistent with the formulation in Reference 1, as:

$$V_{went} \propto \left(\frac{2.4D\ V_{jcI}}{R}\right) \tag{29}$$

(where 2.4D represents the radius of the impingement region at H/D = 4). Figure 35 illustrates that the revised wall jet entrainment velocities exhibit the correct variation of V_{went} with H/D. It should also be noted that V_{went} is invariant with H/D for H/D $\leq$ 6. The reason for this is that the impinging jet centerline flow is still within the potential core, where V_{jcI} is constant.

In order to verify the accuracy of the magnitude of V_{went}, a simple test case was devised for use with the panel methodology. The test case (shown schematically in Figure 36) consisted of a circular disk (with diameter D) emitting an axisymmetric jet (with diameter D) in ground effect. The free jet entrainment velocities used were the corrected free jet entrainment velocities, V'_{fent}, defined by Equation (28). The suckdown force on the disk was then calculated using the wall jet entrainment velocities, V_{went}, of Figure 35 multiplied by various constant scaling factors, K_{went}. The variation of the calculated induced suckdown F_s/T, with K_{went} is shown in Figure 37 for a disk-to-jet diameter ratio (D/D) of 8 and for disk heights of two and four jet diameters above the ground plane. The dashed lines in the figure represent the induced lift determined using the following empirical relation (from Reference 15):

$$\frac{F_s}{T} = -.015\left[\frac{H'/D_e}{(D/D_e - 1)}\right] \exp -[2.2 - .24\ (NPR-1)] \tag{30}$$

The diameter, D_e, represents the equivalent single nozzle exit diameter and is defined as:

$$D_e = 2\sqrt{\frac{\sum_{i=1}^{n} A_{je_i}}{\pi}} \tag{31}$$

where A_{je_i} is the nozzle exit area of the i th nozzle and n is the number of jets. It should be noted that for the single axisymmetric nozzle shown in Figure 36, D is equivalent to D_e.

The points in Figure 37 at which the curves cross the dashed lines determine the value of K_{went} required for adjustment of the uncorrected wall jet entrainment velocities (V_{went}) to yield the empirical value of the induced lift. Curves such as those shown in Figure 37 were also obtained for D/D_e 6 and D/D_e = 12 at H/D_e = 2 and 4. The value of K_{went} required to match the empirical lift loss in ground effect is shown in Figure 38 as a function of plate diameter, D/D_e. A value of K_{went} = 1.50 was selected for use in all future cases in this study. Data obtained later in a MCAIR laboratory study indicate that K_{went} = 1.75. This result was obtained experimentally as a result of hot film anemometer surveys of turbulent wall jets emanating from impinging round jets. These data are shown in Figure 39. The analytical result shown in Figure 39 is the uncorrected AGSF program prediction based on the results presented in Reference 3. Table 2 presents a summary of the procedure used to calculate the total suckdown force on V/STOL aircraft hovering in ground effect.

2. FOUNTAIN FORCE CALCULATIONS - Using the MCAIR V/STOL force prediction methodology, the total multiple jet fountain upwash momentum flux incident upon the aircraft, $\dot{M}_{fI}$, is calculated as the sum of an inner region contribution $\dot{M}_{fI_{in}}$ and an outer region contribution, $\dot{M}_{fI_{out}}$. The fountain upwash momentum flux contributions emanating from the inner region and outer region are determined graphically (Figure 40) using the data determined using the AGSF methodology. However, only a fraction of the total impinging fountain momentum flux is converted to a force on the aircraft. This fraction is accounted for in the methodology by employing the fountain impingement momentum flux transfer coefficient, λ_{fI}.

a. Inner Region Fountain Impingement Momentum flux - To calculate $\dot{M}_{fI_{in}}$, all of the wall jet momentum flux within the inner region is assumed to be turned upward in a circular central fountain and to exhibit the same spreading characteristics as described below for the two-jet fountain. The total momentum flux contained within the central fountain upwash is determined as

$$\dot{M}_{f_{in}} = \lambda_{\dot{M}} \sum_{i=1}^{n} \frac{\Delta\phi_i}{2\pi} \dot{M}_{je_i} \tag{32}$$

where $\dot{M}_{je}$ is the jet exit momentum flux, $\lambda_{\dot{M}}$ is the fountain formation momentum flux recovery factor determined for two-jet fountains in Reference 4 and n is the number of lift jets. (The factor $\lambda_{\dot{M}}$ was found to be equal to approximately 0.55 for two jets impinging vertically with equal thrust and this value increased as the thrust differential between the two impinging jets increased; see Figure 24.) The inner region fountain impingement momentum flux is then calculated based on the ratio of the cross-sectional area of the central fountain at impingement, A_{fc}, and the planform area intercepted by the central fountain, A_{ff} as:

$$\dot{M}_{fI_{in}} = \left(\frac{A_{ff}}{A_{fc}}\right) \dot{M}_{f_{in}} \tag{33}$$

b. Outer Region Fountain Impingement Momentum Flux - To calculate $\dot{M}_{fI_{out}}$, the fountain upwash momentum vectors are projected upward from the ground plane stagnation line to intersect the aircraft planform yielding the fountain fountain impingement centerline (Figure 40). Application of an empirical two-jet fountain spreading rate yields the effective fountain upwash boundaries and, consequently, the fountain "footprint" or that area of the aircraft planform intercepted by the fountain upwash. The two-jet fountain spreading rate was determined based on the data obtained in Reference 4 (see Figure 41) and is given as:

$$\frac{nf}{D} \equiv 2\,\frac{nv/2}{D} \tag{34}$$

where

$$\frac{nv/2}{D} = .50 + .35\,\frac{\zeta}{D} \tag{35}$$

To calculate the total momentum flux impinging on the aircraft in the outer region ($\dot{M}_{fI_{out}}$), the non-uniform two-jet fountain upwash momentum flux distribution curve shown in Figure 42 is applied between each jet pair. This curve was developed by integrating the universal (empirical) two-jet fountain upwash dynamic pressure profile shown in Figure 43 which was, in turn, defined based on data obtained in an unpublished MCAIR Independent Research And Development (IRAD) experimental program. The data from this study indicated that two-jet fountain upwash dynamic pressure profiles are similar for variations in fountain height and are essentially similar for variations in S/D and H'/D as well.

The two-jet fountain upwash momentum flux distribution curve shown in Figure 42 is used to graphically determine $\dot{M}_{fI_{out}}$ as:

$$\dot{M}_{fI_{out}} = \int_{0}^{\dot{M}_{fn_{out_I}}} \frac{\dot{M}_{f\ (n)}}{\dot{M}_{f_{tot}\ (n_f)}}\, d\left(\dot{M}_{fn_{out}}\right) \tag{36}$$

where $\dot{M}_{fn_{out}}$ is the fountain normal momentum flux incident upon the aircraft in the outer region and $\frac{\dot{M}_{f(n)}}{\dot{M}_{f_{tot}}(n_f)}$ is obtained from Figure 42.

The total fountain impingement momentum flux is then calculated as:

$$\dot{M}_{fI} = \dot{M}_{fI_{in}} + \dot{M}_{fI_{out}} \tag{37}$$

3. CALCULATION OF λ_{fI} - Using the approach described above, the fountain impingement momentum flux transfer coefficient, λ_{fI}, was calculated for the YAV-8B, the MCAIR Model 260 and the Grumman Model 698 V/STOL aircraft at three aircraft heights above ground. The height, H', is measured normal to the ground plane surface to the point on the fuselage undersurface directly beneath the aircraft center of gravity. The diameter, D_e, is the equivalent single nozzle exit diameter defined in Equation (31). The three aircraft configurations analyzed are shown in Figure 44.

a. YAV-8B - The fountain impingement momentum flux transfer coefficient was determined for the YAV-8B in hover IGE at an aircraft height of H/D_e = 2.76 in a MCAIR IRAD study. This study was extended in Reference 10 to include calculations of λ_{fI} for the YAV-8B at H'/D_e = 1.72, 3.80 and 4.84. Figure 45 presents the paneled representation of the YAV-8B in the clean configuration without wing pylons, gun pods or fuselage strakes. The horizontal and vertical tail surfaces were assumed to contribute little to the overall suckdown force, and these surfaces were omitted from the paneled model to reduce the paneling effort and computational costs. This groundrule was adopted for the paneling of all three aircraft. For the IGE analyses, the wall jet surfaces were represented as flat, zero-thickness plates extending approximately 60 nozzle exit diameters downstream from the jet impingement points.

Unfortunately, no experimental data are available for the YAV-8B aircraft in a clean configuration (without gun pods or LID's). The fuselage contours, nozzle sizes and nozzle locations, however, are virtually identical on both the AV-8A and the YAV-8B aircraft. Consequently, the induced forces on the two aircraft were assumed to be the same, and the AV-8A data were utilized for the calculations of λ_{fI} for the YAV-8B in the clean configuration. Figure 46 presents the experimental data for the AV-8A in the clean configuration and for the YAV-8B configured with two 16 inch fuselage strakes. Also shown in Figure 46 is the variation with height of the suckdown force, F_S/T, and the incident fountain momentum flux, $\dot{M}_{fI}/T$, calculated using the MCAIR V/STOL methodology. Figure 46 indicates that approximately 19% of the total jet exit momentum flux (thrust) is recovered in the fountain upwash at H'/D_e = 1.72 and that this value decreases to 13% at H'/D_e = 4.84.

The fountain impingement momentum flux transfer coefficient was calculated for the YAV-8B by rearranging Equation (27) to yield:

$$\lambda_{fI} = \frac{\Delta L/T - F_S/T}{\dot{M}_{fI}/T} \tag{38}$$

Figure 47 presents the variation of λ_{fI} with H'/D_e for the YAV-8B in both the clean configuration and with the 16 inch fuselage strakes. The presence of the strakes was assumed to have negligible effect on the calculated values of F_S/T and $\dot{M}_{fI}/T$. Consequently, the curves presented in Figure 46 were used to calculate λ_{fI} for both configurations. Figure 47 indicates that only 29% of the momentum flux within the fountain upwash is converted to a fountain impingement force on the clean configured aircraft at H'/D_e = 1.72. At H'/D_e = 4.84, the fountain effects are shown to be practically nonexistent on the clean aircraft with λ_{fI} = 0.05. The effect of adding the fuselage strakes is seen to increase the effectiveness of the fountain impingement process by capturing approximately an additional 38% of the fountain upwash momentum flux.

b. MCAIR MODEL 260 - The fountain impingement momentum flux transfer coefficient was determined for the Model 260 aircraft at aircraft heights, H'/D_e, of 0.92, 2.42 and 3.92. The calculations were made for the aircraft in both a clean configuration and in a configuration with lift improvement devices (LIDs) consisting of two vertical longitudinal fuselage strakes and a forward lateral vertical fence. Figure 48 presents the paneled representation of the Model 260 aircraft (without tail surfaces) in the clean, hover configuration that was utilized for the suckdown calculations. For the IGE analyses, the wall jets were again paneled as zero thickness flat plates and extended approximately 30 nozzle exit diameters downstream of the jet impingement points.

The experimentally determined induced lift ($\Delta L/T$) obtained using a 4.1% scale model of the Model 260 aircraft, with and without LIDs, is presented in Figure 49. The data are shown for the case of all three jets impinging vertically with each jet operating at a nozzle pressure ratio of 1.50. Also shown in the figure are the calculated values of F_S/T and $\dot{M}_{fI}/T$. Figure 49 indicates that the Model 260 experiences approximately one third of the suckdown force of the YAV-8B and, likewise, recovers only about one third of the jet exit momentum flux in the fountain upwash.

The fountain impingement momentum flux transfer coefficients calculated for the Model 260, both with and without LIDs, are presented in Figure 50. Once again, λ_{fI} is found to decrease with increasing H'/D_e. For the configuration without LIDs, approximately 50% of the impinging fountain momentum flux is converted to a fountain impingement force at H'/D_e = 0.92. However, at H'/D_e = 3.92 only 2% of the impinging fountain upwash momentum flux is effective as a fountain impingement force. The LIDs are seen to increase the efficiency of the fountain impingement process up to an aircraft height of approximately $2.5D_e$. Above this height the increase in λ_{fI} is less than .05 over that found for the clean configuration.

c. GRUMMAN MODEL 698 - Calculations of λ_{fI} were made for the Grumman Model 698 aircraft at aircraft heights of H'/D_e = 0.48, 0.83, 1.89, 2.50 and 3.61. The effect of fuselage corner radius was also investigated by examining the Model 698 with both round and square fuselage corners (chines). Figure 51 presents the paneled representation of the Model 698 in the clean hover configuration (without vertical tail) for a nozzle exit centerline spacing (S/D) of 2.8. The aircraft nozzles were paneled to simulate the experimental test installation.

The experimentally measured induced lift obtained from Reference 16 for the Model 698 with both round and square chines is presented in Figure 52. The data was obtained for the 4.2% scale model with vertically impinging jets operating at a nozzle pressure ratio of 1.06. Also shown in Figure 52 are the suckdown force, F_S/T, and the fountain momentum flux at impingement, $\dot{M}_{fI}/T$, calculated for the Model 698.

The fountain impingement momentum flux transfer coefficients calculated for the Grumman Model 698 aircraft, with both round and square fuselage chins are shown in Figure 53. The effect of fuselage corner radius was assumed to have negligible effect on the suckdown. Consequently, the values of F_S/T

and $\dot{M}_{fI}/T$ shown in Figure 52 were utilized for both configurations to calculate λ_{fI}. For the aircraft with the round chines, λ_{fI} displays an uncharacteristic decrease with decreased H'/D_e below $H'/D_e = 2.5$. For the aircraft with the square chines, λ_{fI} displays the expected trend of increasing with decreasing H'/D_e down to an aircraft height of $H'/D_e = .83$. Below this height, however, λ_{fI} displays an unrealistic decrease in magnitude and is therefore questionable. The advantage of square chines over round chines is evident from both Figure 52 and Figure 53. A possible explanation for this effect is given by Kalemaris in Reference 16.

A summary of the computed values of λ_{fI} for the three aircraft analyzed is shown in Figure 54. The results shown in Figure 54 clearly indicate the sensitivity of λ_{fI} to aircraft configuration geometry and aircraft height above ground. These results also clearly indicate the benefits of lift improvement devices.

As shown in Figure 54, additional lift may be obtained from fountain upwash impingement through the use of airframe undersurface protuberances in the form of fences or strakes which tend to capture the fountain upwash flow. The confining surfaces should extend through 360° of azimuth in an undersurface plane roughly parallel to the ground plane with the aircraft in the proper pitch and (zero) roll attitude for vertical translation. Permanently fixed surfaces suitable for high speed flight such as longitudinal axes strakes and/or pods can be utilized for this purpose, but lateral axis devices should be retractable. The confined undersurface area should be large enough to "capture" the central core of a multi-jet fountain including any fountain impact area translation on the airframe undersurface due to nominal aircraft pitch and roll excursions during hover. Sensitivities of lift improvement device related forces and moments to larger excursions in pitch and roll with and without cross winds should be investigated to assure adequate stability and control margins. This currently must be accomplished through wind tunnel testing of powered aircraft models in ground effect. Tests of this nature require accurate modelling of full scale airframe surface geometry including all undersurface contour details and protuberances. It is also desirable that full scale jet exit conditions in terms of nozzle exit geometry, nozzle exit velocity profiles and jet vector and splay angles be simulated carefully in the reduced scale tests.

The beneficial effect of passive lift improvement devices is demonstrated by the induced lift increment (ΔL) build-up data shown in Figure 55 which was measured in ground effect tests performed with a 15% scale powered model of the AV-8A. The data in Figure 55 indicate the positive lift increments obtained through the addition of gun pod strakes and a forward fence to the baseline vehicle which included gun pods. The data shown were obtained with all four lift jets vectored perpendicularly to the ground plane, however, the nozzles were splayed outward in the nominal splay position (5° forward nozzles, 11.2° aft nozzles). The sensitivity of the fountain forces to changes in nozzle splay angle (or vector) is demonstrated by the data presented in Figure 56 which shows the additional positive lift increment gained by reducing the outward splay angle of all nozzles on the model to 0°. Similar positive lift increments have been measured on models of other aircraft configurations, and in some cases, positive lift improvement can be obtained by simply deflecting existing flaps on the baseline aircraft. Caution must be used to verify that local upwash flowfield changes caused by lift improvement devices do not result in lift engine exhaust gas ingestion.

The mechanism for the increase in fountain lift force due to the use of lift improvement devices (LIDs) appears to be a combination of two effects: (1) the confining surfaces form a concavity which is pressurized at some pressure increment less than or equal to the maximum dynamic pressure in the fountain upwash flow, and (2) the concavity or portions thereof act as turning vanes and increase the local turning of the impinged upwash flow beyond what would normally be obtained by undersurface impingement without the lift improvement devices. In the latter case, an ideally designed LID would double the beneficial force increment obtained by ideal fountain impingement on a flat airframe undersurface parallel to the ground. In the former case, the LID acts like the skirt on a typical ground effect machine. Both mechanisms are theoretically very sensitive to H/D in all multi-jet fountain situations, and the data shown herein tend to confirm this.

II. CROSS-FLOW IN GROUND EFFECT

The impingement on the ground of VTOL aircraft lift jet flows in the presence of cross-winds or the impingement of STOL aircraft vectored jets (considering aircraft forward motion) creates a situation related to, but significantly different from, that discussed in part I of this lecture. The significant difference is the presence of a mean flow (due to the cross-flow or aircraft motion) which is superimposed on the multiple jet impingement flowfield. The interaction of the mean flow with the existing wall jets and fountains produces an additional class of turbulent flow interactions which are more complex than those discussed in part I. Within this class of interactions, there is an additional difference, namely, the effect of forward motion of the aircraft produces a mean flow without a boundary layer, whereas the cross-flow includes a surface boundary layer. In this part of the lecture, empirical and analytical tools for the analysis and prediction of the interaction of a mean flow with a single impinging jet will be presented. Specifically, the interaction of a turbulent wall jet with a cross-flow with and without a boundary layer will be addressed. Analysis and prediction of this type of interaction is vital to the prediction of conditions for which engine exhaust gas ingestion may occur during the landing of a STOL aircraft with thrust reversers. The take-off of STOL aircraft does not create much exhaust gas ingestion potential since the jets are vectored aft, and the mean flow interaction is favorable (tending to convect the jet flows farther aft of the aircraft). In the static situation for a VTOL aircraft take-off or landing, fountain location may be predicted by the methods presented in part I. The remaining area of concern, the effect of a mean flow interaction with a multiple jet fountain currently defies analysis, and exhaust gas ingestion potential for this situation must be investigated in the wind tunnel.

The ground flowfield associated with the use of thrust reversal for STOL landing is depicted schematically in Figure 57. V_c is equivalent to the aircraft forward velocity, and δ_L is the thrust vector angle with respect to the aircraft longitudinal axis. In most applications, δ_L is 115° to 150°

depending on the aircraft configuration. At high values of V_c, the ground stagnation line is located in the aft region of the aircraft flowfield, but as the aircraft decelerates, the ground stagnation line moves forward, and depending on the location of the aircraft inlets, the potential for exhaust gas ingestion by the inlets increases. Since the exhaust jet flow entrains ambient air along its flow path from the nozzle exit to the fountain, and since the cross-flow deflects the fountain upwash in an aft direction, a conservative boundary for exhaust gas ingestion is the condition for which the ground stagnation line is located directly below the aft most portion of the inlet.

Using this criterion for the potential initiation of exhaust gas ingestion, the problem becomes that of predicting under what condition the ground wall jet stagnation line reaches this location. Additionally, once this condition is reached for whatever imposed precautionary margin, the problem becomes that of the actively controlling the flowfield such that exhaust ingestion is precluded. Methods to achieve this control of jet effects will be discussed later.

The basic relationships for the interaction of a uniform cross flow with a wall jet emanating from an impinging jet may be derived for an elemental control volume located on the stagnation line. The control volume for this case is shown in Figure 58. Employing Equation (3) for this control volume:

$$\rho V_c^2 \sin\theta \, dy \, dz = \rho U_R^2 \sin(\phi' - \theta) \, R \, \partial\phi' \, dz \tag{39}$$

Integrating Equation (39) to the wall jet height, h, yields:

$$\rho V_c^2 \sin\theta \, h \, dy = \frac{\gamma f \dot{M}_j}{2\pi} \partial\phi' \sin(\phi' - \theta) \tag{40}$$

where, as before, for the impinging jet

$$\rho R \, \partial\phi' \int_0^h U_R^2 \, dz = \frac{\gamma f \dot{M}_j}{2\pi} \partial\phi' \tag{41}$$

To implement the momentum flux density, MFDM, approach, the left and right hand sides of Equation (40) are divided by their respective momentum flux areas, h dy and h R $\partial\phi'$ yielding:

$$\rho V_c^2 \sin\theta = \frac{\gamma f \dot{M}_j}{2\pi R h} \sin(\phi' - \theta) \tag{42}$$

The above may be solved for the slope of the stagnation line in the ground plane to yield:

$$\tan\theta = \frac{\beta \sin\phi'}{1 + \beta \cos\phi'} \tag{43}$$

where

$$\beta = \frac{\gamma f \dot{M}_j}{2\pi R h \rho V_c^2} \tag{44}$$

For a jet impinging symmetrically with respect to the cross-flow direction, $\phi' = 180°$ and $\theta = 90°$, and the stagnation line distance is given by

$$R = \frac{\gamma f \dot{M}_j}{2\pi h \rho V_c^2} \tag{45}$$

However, h is a function of R, and to solve Equation (45), the relationship between h and R must be considered. Such a relationship may be derived from existing wall jet data, and in general, h may be assumed to be a linear function of R, the simplest form being that of Equation (14). A slightly more complicated expression for h(R) was derived in Reference 1 based on the data of Reference 3. In either case a quadratic equation is obtained which may be solved for R.

Once again, it is instructive to compare the MFDM with the MFM result for this interaction. The MFM result may be derived starting with the fundamental result expressed by Equation (40). Additionally from Figure 59, the following geometric relationships may be obtained:

$$d\ell = \frac{R \, \partial\phi'}{\sin(\phi' - \theta)} = \frac{dy}{\sin\theta}$$

or

$$\partial\phi' = \frac{\sin(\phi' - \theta)}{R \sin\theta} dy \tag{46}$$

Substituting Equation (46) into Equation (40) yields:

$$h \rho V_c^2 \sin^2\theta = \frac{\gamma f \dot{M}_j}{2\pi R} \sin^2(\phi' - \theta) \tag{47}$$

This result was first derived in Reference 1 in which the quantity $\frac{\partial \dot{M}c}{\partial y}$, Figure 59, represented the momentum flux per unit length in the y direction. Equation (47) may be obtained from the results of Reference 1 by selecting

$$\frac{\partial \dot{M}c}{\partial y} = \rho V_\xi^2 \, h \tag{48}$$

Equations (48) and (40) are based on the assumption that the cross-flow momentum flux per unit length in the y direction need include only that amount contained in an area defined by dy and the interacting wall jet height, h. (There is no characteristic height in the uniform cross-flow.)

The relation for the slope of the stagnation line in the ground plane may be obtained for the MFM by solving Equation (47).

$$\tan \theta = \frac{\beta \sin \phi'}{1 + \beta \cos \phi'} \tag{49}$$

where

$$\beta = \sqrt{\frac{\gamma \, f \, \dot{M}_j}{2\pi \, R \, \rho V_\xi^2 \, h}} \tag{50}$$

For a jet impinging symmetrically with respect to the cross-flow direction, $\phi' = 180°$ and $\theta = 90°$, and the stagnation line distance, from Equation (47), is

$$R = \frac{\gamma \, f \, \dot{M}_j}{2\pi \, h \, \rho V_\xi^2} \tag{51}$$

which is identical to Equation (45). Therefore, based on the assumption of Equation (48) both the MFDM and the MFM yield the same result for the distance of penetration of the wall jet into the uniform cross-flow.

Comparisons of stagnation line computations based on the stagnation line slope equations, Equations (43) and (44) versus (49) and (50) show very little effect on stagnation line position or shape. Therefore, the MFDM results have been incorporated into the MCAIR ground flowfield prediction methodology, and the linear relation relating the wall jet height, h, to the radius R developed in Reference 1 is also used, i.e.,

$$h = \sigma_1 + \sigma_2 \, R \tag{52}$$

(see Reference 1).

Comparisons of the above results with the experimental data of Reference 17 indicated that an additional empirical correction was required to obtain agreement with the experimental data for wall jet penetration into a uniform cross-flow. The empirical correction is applied to the cross-flow momentum flux per unit length dy, as given by

$$\frac{\partial \dot{M}c}{\partial y} = C^2 \, \rho V^2 \, h \tag{53}$$

Equations (43), (44) and (45) then become

$$\tan \theta = \frac{\beta \sin \phi'}{1 + \beta \cos \phi'} \tag{54}$$

where

$$\beta = \frac{\gamma \, f \, \dot{M}_j}{2\pi \, R \, h \, C^2 \, \rho V_\xi^2} \tag{55}$$

and

$$R = \frac{\gamma \, f \, \dot{M}_j}{2\pi \, h \, C^2 \, \rho V_\xi^2} \tag{56}$$

The value of C^2 for wall jet penetration into uniform cross-flows and for cross-flows with boundary layers was determined from References 17 and 18 respectively and is discussed in the paragraphs following.

In Reference 17, the penetration of a single impinging jet into a uniform cross flow was studied for both hot and ambient temperature jets. The uniform cross-flow interaction was simulated by moving the impinging jet through ambient air by supporting the jet on a rotary support system. Except for minor centrifugal effects, this test technique correctly simulates the STOL jet impingement situation including the additional retardation of the wall jet due to the relative motion between the nozzle and the fixed

ground plane. The correct simulation can be obtained in a conventional wind tunnel only through the use of a moving ground plane. The correlation of penetration distance into the cross-flow is shown in Figure 60 taken from Reference 17. The geometry and nomenclature are defined in Figure 61. Another empirical correlation from Reference 17 shows that

$$(q_c/q_{wj})^{1/2} \cong 0.5 \tag{57}$$

which indicates, from Figure 61, that the stagnation line in the cross-flow situation occurs at a distance corresponding to the static jet impingement situation where

$$q_{wj} \cong 4\, q_c \tag{58}$$

In other words, the wall jet penetrates into the cross flow much less than would be expected based on an equivalence of local dynamic pressures. This may be accounted for in the analytical models by artificially increasing the cross-flow momentum as shown in Equation (53). From Reference 17 it may be expected that $C^2 \cong 4$ for the uniform cross-flow case without a cross-flow boundary layer.

Equations (54), (55) and (56) were used to determine the value of C^2 to fit the data correlation of Reference 17 shown in Figure 60. The empirically determined value of C^2 was found to be

$$C^2_{\text{uniform cross-flow}} = 3.61 \tag{59}$$

This value of C^2 is used in the MCAIR ground flowfield methodology for the uniform cross-flow interaction with no cross-flow boundary layer and where the wall jet is retarded by the relative motion of the ground plane. A schematic of the interaction with and without a moving ground plane is shown in Figure 62. With a fixed ground plane, the jet impinges statically with respect to the ground plane, and the cross-flow includes a boundary layer. In the moving ground plane situation which simulates the STOL landing situation the stagnation line is shifted aft due to the lack of a boundary layer in the cross-flow and due to the retardation of the wall jet.

In the case of a fixed ground plane, Figure 62a, the value of C^2 would be expected to be less than the value of 3.61 obtained for the moving ground plane case. The data of Reference 18 was used to determine C^2 for this situation. The data of this reference in which a fixed ground plane was utilized is correlated analytically as

$$\frac{R}{D} = 0.61 \left(\frac{q_{je}}{q_c}\right)^{1/2} \tag{60}$$

The data correlated by Equation (60) also included variations in nozzle exit flow temperature.

For this situation, the correlating value of C^2 for use in the MCAIR ground flowfield methodology was determined to be

$$C^2_{\text{fixed ground plane}} = 2.40 \tag{61}$$

These correlations are summarized in Figure 63 in which the variation of the wall jet stagnation line or separation distance is shown as a function of the nozzle exit to cross-flow dynamic pressure ratio. The curve labeled uncorrected MFDM corresponds to $C^2 = 1.0$ which usually overpredicts the penetration of the wall jet into the cross-flow. The correlations corresponding to the moving ground and fixed ground plane situations were obtained using the values of C^2 given in Equations (59) and (61) respectively based on the data of References 17 and 18. Shown also in Figure 63, are data correlations for two values of H/D from wind tunnel and moving ground vehicle tests of ingestion boundaries for the Concorde aircraft configuration with $\delta_L = 115°$. These correlations contain both fixed and moving ground data (Reference 19).

The need for the degree of empiricism used in the results shown in Figure 63 is not surprising due to the complex nature of this turbulent interaction. It is hoped that these correlations will be further verified or modified as required as new data is acquired. The purpose here has been to unify the treatment of the analytical modelling of the interaction. The unified analytical modelling allows consistent parametric variation of the many independent variables associated with this problem with a minimum of additional empiricism.

Additional useful information on the effects of fixed versus moving ground plane testing may be found in References 20 and 21 for example. Reference 21 contains an extensive list of earlier pertinent work. Figure 64 taken from Reference 20 substantiates the results presented in Figure 63 in terms of the STOL aircraft landing rolling speed at which ingestion may first occur. This was established for a particular thrust reverser configuration shown in the Figure which included forward vectoring for reverse thrust plus outboard splay of the reverser jets. It is seen from the Figure than an approximate 15% reduction in rollout speed for ingestion is indicated with the moving ground plane simulation compared to the fixed ground plane simulation. The effect of NPR is also indicated for this reverser configuration, and in general indicates the expected trends with forward vectored reverser jet impingement for a wide range of configurations. The differences between moving and fixed ground plane simulations may not appear to be large; however, the desired landing rollout distance goals are quite short compared to CTOL high speed aircraft landing distances, and these differences must be considered in the aircraft rollout performance analysis.

An alternative empirical method is also used by MCAIR to predict the boundaries for exhaust gas ingestion potential for STOL aircraft landing rollout for configurations employing thrust reversers. This method is based on the balance of local dynamic pressure in the turbulent wall jet with the dynamic pressure of the cross-flow. A typical decay of wall jet dynamic pressure with radius from the jet impingement point is shown in Figure 65. These data also include cases with elevated nozzle exit flow temperatures. Here q_j is the free jet dynamic pressure locally at the distance down the jet corresponding to the distance from the nozzle exit to the jet impingement point. $R_{v/2}$ is also determined from the free jet velocity profile at this point.

In the fixed ground plane situation, the location of the stagnation line is taken to be at the point where

$$q_c = q_{wj}\Big|_{\text{average}} = 0.457\, q_{wj}\Big|_{\text{max}} \tag{62}$$

In the moving ground plane or STOL situation, Equation (62) is also used, but, additionally, the cross flow dynamic pressure is multiplied by a factor of four, i.e.,

$$q_c\Big|_{\text{moving ground}} = 4\, q_c \tag{63}$$

which relates to Equation (58) based on the data of Reference 17.

Figure 66 presents ground stagnation line computations for a typical high speed fighter configuration employing aft located thrust reversers. Stagnation line locations predicted by the MCAIR empirical method are shown as a function of aircraft ground roll speed (headwind velocity) for thrust reversal with and without lateral splay. The beneficial effect of splay is apparent, however a component of reverse thrust can be lost through the employment of splay if the splay is not obtained through a rotation of the reverser about the aircraft longitudinal axis.

The potential for exhaust gas ingestion may be reduced and, in fact, eliminated on ground roll out through thoughtful configuration design, and, additionally, through active control of exhaust jet efflux direction. Thrust reverser designs employing variable vectoring vanes can direct the jet efflux to maintain the ground stagnation line aft of the aircraft inlet location as the rollout velocity is reduced while still providing significant reverse thrust. These systems combined with conventional mechanical wheel braking can provide excellent STOL landing performance.

In addition to the exhaust gas ingestion problem addressed above, the aerodynamicist must be concerned with the jet efflux induced effects on the aerodynamics of the vehicle, including stability and control considerations. These are important both in and out of ground effect. Additionally, surface heating caused by jet efflux or fountain impingement on the airframe must be considered in the vehicle design and development process. Consideration of all of these design and performance factors, at this time, and for the forseeable future ultimately results in a series of wind tunnel simulations. However the analytical modelling of these effects, including the available empirical data base, can be used to minimize the amount of wind tunnel simulation required.

III. UNIFORM CROSS-FLOW OUT OF GROUND EFFECT (FLIGHT TRANSITIONAL FLOW FIELDS)

A method is presented for predicting the aerodynamic performance of complete V/STOL aircraft operating out of ground effect in the transition regime between hover and conventional forward flight. In transition, the large jet deflection angles, low aircraft velocity, relatively low Reynolds number, and high trailing edge flap deflections lead to strong viscous aerodynamic-propulsion interactions that have a substantial effect on aircraft forces and moments (Figure 67). The data of Figure 67 indicate a small effect of jet induced flows on lift for the YAV-8B (power off versus power on), however, the jet induced flows have an appreciable effect on aircraft pitching moment, producing a "pitch-up" increment which must be considered when trimming the aircraft. Although a positive pitching moment increment is induced by the jet flows, the basic stability of the aircraft, dC_M/dC_L, is not changed.

The specific jet induced flow phenomena that produce these large interactions are presented in Figure 68. Although the blockage and mass entrainment of the jets have a substantial effect on the surrounding aerodynamic flow field, the effect of the airframe on the properties of the jets-in-cross-flow is typically weak. This fact allows the jet centerline trajectory, cross-section geometry, and entrainment rate to be calculated by an independent (decoupled) jet-in-cross-flow method.

There have been a multitude of reports, papers and survey papers written on V/STOL transitional jet induced flowfields. Many of these report the jet induced effects on specific or generic aircraft configurations; others report the results of investigations of elements of the overall problem such as the numerous studies of turbulent jets in cross-flow. No attempt will be made here to review all of these contributions, however, References 21 and 22 present recent surveys.

The vectored jets can produce local, relatively direct effects on the airframe such as, in the case of a jet exiting from the lower surface of the airframe, a region of increased static pressure in front of the jet with a region of reduced static pressure behind the jet due largely to the blockage effect of the jet on the cross-flow. This normally results in a "pitch-up" increment to the aircraft longitudinal moment. The entrainment of the jets due to turbulent mixing and the velocities induced by the jet-in-cross-flow vortex structure generally induce a down wash over the aft fuselage and empanage of the aircraft. This generally produces a "pitch-up" increment, and requires a longitudinal trim adjustment. The jet induced downwash for the V/STOL configurations of Reference 23 is shown in Figure 69. The downwash angle, ε, is shown as a function of ψ at three horizontal tail locations for the configuration studied. As would be expected, the downwash angle is greatest for low values of ψ and low "water-line" horizontal tail positions. For the configuration shown and the aircraft attitude selected for the data of Figure 69, the "power-off" ($\psi = \infty$) downwash was 1° or less, therefore, the induced downwash shown is due to jet induced effects. Data of this nature must be developed to establish required horizontal tail deflection ranges for longitudinal balance and stability and control requirements. Although these data may suggest a preference for a high tail position, high angle of attack requirements for highly maneuverable fighter aircraft necessitate a horizontal tail position at or below the wing plane position.

The AV-8B V/STOL aircraft was evolved from the AV-8A Harrier aircraft through the incorporation of a number of aerodynamic changes. Changes to the wing of the aircraft included the adoption of a supercritical airfoil section, an increase in wing area and span, and a change from plain 50° trailing edge flaps to larger, single slotted flaps with 60° maximum deflection. These modifications, and their effect on the aircraft's basic aerodynamic characteristics are discussed in Reference 24. As a result of these modifications, the lift coefficient of the AV-8B was increased over the AV-8A by an increment of $\Delta C_L \approx 0.7$ in the 0° to 12° angle of attack range. To illustrate the sensitivity of V/STOL aircraft performance to small changes in the powered lift system configuration, Figure 70, from Reference 24, illustrates the benefit of simply removing the scarf from the basic AV-8A forward nozzle by extending the outboard wall of the nozzle duct. On the AV-8B with the slotted trailing edge flap, the scarfed forward nozzle flow interacting with the wing undersurface and inboard pylon caused a flow separation upstream of the flap. Removal of the scarf directed the forward jet to a position farther below the wing and produced the C_L increment shown in Figure 70.

Current aerodynamic prediction techniques cannot accurately model all aspects of the V/STOL aircraft jet induced flowfield including all of the viscous phenomenon occuring on the airframe. However, if the vectored jets are directed away from the airframe such that the induced flowfield over the airframe is essentially inviscid and irrotational, the primary induced aerodynamic effects such as ΔC_L, ΔC_m, and the induced downwash, ε, can be predicted. The following paragraphs outline the V/STOL transition mode prediction methodology currently under development at MCAIR. A discussion of the predictions of separated flow effects on the wing of the aircraft due to trailing edge separation with plain flaps is included.

If the complete aerodynamic flow field were incompressible and inviscid, a surface panel method could be applied to calculate the induced forces and moments on the airframe surface. Panelled jets with surface suction would represent the effects of jet blockage and entrainment. However, in the transition mode there can be regions of separated flow associated with highly deflected control surfaces or high angles-of-attack. Panel methods are appropriate for analyzing the flow in the presence of regions of separation if the panelled geometry includes the viscous displacement surface. The problem is to solve for the displaced surface; the difficulty is that the solution is dependent upon strong viscous-inviscid interactions.

In the past decade several methods have been developed for predicting the incompressible aerodynamic forces and moments of two dimensional airfoils in the presence of turbulent flow separation (References 25-29). Most of these methods empirically model the turbulent flow separation region by constant static pressure from the separation point to the airfoil trailing edge with some method for closing off the wake downstream. This bypasses the need to perform complex computations within the viscous separated flow region. An inverse two-dimensional potential flow method is used to "design" the streamline contour that satisfies the constant pressure conditions on the separated wake.

With the development of three-dimensional wing inverse potential flow (or design) methods (References 30-33), the expectation was that finite wing viscous-inviscid interactions including turbulent flow separation would be forthcoming. However, reliable methods have not been developed for several reasons. First, most of the two dimensional viscous-inviscid interaction procedures utilize simple iteration between distinct viscous-only and inviscid-only calculation steps. This procedure can be numerically unstable and often requires man-in-the-loop corrections to insure accuracy and numerical stability. Second, accurate three-dimensional conventional panel methods and design methods are expensive to use. Iterating between a panel method, a viscous calculation method, and a design method for five or more iterations for each angle-of-attack can be prohibitively expensive. Third, until recently, the design methods suffered from numerical instabilities that precluded the accurate and efficient coupling to viscous methods. All of these difficulties should be dealt with simultaneously when considering the finite wing viscous-inviscid interaction problem.

Three recent advances have overcome the major difficulties with three dimensional viscous-inviscid interaction predictions. In 1980 the MCAIR Stalled Airfoil Analysis Program (Reference 29) was developed for the reliable prediction of 2-D airfoil forces and moments in fully attached or turbulent separated flow. In 1981, the MCAIR 3-D Perturbation Analysis Method (Reference 34) was developed for the accurate and inexpensive inviscid solution corresponding to arbitrary small perturbations to wing-fuselage geometries. In 1982, the MCAIR 3-D Subsonic Wing Design Program (Reference 33) was developed for the accurate, inexpensive, numerically stable design of wing-on-fuselage geometries corresponding to prescribed pressure distributions.

The MCAIR V/STOL Transition Mode Methodology represents the synthesis of these three advances that make possible numerically stable solutions to the 3-D viscous flow problem. Furthermore, by incorporating complex aircraft configurations through the use of the panel method, the approach is applicable to wings, wing-fuselage combinations, and wing-fuselage-jet configurations.

The computation of the aerodynamic performance of V/STOL aircraft in transition out of ground effect requires the use of four computer programs:

(a) Adler-Baron Jet-In-Cross-Flow Program (JICP; Ref 35),

(b) MCAIR 3-D Subsonic Potential Flow Program (SPFP; Ref 34),

(c) MCAIR 3-D Geometry Influence Coefficient Program (GICP; Ref 34), and

(d) MCAIR 3-D Stalled Wing Analysis Program (SWAP).

It is assumed that the flow is incompressible and that the following quantities are known: (1) airframe geometry, (2) the freestream angle of attack and unit Reynolds number, (3) the engine inlet mass flow, and (4) uniform nozzle exit conditions (injection angle and freestream to jet velocity ratio). Furthermore, it is assumed that the jets are incompressible and turbulent, and any trailing edge device is unslotted.

The calculation procedure is depicted in Figure 71. The first step is to determine the jet properties under the assumption that airframe influence on the jets is negligible. Each jet injection angle, δ_{je}, and freestream-to-jet velocity ratio, Ψ, is converted by JICP to jet centerline trajectory, cross-sectional geometry, and mass entertainment rate. The jet geometry is panelled and connected to a panelled representation of the baseline aircraft geometry (aircraft without viscous displacement thickness). The mass entrainment of the jet is represented by suction distributed over the jet panels.

The baseline configuration is converted to a distribution of inviscid surface pressure and an aerodynamic influence coefficient matrix by SPFP. The output from this program is used as input to GICP, which calculates a matrix of partial derivatives. Each element of this matrix represents the rate of change of the inviscid perturbation potential on the surface with respect to arbitrary changes in the wing displacement. GICP is executed twice corresponding to angles-of-attack of zero and ninety degrees.

The output from SPFP and GICP are used as input files to SWAP, which uses the inviscid perturbation matrices from GICP to extrapolate for the pressure solution corresponding to the desired angle-of-attack and calculated wing displacement surface. The wing effective shape is determined iteratively along with the distribution of pressure over the aircraft surface. Forces and moments are determined by integration of pressure over the aircraft and surface shear stress over the wing.

The discussion following will concentrate on the empirical data base and computational models used for determining the pertinent flowfield properties for turbulent jets-in-cross-flow. This is followed by a description of the basic MCAIR three dimensional panel method for the computation of subcritical potential flows. A detailed description of the MCAIR 3-D Geometry Influence Coefficient Program and the 3-D Stalled Wing Analysis Program may be found in References 34 and 36 respectively.

JET-IN-CROSS-FLOW MODEL

The MCAIR V/STOL Transition Mode Methodology currently derives required jet-in-cross-flow information for jets emanating from circular or nearly circular nozzles from the Adler-Baron Jet-In-Cross-Flow program, JICP, (Reference 35). The basic method was developed for incompressible jets submerged in a uniform cross-flow. The jet injection angle, δ_{je}, and freestream to jet exit velocity ratio, Ψ, are variable over a useful range for the V/STOL transitional mode application. (MCAIR has modified the basic Adler-Baron formulation to include some non-circular jet exit shapes, and also to permit forward jet injection angles for analysis of thrust reverser flow fields).

A schematic of jet-in-cross-flow development is shown in Figure 72. The jet is deflected downstream by the momentum of the cross-flow. As the jet develops downstream, the vorticity generated by the basic jet injection combined with the flow of the cross-flow around the jet results in the formation of a pair of contra-rotating vortices, which tend to dominate the downstream development of the jet. Induced flowfield velocities result from:

(a) the basic blockage of the jet,

(b) the turbulent entrainment (similar to a free jet), and

(c) vortex induction.

In general, the centerlines of the vortices lie above the nominal jet centerline. Trajectories of both the jet centerline and the vortex centerlines are given in Reference 37 for round jets-in-cross-flow.

The basic Adler-Baron model (Reference 35) is developed on the basis of some simplifying assumptions, namely: 1) external flowfield is irrotational; 2) the mixing field is isothermal and of uniform composition (no heat transfer or diffusion); 3) the flow is turbulent; 4) the flow is incompressible and steady; 5) the jet centerline is defined as the locus of the momentum centers of cross sections; 6) velocities are parallel to the centerline; 7) cross-section boundary of the jet is the locus of points at which the velocity excess in the direction of the centerline vanishes (or is smaller than a prescribed small value); 8) pressure on cross sections is uniform and proportional to $V_c \cos\theta_{jc}$; 9) most of the entrainment takes place in the vortex pair tail.

A control volume in the jet is used to derive the governing two momentum equations of the integral model. These two integral momentum equations, together with four additional equations - i.e., the expansion rate equation, the shape equations, and the normalized velocity profile equation - describe the jet mixing field completely.

Two momentum equations are developed; one parallel to the jet centerline and one perpendicular to it. The momentum balance includes entrained momentum, surface forces on the jet (drag force) and centrifugal body forces. To complete the formulation, the rate of the jet growth, the shape of the cross sections, and the velocity profiles have to be determined. It is assumed that the jet cross-section area growth is a linear superposition of two growing mechanisms: 1) growth of a straight turbulent jet in a quiescent environment; and 2) growth of a vortex pair (in accordance with assumption 9). Although this model of jet growth seems to be an over-simplification, it yields acceptable results.

The cross-section shape calculation predicts approximately the development of the geometry (but not the areas) of these shapes from a circle into the developed norseshoe configuration. This shape development contains much of the nonsimilarity of the mixing process, so that its prediction is essential for a representative model. The cross-section distortion is determined by evenly seeding a finite number N of vortices on the instantaneous boundary of the jet and calculating their displacement over a small time period due to their induced velocity. The induced velocity components of each vortex are calculated, and the vortices are displaced accordingly as the computation progresses down the jet.

The internal jet velocity profiles are obtained from a solution of Poisson's equation within the jet cross-section combined with empirical parameters.

The Adler-Baron solution approach is summarized in Table 3.

The Jet-In-Cross-Flow Program is restricted to one isolated jet issuing from a flat plate into the freestream. Due to the weak effect of the airframe on the jet, it is reasonable to calculate the jet properties in isolation. For multiple jets, the program is executed once for each jet. Furthermore, for tandem jets, as is the case for the YAV-8B, the upstream jet exerts a large influence on the downstream one, and the jets tend to coalesce. For multiple jets with interaction and coalescence, the method of Wooler (Reference 38) is used to determine the blockage effects of the upstream jet on the downstream jet. The merged single jet properties are determined to a first approximation by simply combining the effects of the individual jets without coalescence.

A demonstration of the accuracy of the Adler-Baron JICP is shown in Figures 73-76, where the predicted jet centerline trajectory, cross-sectional area ratio, entrained mass flux and jet velocity profiles are compared with experimental data. (Reference 39). The agreement is good for the cases examined.

MCAIR extensions of the Adler-Baron JICP for non-circular nozzle exits and upstream jet injection angles are shown in Figures 77 and 78 respectively.

Implementation of the MCAIR V/STOL transition mode methodology requires that the jet-in-cross-flow characteristics obtained from the Adler-Baron JICP be modelled in the MCAIR three dimensional Subsonic Potential Flow Program (SPFP). Figure 79 demonstrates the panelling model of the jet-in-cross-flow. The three dimensional outer surface of the jet is obtained from the JICP. The "windward side" of the jet is panelled as a solid surface which models the blockage effect of the jet-in-cross-flow. The "leeward side" of the jet (shaded panels in Figure 79) is made up of panels with a prescribed distribution of normal velocities to simulate the entrainment and velocity distribution induced by the jet-in-cross-flow vortex structure. The jet axial segment control volume shown in Figure 80 is used to establish the total entrainment per unit length of the jet based on the entrainment distribution obtained from the JICP as shown, for example, in Figure 75. A distribution of normal velocities on these entrainment panels such as that shown in Figure 81 is defined to complete the entrainment modelling for the jet-in-cross-flow. This entrainment distribution model, although somewhat arbitrary, places the entrainment "sinks" on the leeward side of the jet-in-cross-flow and nearest to the airframe under-surface as the jet and its vortex structure pass below the aircraft. Results obtained with this model will be shown in the paragraphs following.

Discussion of the modelling of jets-in-cross-flow and the use of the JICP has, to this point, been limited to jets emanating from circular nozzles, except for the results presented in Figure 77. The characteristics of jets-in-cross-flow emanating from rectangular nozzle exits were studied extensively in the work reported in Reference 40. Equations for jet centerline and jet vortex trajectories for the aspect ratio 4 nozzles studied in Reference 40 are contained in that Reference. The relationship of these trajectories to those of circular jets was found to be dependent on the orientation of the rectangular nozzle with respect to the cross-flow direction. When the nozzle exit major axis was placed parallel to the cross-flow direction (streamwise orientation) the jet penetrated further into the cross-flow than the equivalent circular jet. A 90° rotation of the nozzle exit (blunt orientation) showed that the blunt rectangular jet does not penetrate into the cross-flow as far as the equivalent circular jet. In general, it was found that the jet decay (reduction of jet centerline total pressure with distance from the jet exit) data indicated that rectangular jets decay much faster than circular jets of the same equivalent diameter. The increased decay rate is due primarily to increased viscous mixing due to the larger perimeter surface of the rectangular nozzles and jets.

Figure 82 and 83 present measurements (from Reference 40) of surface pressures in the region of the jet exit for a circular and rectangular jet (both streamwise and blunt orientation (Figure 82) and the effect of Ψ on the surface pressures in the vicinity of a blunt rectangular jet exit (Figure 83)). The blunt nozzles are characterized by a significant low-pressure wake region, a region of positive pressure forward of the nozzle, and a region of low pressure which spreads laterally from the sides of the nozzle. The pressure fields induced by the streamwise jets were quite different. The primary effect was a low-pressure region which spread laterally from the sides of the jet. There was almost no wake and only a small region of positive pressure forward of the nozzle exit. Comparisons of the three distributions in Figure 82 shown that the rectangular jet distributions tend, in a qualitative sense, to "bracket" the circular jet results. The circular jet had a low-pressure wake region similar to that exhibited by the blunt rectangular jet, while the lateral spread of low pressure and small upstream positive-pressure region are more characteristic of streamwise-oriented rectangular jets.

The influence of velocity ratio, Ψ, for the blunt orientation Figure 83, indicates three principal effects: 1) the total surface area affected increases as Ψ decreases; 2) the negative pressure field expands forward and outward as Ψ decreases while the positive pressure field contracts; 3) the pressure gradients tend to steepen with decreasing ψ, particularly in the negative pressure region.

SUBSONIC POTENTIAL FLOW PROGRAM

The MCAIR 3-D Subsonic Potential Flow Program (Reference 34) is a surface panel method that is based on the combined source-doublet distribution of the classical third identity of Green (Reference 41). The advantages of this combined source-doublet distribution for a surface panel method are well documented (Reference 42). The mathematical formulation employs a constant source distribution and a quadratic doublet distribution on each panel, where the solution singularity strengths are determined by satisfying indirect internal perturbation potential boundary conditions (Reference 43). The flow velocity on each panel is then established from local velocity-singularity relationships associated with Green's third identity, instead of direct summation of the influences of the singularities on all the panels. The method is formulated with a Gothert type compressibility correction; however, this option is not used in the present method. A detailed discussion of the method is found in Reference 34.

This panel method is used to calculate the airframe inviscid pressure distribution induced by the aircraft forward velocity plus the blockage and mass entrainment effects of the jets. A demonstration of the accuracy of the panel method is presented in Figure 84, where the YAV-83 wing pressure distribution in conventional flight (.50 M_∞, 6.4° angle-of-attack) is compared to wind tunnel pressure data. The ability of the panel method to model geometric details is reflected in the accuracy of the lower surface pressures at 25% semispan, where the effect of the protruding nozzles is substantial. Wind tunnel surface pressure data for the YAV-8B in V/STOL transition is not available for comparison with analytical predictions; however, detailed pressure data are available for a single circular jet emanating from a flat plate into a uniform crossflow (Reference 44). As shown in Figure 85, the geometry for the panelled jet was calculated by the Adler-Baron JICP method. In the surface panel method, the effect of the mass entrainment is simulated by distributed normal velocities on the jet panel surfaces. The pressure distribution on the plate calculated by the panel method agrees well with experimental data, except in the wake of the jet (Figure 86). Although the separated wake of a jet-in-cross-flow represents an important aerodynamic problem that requires further investigation, it is beyond the scope of the present effort. (This problem has recently been addressed in Reference 45.) The good agreement for this jet-plate combination demonstrates that the treatment of the jet decoupled from plate is satisfactory.

EXAMPLE CALCULATIONS

To be able to assess the accuracy of the jet-airframe-wing viscous effects predictions, several wing alone calculations were performed prior to analyzing the YAV-8B powered model. These example computations were supported by the MCAIR Independent Research and Development Program. The wing along geometric parameters chosen for analysis are shown in Table 4 along with the YAV-8B supercritical wing. Each of these solutions is discussed.

The first wing along geometry analyzed was a rectangular planform, NACA 4412 section, aspect ratio 6 wing. Since experimental force and moment data were available for this wing at midspan, it was possible to assess the accuracy of the method without having to deal with strong three dimensional boundary layer effects. The predicted force and moment at midspan are compared with experiment (Reference 46) in Figure 87. The predictions agree well with experiment. Furthermore, this section geometry was analyzed by the Stalled Airfoil Analysis Program (Reference 29) with results depicted in Figure 88. Comparison of Figures 87 and 88 shows that the present method exhibits the same trends as the two dimensional method. This result provides confidence in using the polynomial curve fits to represent the boundary layer thickness and the Perturbation Analysis Method to calculate the inviscid parameters, since the Stalled Airfoil Analysis Program does not use either of these approximations.

The next case analyzed was a 20° swept, NACA 0012 section, aspect ratio 5.5 wing on a wall. The predicted forces and moments are depicted in Figure 89. While experimental data in the form of pressure distributions along lines normal to the leading edge are available (Reference 47), overall force and moment data are not available. The only force data found in this data set was the normal force, C_N, on an unswept, NACA 0012 section, aspect ratio 6 wing. Thus, this wing geometry was analyzed and the predicted normal force is compared with experiment in Figure 90. Also shown is the predicted normal force for the swept wing case, which follows reasonable trends when compared to the unswept data.

While analyzing the swept wing case, it was discovered that the laminar boundary layer calculations tended to become numerically unstable near the suction peak at high angles-of-attack (> 15)°). It is believed that the primary cause for the instabilities was that the transition constraint equations did not move the transition location far enough forward to preclude the presence of very strong adverse pressure gradients within the laminar viscous regions. Successful analysis was accomplished by considering the flow to be fully turbulent from the attachment line and fixing the beginning of the upper surface turbulent region at the leading edge. This procedure was also used for the remaining cases.

The last wing alone case analyzed was a wing with an aspect ratio of 6, 37.25° leading edge sweep, 0.5 taper ratio, and NACA 64$_1$-212 sections normal to the leading edge. The geometry is shown in Figure 91. Comparison of predicted forces and pitching moment with experiment (Reference 48) are depicted in Figure 92. Separation occurs at an angle-of-attack of twelve degrees. The predictions do not fully account for the detrimental effects of the flow separation. However, comparison of the viscosity included predictions with the viscosity ignored predictions indicate that a substantial portion of the viscous effects are predicted.

The final test case, the YAV-8B powered model, was accomplished to assess the accuracy of the complete jet-airframe interaction method. One of the most important interference effects in V/STOL aerodynamics is the lift increment or decrement due to power effects in the transition flight regime. If the strong interaction effects are properly modelled, this interference can be accurately predicted.

The YAV-8B powered model with flaps deflected 50° was analyzed with the MCAIR V/STOL Transition Mode Methodology for both power off and power on conditions. Viscous corrections were not included in these calculations due to the presence of part span flaps, which are not included in the current SWAP capability. The panelled representation of the aircraft geometry with the jets is shown in Figure 93.

The predicted lift coefficient at various angles-of-attack is shown in Figure 94 for the YAV-8B with power off. Also shown is the range of experimental data. While the slope of the lift curve is nearly correct, the level is off significantly for not allowing for viscous flow separation on the flap. The ultimate goal of SWAP is to calculate this lift decrement; however, further development is required.

Two different approaches were used to predict the lift coefficient versus angle-of-attack for the YAV-8B with power on (Figure 95). A well designed V/STOL aircraft, such as the YAV-8B, uses the large downwash induced by the jet-entrainment to keep the flow on the flap attached. Thus, an inviscid method should be able to predict the lift curve. The first approach used was to utilize a single calculation of the jet effects at an injection angle corresponding to 0° aircraft angle-of-attack. The solid line in

Figure 95 is the predicted result. The predicted lift coefficient at 0° angle-of-attack is accurate, but the slope of the lift curve is poor. The reason for this descrepancy is that as the angle-of-attack i, increased the jet modelling is not correct. A remedy to this would be to recalculate the jet propertie at each angle-of-attack. However, an alternative to this expensive procedure is to superimpose the powe off calculated slope of the lift curve starting at the predicted lift coefficient at 0° angle-of-attack. This procedure results in the dotted line in Figure 95, which is quite accurate. The good results are not surprising since the jets act primarily by changing the effective flap deflection, which does not change the slope of the lift curve.

REFERENCES

1. Kotansky, D. R., Durando, N. A., Bristow, D. R., and Saunders, P. W., "Multi Jet Induced Forces and Moments on VTOL Aircraft Hovering In and Out of Ground Effect", Final Technical Report, Naval Air Development Center, NADC Report No. 77-229-30, June 1977.

2. Kleis, S. J., and Foss, J. F., "The Effect of Exit Conditions on the Development of an Axisymmetric Turbulent Free Jet", Third Year Technical Report, NASA Grant NGR 23-004-068, Michigan State University, 15 May 1974.

3. Donaldson, C. du P., and Snedeker, R. S., "A Study of Free Jet Impingement, Part I - Mean Properties of Free and Impinging Jets", Journal of Fluid Mechanics, Vol. 45, Part 2, pp 281-319, 1971.

4. Kotansky, D. R., and Glaze, L. W., "Investigation of the Effects of Ground Wall Jet Characteristics on Fountain Upwash flow Formation and Development", Report No. ONR-CR-212-261-IF, Office of Naval Research, June 1980; Also AIAA Paper No. 81-1294, AIAA 14th Fluid and Plasma Dynamics Conference, Palo Alto, CA, 23-25 June 1981.

5. Kotansky, D. R., and Glaze, L. W., "Investigation of Impingement Region and Wall Jets Formed by the interaction of High Aspect Ratio Lift Jets and a Ground Plane", Report No. NASA CR152174, Ames Research Center, September 1978.

6. Kotansky, D. R., and Glaze, L. W., "Investigation of the Interaction of Lift Jets and a Ground Plane", Report No. NASA CR 152343, Ames Research Center, April 1980.

7. Kotansky, D. R., and Glaze, L. W., "Characteristics of Wall Jets Produced by the Impingement on a Ground Plane of Rectargular Jets of Aspect Ratio One through Eight", AIAA Paper No. 81-0012 presented at the AIAA 19th Aerospace Sciences Meeting, St. Louis, MO, 12-15 January, 1981.

8. Private Correspondence, K. A. Green, Naval Air Development Center to D. R. Kotansky, 24 August 1978.

9. Moran, J., Tinoco, E. N., and Johnson, F. T., "User's Manual Subsonic/ Supersonic Advanced Panel Pilot Code", NASA CR-152047, Ames Research Center, February 1978.

10. Glaze, L. W., Bristow, D. R., and Kotansky, D. R., "V/STOL Fountain Force Coefficient", Naval Air Development Center Report No. NADC-81106-60, January 1983.

11. Hill, B. J., "Measurement of Local Entrainment Rate in the Initial Region of Axisymmetric Turbulent Air Jets", Journal of Fluid Mechanics, vol. 51, Part 4, pp 773-779, 1972.

12. Ricou, F. P., and Spalding, D. B., "Measurements of Entrainment by Axisymmetric Turbulent Jets", Journal of Fluid Mechanics, Vol. 11, Part 1, p. 21, 1961.

13. Wygnanski, I., "The Flow Induced by Two-Dimensional and Axisymmetric Turbulent Jets Issuing Normally to an Infinite Plane Surface", Report No. 63-12, Mechanical Engineering Research Laboratories, McGill University, Montreal, Canada, December 1963.

14. Trentacoste, N., and Sforza, P., "Further Experimental Results for Three-Dimensional Free Jets", AIAA Journal, Vol. 5, No. 5, p. 885, May 1967.

15. Henderson, C., Clark, J., and Walters, M., "V/STOL Aerodynamics and Stability and Control Manual", Report No. NADC-80011-60, Naval Air Systems Command, 15 Janaury 1980.

16. Kalemaris, S. G., "Evaluation of the Effects of Model Scale and Test Technique on Jet Induced Effects", AGARD-CP-308, Proceedings of fluid Dynamics of Jets with Application to V/STOL, January 1982.

17. Abbott, W. A., "Studies of Flow Fields Created by Vertical and Inclined Jets when Stationary or Moving Over a Horizontal Surface", Aeronautical Research Council Current Paper No. 911, Great Britian, October, 1964.

18. Weber, H. A., and Gay, A., "VTOL Reingestion Model Testing of Fountain Control and Wind Effects", AIAA Paper No. 75-1217, Presented at the AIAA/SAE 11th Propulsion Conference, Anaheim, CA, September, 1975.

19. Willmer, A. C., and Scotland, P. L., "Reverse Thrust Experience on the Concorde", AGARD-CP-150, March, 1975.

20. Lotter, K., and Kurz, W., "Aerodynamic Aspects and Optimization of Thrust Reverser Systems", AGARD-CP-150, March, 1975.

21. Margason, R. J., "Jet V/STOL Wind-Tunnel Simulation and Ground Plane Effects", AGARD-CP-308, January, 1982.

22. Kuhn, R. E., "The Induced Aerodynamics of Jet and Fan Powered V/STOL Aircraft", Presented at the International Symposium on Recent Advances in Aerodynamics and Aeroacoustics, Stanford University, August, 1983.

23. Mineck, R. E., and Schwendemann, M. F., "Aerodynamic Characteristics of a Vectored Thrust V/STOL Fighter in the Transition-Speed Range", NASA TN D-7191, January, 1966.

24. Lacey, T. R., and Miller, K., "The AV-8B Wing: Aerodynamic Concept and Design", AIAA Paper No. 77-607, Presented at the AIAA V/STOL Conference, Palo Alto, CA June 1977.

25. Maskew, B., and Dvorak, F. A., "Investigation of Separation Models for the Prediction of $C_{L_{MAX}}$", Journal of the American Helicopter Society, Vol. 23, pp 2-8, April, 1978.

26. Henderson, M. L., "A Solution to the 2-D Separated Wake Modeling Problem and Its Use to Predict $C_{L_{MAX}}$ of Arbitrary Airfoil Sections", AIAA Paper 78-156, January, 1978.

27. LeBalleur, J. C., and Neron, M., "Cacul D'Ecoulements Visqueux Decolles sur Profils D'Ailes par une Approche de Conplage", AGARD Conference Proceedings, No. 291, February, 1981.

28. Carlson, L. A., "A Direct-Inverse Technique for Low Speed High Lift Airfoil Flowfield Analysis", AGARD Conference Proceedings, No. 291, February, 1981.

29. Gilmer, B. R., and Bristow, D. R., "Analysis of Stalled Airfoils by Simultaneous Perturbation to Viscous and Inviscid Equations", AIAA Journal, Vol. 20, No. 9, pp 1160-1166, September, 1982.

30. Johnson, F. T., "A General Panel Method for the Analysis and Design of Arbitrary Configurations in Incompressible Flow", NASA CR-3079, May 1980.

31. Fray, J. M., and Sloof, J. W., "A Constrained Inverse Method for the Aerodynamic Design of Thick Wings with Given Pressure Distribution in Subsonic Flow", AGARD Conference Proceedings, No. 285, May, 1980.

32. Malone, J. B., "An Optimal-Surface-Transpiration Subsonic Panel Method for Iterative Design of Complex Aircraft Configurations", AIAA Paper 81-1254, June 1981.

33. Hawk, J. D., and Bristow, D. R., "Subsonic Surface Panel Method for Airframe Analysis and Wing Design", AIAA Paper 83-0341, January, 1983.

34. Bristow, D. R., and Hawk, J. D., "Subsonic Panel Method for the Efficient Analysis of Multiple Geometry Perturbations", NASA CR-3528, March, 1982.

35. Adler, D., and Baron, A., "Prediction of a Three-Dimensional Circular Turbulent Jet-in-Cross-Flow", AIAA Journal, Vol. 17, No. 2, pp 168-174, February 1979.

36. Gilmer, B. R., Miner, G. A., and Bristow, D. R., "Aircraft Aerodynamic Prediction Method for V/STOL Transition Including Flow Separation", NASA Contractor Report No. 166467, Ames Research Center, April, 1983.

37. Fearn, R., and Weston, R. P., "Vorticity Associated with a Jet in Cross-flow", AIAA Journal, Vol. 12, No. 12, December, 1974.

38. Wooler, P. J., "Development of an Analytical Model for the Flow of a Jet into a Subsonic Crosswind", NASA SP-218, September, 1969.

39. Kamotani, Y., and Greber, V., "Experiments on a Turbulent Jet-in-a-Cross-Flow", NASA CR-72893, June, 1971.

40. Weston, R. P., and Thames, F. C., "Properties of Aspect-Ratio-4.0 Rectangular Jets in a Subsonic Crossflow", Journal of aircraft, Vol. 17, No. 10, October, 1979.

41. Kellogg, O. D., Foundations of Potential Theory, Dover Publications, Inc., 1953.

42. Bristow, D. R., And Grose, G. G., "Modification of the Douglas Neumann Program to Improve the Efficiency of Predicting Component Interference and High Lift Characteristics", NASA CR-3020, August, 1978.

43. Morino, L., and Kuo, C. C., "Subsonic Potential Aerodynamics for Complex Configurations: A General Theory", AIAA Journal, Vol. 12, No. 2, February, 1974.

44. Fearn, R. L., and Weston, R. P., "Induced Pressure Distribution of a Jet-In-Cross-Flow", NASA TN D-7916, July, 1975.

45. Walters, M. M., and Yen, K. T., "Prediction of Propulsion Induced Effects in Transition Using a Modified Jet Wake Model", AGARD-CP-308, January, 1982.

46. Pinkerton, R. M., "Calculated and Measured Pressure Distributions Over the Midspan Section of the NACA 4412 Airfoil", NACA Report 562, 1936.

47. Yip, L. P., and Shubert, G. L., "Pressure Distributions on a 1-by-3 Meter Semispan Wing at Sweep Angles from 0° to 40° in Subsonic Flow", NASA TN D-8307, December, 1976.

48. Edwards, G. G., And Boltz, F. W., "An Analysis of the Forces and Pressure Distribution on a Wing with the Leading Edge Swept Back 37.25°", NASA RM A9K01, March, 1950.

ACKNOWLEDGEMENT

The author wishes to acknowledge contributions to this lecture on V/STOL Aerodynamics from the following researchers: Lloyd Glaze of MCAIR for his work related to Jet Impingement and Ground Flow-fields; Dean Bristow, Brad Gilmer, Dennis Hawk and Gary Miner of MCAIR for their work related to Advanced Panel Methods, Modelling of Separated Flows, and Three Dimensional Jet/Airframe Computations; and Bob Weston of NASA Langley Research Center for his work related to Studies of Turbulent Jets-in-Cross-Flow.

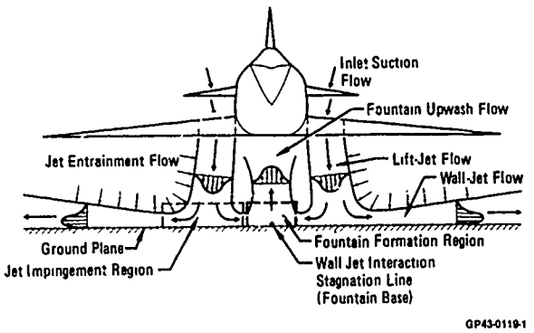

Figure 1. Flowfield About a VTOL Aircraft Hovering in Ground Effect

- Lift Loss (Suck-Down) → Turbulent Jet Entrainment
- Lift and Moment Sensitivity to Pitch and Roll → Deflection of Fountains
- Lift and Moment Sensitivity to Cross-Winds → Deflection of Jets and Fountains by Cross-Winds and Cross-Wind Induced Aerodynamic Loads
- Engine Thrust Loss from Exhaust Gas Ingestion → Fountain, Cross-Wind and Buoyant Convection of Hot Exhaust Gas

GP43-0119-2

Figure 2. VTOL Flowfield Interactions in Ground Effect

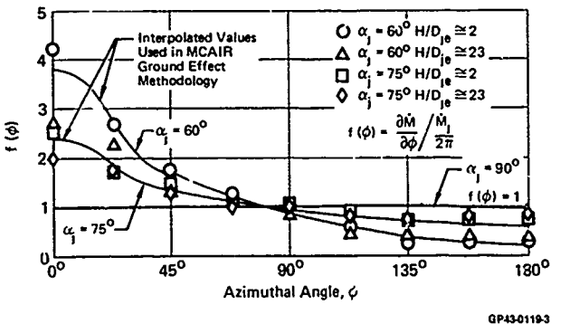

Figure 3. Azimuthal Distribution of Wall Jet Radial Momentum Flux for an Impinging Round Jet

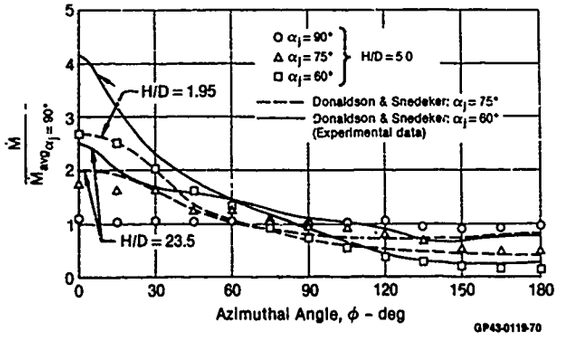

Figure 4. Azimuthal Distribution of Wall Jet Radial Momentum Flux for an Impinging Round Jet

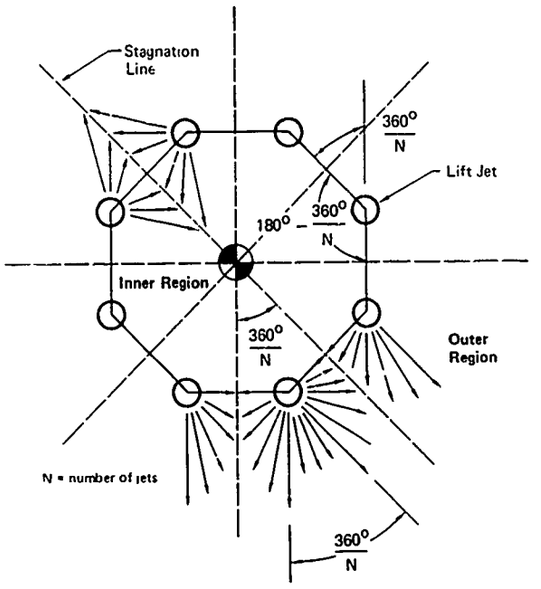

Figure 5. Idealized 8-Jet Lift System Impinging on a Ground Plane

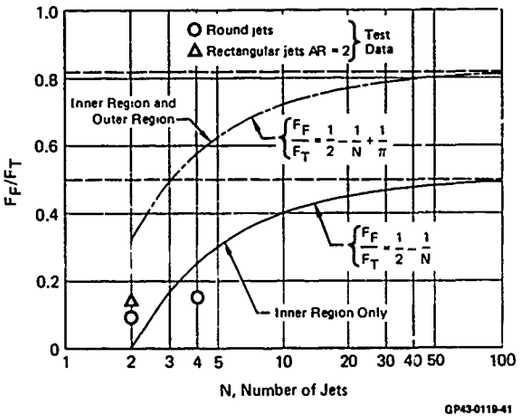

Figure 6. Variation of Maximum Ideal Fountain Force With Number of Round Jets

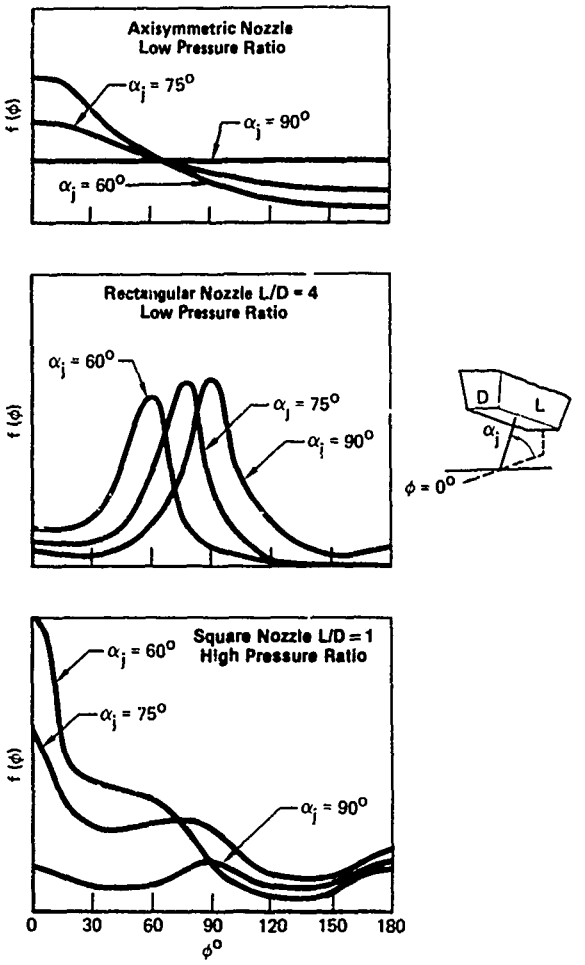

Figure 7. Jet Impingement Radial Momentum Flux Distributions

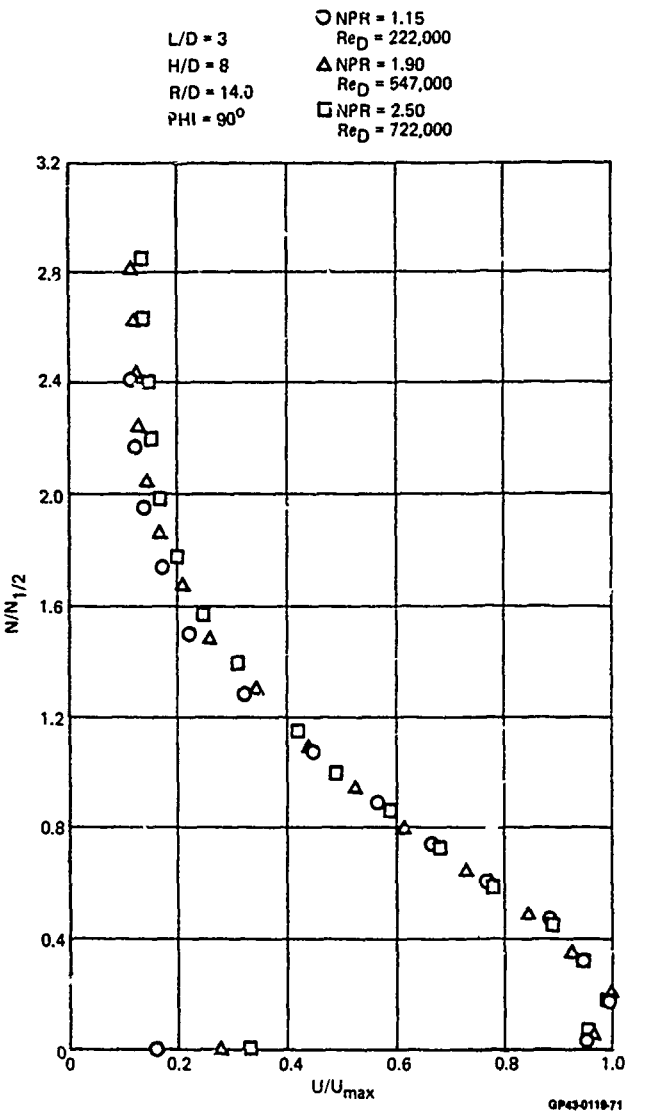

Figure 9. Wall Jet Velocity Profile
Effect of Reynolds Number – Vertical Impingement

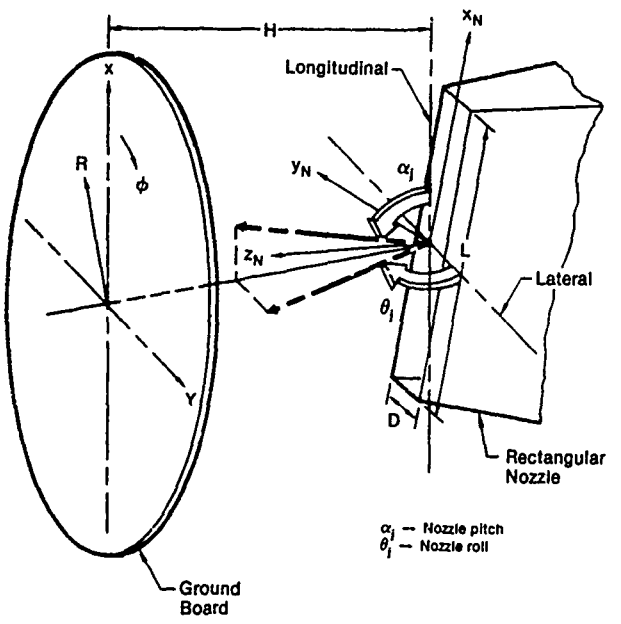

Figure 8. Test Nomenclature

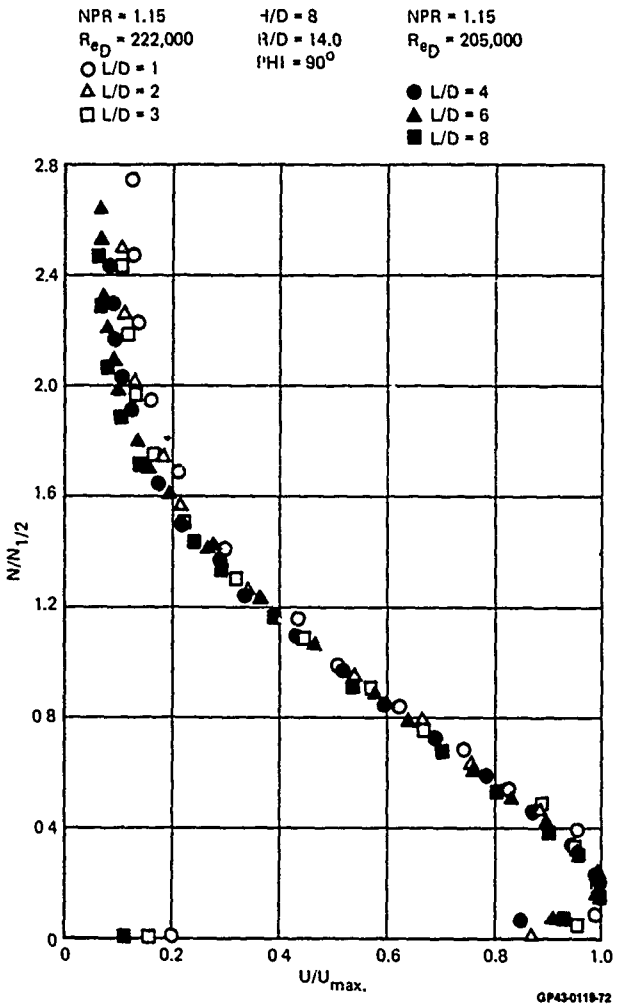

Figure 10. Wall Jet Velocity Profile
Effect of Nozzle Aspect Ratio – Vertical Impingement

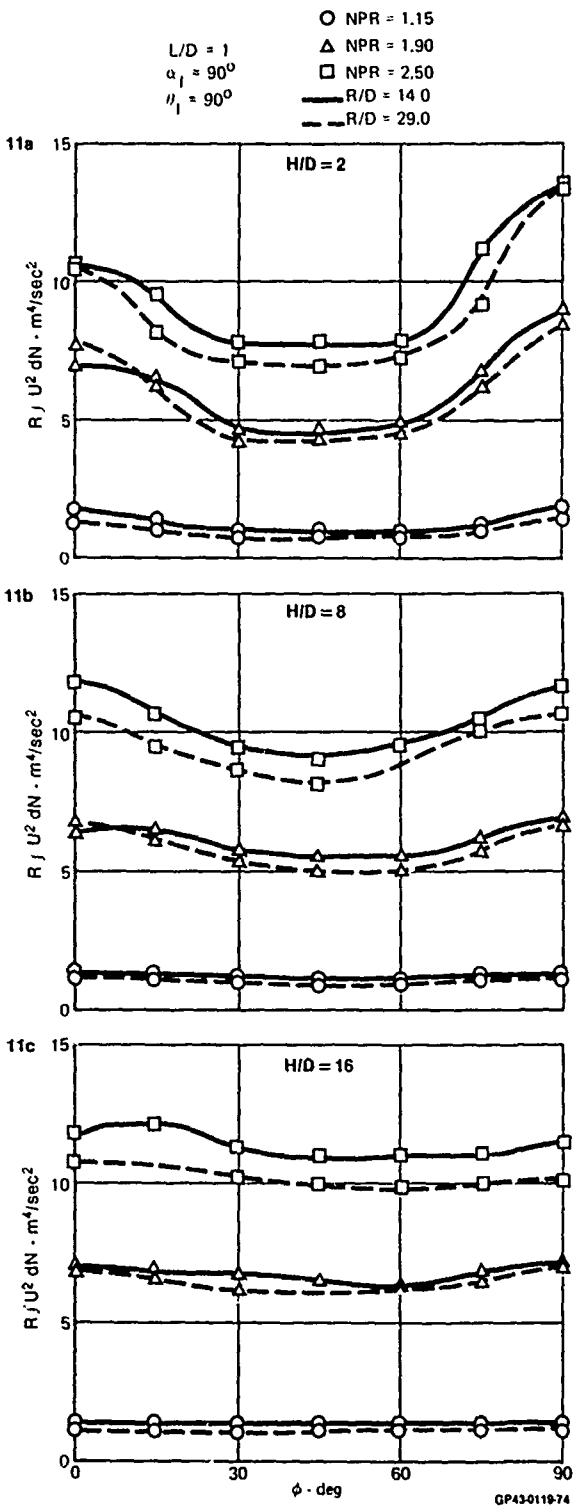

Figure 11. Azimuthal Distribution of Wall Jet Radial Momentum Flux
L/D = 1 Nozzle: Vertical Impingement

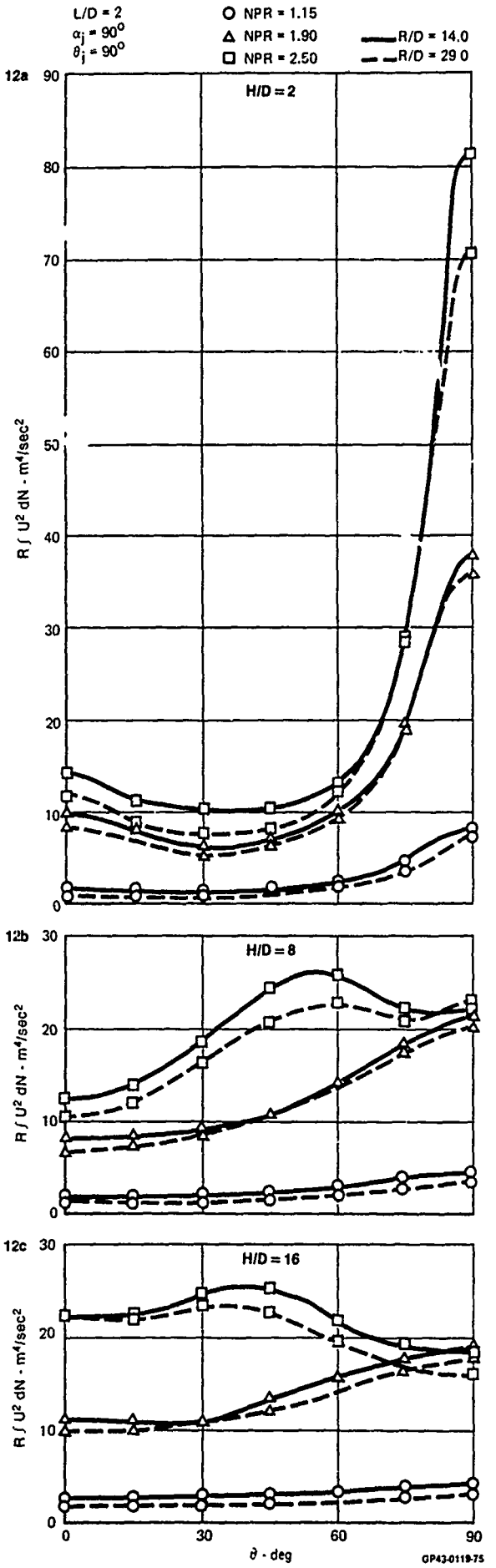

Figure 12. Azimuthal Distribution of Wall Jet Radial Momentum Flux
L/D = 2 Nozzle: Vertical Impingement

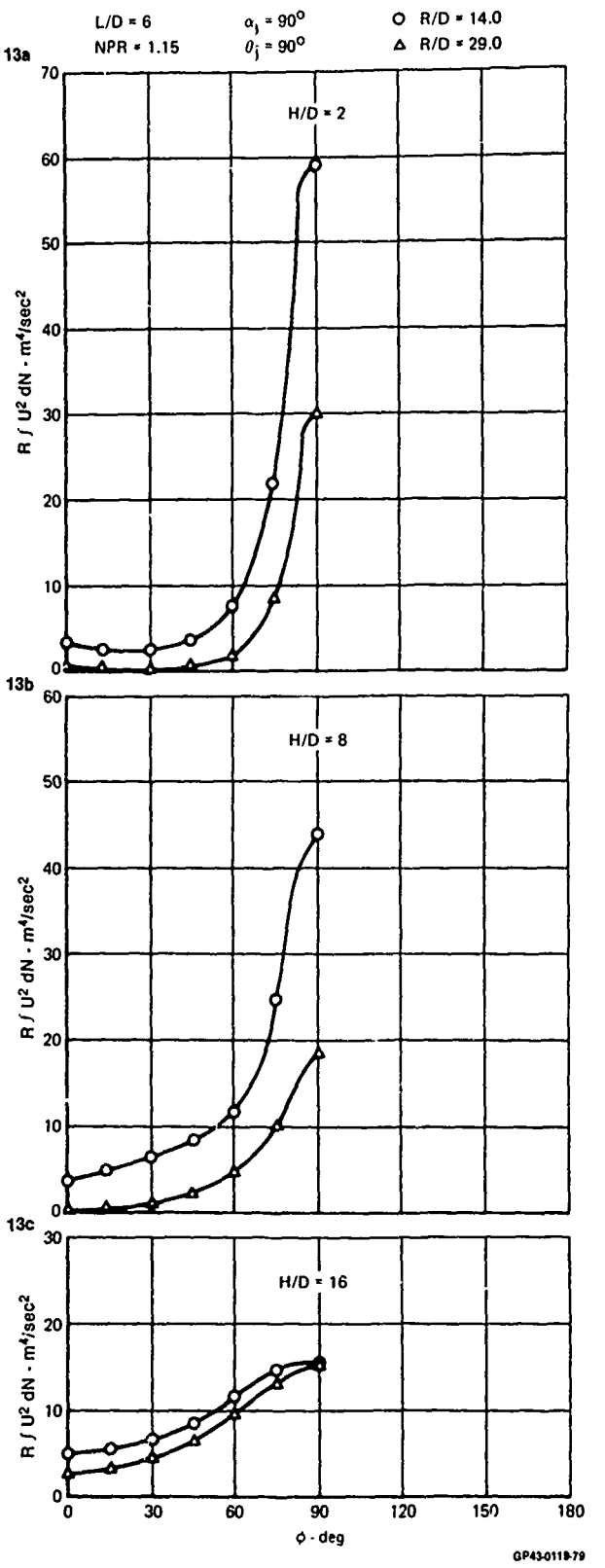

Figure 13. Azimuthal Distribution of Wall Jet Radial Momentum Flux
L/D = 6 Nozzle: Vertical Impingement

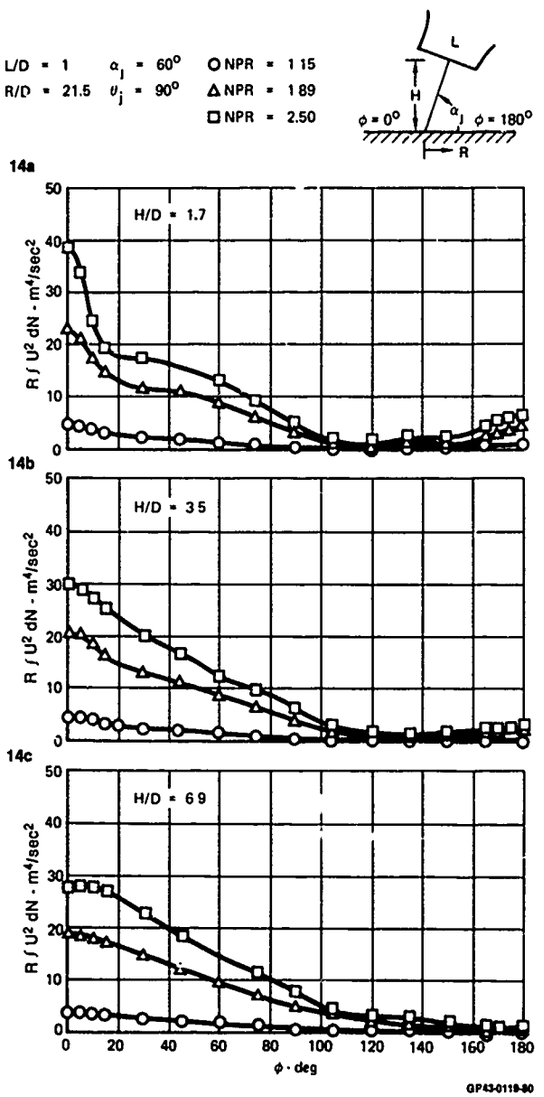

Figure 14. Azimuthal Distribution of Wall Jet Radial Momentum Flux
L/D = 1 Nozzle: Oblique Impingement – Pitch

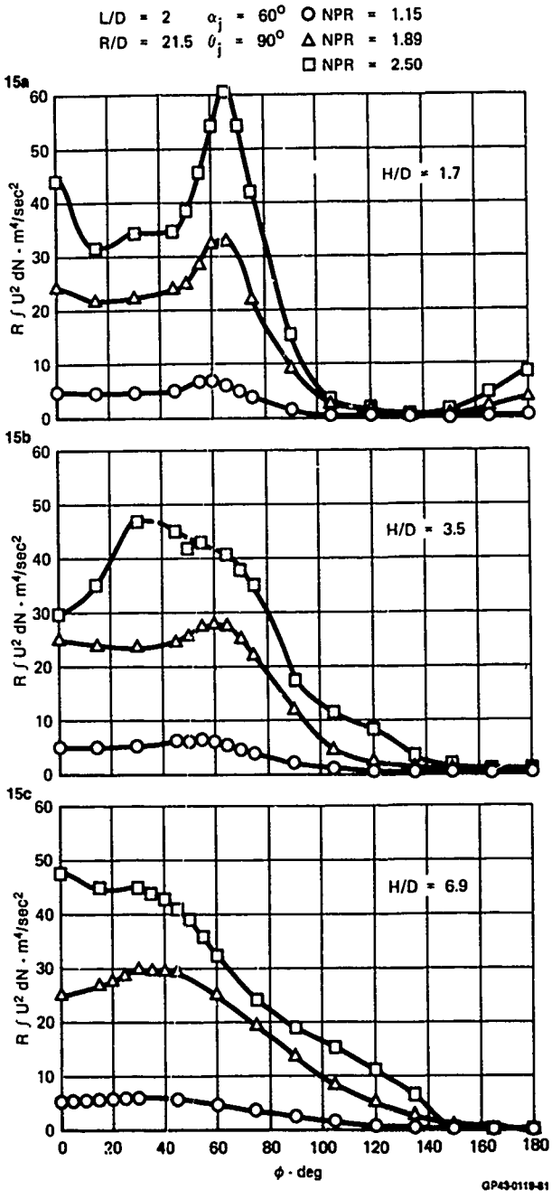

Figure 15. Azimuthal Distribution of Wall Jet Radial Momentum Flux
L/D = 2 Nozzle: Oblique Impingement – Pitch

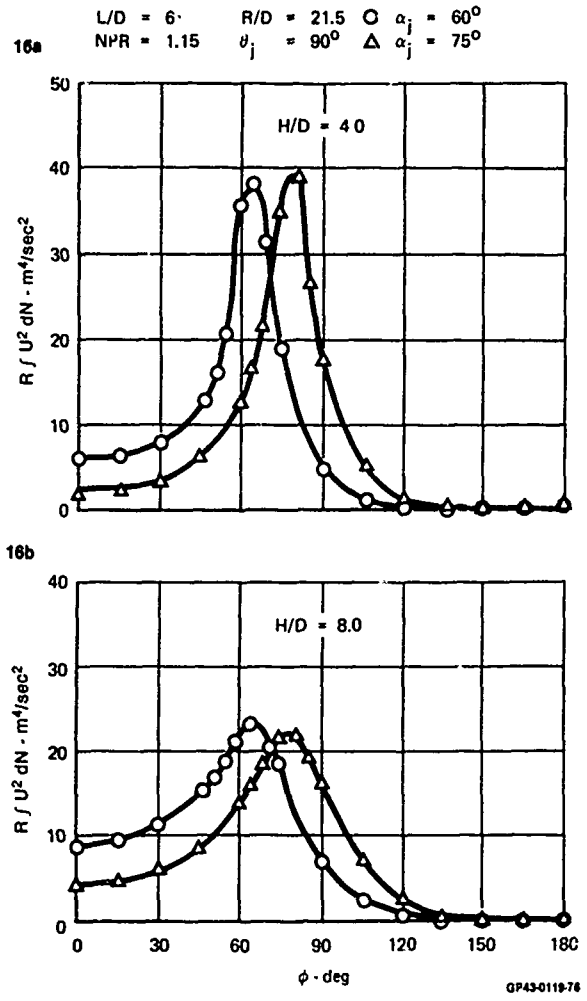

Figure 16. Azimuthal Distribution of Wall Jet Radial Momentum Flux
L/D = 6 Nozzle: Oblique Impingement - Pitch

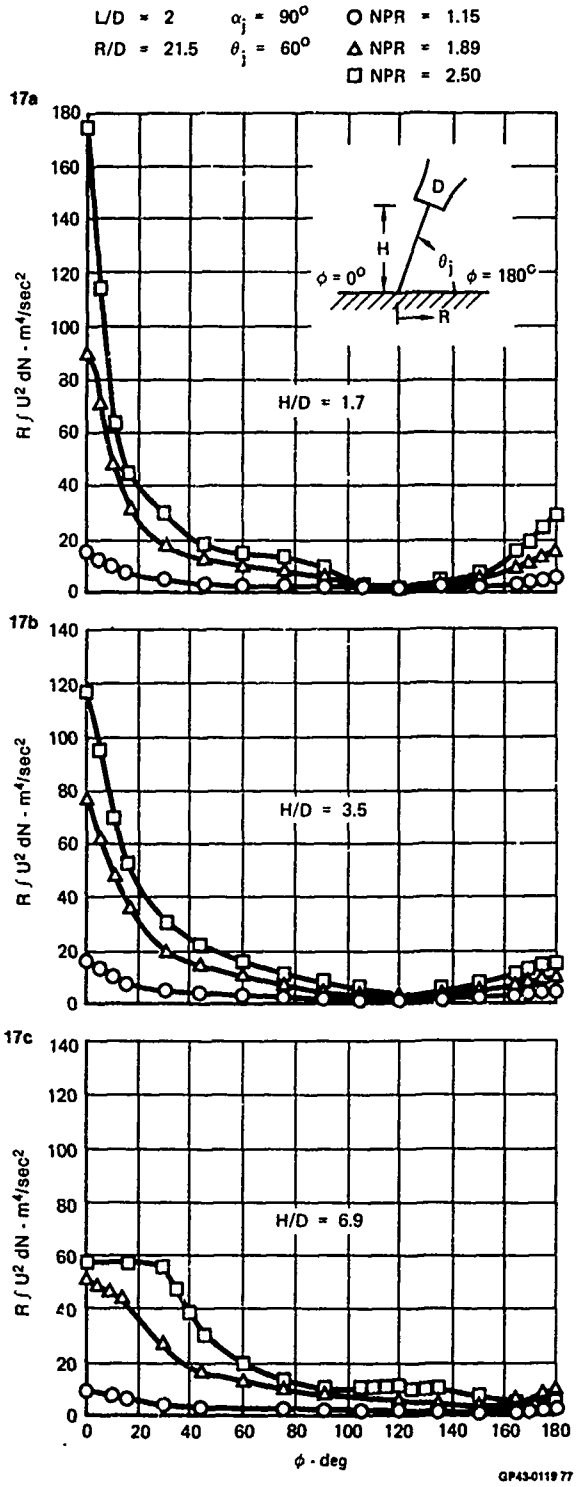

Figure 17. Azimuthal Distribution of Wall Jet Radial Momentum Flux
L/D = 2 Nozzle: Oblique Impingement - Roll

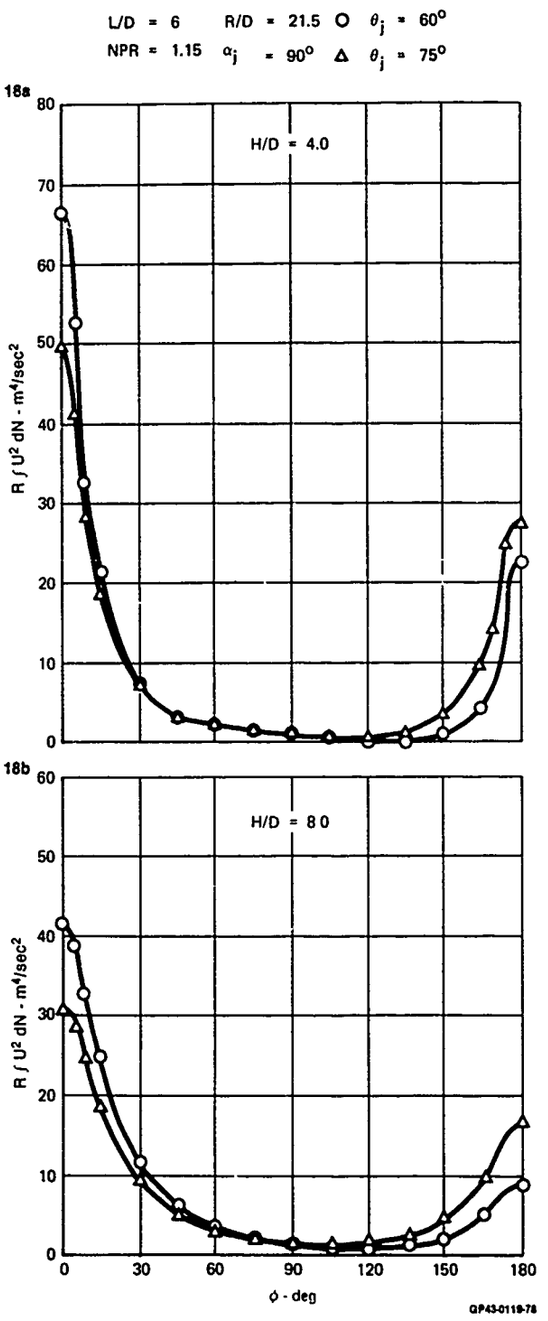

Figure 18. Azimuthal Distribution of Wall Jet Radial Momentum Flux
L/D = 6 Nozzle: Oblique Impingement – Roll

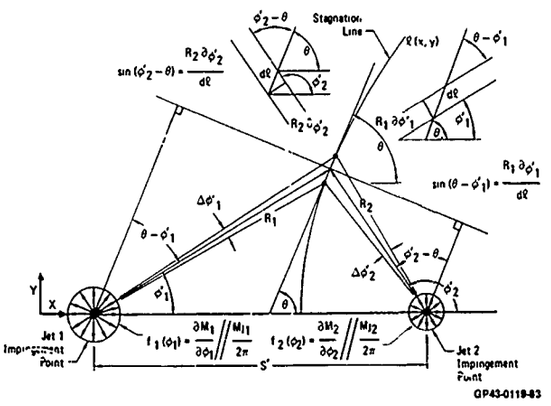

Figure 19. Wall Jet Interaction Geometry

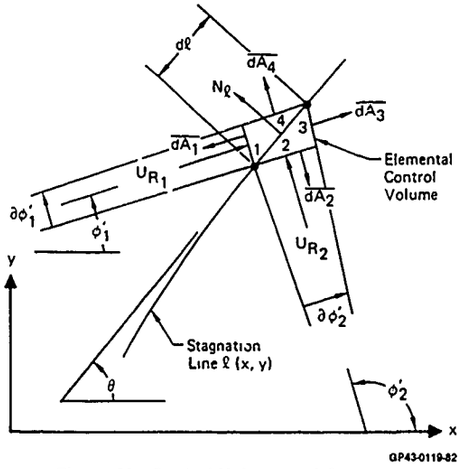

Figure 20. Control Volume and Geometry for Stagnation Line Momentum Balance

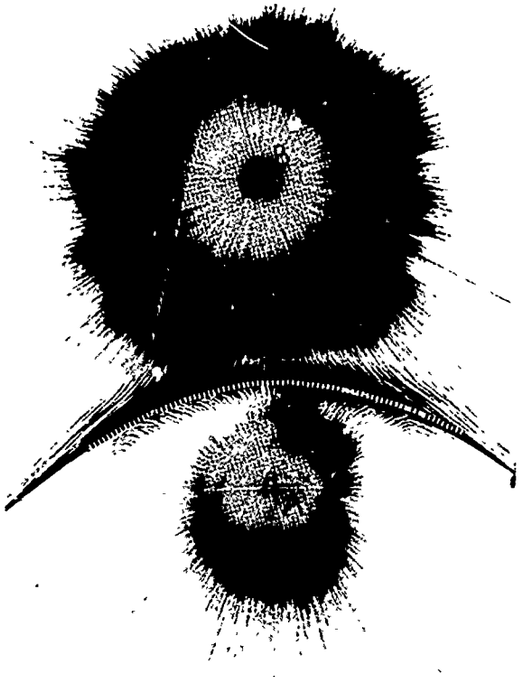

Figure 21. Flow Visualization

GP43-0119-89

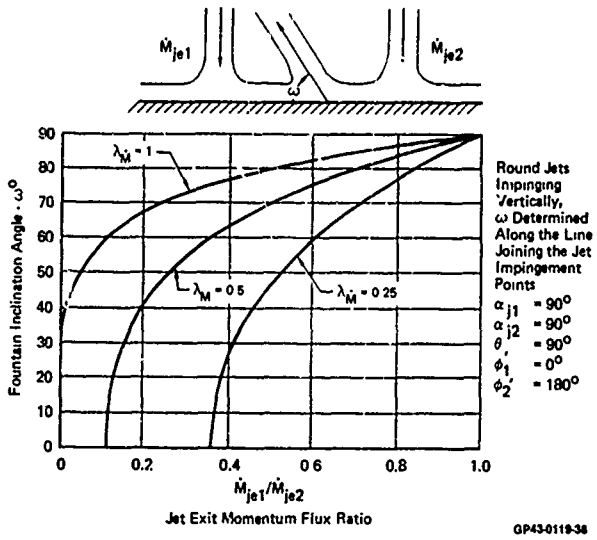

Figure 22. Fountain Inclination Angle

Figure 23(a). Wall Jet Velocity Profiles

Figure 23(b). Fountain Velocity Profiles

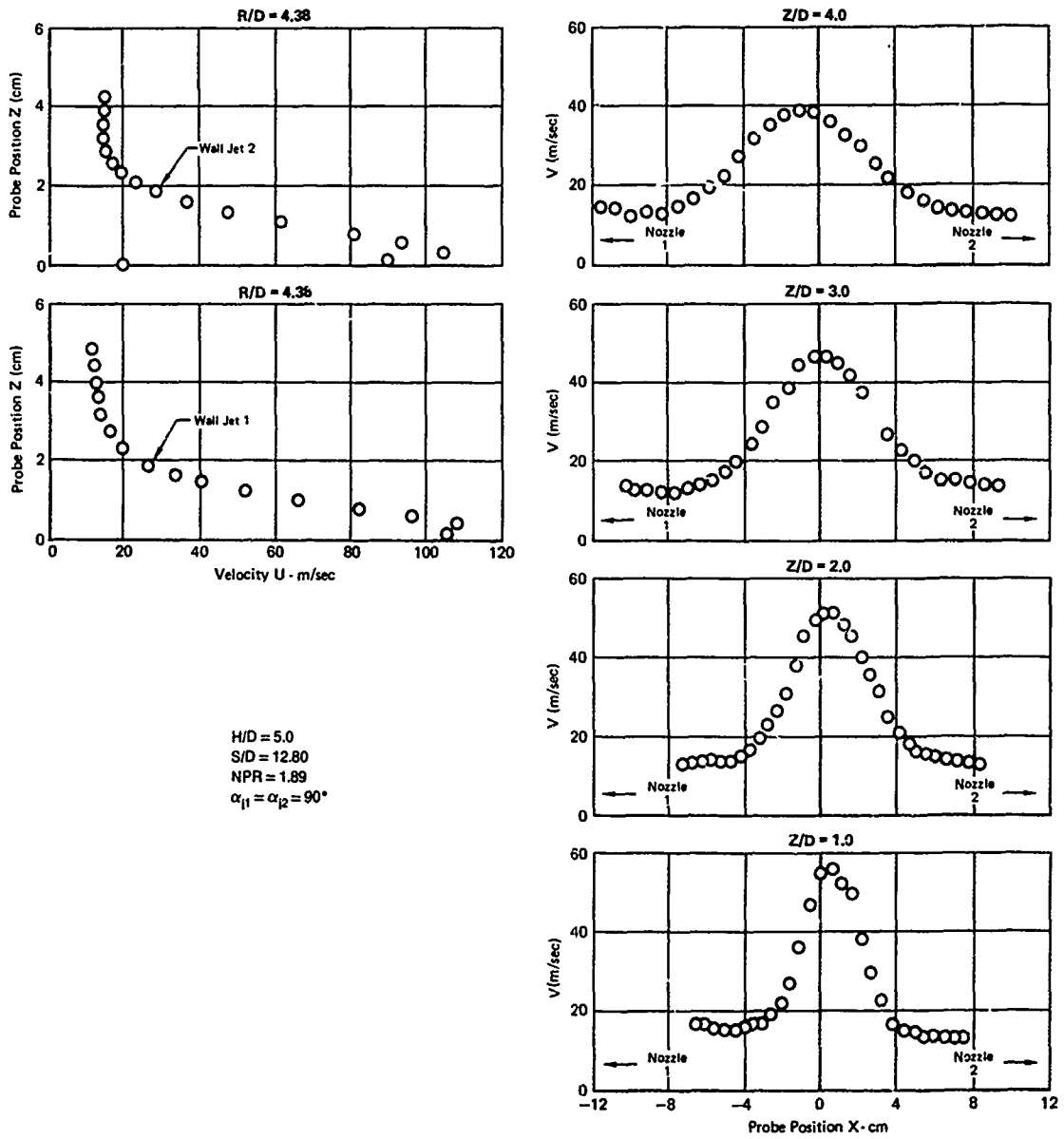

Figure 23. Symmetrical Two-Jet Fountain

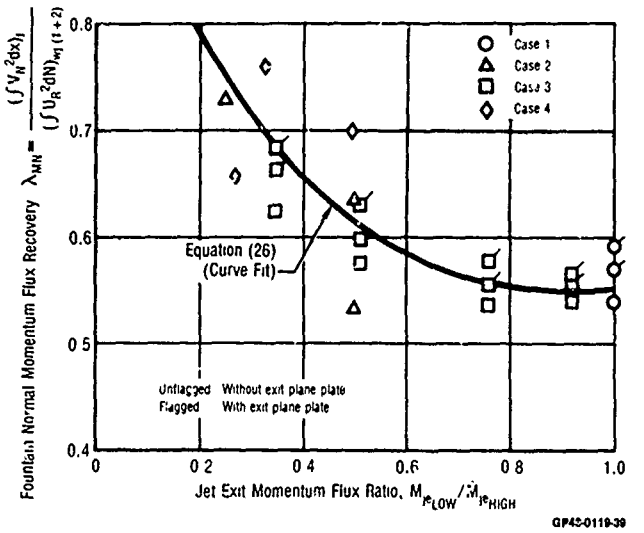

Figure 24. Fountain Normal Momentum Flux Recovery Based on Conservation of Mass Flux Through the Fountain Formation Region

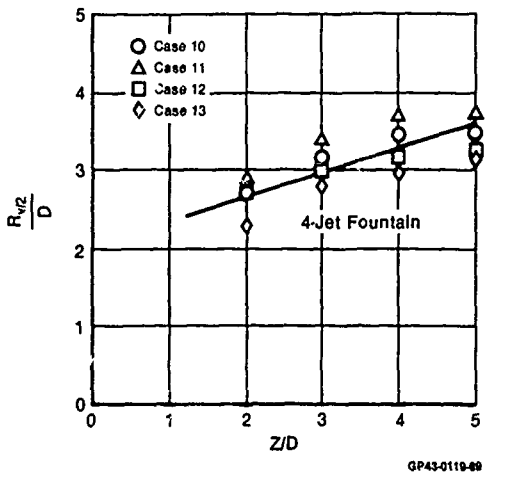

Figure 26. Fountain Spreading Characteristics Four-Jet Fountains

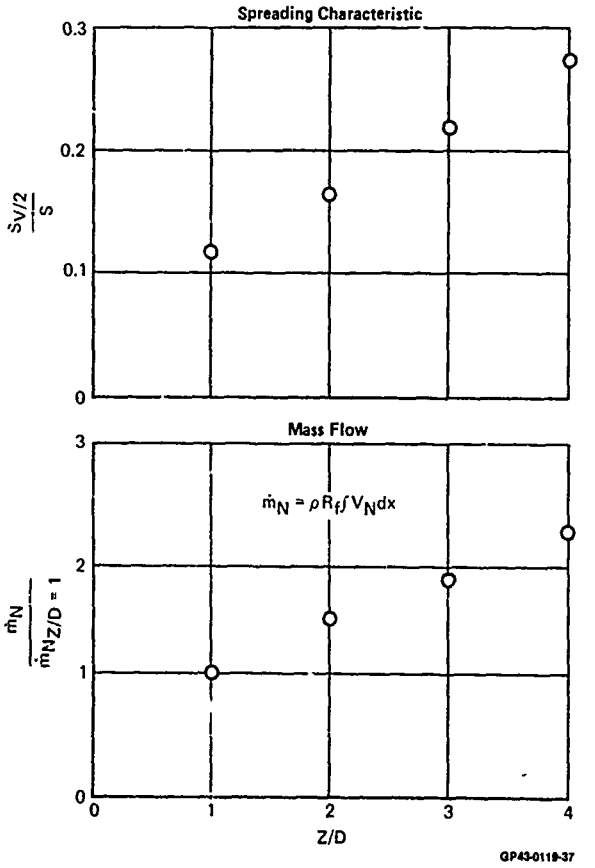

Figure 25. Fountain Upwash Characteristics Symmetrical Two-Jet Fountain

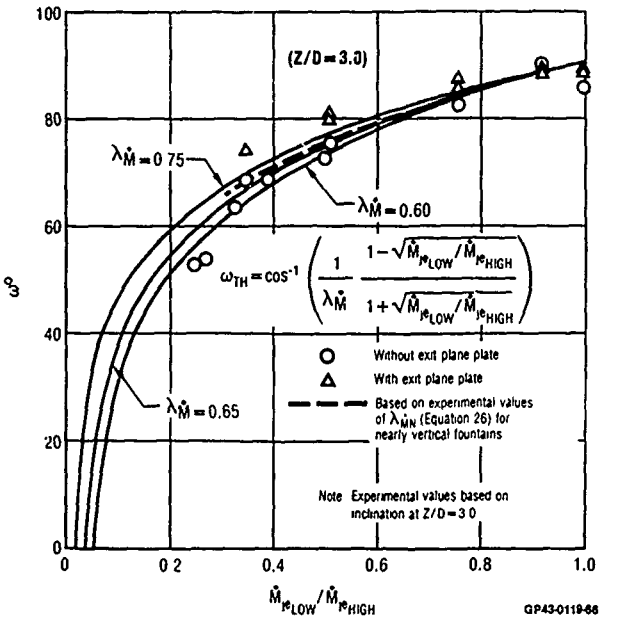

Figure 27. Two-Jet Fountain Inclination - Vertical Impingement

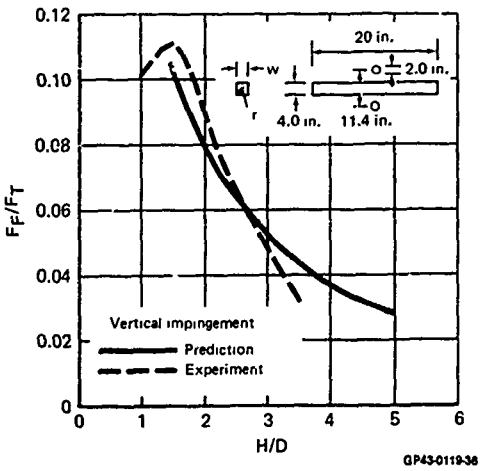

Figure 28. Accuracy of Two-Jet Fountain Impingement Force Prediction

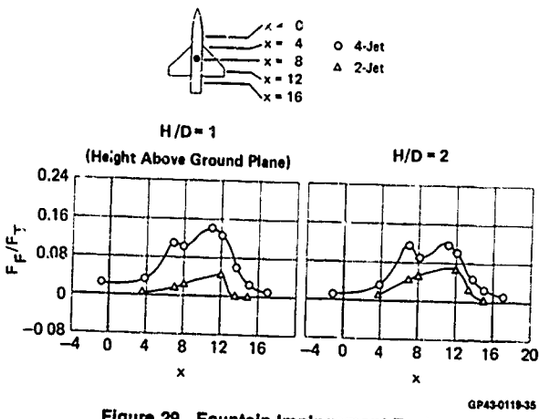

Figure 29. Fountain Impingement Test
2 and 4-Jet Fountain Impingement on a Fuselage/Wing

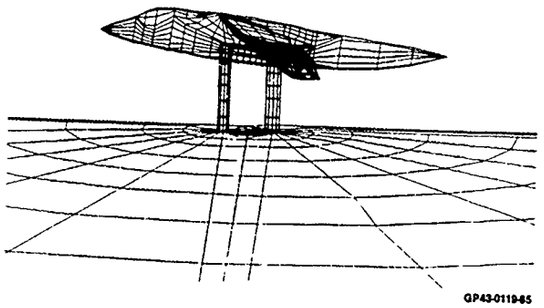

Figure 30. Paneled Representation of YAV-8B in Hover in Ground Effect
$H'/D_e = 2.76$

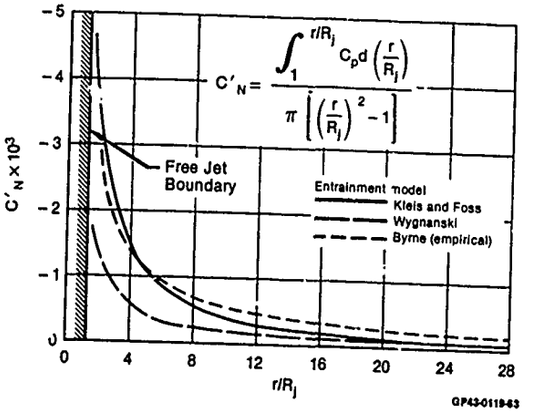

Figure 32. Normal Force Due to an Axisymmetric Jet Issuing From a Flat Plate

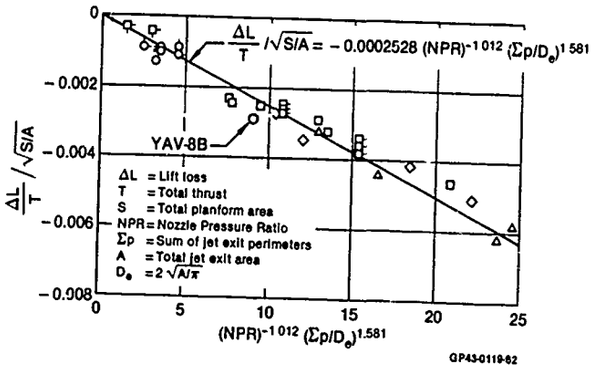

Figure 33. Hover Lift Loss Correlation

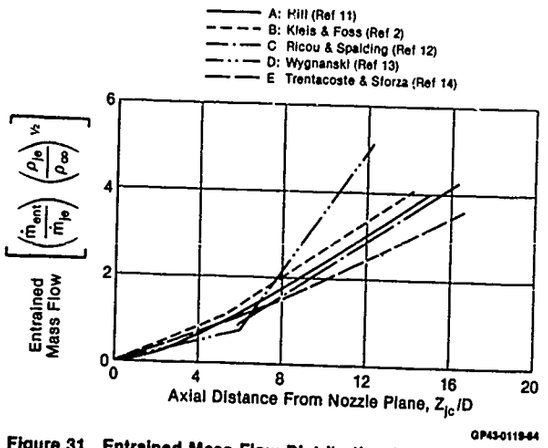

Figure 31. Entrained Mass Flow Distribution for Circular Jets

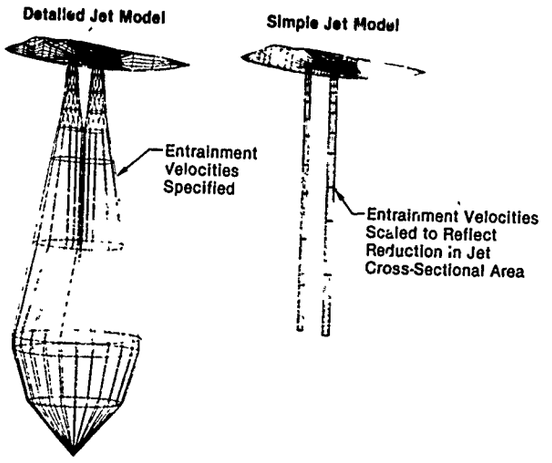

Figure 34. YAV-8B in Hover Out of Ground Effect
Alternate Jet Models

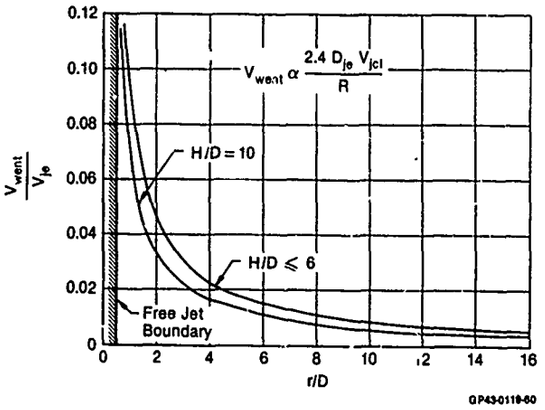

Figure 35. Wall Jet Entrainment Velocities From Modified AGSF Methodology
NPR = 2.0

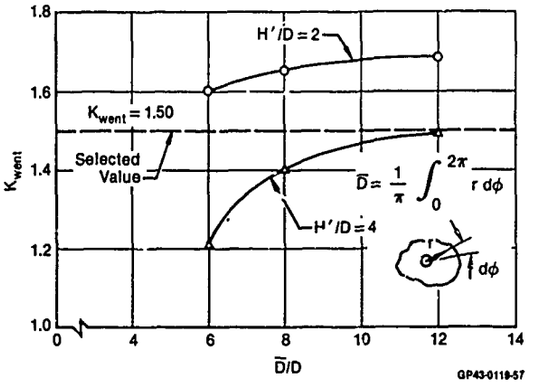

Figure 38. Wall Jet Entrainment Velocity Correction Factor Required to Match Empirical Lift Loss
Circular Plate IGE

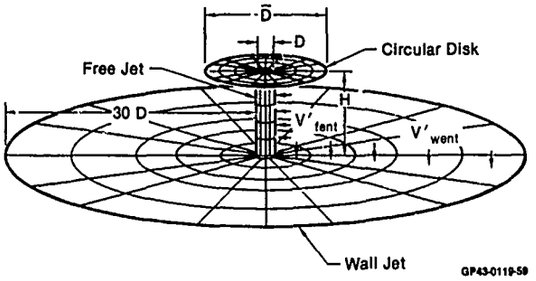

Figure 36. Paneled Representation of Axisymmetric Jet Issuing From a Circular Plate In Ground Effect

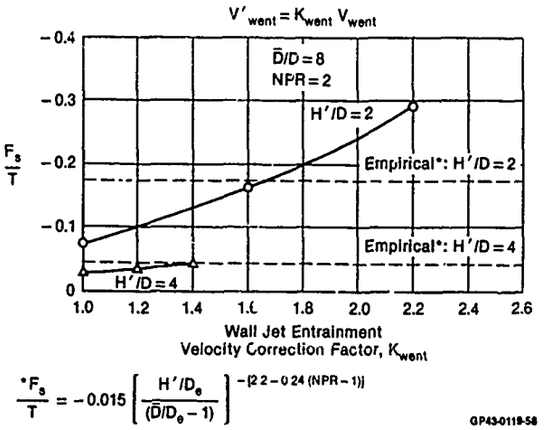

Figure 37. Wall Jet Entrainment Velocity Correction Factor

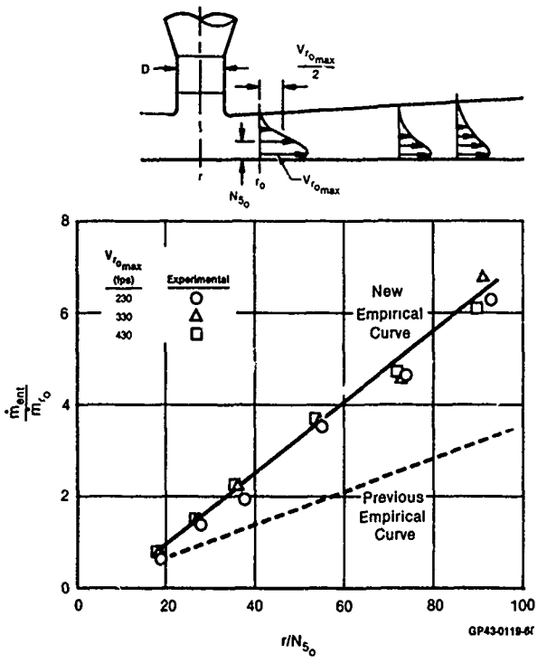

Figure 39. Variation of Wall Jet Mass Entrainment With Radial Distance

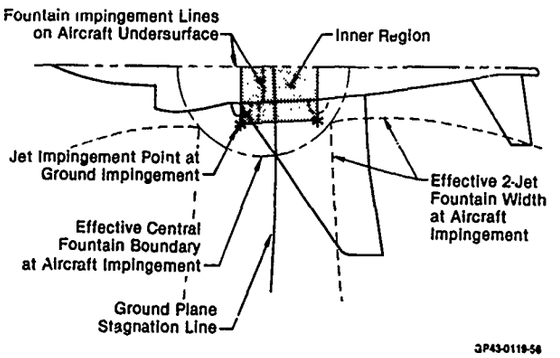

Figure 40. Fountain Impingement Force Calculation Model

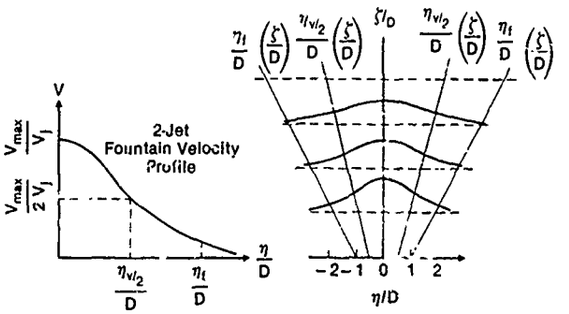

Figure 41. 2-Jet Fountain Spreading Characteristics

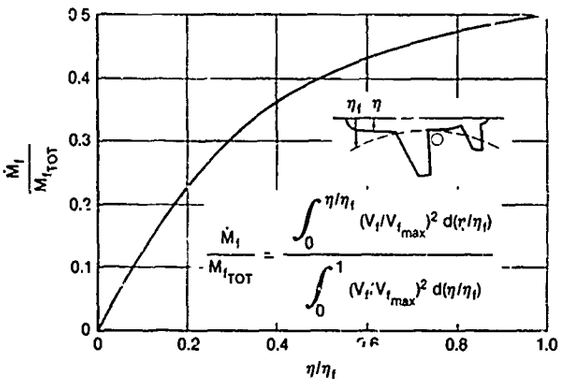

Figure 42. 2-Jet Fountain Upwash Momentum Flux Distribution

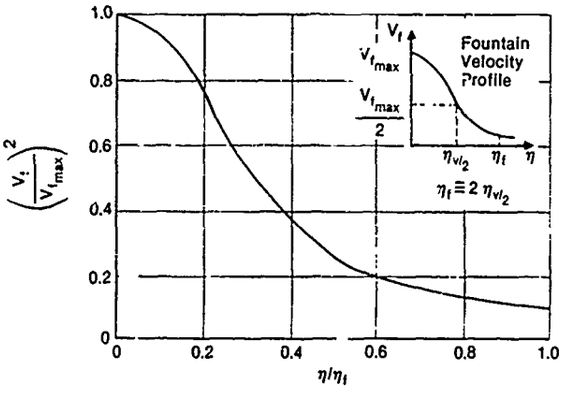

Figure 43. Empirical 2-Jet Fountain Dynamic Pressure Profile

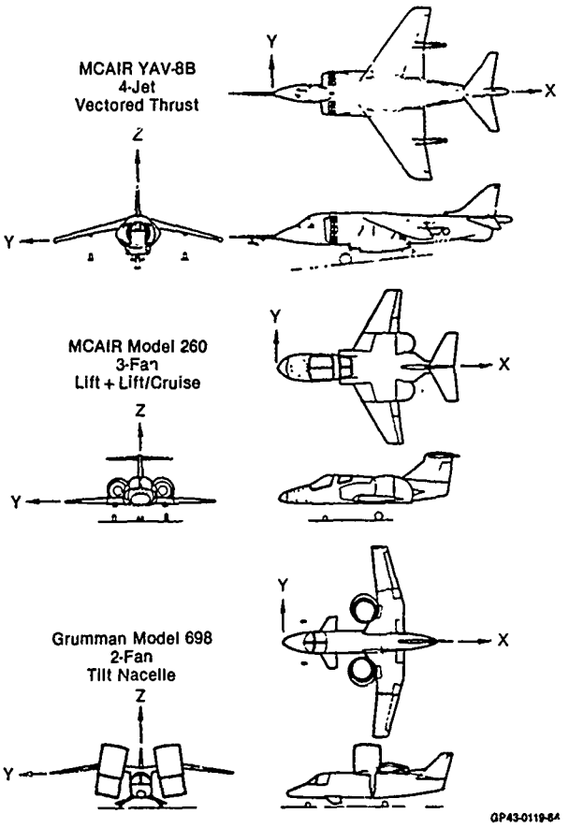

Figure 44. V/STOL Aircraft Selected for Analysis

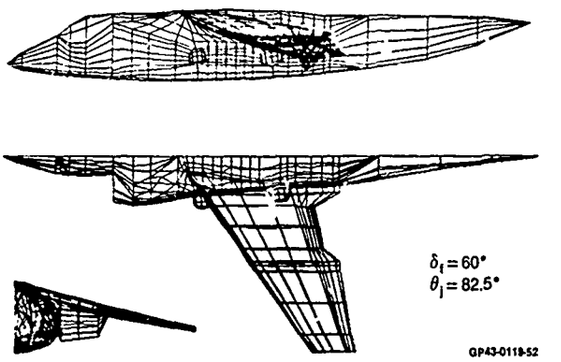

Figure 45. Paneled Representation of YAV-8B
(Without Tail)

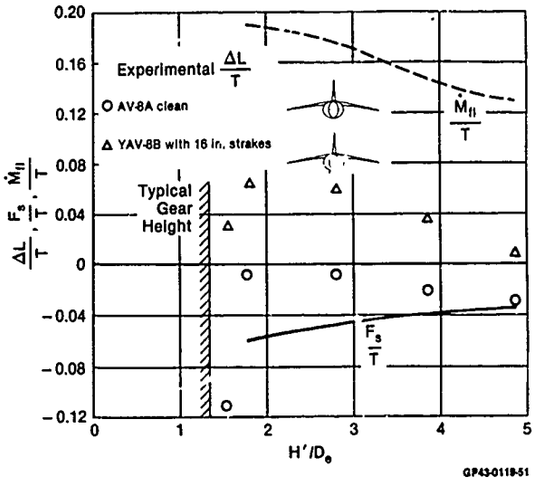

Figure 46. YAV-8B Induced Lift in Ground Effect

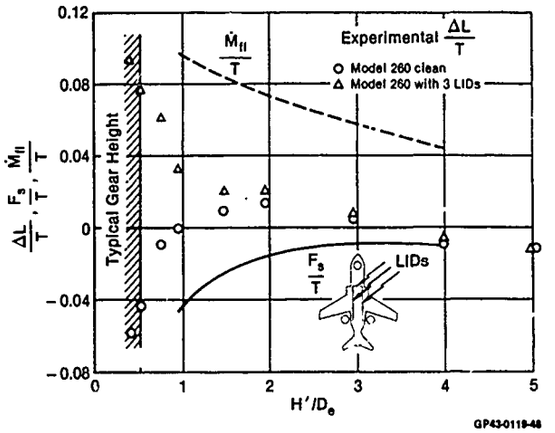

Figure 49. Model 260 Induced Lift in Ground Effect

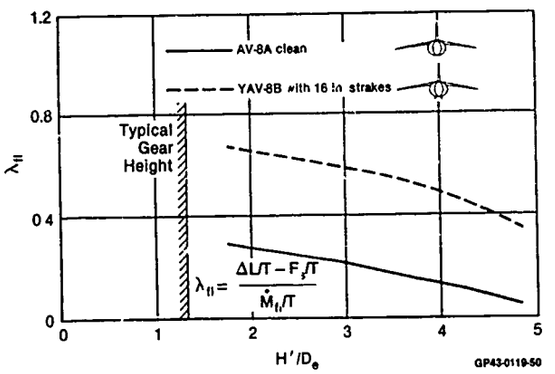

Figure 47. Fountain Impingement Momentum Flux Transfer Coefficient
YAV-8B

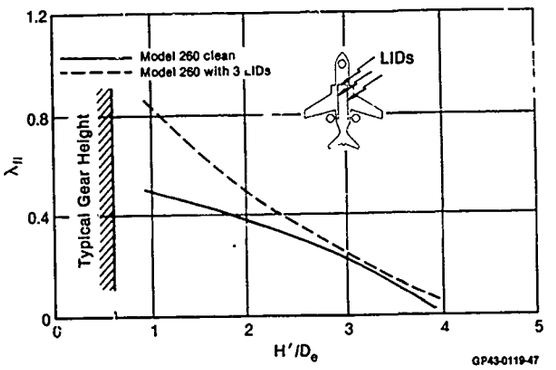

Figure 50. Fountain Impingement Momentum Flux Transfer Coefficient
Model 260

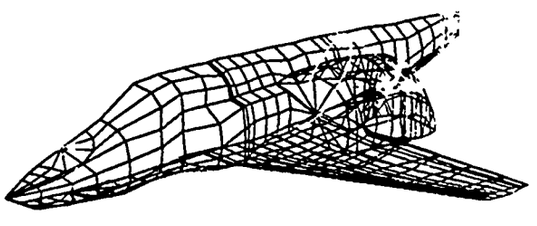

Figure 48. Paneled Representation of MCAIR Model 260

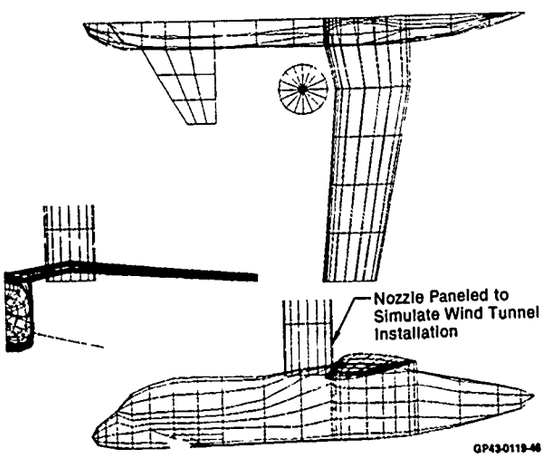

Figure 51. Paneled Representation of Grumman Model 698

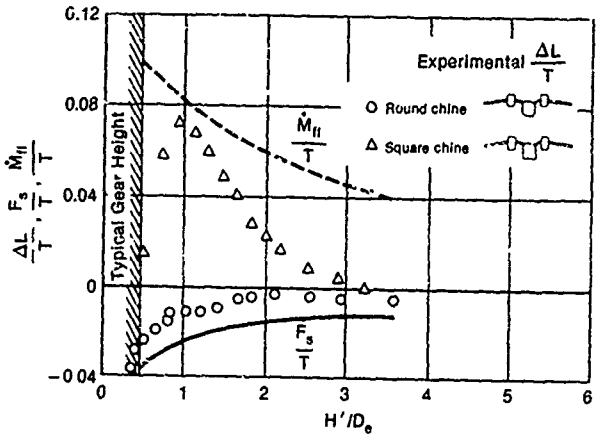

Figure 52. Grumman Model 698 Induced Lift in Ground Effect

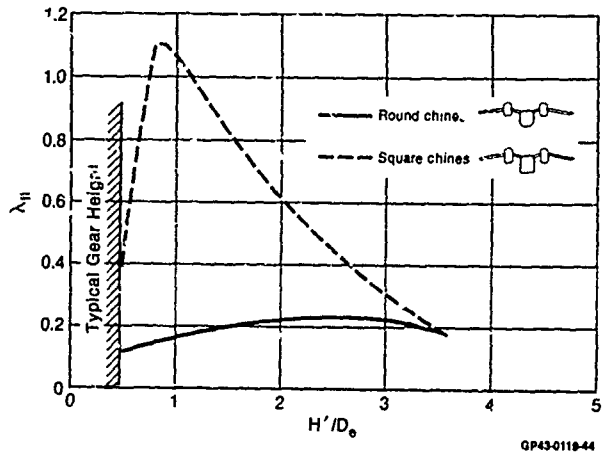

Figure 53. Fountain Impingement Momentum Flux Transfer Coefficient
Grumman Model 698

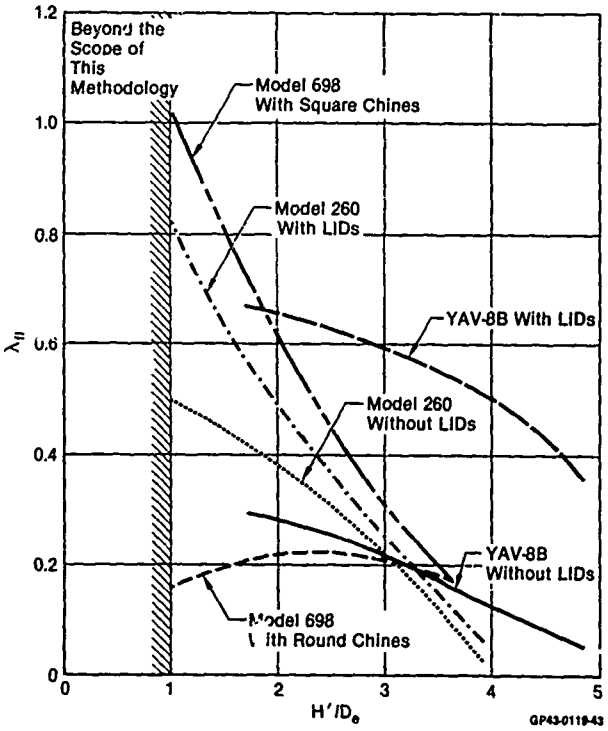

Figure 54. Fountain Impingement Momentum Flux Transfer Coefficient Summary

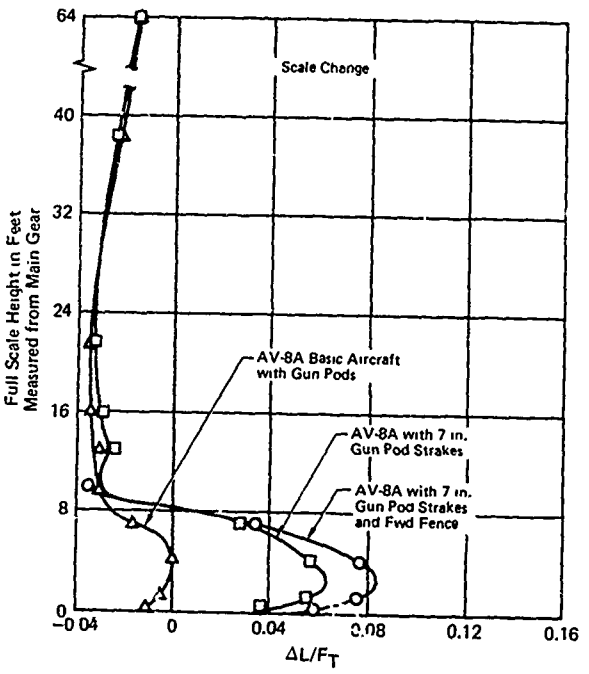

Figure 55. Fountain Capture With Lift Improvement Devices

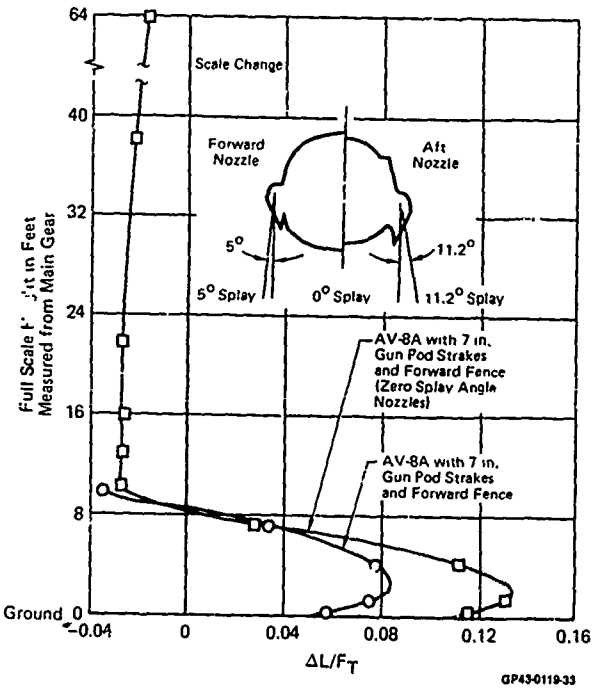

Figure 56. Effect of Changing Nozzle Splay Angle

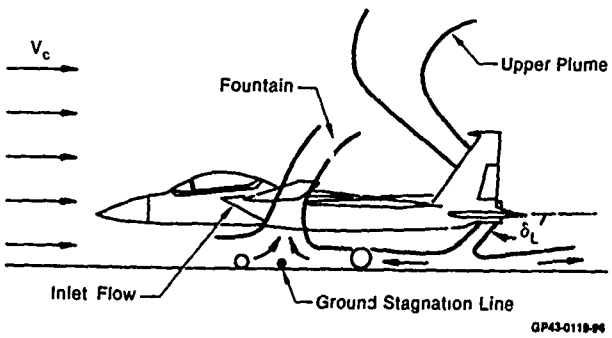

Figure 57. Ground Flowfield With Thrust Reversal

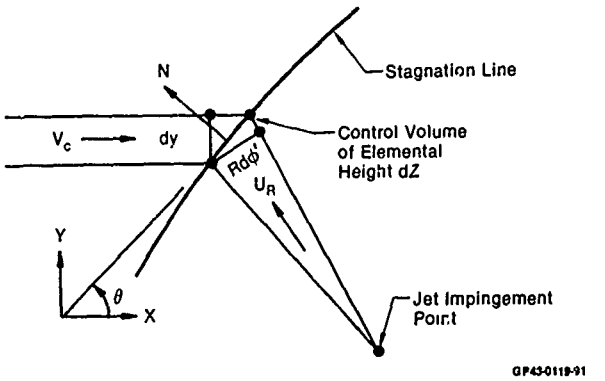

Figure 58. Control Volume for Cross-Flow/Wall-Jet Interaction

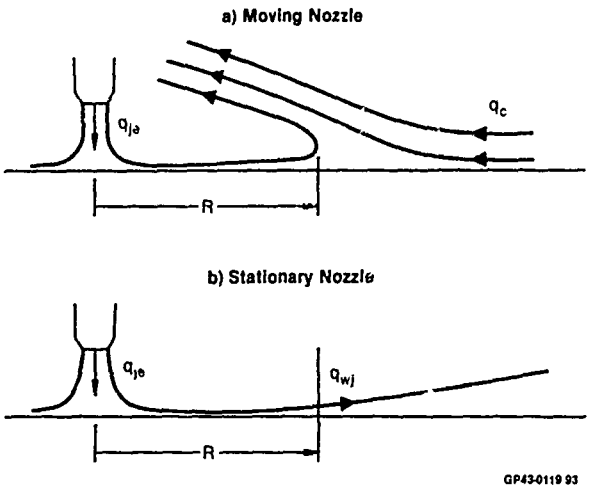

Figure 61. Jet Penetration Nomenclature

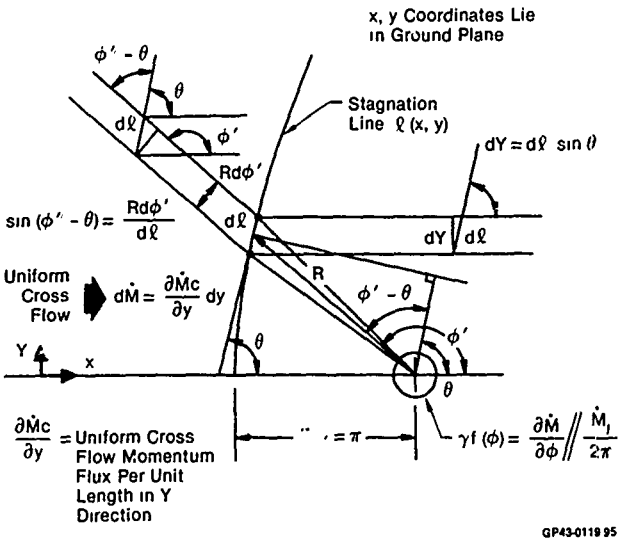

Figure 59. Interaction Geometry - Radial Wall-Jet and Uniform Cross-Flow

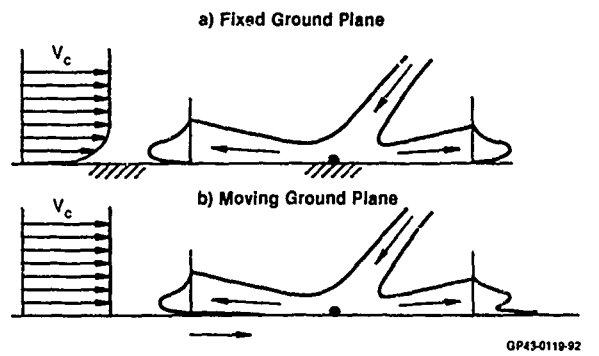

Figure 62. Fixed vs Moving Ground Plane Interactions

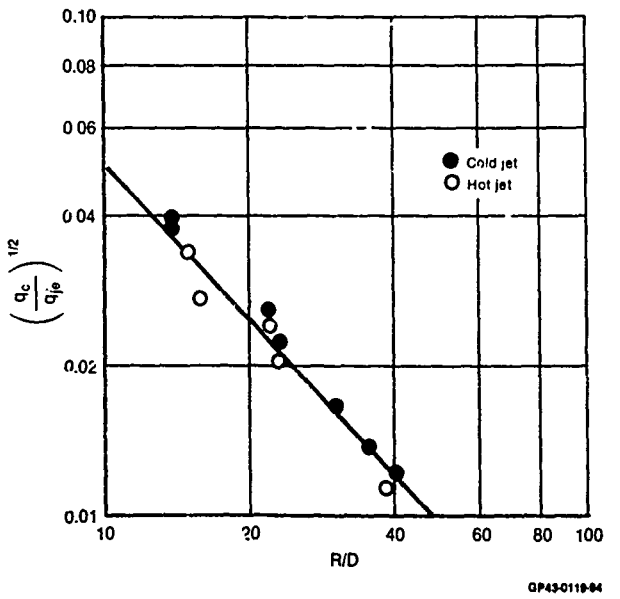

Figure 60. Jet Penetration Into Uniform Cross-Flow for Hot and Cold Jets

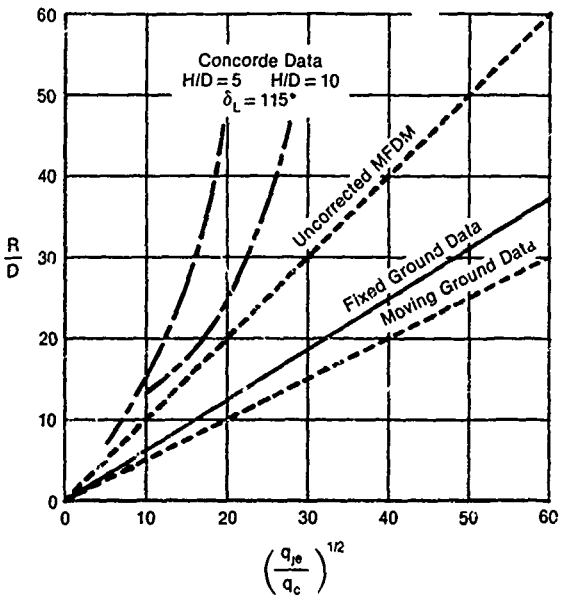

Figure 63. Correlation of Wall-Jet Penetration Results - Cross-Flow/Wall-Jet Interaction

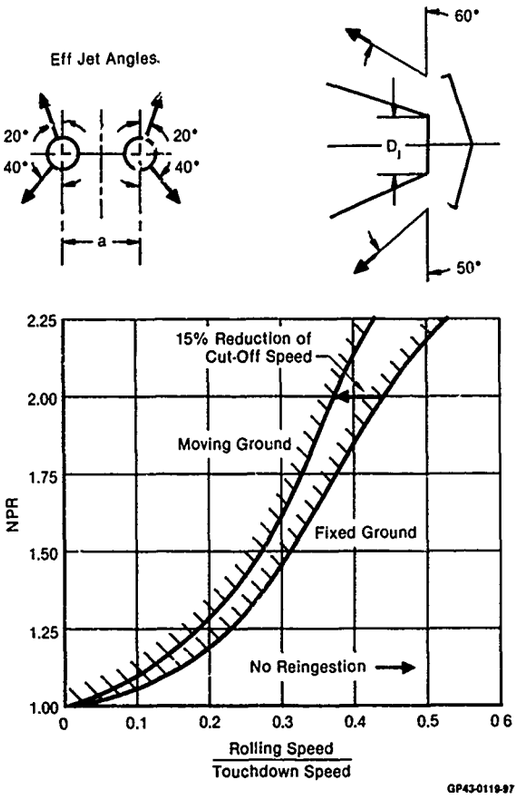

Figure 64. Thrust Reverser Operation Boundary Due to Ingestion for Fixed and Moving Ground Plane Simulations

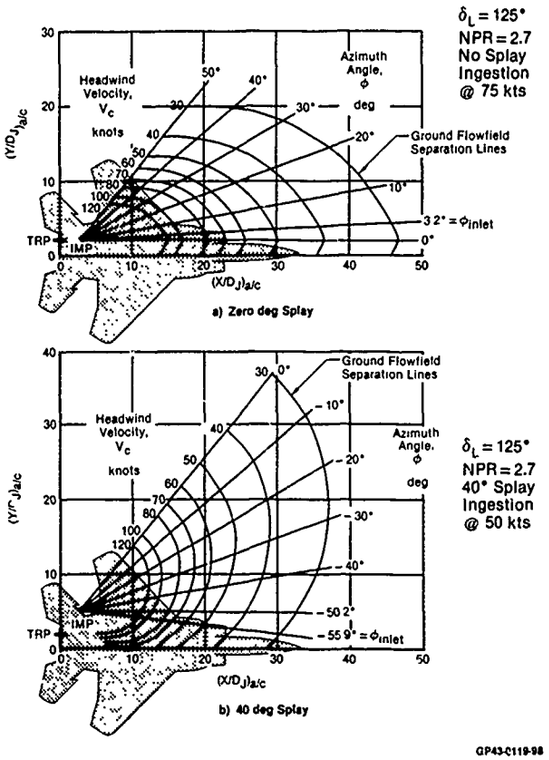

Figure 66. MCAIR Empirical Method Ground Separation Line Predictions

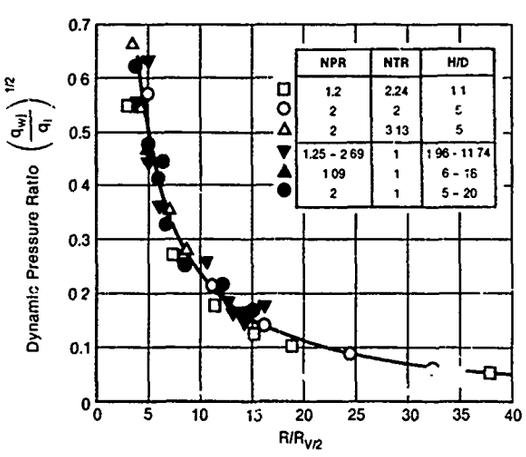

Figure 65. Dynamic Prossure vs Radial Position – Vertical Impingement

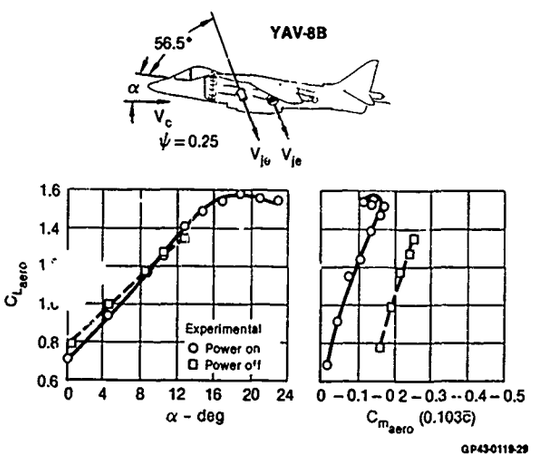

Figure 67. V/STOL Transition: Effect of Jets on Aerodynamic Force and Moment

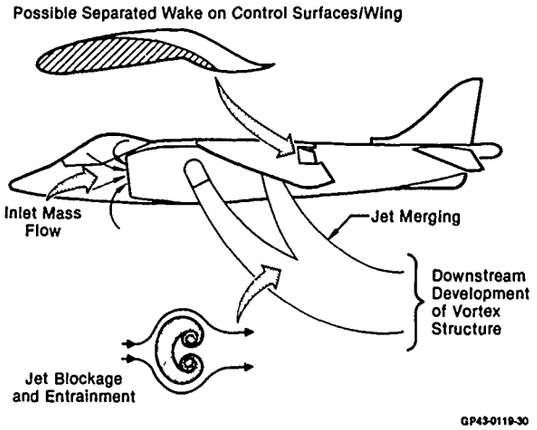

Figure 68. Problem Description: V/STOL Transition Flowfield

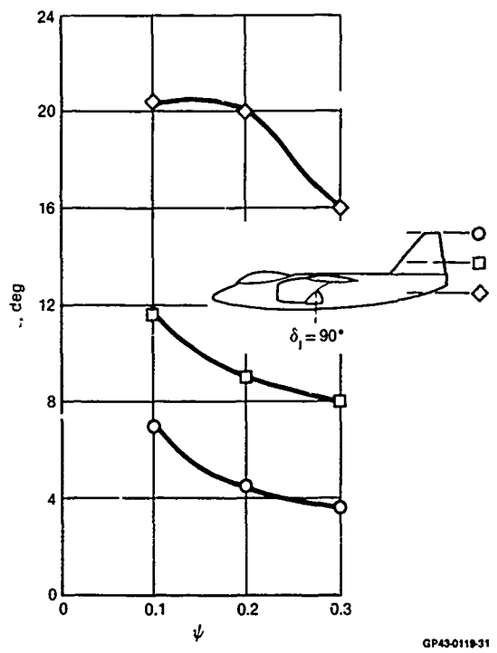

Figure 69. Jet Induced Downwash Showing Effect of Tail Height

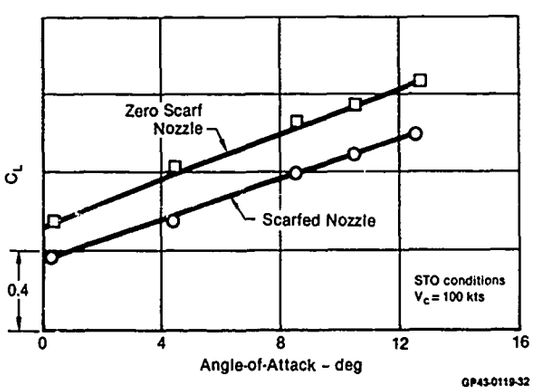

Figure 70. Effect of AV-8B Nozzle Modification
(4) Pylons + (2) 300 Gallon Tanks

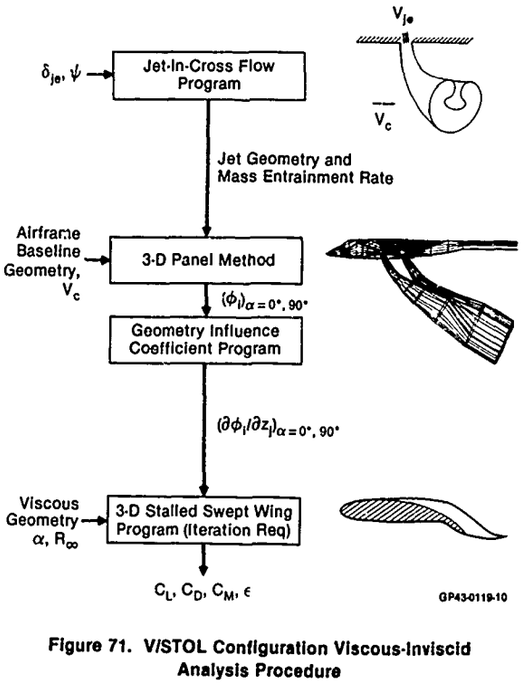

Figure 71. V/STOL Configuration Viscous-Inviscid Analysis Procedure

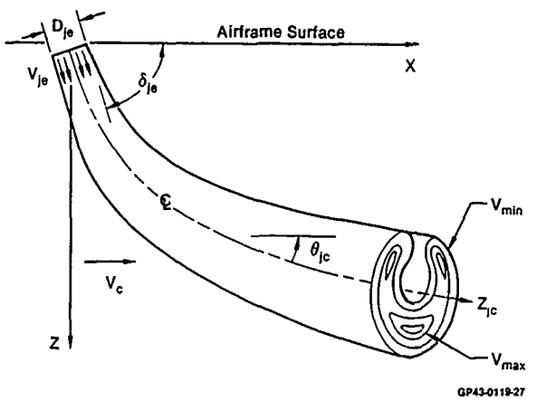

Figure 72. Jet-In-Crossflow at High Injection Angle

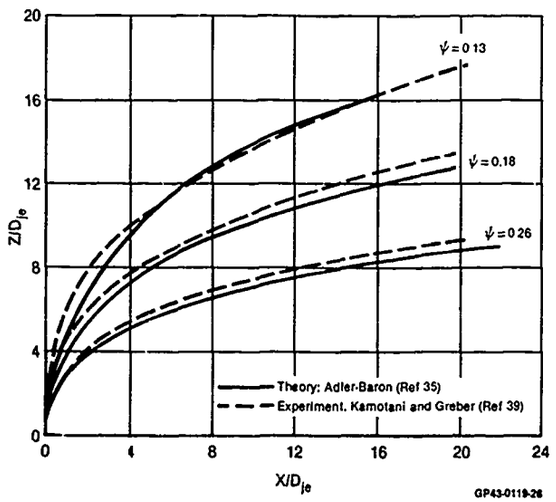

Figure 73. Locus of Peak Jet Velocity Centerline Trajectory
90° Injection Angle

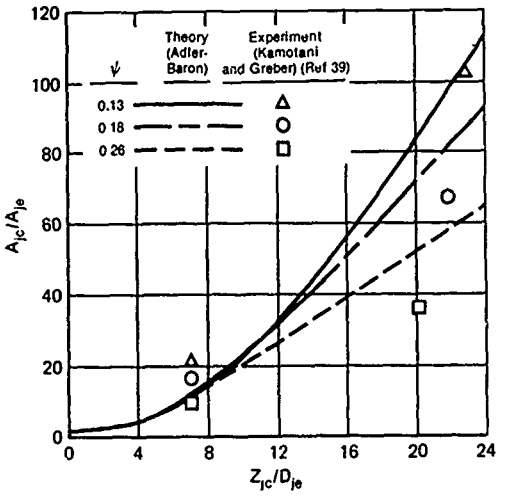

Figure 74. Jet Cross-Sectional Area Ratio Comparison 90° Injection Angle

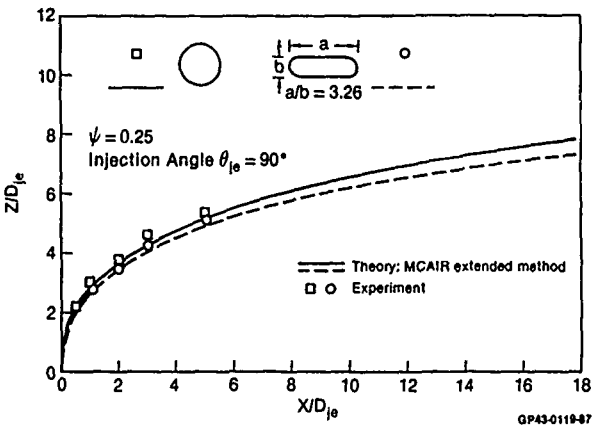

Figure 77. Effect of Nozzle Cross-Section on Velocity Centerline

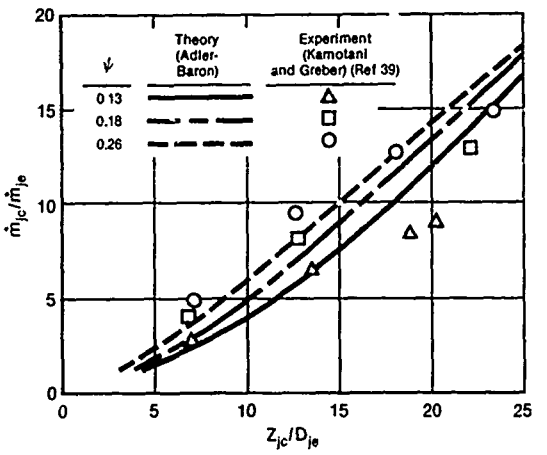

Figure 75. Entrained Mass Flux Comparison 90° Injection Angle

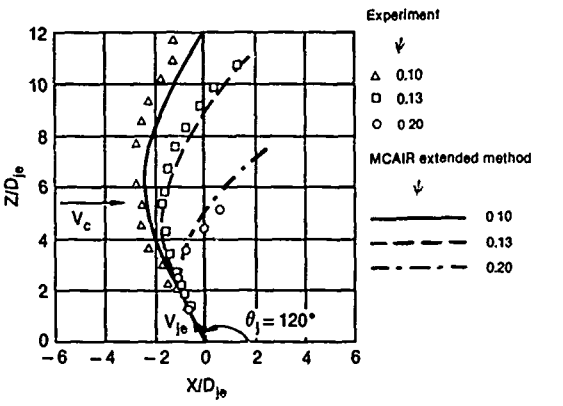

Figure 78. Peak Jet Velocity Centerline Trajectory for Jet Injection Against the Freestream

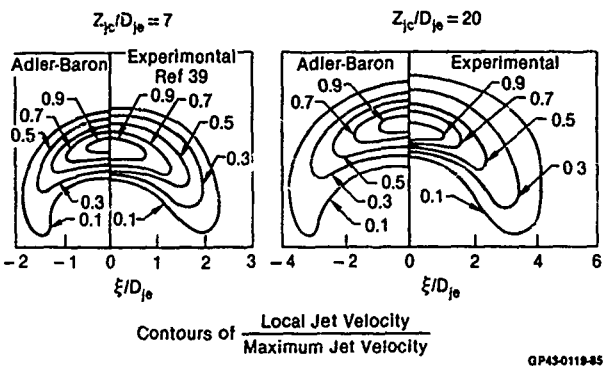

Figure 76. Jet Velocity Profile Comparison 90° Injection Angle $\psi = 0.26$

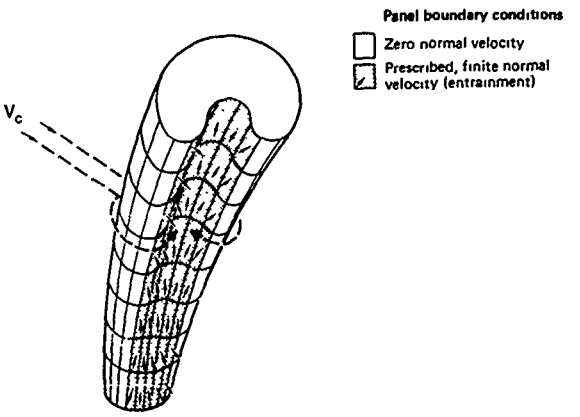

Figure 79. Paneled Representation of a Jet-In-Crossflow

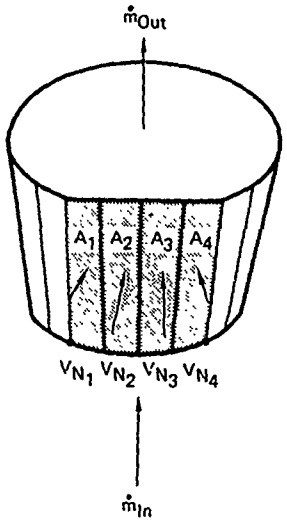

$$\dot{m}_{Out} = \dot{m}_{In} + \dot{m}_{Entrainment}$$

$$\dot{m}_{Entrainment} = \sum_{i=1}^{n} V_{N_i} A_i$$

GP43-0119-23

Figure 80. Jet Segment Control Volume

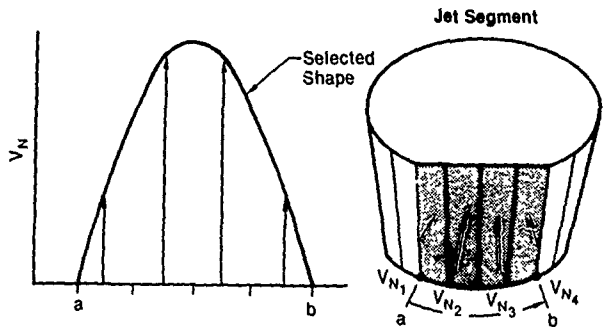

GP43-0119-18

Figure 81. Jet Entrainment Profile Modeling

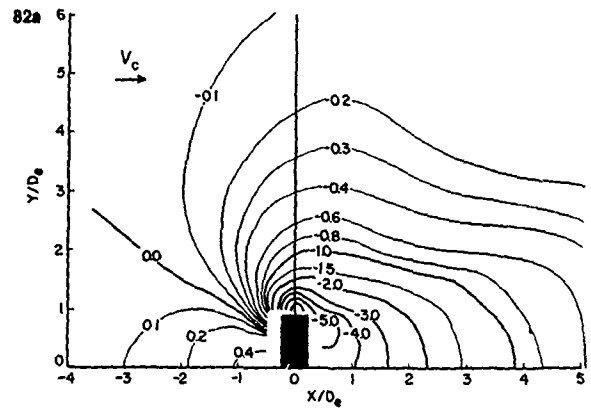

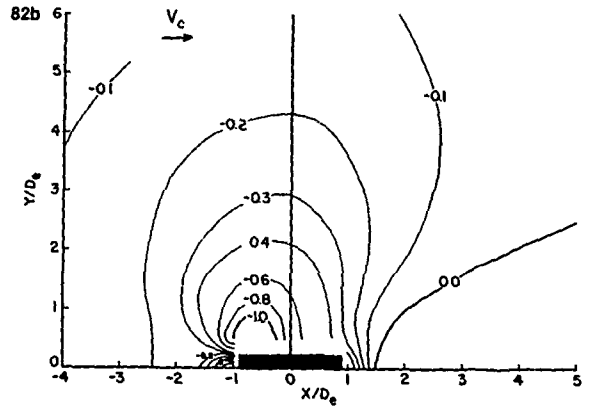

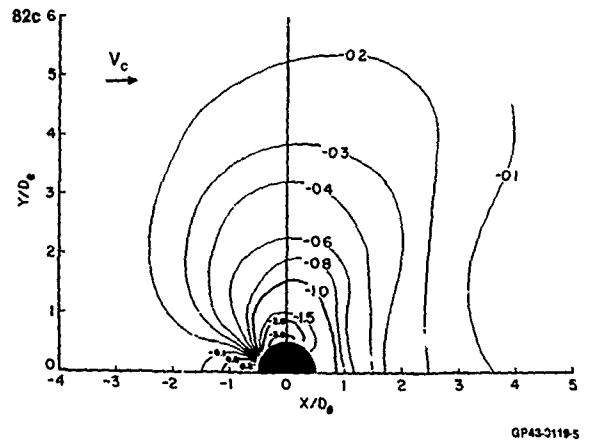

GP43-0119-5

Figure 82. Comparison of Induced Pressure Distributions of Rectangular and Circular Nozzles
$\psi = 0.25 \quad \delta_{je} = 90°$

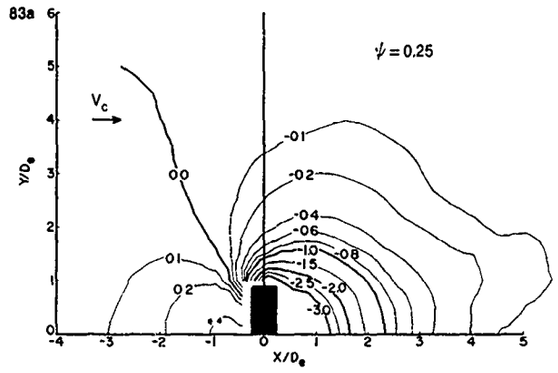

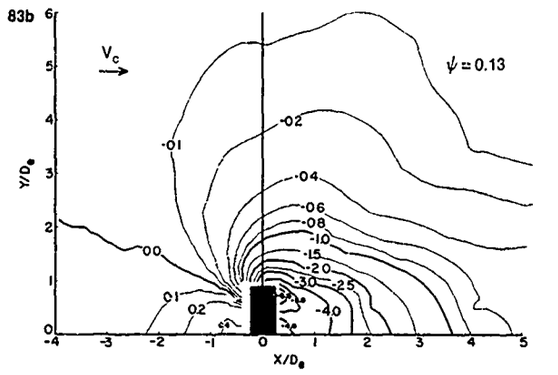

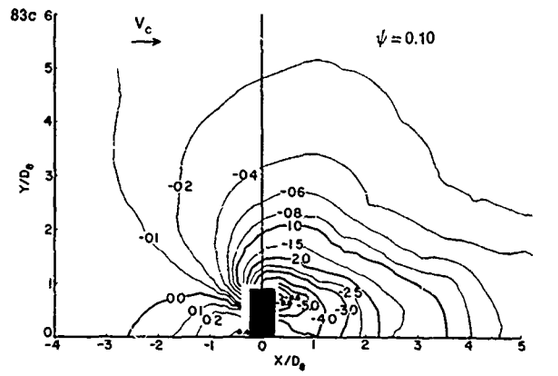

Figure 83. Influence of Velocity Ratio ψ on Induced C_p Contours
$\delta_{je} = 75°$

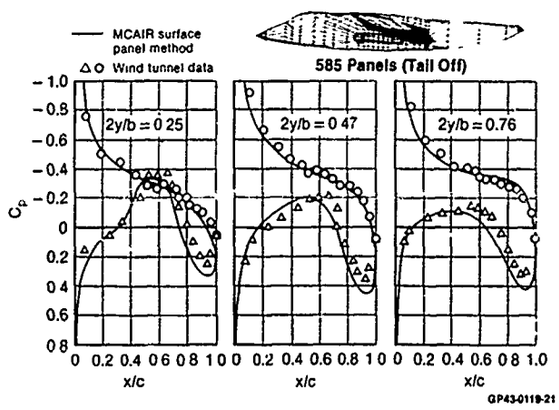

Figure 84 YAV-8B at 6.4° Angle-of-Attack in Cruise Mode
$M_\infty = 0.50$

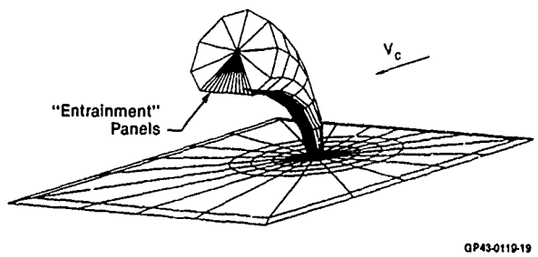

Figure 85. Paneling for a Flat Plate and Circular Jet-In-Crossflow
$\psi = 0.14$ $\delta_{je} = 90°$

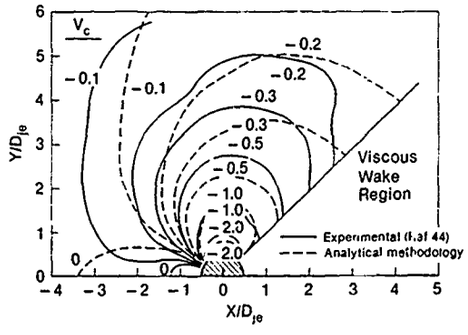

Figure 86. Induced Pressure Distribution Comparison
$\psi = 0.14$ $\delta_{je} = 90°$

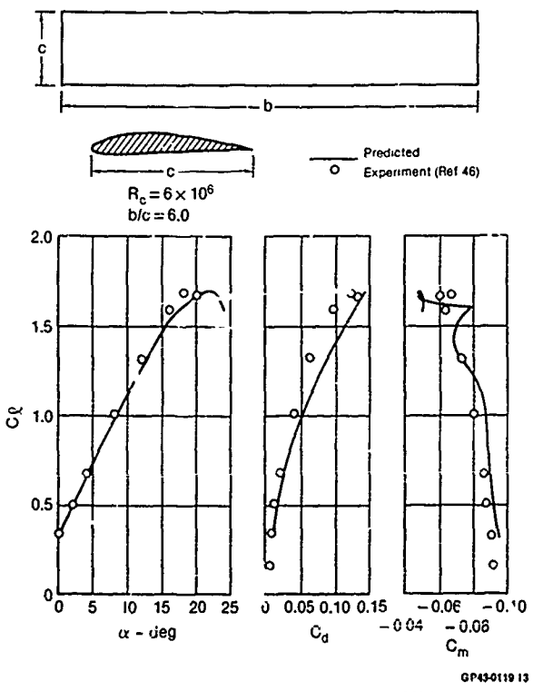

Figure 87. Force and Moment Prediction at Midspan of a NACA 4412, Aspect Ratio 6, Rectangular Wing

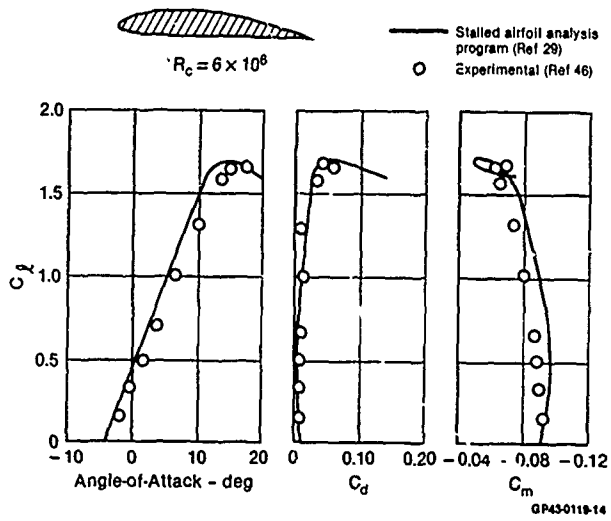

Figure 88. Force and Moment Predictions
NACA 4412 Airfoil

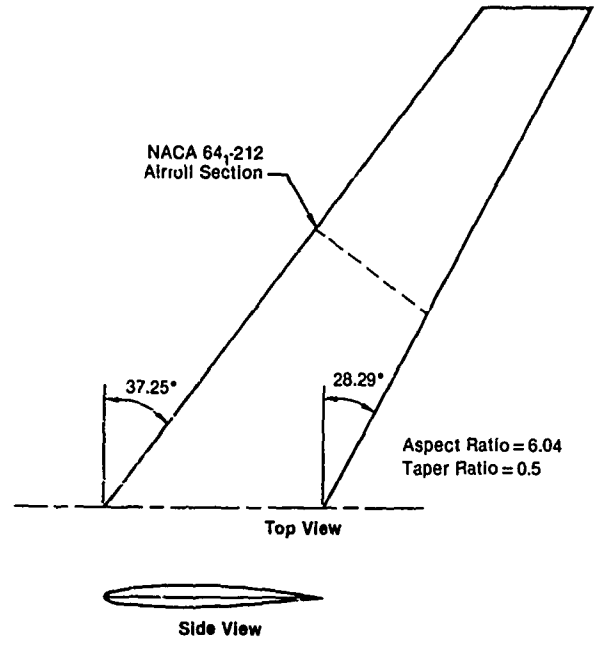

Figure 91. Geometry of Swept and Tapered Wing

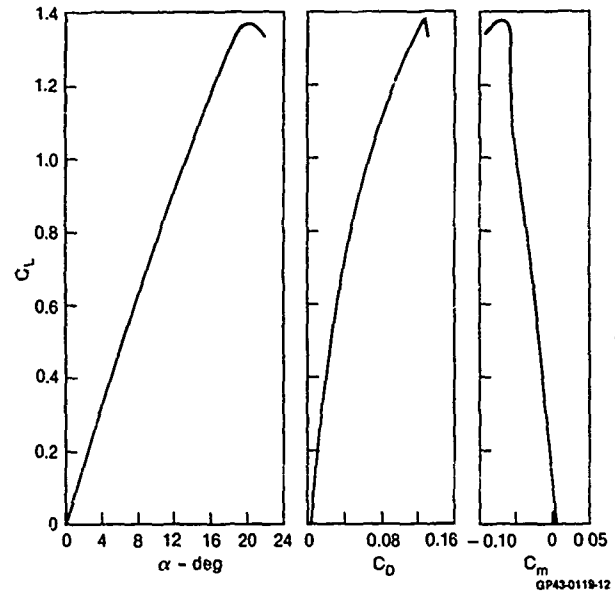

Figure 89. NACA 0012, $\Lambda = 20°$, AR = 5.5 Force and Moment Predictions
$R_\infty = 6 \times 10^6$

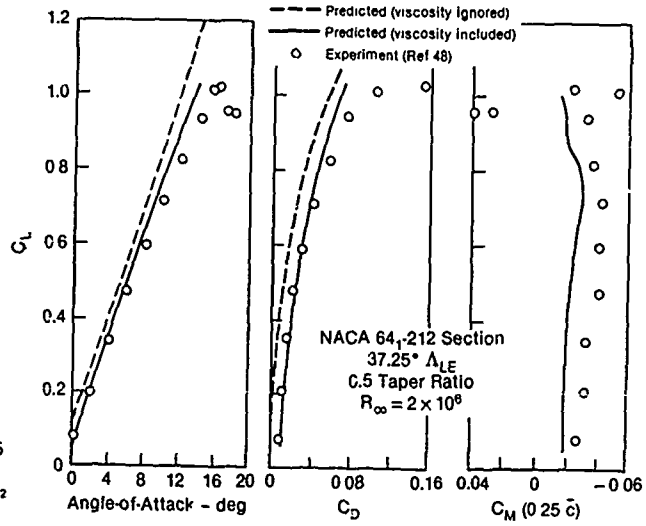

Figure 92. Comparison of Predicted Force and Moment With Experiment for a Swept and Tapered Wing

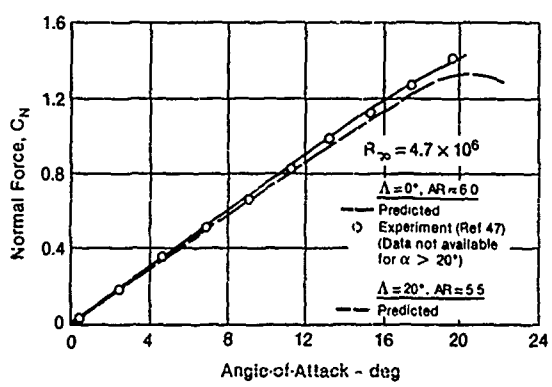

Figure 90. Comparison of Predicted Normal Force Coefficient With Experiment for Wings With NACA 0012 Sections

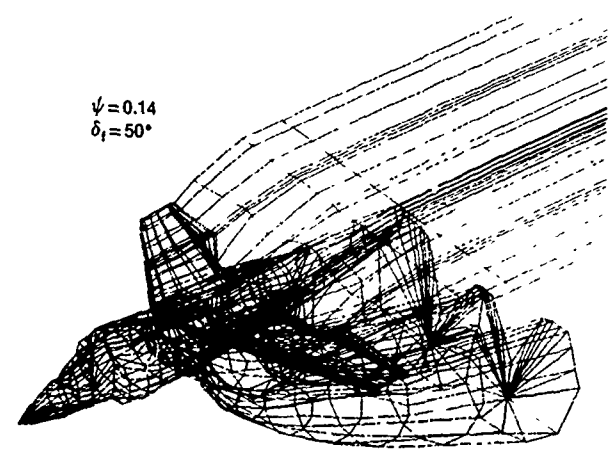

Figure 93. Paneled Representation of YAV-8B Powered Model

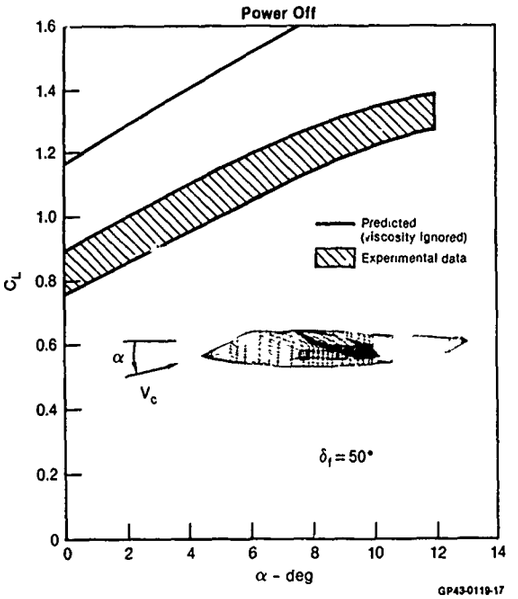

Figure 94. YAV-8B Power Off

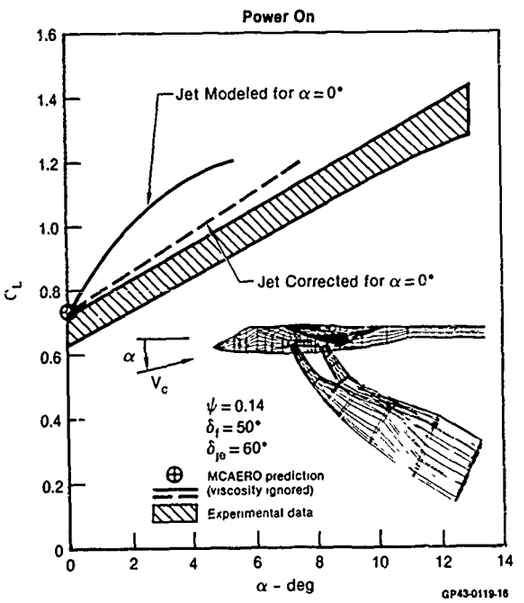

Figure 95. YAV-8B in Transition

Table 1. Two Methods for the Computation of Stagnation Line Location

Momentum Flux Method (MFM)	Momentum Flux Density Method (MFDM)
Stagnation Line Slope	
$\tan\theta = \frac{\beta \sin\phi_2'}{1+\beta\cos\phi_2'}$ where $\beta = \frac{R_1}{S'}\sqrt{\frac{\gamma_2 f_2(\phi_2) M_{je2}^2/\gamma_1 f_1(\phi_1) M_{je1}}{R_2/R_1}} + \frac{R_2}{S'}$	$\tan\theta = \frac{\beta \sin\phi_2'}{1+\beta\cos\phi_2}$ where $\beta = \frac{R_1}{S'}\left[\frac{\gamma_2 f_2(\phi_2) M_{je2}^2/\gamma_1 f_1(\phi_1) M_{je1}}{R_2^2/R_1^2}\right] + \frac{R_2}{S}$
On the Line Joining the Jet Impingement Points	
$\frac{R_2}{R_1} = \frac{M_{je2} f_2(\phi_2)\gamma_2}{M_{je1} f_1(\phi_1)\gamma_1}$	$\frac{R_2}{R_1} = \sqrt{\frac{M_{je2} f_2(\phi_2)\gamma_2}{M_{je1} f_1(\phi_1)\gamma_1}}$

GP43-0119-4

Table 2. Summary of Procedure for Calculation of Suckdown Force in Ground Effect

MCAIR Suckdown Methodology:

1. Panel Aircraft and Lift Jets
2. Determine $(\Delta L/T)_{calc}$ Out of Ground Effect (OGE) Using Uncorrected V_{fent} of Kleis and Foss
3. Correct V_{fent} to Match Empirical Lift Loss, $(\Delta L/T)_{exp}$, as:
$$V'_{fent} = \sqrt{\frac{(\Delta L/T)_{exp}}{(\Delta L/T)_{calc}}}\, V_{fent}$$
4. Panel Wall Jets
5. Determine V_{went} Using AGSF Program and Correct as:
$V'_{went} = 1.5\, V_{went}$
6. Calculate Total Suckdown Force IGE, F_s, Using Panel Method With V'_{fent} and V'_{went}

GP43-0119-07

Table 3. Adler/Baron Solution Approach

Given: Jet Properties at Centerline Station Z_c

Calculate: Properties at $|Z+\Delta Z|_{jc}$

Unknowns	Equations
$\Delta\theta_{jc}$ (℄ Path)	Momentum Balance ∥ ℄
ΔV_{jc} (Max Jet Velocity)	Momentum Balance ⊥ ℄
ΔA (Cross-Sectional Area)	Mass Entrainment
ΔShape	2-D Vortex Tracing
Velocity Distribution Within the Jet	Empirical Poisson Equation Solution

GP43-0119-28

Table 4. Wing Geometries Analyzed

Wing Section	Aspect Ratio	Leading Edge Sweep Angle (deg)	Taper Ratio	Twist (deg)
NACA 4412	6.0	0	0	0
NACA 0012	5.5	20.00	0	0
NACA 64_1 - 212	6.0	37.25	0.5	0
YAV-8B Supercritical (0.11 t/c Root, 0.07 t/c Tip)	4.0	36.00	0.3	−8.0

GP43-0119-15

V/STOL MANEUVERABILITY AND CONTROL

James A. Franklin and Seth B. Anderson
Ames Research Center, NASA
Moffett Field, California, 94035, U.S.A.

SUMMARY

This paper deals with maneuverability and control of V/STOL aircraft in powered-lift flight, and in addition, with specific considerations of maneuvering in forward flight. A review of maneuverability for representative operational mission tasks is presented and covers takeoff, transition, hover and landing flight phases. Maneuverability is described in terms of the ability to rotate and translate the aircraft and is specified in terms of angular and translational accelerations imposed on the aircraft. Characteristics of representative configurations are reviewed, including experience from past programs and expectations for future designs. The review of control covers the characteristics inherent in the basic airframe and propulsion system and the behavior associated with control augmentation systems. Demands for augmented stability and control response to meet certain mission operational requirements are discussed. Experience from ground-based simulation and flight experiments that illustrates the impact of augmented stability and control on aircraft design is related by example.

NOTATION

a_y	lateral acceleration
a_z, Δg	incremental normal acceleration
C_D	drag coefficient
C_L	lift coefficient
C_Z	normal force coefficient
C_{Z_w}	normal force coefficient derivative with vertical velocity
d_e	equivalent jet exhaust diameter
g	acceleration due to gravity
h, z	altitude, vertical position
IMC	instrument meteorological conditions
$j\omega$	imaginary component of complex root
$K_{(\ )}$	feedback gain for variable ( )
M_q	pitch damping derivative
M_u	pitch acceleration derivative with axial velocity
M_{δ_e}	longitudinal control sensitivity derivative
OVC	outside visual cues
q	freestream dynamic pressure
q_{jet}	local dynamic pressure in jet
s	Laplace operator
T	total thrust
T/W	thrust-to-weight ratio
T_h	vertical velocity mode time constant
T_λ	longitudinal velocity mode time constant
T_1	engine inlet temperature
$t_{\phi = 30^o}$	time for 30^o bank angle change
$t_{\psi = 15^o}$	time for 15^o heading change
$t_{50\% \Delta Y_{MAX}}$	time to reach 50% of peak flightpath increment
$t_{0.9 \Delta Y_{SS}}$	time to reach 90% of steady-state flightpath increment

$\dot{u}_{SHEAR}$	rate of change of wind velocity (wind shear gradient)
V	airspeed
VMC	visual meteorological conditions
V_{e_j}	equivalent jet velocity ratio $(q/q_{jet})^{\frac{1}{2}}$
W/S	wing loading
X_u	axial acceleration derivative with axial velocity
X_w	axial acceleration derivative with vertical velocity
x, x_c	actual and commanded longitudinal position
Y_{p_θ}	pilot transfer function for attitude control
Z_w	vertical velocity (heave) damping derivative
Z_{δ_T}	throttle sensitivity derivative
α	angle of attack
β	sideslip angle
γ	flightpath angle
$\Delta(\ )$	incremental value of ( )
$\Delta L/T$	normalized lift in ground effect
$\Delta \mathcal{L}/Td_e$	normalized rolling moment in ground effect
ΔV_A	airspeed change due to wind shear
$(\Delta V/\Delta T)_\theta$	steady-state change in airspeed with thrust at constant pitch attitude
$(\Delta \gamma/\Delta V)_T$ $(d\gamma/du)$	steady-state change in flightpath with airspeed at constant thrust
$(\Delta V/\Delta \gamma)_{ss}$	steady-state flightpath-airspeed coupling in response to thrust at constant attitude
$(\Delta V/\Delta \theta)_T$	steady-state change in airspeed with pitch attitude at constant thrust
ΔX	incremental axial force
ΔZ	incremental normal force
δ_H	stabilator (tailplane) position
δ_{LAT}, δ_a	lateral control position
δ_{MP}, δ_{LONG}, δ_e	longitudinal control position
δ_r	directional control position
δ_T, σ_T	throttle position, main engine throttle position
δ_v	nozzle angle
ζ	damping ratio
θ	pitch attitude
$\theta(1)$	pitch attitude change in 1 sec
θ_T	thrust vector inclination
ρ	air density
σ	real component of a complex root
σ_{FC}	lift engine fuel control position
σ_M	nozzle lever position
τ_e	thrust response time constant
τ_u	time constant for airspeed response to wind shear

τ_x	translational velocity time constant
ϕ	bank angle
$\phi(1)$	bank angle change in one second
ψ	heading change
$\psi(1)$	heading change in one second
ω	natural frequency
$(\dot{\ })$	$d(\ )/dt$
$(\ddot{\ })$	$d^2(\ )/dt^2$

1. INTRODUCTION

The operational requirements for an aircraft's mission define the aircraft's flight envelope and the ability to change from one flight condition to another within this envelope. Maneuverability is associated with the capability to execute these changes in flight condition through changes in the aircraft's attitude, translational velocity, and position in space as demanded by the mission requirement. V/STOL aircraft, in particular, have unique operational maneuvering requirements in addition to those for conventional aircraft. These include the need to hover precisely; move fore and aft, sideways, and vertically for landing; air taxi; transition from powered lift to aerodynamic lift; and perform relatively steep descents and climbouts from confined areas. The precision with which these maneuvers can be accomplished and the effort that the pilot must exert to execute them determines the aircraft's controllability. It is inevitable that certain V/STOL configurations are difficult to control at low-speeds due to low levels of angular damping, little angle-of-attack or directional stability, and too much dihedral effect (Ref. 1). Control is also influenced by the need to counteract forces and moments associated with thrust-induced effects, ground-effect, and flap and speed changes. Environmental effects place extremely severe demands on control for certain V/STOL tasks, such as landing on a small ship in a high sea state with a rolling, pitching, and heaving deck; wind gusts; and wakes from the ship's superstructure. Providing sufficient control to compensate for the lack of inherent stability and to counteract various sources of disturbances is not without penalty because control for low speed operation must be extracted in some form from the propulsion system.

Requirements for V/STOL flying qualities that attempt to define maneuverability and controllability criteria have been developed from a background of flight experience using a wide variety of V/STOL concepts. The specifications in the two documents, AGARD Report 577 (Ref. 2) and MIL-F-83300 (Ref. 3), have been operationally evaluated for recent V/STOL designs but lack clear definition for shipboard operation. Nevertheless, they have served to guide some V/STOL flight test programs and have been used extensively in recent design studies for advanced V/STOL concepts.

The intent of this paper is to describe the environment in which modern V/STOL aircraft will be expected to operate, to establish the nature of maneuvers that are appropriate to execute tasks associated with these operations, and then to relate these maneuvers to control authority demanded for modern V/STOL designs. Given this maneuver environment and required capability, the controllability to permit the desired precision of maneuvering is assessed. Characteristics of the basic aircraft and control augmentation systems that contribute to or detract from control precision are reviewed. The full V/STOL flight regime will be covered in these assessments, including takeoff, transition, approach, and landing. Furthermore, contributions of V/STOL configurations to combat maneuverability are noted in general terms. The paper describes experience that has been gained since AGARD 577 and MIL-F-83300 were published. The results compiled in these two documents are summarized and recent information from ground-based simulation, flight research, concept evaluations, and development test programs are discussed. Conclusions concerning future requirements for flight control research for V/STOL aircraft are mentioned in closing.

2. OPERATIONAL MANEUVER REQUIREMENTS

2.1 Operational Environment

Maneuver requirements for V/STOL aircraft are predicated on the operational environment to which they are exposed. For military use, these aircraft may be required to operate from major military airfields, austere forward sites, large aircraft carriers, or small aviation-capable vessels. Airfields and aircraft carriers provide ample space for takeoff and landing and precision approach guidance for operations conducted under low-visibility conditions and, as such, pose no great challenge to V/STOL operations. The capability for hover and slow-speed flight and for rapidly accelerating between

conventional wing-borne to fully propulsion-borne flight that characterizes V/STOL aircraft permits operation into more confined spaces associated with austere land-based sites and from platforms or decks of small ships. However, these operations enforce a greater precision of control and capability for rapid deceleration to hover than are associated with more generously proportioned facilities. For forward land bases, these aircraft may operate from temporary pads with dimensions of 70x70 ft, in close proximity to trees, buildings, equipment, or other obstacles to flight, as shown in Fig. 1. As a consequence, the ability to position the aircraft, to control height precisely, to stop quickly when approaching obstacles, and to do so under conditions of winds, turbulence, and low visibility is essential to ensure routine operational capability.

Operation at sea may entail vertical takeoff, short takeoff, and ski jump launch and vertical landing, and may take place from the decks of large carriers (70- 80 metric ton) to 15-ton amphibious assault ships, or even destroyers having landing pads of dimensions as small as 40x40 feet. As such, ample space may be available for launch and recovery, or these operations may take place in a confined space surrounded by the ship's structure. Figure 2 illustrates ski jump takeoff from the forward deck of H.M.S. Hermes, and as described by the pilots, is a rather uneventful experience. For vertical takeoffs, the primary concern is to avoid the ship's superstructure at liftoff and at translation away from the ship. For flat-deck, short-takeoff, pitching motion of the deck poses the greatest challenge, since downward excursions reduce clearance margins above the sea and enforce greater maneuver requirements after leaving the deck. In general, however, air operations aboard a ship this size or of that of the U.S.S. Guam, shown in Fig. 3, affords ample space for maneuvering during launch and recovery. When operations take place aboard smaller ships such as those shown in Fig. 4, the proximity of the ship's structure makes it imperative to be able to quickly arrest translational motions when maneuvering during departure or landing on the small pad astern. It should also be noted that, in all cases, air disturbances induced by the ship's superstructure increases the difficulty of precise control, and operation in poor visibility will make the pilot's task of positioning the aircraft in relation to the ship a challenging task.

During recovery to the ship, the vertical, lateral, and rolling motion of the landing pad may present a significant control challenge for the pilot. Figure 5 presents examples of the magnitude of these motions as derived from predictive models of Fortenbaugh (Ref. 4) and Brown et al. (Ref. 5). These motions are shown as functions of significant wave height, which is correlated with the measure of the sea state. For the smaller destroyer-class ship, peak heave motions may reach 10-15 ft, lateral motions as much as 5 ft, and roll amplitudes of nearly 10^{0}, for significant wave heights of 15 to 20 ft. Under current operational guidance, launch and recovery would normally take place in sea states of 4 or less, for which case the ship motion poses much less of a challenge. Although the larger amphibious assault ship has a more benign rolling motion, linear motion at the pad is as large as for the destroyer. Thus, if operations are to be conducted in more adverse weather conditions, it may be necessary for future aircraft to accommodate to the more active deck of the small ship in sea state 5.

V/STOL operation in confined spaces and near obstacles in a steady wind will expose the aircraft to strong wind gradients and turbulence. Figure 6 illustrates the nature of this environment in proximity to the fantail landing spot on a DD-963-class destroyer. In the presence of a 20-knot quartering wind 30 degrees to port, the character of the mean wind for an approach into the wind at an altitude of 100 ft above the sea and during descent onto the landing pad are shown at the left of the figure. Peak wind gusts experienced during descent onto the pad are shown at the right. These data were obtained from the model of Ref. 4 as derived from scale-model wind tunnel tests of this class ship described by Garnett (Ref. 6). When the aircraft enters the wake of the superstructure within a few hundred feet of the ship, a wind gradient is encountered for the example shown that consists of a wind deficit of approximately 6 knots. This change in the steady wind does not present a serious problem in moving up to and establishing a hover position with respect to the ship. At higher altitudes, wind variations induced by the ship would be even less. The major difficulties are encountered during descent onto the landing pad. For this example, the wind decays to essentially a calm condition at the deck, meaning that during the descent of approximately 50 ft, the pilot must correct for a relative velocity of 20 knots with respect to the ship to hold position and avoid moving into contact with its aft structure. Turbulence in the wake increases to a significant extent during descent, compounding the attitude and position control process. While these conditions are among the most extreme encountered in V/STOL operations, they do represent situations which must be taken into consideration. Along with details of the aircraft's design, operational procedures must be developed to provide options for defining an aircraft's controls to deal with this situation.

Visibility in adverse weather is another factor which will influence the manner in which the aircraft is maneuvered and controlled. Figure 7 from Hoh and Ashkenas (Ref. 7) condenses the definition of these conditions and their implications for design and operation. In fully visual flight (visual meteorological conditions - VMC) visual cues for attitude and translational control are easily obtained and no constraints are imposed on the aircraft or its operation. As visual information degrades to partial instrument meteorological conditions (partial IMC), cues for attitude control begin to degrade and translational rate information becomes marginal, and eventually only intermittent. Position cues may be only marginal for outside visual cues (OVC) Level 4. At the extreme is full IMC where all information for control of the aircraft must be presented to the pilot in the cockpit. For aircraft designed to operate in poor visibility, it is implicit that the control system provide stability to offset the lack of visual information. Otherwise, as will be noted later in the paper, additional control authority may be

required for the pilot to provide the stabilization function. Maneuver implications include restricting operations to more docile procedures, or, if full maneuver capability is to be retained, providing the necessary control stabilization and artificial display of information to support more aggressive maneuvers.

2.2 Operational Maneuvers

Given the operational environment discussed in the foregoing paragraphs, the maneuvers peculiar to the V/STOL or powered-lift portion of the aircraft's operation are concerned with takeoff, transition, approach, and landing. Within each phase are particular maneuvers that may have a specific impact on airframe, propulsion, or control system design. In the takeoff, primary concern is devoted to clearing the ground in the presence of ground-induced disturbances, avoiding obstacles near the launch area, and initiating the accelerating transition to cruise flight. Figure 8 presents examples of vertical and short takeoff maneuvers for the AV-8 Harrier described by Lacey (Ref. 8) and in Ref. 9. Sufficient performance and control authority must be available to accelerate vertically near the ground, to suppress the effects of steady winds, turbulence and ground induced disturbances arising from aerodynamic ground effects or from hot-gas-flow ingestion into the propulsion system and to assure aircraft stability at low speed. It is apparent from the examples that control is exercised in relatively large discrete steps for attitude, thrust, and thrust vector angle (nozzle). It can also be stated that in most instances precise control of attitude, heading, and vertical velocity is not demanded to the extent that is associated with the approach and landing.

For the transition to cruise or from cruise to powered-lift flight, it is important to ensure a sufficient performance envelope for maneuvering with satisfactory angle of attack or stall margin. This performance envelope must provide the ability to accelerate or decelerate in level flight, and to climb or descend at constant airspeed, or an appropriate combination of both. One means of presenting this performance envelope is shown in Fig. 9 for the X-22A aircraft (Ref. 10) in terms of duct angle tilt for a given airspeed. The range of duct angles for a given airspeed, or the range of airspeeds at a given duct angle, is a measure of the ability of the aircraft to maneuver through transition. Each range implies a reserve of thrust vector, attitude, and thrust control to generate accelerations for changing airspeeds or for changing flightpath angle. An alternate presentation of this envelope would illustrate the variation in flightpath angle and airspeed against parameters of thrust vector magnitude and angle. The X-22A has an ample transition corridor and corresponding operational flexibility as a consequence of the ability to climb and accelerate and to descend and decelerate within this envelope. A much narrower corridor would restrict the flightpath and speed profiles that could be flown, or even the ability to halt and reverse the process once initiated. Control authority in addition to that for flightpath and airspeed must be sufficient to stabilize the aircraft. Operations tend to be carried out in discrete steps as illustrated for the example from a Harrier at the right of the figure, and, in general, nonprecision control of attitude and heading, as well as airspeed and altitude, is all that is demanded.

The landing approach is concerned with the portion of the flight envelope that encompasses mid-transition to hover. Here, it is important to ensure sufficient capability for steep descents and for ability to decelerate to hover with some margin for climb and descent at low speed. Figure 10 shows a representative approach envelope with parameters of thrust magnitude and vector angle as suggested in the previous paragraph. Constraints may be imposed by aerodynamic lift, flightpath control authority about the nominal approach condition, and maximum allowable descent rates during the approach and near the ground. Within these constraints, it should be possible to manipulate the thrust vector to perform a decelerating descent to hover. Under these circumstances, it should also be possible to make large changes in aircraft attitude and heading rapidly and precisely, as well as flightpath and airspeed. The time history at the right of the figure shows an example of a decelerating approach executed by the Do-31 (Ref. 11). Note the frequent and rapid adjustments of the controls required to maintain precise approach path and speed control in the presence of winds and turbulence encountered during the approach.

For the hover and landing, the aircraft must have essentially the same height-and speed-control capability as for takeoff to successfully accomplish the landing in the presence of ground effect or to abort or wave-off and accelerate to conventional flight. The precision of control for attitude, heading, and horizontal and vertical velocities is greatest in this phase of flight, and it is important to be able to initiate, arrest, and stabilize all these motions rapidly to achieve acceptable hover position control. Control authority must also be sufficient to counter disturbances from air wakes, hot gas reingestion, and ground effect. Another example from a Do-31 landing is included in Fig. 11 to demonstrate the magnitude of control used and the activity of controls during the final approach to hover and at the landing. Note the abrupt rise in engine inlet temperature that indicates the encounter with the engine exhaust flow near the ground. In this case, maximum thrust was not sufficient to arrest the rate of descent once the aircraft was in this environment.

One aspect of maneuvering flight that is not associated with V/STOL flight, but which deserves mention in this discussion, is the use of V/STOL controls for air combat. While specific performance characteristics cannot be discussed in this forum, some of the general characteristics that are sought in good combat aircraft are available in V/STOL aircraft and prove to be beneficial in combat encounters. Hooper (Ref. 12) noted the importance of being able to rapidly achieve large changes in normal and axial acceleration within a performance envelope such as that shown in Fig. 12. The particular example

might be associated with a high-performance aircraft equipped with a speed brake. This acceleration envelope in turn determines the specific excess power, turn rate at a specific flight condition, and the ability to rapidly change flight conditions. Turn rate associated with normal acceleration capability over a range of flight conditions is presented at the right of the figure. The utility of features related to a V/STOL aircraft, such as thrust vectoring, lies in the expansion of this acceleration envelope, which could substantially enhance acceleration and deceleration, and, to a lesser extent, increase maximum normal acceleration and thereby improve turn performance. It should also be noted that the attitude changes required with any of these maneuvers, or with weapon pointing, must be executed rapidly and precisely.

Based on this review of the operational environment and the associated maneuver demands for V/STOL aircraft, the requirements on control authority to achieve this maneuver capability may be discussed.

3. CONTROL AUTHORITY REQUIREMENTS

It is well recognized (e.g., Refs. 2 and 3) that the total control authority of a V/STOL aircraft must be sufficient to trim the aircraft at a stabilized flight condition, to suppress external disturbances imposed on the aircraft, and to provide for maneuvering the aircraft as dictated by the mission and the particular phases of flight. Each of these demands on control authority are important to the designer and must be dealt with in the course of an aircraft's configuration definition and refinement. Control necessary to trim throughout the flight envelope is associated with specific details of a particular configuration and must be considered on an individual basis. The appropriate generalization to be made concerning trim control is that considerable attention should be given in the design process to minimize this requirement. Control authority frequently comes at considerable cost in propulsion system and airframe weight and overall aircraft performance, and the greatest fraction possible should be available for executing maneuvers associated with the mission tasks and for operating in the mission environment. Examples of pitch and roll trim control are shown in Fig. 13 and are representative of jet V/STOL designs. In these cases, trim requirements absorbed so much of the total control available that the control remaining was only marginally adequate for longitudinal path and speed control, lateral maneuvers, and for counteracting vertical and lateral wind disturbances. More recent designs of this class of aircraft, including the advanced Harriers such as the AV-8B and GR MK 5, have substantially reduced these trim requirements, and their operational flexibility and acceptability to pilots have improved accordingly.

Control utilization for suppressing external disturbances that is peculiar to V/STOL aircraft is associated with wind gradients and turbulence in the wake of obstacles, with forces and moments imposed near the ground, and with thrust variations due to hot gas reingestion. Figure 13 illustrates the increase in control activity for the Harrier as it approaches and lands vertically on a CV- class carrier with approximately 40 knots of wind over the deck (Ref. 13). Large control inputs were used to maintain tight control of roll attitude during the hover and landing. Examples of ground effect, including normal force and rolling moments are also shown (Ref. 9). A small initial suck-down, followed by a substantial and abrupt buoyancy, characterizes the normal force. Although the buoyancy is favorable in terms of thrust required to arrest sink rate, the variation in sink rate associated with the force perturbation must still be compensated. In the roll axis, the moment disturbance is abrupt and unstable. If this moment is not counteracted, objectionable roll attitudes and excessive lateral drift may develop during landing.

Control authority reserved for maneuvers is the primary subject of this section. For V/STOL operations, it has been possible to associate these manuever demands with tasks the pilot must perform in the hover and in the transition flight phases. For each phase, the force and moment authority to develop rotational and translational accelerations must be defined consistent with the individual maneuver requirements. Types of maneuvers that dictate control authority are large and rapid attitude and translational velocity changes. An example for hover is provided in Fig. 13 in the form of a quick stop that is required to arrest an increasing drift in speed that has developed inadvertently due to a mistrim condition or an external disturbance. Although the control mistrim may have been small, the buildup in speed that occurs over a period of time requires considerably greater control when the pulot needs to stop quickly. This capability is important for operation in confined space and can be a major factor in determining control utilization. During transition, the width of the operational corridor and the related flightpath acceleration capability is of primary concern. For air combat, the dominant factors involve the ability to produce normal accelerations to turn the aircraft rapidly, axial accelerations to quickly change flight condition and speed relative to an opponent, and rotational accelerations to enable rapid and precise pointing of the aircraft. In the subsections to follow, each of the three flight phases, with their appropriate manoeuvre control authority will be considered.

3.1 Hover

The preponderance of criteria and requirements for control authority in hover is contained in the AGARD V/STOL Handling Criteria (Ref. 2) and in the U.S. Military Flying Qualities Specification for V/STOL aircraft (Ref. 3). The information in these two documents was obtained from a [illegible] of flight tests of fixed-wing and rotary-wing V/STOL aircraft and from ground-based [illegible]ulator tests of specific aircraft models and of generic V/STOL control characteristics. Much of the data were obtained under fully visual flight

conditions and in relatively calm air. Ground effects and hot gas reingestion are peculiar to each configuration. None of the experience in Refs. 2 and 3 includes shipboard operation; hence the influence of air wake and ship motion environment are not reflected in the data or the criteria derived from them. In the case of Ref. 2, the stated control authority criteria are defined separately for maneuver and stabilization in the presence of turbulence. Ref. 3 requirements for control power include demands for maneuvering and stabilization in gusty air.

In the material to follow, each control axis (pitch, roll, yaw, and heave) is addressed individually, followed by a summary of the combined authority requirements for all axes and implications for total installed propulsion system thrust necessary to meet the combined control demand. Based on the categorization of maneuvers in the preceding section, the control utilization and requirements which are about to be described are determined by the following control tasks. For pitch and roll control, the primary concern lies with precision hover positioning and with the execution of longitudinal and lateral quick-stop maneuvers. Any control cross-coupling resulting from maneuvers about other axes must also be accommodated. Yaw control is used to make heading changes, to hold heading during lateral translation, and to reduced undesired sideslip. Propulsive thrust, deflected vertically, is used for height control to maintain vertical clearance and to control rate of descent during the landing. While some of these maneuvers can be described analytically, and control authority can be derived from the analysis, the overall task of the pilot in controlling the aircraft in the hover cannot be reduced to a simple analytical expression. Consequently, the criteria and requirements that follow are based on pilots' assessments of control demands while performing hover control tasks in the framework of a complete operational situation. The pilots' evaluations of control capability in hover account for the precision of control judged to be acceptable for the specific task and for the effort the pilot must expend in terms of attention, mental anticipation, and physical effort that must be devoted to compensate for deficiencies in the aircraft's inherent response to the pilots' control commands. The pilots' evaluations are quantified in terms of the Cooper-Harper rating scale (Ref. 14), and are ultimately interpreted as levels of flying qualities that may be characterized as follows:

Level 1: Flying qualities clearly adequate for the mission flight phase.

Level 2: Flying qualities adequate to accomplish the mission flight but with some increase in pilot workload of degradation in mission effectiveness, or both.

Level 3: Flying qualities such that the aircraft can be controlled safely, but with excessive pilot workload or inadequate mission effectiveness, or both.

These levels have direct correspondence to the major ranges of flying qualities quantified in the Cooper-Harper scale, namely: Satisfactory - Level 1; Adequate - Level 2; Inadequate - Level 3. With satisfactory flying qualities, no improvement in the aircraft's characteristics is necessary. With adequate flying qualities improvement in the aircraft's characteristics is warranted. When flying qualities are inadequate, improvement is required.

Pitch control authority for maneuvering in hover is presented in Fig. 14. The table included with the figure summarizes the AGARD criteria of Ref. 2 and the military (MIL) specifications of Ref. 3. The AGARD criteria are presented alternately in terms of maximum angular acceleration initiated from trimmed flight, or in terms of pitch attitude achieved in 1 sec following an abrupt control input. MIL requirements are stated solely as pitch attitude in 1 sec. An example time history of pitch rate and attitude response to an abrupt (0.3-sec) ramp-control input is provided to illustrate the interpretation of the maximum angular acceleration and attitude change in 1 sec. The attitude change in 1 sec accounts both for the angular acceleration produced by the control and the restoring moment proportional to angular rate that opposes the control moment. AGARD criteria are provided for only Level 1 (fully satisfactory) flying qualities. The lower end of the AGARD criteria apply to configurations which permit longitudinal translation to be accomplished through thrust deflection, while the upper end of the range applies to translation assumed to be performed using pitch rotation. The alternate criteria are self-consistent if the aircraft responds to the longitudinal control as a rate command as indicated in the time history, with a first-order time constant of approximately 0.6 sec. Since the MIL-F-83300 values include some provision for gust disturbances, they are somewhat more lenient than those of AGARD which only account for maneuvering.

Characteristics of several fixed-wing jet V/STOL aircraft are presented at the right of Fig. 14, in terms of the alternate criteria. They include the prototype and current operational versions of the Harrier (Ref. 2 and 8), the VAK-191B (Ref. 15), the X-14A and B (Ref. 16 and 17), and the XV-5A (Ref. 2). These values represent maximum available control authority and do not have trim control extracted. With the exception of the AV-8A nose-down control, all the aircraft substantially exceed both requirements. The AV-8A nose-down capability is lower than the rest because it is determined for the case of maximum bleed in all axes, which reduces the maximum reaction control authority in the individual axes. Various values shown for the X-14A and B represent ranges of control authority that have been evaluated with that aircraft in its variable stability mode. All of these aircraft were considered to have marginal Level 1 or better control power in hover. The fact that all seem to have an excess is attributable to the requirement to trim under various hover and low-speed translational flight conditions and for various loadings. Thus this magnitude of control authority is not always available for

maneuvering. With the exception of the AV-8A under maximum bleed, all the aircraft have total control authorities that agreed with the upper-level recommended in Ref. 2 to accommodate trim, counteract gust upsets, and to maneuver.. While it would be desirable to more clearly define the individual maneuver and turbulence control demands, credible experimental data are just now being acquired from ground-based simulation experiments and, potentially, from Harrier flight experience. In the absence of more definitive criteria, the recommendations of Refs. 2 and 3 stand as the best guides for maneuver control authority.

With the exception of the VAK-191B, all the example aircraft in Fig. 14 had pitch-control systems of the rate-command type. Some experimental evidence from ground-based simulation experiments suggests that maneuver and turbulence-suppression control authority may be reduced if attitude command and stabilization is provided by the flight control system. In Fig. 15, the influence of attitude stabilization on turbulence suppression is noted, both in terms of control utilization and attitude variations. Specifically, these are analytical predictions of the root-mean-square control activity and attitude variations in proportion to the rms gust disturbance magnitude for a range of attitude retention or stabilization control bandwidths. The gust environment represented in this analysis is a random horizontal component with frequency content up to 0.1 rad/sec, which is a reasonable approximation for this component of atmospheric turbulence. Attitude stabilization bandwidths above 1.0 rad/sec dramatically reduce attitude variations and also reduce to some extent the amount of control used to counter the gust upsets. At the right of the figure, the effect of attitude command systems on flying qualities level for aggressive quick-stop maneuvers is shown. For Level 1 flying qualities, the amount of control authority, expressed in terms of maximum angular acceleration, is approximately half that for the rate-command system. This reduction in control required is not so dramatic for Level 2 flying qualities, but it is still significant. These results were obtained from moving-base simulator experiments reported by Greif et al. (Ref. 18) and apply to optimized dynamic characteristics for each of the control systems. The piloting task included aggressive quick-stop maneuvers which produced a higher level of control demand than for the precision control requirements of Refs. 2 and 3. While the absolute magnitude of control for a given level of flying qualities to accomplish the task exceeds the AGARD criteria and the MIL specification of Refs. 2 and 3, the relative control demands for rate and attitude command systems may be correct. Current simulation and prospective future flight experiments are expected to provide information to verify this supposition.

Roll control authority in hover is the subject of Fig. 16. The table provides the AGARD criteria (Ref. 2) and the MIL specification (Ref. 3) results in the same form as for the pitch axis. Again, since the MIL specification values provide for some gust suppression, they are also more lenient than the AGARD criteria. At the right of the figure, characteristics of the same aircraft noted in the discussion of pitch control are presented. In all cases, they substantially exceed the Level 1 criteria, primarily because of the provision for countering rolling moment due to sideslip in low-speed translational flight, or, in the case of the X-14, for variable stability research purposes. With the exception of the lowest control power case for the X-14A, all these aircraft have Level 1 flying qualities for roll control in hover. The X-14A with 0.8 rad/sec^2 angular acceleration was rated to have only marginal Level 2 flying qualities for precision hover. All the other aircraft have control authorities that fall within the range of angular acceleration (0.8 to 2.0 rad/sec^2) that is suggested by the AGARD criteria for trim, upset, and maneuvering. Until more definitive experimental results are available, the criteria for roll control presented in Refs. 2 and 3 stand as the best guides for control authority in hover.

As in the case of pitch control, some prospect for reducing control authority requirements may be provided by attitude stabilization (Fig. 17). In Ref. 11, it was noted that the Do-31, which incorporated pitch and roll attitude stabilization, was considered to have satisfactory roll maneuvering capability in hover using a control power of 0.4 rad/sec^2.Results from Ref. 18 reveal fractions of attitude to rate command control to achieve Level 1 flying qualities that are similar to results obtained for the pitch axis. These data also show the effect of turbulence magnitude on the level of flying qualities , and indicate that in comparison to rate command systems, attitude command systems provide the same level of flying qualities at approximately twice the level of gust disturbance. Rolling moments induced by turbulence that are one-third of the total roll control authority of the aircraft can be encountered while retaining Level 1 flying qualities. Although the absolute value of these roll control requirements are subject to further experimental verification, the influence of attitude control in reducing the total roll control demand is likely to be valid for maneuvering in hover and for suppressing the influence of turbulence.

Criteria for yaw control in hover are given in Fig. 18 for both the AGARD and the MIL specification documents (Refs. 2 and 3). In this case, the AGARD criteria are given in terms of the maximum angular acceleration or the time to achieve a 15° change in heading angle. The MIL specification, as before, refers to the attitude (heading) change achieved in 1 sec. The three criteria are reasonably self-consistent, assuming yaw damping that produces yaw rate time constants of 0.5 to 1.0 sec. Characteristics for the same example aircraft are shown at the right of the figure. With exception of the AV-8A under maximum bleed conditions, all these aircraft exceed Level 1 values for heading change in 1 sec and fall within the satisfactory range of angular acceleration capability suggested by AGARD. The two points for the X-14A represent the extremes of yaw control characteristics evaluated with the variable stability system. The X-14A (at its highest control power) and the AV-8A (single-axis bleed) are considered by pilots to have satisfactory yaw

control characteristics in hover. The X-14A at its lowest control power was rated by pilots to be marginally adequate to inadequate for yaw control in hover; however, this assessment may have been due to a particularly low level of yaw damping for this configuration. With the damping increased to an acceptable level, this same control authority was felt to be adequate (Level 2) by the pilots. Most interesting is the fact that the VAK-191B, with its apparently quick response, was considered to have somewhat sluggish yaw control. This impression is in contrast to a more widely held view, expressed by Lacey (Ref. 8) and Hutchins (Ref. 19), among others, that the AGARD and MIL specification yaw control requirements are more stringent than necessary. It is more likely that the VAK-191B experience reflects a low control sensitivity rather than a deficiency in total control authority. When it is necessary to establish priority for control authority among the three axes, the requirement for yaw acceleration capability will ordinarily be less than for roll and pitch. As a final observation, all these values, with exception of the AV-8A at maximum bleed, fall within the range noted by AGARD to account for trim, gusts, and maneuvering.

Control utilization in heave for height control and stabilization in hover is presented in Fig. 19. For this control axis, both AGARD and the MIL specification cite criteria for minimum thrust-to-weight ratio. In addition, AGARD recommends a minimum steady climb rate, and both AGARD and the MIL specification note the same minimum incremental normal acceleration (though only the MIL value is shown in the table). The heave response characteristics shown in the table are not independent of other heave axis characteristics. Both AGARD and the MIL specification note a dependence of thrust/weight on the level of heave damping inherent in the airframe. This interaction is apparent in the boundary for satisfactory (Level 1) flying qualities at the right of the figure. The lower thrust/weight is considered satisfactory only for sufficient damping in the vertical axis. This trade-off is similar to the variation in control authority for the pitch and roll axes for rate and attitude command systems in the sense that increased damping, like attitude command, improves stability for that control axis. However, it is unlikely that little or no heave damping can be tolerated, no matter how large the thrust/weight. As Hoh and Ashkenas suggest (Ref. 20), a minimum tolerable heave damping on the order of -0.3 sec^{-1} will likely be imposed for height control. These implications on the dynamics of height control will be covered in a later section of this paper.

No aircraft configurations were included on Fig. 19 because of the wide variation in thrust/weight for a given aircraft, depending on its loading condition. For the aircraft listed previously in the paper, a range of thrust/weight from 1.0 to 1.2, and heave damping from nearly zero to -0.3 sec^{-1} was covered. In no case could Level 1 flying qualities be obtained for a precision hover if thrust/weight was less than 1.05. According to Ref. 15, the VAK-191B was considered to have Level 2 flying qualities in hover for thrust/weight of 1.05. In cases in which these aircraft were hovered in calm air, heave damping less than -0.3 sec^{-1} could be tolerated while retaining satisfactory flying qualities. However, it should be emphasized that no significant ground effects or hot gas reingestion were encountered in these cases. The criteria are meant to provide height control capability in excess of heave forces imposed by ground effect of reingestion. Holzhauser (Ref. 11) comments that the Do-31 had unacceptable height control approaching the ground because of reingestion, even though its lift engines provided a hover height control reserve of 0.1 g. For nonprecision maneuvers such as takeoff, it may be adequate for incremental normal accelerations in excess of ground effect to be less than 0.05 g as suggested in Ref. 8. However, for tasks that require precise control, which are performed during a sustained hover near the ground, minimum thrust/weight of 1.05, and incremental normal acceleration of 0.1 g over that necessary to counter ground effects and reingestion of hot gasses is reasonable.

As the MIL specification (Ref. 3) states, the aircraft's control system must be capable of trimming the aircraft in a steady hover in the presence of a wind from the most critical direction, and hold sufficient control in reserve to meet the pitch, roll, yaw, and thrust control demands simultaneously. The wind magnitude most frequently cited for this requirement is 35 knots. This combined requirement for trim and maneuver is assumed to account for stabilization in the presence of gusts and does not require an additional control increment to be added to counteract gust upsets. Since the entire control capability in hover is derived from the propulsion system, either through direct use of thrust or through bleed air from the compressor, this combined control requirement is of serious concern to the designer. An example of the impact on a Level 1 flying qualities requirement for a conceptual design of a four-poster lift-cruise fan aircraft is cited by Shaw and Craig et al. in Ref. 21. The individual contributions to the aircraft's installed thrust/weight are reproduced from their paper at the right of Fig. 20. The combined requirement for trim and maneuver control for attitude and height is over 30% of thrust in excess of weight. To meet this requirement for vertical takeoff would seriously penalize the aircraft's range/payload performance. The thrust necessary to meet Level 2 flying qualities is not reduced substantially. Not all designs present a concern of such magnitude; however, any thrust held in reserve for control often reduce the aircraft's mission effectiveness, and, if excessive, could prevent it from proceeding beyond the design stage. However, the reserve thrust associated with the Level 1 requirement is available for meeting unforseen operational situations, particularly in adverse weather aboard ship, and may permit a V/STOL aircraft to operate routinely in these conditions for the first time.

Other options may be considered as a means for alleviating this substantial demand on the propulsion system for control. Short takeoff will unlikely impose a stringent demand for control reserve as does sustained hover in ground effect. If heavyweight takeoffs are performed with some ground roll, the vertical takeoff demand must no longer be met at

those weights. Meeting the vertical landing requirement will be substantially easier on the propulsion design. Another option is to prioritize the axes for control demand and meet their individual needs accordingly. Hutchins comments (Ref. 19), and it is generally appreciated, that the yaw axis is less critical for control than roll or pitch, and may be treated accordingly. Roll is considered to have first priority, followed by pitch. The Harrier is a good example of a design that has successfully adopted the approach of shared reaction control demand. In that aircraft, an individual control axis has full authority, available when the aircraft is operating below maximum thrust and no other controls are activated. When the aircraft is at maximum thrust and more than one control is demanded, the demand is shared, with the least proportional reduction applied to roll, then to pitch and yaw in that order. Figure 21, taken from Fozard's case study of the Harrier design (Ref. 22), illustrates the time that compressor bleed flow exceeds a fraction of the total available. These characteristics were used to establish a time mean bleed for all three axes which would be provided without any reduction in gross thrust. For bleed demand exceeding this level, maximum thrust would be reduced rapidly as indicated at the right of the figure. In the case of maximum bleed, and for the normal lift dry condition, this penalty would be considerable. In fact, as momentary demands approach this level, transient disturbances would be introduced to other axes as their control was momentarily reduced. However, for operation at the extreme of the control envelope, this design approach has proven to allow the essential control demands to be met without unduly compromising control in other axes. This points out the need to reduce trim requirements, including those for crosswinds, to a minimum during the design phase.

3.2 Transition

Given the nature of maneuvers associated with transition control tasks in Section 2, the AGARD criteria and MIL specification attempt to ensure sufficient control margins as the aircraft accelerates or decelerates between wing-borne and fully propulsion-sustained flight, and to accommodate those maneuvers associated with precision flight at low airspeed. With regard to the latter objective, the AGARD criteria deal primarily with STOL operations and are based on a substantial body of data on powered-lift STOL operations contained in the report by Innis, Holzhauser, and Quigley on STOL aircraft airworthiness considerations (Ref. 23). Pitch axis concerns are related to the need to control either angle of attack, airspeed, or flightpath, and to counteract cross-coupling from thrust to thrust vector angle control activity. Roll control demands arise from the precise lateral flightpath control associated with a precision approach, from yaw to roll coupling during directional maneuvering, and from the need to counteract asymmetric thrust transients. Yaw control is required for de-crab maneuveres, to counteract roll-yaw cross-coupling during lateral maneuvers, and also to suppress asymmetric thrust transients. Flightpath control, obtained from whatever source is identified as the primary flightpath controller (thrust or thrust deflection, or even pitch control), is related to either precision or nonprecision approach and to the need for adequate climb and descent authority and normal acceleration to complete or abort the approach and to execute the landing flare, if required. Longitudinal (axial) acceleration, along with flightpath authority, defines the transition corridor and determines how quickly the aircraft can transit from powered-lift to wing-borne flight and how readily the transition can be arrested or reversed. Criteria for each of these controls will be covered in the following discussion.

AGARD criteria for pitch control during transition are of the same form as used for hover. The values shown in Fig. 22 for attitude change in 1 sec are identical to those for hover whereas the angular acceleration capability is slightly less. They are considered sufficient to accomplish speed or angle-of-attack control during takeoff and approach and to rotate the aircraft for takeoff and landing flare. U.S. Air Force STOL transport flying qualities requirements (Ref. 24) are consistent with the attitude change in 1 sec. The MIL specification (Ref. 3) takes the approach of requiring a 50% control margin in excess of trim through the transition envelope. This is a more general requirement, and, though somewhat arbitrary, has support among the designers. Examples of pitch control used for trim during transition for the AV-8A (Ref. 8) and VAK-191B (Ref. 25) are presented at the right of Fig. 22. At the high end of the transition range, the AV-8A uses somewhat more than half its longitudinal control for trim. Although the aircraft's control margins are considered to be adequate, they have been observed to be less than desired (Refs. 8 and 13), as would be anticipated given the MIL specification values. The VAK-191B longitudinal trim approaches 50% toward the upper end of its transition; however, its longitudinal control margins are considered to be adequate (Ref. 15). The AV-8B requires substantially less control to trim through transition than its predecessor, and it felt by pilots to have fully satisfactory pitch control margins.

AGARD roll control criteria are also of the same form as for hover. The range of angular acceleration shown in Fig. 23 is somewhat greater than for hover, whereas the attitude change in 1 sec remains the same. AGARD also adopts the MIL specification philosophy and includes a 50% control margin criteria to be applied for sideslips produced by full rudder authority. The MIL specification includes this 50% margin as an alternative, but introduces time to bank to 30^{0} as the primary requirement. The latter is an alternative to attitude change in 1 sec as a metric by which to judge roll maneuver capability. Both metrics account for the amount of control authority and for opposing moments produced by roll damping. The range of values contained in the MIL specification encompass aircraft ranging in size from fighter to heavy transports.

Data for angular acceleration and time to bank for recent STOL transport designs in the medium weight class are indicated at the right of the figure. The NASA/Boeing-deHavilland Augmentor Wing Research Aircraft (Ref. 26), the NASA/Boeing Quiet

Short-Haul Research Aircraft (Ref. 27), and the Breguet-941 (Ref. 28) all were determined to have satisfactory Level 1 roll control power and response. The STOL transport flying qualities requirements of Ref. 25 correspond to the upper range of the MIL specification values. The inset at the right of the figure provides data from the AV-8A (Ref. 9) and the VAK-191B (Ref. 25) to illustrate the control margin during sideslip at two speeds within the transition. At 100 knots, both aircraft have lateral control requirements that are extremely sensitive to sideslip and both are considered to have inadequate control remaining during uncoordinated flight (Refs. 8 and 15). The AV-8B, by contrast, has substantially less effective dihedral during transition and its lateral control margins are twice those of the AV-8A (Ref .9).

Yaw control criteria are of the same form as for hover, and include the 50% control margin as an alternate requirement for the MIL specification. AGARD values shown in Fig. 24 are less than stated for hover, reflecting less of a demand for rapid heading change during a landing decrab than during the hover maneuvering. MIL specification values are the same in both cases. Two examples of yaw response for STOL aircraft are provided at the right of the figure. Both the Breguet-941 (Ref. 28) and the Augmentor Wing Research Aircraft (Ref. 26) meet the AGARD criteria; however, the Breguet-941 would fall somewhat short of the MIL Level 1 requirement. Specific pilot evaluations were not obtained for either aircraft, although no objections have been raised concerning their yaw response.

Flightpath control authority is specified by AGARD in terms of steady climb and descent capability at the selected approach condition and the incremental normal acceleration that can be generated. In Fig. 25, the 6° climb capability was derived by analogy from FAA operational requirements for multiengine transport aircraft, and was intended to permit the approach to be aborted without resort to changing the aircraft's configuration. Descent capability below the intended approach path is specified to permit control authority for flightpath tracking. Recently, the FAA and NASA have developed tentative powered-lift airworthiness criteria (Ref. 29) from extensive moving-base simulation experiments to evaluate a variety of STOL aircraft characteristics. These criteria suggest that enough flightpath control be available to achieve level flight with no configuration change, and to descend to 4° below the nominal approach path. The diagram at the right of the figure illustrates the most recent criteria. The ability to achieve level flight without changing configuration was felt to be sufficient to permit the pilot to discontinue the approach, and that a configuration change would be permissible for initiating the subsequent climb. This proposal imposes less demand on excess thrust than does the AGARD criteria, and it is believed to offer adequate safety for operations. The FAA criteria include a greater descent capability than is suggested by AGARD because of results from the simulation program that indicated the need for 4° incremental descent authority for control to the approach path in moderate turbulence. The AGARD requirement was based on flight data that were obtained under essentially calm air conditions. These proposals await further substantiation from flight experience. It should be noted that the descent condition should not violate safe angle-of-attack or airspeed margins described in Ref. 29.

Longitudinal acceleration capability during transition is specified in Fig. 26. Both the AGARD and MIL specification cite the need to accelerate and decelerate rapidly and continuously through transition, and to easily reverse the direction of the transition. AGARD suggests 0.5 g to be a desirable capability. This criterion is largely subjective and it is only possible to cite good and bad experiences in support of this conjecture. The example at the right of the figure is the corridor of the XV-15 tilt rotor, and it represents a very generous transition maneuver capability (Ref. 30). The aircraft accelerates and decelerates well within the envelope, and the pilot is not required to observe a precise conversion schedule. The various models of the Harrier also provide excellent acceleration authority during transition. Capability exceeding 0.5 g has been achieved for these aircraft. The X-22A, whose envelope was given as an example in Fig. 9 also has good acceleration and deceleration capability. The VAK-191B could accelerate at about 0.5 g during the low-speed end of its envelope; however, this capability diminished to nil at higher transition speeds and was considered objectional to the pilot (Ref. 15). Deceleration authority was of no concern. The XV-5A had a limited acceleration capability in transition due to limited thrust, a complex angle-of-attack schedule, and a slow thrust deflection rate (Refs. 1 and 2). Accelerations of 0.13 g were observed during operational experience. Based on these examples, and the body of data on which the AGARD and MIL specification rest, it is possible to say that 0.5 g acceleration and deceleration capability will assure good transition control authority. If this authority is as low as 0.1 g, it will clearly be inadequate. Where the capability to assure adequate acceleration authority lies must be determined more definitively.

3.3 Combat Maneuvering

It is not the intent of this section to discuss requirements for combat maneuvering of V/STOL aircraft, but rather to note some of the favorable contributions that features of a V/STOL configuration may provide in this regard. Quantitative results are not available in the open literature; however, selected references cite advantages of thrust vectoring in qualitative terms that relate to deceleration and reacceleration, turn rate, weapons pointing, and controllability at low airspeed (Refs. 12, 31, and 32). More definitive information is available in the classified literature. Hooper (Ref. 12) notes the approximate magnitude of the expansion of the acceleration capability due to thrust vectoring. In his acceleration vector envelope, which is reproduced at the left of Fig. 27, a great increase in deceleration potential is indicated, and, given a basic 8 g airframe, approximately a 15% increase in normal acceleration is realized. This capability converts to maneuver performance in the proportions shown at the right of the

figure. Full thrust vectoring produces modest fractional increments in turn rate in the combat flight envelope and substantial reductions in time to decelerate or to force an overshoot by an opponent. This capability is available to the pilot essentially as fast as the cockpit control can be manipulated. No time delays of the order required to change thrust or change the aircraft's attitude are required. The use of the deceleration capability is not without its penalties, since it implies a reduction in the aircraft's energy state. It is a capability to be used with discretion, depending on the adversary or adversaries' relative aspect and energy, and is not to be used indiscriminately. Nevertheless, it is an option that may be inherent in some V/STOL aircraft that may be used to advantage against a conventionally equipped opponent.

Another aspect of V/STOL design that may be of value is the ability of some concepts to use the thrust vector to generate moments for rotation of the aircraft to attitudes that could not be sustained by purely aerodynamic controls. Figure 28 illustrates this feature qualitatively for either pitch or yaw control in relation to angle of attack. Trends of the aerodynamic moments with increasing angle of attack as shown in the figure are typical of advanced fighter designs. The proportion of thrust vector moment to that of the aerodynamic control at low angle-of-attack is also reasonably well established. The advantage in ability to rapidly rotate the aircraft in pitch and yaw over a wide range of attitudes of the thrust vectoring VSTOL aircraft over a conventional adversary is clear. Although the contribution of reaction controls to moment generation are not shown for comparison, they have been found to provide similar benefits at lower airspeeds (Ref. 33).

4. V/STOL CONTROL ARRANGEMENTS

With the background of requirements for control forces and moments to achieve maneuver capability that has been discussed earlier in the paper, this section will provide examples of the approaches to control system design for an existing V/STOL aircraft and for several conceptual V/STOL configurations. To focus the discussion, these aircraft will be associated with one of two groups: fighter-attack or subsonic multimission configurations. Although this grouping is somewhat arbitrary, it recognizes that fighter-attack aircraft obtain most, if not all, of their control moments through bleed reaction controls, and that the multimission configurations achieve most of their moment control through redistribution of thrust among the various force generators. The grouping is not intended to infer superior capability for either approach to control design. A general description of these configurations is presented in Nelms' paper in this lecture series (Ref. 34).

4.1 Fighter-Attack Configuration

It is appropriate that the first example deals with the only operational jet V/STOL fighter-attack aircraft, the AV-8 and GR MK series Harriers, originally designed by Hawker Aircraft and most recently modified in design and produced by British Aerospace and McDonnell-Douglas. This aircraft, shown in Fig. 29, relies on high-pressure compressor bleed for reaction controls as well as conventional stabilator (tailplane), ailerons, and rudder for pitch, roll, and yaw moment generation. Bleed flow for the reaction controls is fully selected when the Pegasus engine nozzles are deflected beyond 20°. The reaction controls, along with thrust modulation and thrust deflection, produce control required for hovering flight. During transition, both reaction and aerodynamic controls are effective. In conventional flight, with the Pegasus nozzles undeflected, bleed flow to the reaction controls is shut off and pitch, roll, and yaw control is provided only by the aerodynamic surfaces (Refs. 9 and 22).

The reaction control system uses variable shutter valves located at the extremities of the airframe and which are supplied bleed air on demand. Pitch control is produced through downward exhausting valves in the nose and tail extension. Roll control is provided by valves in the wing tips that thrust either up or down. Yaw control is derived from a single valve in the tail extension. Bleed flow demand is scheduled such that any single axis can achieve its full bleed authority, and that combinations of axes receive proportionally less than their full capacity based on a priority of roll/pitch/yaw. Reaction control does not begin to reduce maximum available thrust from the engine until the level of bleed exceeds 50% of full authority. When water injection is selected, or short lift ratings are used, maximum rated thrust is sustained at higher bleed levels.

Height control in hover is obtained by modulating engine thrust. Longitudinal translation can be performed either by rotating the Pegasus nozzles fore or aft of the hover setting, or by rotating the aircraft in pitch. During transition, flightpath and longitudinal acceleration are controlled by a combination of thrust modulation and deflection. In forward flight, the aerodynamic controls are used conventionally to maneuver the aircraft. Thrust vectoring may be employed to augment turn capability, generate rapid deceleration and reacceleration, and to assist the stabilator in rotating the fuselage in pitch. In its later designs, the Harrier's longitudinal and lateral control margins during transition have been improved considerably. Both longitudinal trim and effective dihedral have been reduced to permit more of the respective controls to be available for maneuvering.

A conceptual design of a single-engine supersonic, V/STOL fighter/attack aircraft of the deflected-thrust class like the Harrier is reviewed next. This configuration is shown in Fig. 30, and, similar to the Harrier, it incorporates a combination of bleed reaction and aerodynamic controls. Reaction control valves are placed in the same locations as for the Harrier and, with exception of the rear pitch valve, the valves exhaust bleed air in a

similar manner. The rear pitch valve exhausts up as well as down. Aerodynamic surfaces include canards, trailing edge flaps, ailerons, and a rudder. Two additional means of control are provided during hover and transition to relieve pitch trim demands on the reaction control system. Differential thrust modulation between the front fan stream burning nozzles and the aft core flow nozzles provides pitch trim in hover. During transition, differential deflection of the front and rear nozzles affords similar trim capability. Engine sizing allows approximately 10% of thrust for control and 5% for ground effect and reingestion during heavy-weight vertical takeoff. The control allowance is increased 4.8% for landing. Reaction controls were sized to meet maximum simultaneous control demands at the vertical takeoff weight and provided the following angular acceleration for each axis: pitch = +0.33, -0.21 rad/sec^2; roll = 0.32 rad/sec^2; yaw = 0.21 rad/sec^2. Maximum single axis capabilities that result from this design are: pitch = +0.7, -0.56 rad/sec^2; roll = 1.35 rad/sec^2; yaw = 0.44 rad/sec^2. This configuration is described in more detail in Ref. 35.

Another supersonic fighter concept that uses a wing-root chordwise ejector for V/STOL capability is shown in Fig. 31. In hover, all moment control is derived from reaction controls arrayed at the wing tips, under the cockpit, and in the tail. The wing tip and cockpit control valves exhaust downward only for pitch and roll control. The tail valves exhaust laterally for yaw control. These controls were sized in accord with the AGARD criteria of Ref. 2 and the MIL specification (Ref. 3). In conventional flight, elevons are used for pitch and roll control and a rudder is used for yaw. While in hover, engine thrust modulation provides height control and attitude rotations are used to translate the aircraft horizontally. During transition, flightpath and longitudinal acceleration are controlled through a combination of thrust modulation, deflection of the core flow, and diversion of fan air from the ejector to the aft nozzle. Engine sizing allows approximately 6% thrust margin at the maximum vertical takeoff weight. A more complete discussion of this concept is provided in Ref. 36.

The other fighter concept to be discussed in this section is based on the tandem-fan propulsion arrangement described in Ref. 37 and shown in Fig. 32. During hover, this concept produces pitch control by differential modulation of thrust between the forward fan and rear fan and core exhaust using variable inlet guide vanes at the fore and aft fans. Yaw control is produced by differential deflection of the exit flaps at the front nozzle and the deflector vanes in the aft nozzle. Height control is achieved through thrust modulation. A demand-bleed reaction-control system feeds valves at the wing tips which exhaust up and down for roll control. In conventional flight, pitch control is produced by a blend of canard and elevons, and a blend of elevons, fore and aft ventral fins, and the vertical fin may be used to generate roll and yaw moments as well as side forces. During transition, thrust modulation and thrust deflection through the forward fan and the aft core and fan exits provide control of flightpath and longitudinal acceleration. At the preliminary design stage, single-axis control powers in hover are marginally satisfactory by MIL specification standards. The thrust margin for maximum vertical takeoff weights is 17%.

Other single-engine fighter concepts noted in Nelms' paper (Ref. 34) may employ different propulsion system arrangements than have been discussed here. The remote augmented lift system shown in Fig. 33 is one that may afford some of the longitudinal control flexibility in hover that was shown for the deflected thrust with fan stream burning and the tandem fan. However, other characteristics of aircraft designs associated with this propulsion system are likely to include those of bleed reaction control discussed previously. They will not be dwelt upon further at this point.

4.2 Subsonic Multimission Configurations

During the U.S. Navy Type A V/STOL concept definition phase, several lift/cruise fan designs were presented for consideration. An example of one of these configurations is provided in Fig. 34. Both gas-coupled and shaft-coupled versions of twin-engine, three-fan aircraft were defined that made use of differential and vectored thrust from each of the fans to produce pitch, roll, and yaw control moments in hover. Symmetric deflection of the fan thrust fore and aft or to either side could be used to generate longitudinal and lateral forces for horizontal translation. Collective control of thrust provided height control. Either variable fan pitch or variable-inlet guide vanes were used to permit rapid modulation of thrust for these control purposes. For transition, the combination of thrust modulation and deflection from all of the fans was used for climb, descent, and acceleration. Control authorities for V/STOL operations were designed to the AGARD and MIL specifications. A description of a typical control design for this configuration is given in Ref. 38.

Another of the lift/cruise fan designs that has attracted considerable attention recently is the twin-tilt-nacelle aircraft. Its control arrangement is presented in Fig. 35 and is distinguished by a set of control vanes located in the engine exhaust flow. These vanes are used to produce pitch, roll, and yaw moments as illustrated in the figure. In generating pitch and roll moments, the vanes also produce forces that would translate the aircraft in the opposite direction intended by the pitch or roll rotation. To compensate for this undesirable characteristic, nacelle tilt and differential thrust modulation with variable-inlet guide vanes act to permit independent control of these forces and moments. Wind tunnel tests (Ref. 39) indicate that the vanes have sufficient effectiveness for trim and maneuvering during hover and transition. Ground-based simulations are being conducted to refine the control design and to confirm the effectiveness of the pitch and roll control blending described above (Ref. 40).

5. BASIC AIRCRAFT STABILITY AND CONTROL

With an understanding of the control authority necessary to accomplish maneuvers associated with V/STOL operations, attention can be given to the influence of basic aircraft stability and control on the pilot's ability to perform specific flight tasks. The low inherent static and dynamic stability at low airspeed, control cross-coupling, and sensitivity to disturbances are all significant influences on the precision of control that the pilot can achieve and the effort that must be devoted to control undesired responses due to poor stability, unwanted coupling, and external disturbances. These characteristics are reviewed in this section as are specific control requirements for height and translational velocity control in hover, and flightpath and airspeed control in transition. Before these characteristics are discussed, it is useful to review the contribution of lift and drag to aircraft controllability at low airspeed. The influence of lift and drag on performance is primary; however, it is also important to appreciate their significance to stability and control at low speed.

5.1 Influence of Lift and Drag on Low-Speed Control

The relationship of steady-state flightpath and airspeed to the lift-drag polar of an aircraft is well understood. Figure 36 provides an illustration of the mapping of a polar for a representative jet V/STOL aircraft into the flightpath-airspeed plane that is appropriate for operationally assessing performance and control. The polars are functions of angle of attack and the equivalent jet velocity ratio for a thrust vector deflection of 55^{o}. Flightpath-airspeed curves at the right of the figure are shown for a representative range of thrust settings and have lines of constant-pitch attitude superimposed. From the path-speed plot, it is possible to determine some of the factors of importance to precision control during the low-speed transition. For example, once the operating flight condition is located, the local gradients of flightpath and airspeed for variations in thrust and attitude control will determine the appropriate control technique that the pilot must use and will establish the steady-state control coupling at this condition. The variation of flightpath angle with airspeed at constant rpm is an indication of whether the aircraft is operating on the front or backside of the drag curve (or thrust or power required curve). Negative gradients represent frontside and positive gradients denote backside conditions. This characteristic has a bearing on whether thrust (rpm) or attitude will be the primary flightpath control. Typically, thrust is used as the primary path control for backside operations whereas attitude is frequently used to control flightpath on the frontside. The delineation between these regions occurs at the peak of the path-speed curve; however, the transition between control techniques is also dependent to a great extent on dynamic response characteristics of the two controls. Gradients of flightpath and airspeed with their respective controls establishes control sensitivity. Cross-coupling is represented by the gradient of either path or speed with the opposite controller. For example, the variation of speed with thrust at constant attitude defines speed cross-coupling when thrust is the primary flightpath control. The cross-coupling illustrated in the figure is conventional and is not objectionable to pilots. Coupling of the opposite sense (speed decrease for an increase in thrust) is of concern for low speed operations and generally leads to poor flying qualities (Refs. 24, 41, and 42).

Influences of lift and drag on flightpath and airspeed dynamic response are indicated in Fig. 37. Characteristics of interest are the initial flightpath time response, the relationship of steady-state to short-term path response to thrust, and the variation of airspeed with flightpath response to thrust. Initial flightpath response is related to the control sensitivity of normal acceleration to thrust and the heave damping that is determined by the incremental normal acceleration due to change in angle of attack. Relation of long-term to short-term flightpath response is defined by flightpath overshoot ratio. As the diagram at the right of the figure indicates, this overshoot is aggravated by deflection of the thrust vector beyond angles of $70\text{-}75^{o}$. A summary of flight and simulation data in Ref. 42 suggests that overshoot ratios should not exceed 2.5 to maintain at least adequate flying qualities (Level 2) for performing a precision instrument approach. Coupling of speed with flightpath response is also sensitive to thrust deflection angle, and changes from a conventional (favorable) to an adverse sense when thrust deflection exceeds the ratio expressed in the relationship at the bottom of the figure. This ratio is a function of lift curve slope, speed, wing loading, and induced drag. The thrust deflection angle for the approach can be chosen considering these interrelationships to minimize coupling of speed to flightpath.

In hover, the influence of lift-drag aerodynamics on controllability becomes more subdued for a high-density V/STOL configuration; these aerodynamics are also influenced to a great extent by propulsion-induced flows. Although it is possible to see some effect on the dynamics of translational motions attributed to aerodynamic forces, the time constants of the translational aerodynamic damping in the respective axes are generally too long to be acceptable for control of height or horizontal position. Illustrations of these dynamic response relationships to the thrust and attitude controls in Fig. 38 indicate the disparity in time between the propulsion and attitude response and the translational motions they are intended to command.

From these few examples, it is possible to appreciate the effect that propulsion-induced aerodynamics, or the lack thereof, have on V/STOL control. They are an indication of the extent to which the aircraft's flying qualities are determined by performance design for V/STOL operation.

5.2 Stability at Hover and Low Speed

To consider stability of the aircraft in hover, it is helpful to review an example of the hover equations of motion and some typical control response relationships that may be derived from them. An example is presented in Fig. 39 for the longitudinal motions of the aircraft. These are in the form of linear differential equations for the axial, vertical, and pitch rotational degrees of freedom and assume small perturbation motions that are decoupled from the lateral and directional motions by virtue of symmetry and uncoupled aerodynamics. Aerodynamic and propulsion-induced forces and moments are included that provide translational and angular velocity damping and pitching moment due to longitudinal translational velocity. Control inputs from thrust and pitch controls provide vertical force and pitching moment and are decoupled from the rest of the axes. In fact, vertical response is entirely decoupled from the pitch and axial motion of the aircraft in this example.

These equations yield characteristic roots that consist of a third-order set that represents the coupled pitch and axial velocity motions, and an uncoupled aperiodic mode that describes the vertical velocity response.

The third-order set typically factors into an aperiodic root and a complex pair, of roots, the latter of which may or may not be stable. The two aperiodic roots generally are stable, although they may have long time constants as a consequence of low axial and vertical velocity damping. Control response relationships are shown at the bottom left of the figure. When appropriate cancelling of numerator and denominator factors is done, it may be seen that height control is second order, pitch attitude control is third order and axial position control is fourth order.

The significance of the order of response to the controls may be more evident if the simplified example at the right of the figure, which neglects aerodynamics entirely, is considered. When the pilot's pitch control applies a pure moment as shown here, the eventual pitch attitude change occurs solely as a result of two integrations of the control input. The axial degree of freedom is still coupled to pitch and, similarly, in the absence of aerodynamic forces, change in axial position is a result of two integrations of the change in pitch attitude. Hence, the fourth-order relationship of the pitch control to axial position means that the pilot must control the intended response of the aircraft through four integrations. In addition, height control must be accomplished through two integrations of the thrust controller. Even if the simplifying assumption is not taken and aerodynamic contributions are included, the resulting stabilizing forces and moments are generally so weak in hover that the pilot observes the control response to be the same as if the aerodynamic effects were neglected.

The significance of control through an integration is that the pilot must anticipate the time to apply and remove the control input to achieve the intended response. A considerable body of literature has shown that a human controller can easily operate through one integration; the response to control application appears as a rate of motion which may be stopped at the desired value when the control input is removed. Little mental or physical effort is required to accomplish this control task. For each subsequent integration, the control effort increases substantially. Figure 40, inspired by a similar example from Ref. 43, provides an example of the control activity the pilot must expend to accomplish a change in position with control characteristics typical of early V/STOL aircraft. Eight control inputs and reversals are required to initiate and establish the change in aircraft position for the situation in which the pilot's control commands pitch angular acceleration. If the control commanded pitch rate instead, the number of control applications and reversals would be halved. For an attitude command, only two inputs and reversals would be required. If the pilot were provided the luxury of translational rate command (returning to the simple rate command example), a single input and reversal would accomplish the task. Hopefully, this example provides an indication of the difficulty a pilot encounters in controlling and stabilizing a hovering aircraft. It should also illustrate the reduction in effort the pilot expends for this control task for some of the higher levels of control augmentation such as attitude and translational rate control. That subject will be covered in more detail in a later section of the paper.

The conclusion should not be drawn that it is impossible to hover an aircraft that has little or no inherent aerodynamic stability or damping. As noted in Ref. 1, numerous aircraft were flown with only inherent rate damping. As shown at the left of Fig. 41, the MIL specification (Ref. 3) allows a slight dynamic instability at low frequency for Level 1 flying qualities in visual flight conditions and accepts exponential divergences of time to double amplitude greater than 12 sec for Level 2 VFR. For instrument operations, Level 2 requirements are equivalent to Level 1 for VFR. It is possible for a well trained pilot to hover an unstable aircraft when full visual and motion cues are available, although considerable effort may be expended in the process. However, as visual cues degrade and when external disturbances are imposed on the aircraft, the benefits of good stability and control response are appreciated. Many of the results on which this specification is based were obtained in fully visual flight in calm air and with a great deal of freedom to maneuver the aircraft. They do not reflect the more challenging operational requirements imposed by a shipboard environment.

Basic static and dynamic stability that may characterize a number of fixed-wing V/STOL configurations is illustrated at the right of Fig. 41. The aircraft's characteristic roots are stable when axial and angular velocity damping are positive and pitching moments due to forward speed (an inlet momentum contribution) are neglected. Increasingly positive pitching moment with forward speed destabilizes the aircraft and may

eventually lead to a low-frequency oscillatory instability of the type restricted by the MIL specification at the left of the figure. As Ref. 8 indicates, the AV-8A dynamic stability at low airspeed does not meet Level 2 flying qualities requirements of the MIL specification because of a rapid pitch divergence. While these characteristics were considered to be adequate for visual flight, they are inadequate for operation in poor visibility at low speed or for operation aboard ship in strong winds and heavy seas (Refs. 13 and 44). Because of low dynamic pressures and the dominance of propulsion-induced flows at low speed, it is unlikely that the basic airframe can be endowed with sufficient inherent stability to provide precision flying qualities in hover and low speed. In most cases, the stability augmentation system must be used to achieve the desired stability for precise control in this portion of the flight envelope.

5.3 Cross-Coupling

Coupling of response to the pilot's controls that produces undesired motion of the aircraft is detrimental to flying qualities for precision tasks. Coupling of this nature may occur as a consequence of aerodynamic characteristics, control effector arrangement, propulsion system geometry, or gyroscopic effects. An example of aerodynamic influence on the coupling of flightpath and airspeed response was cited previously in this section. Other examples are shown in Fig. 42 for hover and transition, and are taken from simulation time histories of the AV-8A with its basic stability augmentation system operating. At the left of the figure, the response to a step increment in rpm in hover shows the coupling into the pitch axis that arises from pitching moments due to thrust. The same sort of influence can be seen in the response to a step change in nozzle during transition. While this control input had the intended effect on airspeed response, both pitch attitude and flightpath angle were also changed to a substantial extent. At the right of the figure, the familiar coupling of roll to yaw that requires a large portion of the lateral control to hold bank angle for a steady heading during moderate sideslips is noted. These are three frequently encountered examples of cross-coupling that force the pilot to direct attention away from the primary control task to counter unintended responses in other axes. When they are of sufficient magnitude, such as the roll-yaw example, they degrade flying qualities and may leave the aircraft unacceptable for operation other than day, VFR, calm air conditions. Except for coupling due to lateral control yawing moments, the AGARD and MIL criteria are not particularly definitive on this subject. Suffice to say, the designer should attempt to minimize undesired coupling in the basic configuration. When that is not possible, control augmentation must be used to achieve satisfactory characteristics.

5.4 External Disturbances

External disturbances imposed by winds and turbulent air wakes, ground effect, and ingestion of hot propulsion gases are another source of unwanted response that affect precision control tasks. The example provided in Section 3 of control response in the turbulent wake behind a ship's superstructure represents a situation in which it is difficult to maintain the desired hover control precision. For precision approaches at slow speed, wind gradients may be a cause of large and rapid excursions in flightpath (Refs. 42 and 45). Figure 43 presents the results of a simple analysis to compare the flightpath and speed response of conventional and powered-lift STOL aircraft when encountering wind shear. For this example, pitch attitude is assumed to be constant. As indicated in the equation at the top of the figure (from Ref. 42), flightpath response is composed of an increment required to counter the inertial acceleration due to the shear and an increment associated with the change in lift-drag ratio with the variation in airspeed. For a typical STOL aircraft that operates on the backside of the drag curve, the magnitude of the flightpath perturbation for a given wind gradient is two-thirds larger than for its conventional counterpart. Furthermore, the disturbance is fully developed for the STOL aircraft in half the time associated with the CTOL aircraft. The comparison is intended to emphasize the concern for low speed operation in these wind environments under circumstances in which the pilot may have insufficient information concerning the aircraft's situation during the approach, or may be distracted by secondary tasks that prevent prompt control action to counter this disturbance. There are few choices in the basic airframe design for reducing any of these disturbances imposed by air wakes, gusts, and wind shears. If the control augmentation system is incapable of suppressing these disturbances, operational restrictions must be based on the severity of the environment.

Forces and moments imposed on the airframe by propulsion-induced flows in proximity to the ground create considerable difficulty for control in hover during landing. The report by Henderson, Clark, and Walters (Ref. 46) provides a concise description of the contributions to these disturbances, including configuration influences on suck-down or buoyancy and on destabilizing pitch and roll moments. The arrangement of the jet exhausts and the contouring of the lower surface of the airframe are particularly important. Because of the influence of height above the deck, jet velocity, and pitching and rolling motions of the aircraft relative to the landing pad, it is possible for the pilot's control application to couple with the upsetting forces and moments and to seriously degrade controllability. For this reason, it is important for the designer to give consideration in the definition of features of the configuration that help to minimize unfavorable interactions.

5.5 Hover Control

After reviewing the character of stability of motion in hover and low speed and the nature of uncommanded motions of the aircraft, the features of the primary, or intended, response to the pilot's controls may now be considered. The example time response of thrust and vertical velocity to the pilot's power lever is repeated from Fig. 38 at the right of Fig. 44. This response is characterized by the initial lag in thrust response to the power lever input, and by the time lag in vertical velocity response to thrust. Thrust response lag is inherent in the acceleration and dynamic response of the fan and core flow of the propulsion system and its associated force generators. For a powered-lift aircraft, basic design philosophy dictates that dynamic response of forces and moments produced by the propulsion unit meet the same requirements as primary flight control. For height control, the MIL specification (Ref. 3) indicates that the force producer respond with an effective first-order time constant of 0.3 sec to achieve Level 1 flying qualities. This requirement, and that for Level 2, is shown at the left of the figure. AGARD criteria suggest that this time constant should be less than 0.5 sec. The subsequent vertical velocity time constant of the airframe is dominated by vertical velocity damping. An approximate representation of this damping shows the influence of the normal force coefficient, the dynamic pressure of the local flow, and the aircraft loading condition. A crude approximation of this term would indicate that it is inversely proportional to the square root of disk loading. For compact aircraft such as jet fighters, this level of damping converts to time constants of 10-30 sec. Recall from Fig. 19 that levels of damping of $-0.3\ sec^{-1}$ or greater were recommended. That level converts to time constants of approximately 3 sec or less as is shown in Fig. 44. The lines of time to reach 50% of the maximum vertical velocity that are superimposed on the plot at the left show that the combination of the thrust and vertical velocity time constant criteria yield vertical velocity rise times between 2.5 and 3 sec. These values are in reasonable agreement with the 3-sec rise time recommended by the powered-lift STOL airworthiness criteria (Ref. 29) as minimally acceptable for precision instrument approach path control. It would appear unlikely that this criteria could be met by most fixed-wing V/STOL aircraft considering their high disk loadings. Thus, this class of aircraft must rely on height control augmentation to achieve acceptable response for precision height control. Additional criteria for thrust time response for height control of aircraft with lift-cruise propulsion systems are given in Ref. 47.

Translational velocity control for hover positioning may be accomplished either through control of aircraft attitude, as discussed at length at the beginning of this section, or may be performed by deflecting the thrust vector about the vertical. Given the lack of stability of the basic airframe for hover control, this is a difficult task when it is performed using attitude control. Even if some level of stability is provided by an attitude rate or attitude command control, the low axial velocity damping means that translational velocity time constants will be long and that the pilot will have difficulty in establishing steady translational rates. This response characteristic is seen at the left of Fig. 45. If the translation is to be performed by thrust vector control, the response is still governed by the axial velocity damping and associated time constant. The advantage of this mode of control is that the dynamics of attitude control are circumvented. However, any pitching moment changes associated with thrust vector angle will disturb the aircraft's attitude and cause the pilot to devote some attention to attitude control. Requirements for translational velocity control do not exist in either the AGARD criteria or the MIL specification. Tentative criteria have recently been developed for this mode of control and will be reviewed in a following section on control augmentation.

5.6 Transition Control

The major concerns for control during transition relate to changing the aircraft configuration and the precision control of flightpath and airspeed within this flight regime. The issue of flightpath and longitudinal acceleration control authority during transition, covered previously in this paper, determines the ability to achieve a range of operating conditions or to transit this part of the flight envelope. The acceptability of control during transition is dependent, in part, on the number of controls the pilot must manipulate and the difficulty of procedures required to change the aircraft control configuration from one that is appropriate for wing-borne flight to one that is suitable for the powered-lift regime (Ref. 48). The transition envelope at the left of Fig. 46 illustrates the selection of thrust setting and thrust vector angle to establish a descending approach condition. To perform this control task for the Harrier, the pilot uses the throttle and nozzle control levers on the throttle quadrant shown in Fig. 47. The manipulation of two controls to accomplish this configuration selection is acceptable so long as the transition profile is not demanding. If the profile is complicated, such as a continuous deceleration on a precise flightpath under instrument conditions, then the continuous and precise manipulation of these two controllers could become an objectionable task for the pilot. If, as for some designs, the pilot has redundant controls for flaps, thrust vector angle, lift and cruise engine thrust, the complexity of the control task becomes insurmountable for all except the most simple transition profiles. Thus a tradeoff is made between operational demands and control complexity.

As shown in Fig. 46, the control of flightpath and airspeed for the example shown is partioned for thrust and pitch attitude. With attitude held constant, flightpath responds to thrust with the characteristics described in Fig. 37. When thrust is fixed, airspeed control with attitude is accomplished as shown at the right of Fig. 46. For airspeed control, the steady speed change per degree of attitude is the significant feature. Flightpath will also respond to the attitude change with a short-term response determined

by the aircraft's normal acceleration sensitivity to angle of attack. The long-term response as shown is indicative of operation on the backside of the drag curve, and the reversal between short-term and steady-state response is a primary reason pitch attitude is not used to control flightpath under these conditions. As discussed in Section 5.1, these flightpath and airspeed control characteristics are established primarily by the propulsion-induced flow effects on lift and drag in low-speed flight. Assuming that there is little flexibility for altering the lift and drag of the basic configuration for control purposes, it remains to use the control system to modulate lift and drag so as to produce response consistent with good flying qualities.

6. STABILITY AND CONTROL AUGMENTATION SYSTEMS

As noted throughout the previous section, deficiencies in the low-speed flying qualities of V/STOL aircraft require the use of the flight-control system to improve the precision of control, reduce the effort the pilot must devote to control of the aircraft during hover and transition, and desensitize the aircraft to external disturbances. Over the past 15 to 20 years, several experimental V/STOL aircraft have used stability and control augmentation systems of varying degrees of complexity and have demonstrated their benefits in flight. The Harrier prototype P-1127 started with a simple rate-damping system which was eliminated from the Kestrel development prototype. However, the poor flying qualities of the Kestrel for precision instrument flight and for operations aboard ship led to the installation of an improved system in the first operational versions of the aircraft (GR MK 1 and AV-8A). Substantial improvements to that system have been incorporated in the Sea Harrier and the AV-8B (Refs. 9 and 22). The AGARD advisory report on displays for approach and landing of V/STOL aircraft (Ref 49) summarized the anticipated requirements for stability and control augmentation and the necessity for an integrated control and cockpit display design approach for aircraft of this class to operate in adverse weather. Figure 48, taken from Ref. 49, illustrates the importance of the interaction of augmented controls and displays with the aircraft's flying qualities for precision instrument flight tasks. Since that report was published in 1972, several research programs have been conducted that have helped to quantify the contribution of control augmentation and displays to flying qualities for these precision operations. This section provides a review of this research and the operational experience obtained over that period.

6.1 Conventional Stability Augmentation

To alleviate some of the deficiencies in flying qualities of the basic aircraft, stability augmentation concepts have been adapted from conventional military fighter aircraft. Pitch, roll, and yaw rate dampers have been used for this purpose, and turn coordination logic has also been included in the yaw axis control. Control-force-feel systems have been used to produce effective "control free" stability at low speed and in transonic flight.

A simple illustration of the characteristics of a rate-damping stability augmentor is provided in Fig. 49. The example shown is for a roll damper that in concept consists of feedback of roll rate from a rate gyro, and feed forward of control position or force from an appropriate control sensor. Although an actual system would incorporate additional filters and gain scheduling, the diagram at the top left of the figure captures the essential design features of the system. The roll equation of motion derived from this simplified diagram is shown below. Any angular rate damping or control sensitivity inherent in the airframe would be included in the appropriate constants in this equation. A time history of roll rate response to a step control input shows that the initial response is proportional to control sensitivity, the response time constant is inversely proportional to the inherent and artificially supplied damping, and the steady- state response depends on the ratio of control sensitivity to damping constants. These characteristics are sufficient to define design criteria for a rate damping augmentation system, and both the AGARD criteria and MIL specifications (Refs. 2 and 3) are shown as examples at the right of the figure. AGARD notes the desired damping and control sensitivity, and the MIL value is expressed in terms of bank angle achieved in 1 sec in response to an abrupt 1-in. step input. With the exception of the X-14A example at the lowest value of damping, all the other aircraft were evaluated to have Level 1 flying qualities for visual flight operations. The lowest damping evaluated for the X-14A was considered to be only marginally adequate even though it does fall within the MIL Level 1 boundary. Thus, a minimum amount of damping, though perhaps not as much as the AGARD criteria suggest, would be appropriate. The recent recommendation of Hoh (Ref. 20) and Clark (Ref. 50) for effective damping of 1.5 sec^{-1} would be about the desired value for Level 1.

For a demanding task such as a precision decelerating approach under instrument conditions, simple rate-damping augmentation will not be sufficient to provide fully satisfactory flying qualities. The diagram at the bottom of Fig. 49 summarizes a range of pilot evaluations from Lebacqz and Aiken's flight experiment on the Calspan X-22A (ref. 10) and the moving-base simulation experiments of Merrick and Gerdes (Ref. 51) and Stapleford, et al. (Ref. 52). These results show that only Level 2 flying qualities can be achieved at best, and that degradation to Level 3 occurs in moderate turbulence. Flight experience with the Do-31 (Ref. 11), the Kestrel (Ref. 44), and the XV-5B (Ref. 53) agrees with these findings. To achieve further improvement in precision approach and hover flying qualities, all these results indicate that some form of attitude stabilization is required.

Another form of stability augmentation that has frequently been applied to V/STOL aircraft is the yaw damper-turn coordinator. The intended benefits of this system were improved dutch roll mode damping during transition, elimination of yaw-roll coupling in the form of adverse sideslip caused by lateral control yawing moments, and yaw rate command and stability in hover. The system concept is shown in the diagram at the right of Fig. 50, and consists of feedback to the directional control (rudder or yaw reaction control valve) of lateral control position, roll and yaw rates, bank angle, and lateral acceleration. Criteria for suppressing sideslip excursions during turn entry are presented in terms of the relative magnitude of sideslip to roll excursions and the phasing of the sideslip transient (Ref. 3). The criteria are more tolerant when sideslip phasing is such that conventional coordination can be performed with the rudder. These criteria are made considerably more stringent in the MIL specification when large roll-yaw coupling exists in the dutch roll mode and are reduced by a factor of 5 below the level shown here. The time history at the bottom of the figure defines the sideslip and bank angle excursions upon which the criteria are based. The effect of the yaw stability augmentation in suppressing the yaw-roll coupling and in damping the dutch roll oscillation is apparent.

This form of yaw axis control augmentation has been very effective in improving lateral-directional flying qualities for precision flight. For demanding hover control tasks, the inclusion of a heading hold feature in combination with the yaw rate command has been investigated extensively (Refs. 10, 51, and 52). This type of system can provide Level 1 flying qualities in the most demanding operational environment in hover; however, the heading hold feature conflicts with the need to minimize sideslip during transitions. Therefore, if heading hold is to be provided in hover, it must be phased out as the aircraft enters the transition. This conversion in control mode is generally accomplished at an airspeed of approximately 30 knots.

It was noted previously that the aircraft's artificial force feel system is used to impart artificial "control free" stability to the aircraft during low-speed flight. Another contribution of this system is to compensate for large trim changes during transition. Most of the stability augmentation systems designed for V/STOL aircraft to date have been of limited control authority. These systems are not capable of providing large trim control requirements; thus to avoid saturating the stability augmenter with these demands, the detent of the force feel system may be repositioned to produce the trim control position desired.

6.2 Advanced Stabilization and Command Augmentation

Investigations of the contribution of advanced stabilization and command augmentation concepts to the improvement of flying qualities for precision hover and transition operations have been carried out over the past 10 years in a number of ground-based and flight research facilities. During this time, the predominant moving-based simulation experiments have been conducted using the three, six-degree-of-freedom simulators at NASA Ames Research Center shown in Fig. 51. The open cab facility at the center of the picture was initially used in Greif's hover control experiments (Ref. 18) and has been employed over the years for similar research on V/STOL control concepts. This simulator has a motion envelope defined by an 18-ft cube, and, within those constraints, it is maneuvered without distortion by motion washout. When flown open cockpit, visual cues have the highest degree of realism.

The Flight Simulator for Advanced Aircraft (FSAA) was used to explore the flying qualities and flight control systems of a variety of V/STOL configurations starting in the early 1970s. Until 1980, it was also the facility from which Merrick's data on advanced control and display concepts for V/STOL shipboard operations (Refs. 51 and 54) were obtained. Stapleford (Ref. 52) and Donley (Ref. 55) investigated criteria for the design of control augmentation systems for operation from small ships in adverse weather in this simulator. It was also used extensively for research on powered-lift STOL transport flying qualities by Franklin and Innis (Ref. 41) and Hoh et al. (Ref. 56) and research on airworthiness criteria by Scott and Hynes (Ref. 29) and Heffley et al. (Ref. 57). The distinguishing features of this simulator are its large lateral motion envelope and a fully enclosed cockpit with a dual-window visual scene produced by a camera-model board system and displayed on side-by-side color television monitors. Complete representation of hover and transition operation is provided by this facility.

The Vertical Motion Simulator (VMS) shown at the right of Fig. 51 has been used since 1981 for all of NASA's V/STOL simulation experiments. It has very large vertical and lateral motion freedom (60x40 ft) and accommodates a cockpit with a four-window, computer-generated visual scene. An example of a scene from the deck of an Amphibious Assault Ship (LHA) is shown at the bottom of the figure. Recent experiments by Farris and Merrick (Ref. 58) on advanced V/STOL controls and evaluations of the flying qualities of the tilt nacelle V/STOL configuration (Ref. 40) were all carried out on the VMS.

Over this same period of time, several flight research programs in the U.S. and U.K. have complemented and extended the ground-based research. The most extensive of the V/STOL flight programs was performed by Lebacqz, Aiken, Radford, and Andrisani with the variable stability X-22A at Calspan through the mid-to-late 1970s (Refs. 10, 59, and 60). This aircraft has the capability to alter its pitch, roll, yaw, and heave response over a wide range of characteristics and thereby to generate data over a range of flying qualities from Level 1 to Level 3. The aircraft also employs a programmable head-up display that is used to provide situation and command information that is compatible with the control concept under evaluation.

The NASA/Army X-14B at NASA Ames was used by Corliss et al. (Ref. 17) as a variable stability facility to evaluate in-flight hover control configurations that had been investigated earlier on NASA's Six-Degree-of-Freedom simulator. The X-14B provided the capability to alter the pitch, roll, and yaw response of the basic aircraft over a broad range of characteristics. Because the aircraft retained its open cockpit design, it was used exclusively for hover control research.

The NASA/Army CH-47B helicopter was involved in control and display research that is relevant to fixed-wing V/STOL control technology. This work was carried out by Kelly, Niessen, and Garren at NASA Langley (Refs. 61 and 62) to assess control and display requirements for manual and automatic instrument decelerating approaches. The aircraft has variable-stability capability in the pitch, roll, yaw, and heave axes, with sufficient control authority to represent a wide range of control configurations. It also provided a head-down electronic display for situation and command information.

A two-seat research version of the T MK 4 Harrier has been used by the staff at RAE-Bedford for V/STOL controls and displays research since the mid-1970s. At various times it has incorporated pitch attitude stabilization and integrated control for the nozzles in hover, along with a programmable head-up display for changing symbology and display formats. Research has been devoted to supporting evolutionary development of control augmentation and head-down displays for Sea Harrier and the recent GR MK5 aircraft.

Powered-lift STOL aircraft flight control research has been conducted at NASA Ames using the Augmentor Wing Research Aircraft. Pitch, roll, yaw, heave, and axial forces and moments could be altered on that aircraft to permit the evaluation of flying qualities and flight control characteristics. Programmable head-down electronic dislays were available to present situation and command information to the pilot. Flying qualities criteria and flight control concept evaluation and design guidelines were developed by Franklin (Refs. 42 and 63) and Hindson (Ref. 64) from these flight experiments.

From this collection of simulators and research aircraft, data have been generated on advanced control augmentation concepts. In the hierarchy of control sophistication, pitch and roll attitude command systems are the simplest of the concepts to be considered. Figure 52 provides an illustration of the characteristics of a roll attitude command system, as an extension of the rate command example of Fig. 49. The additional feature that has been included is the feedback of roll attitude from the vertical gyro. This system is described by the second-order equation of motion at the left of the figure and by the time response at the bottom. Inherent and artificial angular rate damping determine the subsidence of the exponential envelope of the response, and the attitude feedback establishes the speed of the initial response and the period of any apparent oscillatory motion. The steady-state attitude response to a control input depends on the ratio of the control sensitivity to attitude feedback constants. These characteristics are the basis for design criteria proposed in Ref. 3 and by Hoh and Ashkenas (Ref. 20) and Clark (Ref. 50). Level 1 flying qualities criteria from the latter two sources are given by the boundaries on the plot at the right of Fig. 52. Evaluations of the flying qualities of the four aircraft on the plot indicated that the Level 1 attitude control capability was obtained for all in hover. The X-22A and Do-31 were both evaluated during instrument approaches, and attitude stabilization resulted in good attitude control for both aircraft. The overall flying qualities of the Do-31 for a constant-speed approach were not considered to be satisfactory because of poor flightpath control characteristics and the use of raw data displays. The X-22A was given satisfactory ratings for the decelerating approach when a well integrated display was also provided to the pilot. The diagram at the bottom of Fig. 52 presents data collected from the X-22A (Ref. 10) and from simulator experiments (Refs. 51 and 52) that indicate that it is possible to achieve Level 1 flying qualities for the decelerating approach up to moderate levels of turbulence. As turbulence intensity increases further, flying qualities degrade to a marginal Level 2. Recent experience by RAE-Bedford with their research Harrier, and by McDonnell-Douglas/Sperry with the AV-8B prototypes, reaffirm the favorable contribution of attitude command. Again, it should be understood that the ability to achieve the most favorable ratings is dependent upon the proper display of situation and command information to the pilot. A poor choice of display design can negate the improvements in flying qualities for precision instrument operation provided by attitude command systems.

The most complex control augmentation systems to be evaluated to date are those that provide translational velocity command. This class of controls includes horizontal (axial and lateral) and vertical velocity systems. Characteristics of vertical velocity command were covered in the discussion of hover height control dynamics for Fig. 44. Axial and lateral velocity command systems that are reviewed in this section produce translational rates either through changes in body attitude or through deflection of the thrust vector. Figure 53 includes schematic descriptions of the two types of velocity command. The attitude-control-based concept adds an inertial or air-mass-derived velocity feedback to the structure of the attitude command system of Fig. 52. The thrust-vector controller is of the rate command type and uses the velocity feedback in combination with appropriate control gearing of the thrust vector input. The essential response characteristics of either system are described by the first-order equation of motion at the left of the figure. To represent velocity response to attitude in this fashion, it is necessary for the attitude control to be designed based on the attitude command criteria of Fig. 52. The time response shown at the bottom of the figure is characterized by the initial response gradient that is proportional to control sensitivity gain, the time constant that is inversely proportional to the rate feedback, and the steady-state response that is defined by the ratio of the control to the rate feedback gain. Given these essential

features that describe the system response, Radford and Andrisani (Ref. 60) and Clark (Ref. 50) have proposed criteria for Level 1 and 2 flying qualities based on flight data from the X-22A. The analyses of Hoh and Ashkenas (Ref. 20) that included data from two major simulation experiments (Refs. 65 and 66) and from helicopter flight tests (Refs. 67 and 68) also are a source of criteria. This body of results is derived from various land-based precision hover tests of these systems. Simulation experiments by Merrick (Refs. 51 and 54) and Stapleford (Ref. 52) for shipboard landings on a DD-963-class vessel are summarized at the left of Fig. 53. These results indicate that it is feasible to achieve Level 1 flying qualities for the most demanding precision V/STOL operations. Marginal Level 1 flying qualities were maintained in conditions equivalent to sea state 4 and in an air wake environment associated with 25 knots of wind over the deck. Subsequent experiments by Donley (Ref. 55) suggest that a hover position hold feature be included in these systems to compensate for imperfect inertial velocity information, considering the precision required for landing on this size ship. RAE-Bedford has had experience with a simple nozzle controller integrated with the throttle lever on their Harrier research aircraft. This device provides an easy means of adjusting both thrust magnitude and deflection in the hover. Although it does not provide increased vertical or axial velocity damping, it has reduced the pilot's effort for hover control. It has been adopted in the design of the Sea Harrier power management system. To conclude this discussion, it should again be emphasized that a poor choice of cockpit display format or information can reduce the potential benefits of the contol augmentation systems.

To accomplish these higher levels of control augmentation on a V/STOL configuration, some degree of integration of the flight and propulsion control systems is required. In its simplest form, this integration could be provided by a servo link to the power and thrust vector control levers. Even in this simple example, the dynamic response characteristics of the fan and core elements and the thrust deflection control must be taken into consideration in the flight control system design. In turn, the propulsion designer must consider the likely force and moment control demands and treat that aspect of the propulsion system as a primary flight control element as regards rates and accuracy of response. To achieve the required dynamic response for forces and moments from some of the advanced V/STOL concepts reviewed in Section 4 and Ref. 34, it will be necessary to conduct a more integrated design of the flight and propulsion control systems than has been done before. Digital control technology makes it feasible to undertake such a design, in which the integration to comparable degree of hydro- and electromechanical systems of current aircraft would have made the task impossible. The flight test of an experimental Dowty-Smiths digital fuel control on a Harrier/Pegasus in the U.K. proved to be a successful first step in this regard. In the U.S., a joint research effort between NASA Ames and Lewis Research Centers has been under way since the late 1970s to investigate flight-propulsion control integration for this class of aircraft. This work has been encouraged by earlier efforts of this type conducted by NASA and the U.S. military for conventional fighter aircraft. Initial activities involved the full envelope, nonlinear dynamic modeling of a subsonic V/STOL transport aircraft, and a turbofan propulsion system that was used for a nonpiloted simulation investigation. Fully automatic transition, approach, and shipboard landings were performed that provided data concerning precision approach and landing performance, propulsion system demands and performance, and dynamic response characteristics of the propulsion and flight control system (Ref. 69). Most recently, this effort has been directed to the detailed dynamic modeling from piloted simulation of the AV-8 Harrier airframe and Pegasus engine combination. Both models have been developed and brought to operational status for piloted evaluations on NASA's Vertical Motion Simulator, as indicated in Fig. 54. A description of the development of the Pegasus dynamic model for use in real-time digital simulation is provided in Ref. 70. This airframe-propulsion model will be used to acquire data for the assessment of gross thrust demands, internal engine state dynamic behavior, and acceleration and bleed flow demands during takeoff, transition, and landing operations. Thus the experimental capability for evaluating an integrated flight-propulsion control design has been established. It use awaits the initiation of such a design effort on the next generation of V/STOL aircraft.

7. OPERATIONAL CAPABILITY

The ultimate operational utility of future military V/STOL aircraft will be determined to a considerable extent by their ability to operate in an adverse weather and shipboard environment that is at least as demanding as that faced by conventional sea- and land-based aircraft today. Considering the experience with V/STOL aircraft stability and control design and operating characteristics that has been summarized in this paper, it can be concluded that shipboard operations of these aircraft in adverse weather will be constrained by their basic or control augmented flying qualities. Clark (Ref. 50) proposed control augmentation and cockpit display requirements for precision hover and low-speed operations based on the quality of outside visual cues. His suggestion reflects Hoh and Ashkenas' interpretation of these requirements from a large collection of simulation and flight data (Ref. 7) and is shown in Fig. 55. The outside visual cue scale was described previously in Fig. 7. For a given set of visibility conditions that can ultimately be tied to ceiling and visual range, the combination of aircraft control and display design characteristics is determined. It is assumed that each of the control and display designs is optimized. To meet fully satisfactory (Level 1) flying qualities requirements, velocity command controls may be required when visibility is degraded to any extent. In accord with the trade-off between control and display sophistication hypothesized in the AGARD Advisory Report (Ref. 49) and substantiated by several simulation and flight experiments, this demand for highly augmented control may be relieved to a certain extent by employing more sophisticated display presentations of position and velocity situation information and appropriate control commands. To restate

a point made earlier in this paper and emphasized by Farley in his AGARD presentation on display design (Ref. 71), the display of flight information to the pilot is as crucial to the successful control of the aircraft as is the basic or augmented stability and control of the airframe. Improper design or application of the display will negate good control characteristics painstakingly incorporated in the airframe design.

Harrier operational experience is in accord with Clark's proposed requirement. Current and past Harriers (GR MK 1 and 3 and AV-8A) perform their decelerating transition and vertical landing under visual flight conditions (OVC 1 or 2). Even under these conditions, the pilot's workload is high when precision deceleration and hover is required. The next generation of Harrier will have improved capability by virtue of attitude command controls, and should have Level 1 flying qualities in all but the worst visibility conditions.

With regard to the influence of the shipboard environment on operating capability, experiments on the NASA Ames FSAA are summarized in Fig. 56 to illustrate the variation in flying qualities, and hence operational acceptability, over a range of sea conditions for three control command augmentation systems. These results apply for operation aboard a DD-963-class destroyer, and thus represent possibly the most demanding of precision control tasks. To achieve fully satisfactory flying qualities even in calm seas, velocity command augmentation is necessary. Attitude command systems would provide only adequate flying qualities. In moderate seas, decoupled velocity command systems still offer marginally satisfactory flying qualities, and attitude command systems are only marginally adequate under these conditions. Even in heavy seas, the decoupled velocity controls can be expected to provide adequate controllability. Given the limited field of view of the visual display for this simulator, these operations were conducted with the pilot relying entirely on a head-up display for situation and guidance information for landing. Thus, the results effectively apply to fully instrument visibility conditions, and may be somewhat conservative for partial IMC or VMC situations. Experiments that are under way on more advanced simulation facilities at NASA and those planned for the new large motion simulator at RAE-Bedford will serve to clarify this issue. Flight results from the more modern fleet of Harriers that are about to go into service will also provide invaluable data on this challenging sea-going environment.

8. CONCLUDING REMARKS

This paper has provided a summary of the maneuver requirements for V/STOL operations and the related control authority, stability, and controllability demanded of V/STOL designs to achieve this capability. Characteristics of control augmentation systems that enhance operational capability have been reviewed. Based on the existing body of information, several major uncertainties and issues remain to be resolved.

Control authority requirements have not been established for demanding shipboard operations.

- The philosophy of basing the total control authority on the aggregate demands for trim, stabilization or disturbance suppression, and maneuvering is widely accepted in principle. However, it may not be necessary to sum the individual demands for stabilization against disturbances and for maneuvering. Instead, the most stringent of these two requirements may suffice to account for the other.

- Control authority to counter disturbances is amenable to analysis, whether the disturbance is a consequence of air wakes or turbulence, ground effect or hot gas ingestion. Maneuvers are not so easy to specify and describe analytically because of the complex control tasks associated with V/STOL missions. Thus, maneuver requirements need experimental verification. In particular, since quick stop capability can use substantial control authority, realistic requirements for this type of maneuver must be established.

- AGARD Report 577 and MIL-F-83300 pitch and roll maneuver requirements may be reasonably accurate for hover operations; however, those for yaw control seem high based on flight experience.

- The idea of describing maneuver control demands during transition in terms of control margin is an appealing alternative to specifying an absolute value for authority.

Control authority requirements place significant demands on the propulsion system.

- To relieve demands on the installed thrust of the propulsion system, it is desirable to prioritize the use of bleed air or thrust for multiaxis control demands. The order of priority should provide for roll, pitch, height, and yaw control in that sequence.

- Integration of the flight and propulsion controls may be useful in achieving an acceptable design, particularly if the integrated design permits the use of contingency thrust. The potential improvement in mission payload without the sacrifice of control authority or propulsion system reliability is worth investigating.

- The potential indicated in simulation experiments for reducing the overall maneuver and stabilization control authority through advanced control augmentation concepts that exploit the integration of flight and propulsion controls should also be established.

Significant operational benefits may be achieved with advanced control augmentation systems.

- Current indication is that rate command systems are incapable of providing satisfactory flying qualities for a precision control task aboard ship. However, it is not certain whether velocity command augmentation will be required to reduce the pilot's control effort sufficiently.

- It must be determined whether simulation results are unduly conservative and whether attitude command controls can produce at least marginally satisfactory flying.

- The sensitivity of this selection of control mode to cockpit display format and information content has been firmly established. The benefits of good stability and control augmentation design can be negated by a poor display design.

- The influence of the level of control augmentation on operational capability in adverse weather aboard ship requires flight validation. This includes understanding the effect of the visual, air wake, and ship motion environment on the pilot's assessment of a particular control concept.

Based on these major uncertainties and because of the sensitivity of future V/STOL designs to these issues, it is essential that flight validation be performed for the most significant concerns that, to date, are defined only by ground-based simulation. Further, for advanced V/STOL design concepts that appear most promising and are candidates to be carried to detailed evaluation, simulation assessments of their particular flying qualities and operational capabilities are required.

9. ACKNOWLEDGEMENTS

The authors wish to express their appreciation to Dr. J. V. Lebacqz and Mr. V. K. Merrick of NASA Ames Research Center for their suggestions on the scope and their substantive comments on the material presented in this paper. Recommendations on the topics for discussion from Mr. J. W. Clark of the U.S. Naval Air Development Center and Mr. O. P. Nicholas of the Royal Aircraft Establishment - Bedford, U.K. are also gratefully acknowledged.

REFERENCES

1. Anderson, Seth B., "Historical Overview of V/STOL Aircraft Technology." NASA TM 81280, Mar. 1981.

2. Anon., "V/STOL Handling, I - Criteria and Discussion." AGARD R-577-70, Dec. 1970.

3. Chalk, Charles R., Key, David L., Kroll, John Jr., Wasserman, Richard, and Radford, Robert C., "Background Information and User Guide for MIL-F-83300 - Military Specification-Flying Qualities of Piloted V/STOL Aircraft." Technical Report AFFDL-TR-70-88, Nov. 1971.

4. Fortenbaugh, R. L., "Mathematical Models for the Aircraft Operational Environment of DD-963 Class Ships." Vought Corp. Report 2-55800/8R-3500, Sept. 1978.

5. Brown, R. G., and Camaratta, F. S., "NAVAIRENGCEN Ship Motion Computer Program." NAEC MISC-903-8, 1978.

6. Garnett, T. S. Jr., "Investigation to Study the Aerodynamic Ship Wake Turbulence Generated by an FF 1052 Frigate." Boeing-Vertol Report D210-11140-1, Dec. 1976.

7. Hoh, Roger H., and Ashkenas, Irving L., "Effect of Reduced Visibility on VTOL Handling Quality and Display Requirements." AIAA J. Guidance Contr. vol. 4, no. 2, Mar.-Apr. 1981.

8. Lacey, T. R., "MIL-F-83300; View from an Aircraft Designer." Proceedings, Navy/NASA VSTOL Flying Qualities, Apr. 1977.

9. Anon., "YAV-8B Aerodynamic Stability and Control and Flying Qualities Report." McDonnell-Douglas Report MDC A4637, Rev. C, Jan. 1980.

10. Lebacqz, J. V., and Aiken, E. W., "A Flight Investigation of Control, Display, and Guidance Requirements for Decelerating Descending VTOL Instrument Transitions Using the X-22A Variable Stability Aircraft, Volume I: Technical Discussion and Results." Calspan Report AK-5336-F-1, Sept. 1975.

11. Holzhauser, Curt A., Morello, Samuel A., Innis, Robert C., and Patton, James M. Jr., "A Flight Evaluation of a VTOL Jet Transport Under Visual and Simulated Instrument Conditions." NASA TN D-6754, Mar. 1972.

12. Hooper. R. S., "Technology Development to Meet the Military Requirements." AGARD-CP-241, Jun. 1978.

13. Rossetti, A. M. and Iles, J. E., "Shipboard Testing of the AV-8A 'Harrier'." Proceedings, Navy/NASA VSTOL Flying Qualities, Apr. 1977.

14. Cooper, G. E., and Harper, R. P. Jr., "The Use of Pilot Rating in the Evaluation of Aircraft Handling Qualities." NASA TN D-5153, Apr. 1969.

15. Anderson, Seth B., "A Comparison of the V/STOL Handling Qualities of the VAK-191B With the Requirements of AGARD Report 577 and MIL-F-83300." NASA TP 1494, Jul. 1979.

16. Rolls, L. Stewart, and Drinkwater, Fred J. III, "A Flight Determination of the Attitude Control Power and Damping Requirements for a Visual Hovering Task in the Variable Stability and Control X-14A Research Vehicle." NASA TN D-1328, May 1962.

17. Corliss, Lloyd D., Greif, Richard K., and Gerdes, Ronald M., "An In-Flight simulation of VTOL Hover Control Concepts." AIAA Paper 77-610, Jun. 1977.

18. Greif, Richard K., Fry, Emmett B., Gerdes, Ronald M., and Gossett, Terrence D., "Effect of Stabilization on VTOL Aircraft in Hovering Flight." NASA TN D-6900, Aug. 1972.

19. Hutchins, Dale E., "Review of U. S. Navy VSTOL Handling Qualities Requirements." Proceedings, Navy/NASA VSTOL Flying Qualities, Apr. 1977.

20. Hoh, Roger H., and Ashkenas, Irving L., "Development of VTOL Flying Qualities Criteria for Low Speed and Hover." NADC-77052-30, Dec. 1979.

21. Shaw, A. W., Lindbeck, R. K., Craig, S. J., and Booth, G., "The Impact of Current V/STOL Flying Quality Control Requirements on the Propulsion System." AIAA Paper 78-924, Jul. 1978.

22. Fozard, John W., "The British Aerospace Harrier Case Study in Aircraft Design." AIAA Professional Study Series, Jul. 1978.

23. Innis, Robert C., Holzhauser, Curt A., and Quigley, Hervey C., "Airworthiness Considerations for STOL Aircraft." NASA TN D-5594, Jan. 1970.

24. Gerken, G., "USAF Flying Qualities Requirements for a STOL Transport." ASD-TR-78-13, May 1979.

25. Riccius, Rolf, and Sobotta, Werner: "VAK-191-B Experimental Program for a V/STOL Strike-Recce Aircraft." AGARD-CP-126, Apr. 1973.

26. Vomaske, R. F., Innis, R. C., Swan, B. E., and Grossmith, S. W., "A Flight Investigation of the Stability, Control, and Handling Qualities for an Augmented Jet Flap STOL Airplane." NASA TP 1254, Jun. 1978.

27. Flora, C. C., Middleton, R., and Schaer, D. K., "Quiet Short-Haul Research Aircraft Predicted Flight Characteristics." NASA CR 152203, Oct. 1979.

28. Quigley, H. C., Innis, R. C., and Holzhauser, C. A., "A Flight Investigation of the Performance, Handling Qualities, and Operational Characteristics of a Deflected Slipstream STOL Transport Airplane Having Four Interconnected Propellers." NASA TN D-2231, Mar. 1964.

29. Scott, B. C., Martin, P. W., Hynes, C. S., and Bryder, R. B., "Progress Toward Development of Civil Airworthiness Criteria for Powered-Lift Aircraft." FAA-RD-76-100 and NASA TM X-73,124, May 1976.

30. Schroers, L. G., "Initial XV-15 Flight Test Results Compared to Design Predictions." AIAA Paper 80-0235, Jan. 1980.

31. Miller, T. H., and Baker, C. M., "AV-8A Harrier Concept and Operational Performance - U. S. Marine Corps." AGARD-CP-126, Apr. 1973.

32. Gustafson, R. A., "Ten Years of U. S. Marine Corps Harrier Operations." AGARD-CP-313, Jun. 1981.

33. Lacey, D. W., "Air Combat Advantages from Reaction Control Systems." SAE Paper 801177, Oct. 1980.

34. Nelms, W. P., and Anderson, S. B., "V/STOL Concepts in the United States - Past, Present, and Future." Proceedings of the AGARD/VKI Lecture Series on V/STOL Aerodynamics, May 1984.

35. Hess, J. R., and Bear, R. L., "Study of Aerodynamic Technology for Single-Cruise-Engine V/STOL Fighter/Attack Aircraft." NASA CR 166269, Feb. 1982.

36. Foley, W. H., Sheridan, A. E., and Smith, C. W., "Study of Aerodynamic Technology for Single-Cruise-Engine V/STOL Fighter/Attack Aircraft." NASA CR 166268, Feb. 1982.

37. Driggers, H. H., Powers, S. A., and Roush, R. T. "Study of Aerodynamic Technology for Single-Cruise-Engine V/STOL Fighter/Attack Aircraft." NASA CR 166271, Feb. 1982.

38. Konsewicz, R. K., "Rationale for Selection of a Flight Control System for Lift Cruise Fan V/STOL Aircraft." Proceedings, Navy/NASA VSTOL Flying Qualities, Apr, 1977.

39. Betzina, M. D., and Veta, R., "Aerodynamic Effects of an Attitude Control Vane on a Tilt-Nacelle V/STOL Propulsion System." AIAA Paper 79-1855, Aug. 1979.

40. Wilson, S. B. III, Donley, S., Buchmann, W., Valckenaere, W., and Blake, M., "Handling Characteristics of a Simulated Twin Tilt Nacelle V/STCL Aircraft." SAE Paper 831549, Oct. 1983.

41. Franklin, J. A., and Innis, R. C., "Flight-Path and Airspeed Control During Landing Approach for Powered-Lift Aircraft." NASA TN D-7791, Oct. 1974.

42. Franklin, J. A., Innis, R. C., Hardy, G. H., and Stephenson, J. D., "Design Criteria for Flightpath and Airspeed Control for the Approach and Landing of STOL Aircraft." NASA TP 1911, Mar. 1982.

43. Hill, G. C., "Piloted Simulation of Hover and Transition of a Vertical Attitude Takeoff and Landing Aircraft." AIAA Paper 81-2636, Dec. 1981.

44. Morello, S. A., Person, L. H. Jr., Shanks, R. E., and Culpepper, R. G., "A Flight Evaluation of a Vectored-Thrust-Jet V/STOL Airplane During Simulated Instrument Approaches Using the Kestrel (XV-6A) Airplane." NASA TN D-6791, May 1972.

45. Hoh, R. H., and Mitchell, D. G., "Tentative STOL Flying Qualities Criteria for MIL Standard and Handbook." AFWAL-TR-83-3059, Jun. 1983.

46. Henderson, C., Clark, J., and Walters, M.: "V/STOL Aerodynamics and Stability and Control Manual." NADC-80017-60, Jan. 1980.

47. Clark, W. Jr., "Analysis of Response Requirements for V/STOL Lift-Cruise Engines Used to Provide Height and Moment Control." AIAA Paper No. 75-1014, Aug. 1975.

48. Ringland, R. F., and Craig, S. J., "Survey of Piloting Factors in V/STOL Aircraft with Implications for Flight Control System Design." Proceedings of the Navy/NASA VSTOL Flying Qualities Conference, Apr. 1977.

49. Anon., "Displays for Approach and Landing of V/STOL Aircraft." AGARD Advisory Report 51, Nov. 1972.

50. Clark, J. W. Jr., and Goldstein, K. W., "Status of VTOL and VSTOL Flying Qualities Criteria Development-Where are We and Where are We Going?." AGARD-CP-333, Jun. 1982.

51. Merrick, V. K., and Gerdes, R. M., "Design and Piloted Simulation of a VTOL Flight Control System." J. Guidance Contr., vol. 1, no. 3, May-Jun. 1978.

52. Stapleford, R. L., Clement, W. F., Heffley, R. K., Booth, G. C., and Fortenbaugh, R. L., "Flight Control/Flying Qualities Investigation for Lift/Cruise Fan V/STOL." NADC Report 77143-30, Aug. 1979.

53. Gerdes, R. M., and Hynes, C. S., "Factors Affecting Handling Qualities of a Lift-Fan Aircraft During Steep Terminal Area Approaches." NASA TM X-62,424, Apr. 1975.

54. Merrick, V. K., and Gerdes, R. M., "VTOL Controls for Shipboard Operations." SAE Paper 831428, Oct. 1983.

55. Donley, S. T., "Evaluation of Several Control/Display Concepts for V/STOL Shipboard Landing." SAE Paper 801205, Oct. 1980.

56. Hoh, R. H., Craig, S. J., and Ashkenas, I. L., "Identification of Minimum Acceptable Characteristics for Manual STOL Flight Path Control." FAA-RD-75-123, Jun. 1976.

57. Heffley, R. K., Stapleford, R. L., and Rumold, R. C., "Airworthiness Criteria Development for Powered-Lift Aircraft." NASA CR-2791, Feb. 1977.

58. Farris, G. G., Merrick, V. K., and Gerdes, R. M., "Simulation Evaluation of Flight Controls and Display Concepts for VTOL Shipboard Operations." AIAA Paper 83-2173, Aug. 1983.

59. Lebacqz, J. V., Radford, R. C., and Beilman, J. L., "An Experimental Investigation and Control-Display Requirements for Jet-Lift VTOL Aircraft in the Terminal Area." NADC-76099-60, Jul. 1978.

60. Radford, R. C., and Andrisani, D. II, "An Experimental Investigation of VTOL Flying Qualities Requirements in Shipboard Landings." AIAA Paper 80-1625, Aug. 1980.

61. Kelly, J. R., Niessen, F. R., Thibodeaux, J. J., Yenni, K. R., and Garren, J. F., Jr., "Flight Investigation of Manual and Automatic VTOL Decelerating Instrument Approaches and Landings." NASA TN D-7524, Jul. 1974.

62. Niessen, F. R., Kelly, J. R., Garren, J. F., Jr., Yenni, K. R., and Person, L. H., "The Effect of Variations in Controls and Displays on Helicopter Instrument Approach Capability." NASA TN D-8385, Feb. 1977.

63. Franklin, J. A., Innis, R. C., and Hardy, G. H., "Flight Evaluation of Stabilization and Command Augmentation System Concepts and Cockpit Displays During Approach and Landing of a Powered-Lift STOL Aircraft." NASA TP 1551, Nov. 1980.

64. Hindson, W. S., Hardy, G. H., and Innis, R. C., "Flight-Test Evaluation of STOL Control and Flight Director Concepts in a Powered-Lift Aircraft Flying Curved Decelerating Approaches." NASA TP 1641, Mar. 1981.

65. Corliss, L. D., and Dugan, D. C., "A VTOL Translational Rate Control Systems Study on a Six Degree of Freedom Motion Simulator." NASA TM X-62,194, Oct. 1972.

66. Bridadier, W. L., "Analysis of Control Actuator Authority Requirements for Attitude and Translational Rate Command Augmentation Systems for the XV-15 Tilt Rotor Research Aircraft." NASA TM 81243 and AVRADCOM TR-80-A-13, Dec. 1980.

67. Davis, J., Garnett, T., and Gaul, J., "Heavy Lift Helicopter Flight Control System. Vol. III: Automatic Flight Control System Development and Feasibility Demonstration." USAAMRDL-TR-77-40C, Sept. 1977.

68. Anon., "Tactical Aircraft Guidance System Advanced Development Program Flight Test Phase Report, Vol. I." USAAMRDL-TR-73-89A, Apr. 1974.

69. Tinling, B. E., and Cole, G. L., "Simulation Study of the Interaction Between the Propulsion and Flight control Systems of a Subsonic Lift Fan VTOL." NASA TM 81239, 1980.

70. Mihaloew, J. R., Roth, S. P., and Creekmore, R., "A Real Time Pegasus Propulsion System Model for VSTOL Piloted Simulation Evaluation." AIAA Paper 81-2663 and NASA TM 82770, Dec. 1981.

71. Farley, J. F., "Modern Flight Instrument Displays as a Major Military Aviation Flight Safety Weakness." AGARD-CP-347, Oct. 1983.

Figure 1. Harrier operation at a forward site (Photo courtesy of McDonnell-Douglas Corp.).

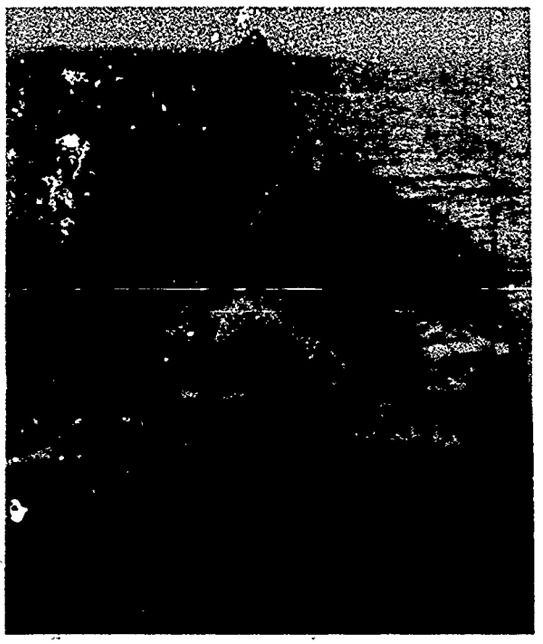

Figure 2. H.M.S. Hermes in the South Atlantic, 1982. (From the 25th Sir Charles Kingford Smith Memorial Lecture, University of New South Wales, Sydney, Australia, September, 1983, by J.W. Fozard.)

Figure 3. U.S. Marine Corps AV-8As on U.S.S. Guam. (From the 25th Sir Charles Kingford Smith Memorial Lecture, University of New South Wales, Sydney, Australia, September, 1983, by J.W. Fozard.)

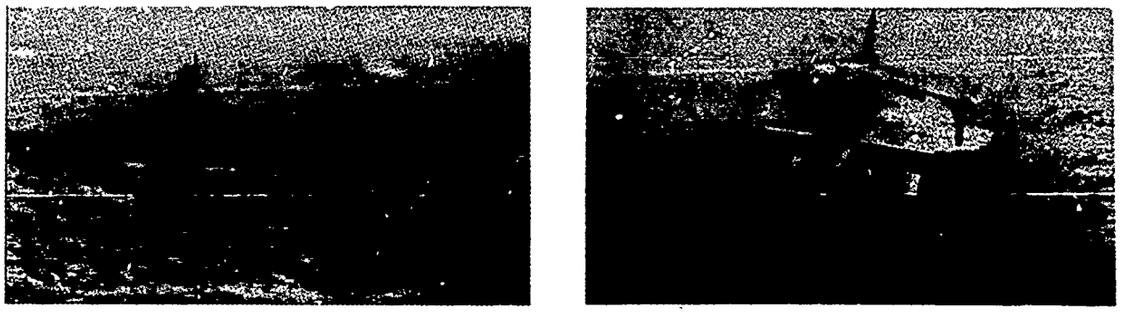

a. Vertical takeoff.

b. Vertical landing.

Figure 4. Harrier operations aboard H.M.S. Blake (from Ref. 22).

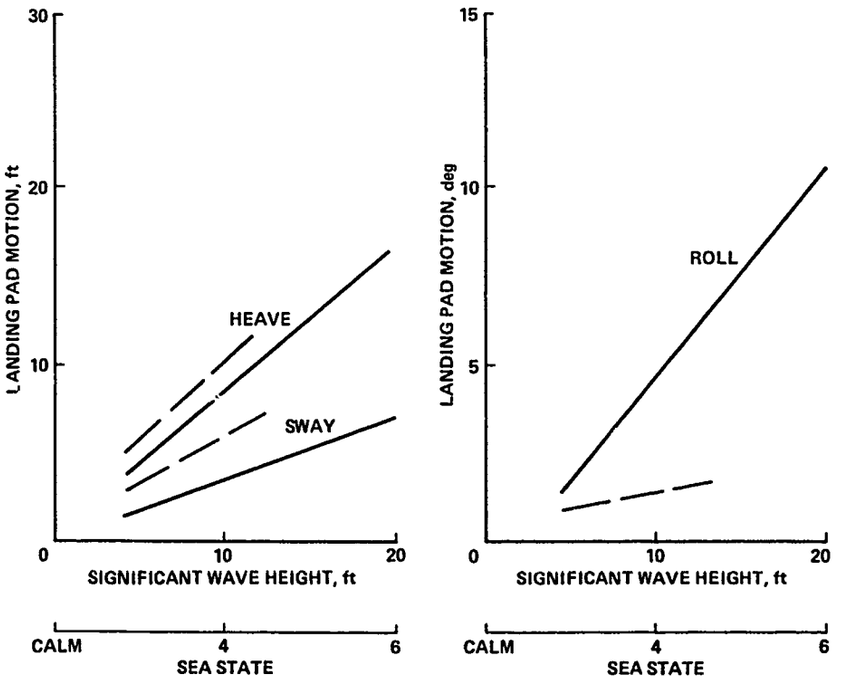

Figure 5. Landing pad motion characteristics for DD-963 destroyer.

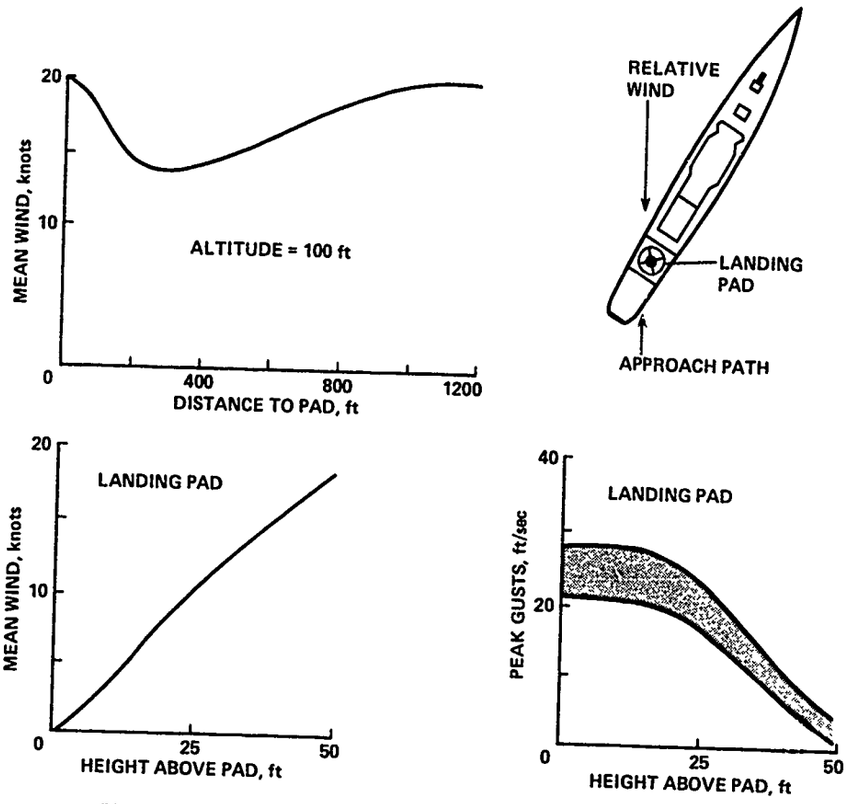

Figure 6. Ship airwake characteristics for DD-963 destroyer.

	ATTITUDE CUES	POSITION AND VELOCITY CUES	OVC LEVEL
VMC	EASILY OBTAINED.	EASILY OBTAINED	①
VMC	SOMEWHAT OBSCURED. REQUIRES FULL CONCENTRATION TO OBTAIN CONTINUOUS ATTITUDE INFORMATION.	EASILY OBTAINED	②
PARTIAL IMC	INADEQUATE IN SOME SECTORS OF THE VISUAL FIELD.	ADEQUATE POSITION. MARGINAL RATE CUES.	③
PARTIAL IMC	INADEQUATE OVER MOST OF VISUAL FIELD.	POSITION AND RATE CUES ARE MARGINAL. RATE CUES ARE INTERMITTENTLY UNAVAILABLE.	④
IMC	NOT AVAILABLE.	NOT AVAILABLE.	⑤

a. Quantification of outside visual cues.

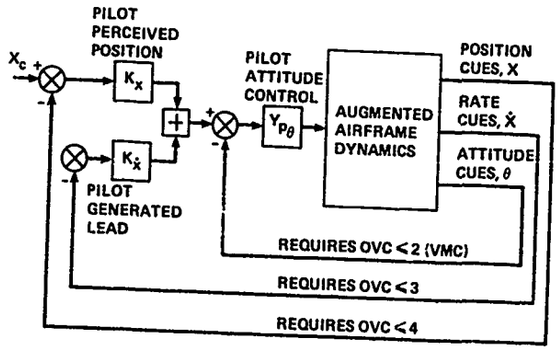

b. Outside visual cues required for control.

Figure 7. Outside visual cue scale (from Ref. 7).

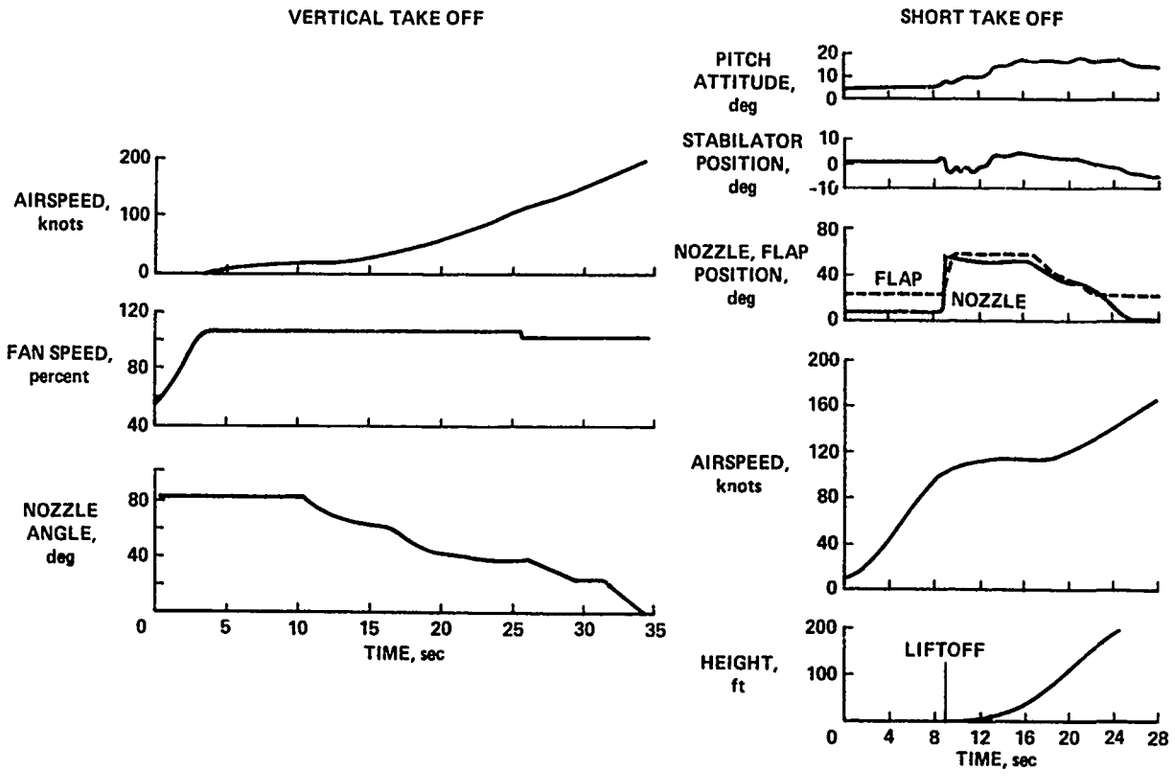

Figure 8. Vertical and short takeoff maneuver.

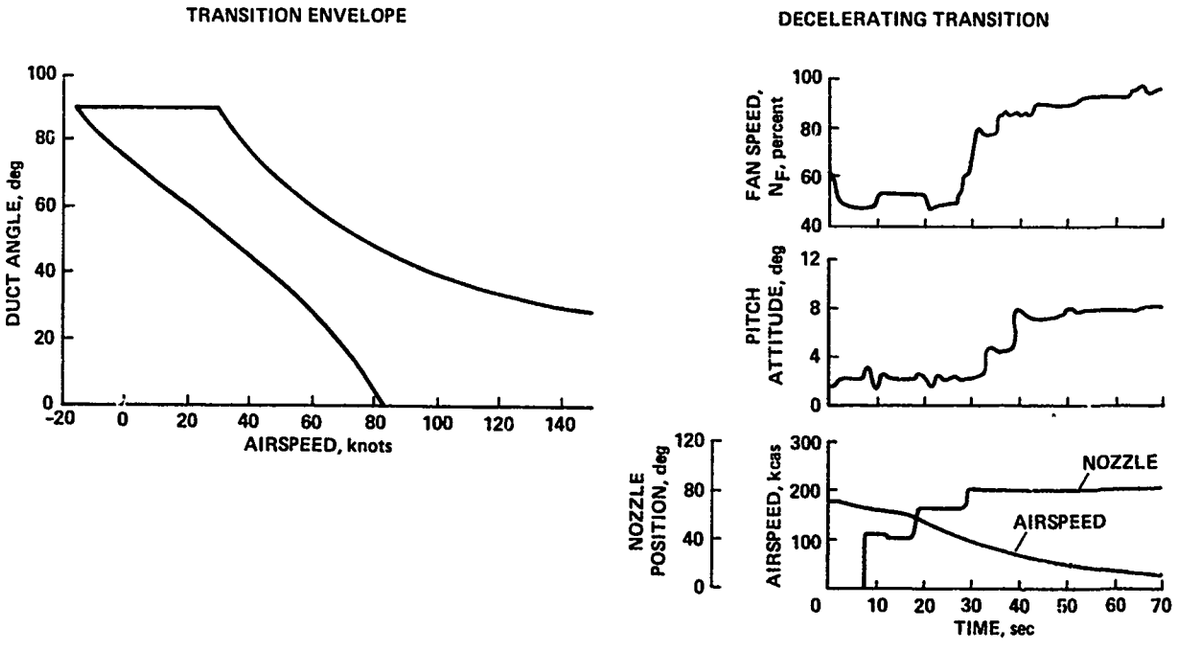

Figure 9. Transition envelope and maneuver.

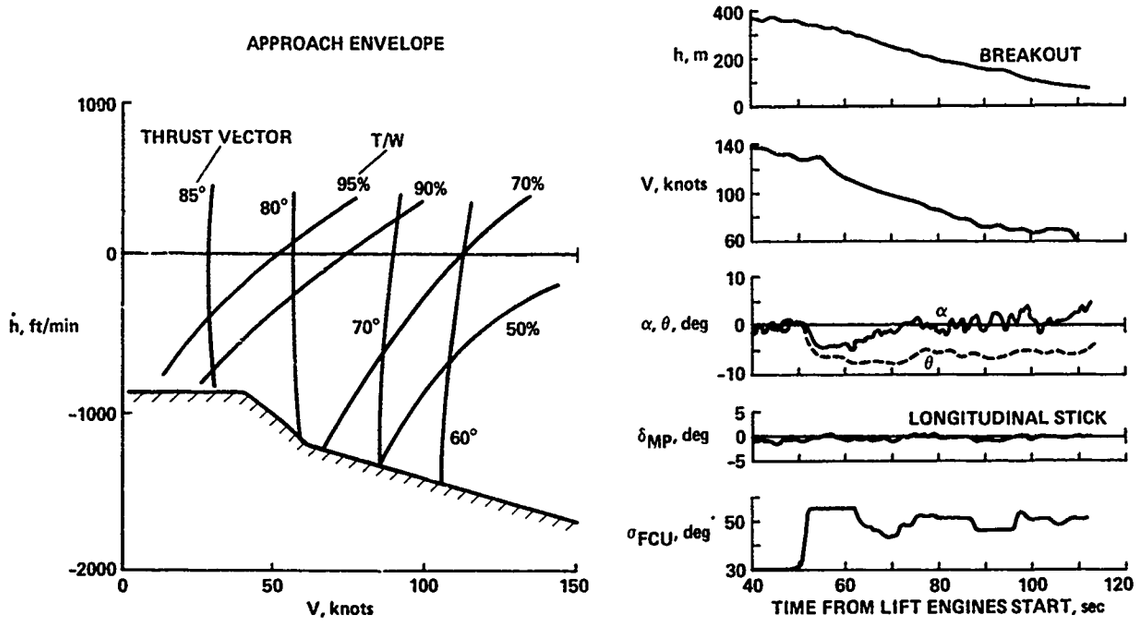

Figure 10. Landing approach envelope and maneuver.

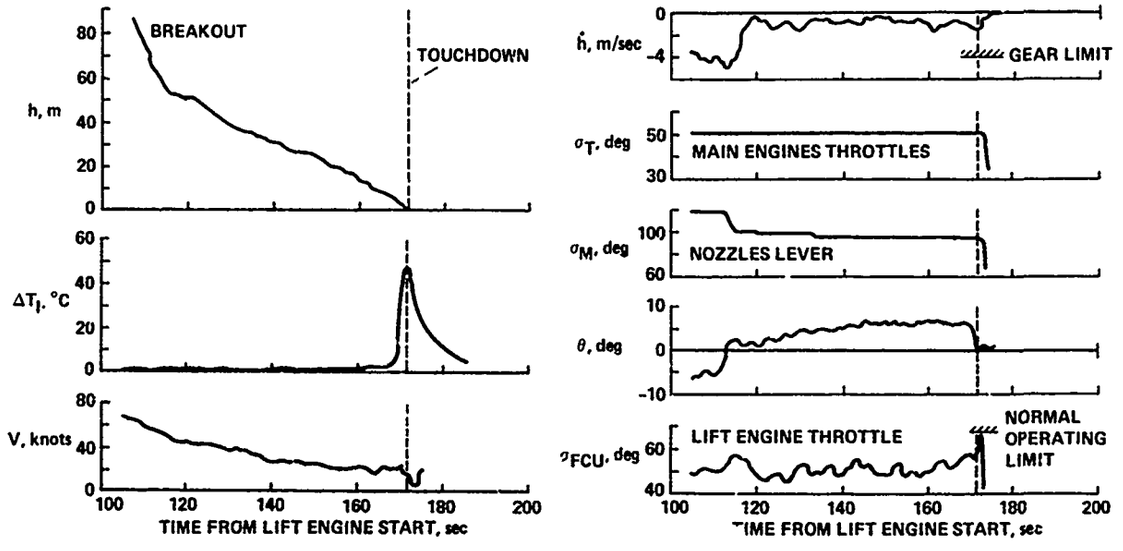

Figure 11. Hover and landing.

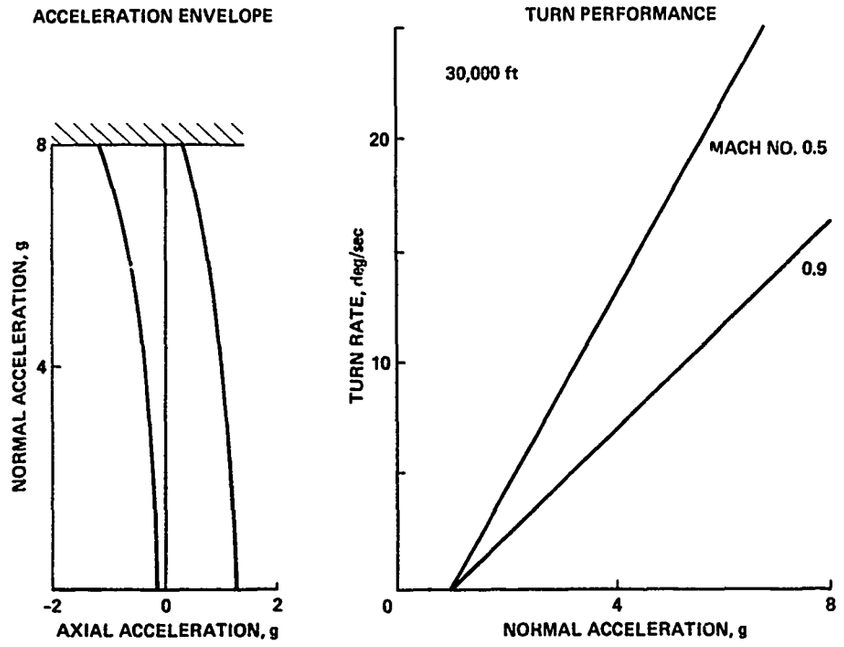

Figure 12. Forward flight maneuver performance.

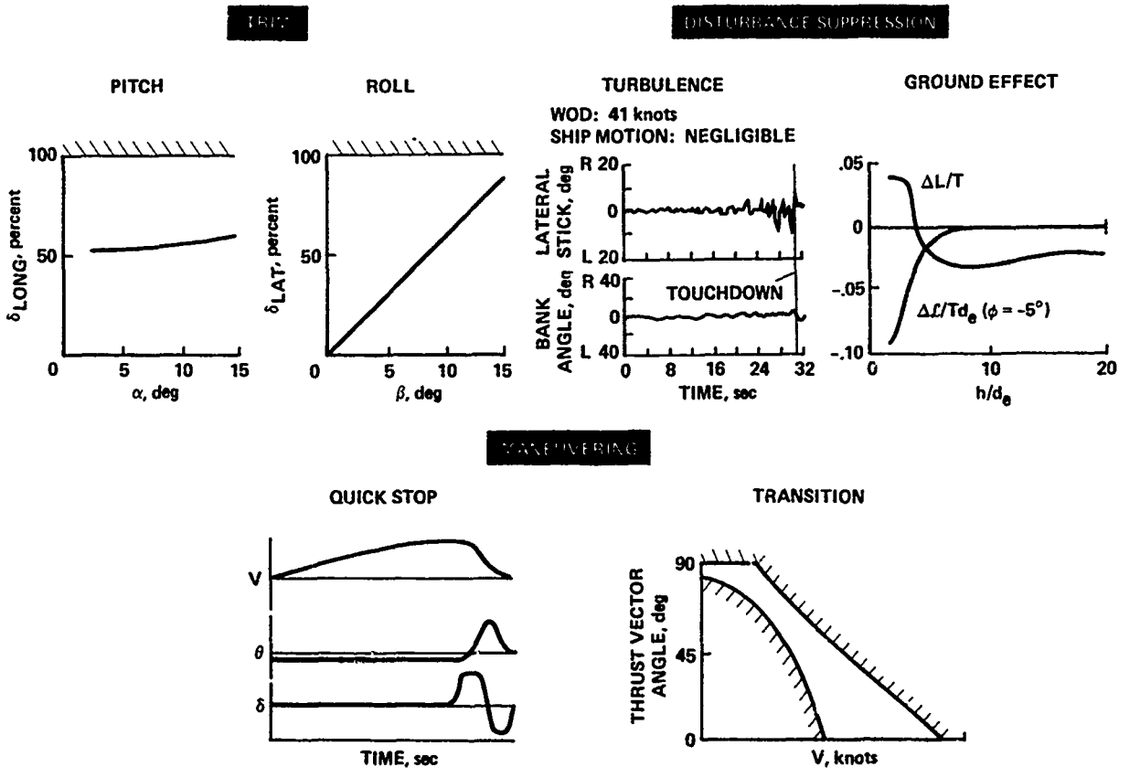

Figure 13. Demands on control authority.

FLYING QUALITIES REQUIREMENT	AGARD 577		MIL-F-83300
	$\ddot{\theta}_{MAX}$, rad/sec^2	$\theta(1)$, deg	$\theta(1)$, deg
LEVEL 1 SATISFACTORY WITHOUT IMPROVEMENT	0.1-0.3	2-4	3
LEVEL 2 ADEQUATE IMPROVEMENT WARRANTED			2

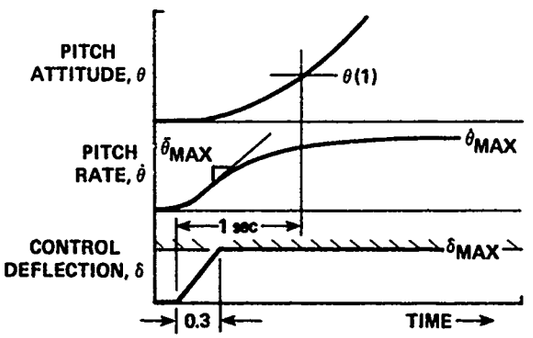

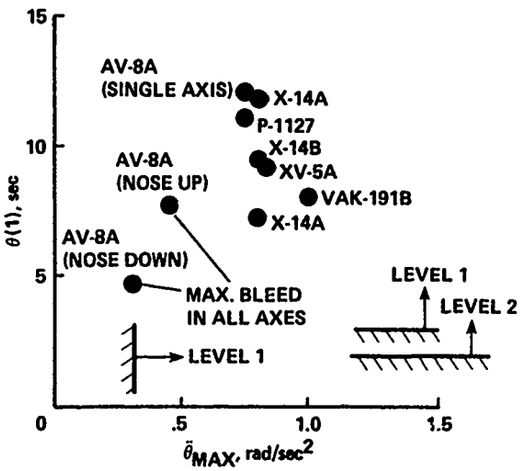

Figure 14. Pitch control authority in hover.

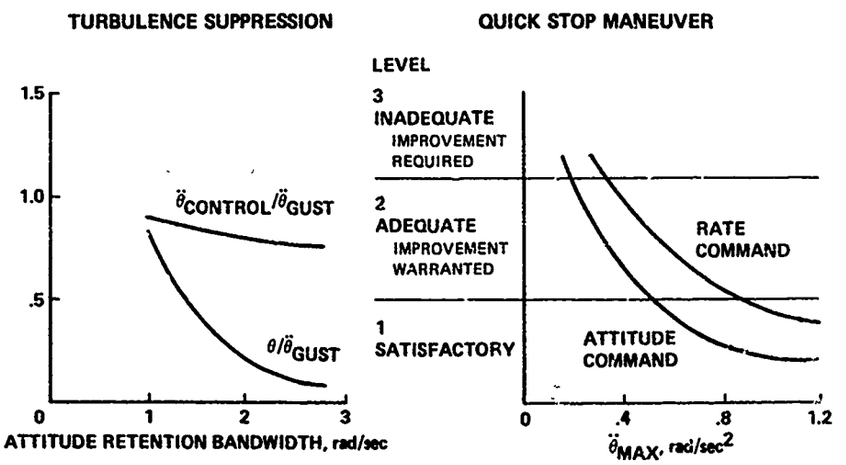

Figure 15. Pitch control utilization in hover.

FLYING QUALITIES REQUIREMENT	AGARD 577		MIL-F-83300
	$\ddot{\phi}_{MAX}$, rad/sec^2	$\phi(1)$, deg	$\phi(1)$, deg
LEVEL 1 SATISFACTORY WITHOUT IMPROVEMENT	0.2-0.4	2-4	4.0
LEVEL 2 ADEQUATE IMPROVEMENT WARRANTED			2.5

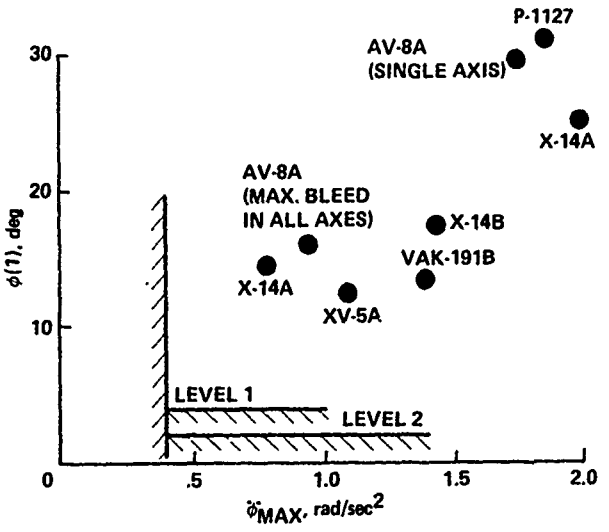

Figure 16. Roll control authority in hover.

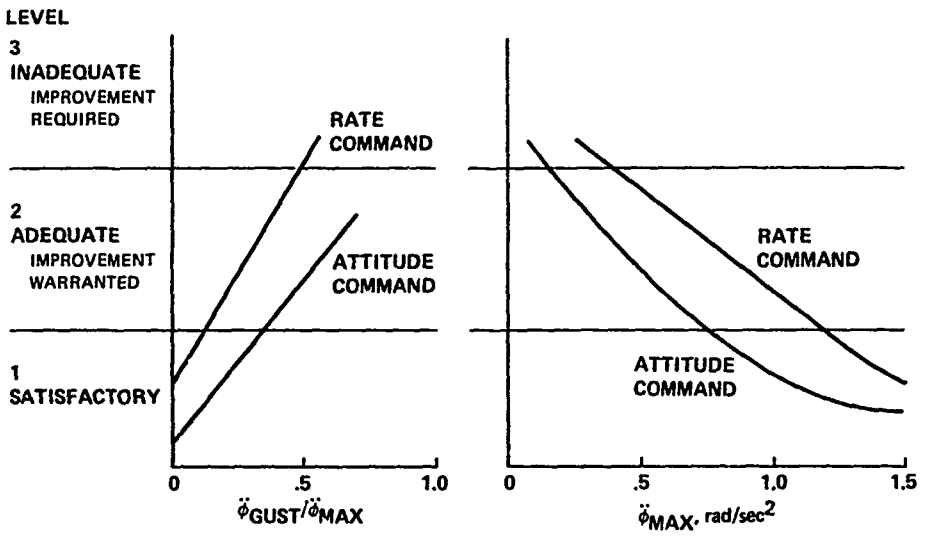

Figure 17. Roll control utilization in hover.

FLYING QUALITIES REQUIREMENT	AGARD 577		MIL-F-83300
	$\ddot{\psi}_{MAX}$, rad/sec^2	$t_{\psi=15°}$, sec	$\psi(1)$, deg
LEVEL 1 SATISFACTORY WITHOUT IMPROVEMENT	0.1-0.5	1.0-2.5	6
LEVEL 2 ADEQUATE IMPROVEMENT WARRANTED			3

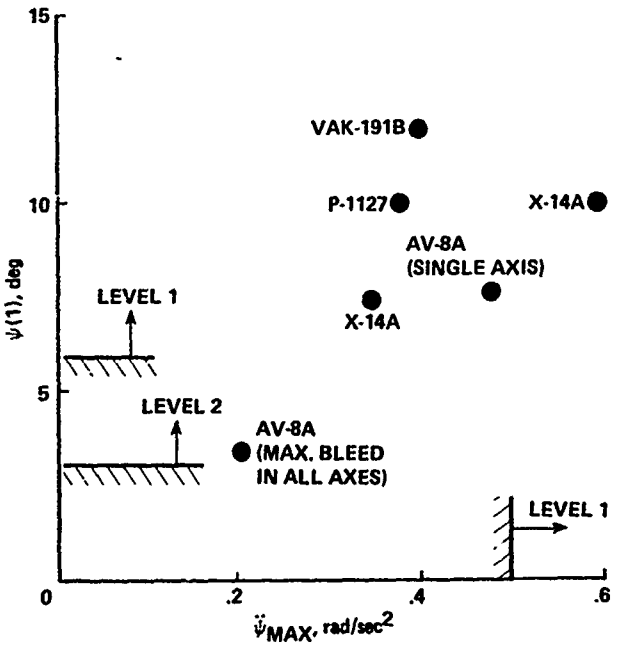

Figure 18. Yaw control authority in hover.

FLYING QUALITIES REQUIREMENT	AGARD 577		MIL-F-83300	
	T/W_{MIN}	$\dot{h}_{MIN}$, ft/sec	T/W_{MIN}	Δg_{MIN}
LEVEL 1 SATISFACTORY WITHOUT IMPROVEMENT	1.03-1.1	600	1.05	0.1
LEVEL 2 ADEQUATE IMPROVEMENT REQUIRED			1.02	0.05

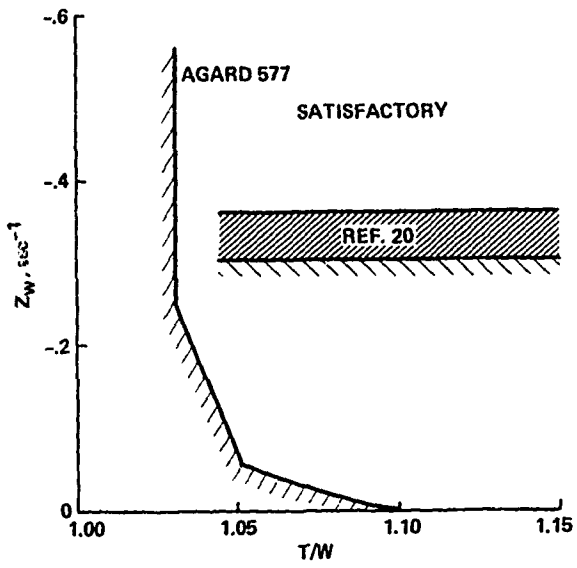

Figure 19. Heave control authority in hover.

FLYING QUALITIES REQUIREMENT	MIL-F-83300				
	PITCH, θ(1), deg	ROLL, ϕ(1), deg	YAW, ψ(1), deg	THRUST, Δg	TRIM WIND, knots
LEVEL 1 SATISFACTORY WITHOUT IMPROVEMENT	3.0	4.0	6.0	0.1	35
LEVEL 2 ADEQUATE IMPROVEMENT WARRANTED	2.0	2.5	3.0	0.05	35

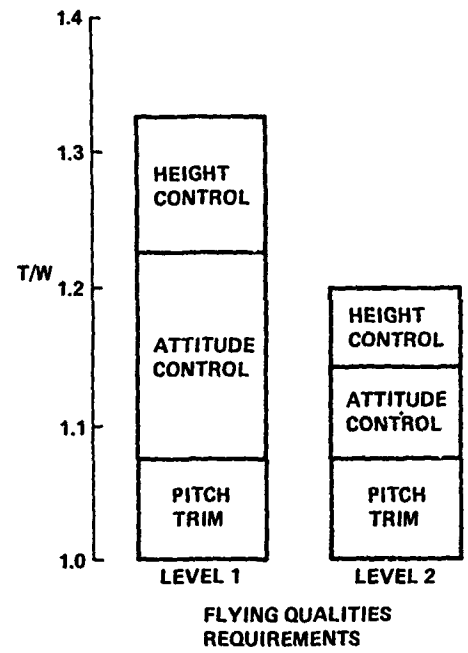

Figure 20. Combined control authority in hover.

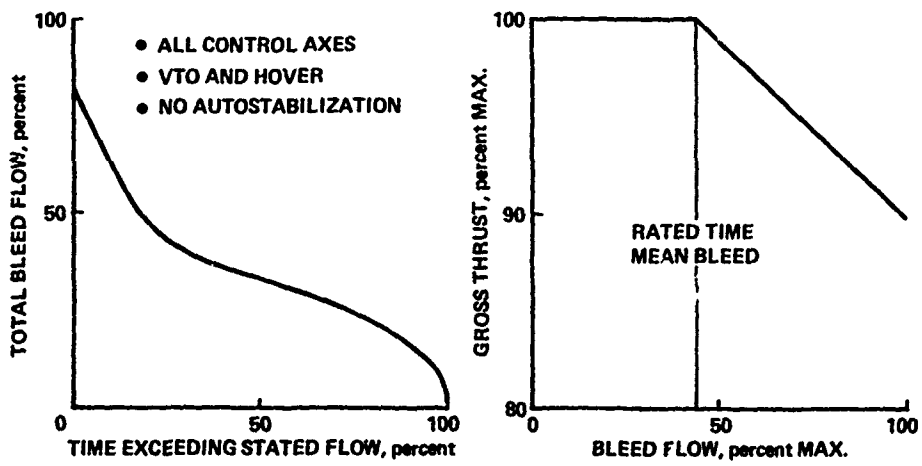

Figure 21. Thrust-bleed tradeoff in hover (from Refs. 9 and 22).

AGARD 577		MIL-F-83300 CONTROL MARGIN IN EXCESS OF TRIM
$\ddot{\theta}_{MAX}$, rad/sec^2	θ(1), deg	
0.05-0.2	2-4	50% OF MAX.

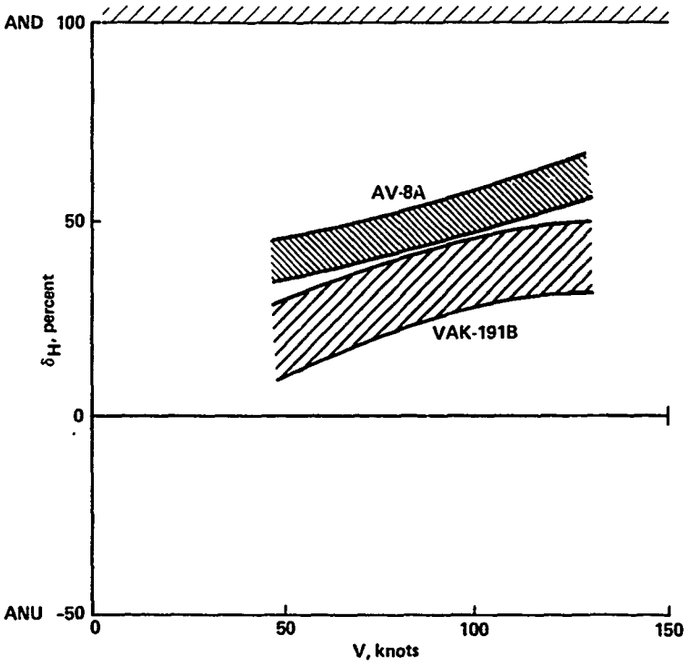

Figure 22. Pitch control authority in transition.

FLYING QUALITIES REQUIREMENT	AGARD 577		MIL-F-83300 $t_{\phi=30°}$*, sec
	$\ddot{\phi}_{MAX}$†, rad/sec^2	ϕ(1), deg	
LEVEL 1 SATISFACTORY WITHOUT IMPROVEMENT	0.1-0.6	2-4	1.0-2.5
LEVEL 2 ADEQUATE IMPROVEMENT WARRANTED			1.3-3.2

*DEPENDS ON AIRCRAFT CATEGORY RANGING FROM FIGHTER TO HEAVY TRANSPORT. ALTERNATE REQUIREMENT – 50% CONTROL MARGIN.

†50% CONTROL AUTHORITY REMAINING FOR FULL RUDDER AUTHORITY SIDESLIP.

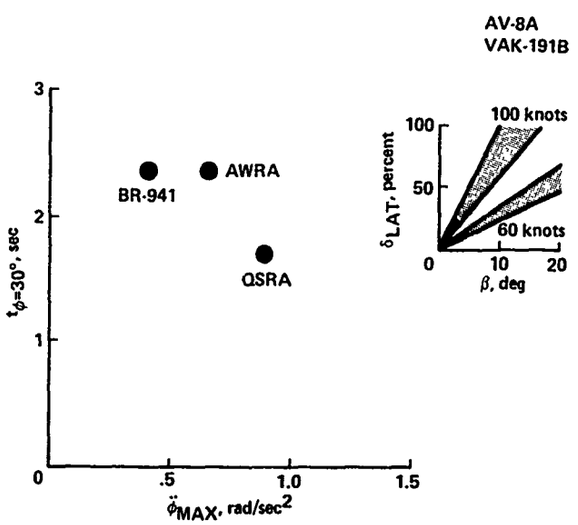

Figure 23. Roll control authority in transition.

FLYING QUALITIES REQUIREMENT	AGARD 577		MIL-F-83300
	$\ddot{\psi}_{MAX}$, rad/sec^2	$t_{\psi=15°}$, sec	$\psi(1)$*, deg
LEVEL 1 SATISFACTORY WITHOUT IMPROVEMENT	0.15-0.25	2.0	6
LEVEL 2 ADEQUATE IMPROVEMENT WARRANTED			3

*ALTERNATE REQUIREMENT 50% CONTROL MARGIN

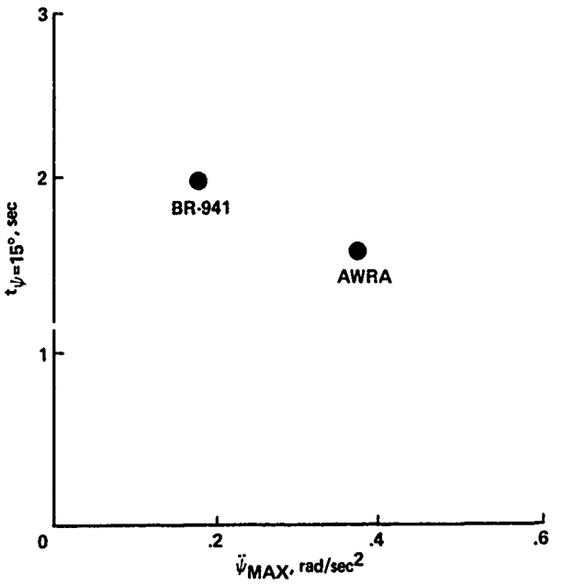

Figure 24. Yaw control authority in transition.

AGARD 577		FAA TENTATIVE POWERED-LIFT AIRWORTHINESS CRITERIA, γ, deg
Δa_z, g's	γ, deg	
±0.1	6° CLIMB -2° GREATER THAN APPROACH PATH ANGLE	LEVEL FLIGHT -4° GREATER THAN APPROACH PATH ANGLE

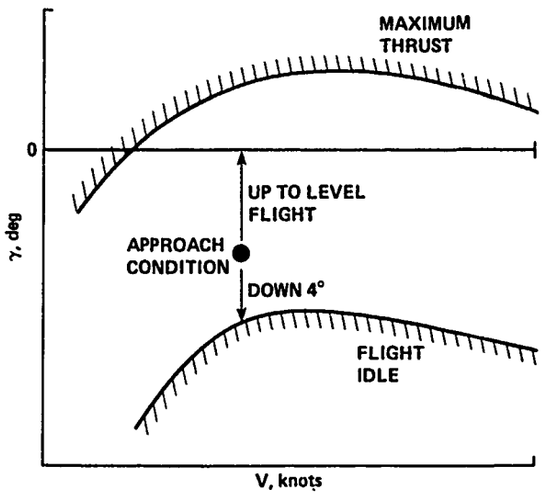

Figure 25. Flightpath control authority in transition.

FLYING QUALITIES REQUIREMENTS	
AGARD 577	MIL-F-83300
ABILITY TO ACCELERATE OR DECELERATE CONTINUOUSLY THROUGHOUT TRANSITION ENVELOPE. ACCELERATION OR DECELERATION UP TO 0.5 g's DESIRABLE DEPENDING ON MISSION. DIRECTION OF TRANSITION SHOULD BE EASILY REVERSED.	ABILITY TO ACCELERATE OR DECELERATE RAPIDLY FROM ANY TRIM POINT WITHIN TRANSITION ENVELOPE. TIME DURATION OF MANOEUVRE IS MISSION DEPENDENT. DIRECTION OF TRANSITION SHOULD BE EASILY REVERSED.

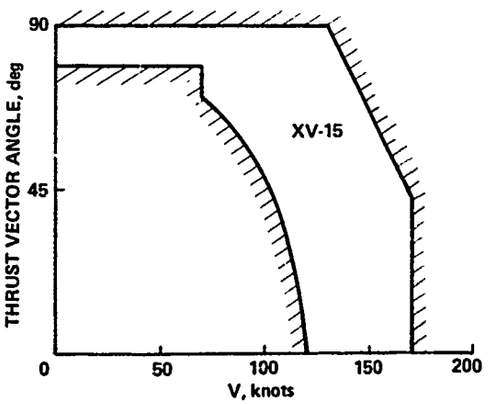

Figure 26. Longitudinal acceleration control authority in transition.

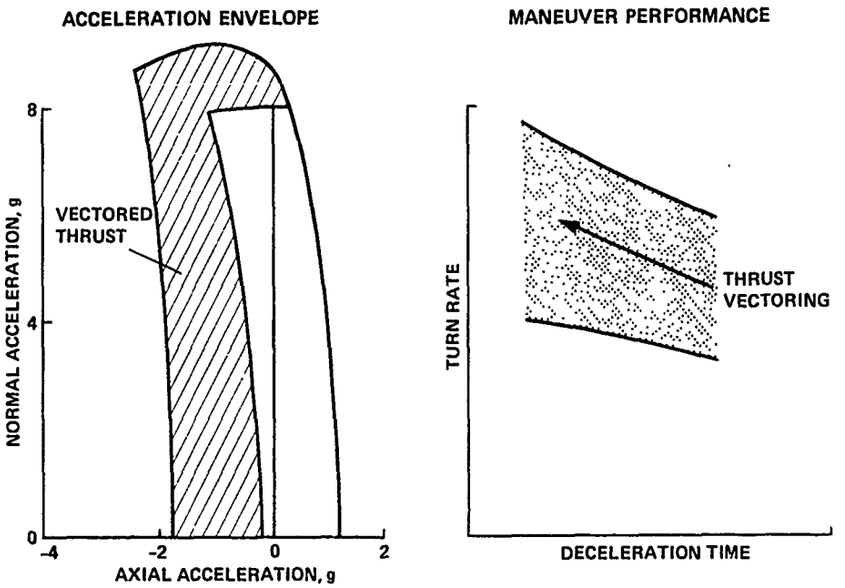

Figure 27. Forward flight maneuver enhancement.

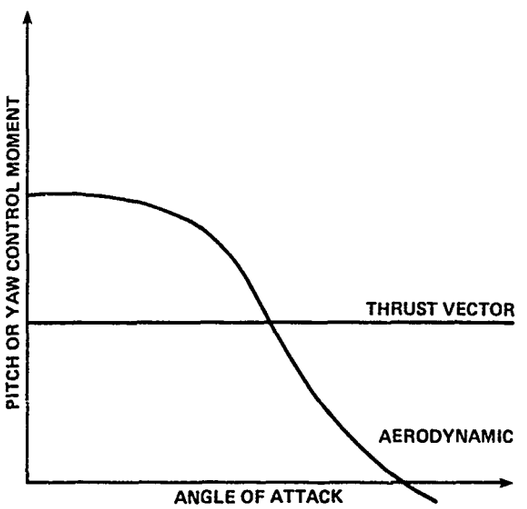

Figure 28. Forward flight attitude control.

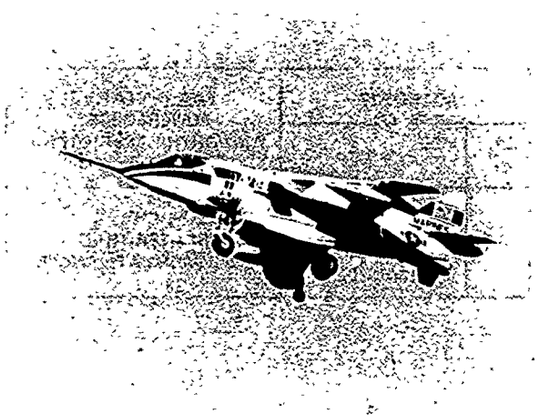

Figure 29. AV-8B Advanced Harrier.

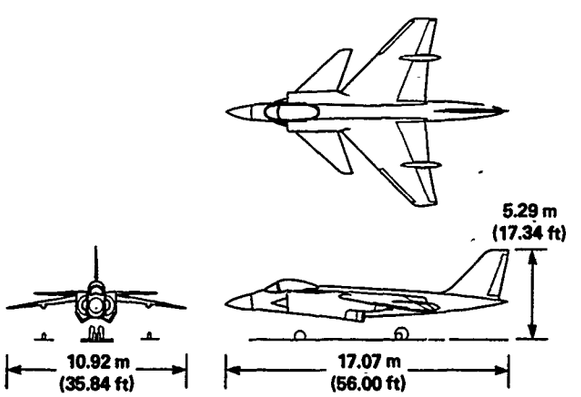

Figure 30. Deflected thrust aircraft configuration.

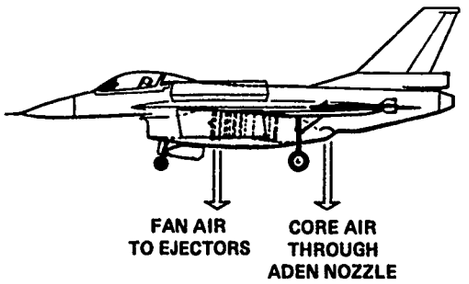

(a) HOVER CONFIGURATION

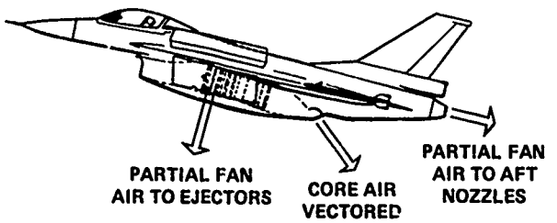

(b) STO AND TRANSITION CONFIGURATION

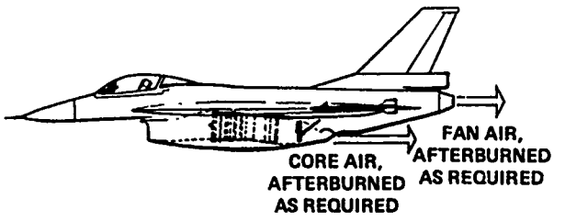

(c) UP-AND-AWAY CONFIGURATION

Figure 31. Augmentor-ejector aircraft configuration.

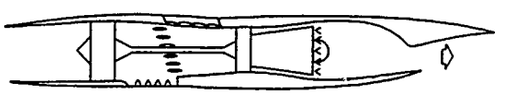

SERIES FLOW MODE - HIGH SPEED

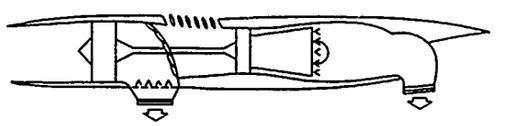

PARALLEL FLOW MODE - V/STOL

Figure 32. Tandem-fan propulsion concept.

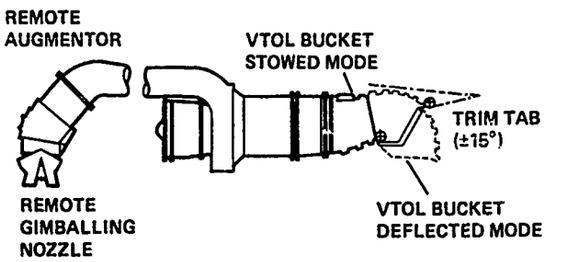

Figure 33. Remote augmented lift propulsion concept.

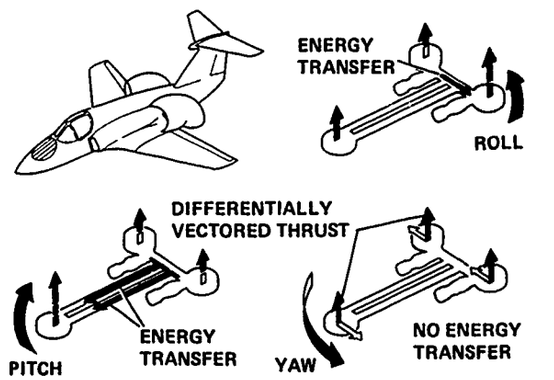

Figure 34. Lift-cruise fan aircraft configuration.

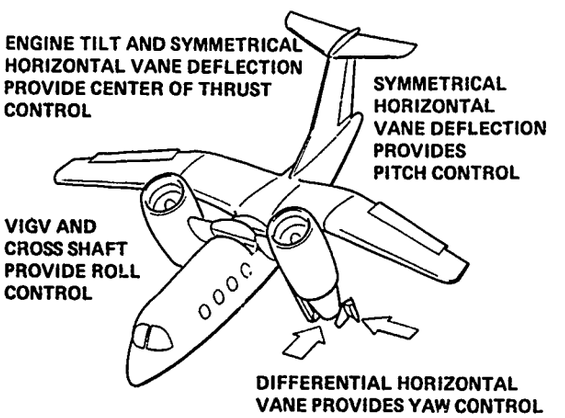

Figure 35. Twin tilt nacelle lift-cruise fan aircraft concept.

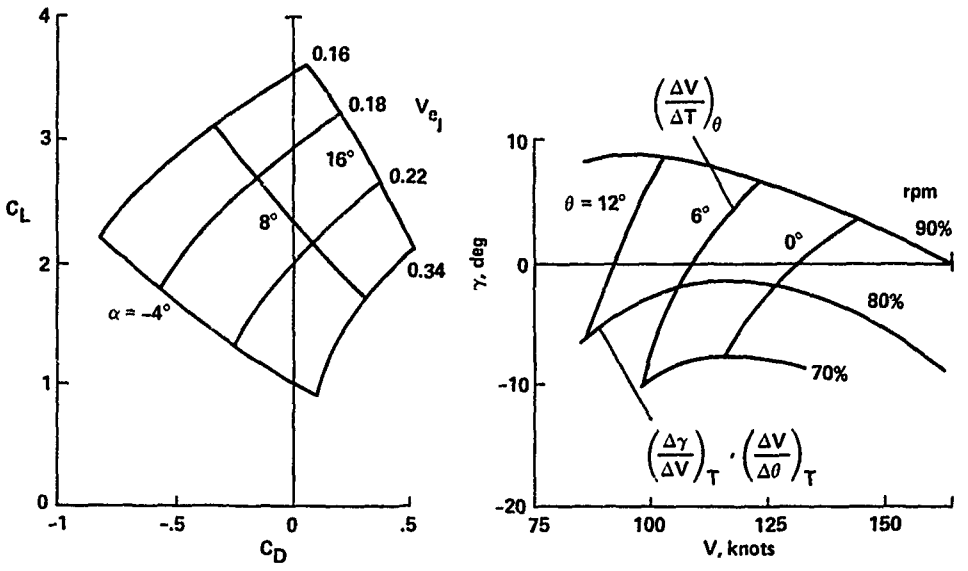

Figure 36. Relationship of steady-state flightpath and airspeed control to lift and drag aerodynamics.

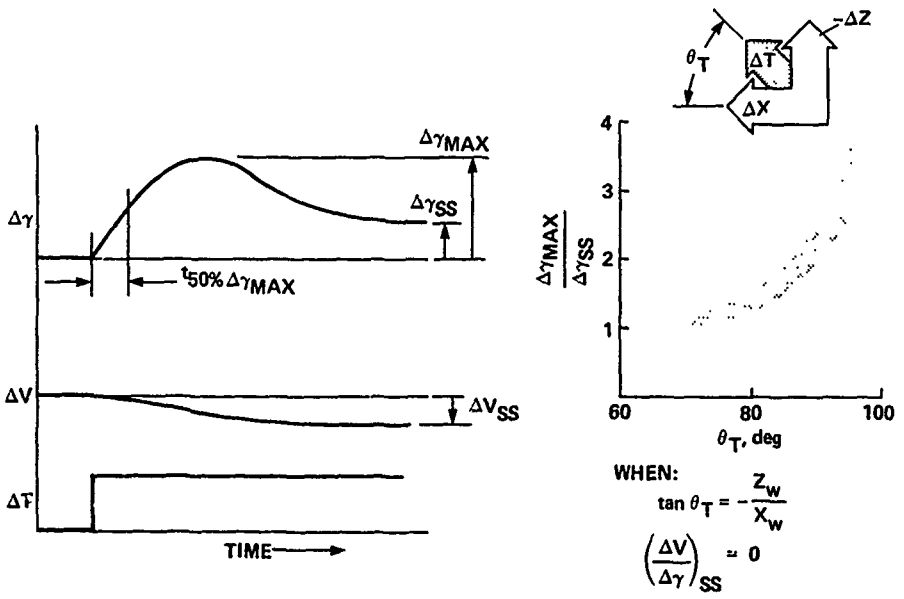

Figure 37. Relationship of flightpath and airspeed dynamic response to lift-drag aerodynamics.

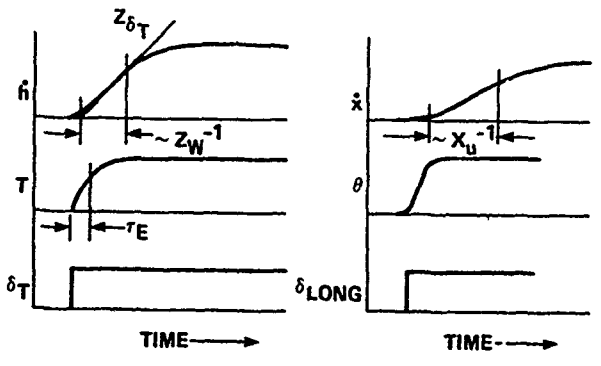

Figure 38. Hover control dynamics

AXIAL $\ddot{x} - X_u\dot{x} + g\theta = 0$

VERTICAL $\ddot{z} - Z_w\dot{z} = Z_{\delta_T}\delta_T$

PITCH $-M_u\dot{x} + \ddot{\theta} - M_q\dot{\theta} = M_{\delta_e}\delta_e$

$$(s - Z_w)(s^3 - (X_u + M_q)s^2 + X_uM_qs + gM_u) = 0$$

OR

$$(s + \frac{1}{T_h})(s + \frac{1}{T_\lambda})(s^2 + 2\zeta\omega s + \omega^2) = 0$$

HEIGHT CONTROL $\quad \frac{z}{\delta_T} = \frac{Z_{\delta_T}}{s(s + \frac{1}{T_h})} \qquad \frac{1}{T_h} = -Z_w$

PITCH CONTROL $\quad \frac{\theta}{\delta_e} = \frac{M_{\delta_e}(s - X_u)(s + \frac{1}{T_h})}{(s + \frac{1}{T_h})(s + \frac{1}{T_\lambda})(s^2 + 2\zeta\omega s + \omega^2)}$

AXIAL POSITION CONTROL $\quad \frac{x}{\delta_e} = \frac{gM_{\delta_e}(s + \frac{1}{T_h})}{s(s + \frac{1}{T_h})(s + \frac{1}{T_\lambda})(s^2 + 2\zeta\omega s + \omega^2)}$

AERODYNAMICS NEGLECTED

$\ddot{x} = -g\theta$

$\ddot{\theta} = M_{\delta_e}\delta_e$

$\ddot{z} = Z_{\delta_T}\delta_T$

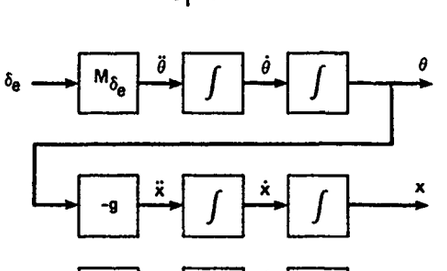

Figure 39. Basic aircraft hover equations.

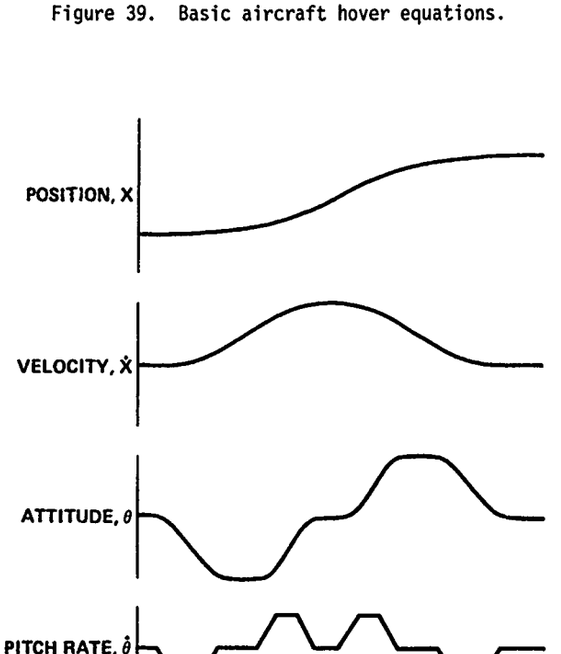

Figure 40. Hover position control.

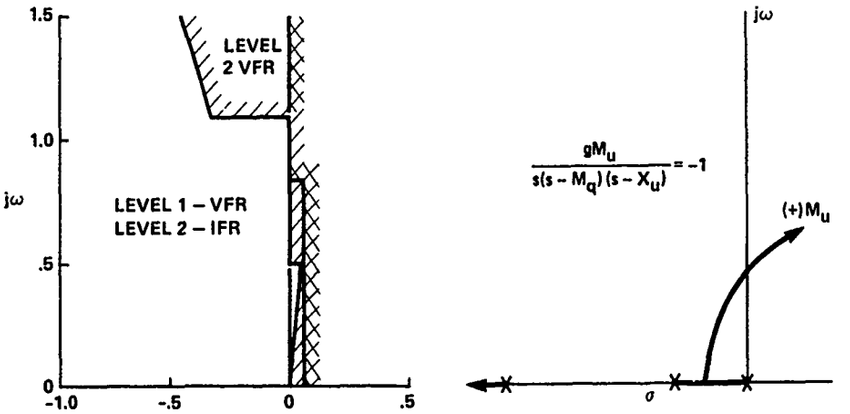

Figure 41. Basic aircraft hover stability.

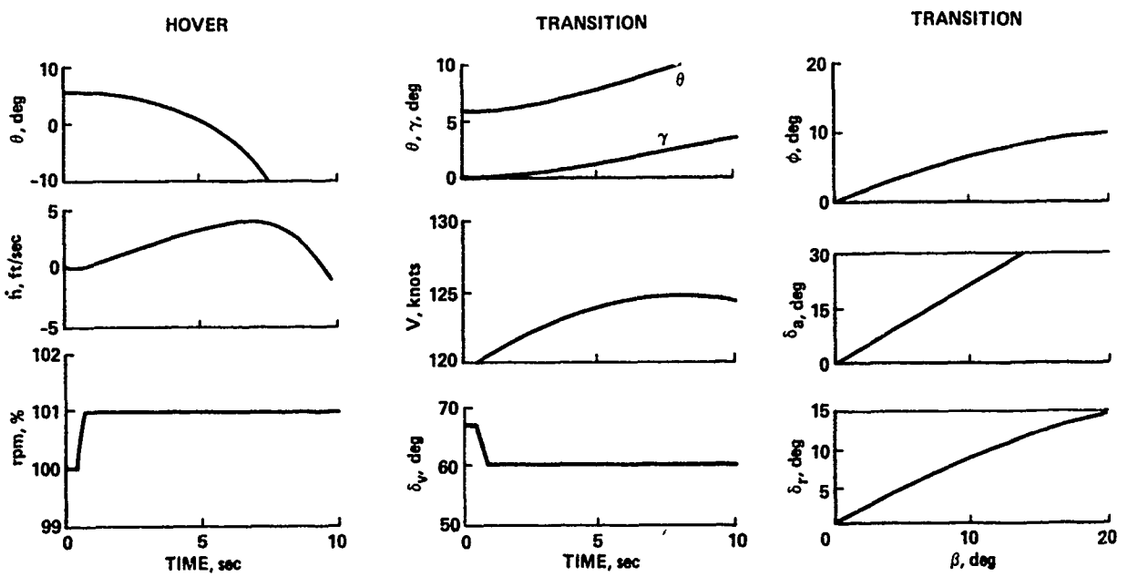

Figure 42. Control cross-coupling examples.

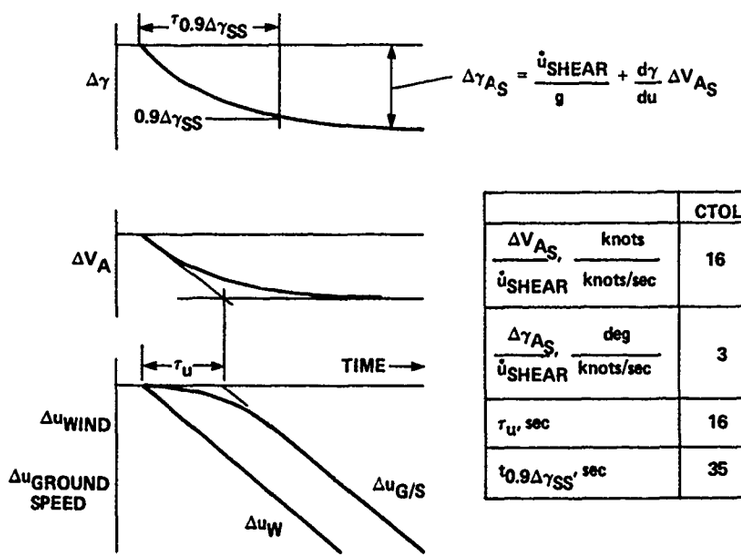

	CTOL	STOL
$\frac{\Delta V_{A_S},\ \text{knots}}{\dot{u}_{SHEAR}\ \text{knots/sec}}$	16	8
$\frac{\Delta\gamma_{A_S},\ \text{deg}}{\dot{u}_{SHEAR}\ \text{knots/sec}}$	3	5
τ_u, sec	16	8
$t_{0.9\Delta\gamma_{SS}}$, sec	35	20

Figure 43. Representative response of CTOL and STOL aircraft to wind shear.

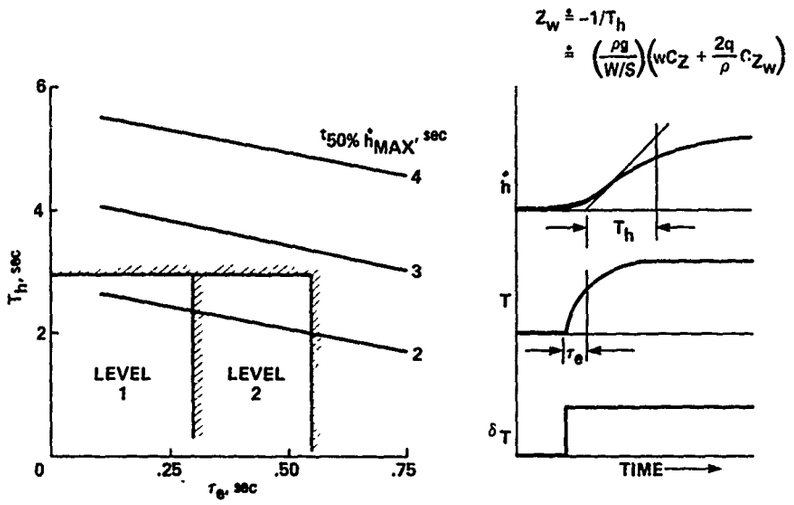

Figure 44. Height control dynamics in hover.

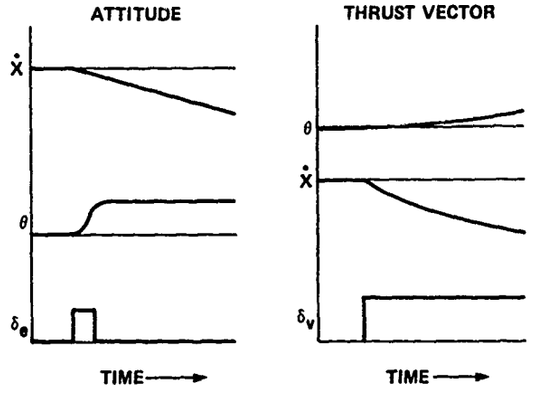

Figure 45. Low-speed translational velocity control.

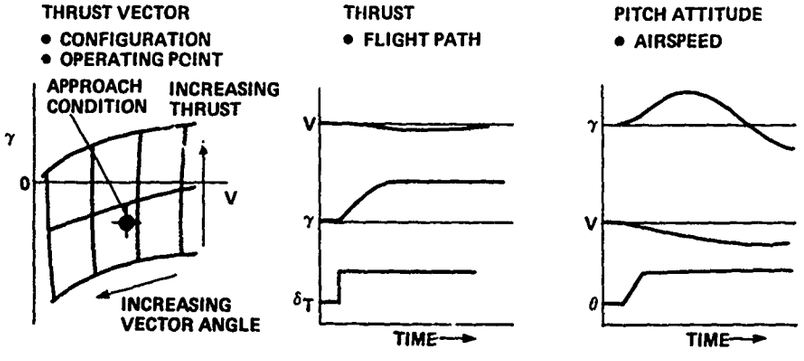

Figure 46. Transition control technique.

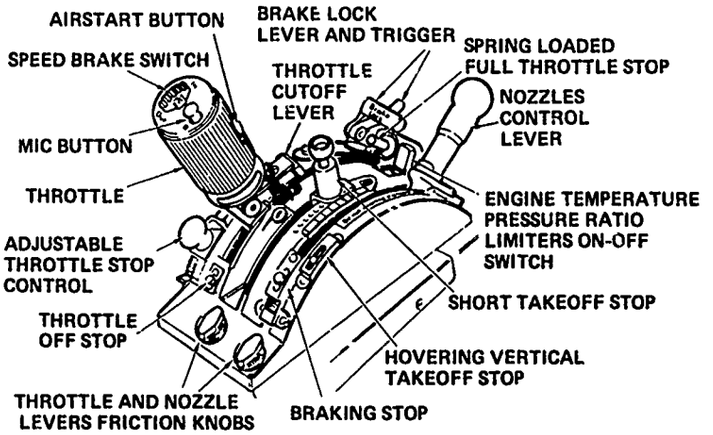

Figure 47. Harrier throttle-nozzle quadrant.

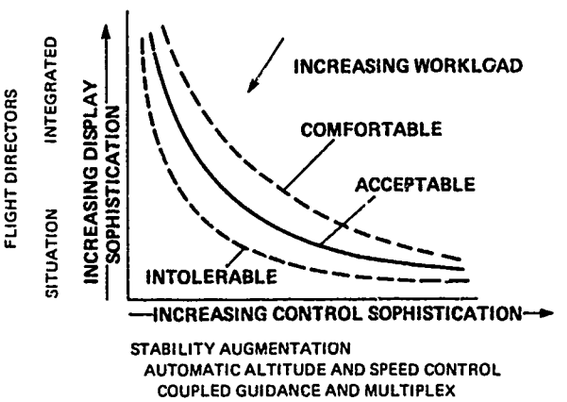

Figure 48. Tradeoff between display and control sophistication (from Ref. 49).

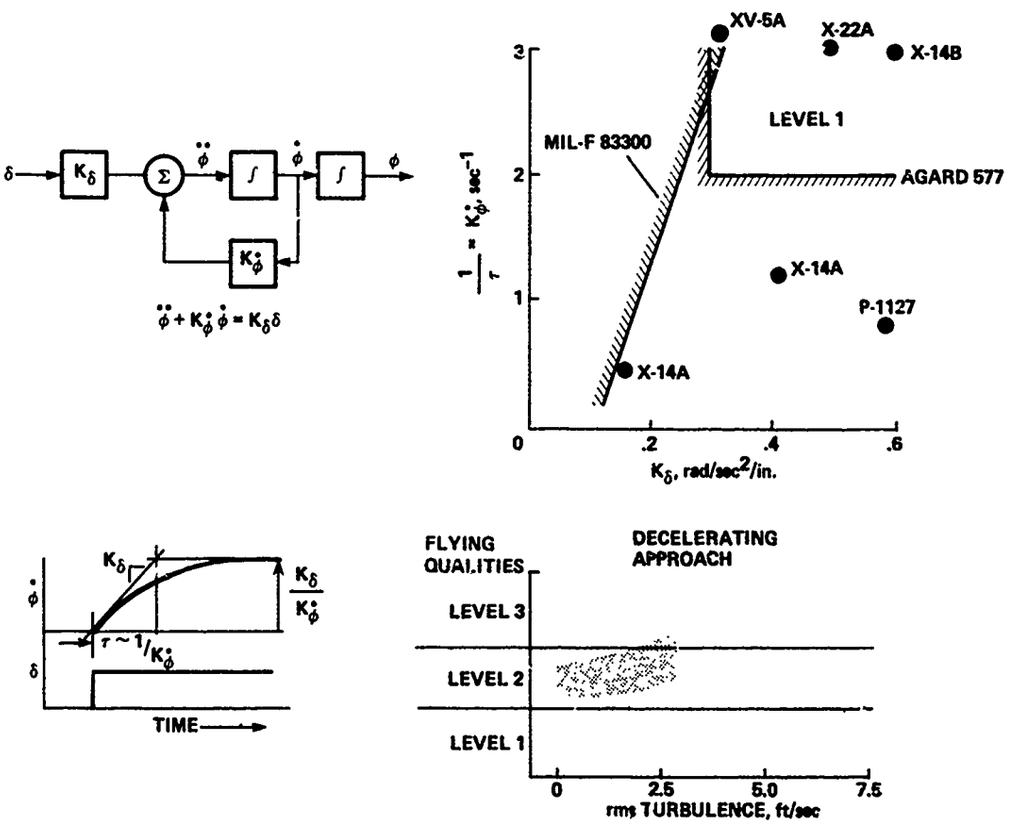

Figure 49. Rate damping stability augmentation.

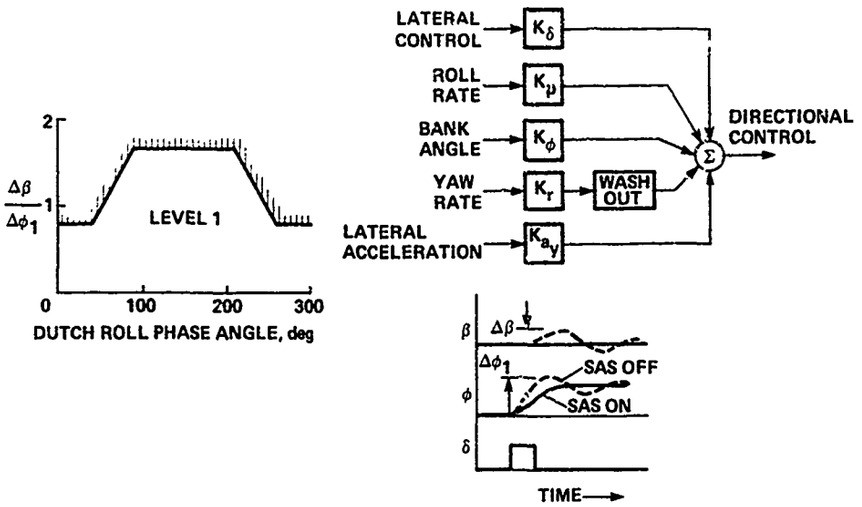

Figure 50. Yaw damper-turn coordinator.

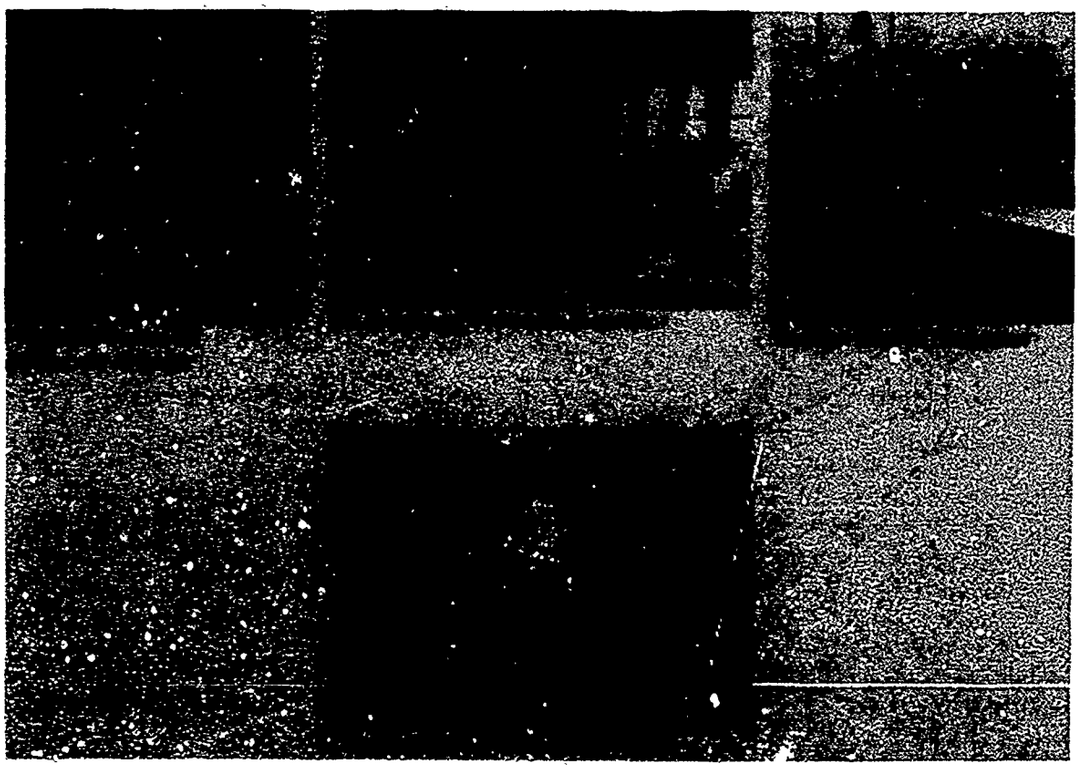

Figure 51. NASA Ames moving base simulators.

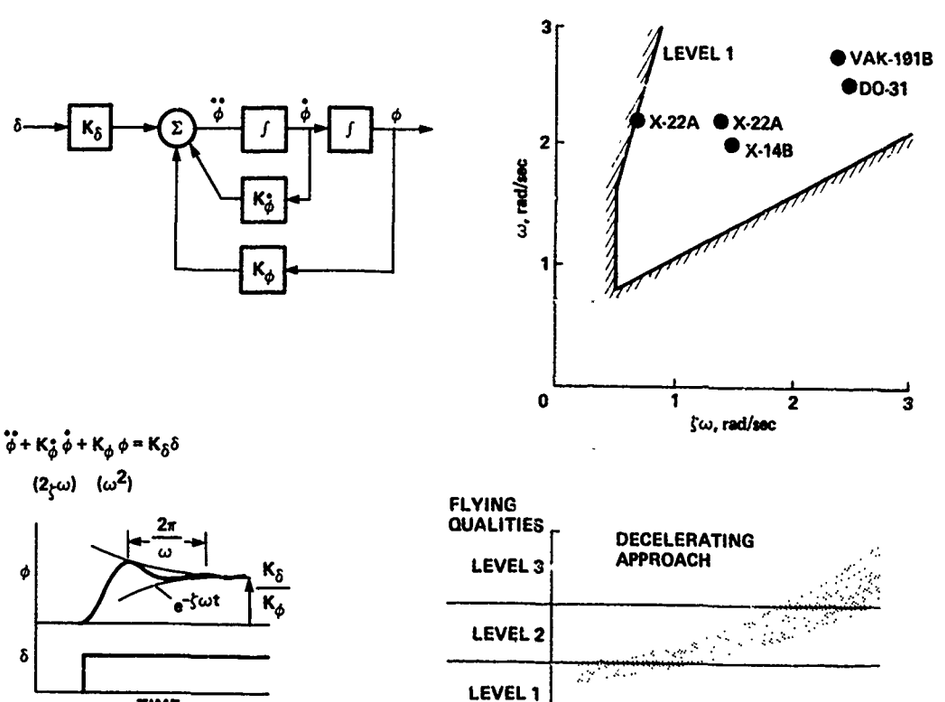

Figure 52. Attitude command systems.

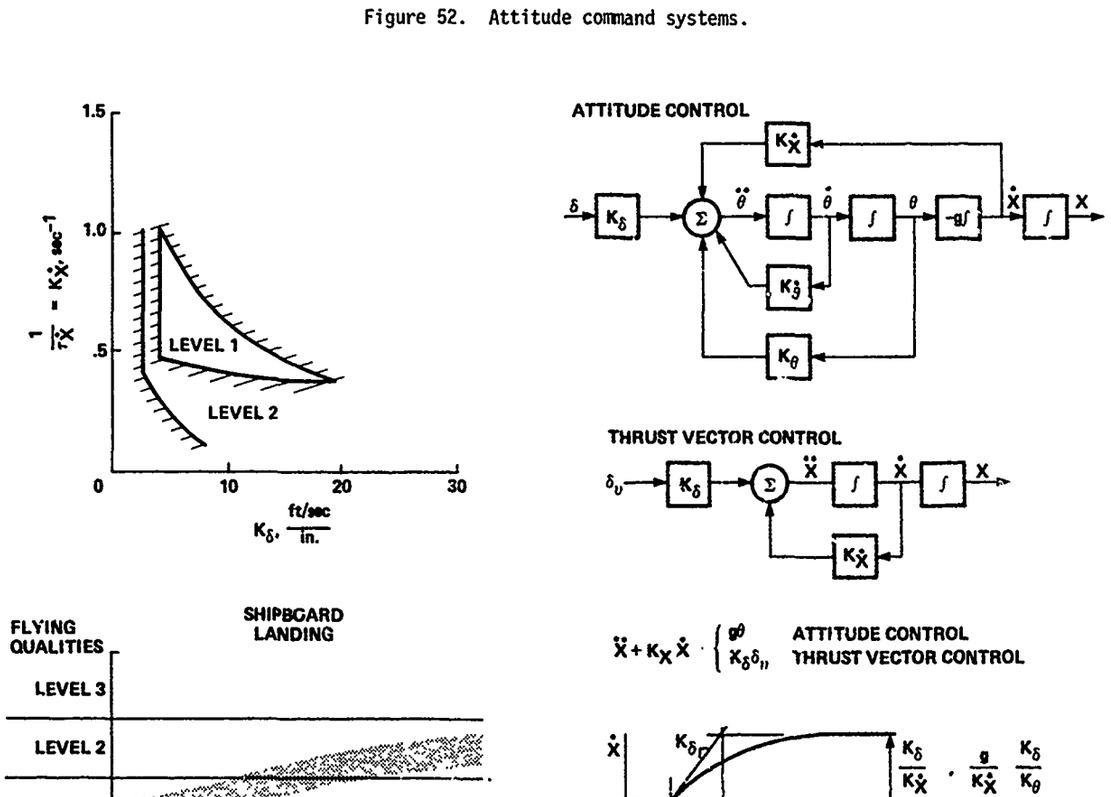

Figure 53. Velocity command systems.

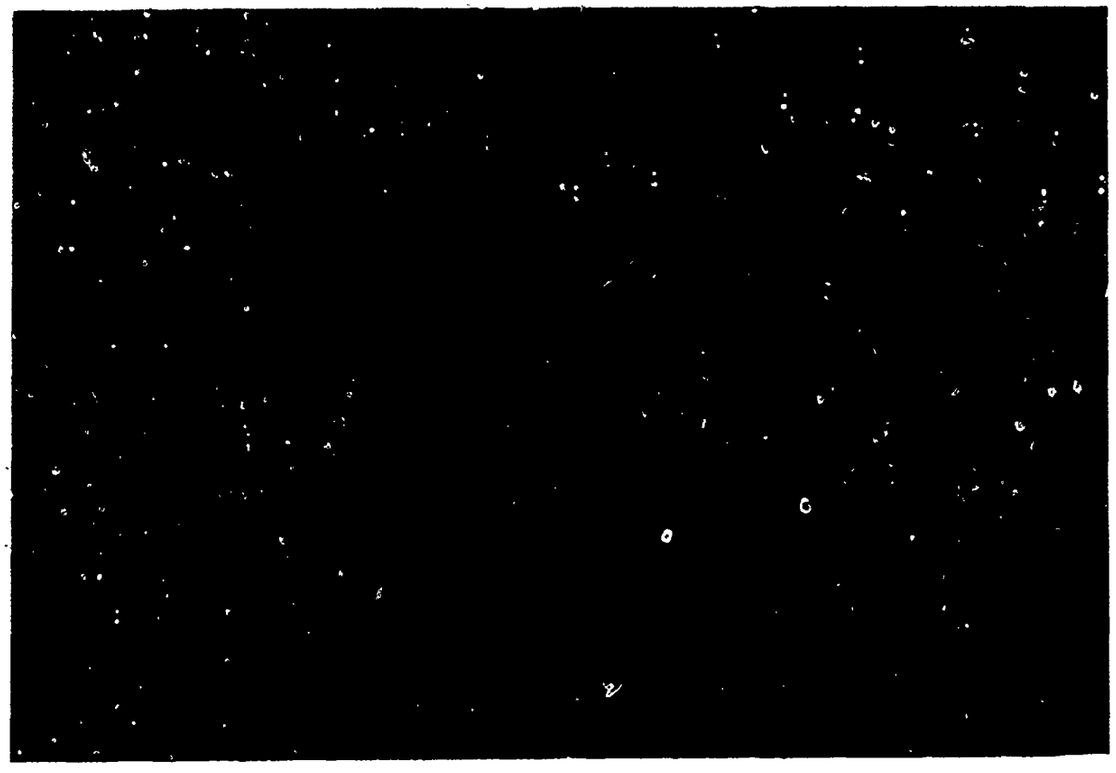

Figure 54. NASA flight/propulsion controls research.

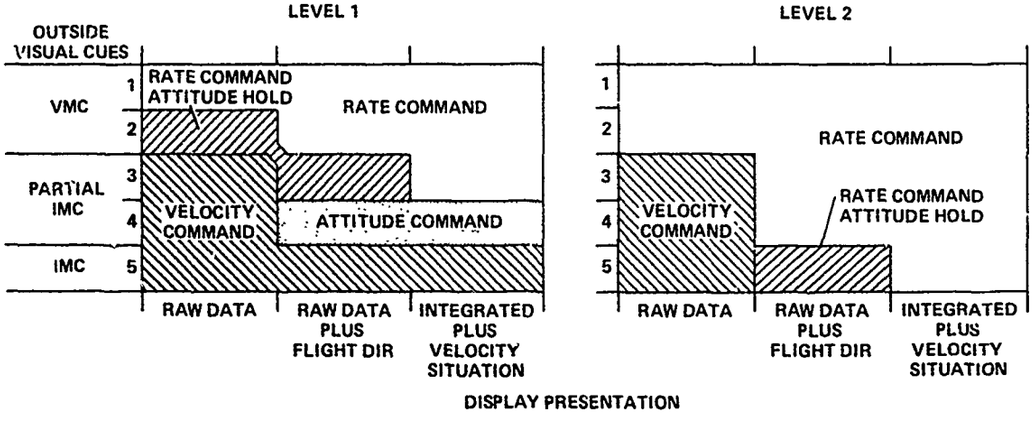

Figure 55. Control/display requirements for low-visibility conditions.

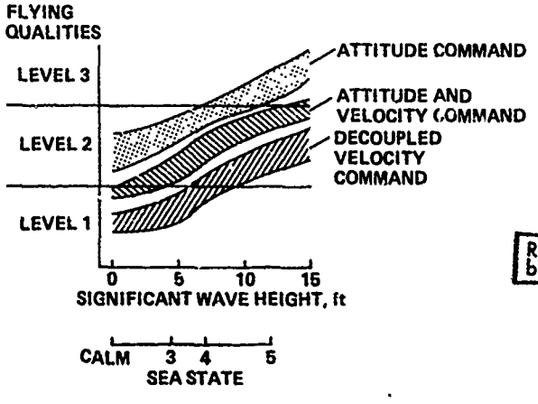

Figure 56. Shipboard landing capability.

V/STOL WIND-TUNNEL TESTING

David G. Koenig
NASA Ames Research Center, Moffett Field, California 94035, U.S.A.

SUMMARY

Factors influencing effective program planning for V/STOL wind-tunnel testing are discussed. The planning sequence itself, which includes a short checklist of considerations that could enhance the value of the tests, is also described. Each of the considerations, choice of wind tunnel, type of model installation, model development and test operations is discussed, and examples of appropriate past and current V/STOL test programs are provided. A short survey of the moderate to large subsonic wind tunnels is followed by a review of several model installations, from two-dimensional to large-scale models of complete aircraft configurations. Model sizing, power simulation, and planning are treated, including three areas in test operations: data-acquisition systems, acoustic measurements in wind tunnels, and flow surveying.

SYMBOLS

A	aspect ratio, b^2/S, nozzle or jet area, m^2 ($in.^2$)
A_L	lifting element area $[n(\pi/4)D_L^2]$, m^2 (ft^2)
A_M	momentum area of aircraft $(\pi b^2/4)$, m^2 (ft^2)
A_N	area of powered lift element, fully expanded; or equivalent nozzle area, m^2 (ft^2)
A_T	cross-sectional area of wind-tunnel test section, m^2 (ft^2)
b	wing span, m (ft)
B	test section width, m (ft)
c	wing chord, cm or m (in. or ft)
$\bar{c}$	mean aerodynamic chord, m (ft)
c_n	section normal force coefficient
c_p	pressure coefficient, $(p - p_\infty)/q$
C_{corr}	corrected coefficients
C_D	drag coefficient, total if not otherwise indicated, drag/(qS)
C_{DA}	aerodynamic drag coefficient, C_D (total) less effects of thrust and ram drag
C_J	jet thrust/qS
C_L	lift coefficient, total, (L/q)S
C_{LA}	aerodynamic lift coefficient C_L (total) less effects of thrust
C_{LAERO}	same as C_{LA}
C_m	total moment coefficient, moment/q $S\bar{c}$
C_{m_A}	aerodynamic moment coefficient less effects of thrust and ram drag
C_{meas}	measured coefficients
C_{si}	see Fig. 71
C_u	jet momentum coefficient $(m_j/q) \cdot (V_j/S)$
d	jet exit diameter ($\approx D_o$)
D	equivalent surface diameter of the suck-down plate, m (ft)
D_e	equivalent exit diameter, diameter of a circle whose area equals the sum of the areas of all jets, m (ft)
D_L	diameter of lifting element, m (ft)
D_n	diameter of nozzle, m (ft)
D_o	outside diameter of annular nozzle slot (the investigation of Ref. 35), m (ft)
F_x	force parallel to free stream, N (lb)
h	ground height, m (ft)
H	test section height, m (ft)
i_t	tail incidence, deg
IGE	in ground effect
K	angle-of-attack correction factor used in Ref. 52, $[3.537 - 1.256(1 - M^2)^{1/2}$
l	length, m (ft)
L	lift, N (lb)
m_j	mass rate of flow of jet, kg/sec (lb/m/sec)
M	Mach number
n	number of lifting elements
NPR	nozzle pressure ratio
OGE	out-of-ground effect
OASPL	overall sound pressure level
p	local static pressure, N/m^2 (lb/ft^2)
Pt	total pressure, N/m^2 (lb/ft^2)
P_∞	free-stream static, N/m^2 (lb/ft^2)
P_o	free-stream total pressure, N/m^2 (lb/ft^2)
PNL	perceived noise level
q	dynamic pressure, free stream unless noted otherwise, $1/2\ \rho V^2$, N/m^2 (lb/ft^2)
s	distance along jet, m (in.)
S	wing reference area, m^2 (ft^2)
SPL	sound pressure level
T	static thrust, N (lb)
Tc	thrust coefficient, [thrust/(q × fan area)]
V_B	moving belt speed, m/sec (ft/sec)

V_e	effective velocity ratio, $[q_o/(T/2A_N)]^{1/2}$
V'_e	value of V_e at which the jet impinges on the floor, (see Fig. 66)
V_j	jet velocity, m/sec (ft/sec)
V_o	free-stream velocity, m/sec (ft/sec)
w_p	primary weight rate of flow, kg/sec (lb·m/sec)
w_s	secondary weight rate of flow, kg/sec (lb·m/sec)
x	streamwise or longitudinal dimension, m (ft)
y	spanwise dimension, m (ft)
z	vertical dimension, m (ft)
α	angle of attack, deg
α_g	geometric angle of attack, deg
β_v	deflector vane setting with respect to fan axis, deg
Γ	vortex circulation strength
δ_j	jet deflection, deg
Δ	difference or change in a parameter
Λ	wing sweep, deg
ρ	mass density of air

Subscripts:

c	corrected
e	effective
i	inlet
n	nozzle
o	free-stream conditions
u	uncorrected

1. INTRODUCTION

Wind-tunnel testing continues to be a key activity in aircraft development. It has been particularly necessary in the development of V/STOL aircraft because our understanding of the complex flow patterns affecting a powered-lifting system and formulations of prediction theories, has continued to lag the requirement to design and build a V/STOL aircraft. Our present ability to predict details of aircraft performance and of stability and control relies heavily on the use of integral flow modeling combined with paneling methods based on potential-flow assumptions. The solutions and computer codes that apply the methods must be efficient enough to be used with aircraft design optimization techniques. As computer capability improves, computational fluid dynamics (CFD) will be used.

In any case, wind-tunnel testing will figure in many stages of the aircraft development from the initial conception of the thrust-vectoring method using quasi-two-dimensional or semispan installations to testing of full or scaled models of the aircraft configuration. Even though we do not have complete and reliable computation methods with which to supplant wind-tunnel testing, they will, in whatever stage of development, be an integral part of the testing phase as means of correlating test results and, possibly, helping to restrict the size of the test matrix.

As indicated by the other lecturers in this series, and in the overviews on V/STOL concepts given in Refs. 1-3, it is a continuing objective in V/STOL development to make efficient use of all available on-board energy for meeting requirements in maneuverability, maximum speed, range, and short field lengths (at an affordable cost). The techniques in testing must be chosen carefully if it is to be ensured that the aircraft designer has well-documented test data (which verify predictions) providing him with sufficient information for preliminary design of the advanced version of the aircraft. At the same time, it is hoped that all the test data can be sufficiently documented using the proper instrumentation to make it valuable as a data base to be used for general aerodynamic study.

Because of these considerations, this lecture will concentrate on methodology with which an experimentalist must be intimately familiar in order to plan and complete a successful V/STOL wind-tunnel test program. The approach draws heavily on some of the factors mentioned in Refs. 4 and 5, and it is assumed that the reader can become familiar with the many other papers on V/STOL wind-tunnel testing, many of which will be cited throughout the lecture. It will also be assumed that the basics of Pope and Harper (Ref. 6) and of Pope and Goin (Ref. 7) are available. The lecture is organized into the following sections: planning: an introductory section outlining the development of a program; wind tunnels: a brief review of typical, moderate-to-large size, testing facilities; V/STOL testing installations: a discussion of options or categories of wind-tunnel installations; model development: a consideration of model sizing criteria, possible power systems, and construction techniques; test operations: a discussion of data acquisition systems, acoustic testing, and flow visualization.

Treatment is limited primarily to fixed-wing (V/STOL) testing as opposed to rotor-wing (helicopter) testing. The author assumes V/STOL also applies to the tilt rotor or even to such designs as the X-wing (which will not be mentioned), but there will be no treatment of rotary-wing testing.

2. PLANNING AND PRETEST PREPARATION

Before all the available tools for V/STOL wind-tunnel testing are evaluated in detail, the essential objectives of the program must be considered, and, to a certain extent, the data analysis be addressed. Unfortunately, such factors as budgets, time restrictions, continual technological advancements, and military/commercial objectives prohibit writing this part in a textbook fashion, particularly for an aircraft development program. This is true for most new experimental efforts, but is particularly true in V/STOL wind-tunnel testing, where the amount of available testing time can be severely restricted because of high wind-tunnel operational costs and costs required to support on-site testing.

The planning sequence will be discussed briefly as follows:

1. Objectives of all testing
2. Test parameters to be considered
3. Model design
4. Wing-tunnel installation
5. Instrumentation and data acquisition
6. Program management

2.1 Objectives

Definition of objectives for V/STOL wind-tunnel testing must include considerations in two areas: (1) establish the overall aerodynamic factors to be obtained from the test that will be essential to the program involved, and (2) obtain an overall feeling for and commitment of the support available for the program (financial and otherwise). For a development program, for example, this can mean obtaining a decision based on studies as to how significant additional aerodynamic lift is related to the aircraft mission weight and cost. Obviously the two are interrelated to the extent that in the end analysis, the available support establishes the complexity of the model and the type of wind tunnel that can be used. Examples of past wind-tunnel programs with various levels of each factor are shown below.

	Factor	
	Aerodynamic scope	Project support
Jet-in cross flow	Component tests	Minimal budget
USB large-scale tests	Complete model	Low budget
Tilt nacelle tests	Component tests	Low budget
Grumman 698	Complete	Large budget
AV-8B 40 by 80 tests	Complete aircraft configuration	Large budget

It should be understood that any of these cases could vary widely in model complexity and instrumentation requirements. The second factor, project support, will not be included in any further discussion but the principals in "aerodynamic scope" will be addressed. An additional item concerning the above test installations is the possible justification for large-scale testing. This will be addressed in a following section.

2.2 Test Parameters

For most wind-tunnel test planning, Margason (Ref. 5) has provided an excellent checklist defining the objectives of an investigation. As is usually the case for any wind-tunnel investigation of complete configurations, the test results will include aerodynamic forces and moments for performance and stability. These characteristics may include aerodynamic propulsion-induced effects for transition flight (Fig. 1) as well as hover. Throughout this flight regime the test parameters must be chosen to define the complete flight envelope with assurance that the thrust effects are obtained. The configuration variables should be chosen and the construction of the model planned so that significant variables, such as flap settings or nozzle deflections, can be evaluated. It is at this point that a judgment in the importance of exact duplication of all aircraft details be made. In planning for either a small wind-tunnel model or in large-scale testing (Ref. 4), this cannot be completely accomplished for a number of reasons; as a result, a concentrated effort should now be made to establish areas in which direct duplication of the full-scale aircraft are not essential for evaluating aircraft flight characteristics.

2.3 Choice of model

It is at this point that the model design factors, such as model size, facility availability and model systems, should be considered as part of the planning. This will be directly influenced by factors discussed in appropriate sections of this lecture. However, there are several general considerations that can be made at this point.

2.3.1 Model size

Anticipated scale effects can have varying significance on the choice of model size depending on how close to production the aircraft to be investigated is, how well defined the details of the final configuration are, and how significant the local areas of flow separation are in their effect on the data. For purposes of discussion, model scale will be referred to as small, less than 0.2 scale, moderate, 0.2-0.5, and large, larger than 0.5 scale. For exploratory investigations with simplified models and for low flap settings and angles of attack, and where accurate corrections are possible, small-scale models can be most economical and produce reliable wind-tunnel test results. This certainly was the case in the early AV-8B development (Ref. 8) in which a powered 0.15-scale model was developed by modifying an available flow-through nacelle model. The resulting comparison with large-scale tests (Fig. 2) showed good comparisons with full-scale data in the linear angle-of-attack range. As might be expected, control and flap lift were slightly lower for the small-scale (Ref. 9) tests. More factors about both the large- and small-scale investigations will be discussed later since they are classic examples of coordinating both large- and small-scale aerodynamic testing in V/STOL aircraft development.

As noted in Ref. 4, there have been several well-documented demonstrations of the significance of scale effects. These are reprinted in Figs. 3 through 7. For components of models, the actual size or local Reynolds numbers may be very small compared with that of the complete aircraft configuration. This was the case for the examples shown in Figs. 3-5, where the small-scale data indicated lower stalling angles for the inlet, deflector vanes, or leading-edge slats. On the other hand, there may be a "size effect" for the complete aircraft configuration such as the one for the small- and large-scale installations of Fig. 6 (deflected slipstream transport model). The large-scale model was powered by PW JT15D engines and tested in the Ames 40- by 80-Foot Wind Tunnel. The small-scale model was powered by ejector propulsion simulators, and the relative size and shape of the 40 x 80 test section were simulated. The differences in the two sets of

longitudinal characteristics, shown in Fig. 7, are probably not only scale effects but may be due to the nonsimilarity in both inlet and exit flow, particularly where jet efflux and its velocity profile effects the induced lift from the flap.

2.3.2 Power Systems

The previous example of the importance of simulating the jet efflux in any powered-lift test is one of many which can probably not be completely documented but in which wind-tunnel testing produced erroneous performance estimations of the aircraft flight characteristics. As is discussed in Sec. 5.2, the current trend is to attempt to simulate the actual engine flow including bypass ratio. The CMAPS (see Sec. 5.2.4) is such a device on which its full application potential is currently being evaluated. The ejectors, developed in the 1960s and which powered the smaller model of Fig. 6 produced a uniform exit flow but were limited in exit pressure ratio and did not simulate the inlet flow rate for a given thrust level. A very valuable workhorse has been the tip-driven fans which have been built in several sizes up to more than 12 in. The driving factor in the use of any of these propulsion simulators is the need to get high-pressure air into the model and, if the forces and movements of the entire lifting system are required, that air must be "jumped" across the sting or wind-tunnel balance. The flexible lines, coil, or other transfer means can have significant effects on the design and cost of the model. At this point, if large- or full-scale testing is contemplated, several schemes of building a large but subscale model such as that of Fig. 8 should be considered. In this case, a model was built using 2-J97 turbojet engines which were 0.7 scale of a two-engine fighter design (see Sec. 5.2). Planning for the power system must be integrated with other considerations, including the compatibility of the facility with the wind tunnel.

For rotary-wing projects, the power systems for some generic rotor tests are variable frequency electric motors. For example, the Ames 40 x 80 rotor test bed shown installed in Fig. 9 is driven by two 1,500 hp variable-frequency motors coupled together. Air-driven and hydraulic-powered motors are also used for small-scale rotor tests.

2.4 Wind-Tunnel Installation

At this point in the planning sequence, the investigator must have a working plan that includes the aerodynamic experiments needed to meet his objectives and must consider what model support and wind-tunnel test facilities are required. A table might be assembled similar to the one shown in Table 1 for in-flight jet noise simulation; it is described in Ref. 10. A section in this lecture covers typical wind-tunnel facilities that are available. Let it be stressed that for the particular demands of V/STOL testing, any choice should include consideration of the equipment and staff that could be made available to the program. Reference 11 or its equivalent will provide important parameters of candidate wind tunnels, but a meeting with the staff of each facility should be held to determine availability. Topics pertinent to V/STOL testing, among many other details should include:

1. Availability of electrical power or high pressure air.

2. Model motors and engine simulators available and maintenance required.

3. Capacity and currency of data-acquisition systems; the value of planned testing depends on reliable documentation of power for each test condition, and this is probably one of the most important topics in the planning.

4. Model support and balance hardware: for rotary-wing testing, few wind tunnels are currently equipped with all the support hardware needed — meaning added cost to the experimenter. For air-driven tests, rotary wing or otherwise, metering and air-transfer equipment are essential topics.

5. For acoustics tests, factors listed in Ref. 10 should be discussed.

6. For large- or full-scale testing, using gas turbine engines, specific items such as maintenance required, fuel, fire control, hydraulics, and start-stop requirements should be discussed. For the Ames 40 by 80, length of testing before temperature limits are reached is an important consideration, although planned improvements in ventilation will extend these limits.

After power systems and wind tunnels have been adequately considered, it is recommended that the combination of model scale or size and type of wind-tunnel support be readdressed. The important factor of magnitude of wall-constraint effects for all projected test conditions may never be answered until after the testing is complete but, as noted in Sec. 5.1., advancements in computational fluid dynamics (CFD) are taking an increasingly essential role in this area. Information that could serve as a guide has been accumulated using the Ames 40 by 80 for tests on widely varying V/STOL aircraft configurations. The resulting wind-tunnel and flight-test data correlations were used to obtain the charts shown in Fig. 10 (Ref. 4 with G698 data added). Data for both lift and momentum, as well as wing-span sizing, were obtained. The lines, representing possible size limits, have been somewhat arbitrarily drawn in the charts to represent guidelines for good wind-tunnel flight comparison under balanced conditions, and all data were obtained on complete lifting systems.

The possible acceptability of using partially complete models or component tests should be considered. Most wind tunnels now in operation have a full stock of the hardware needed for semispan mounts and, if not, it usually is relatively inexpensive to manufacture the needed parts. Where lateral and directional characteristics are not required, the semispan mount is an economical method of studying high-lift characteristics, power-component performances, and loading on all parts. There is enough well-documented testing experience to ensure quantitative measurements and to evaluate most questions concerning effective aspect ratio. As examples, the large- and small-scale installations shown in Figs. 11 and 12 were tested in the Ames 40 by 80 and 7 by 10 wind tunnels, respectively. Objectives of both tests were to evaluate the performance and spanwise effects both in hover and during transition (Refs. 12 and 13). For the 40 by 80 tests, even though the effective wing-span-to-tunnel-width ratio was about 0.4 the wind-tunnel wall effects were minimal caused by the effective depth (80 ft) of the tunnel and the geometric aspect ratio, assuming the end plate (which was fixed and nonmetric) was the reflection plane. For the 7 by 10 tests (Ref. 13), the model size relative to

the wind-tunnel cross section was much larger, but quantitative measurements were still obtained on the ejector performance and its influence on the external aerodynamics of the wing. For this case, accurate evaluation of hovering performance was obtained in the wind tunnel with the large side access door open and blowing the ejector exhaust into the shop area.

2.5 Instrumentation and Data Acquisition

During the foregoing considerations it must be assumed that model instrumentation and data acquiring and processing have been assigned significant roles in the planning. The continuing development of microprocessors and more economical computer systems must be considered in choosing the data-acquisition objective. For example, it is becoming more feasible to obtain a significant amount of pressure data along with the overall force and moment data and a few directly measured component loads. Nevertheless, as indicated by the possible measurement needs for a V/STOL investigation listed in Fig. 13, the advantage of using large-scale solely for the purpose of storing on-board data-acquisition equipment may still offset possible higher model construction costs for the large models. To obtain all the items that can be evaluated on board one large-scale model, it is possible that two-small scale models would have to be built or that at least a force and a pressure model would be built. It is, therefore, essential in planning to evaluate the state of technology of such items as electronic Scanivalves, straingage or capacitance balances or both, or flow-survey equipment.

Most established wind-tunnel facilities are continually evaluating and updating their data acquisition equipment and, during discussions with the wind-tunnel staff the potential limits on instrumentation should be thoroughly discussed. Since current V/STOL testing taxes the most up-to-date computer system, it has been my experience that a program can be enhanced by the experimenter using an auxiliary small computer for some of the measurements that can be correlated using a time-code with the data reduction supplied by the wind tunnel. For rotary-wing testing, dynamic analysis hardware and software are now available at most of the larger wind tunnels. At the NASA 40 by 80, this system is on-line and is an essential part for a safe and successful test procedure.

2.6 Test Program

Having obtained the above information and made the decisions and commitments, a written test plan should be produced and distributed to interested parties to ensure that agreements were as perceived. Except for smaller programs, which are funded and activated in-house, this is good practice for any experimental effort, but it is essential for V/STOL testing to the extent that all those designated in Fig. 14 be informed. The particular examples shown in Fig. 14 were large-scale test programs, but they are still representative in terms of the significance of planning and coordinating most V/STOL wind-tunnel test programs. They are presented in the order of increasing program costs with the numbers listed corrected for 1983 cost-of-living levels with respect to the level existing at the original test dates. The following is a brief description of each as reprinted from Ref. 4.

The test results for the project of Fig. 14(a) are reported in Refs. 14 and 15. This was an internally managed, basic-research, project with the objective of studying stability and control, high-angle-of-attack characteristics through stall, and acoustics. Project management came from Ames Low Speed Aircraft Research Branch (FHA) with both an engine and an airframe manufacturer acting as consultants. Final reporting was done by Ames.

Test results for this project shown in Fig.14(b) are reported in Refs. 16-18. This was a U.S. Navy-NASA funded program, managed by NASA, with the objective of obtaining static (in and out of ground effect) and wind-tunnel data for loads, stability and control, and performance. The model was heavily instrumented to document propulsion and external-surface pressures. The test management came from the Ames Aircraft Project Office, with the FHA serving as advisors. The airframe contractor supported the tests with design, test support, data analysis, and reporting.

Test results for the project of Fig. 14(c) are reported in Ref. 19. This was U.S. Navy funded with test management coming jointly from the FHA, the contractor, and the Navy. The model was equipped primarily for full-scale stability, control, and performance checks with the instrumentation required to document power settings together with a few loads. The cost of the model was an order of magnitude higher than those in the foregoing projects because the model combined a fuselage flight structure with the Rolls Royce F402-R-402 engine and a boiler plate wing-flap system. In addition, since the tests were part of an aircraft development program on a tight schedule, it was highly "visible," and a large number of contractor personnel were required to support the operation of the tests and correlate test results on a daily basis.

Each of these projects has proved to be productive, with the first program being the forerunner of the NASA Quiet Shorthaul Research Aircraft (QSRA); the last program is currently near the production stage. All projects included considerable wind-off testing, as well as wind-tunnel work, and measurements obtained were in the following areas of study.

1. Stability and control
2. Aerodynamic performance
3. Propulsion performance, inlet and nozzle
4. Loads on flaps and control surfaces
5. Surface-pressure measurements on all components
6. Boundary-layer surveys
7. Acoustic studies, near- and far-field
8. Wake surveys, downwash, sidewash
9. Static pressures on tunnel walls to evaluate wall effects
10. Flow visualization
11. Structural static and dynamic loading
12. Aircraft systems check

All of these topics plus those pertinent to rotating-wing systems continue to be subjects of V/STOL wind-tunnel testing, and the remainder of this lecture will address details to be considered in their measurement.

3. WIND TUNNELS

This section presents a short survey of available wind-tunnel test facilities that have, in general, large test sections, are subsonic, atmospheric, and have sufficient support equipment and personnel for testing a complete, powered V/STOL aircraft model through transition speeds. The section is not intended to be a complete survey but rather one that indicates types of wind tunnels and equipment that are available. For this reason, only one large industrial tunnel is mentioned; only the high-speed and pressurized wind tunnels at Ames are listed, though they are not described in detail.

For evaluating the capability of a wind tunnel for V/STOL testing in which flow separation may be occurring at anytime during normal flight operation, it could be assumed that the flow quality in the test section may have a large effect on the power-induced aerodynamics. Because of this, at most of the large wind tunnels, considerable effort has been made to evaluate and improve these characteristics. The significance of flow qualities is discussed in Refs. 20-22 but, for V/STOL, they should include turbulence as well as uniformity of test-section dynamic pressure. Unfortunately, except for the DNW and Langley 4- by 7-m tunne' complete documentation of these characteristics was not available at this time.

3.1 DNW Wind Tunnel

The DNW facility is probably one of the most recently developed. A general description appears in Ref. 23, and a compilation of calibration data is included in Ref. 24. As indicated in Fig. 15, the wind tunnel is a closed-return design and has interchangeable test sections. The latter include 6 x 6 m, 8 x 6 m, and 9.5 x 9.5 m sections as well as an open section for acoustic testing for which longitudinal slots are provided in the walls permitting an open-to-close area ratio variation up to 12%. Flow qualities measured to date are excellent with a deviation of static and dynamic pressure across the test section of less than 0.3% flow angularity ±0.1°, and a turbulence level of 0.1%.

The facility has hardware for either floor or sting mounting. The sting has sufficient degrees of freedom to allow strictly vertical movement without pitch change or pitch and yaw without vertical or lateral displacement. The hydraulic actuation allows a downward velocity of 5 m/sec at 0.5 g for possible use in flare simulation. As with most modern sting arrangements, a high-pressure air-supply line is included to supply compressed air to the model. Floor mounting to the external balance is possible for either strut-supported or semispan models. For gound-effect tests, a 6.3 by 7.6 m (width to length) moving belt can be installed in the two large test sections with a belt speed of 5-60 m/sec. The open-throat feature has been designed for use in acoustics studies. An acoustic evaluation of the facility is reported in Ref. 25.

3.2 8-m ONERA Transonic Wind Tunnel

The ONERA facility has been operating since the 1950s in Modane, France (Ref. 26). The Mach number range is from 0.03 to 1.02, which might enhance its utility for V/STOL testing by making it possible to test with the same model installation from low transition airspeeds to transonic speeds. Although, as discussed in Sec. 5.3, it may not be practical or economical to do this. The facility has a round test section but is equipped with a blown ground board for handling strut- as well as sting-mounted models. An important feature affecting test operations is the ability to exchange test sections, with options such as those shown in Fig. 16(b). For complicated powered models with a network of instrumentation needed, this makes it theoretically possible to make all the pretest checks while another project is occupying the tunnel.

3.3 Langley V/STOL, 4- by 7-m Wind Tunnel

The circuit of the Langley V/STOL facility is shown in Fig. 17. The test section is 4.42 m (14.5 ft) high by 6.63 m (21.75 ft) wide and 15.2 m (50 ft) long. The maximum speed is 103 m/sec (200 knots) and it can be operated in a variety of configurations — closed, slotted, partially open, and open, the latter being open on three sides. Studies have been conducted on methods of improving the flow quality in the test section (Ref. 27). Nevertheless, the wind tunnel has continued to be an essential tool in NASA's low-speed experimental aerodynamics studies and has most of the hardware required for supporting models either by a sting or by using a floor-mounted strut. A moving-belt ground plane is also available. The effort to improve the flow quality and productivity will take a significant step when the wind tunnel undergoes major modifications in late 1984.

3.4 Boeing V/STOL Wind Tunnel

The Boeing tunnel (Fig. 18) is a typical industry-managed facility which is kept uo-to-date as required for company developmental testing, as well as for industry-wide and government-supported programs. There is an option of a 6.6- by 6.6-m (20- by 20-ft) or an open-throat test section, as shown in Fig. 19, with the test section open on both sides. The particular model installation shown is for a small-scale aero-acoustic test for which the model design is discussed in Sec. 4.1.3. This wind tunnel also has the options for either strut- or sting-supported tests. At present, the tunnel is capable of maximum speeds of 250 and 100 knots for the closed and open test sections, respectively.

3.5 Ames 40- by 80-ft/80- by 120-ft System

The Ames 40- by 80-ft has been in operation for about 40 yr, but a recent project (described in Ref. 29) has extended the speed range and added a new test section installed in another "leg" as shown in Fig. 20. To do this, a new drive system has been installed, and vanes are being designed to divert the 80 by 120 test section inlet flow into the fans through the new inlet. It is too early to detail all features of operating in the 80 by 120 test section but the 40 by 80, as it was originally conceived, has proved an invaluable tool for investigating V/STOL aerodynamics, as well as flight-like aircraft systems. With reference to the 40 by 80 test section shown in the elevation view (Ref. 30) of Fig. 21 (updated to show recent changes), the large (and sometimes very heavy) models or aircraft are moved into the outer "high bay" ground level or "2 ft level" and, when readied, hoisted up over the clamshell doors onto the support system. A three-support model installation (the full-scale model of the Grumman tilt-nacelle configuration G698) is shown in Fig. 22. A sketch of the 80 by 120 test section is shown in Fig. 23, viewed from outside the test section.

The size of such a test section as the 40 by 80 has allowed special studies and tests on aircraft components; for example, the acoustic investigation with an installation shown in Fig. 24(a) (see Sec. 6.2.2) and the small-scale hover test in Fig. 24(b). In the latter case a "flying" ground plane was used to incorporate pitch and roll effects into the basic ground-effect study. The data-acquisition support hardware and power systems have been gradually updated through the years, and current data systems include an on-board system that can be made compatible with flight-test installations. Most large- and full-scale models can only be practically supported from below, but for moderately sized models, sting-support hardware has recently been made available. Since aircraft engines at this scale are commonly run in the test section, available support systems include those for fuel, CO_2 and engine servicing equipment, and the power systems usually available, such as air supply and variable frequency power. The facility has a group of qualified aircraft mechanics.

3.6 Langley 30- by 60-ft Wind Tunnel

The Langley 30 by 60 is a classic large-scale installation, and has been in operation since the 1930s. The circuit is shown in Fig. 25. As shown in Fig. 26, it is an open-throat tunnel with the model located just in front of the fans. It has been used for the dynamic stability and control studies described in Refs. 31 and 32 and discussed in Sec. 4.4.1. The wind tunnel has been utilized quite regularly in aviation development as was the case for the installation in Fig. 26. Unfortunately, because of the porximity of the test section to the drive fans, valid acoustic testing has been difficult.

3.7 NRC 9-m V/STOL Wind Tunnel

Except for DNW, the NRC 9-m wind tunnel (Ref. 33) is one of the newest low-speed tunnels, having been in service since 1970. Its development included testing of a 1/10-scale model of the wind tunnel and, although quantitative values of flow turbulence are not available for publication, there is a set of screens immediately upstream of the test section. Most of the V/STOL testing experience to date has incorporated a floor-mounted strut system such as the installation shown in Fig. 27, which is connected to the balance system below the floor. One particular asset for air-driven V/STOL testing is the compressed air supply. It has nearly full use of the NRC Blowdown Wind Tunnel supply which produces dry filtered air at 2050 kPa (300 lb/in.^{2}). At the wind tunnel, this means 1,700 kPa (250 lb/in.^{2}) for 30 kg/sec (45 lb/sec). Unfortunately, heating capability is limited.

3.8 Other Wind-Tunnel Test Facilities

The foregoing brief survey has identified some of the larger wind tunnels that are atmospheric and have complete facilities for both fixed and rotary-wing investigations. Not described were the United Kingdom large subsonic tunnels, the Lockheed tunnel, the high-speed tunnels such as the Ames Unitary System (Fig. 28), and the 12-ft pressure tunnel. The 11-ft test section of the Unitary System is capable of holding a continuous speed down to M = 0.4 so that a program can cover subsonic airspeeds for models designed for transonic and supersonic testing. The CMAPS program, at Ames (see Sec. 5.2.4) is designed to make such testing eventually practical by accurately simulating inlet and exit flows. In addition, ther are several 7 [illegible] wind tunnels in academia, government, and industry which can be useful for small-scale or component tests.

One of the most economical systems of wind-tunnel testing, particularly as it is applied to V[illegible] ing, is the one described by Knott (Ref. 34) and operated by British Aircraft Corporation (BAC), Mi[illegible] Aircraft Division (Fig. 19). The test section is 5.5 m (18 ft) wide and 5.0 m (16.5 ft) high, but the [illegible] operates over a narrow speed range of 11 to 21 m/sec (35 to 70 ft/sec). This requires an installed power of only 200 kW (250 hp). There is some disadvantage in that the existing installation is the open-throat, no-return type and its test-section flow qualities are, therefore, subject to weather. The design trade-off may, then, be one of flow quality required against the cost of screens and flow straighteners resulting in increased power required. The testing and scaling techniques assume that Mach number simulation is not important. Table 2 shows typical values for the test velocities compared with full-scale values. A major advantage could be lower model costs and lower on-board power requirements. This also could mean a "lower profile" support system required to take the lower model loading.

4. TESTING INSTALLATIONS FOR V/STOL

Since the choice of the proper testing installation depends on many factors — not the least of these is cost — it would be meaningless to suggest any given procedure for choosing the model installations. The following are examples of test programs that in most cases, proceed through a variety of wind-tunnel test setups.

Much information can be obtained from such exploratory tests as that shown in Fig. 30 (Ref. 35), which had the objective of evaluating characteristics in hover and forward flight for a ground-effect vehicle — the "Avro" car. This test, in the Ames 7- by 10-ft tunnel was made after 40 by 80 tests showed the full-scale vehicle had a large aerodynamic center location change as it lifted out of ground effect. The small-scale test was a very low-cost effort to investigate the fundamentals. A sampling of the test results is shown in Fig. 31. Ground effect was measured very close to the ground board. Although not done, the data could have been corrected for the displacement thickness of the boundary layer by the method similar to that suggested later by East (Ref. 36):

$$C_{corr} = C_{meas} \times \frac{\delta^*}{h} \frac{\partial C}{\partial(\partial^*/h)} + \frac{\partial \delta^*}{\partial X} \frac{\partial C}{\partial(\partial \delta^*/\partial X)}$$

where the gradients of C are determined by carrying out additional tests with other boundary-layer thicknesses. No moving belt was needed with BLC being planned for but not used and qualitative correlations were made with the full-scale data.

An example of a more sophisticated (and more costly) test is that of the Grumman 698 tilt-nacelle development. It was decided that a full-scale test was needed to verify control which might be available from the 698 control-vane effectiveness design. A component test installation in the Ames 40 by 80 tunnel was used

(Ref. 37). The nacelle was powered by the Q-fan (Ref. 38), and was mounted on the 40 by 80 wind-tunnel turntable as shown in Fig. 32, which provided the nacelle with a large angle-of-attack range. In this case the inlet and fan itself were the subject of another investigation (Ref. 39), so that two test objectives were met using common hardware.

A third example, that of the development of the XFV15 tilt-rotor aircraft (Refs. 40 and 41), included the series of test installations shown in Fig. 33. Going to a higher disk loading and a more usable drive system meant a series of tests varying from small- and large-scale semispan models to testing the actual aircraft in the Ames 40 by 80 tunnel.

The range in possible types of installations varying in complexity and cost between those of the previous examples is large, and the test objectives are diverse. In the following discussion, experience with test installations varying in type and complexity will be discussed in more detail.

4.1 Partial Installations

Even though for V/STOL investigations it is usually essential to simulate the complete aircraft configuration in the final aerodynamic evaluation of the aircraft, component testing, two-dimensional testing, and quasi-two-dimensional testing can take a major part in the program. Examples of these installations follow.

4.1.1 Component testing

In one of the previous examples (Fig. 32) it was necessary to establish the control effectiveness of the pitch-control vane before going ahead with a full-scale model. In that test, the data of Fig. 34 verified predictions that the fan efflux would provide sufficient control effectiveness through a wide range of nacelle attitudes. The vane loads and fan flows were documented with sufficient on-board information to establish design information for proceeding with the program. Note that in this case, it did not seem necessary to simulate the wing or fuselage interference effects. This would be the subject of the next phase — a full-scale model an order of magnitude more costly than this one.

For a two-engine fighter configuration, overhead inlets have recently been investigated by Smeltzer et al. (Ref. 42) and Durston and Smeltzer (Ref. 43), using a component or partially complete model installation, as shown in Fig. 35. The inlet region of the model was sufficiently instrumented to obtain both external flowfield contours forward of the inlet and inlet distortion and pressure recovery. This was done using five-hole cone probes. The forward part of the model was sufficiently simulated to relate changes in leading-edge configuration to flow at the inlet plane for both subsonic and supersonic speeds. The model had flow through the nacelles, but metering plugs were added to vary flow through the inlet.

Certain basic study projects and key experiments can also be placed in this category. Many researchers have been accumulating wind-tunnel data on the jet-in-cross flow problem, as reported in Ref. [illegible] for the installation of Fig. 36. Initially, this type of experiment was started with the use of a flat plate, as shown in Fig. 37, with a 10-cm (4-in.) jet issuing from the center. Then, using a smaller test section (Ames 7 by 10), the body of revolution and another flat plate were tested. All tests have been closely coordinated in objective and scope, that is, to evaluate the pressure on the surface surrounding the jet exit and to study the flow in the jet itself. From this data base, several jet models of the jet-in-cross flow problem are being evaluated, among them being the diffuse vortex model of Fearn and Weston (Ref. 45). The 5-cm (2-in.) jet model has also been used recently to study the flow characteristics using a three-component LDV technique which is described in Sec. 6.3.2.

4.1.2 Two and Quasi-Two-Dimensional Testing

Before the significance of powered-lift effects on airfoil section characteristics was fully realized, airfoil sectional characteristics were accurately evaluated using test installations of constant chord and spanning the width of the wind-tunnel test section. The height of these tunnels was generally much more than their width to minimize blockage corrections. For high or powered lift airfoils the technique has been successfully applied using precautions for preventing flow separation on the end wall. In one case (Ref. 49) for the installation of Fig. 38, a powered nacelle was added to a two-dimensional high-lift externally blown flap (EBF) installation to evaluate leading-edge stall control and turning effectiveness. As in the case of any airfoil adjoining a flat plate, the adverse pressure gradient on the airfoil is transmitted to the wind tunnel or end-plate walls. A positive way of controlling this is to use local BLC at critical locations on the plate itself.

This was also done to the quasi-two-dimensional model shown in Fig. 39. In this instance, the objective was to study effects of airspeed on a span-wise ejector (Ref. 50) and to derive the two-dimensional section characteristics of such a high-lift device for correlation with large-scale tests on a complete model configuration. It was found that although the two-dimensional effective angle of attack could not be evaluated to much closer than ±2°, the effective aspect ratio was sufficiently large, — approximately 8 (based on the power-off drag polar) — to make the power-on data useful in evaluating the ejector performance as functions of both power and angle of attack. The key to such an installation is the design of the end plate. There are very few published data on large end plates except those by Riley (Ref. 51); more recent studies are being directed at drag reduction of higher aspect ratio wings. For the installation of the high-speed evaluation of wing cruise blowing system by Mahal (Fig. 40; Ref. 52) the angle of attack was evaluated as

$$\alpha = \alpha_{geom} - k\,Cn$$

$$k = 3.54 - 1.26(1 - M^2)^{1/2}$$

This is consistent with all the power-on data obtained, and was used in evaluating the effects of blowing on the drag rise Mach number at a target cruise lift. This installation shown installed in the Boeing wind tunnel (Fig. 40) had an end plate that was contoured to minimize drag at high subsonic speeds. All data were in the form of surface pressures integrated to give lift and pitching movement with momentum rake data being used for drag evaluation.

4.1.3 Semispan Installations

Semispan models have been widely used in the conceptual stage of a high-lift concept. In the 1950s very economical installations, such as the one described by Anscombe and Williams (Ref. 53) and shown in Fig. 41 were developed. The advantages over complete aircraft simulations are lower cost plus larger scale potential for a given test-section size. The main disadvantage is lack of any lateral-directional information and, possibly, questionable pitch control-data. Most installations rely on the use of either a mechanical or electrical balance, located below the floor.

A major choice for such an installation is whether to have the model include a half fuselage that is metric, such as the one in the sketch of Fig. 41; a fuselage that is nonmetric, or attached to the wind tunnel floor; or an end plate that is nonmetric with the wing protruding through it. Except for exploratory tests in which the longitudinal characteristics of a canard/tail-wing configuration are needed and each component must be repositioned, the author is partial to the use of the metric half fuselage. Experience in the Ames 40 by 80 with the semispan installation of Fig. 11 (Ref. 12) has been excellent to the extent that approximate correlations were made with a complete jet flap wing-fuselage model. For the installation of Fig. 11, the root or effective plane of symmetry was raised to be clear of the floor boundary layers. The test reported in Ref. 54 and shown in Fig. 42 incorporated a half fuselage that pitched with the wing but was nonmetric and attached to the floor fairing of the tunnel. The disadvantage of this is sealing problems where the root of the wing had to be nonrestrictive in order to avoid affecting the measurements of the wing characteristics. For high-lift conditions, the pressure difference places an additional force on any seal that is installed.

The semispan installation was also used economically in the development of the XV-15 tilt-rotor model mentioned earlier. Using the installation in Fig. 33(c), both power-off and power-on tests were made as described in Ref. 55 to evaluate rotor aerodynamic performance, rotor dynamics, and hardware of the rotor systems. Even though the root of the wing was rigidly fixed, the wing-rotor dynamic measurements could be used to predict operating limits of the complete aircraft. The model shown was unpowered and could be assembled with spars of three different natural frequencies. During the windmilling tests, the effect of damping of the rotor-pylon-wing twist mode was evaluated with step inputs into the rotor tilt actuation system. The rotor performance was later studied using a dynamometer test installation. All test results were correlated with small-scale measurements and predictions.

4.2 Testing Complete Aircraft Configurations

Since the wind-tunnel time for complete aircraft configurations is a major part of the aerodynamic and dynamic development for any aircraft, conventional or V/STOL, any cost saving in this phase can have a major effect on the overall development costs. Powered V/STOL models themselves are inherently more expensive than unpowered conventially configured models. This is a result of additional costs that are incurred not only because of adding power to the model but also because of the additional effort needed to support the tests. Other costs come from the increased amount of on-board instrumentation for which leads have to be "funneled through" or around model supports. As for moving-base or for free-flight operation, the model must be sufficiently light and designed for adequate remote control. Low model weight and light power units are also required for track-supported models such as used at the Princeton track facility. Examples and problems of each of the above will now be discussed.

4.2.1 Sting Supports

For the rigid mourting category, sting supports, in addition to high-speed requirements, are sometimes desirable for minimizing aerodynamic interference induced by model lift, particularly in ground effect. For some test conditions, strut mounts can induce buoyancy or blockage under the model that may be difficult or impossible to evaluate. For V/STOL configurations, it is important that the sting support be downstream of the area generally occupied by lifting jets and flaps. As can be seen by the model support in Figs. 43 and 44 (Refs. 56 and 43), however, the rear end of the model can be adapted to receive a sting of sufficient size to minimize support flexibility and, at the same time, enter the model with a minimum alteration of the rear contour.

In the case of the CMAPS-powered model shown in Fig. 45 (Ref. 57) for the two-engine supersonic fighter, the pressure and instrumentation leads were routed forward under the fuselage. During these tests an attempt was made to set the narrow segment of sting as short as possible to reduce "bounce" and length of high-pressure leads. Lower surface pressures were calculated at the model plane-of-symmetry; a summary of the results is presented in Fig. 46 (Ref. 58). It is evident that lengthening the sting or moving the adapter 0.30 m (12 in.) farther from the model reduced the influence of the adapter to a very small amount ($\Delta C_p = 0.05$) at the model trailing edge.

For some powered fighter configurations, an off-side or overhead mount could minimize restrictions in direct simulation of the rear of the aircraft such as the mount shown in Fig. 47 for a generic fighter investigation. Instrumentation leads and the air for powering the propulsion jets were routed in through a twin support at the vertical tails, thus leaving the lower-rear of the model free of any induced flow generated by the deflector nozzles. This was mandatory in this case because the objective of the test was to evaluate the effect of nozzle configuration on the aerodynamics of the model over a large Mach number range.

A somewhat larger model built for lower speed with a corresponding lighter construction (lower weight per size) was tested in the Ames 40 by 80 as shown in Fig. 48 (Refs. 60 and 61). This was a sting-supported model to be installed on the 40 by 80 turntable, and the model chord plane was vertical so that rotation of the turntable would change angle of attack through high angles. The configuration was a side-by-side twin-engine configuration so that the sting installation required a widening of the rear fuselage slightly beyond scaled width. For this case, it was judged acceptable since aerodynamic corrections could be made using integrated surface pressure measurements. Also, in this case, it is believed that the thrust of the fans had little interaction with the sting since they were used to pump air through the inlets, and the momentum of the exhaust was exceptionally low. A disadvantage of this installation was the asymmetrical lateral/directional effects on the model induced by the vertical strut.

As the full model size capabilities of the large atmospheric wind tunnels are utilized, the models may become large and heavy enough to preclude sting supports. At this stage available sting hardware may produce mounting that is too flexible to maintain a stable platform for the balance. There is probably some model size-weight level for which strut mounts become mandatory for practical reasons and for which the required sting size becomes too large to allow tailoring the rear of the model to scaled aircraft contours. There appears to be no coherent criteria to help in the strut or sting choice but a thorough study of the interaction of possible oscillating aerodynamic loads and the model-support dynamics is an essential part of this choice.

4.2.2 Strut-Supported Installations

For a configuration in which there is a large amount of power-induced circulation from the wing, the single support mount shown in Fig. 49(a) (Ref. 62), a 1/7-scale test of the H126 jet wing aircraft, was used successfully. For comparison purposes, the aircraft itself is shown in Fig. 49(b) mounted in the Ames 40 by 80. The small-scale test was made in the Ames (Army) 7 by 10 and employed a pitch link activated by a rod running parallel to the main strut. The large fairing enclosed instrumentation and the pitch-link actuator. In most cases, this actuator can be located below the floor to reduce the required fairing size. When the lift jet efflux is in the center of the model or it is thought that strut interference effects would be excessive, the model can be inverted, as shown in Fig. 50 (Ref. 63). As with sting mounts, a disadvantage of the heavier models is that the single-strut installation tends to be more flexible in the yaw-roll modes of oscillation.

An interesting type of hybrid mounting system (Fig. 51) has been used by Boeing Vertol for rotary-wing testing. It incorporates the air-driven "power pod" in supporting a helicopter model. The pod itself has been attached to the sting which is equipped for pitching and yawing the entire system. The "pedestal" or vertical strut supports the model through the balance inside the model. An optional setup uses the same power pod for a floor-mounted installation.

Because of model weight, large- and full-scale models at the large-scale test facilities (40 by 80 and 80 by 120 at Ames and the 30 by 60 at Langley) must use floor-mounted struts, usually, a three-strut system as shown in Figs. 22 and 52, respectively. The struts tend to be stiff in yaw if the main struts are mounted to the outer wing, such as in the case for the AV-8B model of Fig. 53. A compromise was made in the landing-gear-type mount for the STOL transport model shown in Fig. 6(a) (as well as with the 698 model of Fig. 22). For these models there was a special effort to design the model with the struts away from the undersurface of the wing in order to minimize any local effect on wing airflow separation.

Even with the effective thickening of the strut tips due to attachment of leads, there has been a wealth of evidence that for the V/STOL configurations tested to date, strut-interference effects have been extremely small. This confidence has come primarily in the comparisons of full-scale wind-tunnel test data for actual aircraft with their corresponding flight-test results (Refs. 64 and 65). Data representing an assortment of V/STOL aircraft have correlated well in both angle of attack for a given lift and power setting, as well as for stability and control. Some of the data for the smaller aircraft, such as the VZ3 and XV3, correlated well without applying any wall constraints or blockage corrections to the data. Concerted efforts to generalize what strut tares exist, as suggested in Ref. 6, have not been successful for V/STOL models, particularly at the low-speed end of transition with high flap settings and jet deflections.

4.3 Ground-Effect Testing

As shown by the experience with evaluation of the flight versus wind-tunnel data of the Augmentor Wing Research Aircraft at Ames and discussed by Cook and Whittley (Ref. 64) a highly deflected jet impinging on the floor of the wind tunnel must be accurately simulated. It must be prevented from migrating too rapidly forward through the low momentum of the floor boundary layer then blowing back up (which may or may not be the case for the actual aircraft in flight) and over the wing. This can be reasonably well simulated by maintaining a small boundary layer by either or both BLC and moving belt (Ref. 66). An additional method is the moving-model technique such as has been used at the Princeton and other towing facilities (Sec. 4.4.2). In 1977, Campbell et al. (Ref. 67) reviewed the status of the use of wind-tunnel measurements to predict aircraft flight characteristics, including initial experience with the C8A just mentioned. Since that time, similar comparisons have been made using both the Harrier and QSRA, results of which have not been well documented. Most of these comparisons varify the so-called Turner criteria which is shown in Fig. 54 (taken from Refs. 29 and 68) or the equivalent if BLC is used to control the boundary layer on the ground plane. Margason (Ref. 5) has also reviewed the need for a moving belt or BLC and concluded that for low-aspect-ratio wing configurations, particularly those using deflected thrust concentrated in a small area, less control of the wind-tunnel floor boundary layer is required. In any case, some of the flow phenomena restricting the measurement of ground effect of V/STOL configuration in a wind tunnel are the same as those governing model sizing (Sec. 5.1). Turner's belt installation (Ref. 68) was in an enlarged inlet of the Langley 7 by 10 300-mph wind tunnel and, as shown in Fig. 55, is close to the inlet of the test section. The result was as expected. As shown in Fig. 56, with the belt speed synchronous to the tunnel airspeed, the boundary layer was completely eliminated. The early development of the moving belt itself, as indicated by Butler et al. (Ref. 69), was tedius, but through advancements in materials and multiple drive systems, current operation is relatively trouble free. At the present time, most of the moderately sized low-speed tunnels having sting supports are equipped with a moving belt similar to the one in the Boeing Vertol tunnel (Fig. 57) where the essential parts of any belt system are noted. As shown, the suction slot provides BLC forward of the front roller.

A more economical method of accounting for the wind-tunnel boundary-layer growth is the placement of BLC on the floor by itself or combined with a raised ground board forward of the model. A study was completed for NASA in 1974 (Ref. 70) to explore the feasibility of a BLC installation in the Ames 40 by 80 wind tunnel. The objective was to facilitate ground-effect testing, as well as to lower the testing airspeed restriction for propulsive systems with highly deflected jets. The finally recommended design was not used for economy reasons, but the design (Fig. 58) is still considered valid, and basic aerodynamic studies by Hackett et al., which were vital in understanding BLC requirements, continued through the 1970s. Other investigations were summarized in a 1973 lecture by Poisson-Quinton (Ref. 71). In most of the studies, small-scale jet flap tests were made, using both a belt and BLC. Typical wind-tunnel results, though preliminary, were updated by Hackett et al. in Ref. 72, and a sample set of pitching-moment data with tail on is shown in Fig. 59 for the case of 2 chord lengths above the floor. The correlation between fixed-ground plus BLC and the moving belt are

good, even though, at $C_\mu = 3$, the jet wake is probably starting to impinge on the floor. When this happens just behind an unswept wing or two-dimensional jet flap model, the flow pattern, which includes a standing vortex, is established and causes suck down. The control and intensity of this flow pattern is affected by floor BLC (or moving-belt velocity), but may not get established during the landing flare or any other transient situation.

4.4 Moving-Base Testing

If the above mentioned flow patterns are not particularly Reynolds-number sensitive, moving-base techniques may be used to evaluate their effects. V/STOL models configured to simulate the power loading as a complete aircraft configuration and at the same time to have sufficient scale to ensure quantitative test results tend to become heavy. An example of hardware needed to move a heavy model in vertical motion is shown in Fig. 60, which was the result of a design study (Ref. 73) to investigate problems of simulating the transient ground effects in the Ames 40 by 80. The design criteria for a 0.11-scale model of a large STOL transport aircraft included the following test conditions and model parameters:

Dynamic pressure, kPa (lb/ft^2)	1.93 (40.3)
Reynolds number, RN	2.24 (10)^6
Model weight, KN (lb)	3.23 (727)
Model span, m (ft)	3.7 (12.1)
Sink rate, m/sec (ft/sec)	5.2 (17)
Rotation rate (for flare) deg/sec	67

Scaling full-scale flare and touchdown maneuvers brought large accelerations; the result is the design of Fig. 60 and prohibitive costs. Even though a trade-off between facility cost and model scale may reduce the size of the support somewhat, studies of some of the questions on transient ground effects and aerodynamic damping using scaled experiments may still have to rely on the use of track facilities and free-flight techniques. The following is a brief discussion of two such facilities.

4.4.1 Free-Flight Methods

Although the term free-flight testing is also applied to high-speed or ballistic testing, or the spin-tunnel testing for V/STOL evaluation, it has usually become synonymous with the wind-tunnel free-flight methods such as used in the Langley 30 by 60. With use of this technique, a qualitative evaluation of flight characteristics of a wide range of aircraft concepts has been made in and out of ground effect. The well-known technique (Fig. 61) incorporates Froude-scaled replicas of the aircraft. Reference 74 includes a concise description of significant factors of the technique, and equations of motion for the models are listed in Ref. 75. For most current aircraft designs, the geometric scale tends to run from 1/10 to 1/5, with lengths 2.1 m (7 ft), wingspans of 1.52 to 1.83 m (5 to 6 ft), and weights of 224 to 267 N (50 to 70 lb). With this scaling, the model angular motions are up to 3 times as fast as those at full scale. This brings the requirement for multioperators. Since the operators must attempt to keep the aircraft in one position or on a predetermined flightpath and, as mentioned, the time-constants are 1/3 full scale, light, quick response actuators have been developed which provide the pilot with tight control. The model is instrumented to measure linear and angular acceleration along with control-surface positions which are transmitted throughout the flight to strip charts. The flight cable also supplies the high-pressure air to the model motors. Motion pictures document the flightpath and representations of desired automatic stability and control augmentation systems are input into the control systems.

Although these techniques have gradually been improved through the years, Paulson (Ref. 76) still gives one of the most detailed descriptions of the technique and its problems for use with the B-58. In a more recent application, the free-flight technique was used to evaluate the high-angle-of-attack characteristics of a forward-swept wing fighter configuration (Ref. 31). The program included the use of two models, one a 0.16-scale model of the complete aircraft and a 0.16-scale flat plate model. The former was both fixed-support tested and tested in free flight. The project was coupled with tests of both models on a free-to-roll apparatus in order to evaluate any unclamped roll oscillations at high angles of attack. The model is shown in Fig. 62 being tested in the free-flight mode. Damping in roll evaluated from the free-flight tests was found to agree quantitatively with the flat-plate measurements for moderate angles of attack.

4.4.2 Moving-Base Track

A major difference between the free-flight facilities and the moving-base track is the latter's capability of restraining certain undesired degrees of freedom of the model motion. Therefore, it pre-programs a flightpath such as a landing flare or a roll oscillation. In the case of the Princeton Track (PDMT), Froude-scaled models are moved along a pre-programmed route that is 246 m (750 ft) long (Ref. 77). The track is enclosed in a building 9.8 m (30 ft) wide and 9.8 m (30 ft) high and, during operation, the building is tightly sealed to ensure still air along the flightpath. The facility has been equipped with a model support system (Fig. 63) that allows small amounts of model translational motion freedom, as well as angular motion about a ball-bearing gimbal system. Any motion with respect to the carriage is measured and used as an error signal in a closed-loop servomechanism which can position the carriage with respect to the model. If everything is working properly, there is, essentially, a free-flying model about a mean free flightpath with which to reference the natural dynamics of the model. Note also that the facility can be used for steady-state (Putnam refers to it as static) testing in which the model moves along the track at a constant vertical position. A version of the subsonic tilt nacelle (Grumman 698) V/STOL aircraft was tested as reported in Ref. 78. The principal objective of the tests was to evaluate transient ground effects. Although the results have not been completely analyzed, experience indicates that with this method of testing, the data should represent those of steady state. For another configuration, a comparison of lift and drag data is reprinted from Ref. 77 in Fig. 64 (coefficients are based on slipstream dynamic pressure). The data show good agreement with wind-tunnel test results.

5. MODEL DEVELOPMENT

The V/STOL wind-tunnel model continues to be one of the most expensive parts of any wind-tunnel program; it will be even more so if we are to take complete advantage of recent advancements in model fabrication techniques and instrumentation. The unpowered high-speed models or those adaptable to pressure tunnels are expensive to contour and finish, particularly if equipped with surface-pressure taps; the high cost is a result of the precision required and large design dynamic pressure. Adding power can double or triple any model costs because of (1) the cost of the engine simulator, (2) the power source (electric, compressed air, etc.) hookup, and control, (3) the added instrumentation needed to evaluate power setting, and (4) the additional effort required for data reduction. Once the above complications are added, there seems to be little direct correlation with the size and cost of the model itself so that, in general, within the restrictions of given available wind-tunnel sizes, scale effects continue to dictate as large a model as possible. Except for possible limitations owing to the available propulsion simulators, the initial approach in model planning is to evaluate the magnitude of wind-tunnel wall constraints. To put all of this together requires proper use of material and construction techniques in order to minimize flexibility, change time, or shop costs. The above considerations will be discussed in more detail.

5.1 Model Sizing

Figure 10 was proposed as a correlation of experience in comparing full-scale wind-tunnel test results with those of actual flight tests using, in some cases, the same airframe. Many investigations have, subsequently, evaluated model size limits and related these limits to the magnitude of wall-constraint corrections. Approaches to wall-constraint correction might be organized into application to type of lifting systems as follows:

1. Power-off or low thrust deflection: use classical corrections from Pope (Ref. 6)
2. Power-on with distributed blowing and limited thrust deflection: use Pope based on C_{L_A}
3. Power-on concentrated or focused thrust deflection: Heyson (see Ref. 79 for summary)
4. High angle of attack, Maskell (Ref. 80) with considerations by Peitzman (Ref. 81) and Stoll (Ref. 60)
5. Blockage for all cases (Ref. 82)
6. Corrections using wall pressure signatures (Ref. 83)

The last two items have shown promise for reliable evaluation of wall-constraint effects combining simple modeling of the lifting system with wall surface-pressure measurements in the wind-tunnel test section. These corrections increase rapidly with relative model size to wind-tunnel cross-sectional area and will be enhanced by the rapidly developing computational methods, such as was done recently by Snyder and Ericksen at Ames (Ref. 84). In the latter case, PAN-AIR (a high-level paneling code), was used to evaluate wall corrections with emphasis on a bump under the model. The basic problem and flow modeling are shown in Fig. 65. Lower-level paneling codes and vortex-lattice simulations of walls and lifting systems are getting more attention for treatment of the wall-correction problem and are being integrated with the data acquisition software of some wind tunnel facilities.

The question now is at what point do these corrections become meaningless or questionable. The physical constraint for highly deflected jets is classically illustrated in the sketches of Fig. 66, which are reprinted from Ref. 5, and are taken from the study done by Tyler and Williamson (Ref. 85). Also included is an example of one jet height and several velocity ratios which were studied for several relative test section sizes. The general flow pattern at the limit of testing consists of a vortex surrounding the point of jet impingement on the wind-tunnel floor. In this case (Fig. 66), for two laterally spread jets, the jet exhaust impinged on the floor at

$$V_e' = 1.31\, D_e/h$$

For the lift-fan data of Hoad and Gentry (Ref. 86), Margason (Ref. 5) runs through an example to keep $\Delta\alpha$ at the tail to 5°, and using Heyson's corrections, $V_{e_{min}} = 0.125$. Testing below this velocity would probably cause a vortex formation. There is a suggestion in Ref. 87 that testing should be limited when the wake impinges 2.5 wing spans downstream from the model. This is consistent with Turner's criteria of Fig. 54 for the moving-belt ground plane.

Carbonaro (Ref. 88) considers limits using Heysons criteria of testing for acceptable amounts of correction. A set of limits of wall corrections was assumed, such as $\Delta i_t = \pm 5°$, $\pm 2°$, and $\pm 1/2°$ for maximum acceptable, moderate, and no corrections, respectively, as listed in Table 3. Values of maximum test lift coefficient are related to ratio of wing span to tunnel width for several semispan and complete lifting systems. In this and previous reviews, Carbonaro concluded that the flow breakdown limit applies mainly to models that are small with respect to the test section; that is, for span-to-width ratios below about 1/4. Typical lift versus test-section width plots are reprinted in Fig. 67. For larger model dimensions relative to test-section size, the wall corrections become too large before flow breakdown occurs.

In the author's opinion, many of these limits can be "pushed" and some valuable information still obtained on power-induced effects for such items as aircraft stability and control, as well as flap and control loadings. Of equal significance is the fact that Heysons early work using a linear wake trajectory has been replaced by a free or "relaxed wake" which tends to move the predicted point of impingement on the wind-tunnel floor downstream. As previously mentioned, low-level CFD methods simulating the complete lifting system as well as the floor are being considered for evaluating both sizing criteria and wind-tunnel wall corrections, including support influence.

The general case of blockage and wall-constraint effects has been studied for some time by Hackett. An updating of this work is published in Ref. 82. The monitoring of wind-tunnel wall pressures and relating the results to an equivalent distribution of sources and sinks continues to be a promising method of evaluating the effective blockage of most conceivable V/STOL aircraft configurations. If properly instrumented, an angle-of-attack correction can also be derived, as illustrated in the block diagrams of Fig. 68(a). The key

is the comparison of the measured pressure imprint on walls (Fig. 68(b)) with results of theoretical modeling of the lifting system.

Investigations into methods of extending these limits have included changes in wind-tunnel design and methods of mounting the models. Off-center mounting, such as moving the model higher in the test section to effectively increase D_e/h, may help in some cases, but as shown by the University of Washington studies (Refs. 89 and 90) it tended to increase the magnitude of the wall-constraint corrections. Adding slots to both the floor and ceiling could be effective in delaying the formation of the floor vortex. Several moderately sized wind tunnels are equipped with hardware needed for this. The systems and correction factors may be similar to those being posed for transonic test sections (Ref. 91). Unfortunately, the amount of suction required through the slots and the system for distributing this suction is still being debated, particularly for the case of high-velocity jet impingement. Along with this debate go proposals of so-called adaptable walls. Sears' concept (Ref. 92), would require linking the wall-constraint porosity and shape to a mathematical model of the wake in order to eliminate any possibility of the wake being ingested by the lifting system (Fig. 69). Small-scale experiments on this concept are now under way, but it seems unlikely that it could be adapted to any of the existing large wind-tunnel facilities.

As the size of the lifting system increases with respect to the tunnel test section, the increase in blockage and, hence, free-stream velocity correction, results from the combined effects of model bulk, deflected jets, or separation wakes. For high-angle-of-attack tests, a model sized for conventional angle-of-attack ranges can have sufficient blockage at angles of attack above 45° to make test results meaningless. For the investigation of Refs. 60 and 61, a correction was used which was based on flat-plate drag data such as those shown in the plot of Fig. 70(a). The gross drag on the model and supports was measured by the tunnel scale system. From this, model-induced drag, less gross thrust and inlet momentum drag, was subtracted and related to a Δq corection in Fig. 70(b). The blockage correction was assumed to act uniformly across the test section. As shown in Fig. 70(b), the resulting Δq correction for the model with $S/C = 3.5\%$ was 12% at 90°. For models having much larger values of S/C, the flow uniformity assumption would be in question.

5.2 Power Simulation

In evaluating V/STOL concepts in the wind tunnel using scaled models, it is becoming evident that the full-scale jet properties must be evaluated in greater detail. Early experimenalists studied engine-airframe aerodynamic interactions using jets of air the quality of which was seldom documented. As a result, there were differences between experimental results which could not always be explained by such things as variances in velocity ratio and placement of the jets.

Ames Research Center has undertaken a major experimental program to evaluate the principal scale effects involved in jet simulation. The initial phase, reported on in Ref. 93, included the full-scale test portion of a full-scale to small-scale comparison program. Measurements of the effects of using actual turbojet/turbofan engines will be evaluated at small scale by attempting to simulate the geometry and jet characteristics of the engine exhaust and evaluating any full-scale differences in suck down and ground effect. The results, using a General Electric YJ-97-GE-100 turbojet engine, are summarized in Fig. 71. Although small-scale experimental results are not yet available for comparison with existing large-scale data, it is evident that the measured suck down is considerably more than the predictions using empirical methods (Ref. 94) which were based on small-scale generic investigations. This program will continue with the small-scale phase and then be extended to co-flowing jets, but until we have answers on the significance of modeling all jet characteristics, including the possible need to simulate jet turbulence, the current objectives should be to model the real jet properties of jet cross-section and velocity profile for a given pressure ratio.

The need to do the latter is demonstrated in the experiments of Kuhlman and Ousterhout (Ref. 95) and Kuhlman and Warcup (Ref. 96). A plug was inserted in a nozzle to change the jet qualities, particularly the total pressure variation across the jet. A typical result is shown in Fig. 72. Inserting the plug near the jet exit added a loss in momentum to the center of the jet and contributed to a more rapid velocity decay and change in jet trajectory in the cross flow.

The foregoing results indicate that simulating jet velocity profile across the jet is mandatory and, possibly, the simulating of jet turbulence could be significant for evaluating jet-airframe interference effects. As the requirement for more quantitative test results increases there is a need for a more careful choice of the propulsion simulator to be incorporated in the model design. In planning the test program, this choice is integral to model size consideration because of the availability of off-the-shelf simulators and the large cost of simulator units already developed.

5.2.1 Simulator Classification

Classification of aircraft engines, and hence engine simulation types, was well organized by Wulf and Melzer (Ref. 97), as shown in Fig. 73.

The choice of simulation is between "self-manufactured motionless systems" and "expensive, purchased rotating systems," with rotary-wing model power and turbofan engines falling in this latter class. Although not listed, hydraulic-powered motors should not be overlooked for driving rotary-wing models or for installations in which a return lead can be installed. Table 4 bridges the two branches for air-driven models classified according to nacelle type. To extend the application to full or large scale, I added the line item, gas-turbine engines. The following three sections cover the fixed blown simulators which include the full, blown jet, and ejector, as well as the turbine powered simulator and gas turbine engines. Electrical power is considered beyond the scope of this lecture though it is a significant factor in model costs. Its application is typically a mechanical problem and one of tying into either an on-board model motor or to a wind-tunnel auxiliary power facility, such as the one available at the Vertol tunnel (Fig. 51) or at the Ames 40 by 80 (Fig. 9).

5.2.2 Fixed Blown Simulators

Fixed blown simulators probably have been and will continue to be used because of their economy, particularly for powering partially complete models. Most initial studies in jet/airframe interference effects have incorporated this type of power for jets, such as the work by Vogler (Ref. 66) and, more recently, in the jet-in-cross-flow studies of Refs. 44 to 48. The simulation of a uniform jet and, at the same time, getting it within the contours of a small model of a complete aircraft configuration, is a difficult task, particularly if the entire assembly must be metric (total forces measured by the balance). Effective designs of the fixed blown simulator were used in the early studies of the Hawker P-1127 using a 1/10-scale model; an illustration of the model is reprinted in Fig. 74 (Ref. 63). In the most recent development of the AV-8B, a 0.15-scale model was powered by the airfeed plenum shown in Fig. 75.

In any of these, and also in similar designs, the quality of the jet is a function of the screen or colander design combined with the size of the settling chamber. A very uniform jet velocity was obtained in the AV-8B model just mentioned. A very compact installation, it still had a settling chamber up stream of the conical screen (Fig. 75). In these installations the desired contraction from screen into the nozzle entrance was difficult to package. For the basic jet-in-cross-flow studies of Aoyagi and Snyder (Ref. 46) and Fearn and Westen (Ref. 47), a very uniform jet velocity profile was obtained by the relatively bulky design shown in Fig. 76. The need for some contraction ratio is always a major problem in designing fixed blown propulsion simulators for complete aircraft models because of limited available space inside the model.

For simulating (approximately) engine inlet velocity, as well as in providing exhaust flow with a minimum of high pressure flow, the ejector should be considered. The application of the ejector was aided by the work published in Ref. 98. The ejector used was fed by air with pressures up to 2.41 MN/m^2 (350 psig) through a large number of primary nozzles in order to maintain uniform flow across the ejector. Ejector performance for one design is presented in Fig. 77. Even though an overall pressure ratio of 1.5 could be obtained, the ratio of ejector inlet flow (secondary flow) to total exit flow (primary plus secondary) was less than 0.5, meaning a subscale inlet area. Jet-pump theory indicates that this ratio would increase rapidly as less exit pressure is required. The effort did show that effective gross thrust for any given ejector configuration could be set to a known value and maintained, providing a complete calibration was made for each exit nozzle or deflector-inlet combination. The ejector is adaptable to packaging into nacelle configurations, as shown in Figs. 78(a) and 78(b) for a turbojet or turbofan, respectively (Refs. 97 and 99). Subsequent development such as the effort by General Dynamics (Ref. 100) has refined the use of the ejector for simulating high bypass ratio engines. (See also Ref. 99 for application to an investigation of the EBF – externally blown flap.) The simulator used here, and shown in Fig. 78(b), simulated the correct exit thrust split but the incorrect inlet flow simulation, though probably close enough to have had little effect on measurements of EBF performance.

5.2.3 Turbine Powered Simulators: Low Pressure Ratio

The tip-drive fans (Fig. 79) are roughly one tenth the cost of the center turbine driven fans but still have a big advantage over the ejectors in being able to move the bypass flow at 5 to 6 times the flow rate of the drive air. As for U.S. designs, a major workhorse has been the 5.5 in. (14 cm) fan shown (Fig. 80) disassembled and installed in an early Rockwell lifting-nacelle configuration (Ref. 101). The fan was also used to simulate the fan flow in the built up nacelle (Fig. 81 from Ref. 102). The 5.5-in. fan was combined with a direct blown simulation of an engine core in a 0.094-scale model of a V/STOL research airplane to be powered by Allison PD 370-16 engines. For this test, the fan turned out to be a reliable performer. One of the largest of the tip-driven type was Tech Developments 12-in. fan (Ref. 103), which was incorporated in the high-angle-of-attack model tested in the Ames 40 by 80 tunnel (Ref. 60) and in ongoing inlet work at NASA Lewis. In both of these cases, it has been used only to suck the inlets rather than provide a propulsive jet since, at this stage of its development, it has a large radial variation in total pressure. Initial calibrations established, however, that it met the design objectives of an effective pressure ratio of 1.4. Air supply required for a full total thrust of 800 lb is 6.5 lb/sec heated to 250°F. Again, testing experience has shown this fan to be reliable.

In the final stages of aircraft aerodynamic development, the turbofan or central powered simulator has had a strong role. Here, the engine bypass and pressure ratios are both closely simulated for given thrust loadings, T/A_L. As a result, for a given nacelle configuration, scaled to the same A_L/S as the aircraft, testing can be accomplished at high subsonic Mach numbers for effective evaluation of cruise drag. The TF 34 simulators are also being used in the small-scale tests of the Grumman 698 (subsonic tactical aircraft) model shown in Fig. 82 mounted for hover testing in the Ames 40 by 80. Results have not been published for these tests, but long-range plans involve comparison with full-scale static and wind-tunnel tests, with documentation of the jet efflux coming from both large- and small-scale models.

5.2.4 Compact Multimission Aircraft Propulsion Simulator

The ejectors and rotating simulators just discussed can be applied only to simulated turbofan engines having subcritical pressure ratios. For power-on testing of high-performance aircraft, techniques used in the past have required direct feed of the air and, if the inlet were to be simulated at the same time, a bulky suction lead would have to be routed outside the wind tunnel. The continuing development and application of the compact multimission aircraft propulsion simulator, CMAPS (Fig. 83), has had the objective of simulating both propulsive jet and inlet flow at total pressure ratios corresponding to those of current high-performance engines. The simulator (Fig. 84) is a miniature four-stage turbocompressor driven by high-pressure air expanded through a single-stage turbine. It has the capability of changing the engine pressure ratio at a constant compressor airflow by changing the fraction of turbine discharge air of the exhaust nozzle. The hardware development started by McDonnell Aircraft Company under the auspices of the Air Force Aero Propulsion Laboratory; a complete history of its development is provided in Ref. 104.

Ames Research Center is funding a major program to develop the technology for the application of the CMAPS to small-scale wind tunnel models. The primary objective in this program is to measure the aerodynamic interaction effects that may result from geometrically close-coupled propulsion/airframe components. A second objective is the development of installation and test techniques for propulsion-equipped wind-tunnel models. A third objective is the expansion of the high-speed V/STOL aircraft aerodynamic data base. The initial

aircraft configuration chosen was that of a two-engine, close-coupled, canard-controlled aircraft similar to the General Dynamics design (GD 205) resulting from the study of Ref. 2. The model is shown installed in the Ames 11-ft transonic tunnel in Fig. 45, and the basic model design features are described by Bailey et al. in Ref. 105.

As the model was developed, the problem of isolating the aerodynamic forces acting on the airframe from the propulsion forces was addressed, as shown in Fig. 85. As it turned out, a single internal balance was used which supported all external surfaces except the boattail. The boattail forces were measured using surface-pressure instrumentation. In this manner, the use of seals was kept to a minimum, with one at each inlet and exit of the simulator and at the intersection of the support and lower fuselage.

A major part of the program has been the development of the calibration tank (Ref. 106) along with the control system itself, and the instrumentation needed to monitor inlet flow (Ref. 107). The general purpose of this facility (Fig. 86) is to obtain pretest relationships between the inlet and exit flow rates and pressure ratios as functions of the CMAPS control air parameters. As may be seen in Fig. 84, it will meter inlet air supply and exhaust extractors. All the required pressure valve controls and pressure instrumentation will be linked to a digital control console adjacent to the calibration tank.

5.2.5 Aircraft Engines

For large subscale or full-scale V/STOL testing, gas turbine engines are needed. It is at this scale that the larger size simulators, such as the 30-cm (12 in.) tip-driven fan, either have limitations in fan pressure ratio or require an excessive amount of compressed air for continuous operation. For direct blowing, most wind-tunnel facilities do not have sufficient compressed air capacity in either amount, pressure ratio, or heat. For large subscale models, the gas turbine engines developed for business jet aircraft adapt well to scales from 0.3 (for light transport aircraft) to 0.7 for tactical fighter designs. For larger models, there is a jump in thrust to the 10,000-lb class engines. Relative geometric profiles for some of the smaller engines are shown in Fig. 87 (Ref. 4). Ames Research Center has used these engines in several large-scale research investigations in the 40 by 80 tunnel. The engines have seldom been flightworthy, but have been maintained sufficiently to run at or near maximum thrust in most cases. An installation of the JT15D engine (as bypass ratio 3) used in a large-scale upper-surface-blowing investigation is shown in Fig. 88 installed in a boiler-plate nacelle without some of the nozzle fairings installed. One disadvantage of using this size of engine is that the fuel control and starter are usually located at the bottom of the engine, making it sometimes difficult to exactly scale the external nacelle contours of an aircraft configuration. However, this gave few problems in simulating the significant USB geometrical parameters needed for the model of Fig. 89 (Ref. 15).

Maximum rated performance is shown in Fig. 90 (Ref. 4) for an assortment of engines and tip-driven lift fans (LF 336 and LF 376). The augmented wing compressor and the Viper compressor are gas-turbine driven pumps which might be too large to be housed in a fuselage of a high-performance fighter model, but they provide cool air at 30 to 50 lbm/sec at pressure ratios up to 3.5. The J97 General Electric engine has been used in the basic research models with one shown in Fig. 8 (Ref. 108) and has a moderate combination of thrust-to-pressure ratio. NASA "inherited" all of these engines from a military program; they were in good enough condition to serve as reliable power sources. As can be seen from Fig. 90, there are no engines immediately available in the 10,000-lb class with sufficient pressure ratio to simulate some of the larger power plants now being planned with pressure ratios of 3 to 3.5. This is forcing the model size to nearly full scale for testing V/STOL supersonic tactical aircraft configurations in order to duplicate pressure ratio.

5.3 Model Planning

The foregoing discussions have attempted to treat model sizing and propulsion simulators separately. This was done primarily to allow emphasis on significant factors for each topic such as scale effects or details of the CMAPS. As was the case for using available engines (previous section), in actual model development, an experimentalist may have to take whatever power simulation is available. Providing it gives him the necessary parameters such as NPR or thrust, with the support equipment in the wind tunnel that is available to him, he will design his model around that particular simulator. The following are a few examples of V/STOL wind-tunnel model design and construction.

An 11% scale model of the Grumman 698 tilt nacelle aircraft is currently undergoing wind-tunnel tests in several U.S. facilities. This high-speed steel and aluminum model was designed and built simultaneously with the hover and wind-tunnel testing of the full-scale boiler-plated model. From previous development of conventional military aircraft using the TF34 simulator, sufficient experience with the unit indicated that it could be a reliable power plant for a V/STOL model. The model was constructed with provisions for both three internal balances and 200 surface-pressure taps, which resulted in the tubing network (Fig. 91) leading to the on-board Scanivalves. The nacelles, shown partly disassembled in Fig. 92, were designed to house the TF34 simulator, supply the required amount of drive air, and attach to the model through a floating or metric frame so that the propulsive forces and moments could be measured independently of those acting on the wing fuselage. In the process, a coil (Fig. 93) for the fan drive air was developed to minimize force and moment tares from the air. This was done before the air entered the model since there was not enough room inside the model to house isolation systems such as flow-through balances (see Sec. 6.1). As might be expected from the complexity of the model, there were several problems that had to be addressed, not the least of which was the excessive time needed to assemble the model on the sting. Tests using the model have been considered successes since reliable data were finally obtained and are now being analyzed. The final cost of this model corrected for 1984 dollars was probably over $800,000, and this did not include the cost of the TF34 simulators (approximately $100,000 per unit).

The prime question is could the above model have been designed in such a manner that the cost would have been lower. The answer is that it probably could not have been, although there were alternative designs which might have included two complete models, one being a force model with no surface-pressure instrumentation and the other strictly a pressure model. This is commonly done for high-speed conventional models, such as that shown in Fig. 94, which shows the model plus some of its components needed for alternative configurations and model changes. However, the principal cost of such models comes from the close tolerances required to

maintain scaled contours and model components that are interchangeable. Rapid advances in computer aided design and manufacture (CAD-CAM) techniques where applied to these complicated wind-tunnel models is reducing some of the time for construction, but there will always be a need for a certain amount of hand fitting, which runs up costs. Another option for the tilt-nacelle model, could have been the use of an unpowered or transition test that if the proper propulsion simulator had been available, could have been of larger scale but sized (about 0.2 scale) to the limits of testing in a moderately sized subsonic tunnel, such as the Langley V/STOL tunnel. The actual contouring tolerances could have been relaxed and wood-plus-foam-fiberglass materials considered. Even so, if the on-board pressure instrumentation were needed in both high- and low-speed models, the total costs of both models would be the same or more than the one that was built.

For large-scaled V/STOL models designed for testing in the NASA large-scale wind tunnels, the options in model design and construction are more numerous. Levels of sophistication and particular examples are shown in Table 6 defining several levels of costs. Level 1 would include the component tests such as the Q-fan (Fig. 32) or the high-angle-of-attack studies using the 0.4-scale model of Fig. 48. Level 2 would include large but probably subscale models of mostly boiler-plate construction and probably powered by the smaller gas turbine or turbofan engines mentioned in the previous section. Level 3 would include full-scale, mostly boiler-plate models using the same or similar power plants as planned for the aircraft, such as the AV-8B flight-like model of Fig. 5. Since this type of model is full scale, it could incorporate flight-weight components where appropriate. Level 4 would be wind-tunnel tests of the actual aircraft remotely controlled as required and adapted to the wind-tunnel support struts, using either the landing gear attachment points or reinforced wing-mounting arrangements. The increasing cost with level applies principally to tactical V/STOL aircraft for level 3 and below since the actual aircraft might be wind-tunnel tested cheaper than the total costs of building and testing a large but subscale fully powered model.

The term boiler plating might wrongfully have the connotation of making something overly heavy and strong with little regard for model weight and some of the aircraft details to be modeled. This is generally not the case at all though some models turn out heavy. What does reduce construction costs is to stay away from complex surface curvatures by using straight-line elements and rolling or multiple bending of the skin. Care must be taken in the planning of the model so that short straight-line elements simulate the scaled, gradually changing, surface contours. Stamped or machined elements are used for sharp curves such as leading edges or inlets. An example was the USB STOL model (Fig. 89) which incorporated the Pratt and Whitney JT15D powered nacelle of Fig. 88. For this model, the wing leading edges and flap skin were formed using multiple bends along straight-line wing elements and the inlets were spun-formed for blending with the skin of the nacelle. Most of the rest of the model was boiler plated, using welded steel construction, as shown in Fig. 95(a) for the two-engine fighter model (Fig. 8, Ref. 108). Where the surfaces are not exposed to hot flow, a rigid and complex surface is obtained by polyurethane foam, which is applied in liquid form between plywood ribs, allowed to expand, and then cured. This is then shaped and covered with several layers of fiberglass and filled. Going one step further, this technique can be incorporated with aircraft parts such as was done for the full-scale AV-8B model shown in Fig. 96 (Ref. 19).

6. TEST OPERATIONS

Planning and carrying out the actual wind-tunnel testing operation must depend not only on the capability and test limitations of the model but must also rely on full use of support and equipment available at the wind-tunnel facility. This is particularly true for the powered V/STOL model, testing at all speeds, where such things as time to set power, tunnel venting (where actual engines are used), change time, or time to take a data point can determine the success or failure of the test operation. Examples of the latter are factors considered in Ref. 4 and reprinted in Fig. 97. The actual data were obtained from experiences with gas-turbine powered models in the Ames 40 by 80, but they are significant factors to be dealt with for any powered-lift testing, particularly, downtime for configurational changes and time per data point. Many other factors influence facility use time. The ones chosen for the following brief discussion are instrumentation and data acquisition, acoustics studies, and flow surveying.

6.1 Instrumentation and Data Acquisition

It will be assumed that the experimentalist has available to him the most up-to-date instrumentation with potential for on-board use such as Scanivalves (if possible to install on the model) or a reliable flow-through balance similar to the one shown in Fig. 98, which was used in the investigation of Ref. 109. For power coming from cool compressed air, this design integrated the force isolation scheme for the drive air with the balance itself. In this case, opposing bellows and seals were used with a metric mass-flow distributor routing the air to various blowing systems in the model. When the air must be heated above about 200°C, the flow-through feature might not be practical, a result of thermal sensitivity of the force-measuring part of the balance. In such a case, drive air might have to be "jumped" through an isolation coil similar to that shown in Fig. 93.

As for Scanivalves, at the date of this lecture, many test facilities are converting to the electronic type which takes advantage of low-cost silicon pressure transducers whose inherent errors (such as thermal zero shift and output drift with time) are corrected by the periodic on-line calibrations. The advantage of this system, particularly for a powered model testing under fluctuating load, is that all pressures can be sampled almost simultaneously within the channel capacity of the data-acquisition system. At first glance, some of the possible installations seem geometrically smaller than the smallest of the mechanically driven ones (although this may not generally be the case). A possible disadvantage for low-speed V/STOL use is a measurement error resulting from the requirement to use a ±5-lb/in.^{2} transducer for a ±1-lb/in.^{2} measurement range. A unit of this range, however, will be available shortly. Other uncertainties are possible adverse effects caused by temperature and by high-frequency vibration of the mount.

For large-scale testing, an on-board data-acquisition system using pulse-code and modulation (PCM) similar to that used in flight testing, has been used for several years with the remote digitizer multiplexer unit (RMDU) which is evolving into the remote millivolt multiplexer and amplifier module (RAMM) (Ref. 110). This allows all conditioned analog signals except those from thermocouples to be digitized and multiplexed so that they can be transmitted to the data acquisition through a minimum of leads. The compatibility of electronic scanners with this system is under evaluation.

The wind-tunnel data-acquisition system that is finding acceptance at Ames Research Center with similar systems in industry was detailed by Cambra and Tolari in the mid-1970s (Refs. 111 and 112). The version finally adapted for the Ames Large Scale Test Facilities (40 by 80) is shown in Fig. 99. It is sufficiently flexible to be applied to both dynamic and steady-state testing. Also shown are the other operating systems, including the inputs from the mechanical (below the floor) wind-tunnel balance (Toledo system) which are transmitted to the data gathering processor (DGP) through the control processor. The real-time executive processor (REP) processes information from the DGP and rapidly returns the result to the displays in the control room. For normal V/STOL testing, real-time updating of the displays, which might include aerodynamic and propulsion parameters, every 1 sec has been found satisfactory. The existing choice in software provides a large range in time for data sampling during the recording process. For dynamic tests such as rotary-wing investigations, the dynamic analysis system (DAS) is available to be used either separately or combined with the DGP.

6.2 Special Requirements for Acoustic Studies

The strength of all possible noise sources on an aircraft should be determined during the final development of the aircraft in order to obtain the acoustic loading and to ensure a safe working environment for both the crew of the aircraft and ground-support personnel. For the USB tests of Schoenster et al. (Ref. 113) there were small but noticeable differences in surface acoustic loads owing to airspeed even though the airspeed tested (in the Langley 30 by 60) was only 16 m/sec. The investigation of the 727/JT8D flight noise (Ref. 114) compared model, full-scale wind-tunnel data, static-test data, and level flyover data for the 727 airplane. The JT8D installation shown in Fig. 100 was used with microphones on a traversing beam 3 m to the right of the engine centerline (looking aft) but still in the near-field. In this way, the angle relative to the noise source could be changed. When the measurements were extrapolated to the far-field, they compared well with the aircraft forward-speed effects, as shown in Fig. 101. The investigation has been one of several which pointed out the need for and value of continued acoustic study in the wind tunnel.

6.2.1 Method

Problems with and techniques for measuring strengths of noise caused by jets and inlets in the wind tunnel were evaluated by Soderman and others in the 1970s (Refs. 115-117). Measurements of noise radiation from powered V/STOL models can, generally, be confined to using incomplete or component models of the primary noise systems as was done for the Boeing 727 study just mentioned. In this way, the study of forward-speed effects on the acoustics of an aircraft can be investigated at full-scale with accurate model simulation of the anticipated noise sources. An exception to this was the evaluation of airframe noise (Ref. 118) where the noise radiating from a large-scale semispan model of the complete lifting system was measured in the 40 by 80.

The principal problem areas in measuring noise in a wind tunnel are source-noise reverberation, background noise owing to the wind-tunnel drive system, and microphone wind noise. To alleviate these, some tunnel facilities are updating the equipment and, in effect, doing the following: (1) acoustically treating the walls, (2) reducing fan-drive noise, and (3) reducing wind noise by refining support struts or eliminating protuberances from the walls. The challenge is one of selecting measuring devices that are directional or discriminate against unwanted sound, and by using special techniques and free-field comparisons to evaluate the reverberant field. An example of the latter is reverberant field simulation in which the reverberant sound field of compact wind-tunnel models is simulated by operating a calibrated loud speaker at the noise source location (Ref. 119). When the reverberant field level is known, the model noise data can be corrected to give approximate free-field noise levels. The technique was verified by wind-tunnel and flight correlations using the actual flyover noise, such as the XV-5 comparison of Fig. 102 (Ref. 120). Unfortunately, where the noise source is large and distributed relative to the size of the tunnel test section, such as for spanwise distributed blowing models, the technique cannot be applied, and reverberation corrections must come from operating both in the wind tunnel (at $V_\infty = 0$) and in the free field.

6.2.2 Forward Velocity Effects on Advanced Inlet Suppression of Fan Noise

The inlet-fan acoustic studies of Falarski and Moore (Ref. 121) and of Moore (Ref. 122) are other examples in which the wind tunnel was effective in evaluating forward-speed effects on acoustic sources. Flight effects on fan noise have been observed by investigators who have compared turbofan flyover noise with static noise, but the details are obscured by the mixture of aircraft-noise and other engine noise sources. Therefore, in order to understand fan noise, the actual flight conditions must be simulated. To suppress compressor noise, advanced inlet designs were devised. One design, the hybrid inlet, had a smaller than normal throat area and acoustic treatment in the diffuser. The other, the deflector inlet, had an extended low inlet lip with acoustic treatment to deflect fan noise up as well as forward. The performance and acoustics of both of these inlets were to be compared with those of a standard inlet with no diffusion. The objectives of the program were to determine the low-speed flight effects as simulated by the 40 by 80 on the forward radiated fan noise and on the acoustic suppression characteristics of the inlets.

The series of test inlets was designed around the requirements of the JT15D, with the resulting basic nacelle shown in Fig. 103. The turbine and the fan exhaust ducts, as well as the skin of the nacelle, were acoustically treated. The simulated flight tests in the Ames 40 by 80 used the test installation shown in Fig. 24(a), which is shown with microphone stands installed and with a circular traversing stand mounted in front of the model. The entire fan-strut assembly was mounted on the turntable of the wind tunnel for angle-of-attack adjustment. In both installations, a foam mat was installed which removed reverberant reflections from the noise data at all frequencies above 500 Hz. As a result, the fan-nacelle installation, using the JT15D as mounted was about 1/4-scale of moderately sized current, commercial turbofan aircraft's engines. To enhance simulation of the larger engine, the core IGV (inlet guide vanes) had been modified. The traversing microphone was kept aligned with the free stream by using a vane-type pivoted mount. The standard 0.25-in. microphone was used with a faired nose cone attached to reduce wind noise. Noise inside the inlet was measured using Kulite pressure transducers (outside tests only) mounted flush to the local surface.

Care with the details just mentioned, as well as with many other factors that influenced the data, eventually produced some interesting results, the foremost being that the hybrid inlet suppressed the high-tip-speed fan noise as much as 18 PNdB on a 61-m (200-ft) side line which was scaled to CF6 size engines. In

addition, it was found that no significant changes in fan-noise suppression for either inlet occurred for forward-velocity changes above 21 m/sec (68 ft/sec) or for angle-of-attack changes up to 15°.

This is another clear instance of wind-tunnel acoustic studies helping in the evaluation of flyover noise. In another sense, it verified some of the noise evaluation techniques prevailing today and which are applicable to acoustic studies of V/STOL aircraft.

6.3 Flow Surveying

For V/STOL wind-tunnel testing operations, flow visualization, if not flow-field surveys, can be a major part of the test program. The traditional method of using surface tufts, tuft or smoke probes, and directional flow surveying are necessary tools in understanding the complicated flow patterns which surround a powered-lifting system, and how they influence the aerodynamic parameters of the aircraft. For example, in the study and modeling of lifting jets, the flow visualization tests of Margason (Ref. 123) have been considered by some to be sufficiently quantitative to define the path of the jet-in-cross flow.

6.3.1 Surface Effects Study

No subsonic test of a lifting system is complete without the model being covered with tufts, oil, or kerosene. Studies such as that shown in Fig. 104 are instrumental in evaluating flap performance (and, in this case, model installation effects). For a review of some of these techniques used near the model surface the reader is referred to Werle (Ref. 124) (a general treatment of all flow-visualization technique) and Merzkirch (Crowder) (Ref. 125), who has specialized in the use of fluorescent minitufts for nonintrusive surface-flow visualization.

In addition to qualitative information that flow visualization has always provided, more quantitative information is now being obtained, from the imaging and numerical processing of flow-visualization pictures (Ref. 126). For two-dimensional flow, flow separation is becoming well understood, but in three dimensions the problem still needs considerable research. For interpreting flow-visualization data in three dimensions, the current trend is to use topological concepts with skin-friction lines. Although these concepts have been with us for some time, Hunt et al. (Ref. 127) initiated more interest in the subject. Recently, Kao and Burstadt (Ref. 128) applied the method to analysis of visualization data for deflected thrust V/STOL nozzles, and others have applied it to flow separation at high speed. More application to analysis of flow patterns on V/STOL aircraft in hover and transition should be continued in view of the economy of obtaining this type of data.

6.3.2 Flow-Field Measuring

Methods incorporating pressure probes, LDV, IR imaging, Schleiren, shadowgraphing, and hot-wire surveying are becoming well established. The use of smoke is becoming more common for evaluating flow fields, and, its use and limitations are thoroughly discussed by Werle (Ref. 124) and Mueller (Ref. 129). Where a quick approximate answer is required, the classical tuft grid should not be forgotten. The results of Naeseth (Ref. 130) were certainly descriptive of the effect of high power induced circulatory lift on the upwash near the engine inlet (Fig. 105). In view of the need of survey equipment and methods that can be used for three-dimensional flow in a hostile environment, such as is the case for V/STOL testing, the first two, pressure probes and LDV, will be discussed. Where there is a need for close study of the flow field involving high-energy jets, particularly at small scale and high speed, a special attempt should be made to utilize the wind-tunnel Schlairen and shadowgraphing equipment.

The use of pressure probes and rakes has been essential throughout the history of experimental aerodynamics. Rake survey equipment, boundary-layer rake probes, and directional pitot tubes have been standard equipment in most wind-tunnel facilities. For evaluating highly deflected flows, the directional pitot tube has continued to be used where more sophisticated methods, such as LDV, are not available. The probes have generally been lacking in three main areas: (1) their possible influence on the flow that is being measured, (2) lack of sensitivity for small-flow velocities, and (3) errors in measurement at high angles with respect to the axis of the probe. The first problem, has been reduced — but will never be eliminated — by the use of very small tubing with off-the-shelf probes of 1/8 D or less now being available. The second difficulty can only be helped with the use of careful calibration and sensitive pressure transducers that are geometrically close to the head of the probe. The third problem has been alleviated recently in two ways. First, the use of the five-hole probe (Fig. 106) (Ref. 47) was enhanced at the high-incidence range by using a potential-flow model to define the form of a calibrating equation. Constants for the equation were then obtained during calibration. Second, the other area has been the development of the seven-hole cone shown in Fig. 106 (Ref. 131), which has been calibrated over a large speed range with good accuracy up to 80° incidence.

Laser Doppler velocimetry (LDV) has been advancing steadily since the early 1970s. At Ames Research Center, Orloff et al. have been extending the measurement capability from the original two-color-two-dimensional backscatter laser velocimeter (2D-LV, 7 by 10 installation) to a 7 by 10 size three-dimensional laser facility and a large scale two-component unit. Because of the capability of obtaining flow velocity and direction measurements with no physical interference with the flow itself, the development of the equipment will continue. In a recent paper, Orloff et al. (Ref. 132) reviewed Ames LVD experience, and plans for and the accuracy of LDV systems are discussed in Ref. 133.

Diagrams of the 7 by 10 three-dimensional laser equipment are presented in Fig. 107. It measures three velocity components by means of three independent dual-scatter channels that operate in the backscatter direction. A combination of mechanical tilt and variable focusing are used to ensure that the focal point of the upper channel remains colocated with the focal point of the lower two-dimensional portion as the lower focal point moves in a cross-flow direction across the test section during a survey. Streamwise and vertical positioning is accomplished by moving the entire package (Fig. 107(a)) on the digitally controlled translation platform of Fig. 107(b). The status of this equipment gives repeatable positioning accuracy to less than 0.5 mm and the probe has a focal volume of 1.5 mm. It is generally operated in a closed-loop mode with the computer performing test-point positioning and path control through communication with five stepping-motor controllers. Rather than use forward scatter, such as the JPL equipment (Ref. 134), to increase

signal-to-noise level for some testing, the signal is enhanced by minimizing the bandwidth, the minimum being controlled by programmable frequency synthesizers. The equipment has been used extensively in the Ames jet-in-cross-flow program, Fig. 108 (Ref. 133), where surveys very close to the flat plate and nozzle have been completed.

The large-scale laser was developed to mount in the large wind tunnels, as shown in Fig. 109 (Ref. 135). It is a single color, dual-beam, scanning, confocal back scatter LDV that directly senses two orthogonal components of velocity; it is shown in operation in Fig. 110. A third component is obtained by further transformation of coupled velocity components. As shown in Figs. 110 and 111, the laser and system optics are mounted and enclosed in a streamline cylindrical shell that is supported along the longitudinal axis. The laser power unit and other components are mounted below the cylinder in a faired structure which also serves as its support. This entire assembly is mounted on a carriage for cross-flow translation. The current options for range are 10 or 20 m. This unit will also be used at the Ames Outside Aerodynamic Research Facility (OARF) to study ground-effect flow fields and ingestion problems being investigated using large-scale models.

7. CONCLUDING REMARKS

Aspects of wind-tunnel testing of V/STOL aircraft configurations have been reviewed. The choice of topics discussed were, generally, based on their significance to the planning stage of a wind-tunnel testing program. Suggestions and comments on techniques to be used during a test program covered a large range in types of testing and possible program costs. Their value would be greatly enhanced as the planning phase of a program matures by obtaining details from the sources listed and, most importantly, thorough consultation with the staffs of the wind tunnels that are being considered.

The material was organized into the given topics as a result of technical consideration with little, though some, discussion treating the economics of testing. Because of ever-increasing cost of wind-tunnel time and model construction, we are always looking for simpler and cheaper ways to construct models and for ways to reduce tunnel use, for example, by faster sampling of the data for each test condition, reduced configurational change time, or reducing the number of data points by improved data analysis methods which incorporate use of advanced prediction methods.

The accelerated use of CFD for isolated multienergy fluid dynamic problems which can apply to powered-lift aircraft concepts combined with a more thorough understanding of scale effects may eventually allow us to feel more confident with hover and transition testing at small scale or models sized for the 7 by 10 size tunnel. This model would then be restricted in on-board instrumentation. Use of the moderately sized wind tunnels, such as the DNW larger test section or the NASA Langley 4 by 7 m requires a model of a complete aircraft configuration which is currently pushing the state of the art in miniaturizing on-board instrumentation and power simulators. In addition, even at this scale for atmospheric wind tunnels there are scale effects, and problems in power simulation which might produce uncertainty in the results. One is therefore led to consider the use of large- or full-scale models powered by gas turbine engines and tested in NASA's large-scale test facilities. In these facilities there is the opportunity to test with both flight-like and flight-weight hardware, and, for some types of tests, the level of total program cost may not be much above small-scale tunnel testing.

Although most of my experience has been with large-scale methods, I will be the first to concede the value of small experiments, not only for exploratory use but sometimes for complete development programs in the design phase. There is ample experience in programs, such as the AV-8B development to show that it is desirable to make good use of small-scale testing in evaluating many of the basic aerodynamic problems and to verify the results using large-scale tunnel tests. During any stage of the aerodynamic development, it is recommended that large-scale testing with flight-like models be phased into the V/STOL wind-tunnel testing program to establish hover and transition characteristics. And, finally (for medium sized aircraft), the aircraft itself should be tested in one of the large-scale wind tunnels, either before or during flight tests, such as was done for the XV-15 tilt rotor or the XFV-5 lift fan aircraft. In this way, aerodynamic predictions, based on small-scale wind-tunnel data enhanced by computational techniques can be continually evaluated.

REFERENCES

1. Hickey, David H., "VSTOL Aerodynamics: A Review of the Technology." AGARD CP-143, V/STOL Aerodynamics, 1974, pp. 1-1 through 1-13.

2. Nelms, W. P., and Durston, D. A., "Preliminary Aerodynamic Characteristics of Several Advanced V/STOL Fighter/Attack Aircraft Concepts." NASA TM-81281, 1980.

3. Roberts, L., Deckert, W., and Hickey, D., "Recent Progress in V/STOL Aircraft Technology. NASA TM-81281, 1981.

4. Koenig, D. G., Aiken, T. N., and Aoyagi, K., "Large Scale V/STOL Testing. AIAA Paper 77-586, 1977.

5. Margason, R. J., "Jet V/STOL Wind Tunnel Simulation and Ground Plane Effects." Paper No. 15, AGARD Conference Proceeding No. 308, Lisbon, Nov. 1981.

6. Pope, A., and Harper, J. J., "Low Speed Wind Tunnel Testing." John Wiley & Sons, Inc., New York, 1966.

7. Pope, A., and Goin, K. L., "High Speed Wind Tunnel Testing." John Wiley & Sons, Inc., New York, 1965.

8. Johnson, D. B., Lacey, T. R., and Vodo, J. J., "Powered Wind Tunnel Testing of the AV-8B: A Straightforward Approach Pays Off." AIAA Paper 79-0333, New Orleans, La., Jan. 1979.

9. Lacey, T. R., and Miller, K., "The AV-8B Wing Aerodynamic Concept and Design." AIAA Paper 77-607, 1977.

10. Clapper, W. S., Mani, R. J., Stringas, E. J., and Banerian, G., "Development of a Technique for Inflight Jet Noise Simulation. Part I." J. Aircraft, Vol. 15, No. 2, Feb. 1978.

11. Pirrello, C. J., Hardin, R. D., Heckart, M. V., and Brown, K. R., "An Inventory of Aeronautical Ground Facilities." Vol. I. Aeronautical Facilities. Vol. II. Airbreathing Engine Test Facilities. NASA CR-1874 and 1875, Nov. 1971.

12. Aiken, T. N., Falarski, M. D., and Koenig, D. G., "Aerodynamic Characteristics of a Large Scale Semispan Model with a Swept-Wing and an Augmented Jet Flap with Hypermixing Nozzles." NASA TM-73236, 1979.

13. Koenig, D. G., Stoll, F., and Aoyagi, K., Application of Thrusting Ejectors to Tactical Aircraft Having Vertical Lift and Short Field Capability." AIAA Paper 81-2629, 1981.

14. Aoyagi, K., Falarski, M. D., and Koenig, D. G., "Wind Tunnel Investigation of a Large-Scale Upper Surface Blown-Flap Transport Model Having Two Engines." NASA TM X-62,296, 1973.

15. Koenig, D. G., and Aoyagi, K., "Maximum Lift of Upper Surface Blowing STOL Aircraft with Swept Wings." AIAA Paper 75-868, Hartford, Conn., 1975.

16. Gambucci, B. J., Aoyagi, K., and Rolls, L. S., "Wind Tunnel Investigation of a Large-Scale Model of a Lift/Cruise Fan V/STOL Aircraft." NASA TM X-73,139, 1976.

17. Gambucci, B. J., Aoyagi, K., and Rolls, L. S., "Wind Tunnel Investigation of a Large-Scale Model of a Lift/Cruise Fan V/STOL Aircraft with Extended Lift/Cruise Nacelles." NASA TM X-73,164, 1976.

18. "Wind Tunnel and Ground Static Investigation of a Large Scale Model of a Lift/Cruise Fan V/STOL Aircraft." NASA CR-137,916, 1976.

19. Hollingsworth, E. G., Aiken, T. N., and Ragget, J., "Validation of AV-8B V/STOL Characteristics of Full-Scale Static and Wind-Tunnel Tests." AIAA Paper 77-597, Moffett Field, Calif., 1977.

20. Steinle, F., and Stanewsky, E., "Wind Tunnel Flow Quality and Data Accuracy Requirements." AGARD-AR=184, Nov. 1982.

21. Mobey, D. G., "Flow Unsteadiness and Model Vibration in Wind Tunnels at Subsonic and Transonic Speeds." C.P. No. 1155, British A.R.C., 1971.

22. Paterson, Robert W., Vogt, Paul G., and Foley, William M., "Design and Development of the United Aircraft Research Laboratories Acoustic Research Tunnel." J. Aircraft, Vol. 10, No. 7, July 1973, pp. 427-433.

23. Seidel, M., and Jaarsma, F., "The German-Dutch Low Speed Wind Tunnel DNW." Aeronaut. J., RAS, Apr. 1978.

24. Duits Nederlands Windtunnel Staff, Noordoostpolder, The Netherlands — Compilation of Calibration Data of the German-Dutch Wind Tunnel. MP-82.01, Mar. 1982.

25. Herkes, W. H., and Strout, F. G., "Acoustic Evaluation of the DNW Free Jet Shear Layer Correction Using a Model Jet." AIAA Paper 83-757, 1983.

26. Christophe, J., "The ONERA Wind Tunnels at Mondane Centre and Le Eouga Centre and Their Utilization in Subsonic Range." Office National d'Etudes et de Recherches Aërospatiales, T.P. n 1983-28. Paper was also presented at the 19th Subsonic Aerodynamic Testing Association, Meeting College Station, Kansas, April 18-20, 1983.

27. Applin, Z. T., "Flow Improvement in the Circuit of the Langley 4- by 7-Meter Tunnel." NASA TM-85662, 1983.

28. "The Boeing V/STOL Wind Tunnel Users Manual." Boeing Vertol Company, Philadelphia, Pa., Oct. 1982.

29. Mort, Kenneth W., Soderman, Paul T., and Eckert, William T., "Improving Large-Scale Testing Capability by Modifying the 40- by 80-Foot Wind Tunnel." AIAA Paper 77-587, 1977.

30. "Guide for Planning Investigations in the Ames 40- by 80-Foot Wind Tunnel Operated by the Large-Scale Aerodynamic Branch." Ames Research Center, Moffett Field, Ca., June 1978.

31. Grafton, S. B., Gilbert, W. P., Croom, M. A., and Murr, D. G., "High-Angle-of-Attack Characteristics of a Forward-Swept Wing Fighter Configuration." AIAA Paper 82-1322, 1982.

32. Phelps, A. E., III, "Summary of Low Speed Aerodynamic Characteristics of Upper-Surface-Blown Jet-Flap Configurations." Paper No. 4, NASA SP-406, 1976.

33. " The 9M V/STOL Wind Tunnel — A Brief Description and Photo Review of Projects." National Research Council of Canada, Ottawa, Canada, July, 1979.

34. Knott, P. G., "V/STOL Aerodynamic Testing Techniques at British Aircraft Corporation." AIAA Paper 77-584, 1977.

35. Grief, R. K., Kelly, M. W., and Tolhurst, W. H., "Wind-Tunnel Tests of a Circular Wing with an Annular Nozzle in Proximity to the Ground." NASA TN D-317, 1960.

26. East, L. F., "The Measurement of Ground Effect Using a Fixed Ground Board in a Wind Tunnel." ARC, R & M 3689, 1972.

37. Betzina, M. D., and Kita, R. D., "Aerodynamics Effects of an Attitude Control Vane on a Tilt Nacelle V/STOL Propulsion System." AIAA Paper 79-1855, 1979.

38. Demers, W. J., Metzger, F. B., Smith, L. M., and Wainauski. H. S., "Testing of the Hamilton Standard Q-Fan Demonstrator (Lycoming T55-L-11A Core Engine." NASA CR-121,265, 1973.

39. Betzina, M. D., and Falarski, M. D., "Aerodynamics of a Tilt-Nacelle V/STOL Propulsion System." NASA TM-78606, 1979.

40. Weiberg, J. A., and Maisel, M. D., "Wind Tunnel Tests of the XV-15 Tilt Rotor Aircraft." NASA TM-81177 (also AVRADCOM TR80-A03, April 1980).

41. Schoers, L. G., "Dynamic Structural Aeroelastic Stability Testing of the XV-15 Tilt Rotor Research Aircraft." NASA TM-84293 (also USAAVRADCOM 82-A-17), 1982.

42. Smeltzer, D., Nelms, W., and Williams, T., "Airframe Effects on a Top-Mounted Inlet System for V/STOL Fighter Aircraft." AIAA Paper 81-2631, 1981.

43. Durston, D. A., and Smeltzer, D. B., "Inlet and Airframe Compatibility for a V/STOL Fighter/Attack Aircraft with Top-Mounted Inlets." NASA TM-84252.

44. Schetz, J. A., and Jakubowski, A. K., "Surface Pressured Induced on a Flat Plate with In-Line and Side-by-Side Dual Jet Configurations." AIAA Paper 83-1849, 1983.

45. Schetz, J. A., Jakubowski, A. K., and Aoyagi, K., "Jet Trajectories and Surface Pressures Induced on a Body of Revolution with Various Dual Jet Configurations." AIAA Paper 83-0080, 1983.

46. Aoyagi, K., and Snyder, P. K., "Experimental Investigation of a Jet Inclined to Subsonic Crossflow." AIAA Paper 81-2610, 1981.

47. Fearn, R. L., and Weston, K. P., "Induced Velocity Field of a Jet in a Cross Flow." NASA TP-1087, 1978.

48. Fearn, R. L., and Weston, R. P., "Velocity Field of a Round Jet in a Cross Flow for Various Jet Injection Angles and Velocity Ratios." NASA TP-1506, 1979.

49. Mavriplis, F., and Gilmore, D., "Investigation of Externally Blown Flap Airfoils with Leading Edge Devices and Slotted Flaps." AGARD V/STOL Aerodynamics, No. 143, Paper No. 7, April 1971.

50. Aiken, Thomas N., "Aerodynamic and Noise Measurements on a Quasi-Two-Dimensional Augmentor Wing Model with Lobe-Type Nozzles." NASA TM X-62,237, 1973.

51. Riley, D. R., "Wind Tunnel Investigation and Analysis of the Effects of End Plates on the Aerodynamic Characteristics of an Upswept Wing." NACA TN-2440, 1951.

52. Mahal, A. S., and Gilchrist, I. J., "Design Integration and Noise Studies for Jet STOL Aircraft — Task VIIB Augmentor Wing Cruise Blowing Valveless System." NASA CR-114,560, Jan. 1973.

53. Anscombe, A., and Williams, J., "Some Comments on High-Lift Testing in Wind Tunnels with Particular Reference to Jet-Blowing Models." AGARD Report 63, Aug. 1956.

54. Schoen, A. H., Kolesar, C. E., and Schaeffer, E. G., "Static, Noise, and Transition Tests of a Combined-Surface-Blowing V/STOL Lift/Propulsion System." NASA CR-151,954, April 1977.

55. "Advancement of Proprotor Technology Task II — Wind Tunnel Test Results." NASA CR-114,363, 1971.

56. Durston, D. A., and Schreiner, J. A., "High-Angle of Attack Aerodynamics of a Strake-Canard-Wing V/STOL Fighter Configuration." AIAA Paper 83-2510, Oct. 1983.

57. Bailey, R. O., Smith, S. C., and Gustie, J. B., "Propulsion Simulation Test Technique for V/STOL Configurations." Society of Automotive Engineers TP-83-1427, Oct. 1983.

58. Mraz, M. R., and Hiley, P. E., "Propulsion Airframe Aerodynamics Interactions of Supersonic V/STOL Configurations, Phase I." McDonnell Douglas MDC A7238, St. Louis, Mo., NASA Contract NAS2-10791, July 1981.

59. Schnell, W. C., Ordonez, G. W, and Smeltzer, D. B., "Axisymmetric and Non-Axisymmetric Exhaust-Jet-Induced Effects on a V/STOL Vehicle Desigh. Part III. Experimental Technique." NASA CR-156,147, 1981.

60. Stoll, F., "Large-Scale Wind Tunnel Tests of a Sting Supported V/STOL Fighter Model at High Angles-of-Attack." AIAA Paper 81-2621, 1981.

61. Stoll, F., Koenig, D. G., "Large-Scale Wind Tunnel Investigation of a Close-Coupled Canard-Delta Wing Fighter Model through High Angles-of-Attack." AIAA Paper 83-2554, 1983.

62. Laub, Georgene H., "Low Speed Wind Tunnel Tests on a One-Seventh Scale Model of the H.126 Jet Flap Aircraft." NASA TM X-62,433, 1975.

63. Trebble, W. J. G., "Technique for the Aerodynamic Testing of V/STOL Models." AGARD, AGARDograph 126, May 1968.

64. Cook, W. L., and Whittley, D. C., "Comparison of Model and Flight Test Data for an Augmented Jet Flap STOL Research Aircraft." NASA TM X-62491, 1975.

65. Hickey, D. H., and Cook, W. L., "Correlation of Wind-Tunnel and Flight-Test Aerodynamic Data for Five V/STOL Aircraft." AGARD, Flight Mechanics Panel Meeting, Oct. 1965.

66. Vogler, R. D., "Ground Effects on Single- and Multiple-Jet VTOL Models at Transition Speeds over Stationary and Moving Ground Planes." NASA TN D-3213, Jan. 1966.

67. Campbell, J. P., Hassell, J. L., and Thomas, J. L., "Recent Research on Powered Lift STOL Ground Effects." AIAA Paper 77-574, 1977.

68. Turner, T. R., "A Moving Belt Ground Plane for Wind Tunnel Ground Simulation and Results for Two Jet-Flap Configurations." NASA TN D-4228, 1967.

69. Butler, S. F. J., Moy, B. A., and Pound, T. N., "A Moving-Belt Rig for Ground Simulation in Low-Speed Wind Tunnels." Aeronautical Research Council, R & M., No. 3451, 1967.

70. Hackett, J. E., Boles, R. A., and Lilley, D. E., "Ground Effect for V/STOL Aircraft Configurations and Its Simulation in the Wind Tunnel." "Pt. I. Introduction and Theoretical Methods." "Pt. II. Experimental Studies." "Pt. III. The Tangentially Blown Ground as an Alternative to a Moving Ground, Application to the Ames 40 by 80." NASA CRs 114,495; 114,496; and 114,497, 1974.

71. Poisson-Quinton, Ph., and Christophe, J., "Special Ground Testing Facilities and Testing Techniques for STOL Aircraft." Von Karman Institute for Fluid Dynamics, Lecture Series 60, STOL Technology, Sept. 1973.

72. Hackett, J. E., Boles, R. A., Lilley, D. E., "Ground Simulation and Tunnel Blockage for a Jet-Flapped, Basic STOL Model Tested to Very High Lift Coefficients." NASA CR-137,857, 1976.

73. Crowder, J. P., Goldhammer, M. I, and Smyth, D. N., "STOL Aircraft Transient Ground Effects. Pt. II. Experimental Techniques Feasibility Study." NASA CR-137,767, 1975.

74. Wolowicz, C. H., Bowman Jr., J. S., and Gilbert, W. P., "Similitude Requirement and Scaling Relationships as Applied to Model Testing." NASA TP-1435, 1979.

75. Gainer, T. G., and Hoffman, S., "Summary of Transformation Equations of Motion Used in Free-Flight and Wind Tunnel Data Reduction and Analysis." NASA SP-3070, 1972.

76. Paulson, John W., "Investigation of the Low-Speed Flight Characteristics of a 1/15 Scale Model of the Convair XV-58 Airplane." NACA RM-SL57K19.

77. Putnam, W. F., and Curtiss, H. C., Jr., "Low Speed Testing-Techniques for V/STOL Aircraft in the Princeton Dynamic Model Track." AIAA Paper 79-0334, 1979.

78. Putnam, W. F., "Tests on a Twin-Turbofan V/STOL Model in Ground Effect in the Dynamic Model Track," Princeton University, Princeton, New Jersey, Final Report for Navy Contract N62269-79-C-0223, Jan. 1983.

79. Heyson, Harry H., "Wind Tunnel Testing of VTOL and STOL Aircraft." NASA TM-7850, 1978.

80. Maskell, E. C., "A Theory of the Blockage Effects on Bluff Bodies and Stalled Wings in a Closed Wind Tunnel." Royal Aeronautical Establishment R&M No. 3400, Nov. 1963.

81. Peitzman, F. W., "Determination of High Attitude Wall Corrections in a Low Speed Wind Tunnel." AIAA Paper 78-810, 1978.

82. Hackett, J. E., "Living with Solid Walled Wind Tunnels." AIAA Paper 82-0583, 1982.

83. Hackett, J. E., Wilsden, D. J., and Lilley, D. E., "Estimation of Tunnel Blockage from Wall Pressure Signatures: A Review and Data Correlation." NASA CR-152,241, 1979.

84. Snyder, L. D., and Erickson, L. L., "PAN-AIR Prediction of NASA Ames 12-Foot Pressure Wind Tunnel Interference on a Fighter Configuration." AIAA Paper 84-0219, 1984.

85. Tyler, R. A., and Williamson, R. G., "Experience with the NRC 10-ft x 20-ft V/STOL Propulsion Tunnel: Some Practical Aspects of V/STOL Engine Model Testing." NAE Quarterly Bulletin, No. 2, 1973, pp. 45-59, 61-75.

86. Hoad, D. R., and Gentry, G. L., Jr., "Longitudinal Aerodynamic Characteristics of a Low-Wing Lift Fan Transport Including Hover Characteristics in and out of Ground Effect." NASA TM X-34020, 1977.

87. "Conference on V/STOL and STOL Aircraft." NASA SP-116, 1966.

88. Carbonaro, M., "Interference Problems in V/STOL Testing at Low Speeds." AGARD-CP-174, No. 40, Oct. 1975.

89. Shindo, S., and Rae, W. H., Jr., "Low Speed Test Limit of V/STOL Models Located Vertically Off-Center." J. Aircraft, Vol. 15, No. 4, April 1978, pp. 253, 254.

90. Shindo, S., and Rae, W. H., Jr., "Recent Research on V/STOL Test Limits at the University of Washington Aeronautical Laboratory." NASA CR-3237, 1980.

91. Steinle, F. W., and Pejack, E. R., "Toward an Improved Transonic Wind-Tunnel Wall Geometry — A Numerical Study." AIAA Paper 80-0442, 1980.

92. Sears, W. R., "Adaptable Wind Tunnel for Testing V/STOL Configurations at High Lift." J. Aircraft, Vol. 20, No. 11, Nov. 1983, pp. 968-974.

93. Christiansen, R. S., "A Large Scale Investigation of V/STOL Ground Effects." AIAA Paper 84-0336, 1984.

94. Henderson, C., and Walters, M., "Development and Validation of the V/STOL Aerodynamics and Stability and Control Manual." AIAA Paper 81-2611, Dec. 1981.

95. Kuhlman, J. M., and Ousterhout, D. S., "Experimental Investigation of Effect of Jet Decay Rate on Jet-Induced Pressures on a Flat Plate." NASA CR-2979, 1978.

96. Kuhlman, J. M., and Warcup, R. W., "Jet Decay Rate Effects on Hover Jet-Induced Loads." J. Aircraft, Vol. 17, No. 8, Aug. 1980, p. 605.

97. Wulf, R., and Melzer, E., "Wind Tunnel Testing with Engine Simulation for V/STOL Airplanes." AGARD, V/STOL Propulsion Systems, No. 135, Paper No. 8, 1973.

98. Margason, Richard J., and Gentry, Carl L., "Static Calibration of an Ejector Unit for Simulation of Jet Engines in Small-Scale Wind Tunnel Modes." NASA TN D-3867, Mar. 1967.

99. Hoad, D. R., "Longitudinal Aerodynamic Characteristics of an Externally Blown Flap Powered Lift Model with Several Propulsive System Simulators." NASA TN D-7670, 1974.

100. Nicoloff, C. B., and Weber, H. A., "Characteristics of an Ejector-Type Engine Simulator for STOL Model Testing." AIAA Paper 72-1038, 1972.

101. Stewart, V. R., "Low Speed Wind Tunnel Tests of Ground Proximity and Deck Edge Effects on a Lift Cruise Fan V/STOL Configuration." NASA CR-152,247.

102. Hunt, D., Clingen, J., Salemann, V., and Omar, E., "Wind Tunnel and Ground Static Tests of a 0.094 Scale Powered Model of a Modified T-39 Lift/Cruise Fan V/STOL Research Airplane." NASA CR-151,923, 1977.

103. "Installation and Operation Manual, Model 1109, 12" Diameter, Tip-Turbine Fan." TM78-114, Tech Development, Inc., Dayton, Ohio, Oct. 1978.

104. Eigenman, M. F., and Bailey, R. O., "Development of the Propulsion Simulator — A Test Tool Applicable to V/STOL Configurations." Society of Automotive Engineers 770984, Nov. 1977.

105. Bailey, R., Mraz, M., and Hiley, P., "The Design of a Wind Tunnel V/STOL Fighter Model Incorporating Turbine Powered Engine Simulators." AIAA Paper 81-2635, 1981.

106. Harper, M., "The Propulsion Simulator Calibration Laboratory at Ames Research Center." AIAA Paper 82-0574, 1982.

107. Smith, S. C., "Determining Compressor Inlet Airflow in the Compact Multimission Aircraft Propulsion Simulators in Wind Tunnel Applications." AIAA Paper 83-1231, 1983.

108. Falarski, M. D., Whitten, P. D., and Harris, P. D., "Aerodynamic Characteristics of a Large Scale Model of a Highly Maneuverable Supersonic V/STOL Fighter: STOL Configuration." AIAA Paper 80-0234, 1980.

109. Dawson, C. R., "Ground Effects and Control Effectiveness Tests of a 0.095 Scale Powered Model of a Modified T-39 Lift/Cruise Fan V/STOL Research Airplane." Boeing Document D 180-20391-1, Boeing Aircraft Company, Seattle, Wash., Feb. 1977.

110. Juanareno, D. B., and Blumenthal, P. Z., "A Remote Millivolt Multiplexer and Amplifier Module for Wind Tunnel Data Acquisition." Pressure Systems Incorporated, Hampton, Va., NASA Lewis Contract, NAS3-22950.

111. Cambra, J. M., and Tolari, G. P., "Real-Time Computer Data System for the 40- by 80-Foot Wind Tunnel Facility at Ames Research Center." NASA TN D-7970, 1975.

112. Cambra, J. M., and Trover, W. F., "The Revolution in Data Gathering Systems." NASA TM X-62,452, 1975.

113. Schoenster, J. A., Willis, C. M., Schroeder, J. C., and Mixson, John S., "Acoustic-Loads Research for Powered-Lift Configurations." NASA SP-406, May 1976, pp. 429-443.

114. Strout, F. G., and Atencio, A., Jr., "Flight Effects on JT8D Engine Jet Noise as Measured in the NASA Ames 40- by 80-Foot Wind Tunnel." AIAA Paper 76-556, 1976.

115. Soderman, P. T., "Instrumentation and Techniques for Acoustic Research in Wind Tunnels." IEEE Publication 75 CHU 993 6 AES, 6th International Congress on Instrumentation in Aerospace Simulation Facilities, Ottawa, Canada, Sept. 22-24, 1975.

116. Falarski, M. D., Koenig, D. G., and Soderman, P. T., "Aspects of Investigating STOL Noise Using Large-Scale Wind-Tunnel Models." Journal of the Canadian Aeronautics and Space Institute, Vol. 19, No. 2, Feb. 1973.

117. Diedrich, J. H., and Luidens, R. W., "Measurement of Model Propulsion System Noise in a Low-Speed Wind Tunnel." AIAA Paper No. 76-91, 1976.

118. Ahtye, W. F., "Wing and Flap Noise Measured by Near- and Far-Field Cross, Correlation Techniques." AIAA Paper 79-0667, 1979.

119. Atencio, A., Jr., and Soderman, P. T., "Comparison of Aircraft Noise Measured in Flight Test and in the NASA Ames 40- by 80-Foot Wind Tunnel." AIAA Paper 73-104.7, 1973.

120. Cook, W. L., and Hickey, D. H., "Correlation of Low Speed Wind Tunnel and Flight Test Data for V/STOL Aircraft." NASA TM X-62,423, 1975.

121. Falarski, M. D., and Moore, M. T., "Acoustic Characteristics of Two Hybrid Inlets of Forward Speed," AIAA Paper 79-0678, 1979.

122. Moore, M. T., "Forward Velocity Effects on Fan Noise and the Suppression Characteristics of Advanced Inlets as Measured in the NASA Ames 40- by 80-Foot Wind Tunnel." NASA CR-152328, 1979.

123. Margason, R. J., "The Path of a Jet Directed at Large Angles to a Subsonic Free Stream." NASA TN D-4919, 1968.

124. Werle, H., "Flow Visualization Techniques for the Study of High Incidence Aerodynamics." AGARD VKI Lecture Series 121, 1982.

125. Merzkirch, W., ed., "Flow Visualization Proceedings of the Second International Symposium on Flow Visualization." Crowder, J. P., "Fluorescent Minitufts of Nonuniform Surfaces Flow Visualization." Proceedings of the Second International Symposium on Flow Visualization, Bochum, West Germany, pp. 663-667, Sept. 1980.

126. Imaichi, K., and Ohmi, K., "Numerical Processing of Flow-Visualization Pictures – Measurement of Two-Dimensional Vortex Flow." J. Fluid Mech., Vol. 129, Apr. 1983, pp. 283-311.

127. Hunt, J. C. R., Abell, C. J., Peterka, J. A., and Woo, H., "Kinematical Studies of the Flows around Free or Surface-Mounted Obstacles: Applying Topology to Flow Visualization." J. Fluid Mech., Vol. 86, May 1978, pp. 179-200.

128. Kao, H. C., and Burstadt, P. L., "Flow Visualization and Interpretation of Visualization Data for Deflected Thrust V/STOL Nozzles." NASA TM-83554, 1984.

129. Mueller, T. J., "Smoke Visualization in Wind Tunnels." Astronaut. Aeronaut., Jan. 1983, pp. 50-62.

130. Naeseth, Roger L., and Hoad, Danny R., "Upwash Angles Near Engine Inlets of an Externally Blown Flap STOL Transport." NASA TN D-8091, 1975.

131. Everett, K. N., Gerner, A. A., and Durston, D. A., "Theory and Calibration of Non-Nulling Seven Hole Cone Probes for Use in Complex Flow Measurement." AIAA Paper 82-0232, 1982.

132. Orloff, K. L., Snyder, P. K., and Reinath, M. S., "Laser Velocimetry in the Low Speed Wind Tunnels at Ames Research Center." NASA TM-85885, 1984.

133. Orloff, K. L., and Snyder, P. K., "Laser Doppler Anemometer Measurements Using Nonorthogonal Velocity Components: Error Estimates." Appl. Opt., Vol. 21, Jan. 1982, pp. 339.

134. Beranl, L. D., and Sarohia, V., "Entrainment and Mixing in Thrust Augmenting Ejectors." AIAA Paper 83-0172, 1983.

135. Reinath, M. S., Orloff, K. L., and Snyder, P. K., "A Laser Velocimeter System for the Ames 40- by 80-Foot and 80- by 120-Foot Wind Tunnels." AIAA Paper 84-0414, Jan. 1984 (also NASA TM-84393, 1984).

TABLE 1.- EVALUATION OF FIXED FRAME FACILITIES (REPRINTED FROM REF. 10)

Facility requirements	Objectives	NASA/ Langley	NASA/ Lewis	NASA/Ames 7' × 10'	NASA/Ames 40' × 80'	GE open throat anechoic wind tunnel
Nozzle weight flow	25 lbm/sec	17 lbm/sec	25 lbm/sec	25 lbm/sec with modification	25 lbm/sec with modification	42 lbm/sec
Nozzle size	4" - 6"	?	4" - 6"	4"	6"	6"
Exhaust gas total temperature range	520°R-2500°R	Burner needs to be provided	Ambient	Ambient	Ambient - 1600°R	Ambient - 3000°R
Nozzle pressure ratio	1.5 - 4.0	?	1.5 - 4.0	1.0 - 2.5	1.0 - 2.5	1.5 - 4.0
Free stream velocity range	0-400 ft/sec	0-400 ft/sec	0-220 ft/sec	0-400 ft/sec	0-325 ft/sec	0-330 ft/sec
Facility wall type	Anechoic	Anechoic	Hardwall	Scottfelt	Partially treated	Anechoic
Performance measurements	Proven nozzle performance system + 1/2% accuracy	Extensive modifications	Will have capability by Dec. 1974	Extensive modifications	Extensive modifications	Feasibility to be studied
Facility availability	1974, 1975, 1976	1974, 1975 1976	1976	1974, 1975, 1976	9 weeks/yr	1975, 1976
Duration of operation	Continuous	Blowdown	Continuous	Continuous	Continuous	Continuous
Capable of performing laser velocimeter measurements	Large window high quality optical glass	Minor modifications	Would require modifications	Yes	Would require modifications	Designed to accept laser velocimeter

TABLE 2.- REDUCED VELOCITY SCALE (FROM REF. 34)

V_o/V_j	0.05	0.075	0.10	0.15	0.20	0.30	0.50
C_μ $(S/A_j = 40)$	20	9	5	2	1.25	0.6	0.2
V_o Full scale, m/sec	20	30	40	60	80	120	200
V_j	400						
V_o Model scale, m/sec	20						
V_j	400	267	200	133	100	67	40
$\left(\frac{V_o \text{ model scale}}{V_o \text{ full scale}}\right)$	1.0	0.67	0.5	0.33	0.25	0.17	0.1

TABLE 3.- ACCEPTABLE LIMITS TO WALL CORRECTIONS (FROM REF. 88)

Parameter	Maximum acceptable corrections	Moderate corrections	No corrections
$\Delta\alpha$	± 5°	± 5°	± 1/2°
q_c/q	1 ± 10%	1 ± 10%	1 ± 5%
Δi_t	± 5°	± 2°	± 1/2°
q_t/q_c	1 ± 10%	1 ± 5%	1. ± 5%
Δi_w	± 2°	± 1/2°	± 1/2°
$d(\Delta i_w)/d(y/b)$	± 5°/semispan	± 1°/semispan	± 1°/semispan
$\Delta q/q_c$	± 10%	± 5%	± 5%

CORRESPONDING LIMITS FOR A JET FLAPPED WING OF ASPECT RATIO 6; B/H = 4/3

	Moderate corrections	Maximum corrections
Normal mounting at the center of a 4:3 test section		
b/B = 1/2	$C_L < 6.3$	$C_L = 14.1$
b/B = 3/4	$C_L < 0.81$	$C_L < 4.14$
Semispan mounting on the floor of a 4:3 test section		
(b/2)/H = 1/3	$C_L < 15$	$C_L < 20.4$
(b/2)/H = 1/2	$C_L < 4.86$	$C_L < 11.0$
(b/2)/H = 2/3	$C_L < 2.4$	$C_L < 5.82$

TABLE 4.- JET THRUST SIMULATION (FROM REF. 5 WITH ADDITIONS)

Nacelle type	Air supply requirement	Principal simulations	Other simulation capabilities	Comment
Flow	None	•Inlet geometry •Inlet V_j/V_∞ at one Mach No.	•Dual flow	•Simple •Good for aerodynamic drag studies
Blown jet	Large	•Exhaust nozzle geometry •Gross thrust	•Dual flow •Hot gas	•Simple operation •Erroneous inlet contribution
Ejector	Moderate	•Inlet geometry/or •Exhaust nozzle geometry/and •Gross thrust	•Dual flow	•Inlet and exhaust flow not simulated simultaneously
Turbine powered	Small	•Inlet geometry or exhaust nozzle geometry •Inlet V_j/V and not gross thrust •Gross thrust and not inlet V_j/V		•Sensitive mechanism •Difficult to simulate inlet and exhaust flow simultaneously
Gas turbine powered	Small	•Inlet and exhaust nozzle geometry •Inlet V_j/V plus gross thrust •Exhaust Mach No. and temperature	•Dual flow	•For subscale use bypass ratio may not always be simulated •For subscale, engine is often over size

TABLE 5.- LEVELS OF SOPHISTICATION: LARGE-SCALE MODELS

Generally Increasing Model Cost >				
Factor	1	2	3	4
Airframe	Approximated configuration	Scaled configuration	Full-scale configuration	
Propulsion	Simulated propulsion	Engine used but small	Including some structure	Aircraft
Controls	Scaled		Same engine	
Dynamics				
Electronics				
Other				
Examples				
Model type	1	2	3	4
Complete configuration	High α (0.4 scale) (VATOL models)	CSRA model	AV-8B 40 by 80	XFV 15 40 by 80
	Q-fan simulation of tilt nacelle	Basic USB/EBF research models	G 698 40 by 80	AV-8B (static)
		M-26C		XFV 12A
		97 powered ejector model		Tether and static
Semispan	Aug Wing 40 by 80	Cooling drag	Cooling drag	NA
Components	Thrust reverser	Acoustic test 40 by 80	698 nacelle "C" nozzle	NA

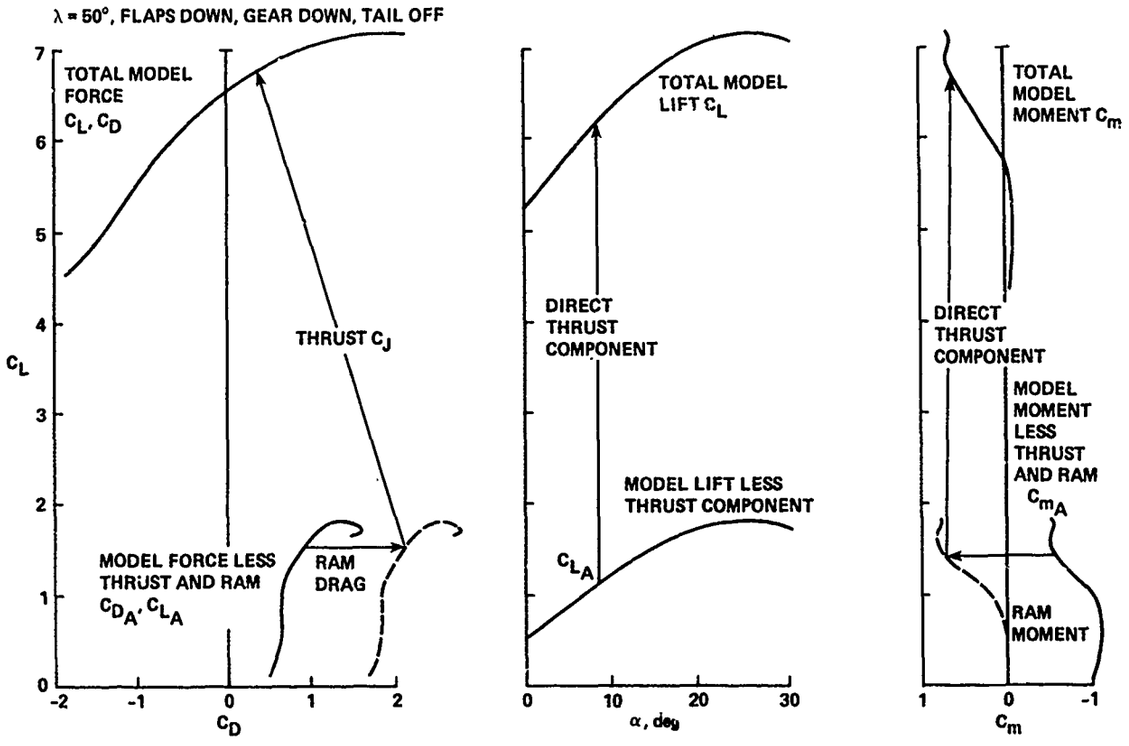

Figure 1. Induced effects for transition flight.

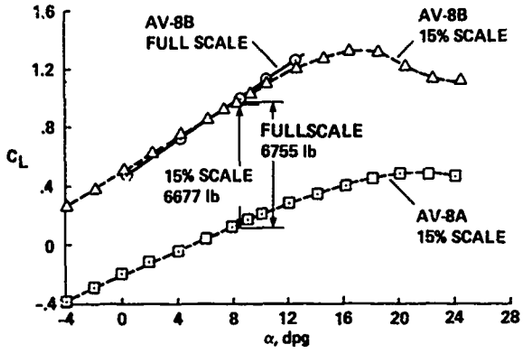

Figure 2. Comparison of large- and small-scale test data for the AV-8B (Ref. 8).

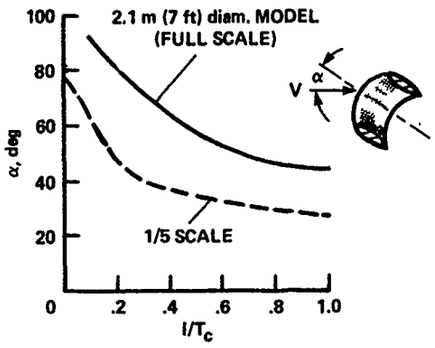

Figure 3. Effect of scale on duct inlet stall boundary (Ref. 4).

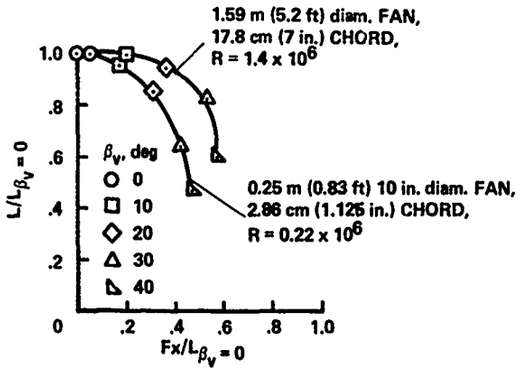

Figure 4. Performance of large- and small-scale exit vanes (Ref. 4).

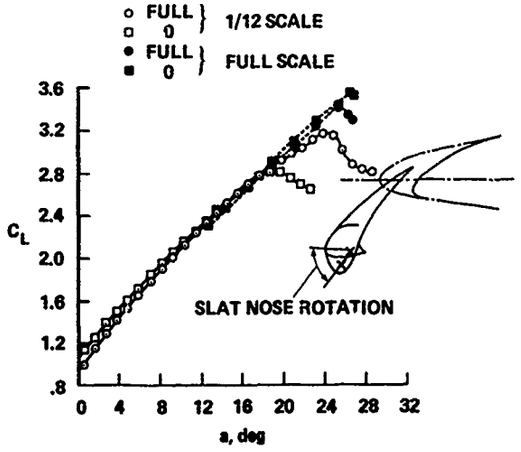

Figure 5. Effect of scale on the lift characteristics of the F111A airplane landing configuration (Ref. 4).

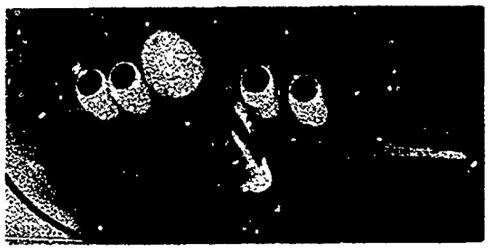

b = 1.91 (6.25) MOUNTED
IN 40 BY 80 INSERT -- LANGLEY
V/STOL TUNNEL

b = 11.62 (38.18) MOUNTED
IN 40 BY 80

Figure 6. Externally blown flap models with the same wing-flap geometry.

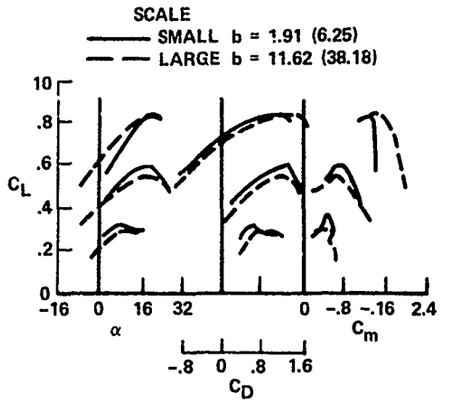

Figure 7. Comparison of wind-tunnel test results on the externally blown flap models of Fig. 6 (Ref. 4).

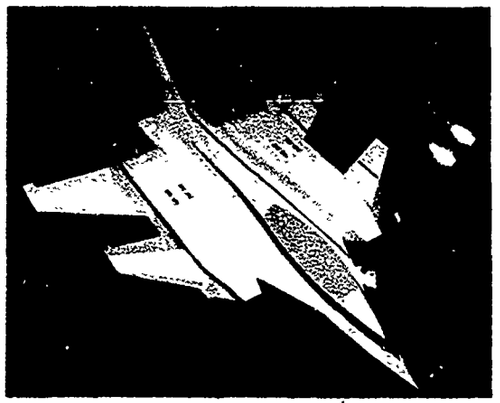

Figure 8. Large-scale J97-powered model of the GD205 two-engine fighter configuration.

Figure 9. Rotor test rig mounted in the Ames 40 by 80 tunnel.

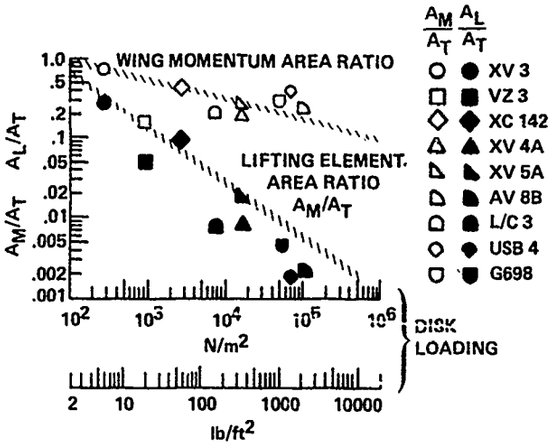

(a) Lift and momentum area sizing.

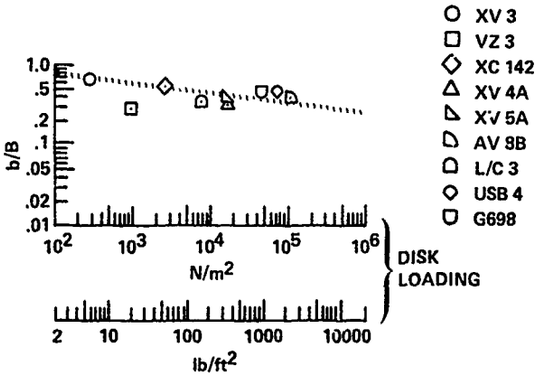

(b) Wing span sizing.

Figure 10. Sizing parameters (Ref. 4).

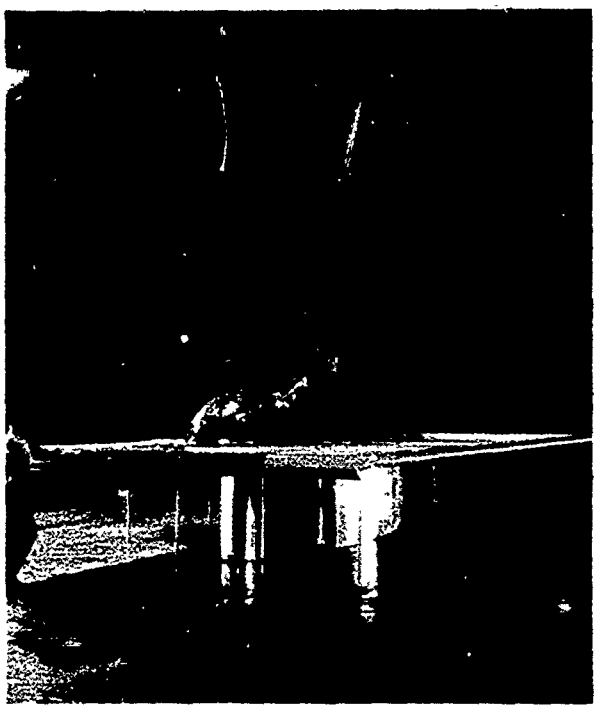

Figure 11. Bell/NASA ejector flap wing semispan model mounted in the Ames 40 by 80 wind tunnel (Ref. 12).

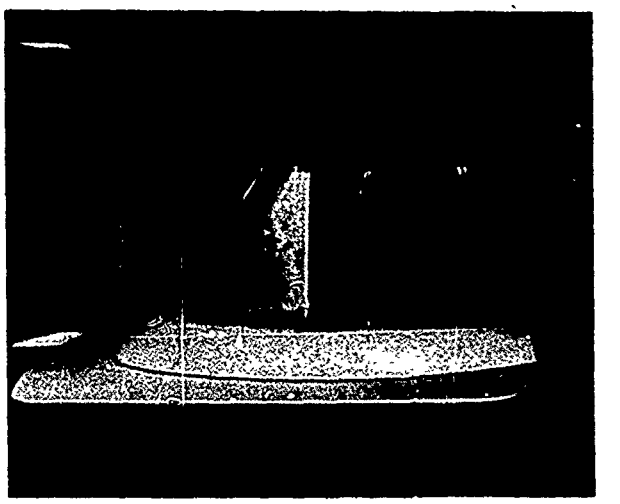

Figure 12. The Air Force ejector mounted in a semispan installation in the Ames 7 by 10 tunnel: $\delta_f = 90^0$ (Ref. 13).

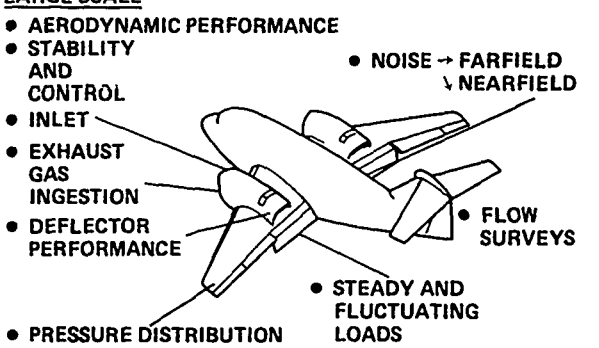

Figure 13. Measurements using large- and small-scale models (Ref. 4).

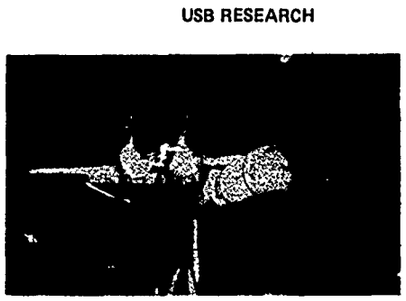

(a) An in-house basic research project.

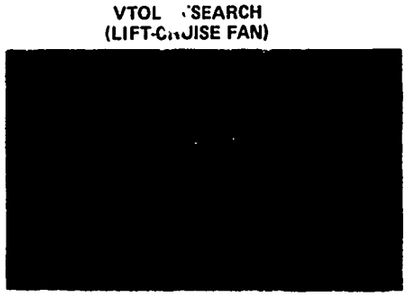

(b) A joint service R. & D. project.

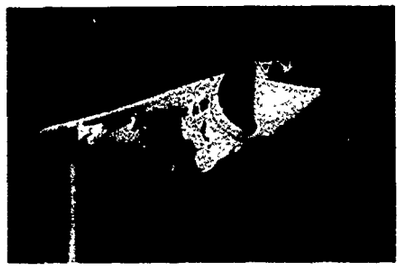

(c) A military development program.

Figure 14. Organization and costs of some large-scale V/STOL wind-tunnel investigations (Ref. 4).

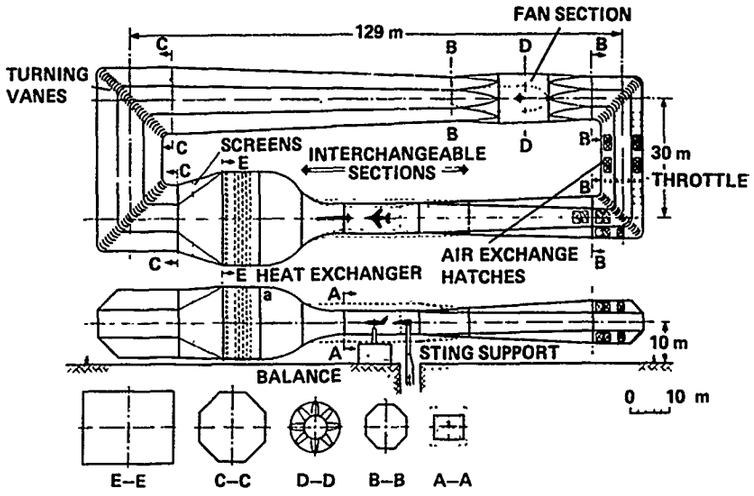

	WORKING SECTION			
CROSS-SECTIONAL SHAPE & SIZE, m X m	9.5 × 9.5	6 × 8	6 × 6	6 × 8
TYPE	CLOSED	CLOSED	CLOSED	OPEN
USABLE LENGTH, m	15	16	9	20
MAX. AIR SPEED, m/sec	62	117	153	80
CONTRACTION RATIO	4.8	9.0	12.0	9.0
MAX. MODEL SPAN, m	≈ 6.5	≈ 5.5	≈ 4.2	≈ 4.0

Figure 15. DNW wind tunnel (Refs. 23, 24).

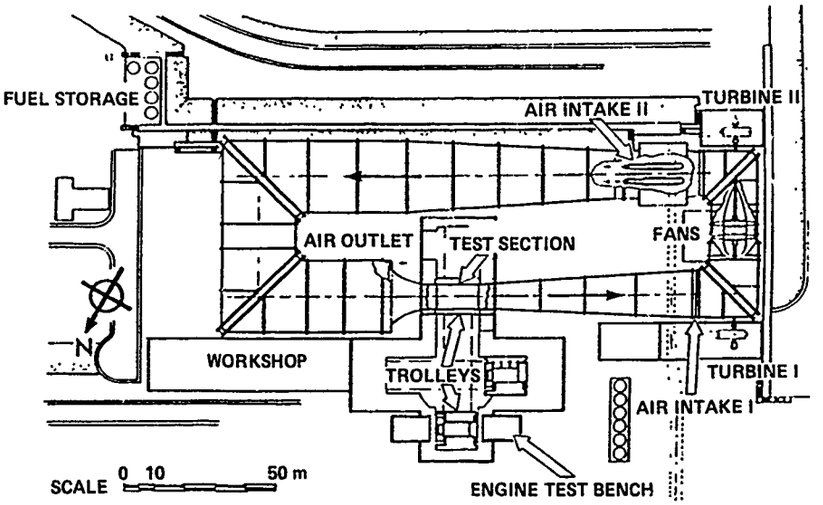

(a) General layout.

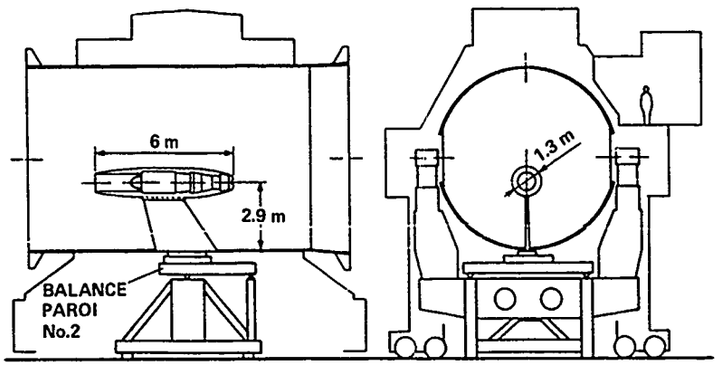

(b) One of the test sections.

Figure 16. ONERA-Modane 8M Facility (Ref. 26).

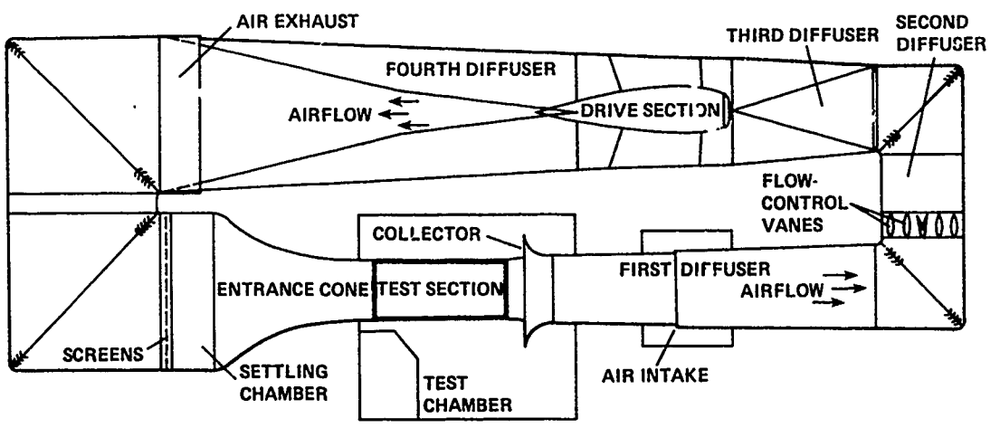

Figure 17. Planview of the Langley 4 by 7 tunnel (Ref. 27).

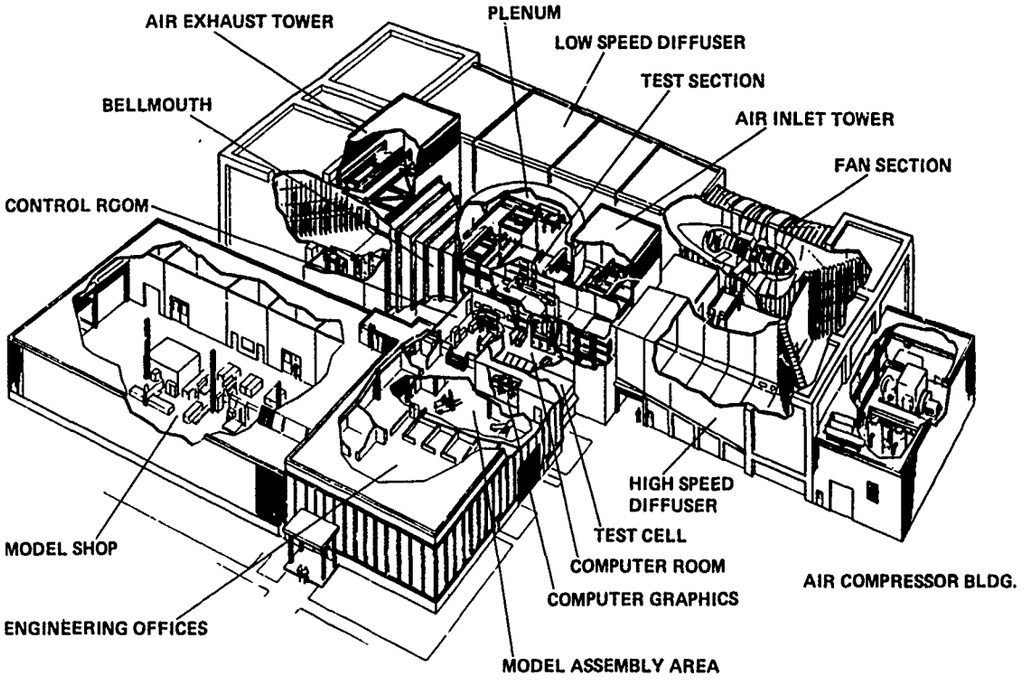

Figure 18. Boeing V/STOL wind tunnel (Ref. 28).

Figure 19. The test section of Boeing V/STOL wind tunnel: open-throat mode.

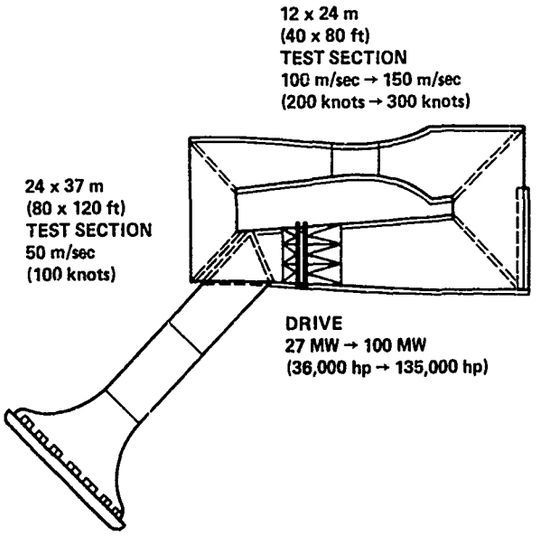

Figure 20. Ames large-scale wind-tunnel system (Ref. 29).

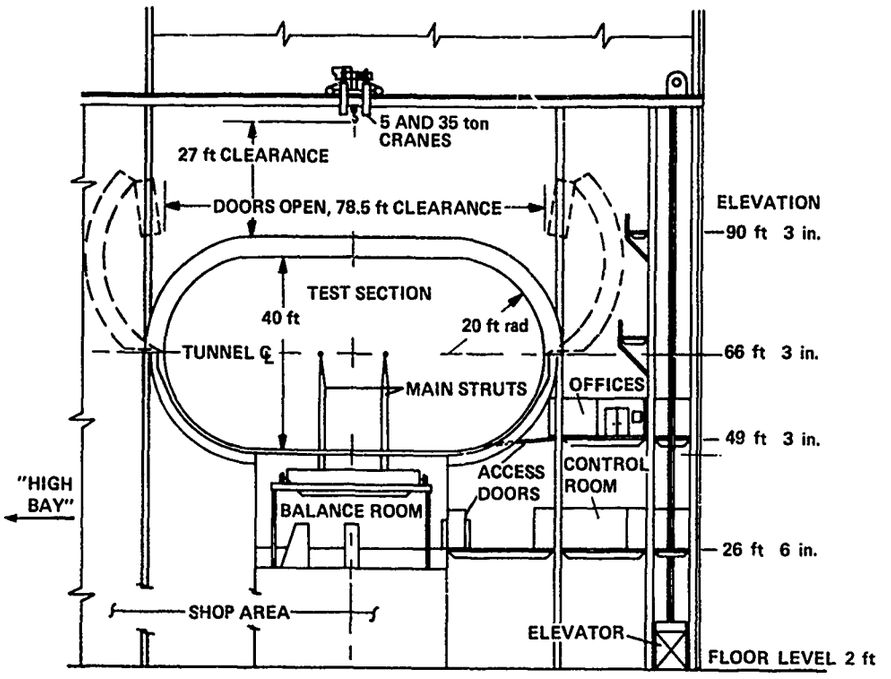

Figure 21. Elevation of Ames 40 by 80 test section.

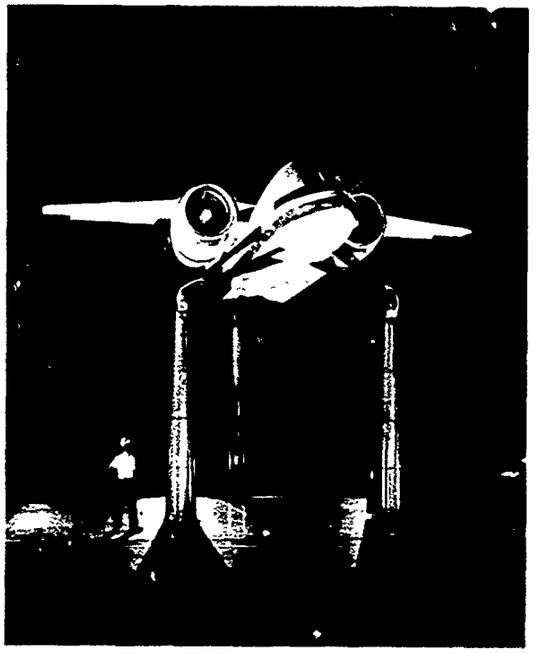

Figure 22. Complete model (G698) installed in the Ames 40 by 80 test section.

Figure 23. Sketch of Ames 80 by 120 test section.

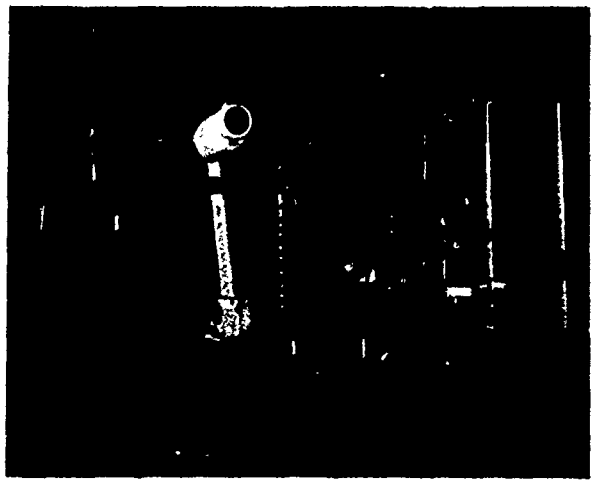

(a) Compressor noise studies: hybrid inlet.

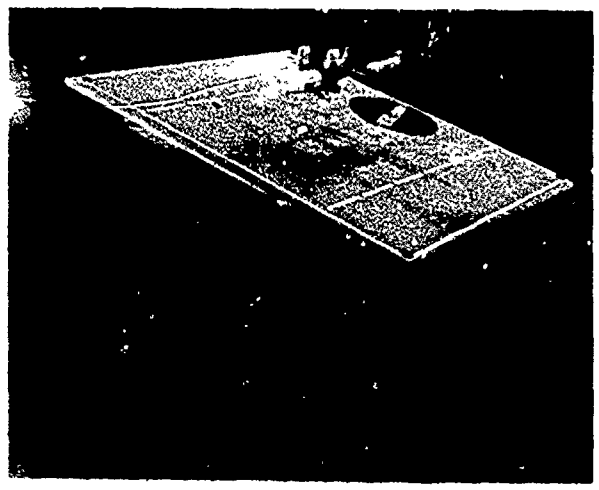

(b) 0.11-scale G698 hover tests.

Figure 24. Special test setups in the Ames 40 by 80 tunnel.

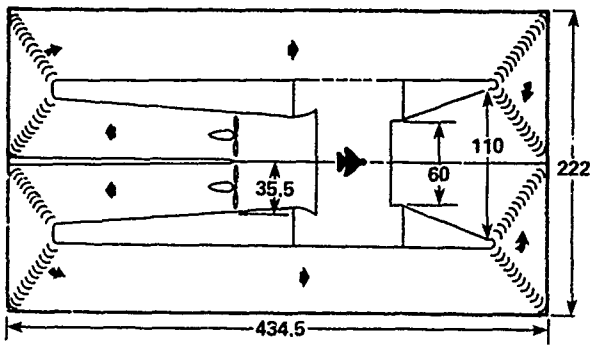

ALL DIMENSIONS IN FEET

Figure 25. Langley 30 by 60 wind tunnel.

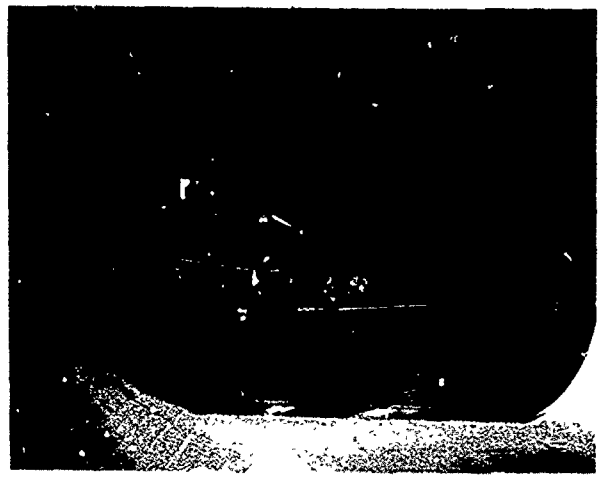

Figure 26. Langley 30 by 60 test section.

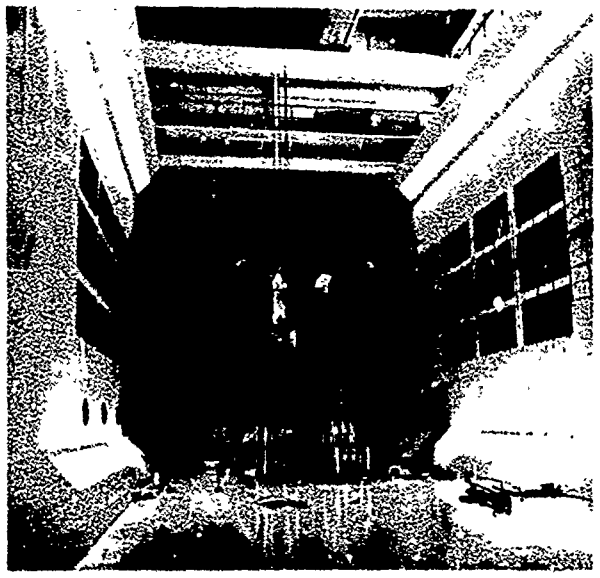

Figure 27. The test section of the NRC 9-m wind tunnel.

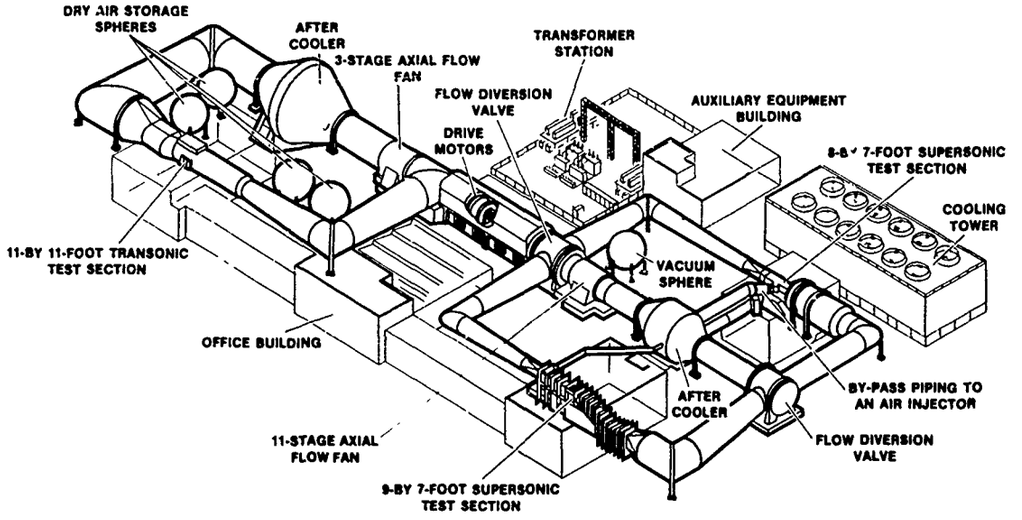

Figure 28. Ames Unitary Wind Tunnel System.

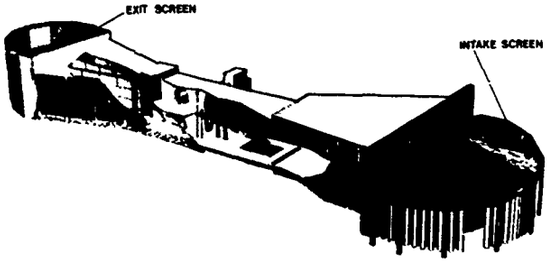

Figure 29. BAC 5.5-m (18 ft) open-throat wind tunnel (Ref. 34).

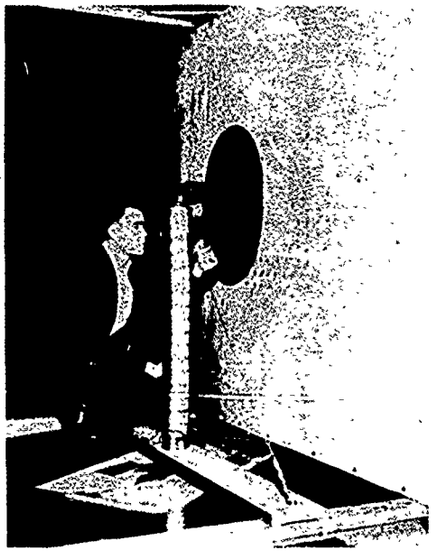

Figure 30. General arrangement of circular wing and ground plane (Ref. 35).

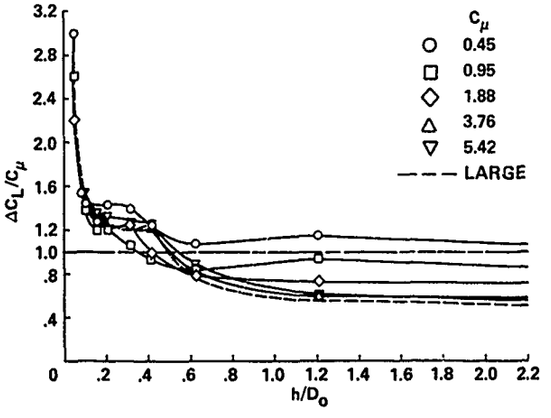

Figure 31. Effect of C_μ on the circular wing vertical thrust variation with altitude: $\alpha = 0^\circ$ (Ref. 35).

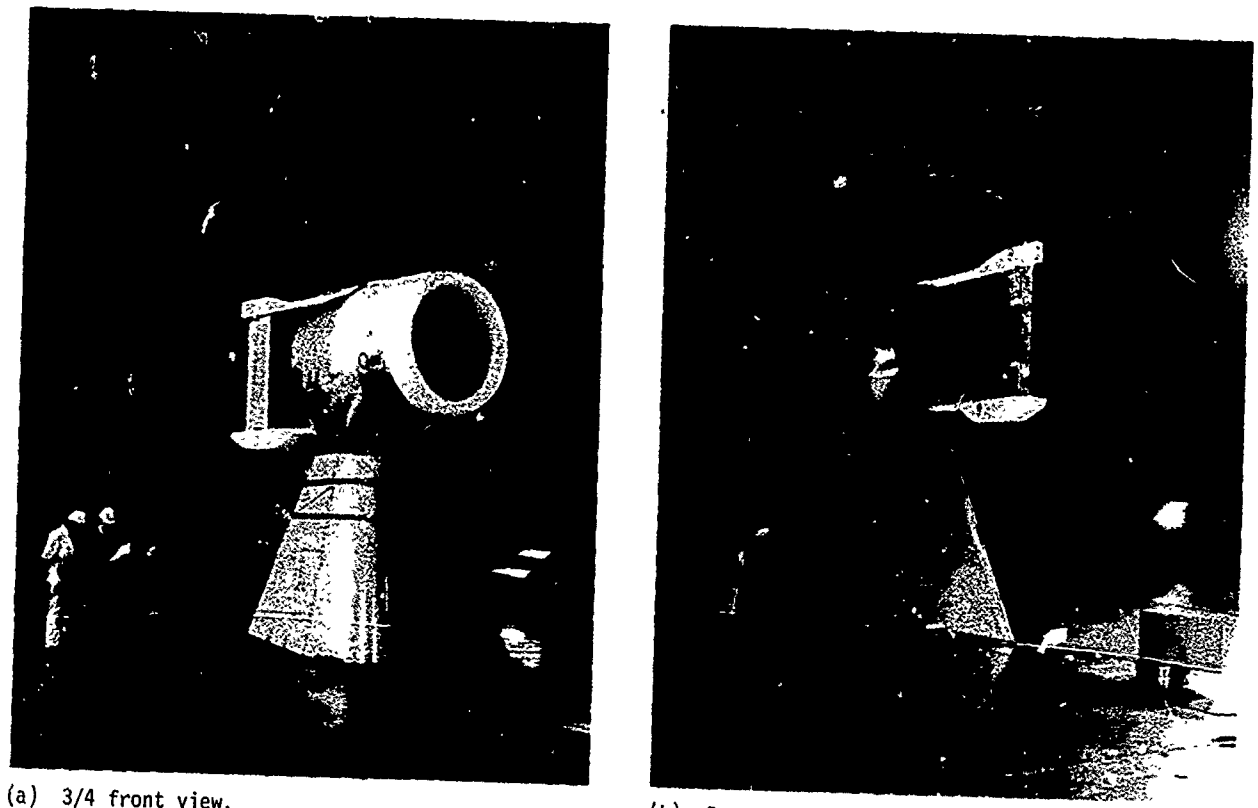

(a) 3/4 front view.

(b) Rear view.

Figure 32. Q fan and a pitch-control vane mounted in the Ames 40 by 80 tunnel (Ref. 37).

(a) XFV3 flight tests.

(b) Small-scale tests.

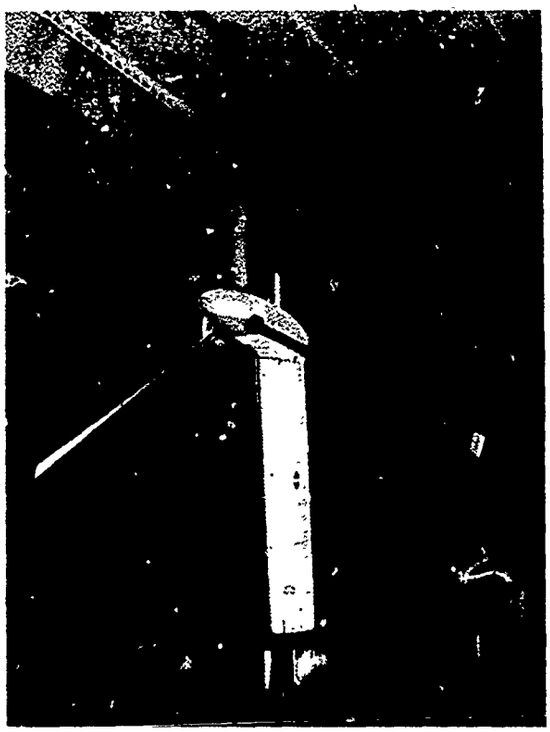

(c) Semispan tests.

(d) Dynamometer tests.

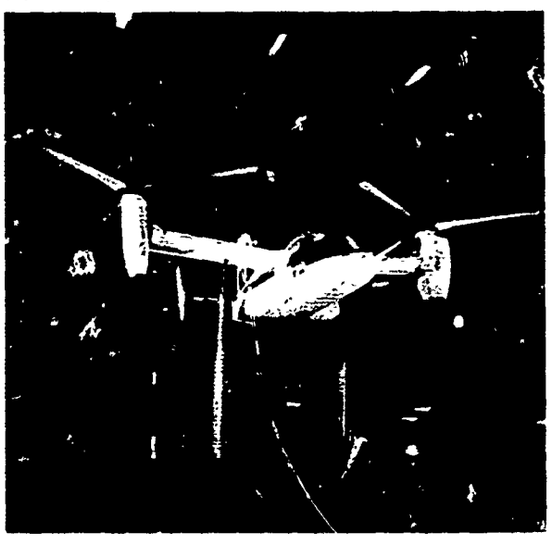

(e) Full-scale wind-tunnel tests.

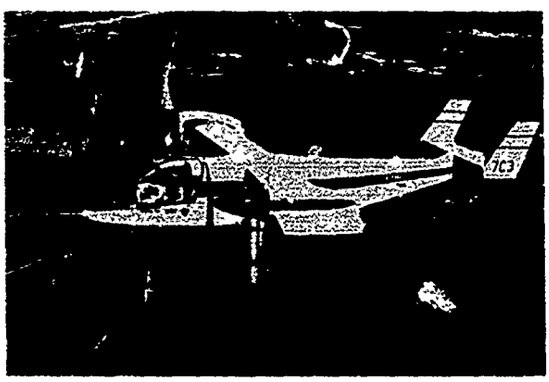

(f) XV15 in flight.

Figure 33. XV-15 development.

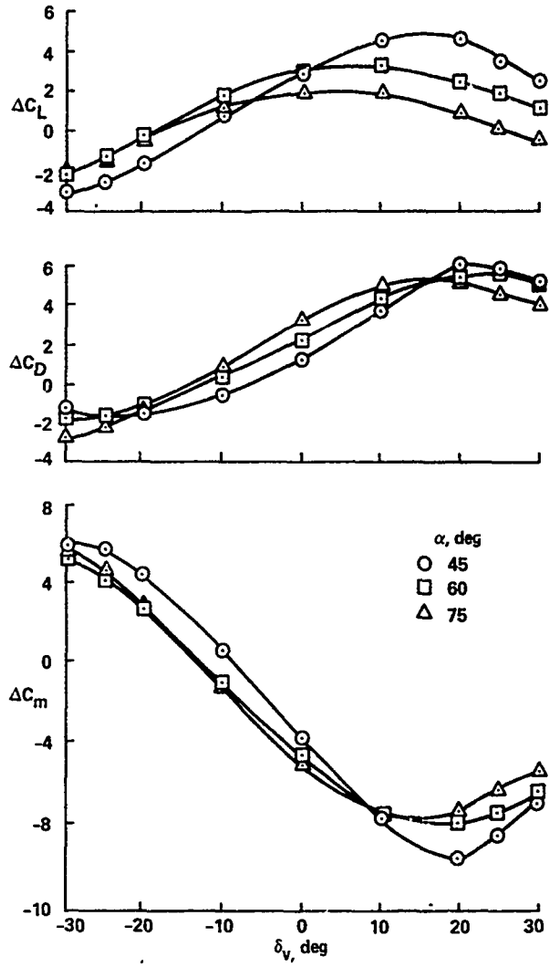

Figure 34. Effectiveness of the pitch-control vane for the subsonic tilt nacelle aircraft: C_J = 10 (Ref. 37).

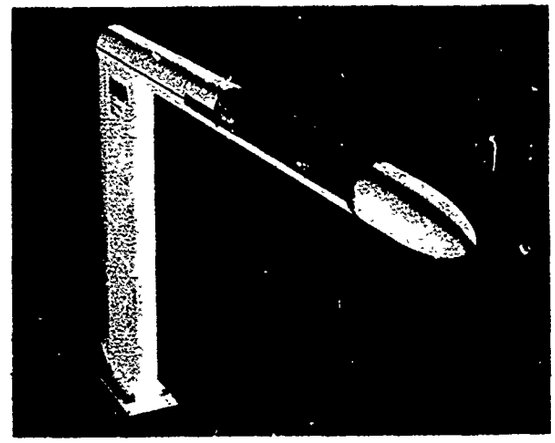

Figure 36. Jet-in-cross-flow body mounted in Ames 7 by 10 wind tunnel (Ref. 46).

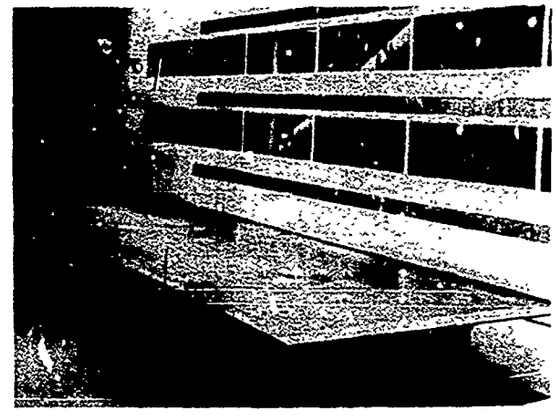

Figure 37. Jet-in-cross-flow installation in the Langley V/STOL wind tunnel (Ref. 47).

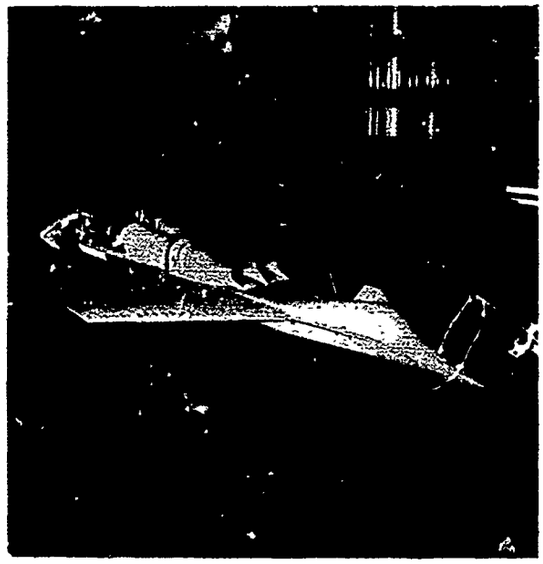

Figure 35. Above the wing inlet study in the Ames 11-ft tunnel (Ref. 42).

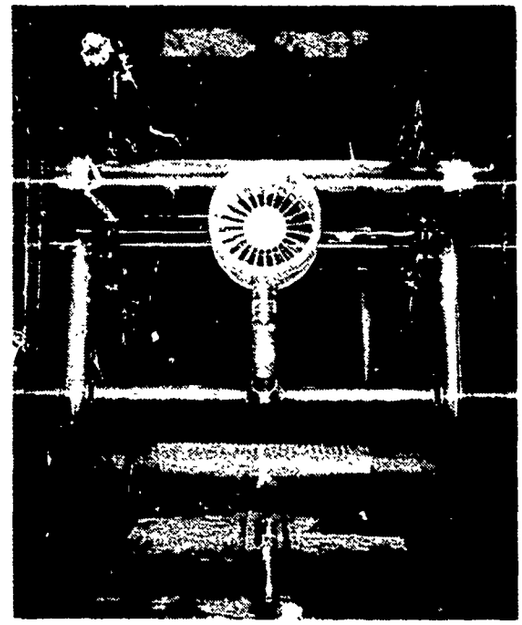

Figure 38. Installation of high-lift wing model and turbine fan between two-dimensional blowing walls (Ref. 49).

(a) Wind-tunnel installation.

(b) Details of model.

Figure 39. A quasi-two-dimensional ejector flap model (Ref. 50).

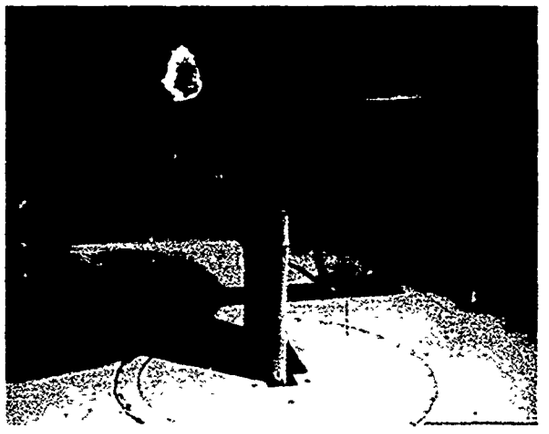

Figure 40. The cruise blowing model in the Boeing transonic wind tunnel (Ref. 52).

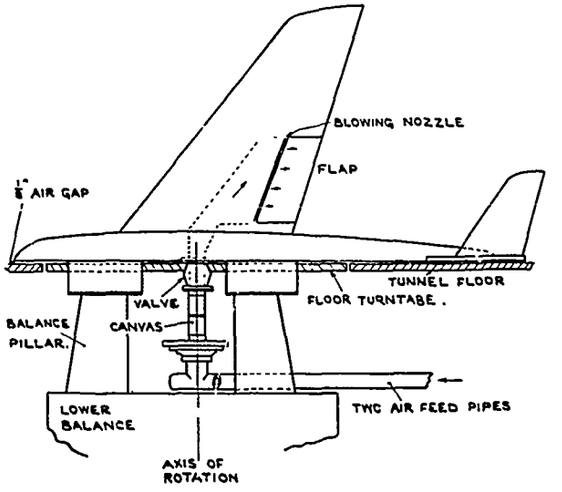

Figure 41. Semispan mount for a wing-fuselage-tail configuration (Ref. 53).

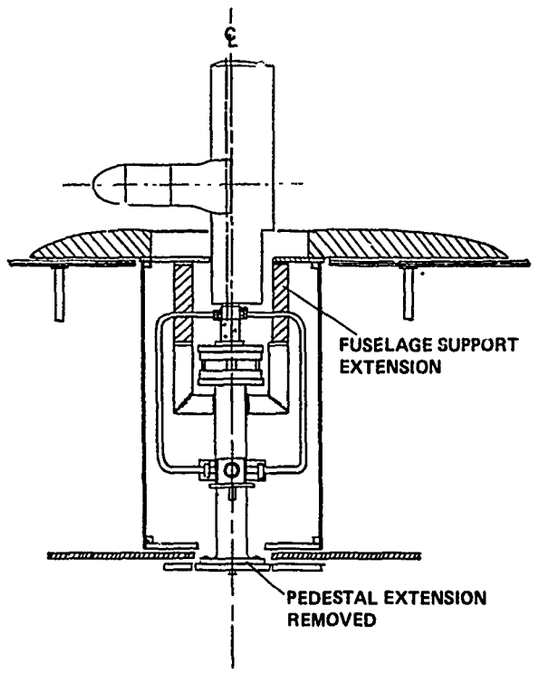

(a) Mounting details

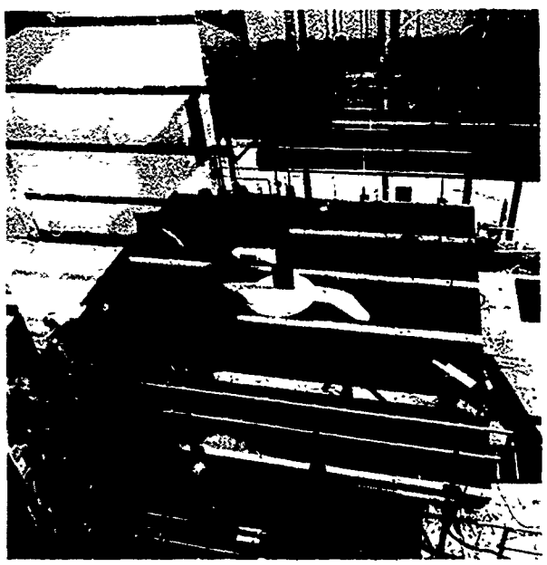

(b) View of installation in the Boeing Vertol wind tunnel.

Figure 42. Wing-fuselage semispan mount with the fuselage nonmetric (Ref. 54).

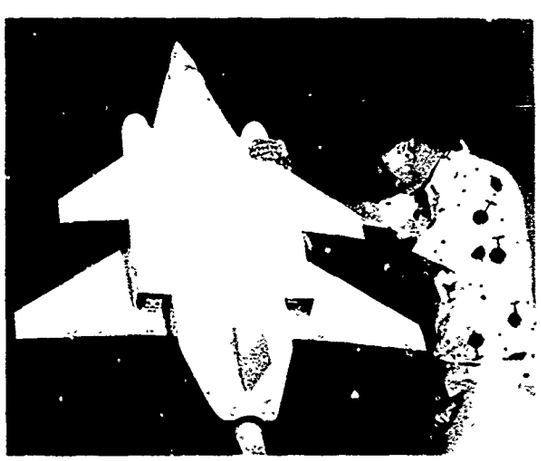

Figure 43. Twin-engine, high-speed model mounted in the Ames 12-ft tunnel (Ref. 56).

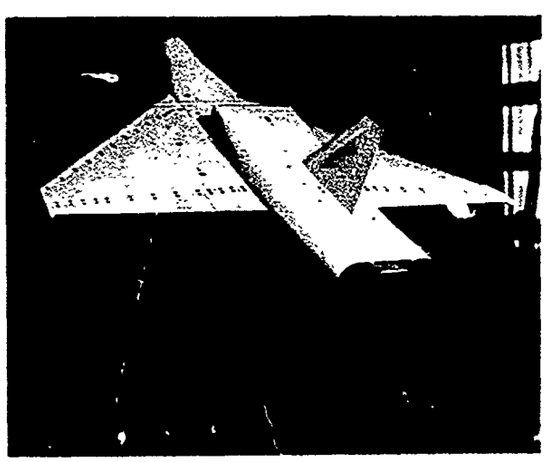

Figure 44. Sting mount of an above-the-wing inlet model in the Ames 11-ft tunnel (Ref. 43).

Figure 45. CMAPS-powered model in the Ames 11-ft transonic tunnel (Ref. 57).

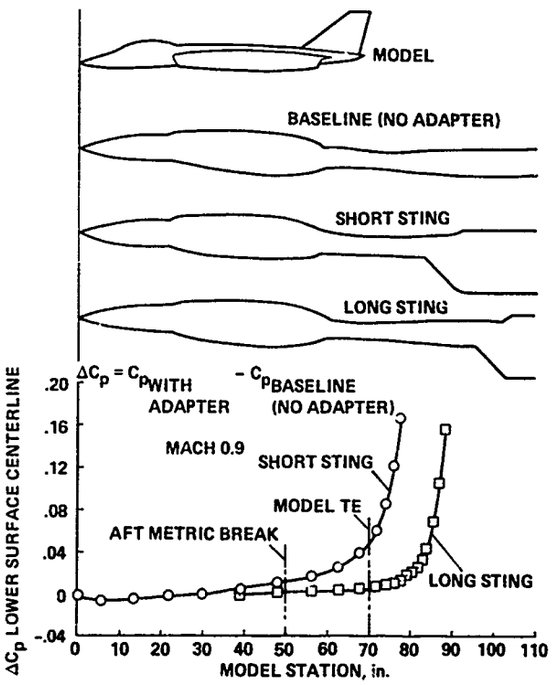

Figure 46. Sting-length effect on adapter-induced pressure increments for the CMAPS-powered model of Fig. 45 (Ref. 58).

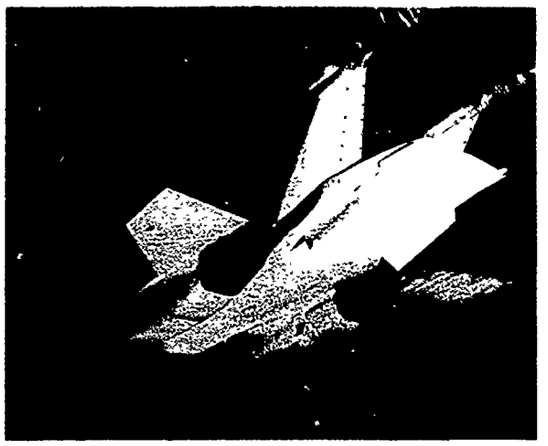

Figure 47. Twin-tail support for a generic fighter model powered by direct blowing (Ref. 59).

Figure 48. A sting mount installation in the Ames 40 by 80 for high-angle-of-attack studies (Refs. 60, 61).

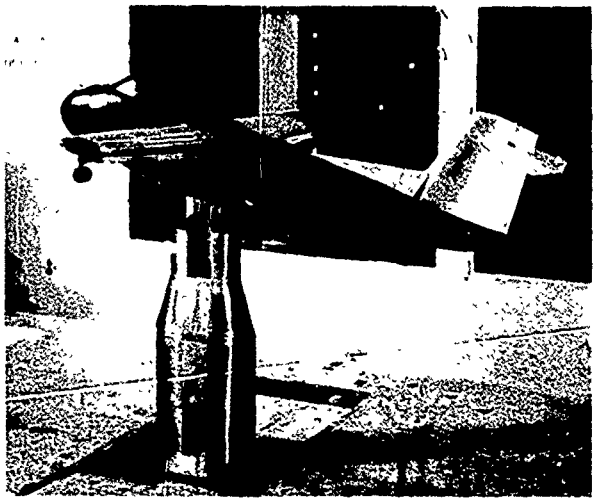

(a) Mounted in Ames-Army Air Mobility Command 7 by 10 1/7-scale (Ref. 62).

(b) The H-126 aircraft mounted in the Ames 40 by 80.

Figure 4: Wind-tunnel mounting of the H-126.

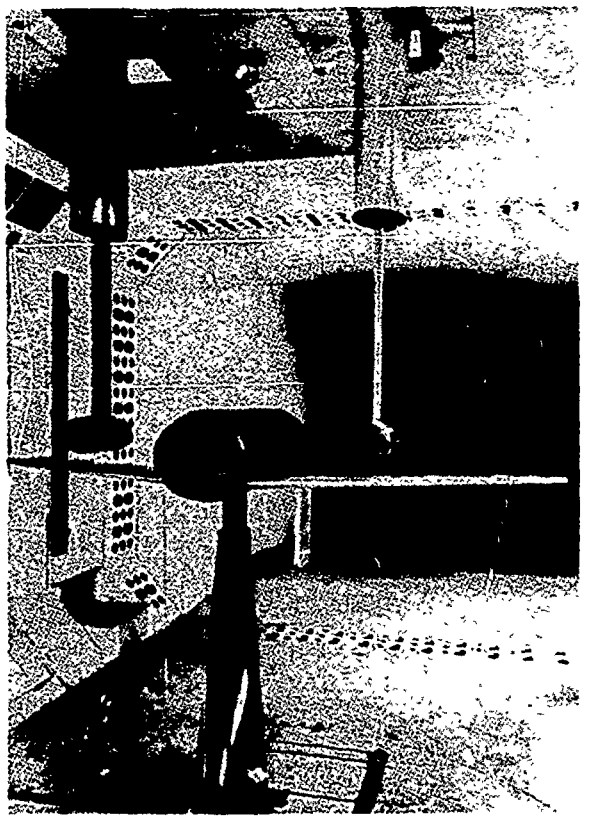

Figure 50. Composite model rig for jet-nacelle model with wing-fuselage inverted (Ref. 63).

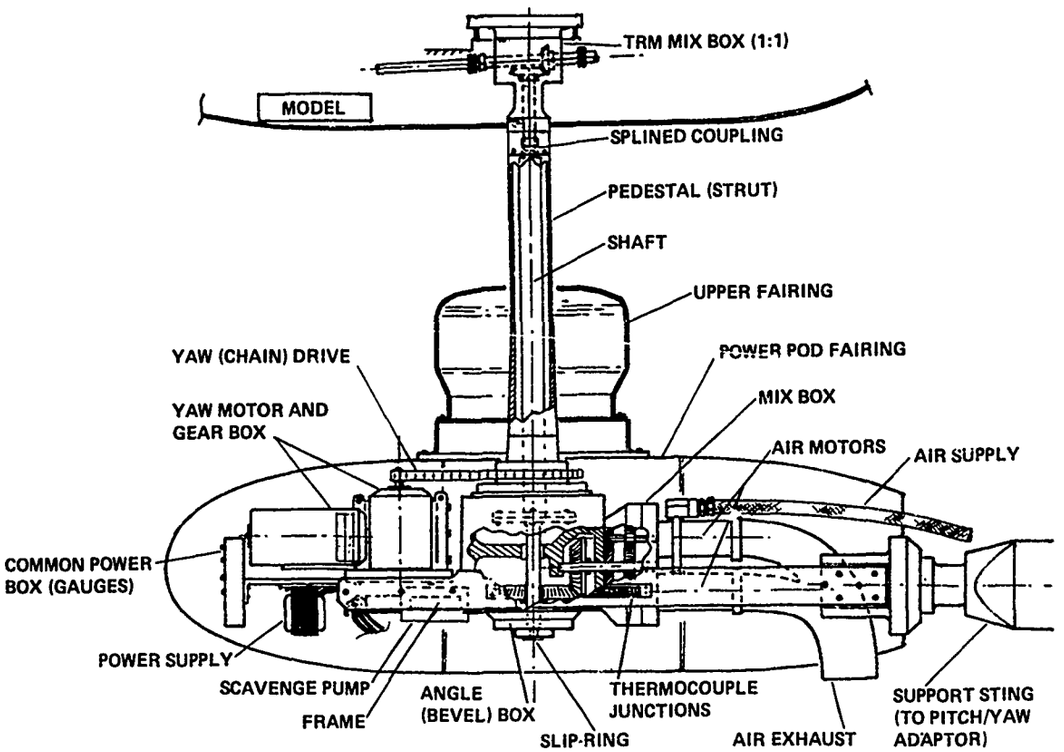

Figure 51. Pedestal-mounted model on the Vertol power pod (Ref. 28).

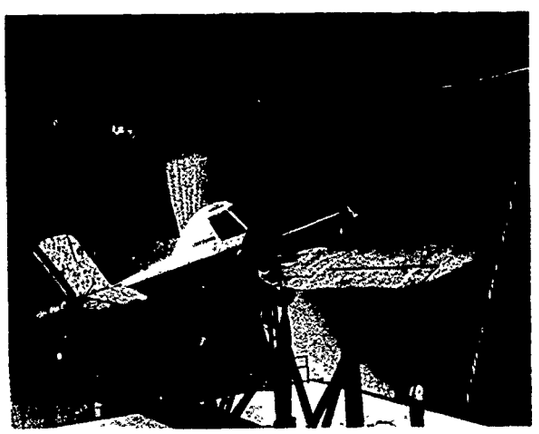

Figure 52. Aircraft installation in the Langley 30 by 60.

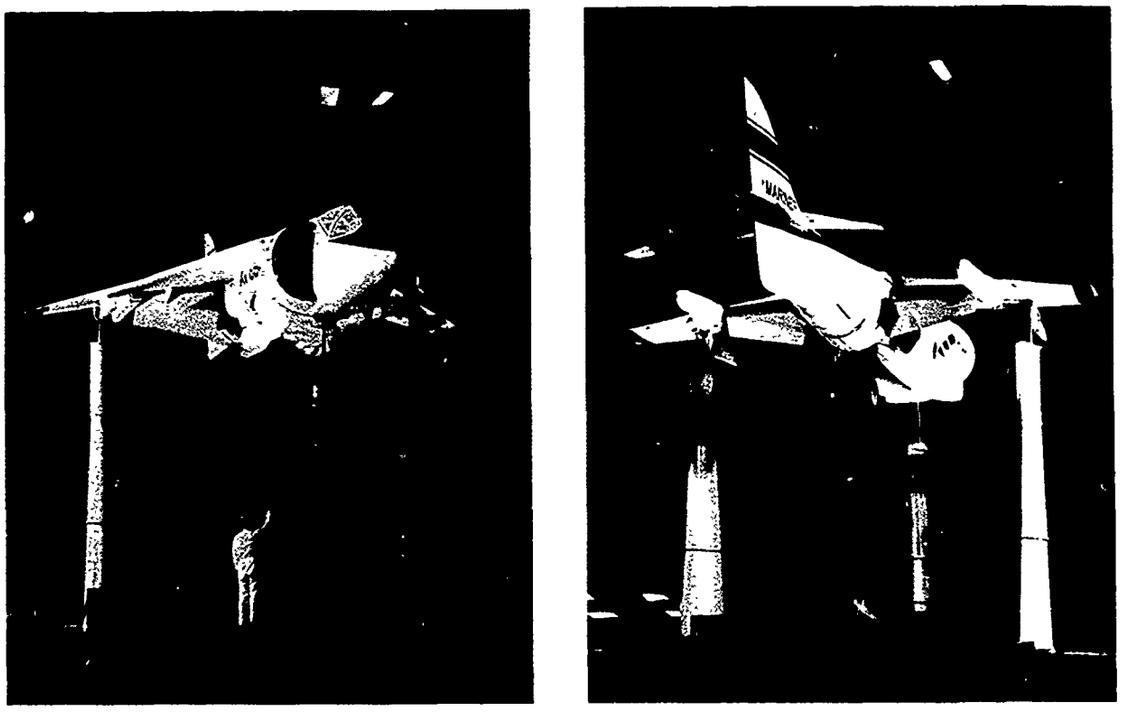

(a) 3/4 front.

(b) 3/4 rear.

Figure 53. Full-scale AV-8B model mounted in the Ames 40 by 80 (Ref. 19).

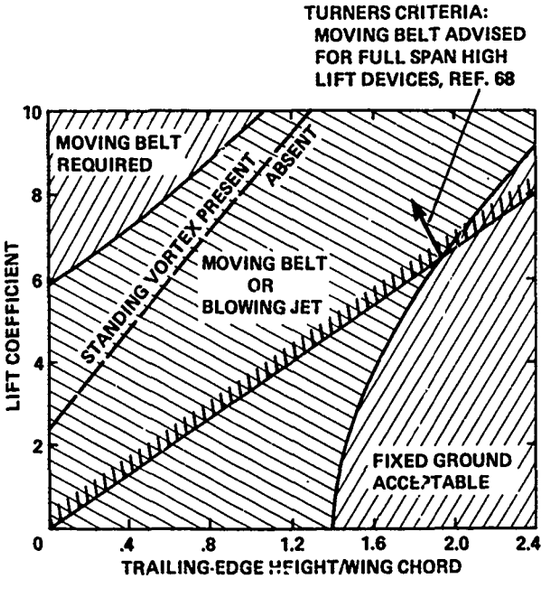

Figure 54. Criteria for ground-effect simulation (Refs. 29, 68).

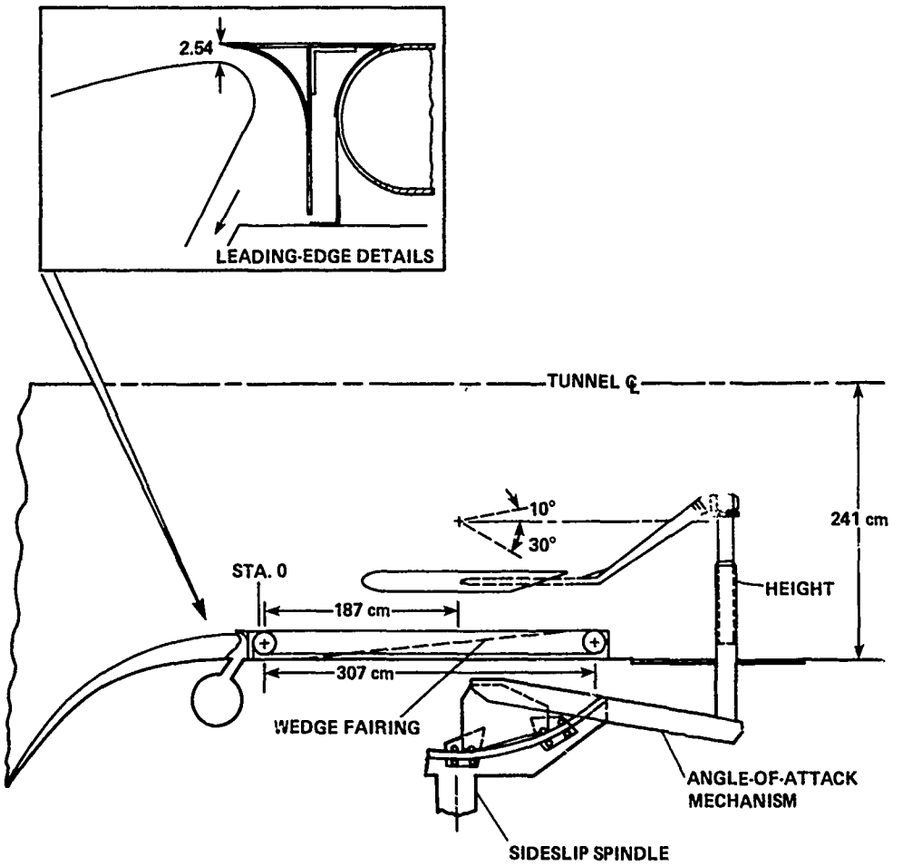

Figure 55. Turner's moving-belt installation (Ref. 68).

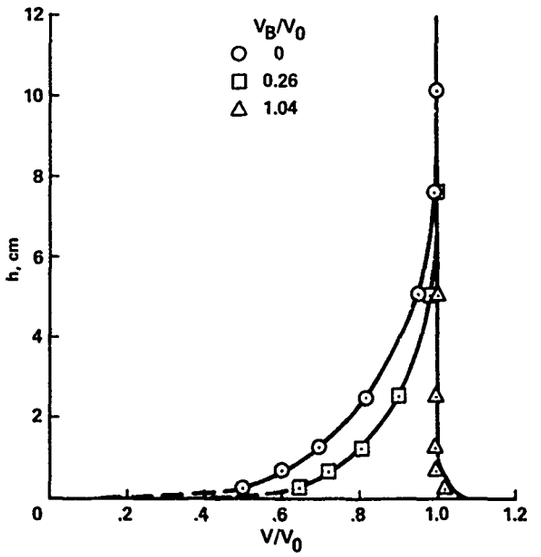

Figure 56. Effect of belt velocity on boundary-layer profiles: station 187; see Fig. 55 (Ref. 68).

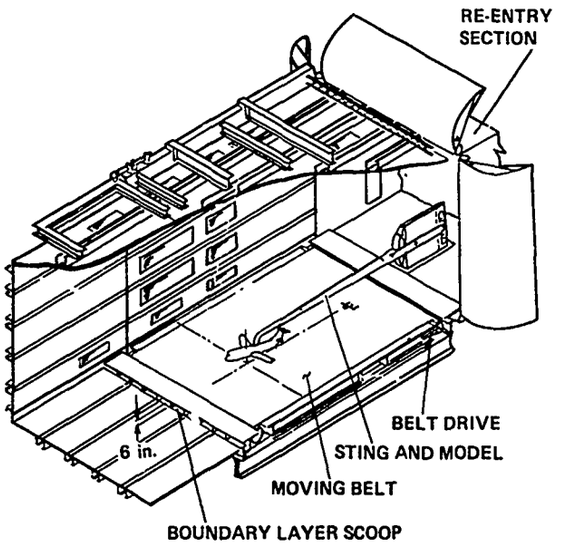

Figure 57.. Moving-belt installation in the Boeing V/STOL wind tunnel (Ref. 28).

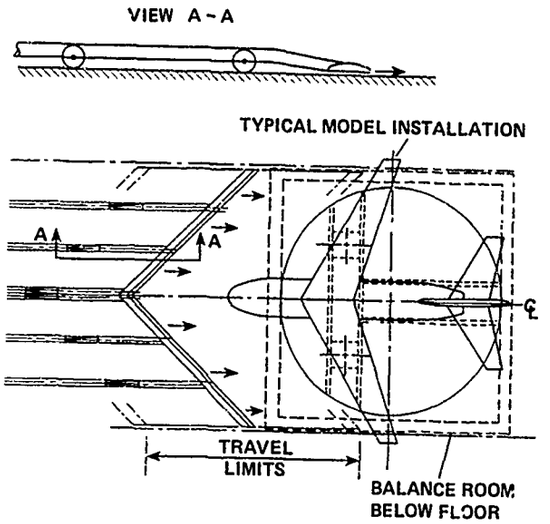

Figure 58. Ames 40 by 80 proposed floor BLC design (Ref. 70).

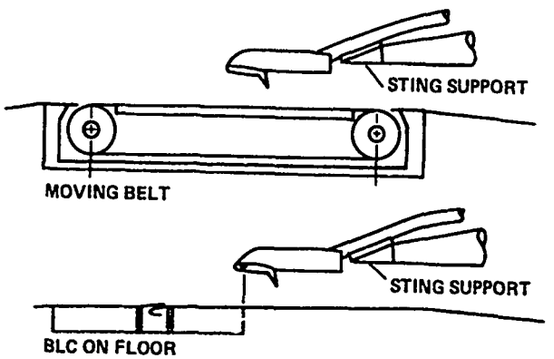

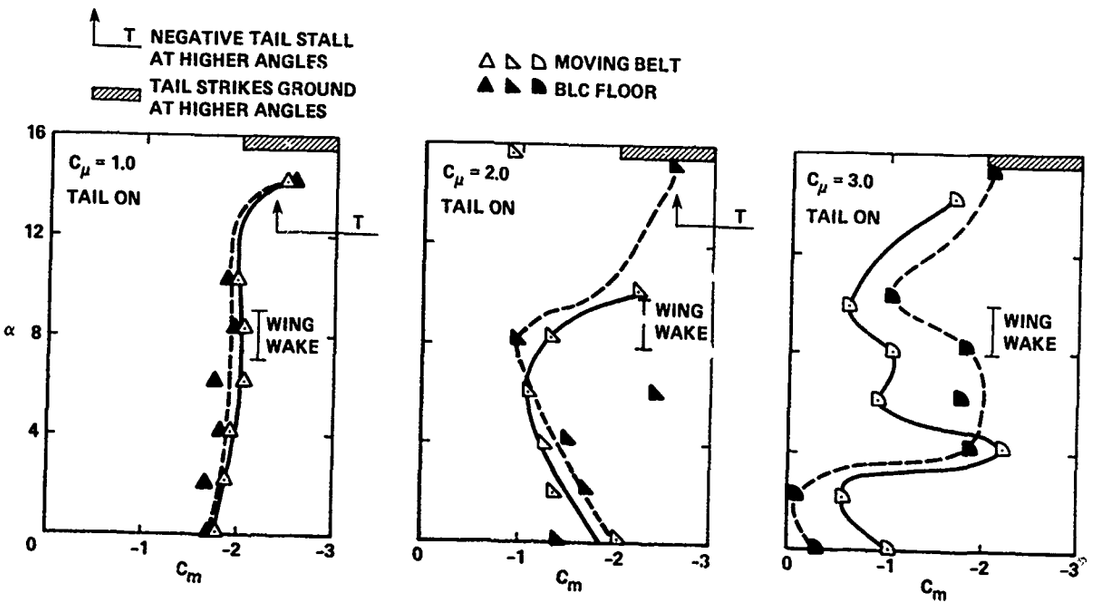

Figure 59. A sampling of data comparing the use of BLC on the wind-tunnel floor with that of a moving belt: h/c = 1.0 (Ref. 72).

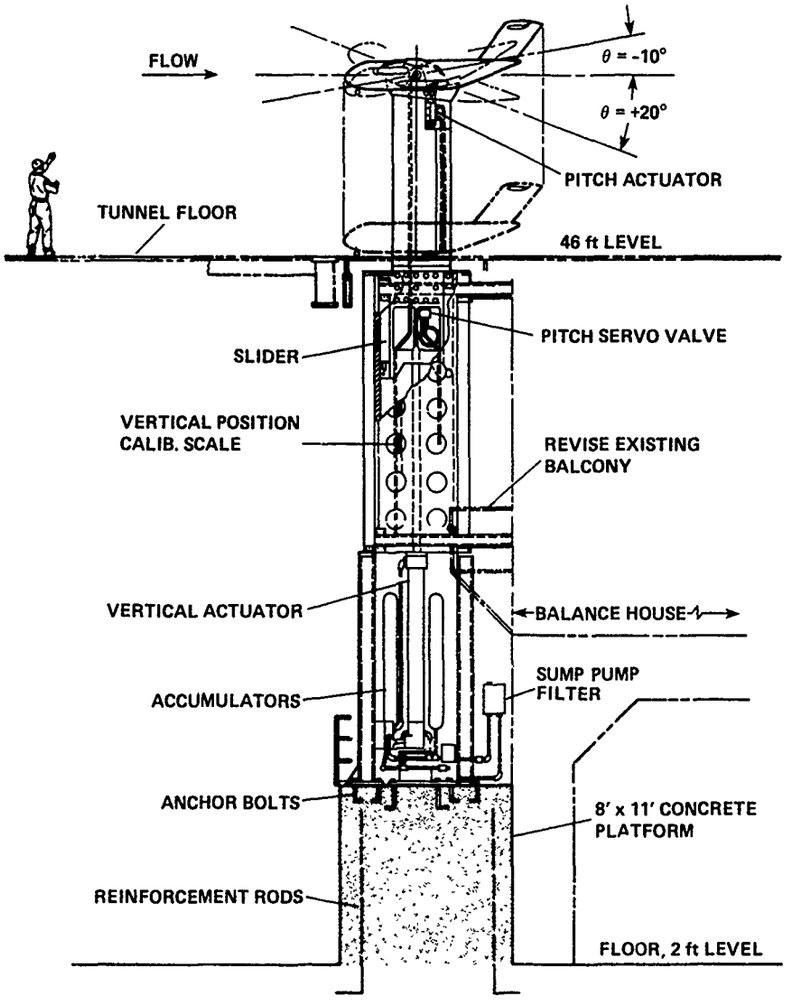

Figure 60. Transient ground-effect support design for the Ames 40 by 80 (Ref. 73).

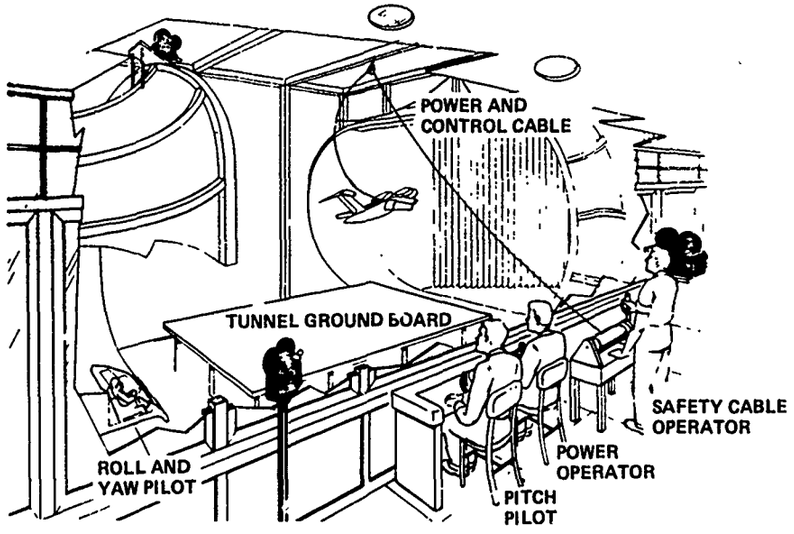

(a) Test setup in test section.

PILOT CONTROLS	DIGITAL FLIGHT CONTROL COMPUTER AND RECORDERS	POWERED DYNAMICALLY-SCALED MODEL
• VISUAL REFERENCE • PENCIL-TYPE CONTROL WITH TRIMMER • SELECTABLE CONTROL MODES – PROPORTIONAL – FLICKER	• PROGRAMMABLE CONTROL LAWS • VARIABLE GAINS AND GEARING • SELECTABLE FEEDBACKS • FAILURE MONITORING	• ELECTROPNEUMATIC ACTUATORS • ONBOARD DATA SENSORS -- MOTIONS – CONTROL POSITIONS

(b) Description of system features.

Figure 61. Free-flight operation in the Langley 30 by 60 wind tunnel (Ref. 74).

Figure 62. An X29A model in flight in the Langley 30 by 60 tunnel (Ref. 75).

(a) Model support.

(b) Grumman 698 model at wheel height.

Figure 63. Use of the Princeton track for ground-effect tests (Ref. 78).

DATA SOURCE	i_t	h (OGE), cm (in.)	h (IGE), cm (in.)
○ DMT (PRINCETON)	20°	42 (16.5)	9.6 (3.8)
□ 40x80 TUNNEL (AMES)	20°	42 (16.5)	9.6 (3.8)
△ 7x10 TUNNEL (LANGLEY)	OFF	22.6 (8.9)	9.6 (3.8)
⍙ 7x10 TUNNEL (15x17 SECT. WITH MOVING BELT)	OFF	22.6 (8.9)	9.6 (3.8)

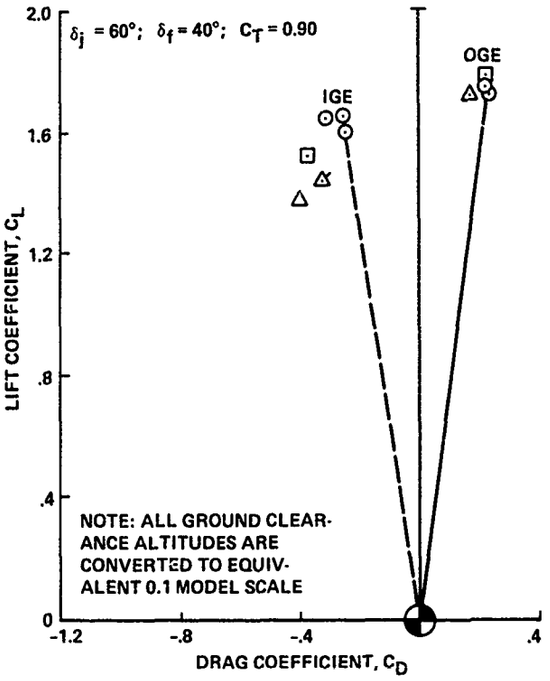

Figure 64. Comparison in ground-effect of results using the Princeton Track with that from three other facilities: tilt-wing model; h measured using Princeton model scale (Ref. 77).

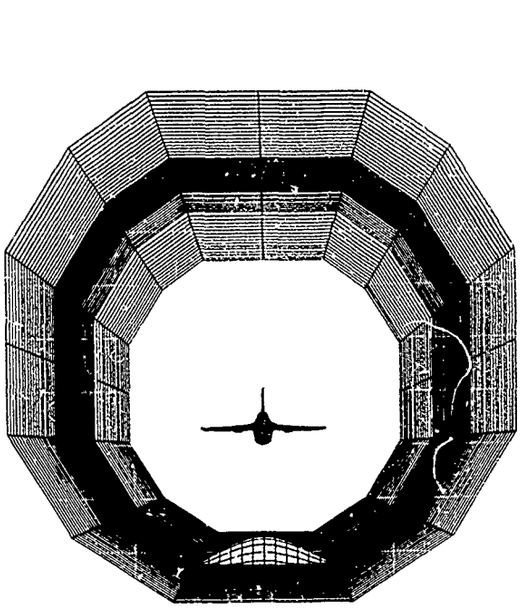

(a) PAN AIR model of Ames 12-ft tunnel (front view).

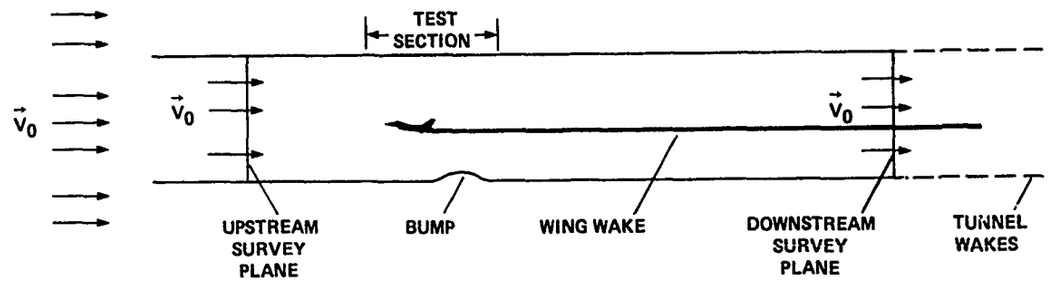

(b) Schematic of complete PAN AIR model; section shown at plane of symmetry.

Figure 65. Evaluation wall constraints using potential-flow paneling method (Ref. 84).

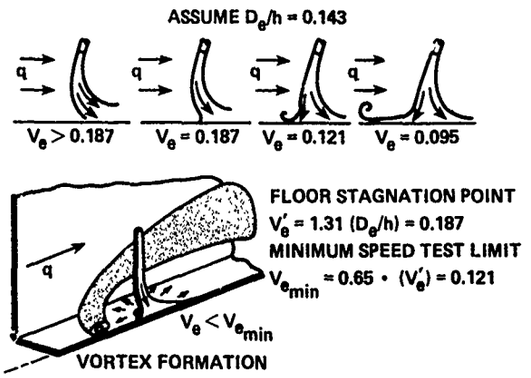

Figure 66. Minimum-speed testing limit for a configuration with two side-by-side lifting jets at h/D_e = 7 (Ref. 5).

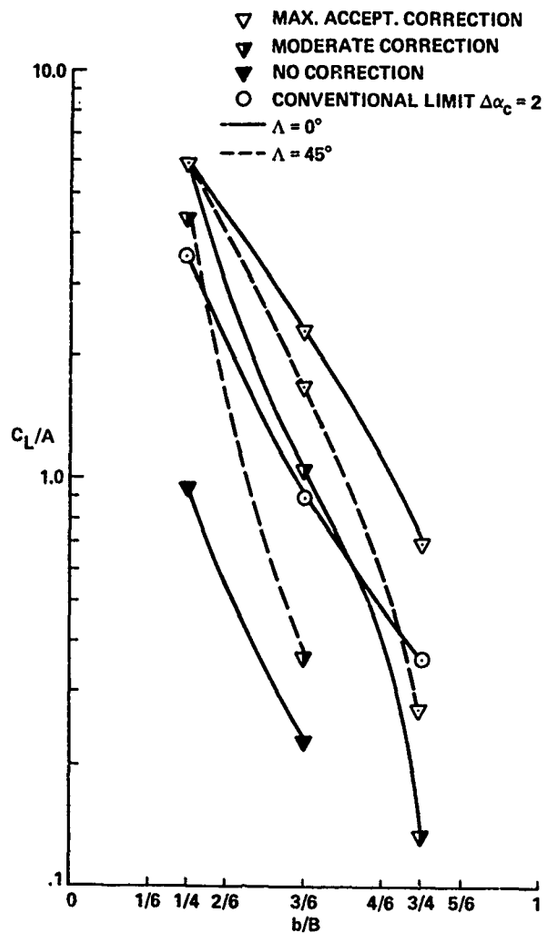

Figure 67. STOL testing limits: $D_i/L = 0$; model in center of wind tunnel; B/H = 4/3 (Ref. 88).

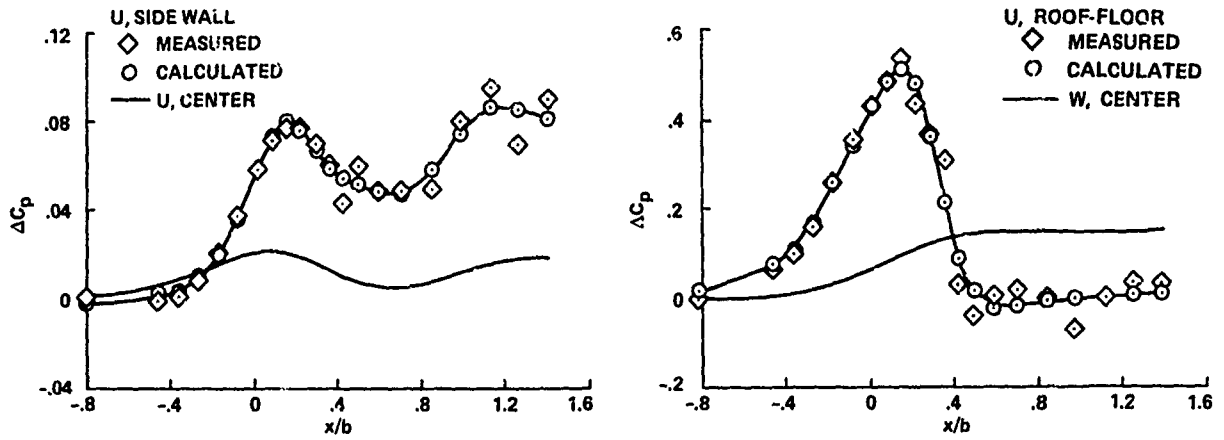

(a) Wall pressure signatures.

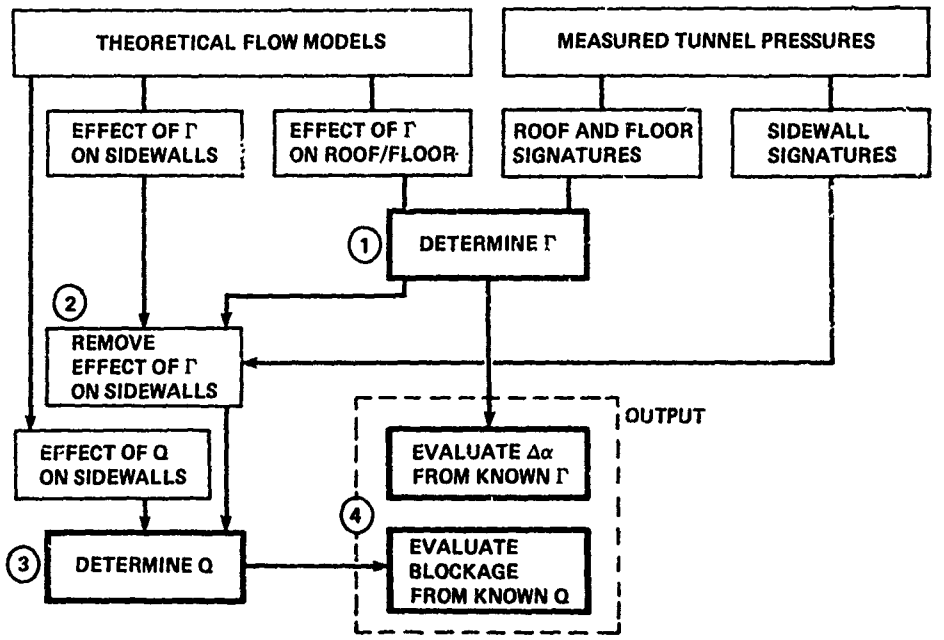

(b) Block diagram of procedure.

Figure 68. Evaluating wall corrections using wind-tunnel surface pressures (Ref. 82).

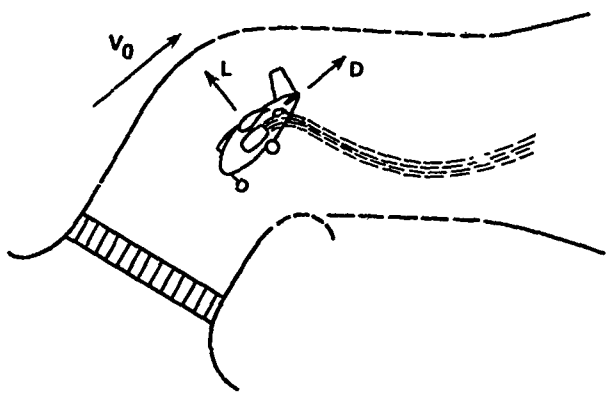

Figure 69. Adaptable wall concept for V/STOL wind-tunnel testing (Ref. 92).

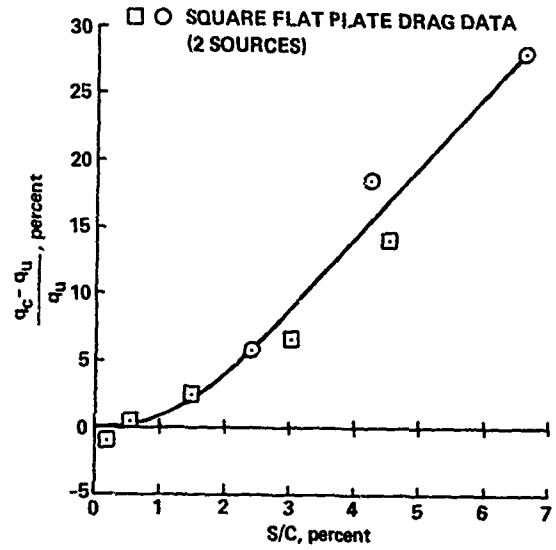

(a) Wake blockage correction to flat-plate drag data assuming $C_{D_c} = 1.17$.

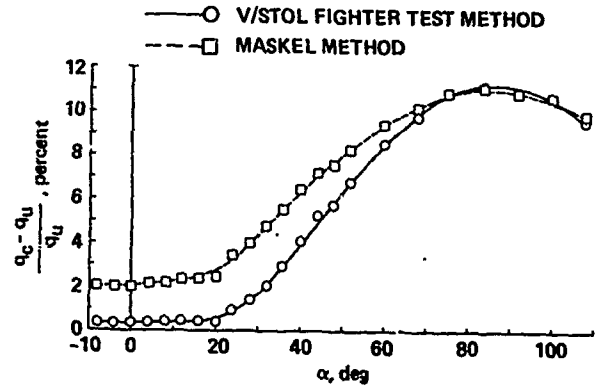

(b) Comparison of Maskell wake blockage correction with method developed for V/STOL fighter model test applied to test run.

Figure 70. Blockage corrections for high-angle-of-attack model (Ref. 60).

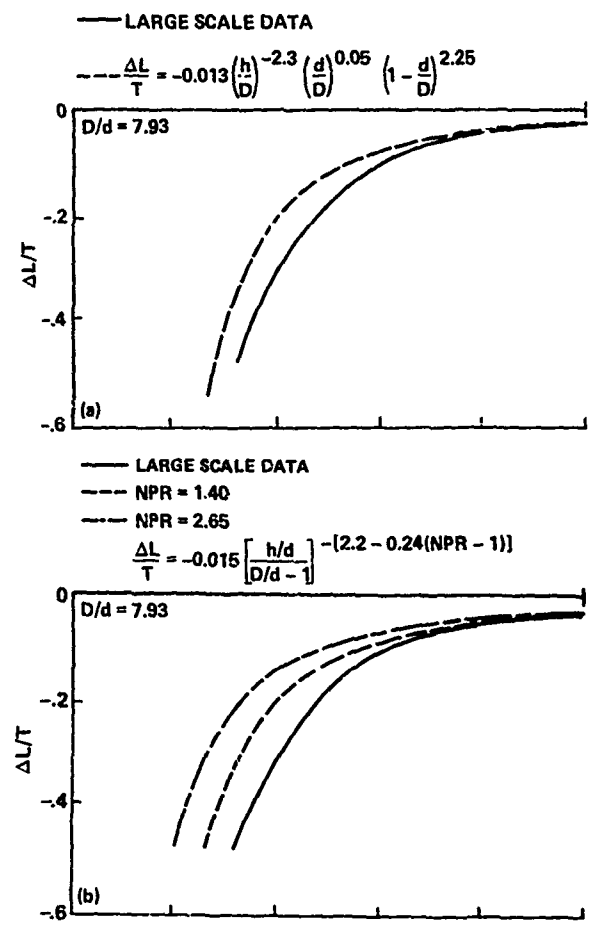

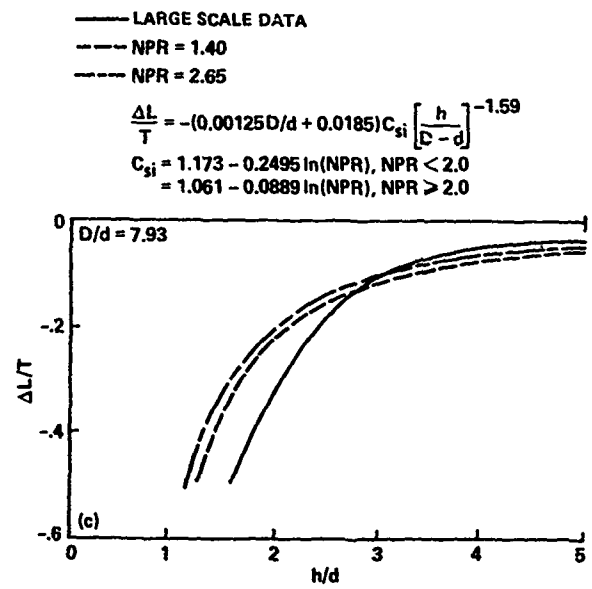

Figure 71. Comparison of large-scale data with predicted lift losses (Ref. 93).

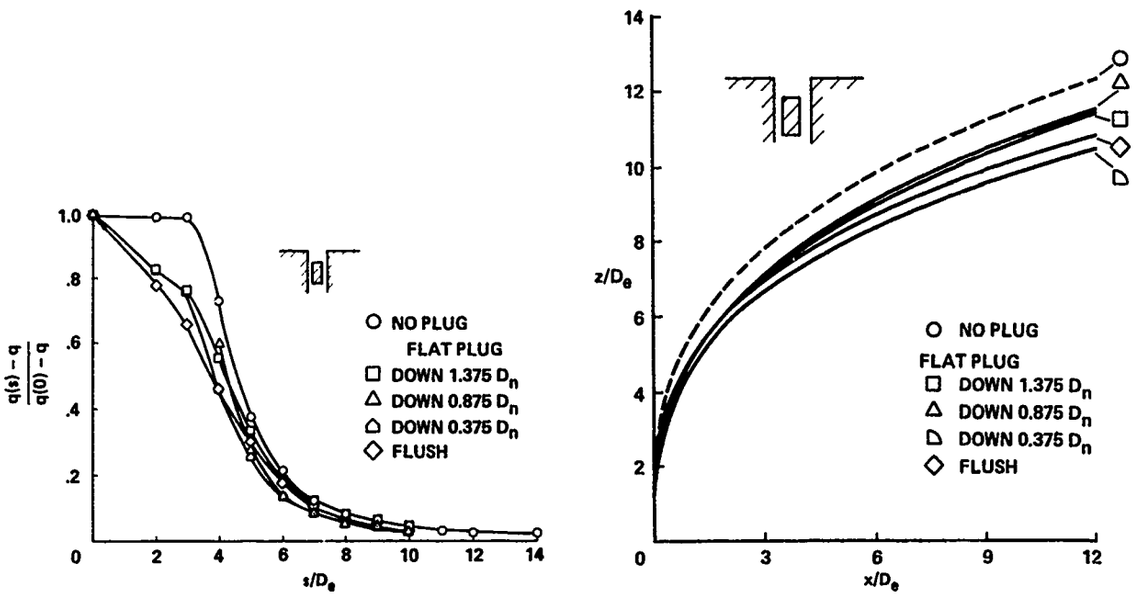

(a) Dynamic pressure decay. (b) Jet centerline trajectories.

Figure 72. Effect of a flat plug on characteristics of a round jet: R = 6 (Ref. 95).

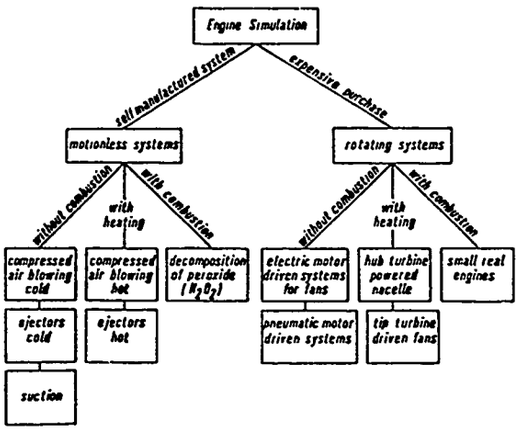

Figure 73. Classification of principal engine simulation techniques (from Ref. 97).

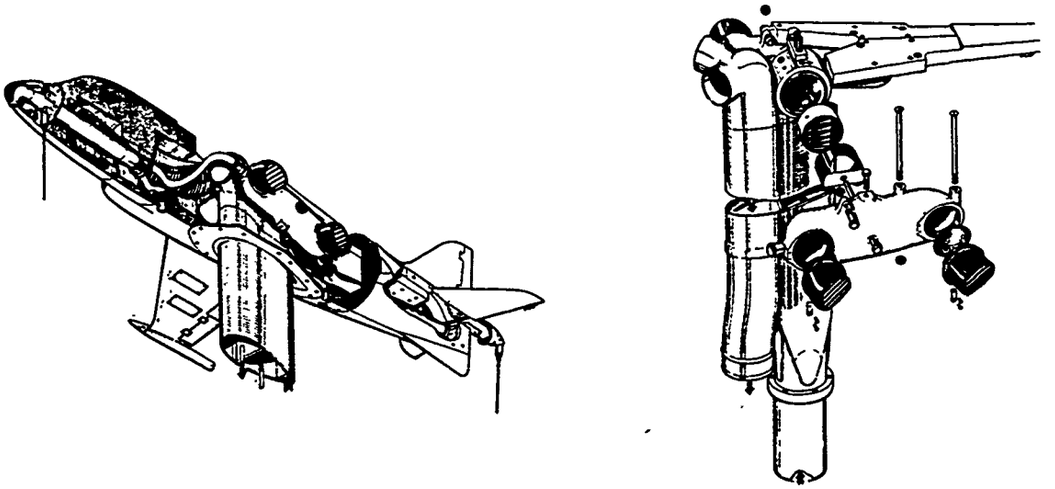

(a) General model arrangement. (b) Ducting and nozzle details.

Figure 74. Hawker P.1127, 1/10th-scale model (Ref. 63).

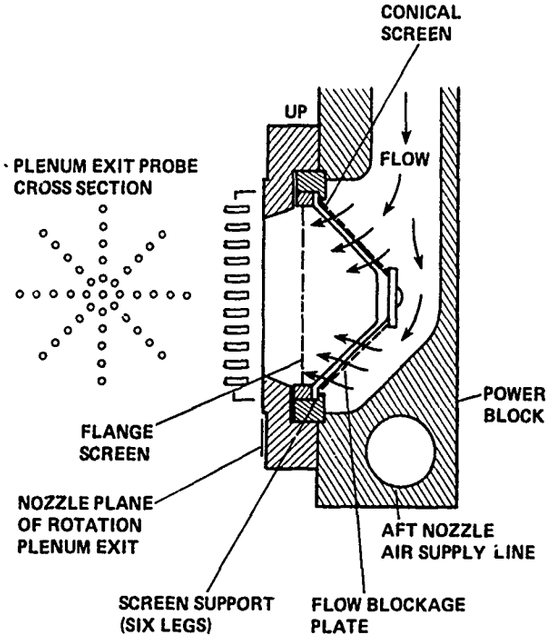

Figure 75. 15% AV-8B model nozzle air-feed design (Ref. 8).

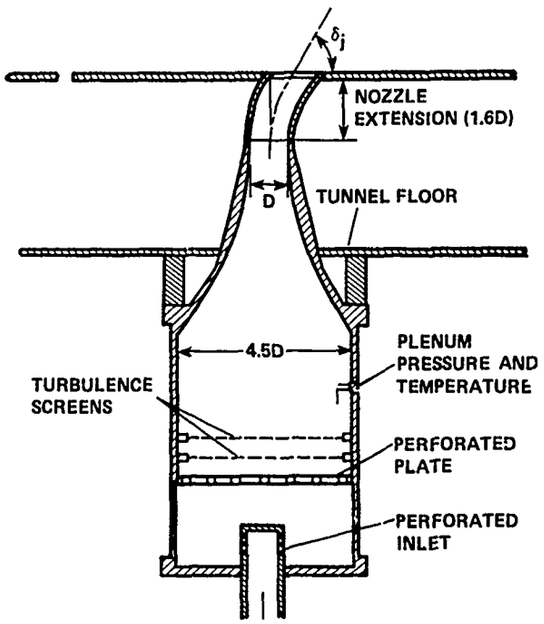

Figure 76. Nozzle and plenum chamber design to insure a jet with uniform velocity profile (Ref. 47).

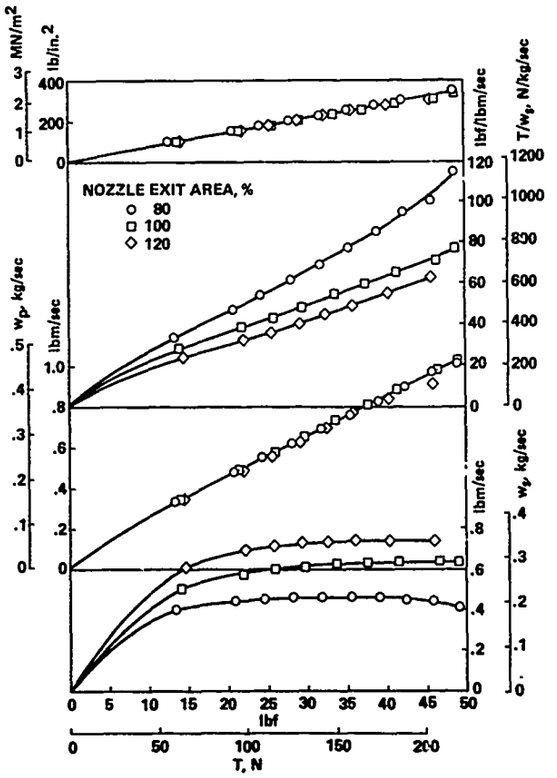

Figure 77. Effect of exit area ratio on ejector performance (Ref. 98).

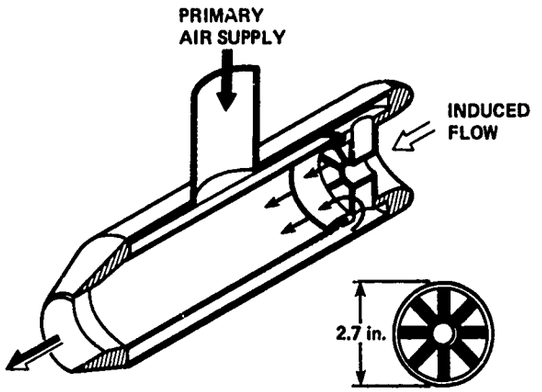

(a) Turbojet (Ref. 97).

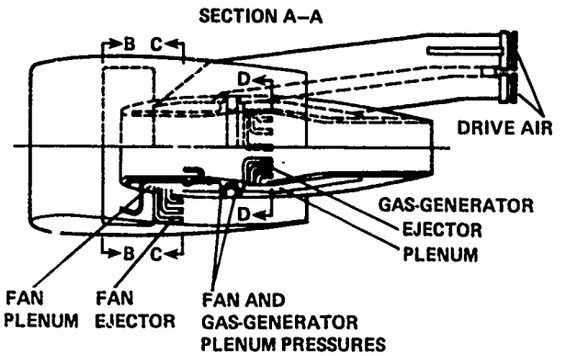

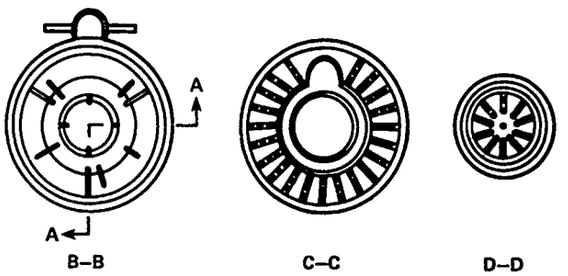

(b) Turbofan (Ref. 99).

Figure 78. Power simulation by ejectors.

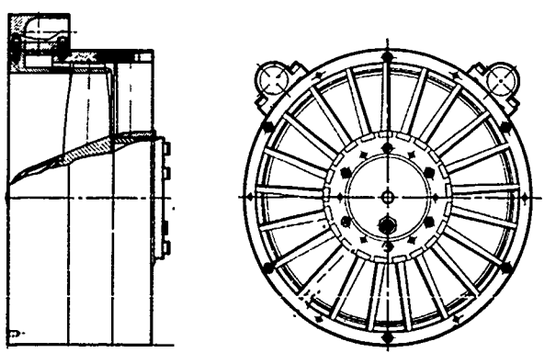

Figure 79. Tip-driven fan assembly.

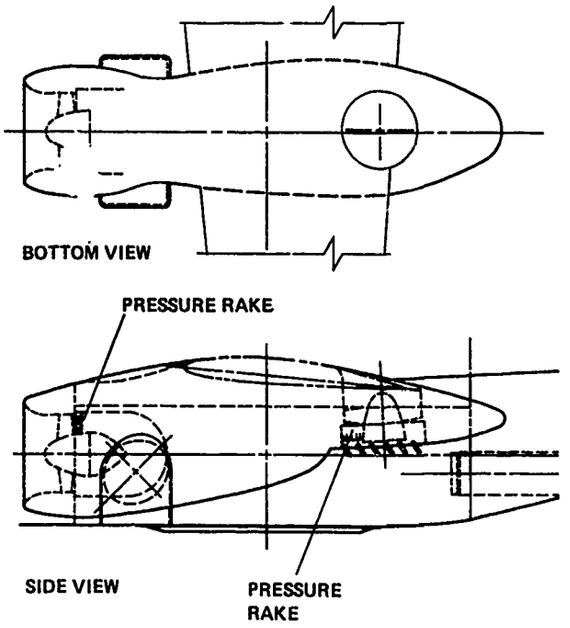

(a) Nacelle details.

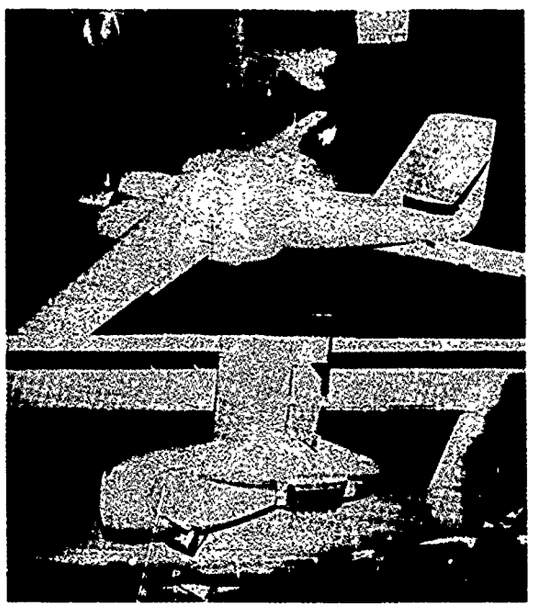

(b) Model installed in the Langley 4- by 7-m tunnel.

Figure 80. Use of tip-driven fan in a lifting-nacelle configuration (Ref. 101).

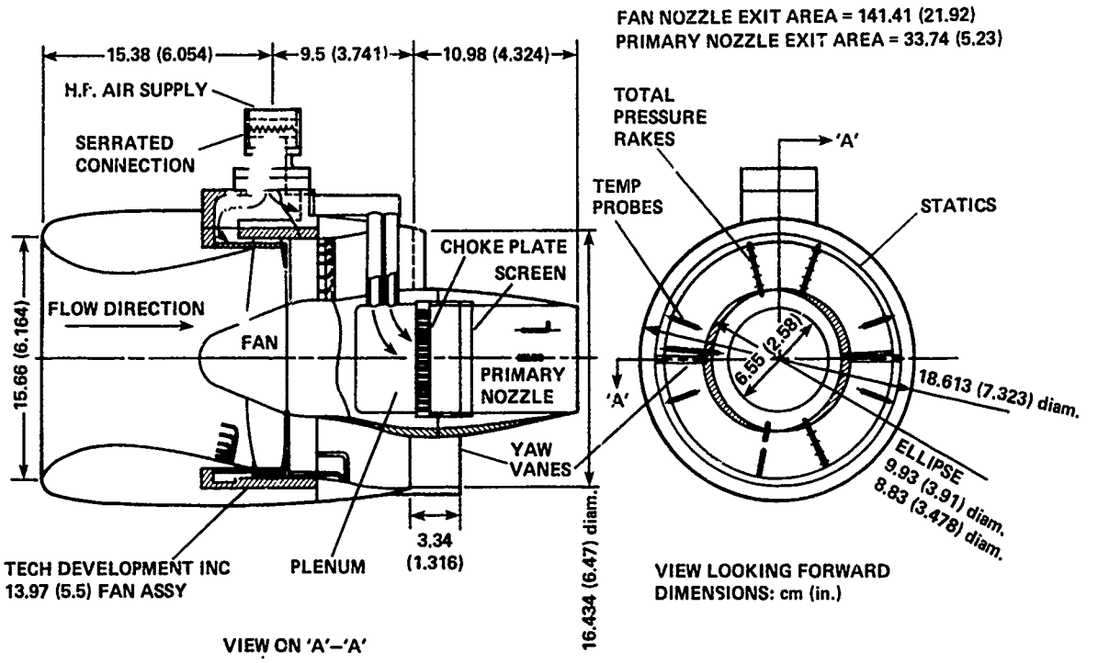

Figure 81. Use of 5.5-in. tip-driven fan in Boeing lift-cruise fan assembly (Ref. 102).

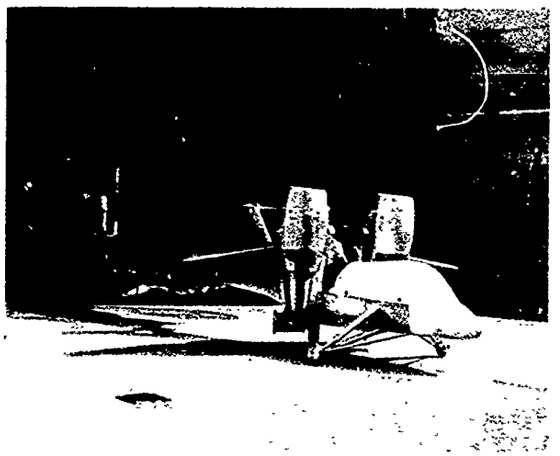

Figure 82. 11% Grumman V/STOL model in ground effect tests.

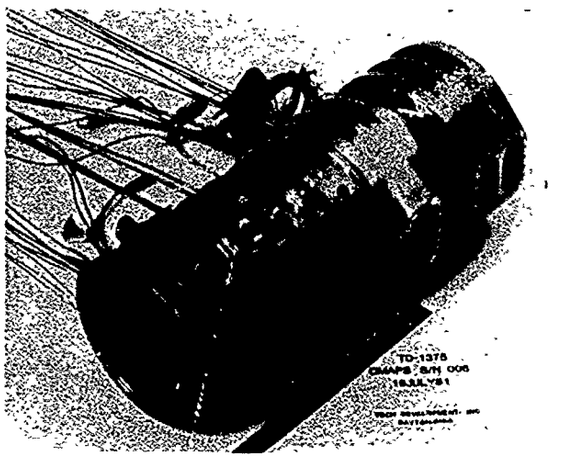

Figure 83. CMAPS before installation into a model.

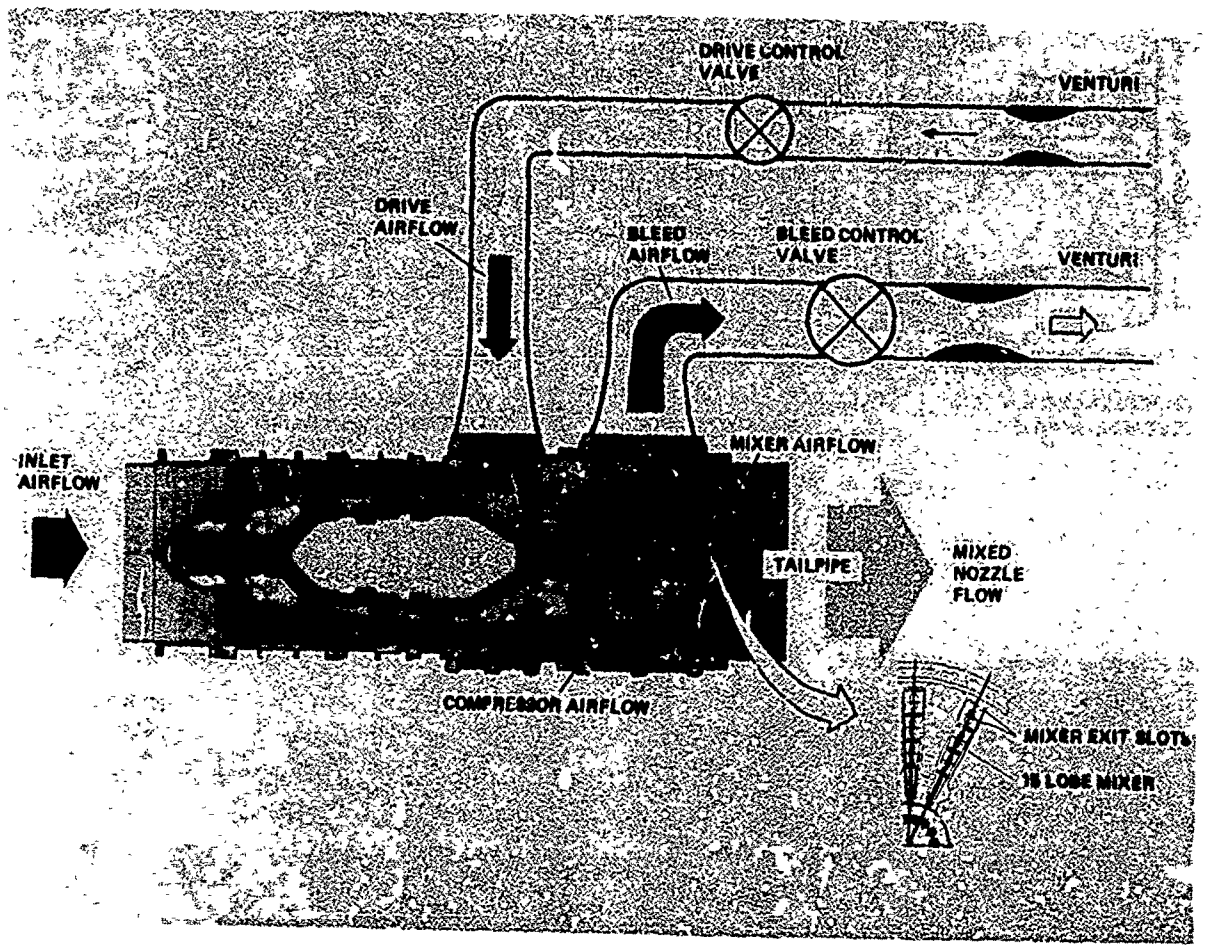

Figure 84. Schematic of CMAPS.

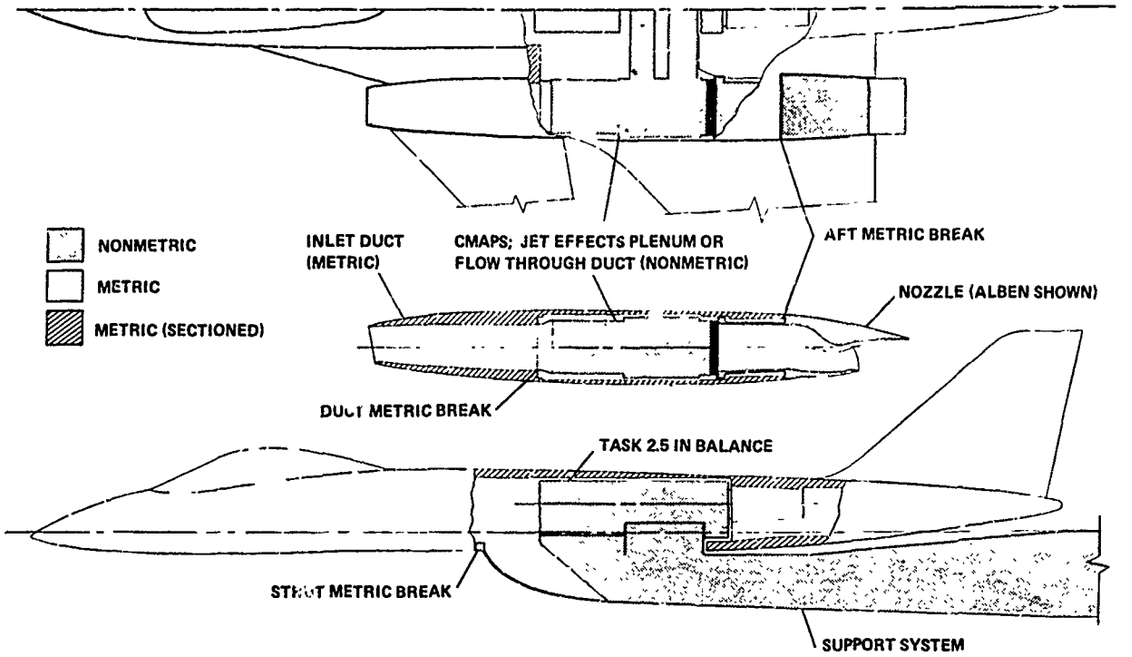

Figure 85. Support system for the CMAPS-powered model shown in Fig. 45 (Ref. 105).

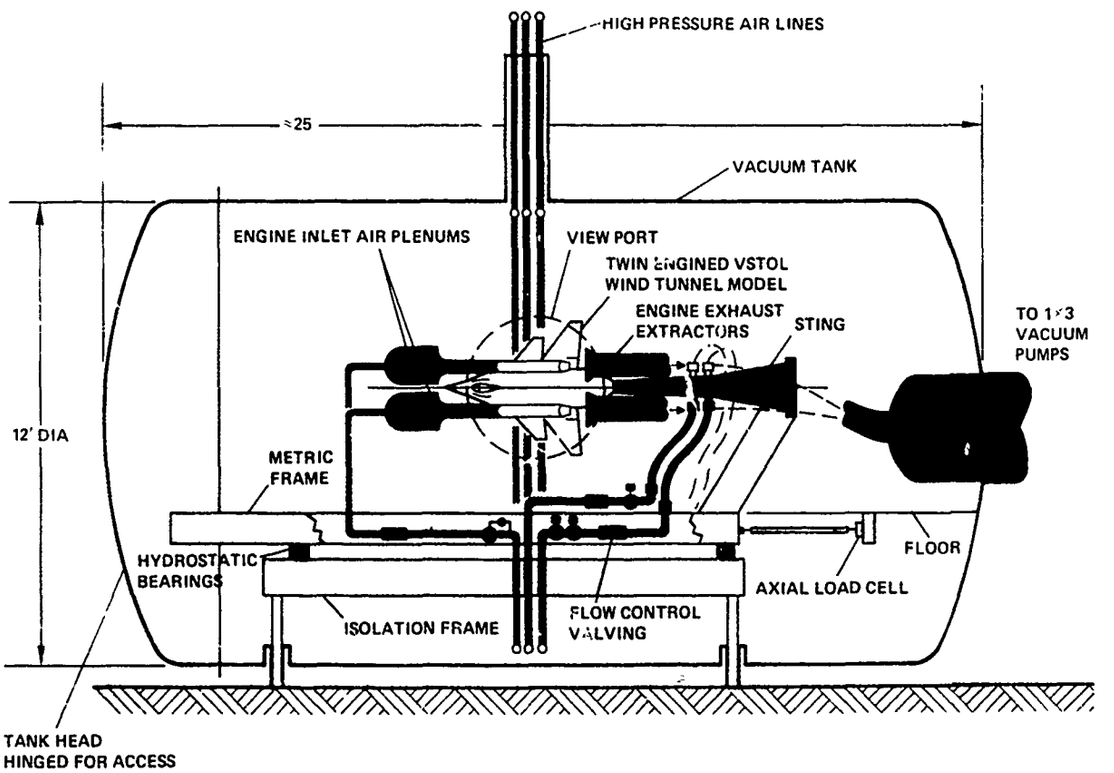

Figure 86. CMAPS calibration tank (Ref. 106).

	THRUST		W		P_T/P_O	A_e	
	N	(lb)	kg/sec	(lb/sec)		m^2	$(in.^2)$
J85-5	11,560	(2600)	19.28	(42.5)	2.24	.0742	(115)
T58	2,670	(600)	5.67	(12.5)	2.1	.0188	(29.2)
J97	20,020	(4500)	31.75	(70)	3.0	.0839	(130)
JT15-D	8,450	(1900)	34.02	(75)	1.35	.1419	(220)

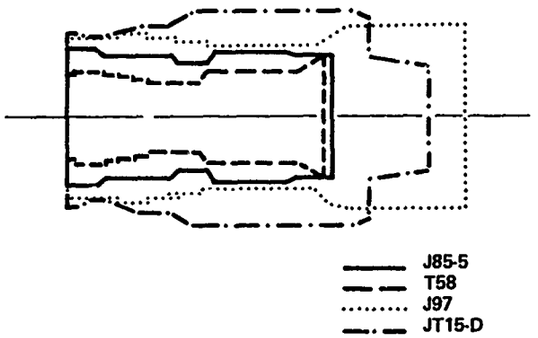

Figure 87. Relative engine sizes of small gas turbines (Ref. 4).

(a) 3/4 front view

(b) 3/4 rear view.

Figure 88. A JT15D installation for an upper-surface blowing model (Ref. 104).

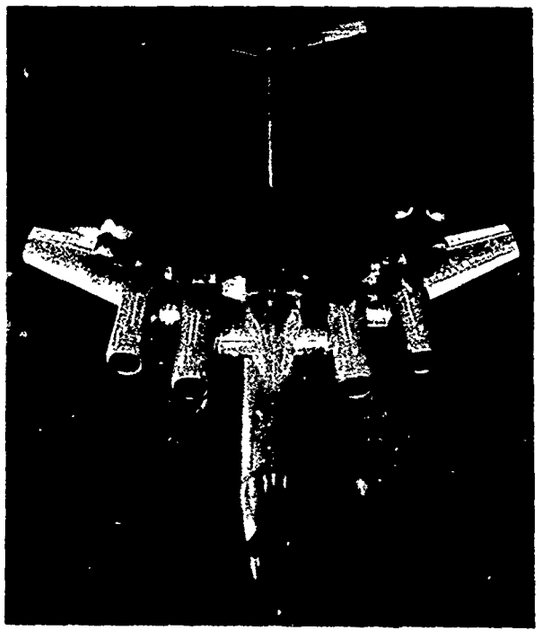

Figure 89. Large-scale upper-surface model using the JT15D engines (Ref. 15).

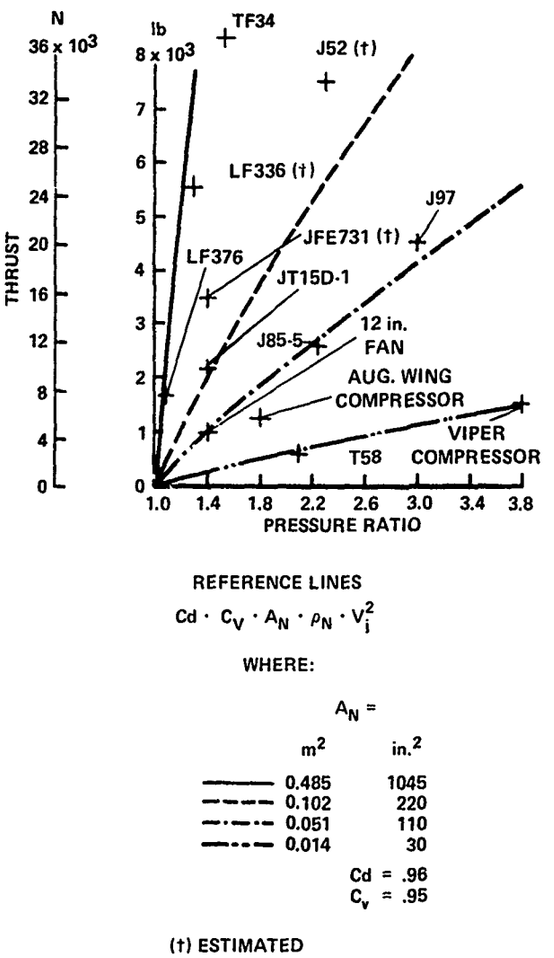

Figure 90. Thrust as a function of pressure for several candidate large-scale rodel engines (Ref. 4).

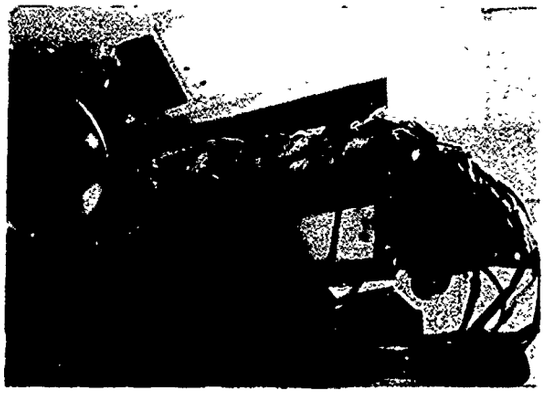

Figure 91. 11% G698 on-board instrumentation shown ready for installation of the fuselage shell.

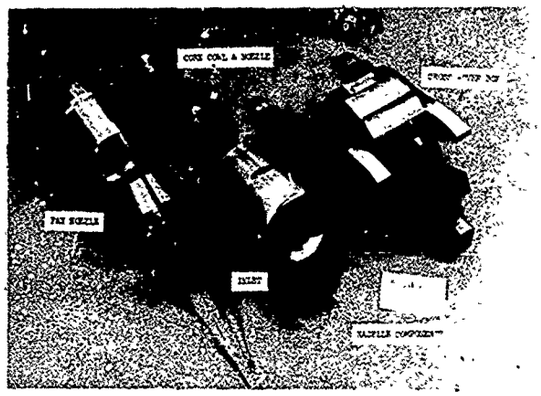

Figure 92. Nacelle components for the 11%-scale G698 model.

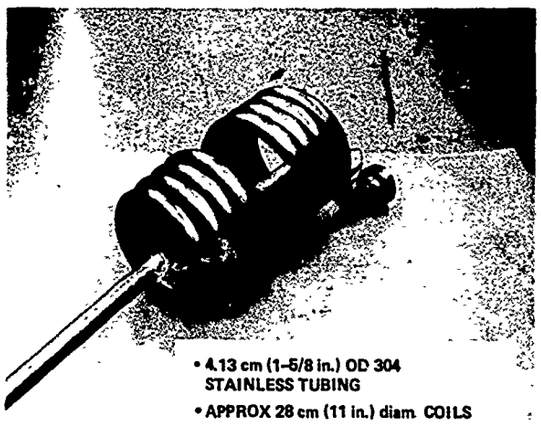

Figure 93. Drive-air force-isolation coil for the 11% G698 model.

Figure 94. Model parts for the high-speed, two-engine fighter model of Fig. 43.

(a) Metal fabrication of model shown in Fig. 8.

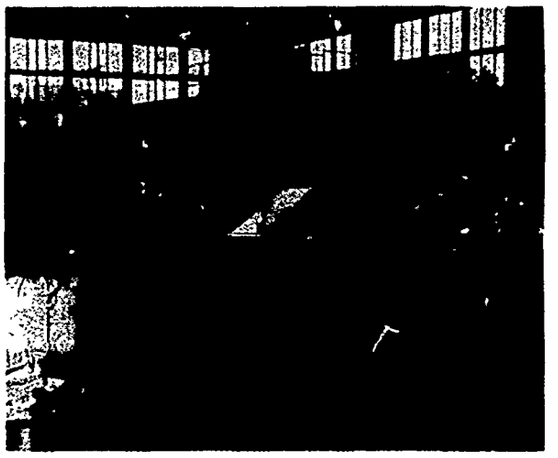

(b) Soft construction use of polyurethane foam.

Figure 95. Boiler-plate model construction.

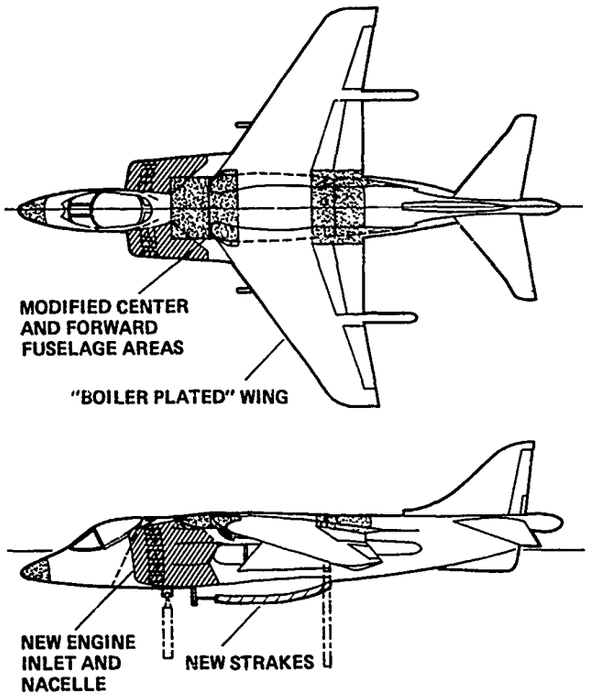

Figure 96. Boiler-plate plan for the full-scale AV-8B model (Ref. 8).

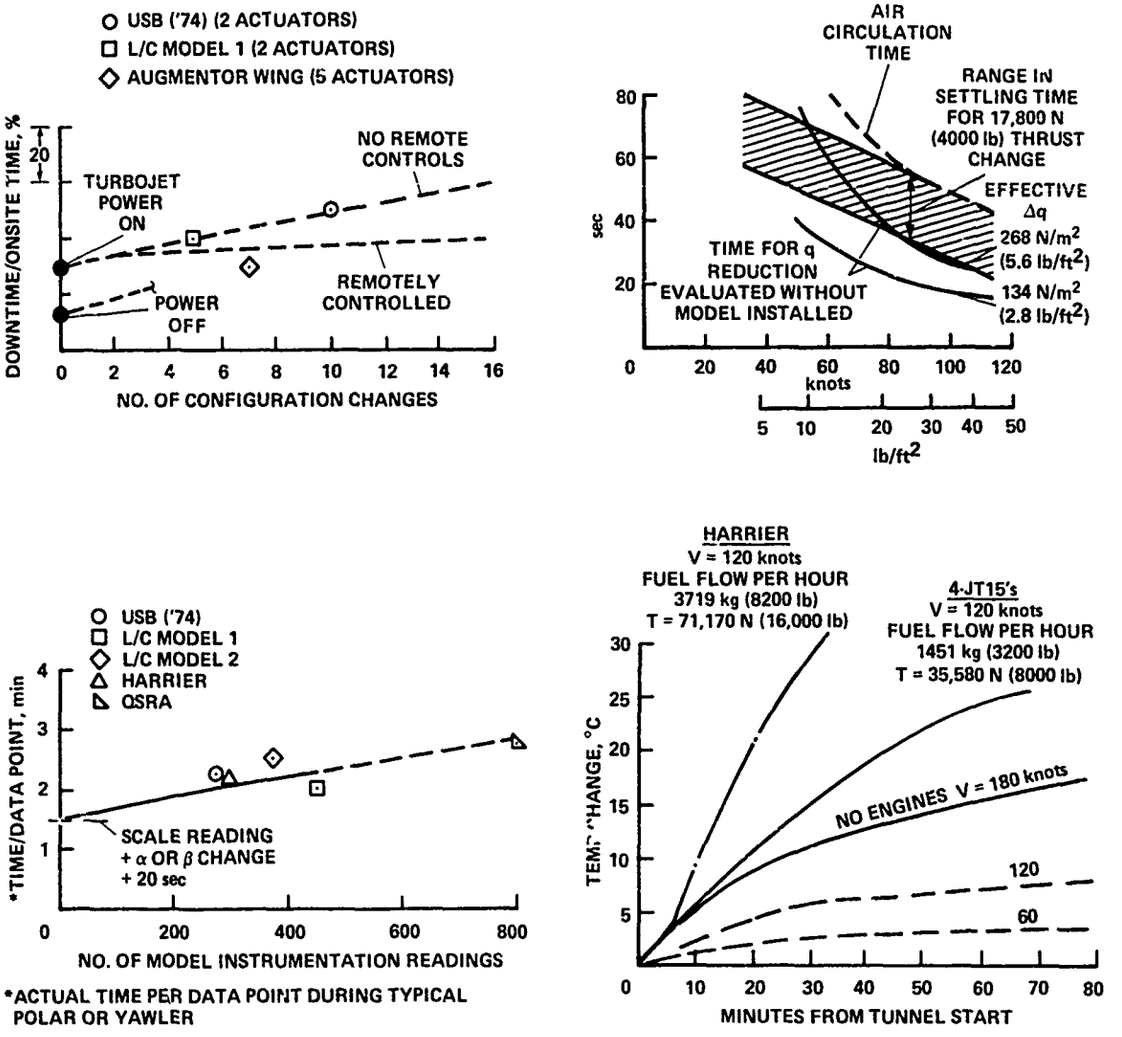

Figure 97. Factors influencing testing time for powered models in the Ames 40 by 80 (Ref. 4).

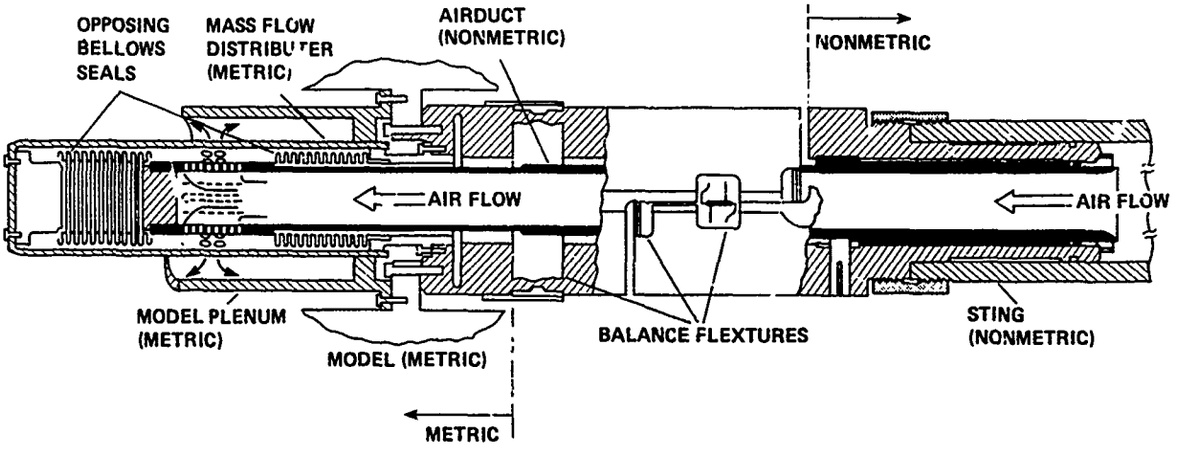

Figure 98. Schematic of flow-through internal balance (Ref. 109).

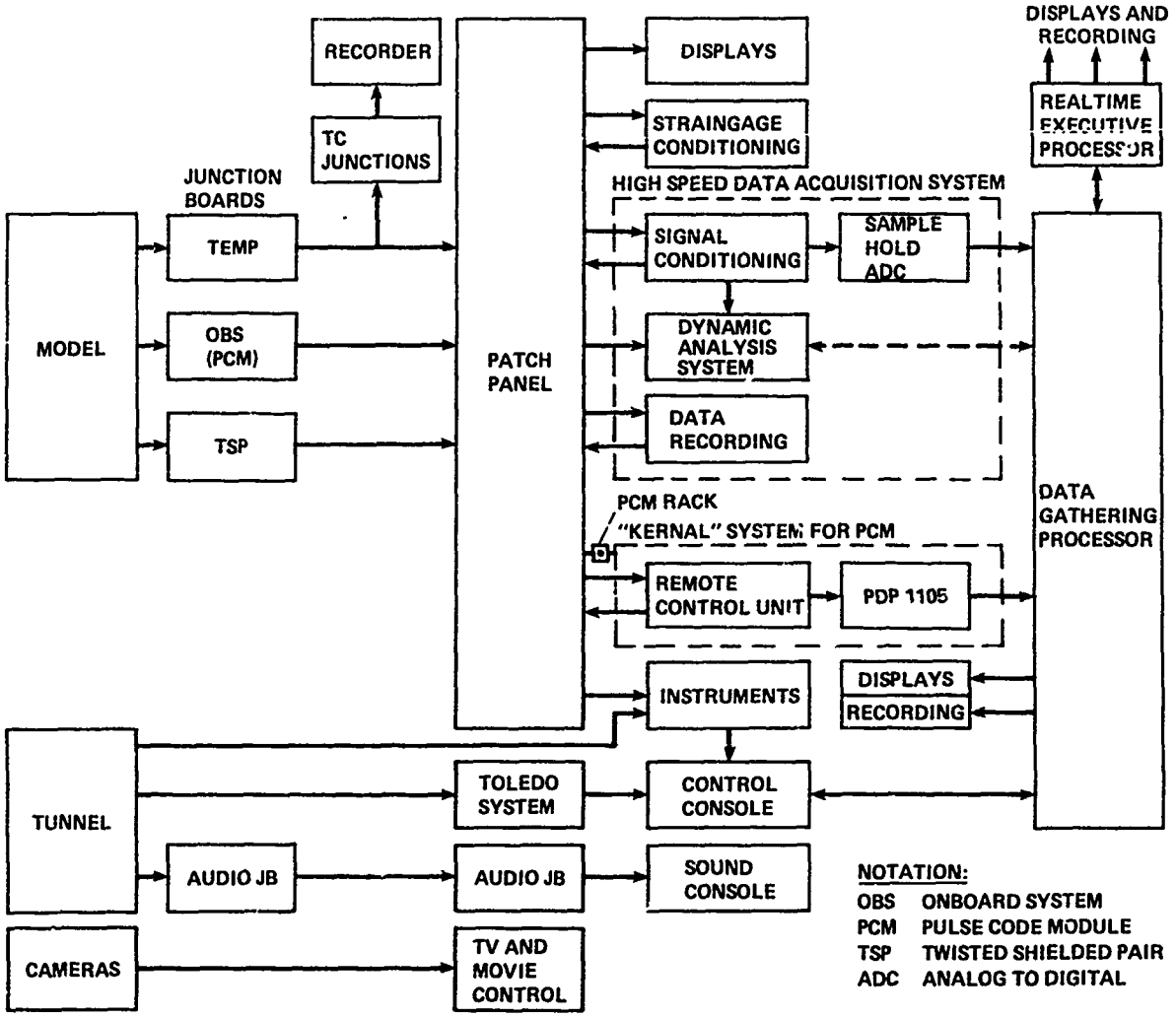

Figure 99. 40 by 80 data-acquisition system.

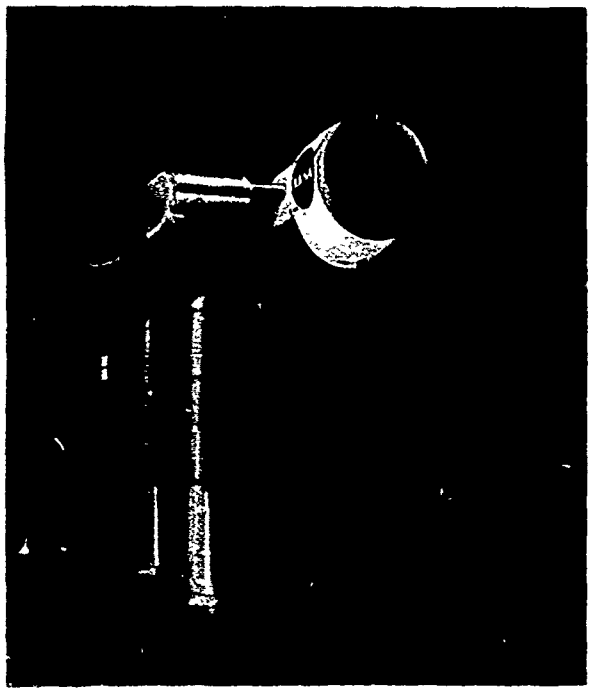

Figure 100. JT8D mounted in wind tunnel for the jet noise investigation (Ref. 114).

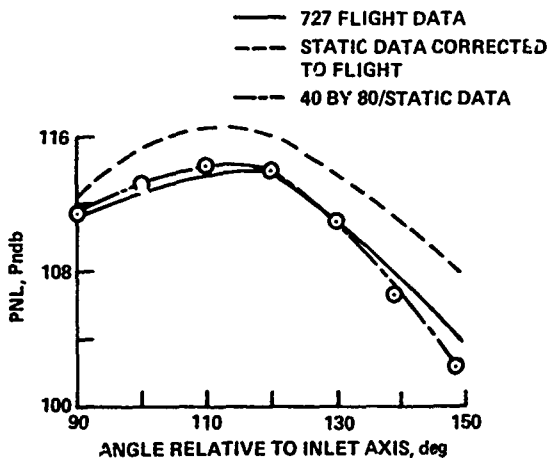

Figure 101. Comparison of 40- by 80-ft wind tunnel and flight-stand data with the 20-lobe ejector suppressor on a JT8D-17 turbofan engine (Ref. 114).

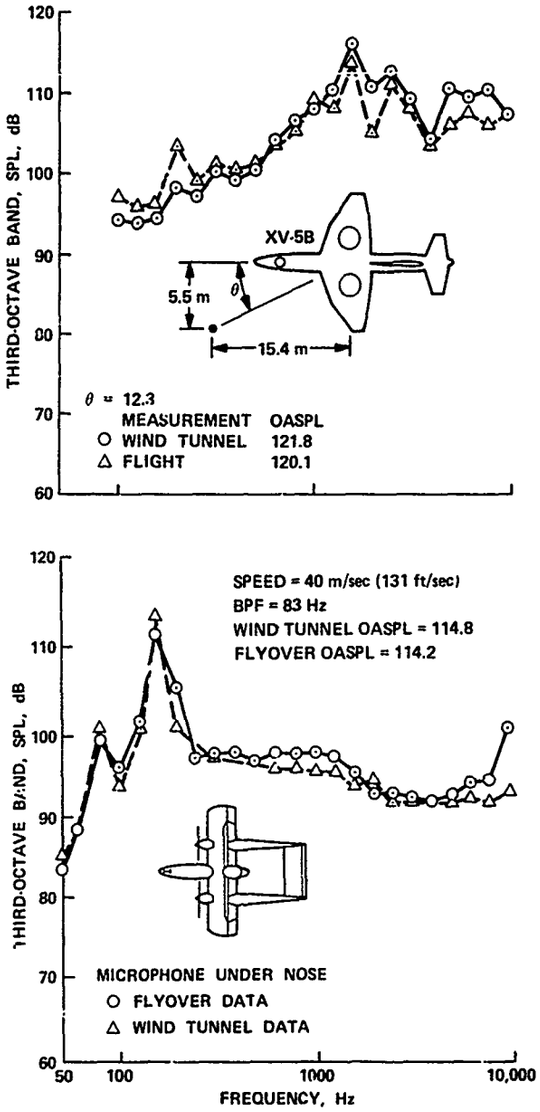

Figure 102. Comparison of corrected flyover and 40- by 80-ft wind tunnel noise data at equal distance for two aircraft (Ref. 120).

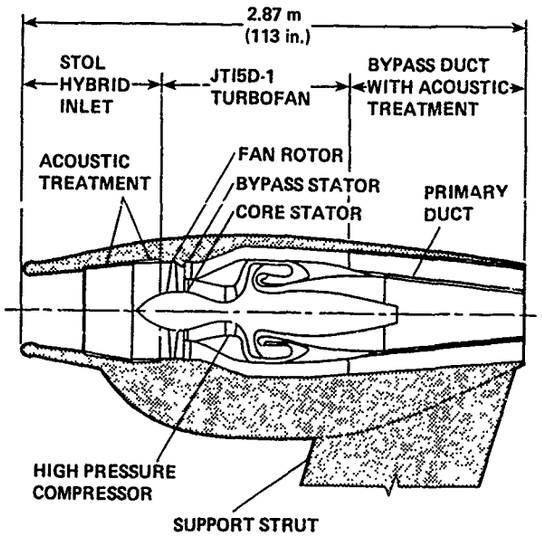

Figure 103. Hybrid inlet nacelle installation (Ref. 122).

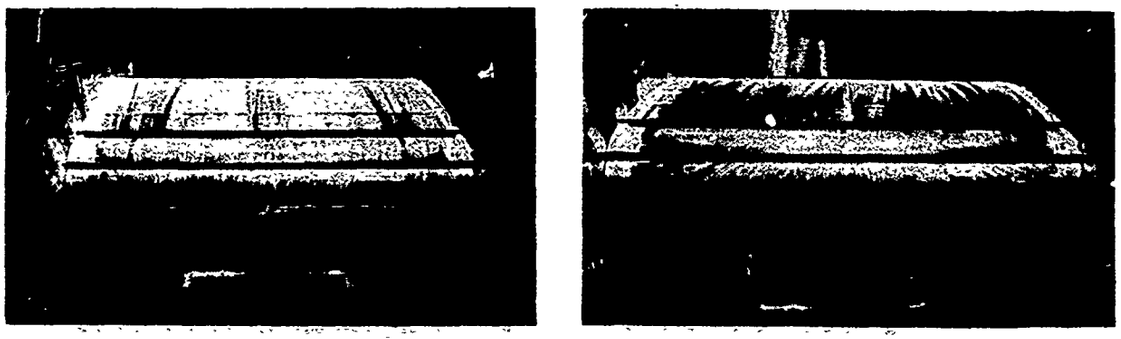

Figure 104. Oil-smear evaluation of flow on multiairfoil two-dimensional model (Ref. 49).

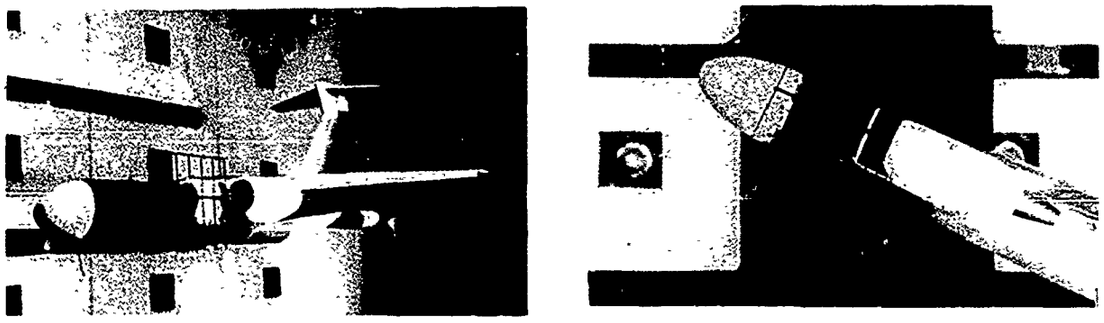

(a) Model instaliation.

(b) Model at $\alpha = 24^{\circ}$, $C_j = 2$, $q = 479$ N/m^2 (10 lb/ft^2).

Figure 105. Tuft grid study for evaluating upwash near inlet of EBF transport model (Ref. 130).

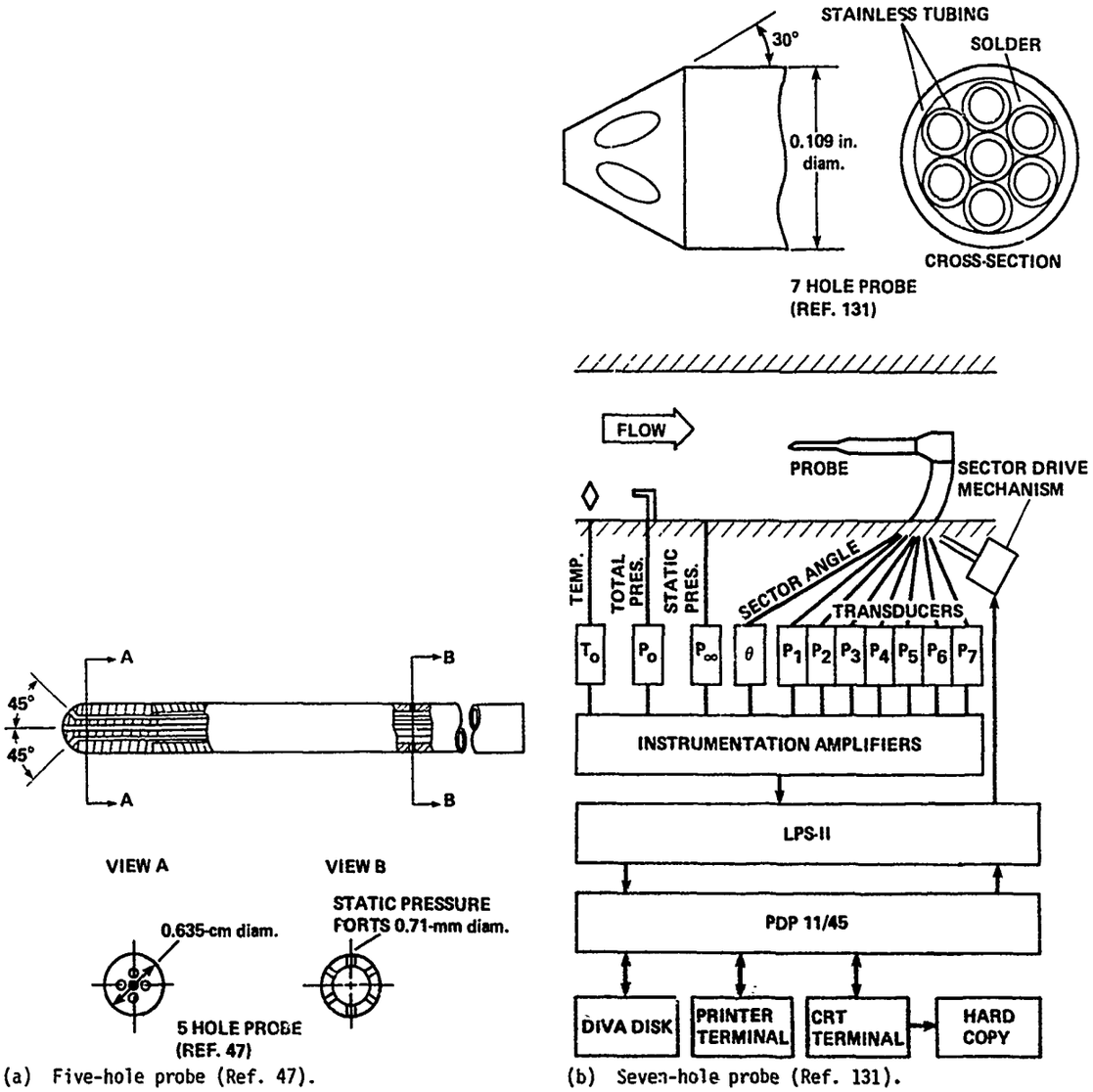

(a) Five-hole probe (Ref. 47).

(b) Seven-hole probe (Ref. 131).

Figure 106. Five- and seven-hole directional probes.

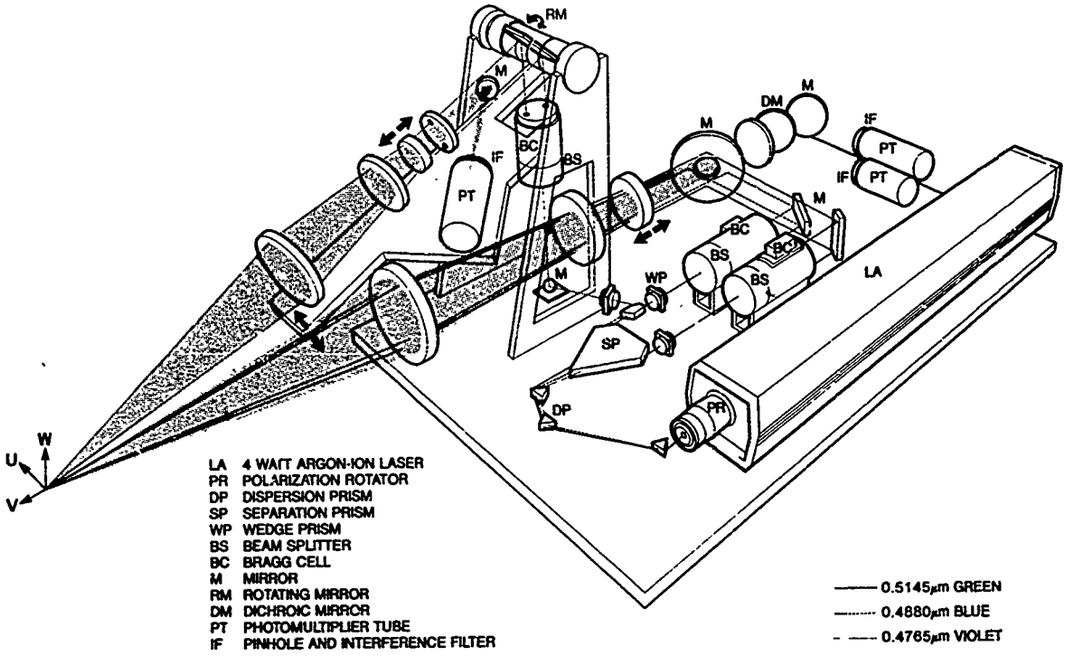

(a) Three-dimensional laser velocimeter. Uses three different colors from a single argon-ion laser to form three independent dual-scatter backscatter channels.

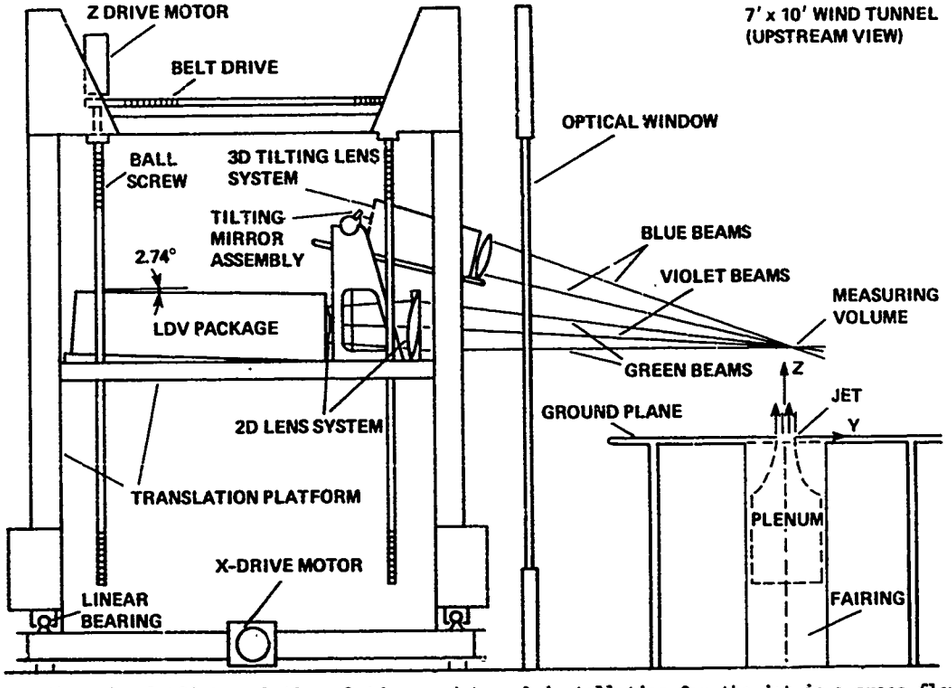

(b) Three-dimensional LDA translation platform and tunnel installation for the jet-in-a-cross-flow test.

Figure 107. Three-dimensional laser velocimeter (Ref. 132).

Figure 108. Three-dimensional laser velocimeter operating in the Ames 7 by 10 wind tunnel; jet-in-cross-flow test.

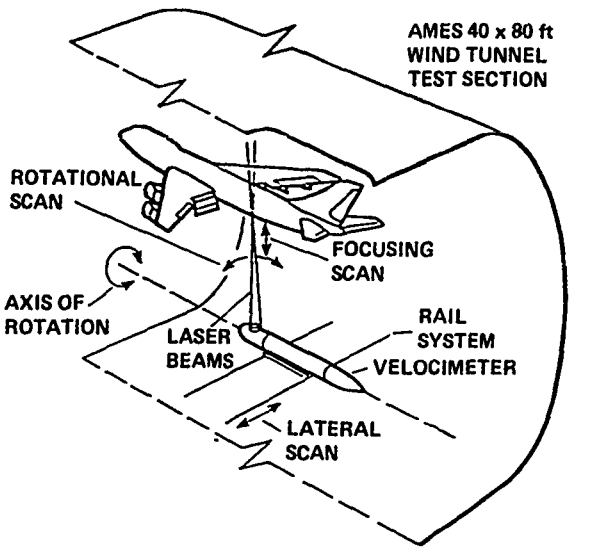

Figure 109. Use of two-dimensional laser velocimeter in large wind tunnel (40 by 80 shown) (Ref. 135).

Figure 110. Large laser velocimeter in operation.

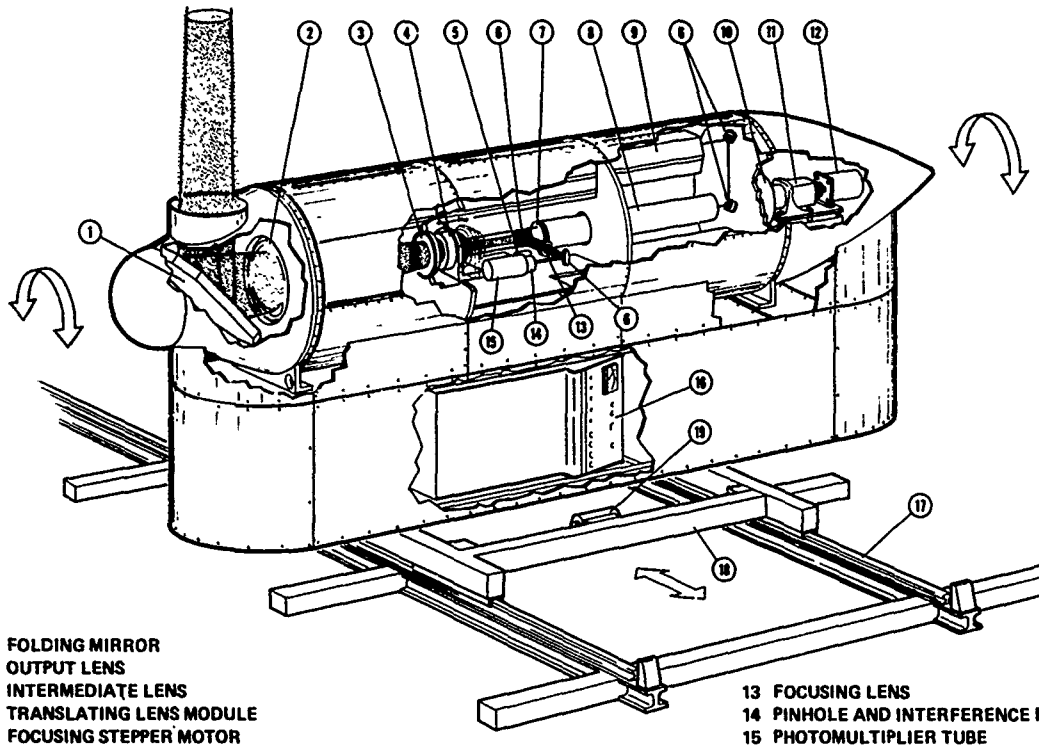

1 FOLDING MIRROR
2 OUTPUT LENS
3 INTERMEDIATE LENS
4 TRANSLATING LENS MODULE
5 FOCUSING STEPPER MOTOR
6 MIRROR
7 RHOMBOID ROTATOR ASSEMBLY
8 BEAM SPLITTER AND FREQUENCY SHIFTER
9 LASER
10 ABSOLUTE ENCODER
11 GEAR REDUCER
12 ANGLE ROTATION STEPPER MOTOR
13 FOCUSING LENS
14 PINHOLE AND INTERFERENCE FILTER
15 PHOTOMULTIPLIER TUBE
16 LASER POWER SUPPLY
17 LINEAR BEARING
18 TRANSLATION STAGE
19 LATERAL TRANSLATION STEPPER MOTOR

Figure 111. Laser-velocimeter system shown mounted on lateral traversing rails; insert shows alternative method of receiving for extended-range configuration (both beam pairs are shown in the insert (Ref. 135).

GROUND BASED TESTING WITHOUT WIND TUNNELS

C.L. Bore
Head of Research
British Aerospace, Kingston

INTRODUCTION

Mr. Koenig has covered thoroughly the special features of V/STOL wind tunnel testing, but there are some important ground based tests which do not require wind tunnels.

- Reaction Controls.
- Air Intake Testing at Very Low Speeds.
- VTO Suckdown Forces and Moments.
- Hot Gas Ingestion.

REACTION CONTROLS

The maximum thrust required from a reaction control may be typically about half a ton, so the efficiency of these is quite important. If the compressed air for the reaction controls is bled from the high pressure compressor (in the Harrier family it is) then at some combinations of control demand, the removal of air from the combustion chamber flow may cause the turbine entry temperature (TET) to rise to its limit. Beyond this point, the TET limiter will cut back the fuel, and the engine thrust with it. Typically, if the mass flow of compressed air bleed could be reduced by one pound per second, the main engine thrust may rise by about 300 pounds for total bleeds above the TET limit, but the Pegasus is flat rated below the TET limit. It follows that considerable development is worthwhile if the compressed air bleed requirement is reduced as a result.

Since the bleed air is hot (typically 700K) the mechanical durability of the reaction control valves undergoing friction, fatigue and heating needs attention. Consequently we use a rig supplied with heated compressed air to measure the thrust of reaction controls, to minimise leakage, measure local temperatures and obtain data for fatigue and acoustic fatigue checks.

AIR INTAKE TESTING AT LOW SPEEDS

The payload and range of an aircraft operating from a vertical take-off is very sensitive to the efficiency of the air intake, and also the distributions of total pressure, total temperature and static pressure across the compressor face. For a STO/VL aircraft (i.e. short take-off/vertical landing) those qualities together dictate the maximum landing weight.

To illustrate this statement, consider some typical trade-offs for the Harrier family. Suppose that the payload for given fuel weight was (say) 20% of the full engine thrust. Then clearly a 2% loss of thrust would lose 10% of payload. Now suppose that the total pressure loss were to be concentrated mainly in the inner annulus of the compressor flow, so that the flow destined to enter the high pressure compressor is mainly affected. Then it may happen that a 1% loss of overall total pressure results in 2% loss of engine thrust, which in turn would mean 10% loss of payload. It follows that meticulous attention to intake performance is merited.

Figure 1 shows the difference that was made to the distribution of total pressure loss in the Harrier intake as the outcome of a very thorough investigation of detailed shaping (see Ref. 1).

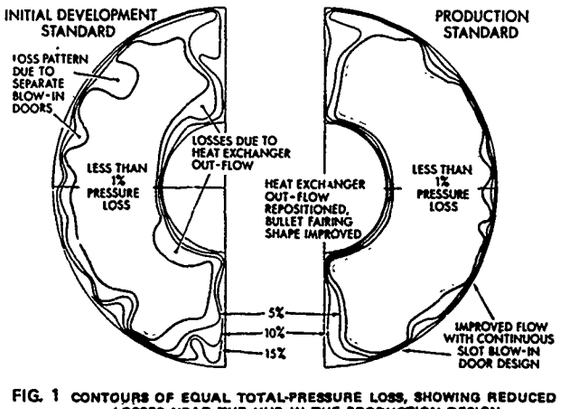

FIG. 1 CONTOURS OF EQUAL TOTAL-PRESSURE LOSS, SHOWING REDUCED LOSSES NEAR THE HUB IN THE PRODUCTION DESIGN

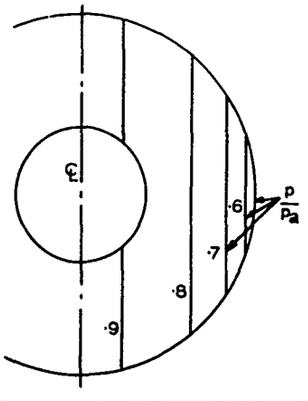

FIG. 2 STATIC PRESSURE DISTRIBUTION ACROSS COMPRESSOR FACE (SCHEMATIC)

Even as long ago as that investigation, I suspected that the distribution of static pressure also might affect the engine thrust, so we measured the static distribution. This involved both static tappings around the intake duct and also static pressure caps for the pitot rakes across the entire engine face. The results of the experimental survey were simple and plain. There was a strong gradient of static pressure across the width of the engine face, with low pressures on the outer ends of the diameter and high pressure near the centre plane (Fig. 2). The static pressure isobars were practically vertical straight lines. (The isobars shown are sketched from memory).

However, the practical significance of this evidence was not taken into account for a long time. For one thing, it was argued that our model results related to an empty air intake duct, without a compressor at the "engine face", and a compressor might even out the static pressure. Indeed, it was conventional to think of a compressor as a device that imposed a constant static pressure across its face! In any case, there was not much we could do about it on the Harrier, for the static pressure distribution was a consequence of high speed flow round a curved duct, and it was too late to alter the ducts.

Later it was found by full scale tests with an engine that such a steep variation of static pressure (which corresponds with a strong gradation of local Mach number) could be responsible for a substantial loss of thrust - in some circumstances over 800 pounds of thrust. Furthermore, it was found to be possible to reduce this loss greatly by lengthening and reshaping the ducts.

All these tests were made by sucking air at full scale Mach numbers through model air intakes of one-quarter scale, using an ejector driven suction tunnel. They have been borne out well by full scale performance.

VTO SUCKDOWN FORCES AND MOMENTS

When a jet lift V/STOL aircraft is close to the ground, the effluxes spreading more or less radially over the ground entrain ambient air, which has to be replaced by a down draught above the aircraft. Since the entire process is driven by momentum exchanges, the anti-lift or suckdown forces induced are proportional to the efflux momentum or thrust. If there is simply one central jet, or a close array of jets, the suckdown can become large: the order of 30% of the jet thrust.

However, if there are two or more widely spaced jets, the sheets of efflux spreading over the ground will meet at some equal-stagnation-pressure loci and spray vigorously upwards, as a "jet fountain", as discussed by Dr. Kotansky. If the aircraft designer exercises enough cunning, he will arrange a cross-dam and a pair of longitudinal strakes near the edges of the underbody, to deflect these "fountain" flows downwards again (Fig. 3). On the Harrier, the extra lift from the fountain flows trapped and deflected in this way fairly neatly offsets the suckdown force, so that the maximum net suckdown is only around 4% of thrust, at a height of over 15 feet, where the fountain flows are too weak to make any difference (see Fig. 4).

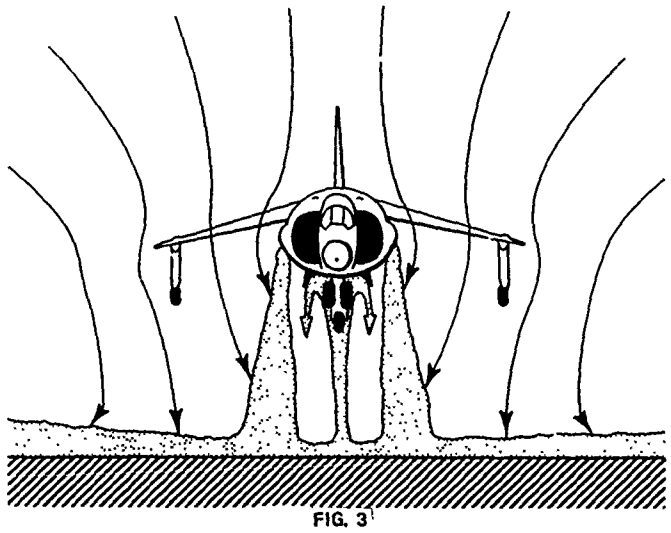

FIG. 3

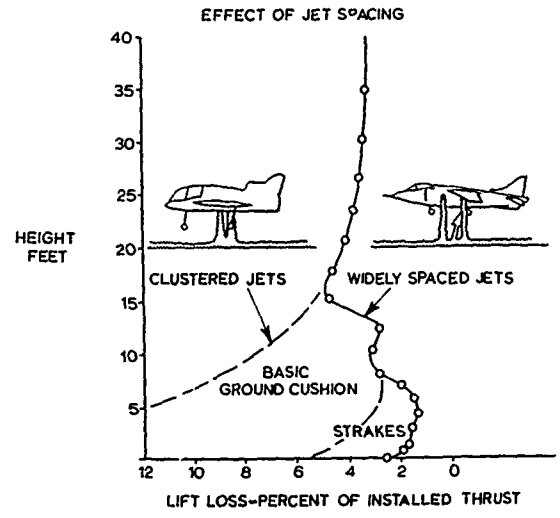

FIG. 4

The point to note here is that the net vertical force on the aircraft (which dictates the landing weight) and the pitching and rolling moments (which dictate the reaction control forces) depend on the angles between the ground and the aircraft, and the ambient wind, and the shape of anything the aircraft is hovering over (such as part of a ship) and details of the nozzles and strakes, and so on.

So there is a lot of work to do, to check out any proposed new feature. As happens often with V/STOL, there is not enough time and money to do all the parametric design variations, so we have to try to judge from experience what may be a useful improvement, and then check it out!

Our original rig was not elaborate (Fig. 5). The main feature, of course, was a model aircraft equipped with jets and an air intake. Ideally one needs the intake momentum scaled to the momentum of the jets, otherwise one would have to extrapolate the air intake force contributions from tests done at reduced intake flow. The model shell is isolated from the nozzles, and the forces and moments are measured. Beneath the model, the ground board could be raised or lowered. A portable fan could be used to simulate wind. For this work the jet pressures need to be fairly high in order to induce measurable forces and moments, so this testing was not done on the hot gas rig.

Often people ask why this sort of work is not done in a wind tunnel. One reason is that rather little of the work requires a wind at all, and few wind tunnels can run at low enough scaled speeds. A more telling reason is concerned with the interferences produced by the walls. As soon as the spreading jet sheets reach the walls, the induced flows would start to be wrong in character, and if the effluxes are hot the hot gas cloud is constrained unrealistically.

After 20 years of use, the old rig has been scrapped and replaced by a much more versatile facility which can be switched readily between suckdown force testing and hot gas ingestion testing. This will be described later in the context of hot gas ingestion.

HOT GAS INGESTION TESTING

On all the Harrier family so far (except the P.1154 supersonic aircraft) the front jets have exhausted only warm air (around 370K). Ingestion of a little air from these front jets does not cause much loss of thrust, though on very rare occasions some unusual manoeuvres have led to engine surge very near the ground.

However, if we wish to boost the engine thrust greatly by using Plenum Chamber Burning (PCB) - that is reheat in the bypass air to the front nozzles - then we have to face a very different prospect. Typically, PCB to high temperatures such as 1600K may increase the thrust of a basic engine by around 50%. This provides high specific thrust, suitable for propulsion of a supersonic aircraft, and also high static thrust to land the supersonic aircraft vertically at the end of its mission (STO/VL). Obviously we do not want much gas at that temperature entering the intake, even if it were uniformly distributed. If it were non-uniformly distributed, then compressor surge may result. Consequently we have done a lot of model testing over the past 20 years, aimed at minimising the adverse effects of Hot Gas Recirculation (HGR), while Rolls-Royce have been investigating the engine aspects.

Naturally this involves an aerodynamic model equipped with hot gas nozzles at appropriately scaled temperatures, and an air intake sucking in an appropriately scaled momentum of air. At the model "compressor face" an array of fast response thermocouples measures the ingested air temperatures. The data is then plotted out by computer in terms of the various parameters concerned, such as the mean temperature rise, and the temperature rise coefficient (such as TC 120).

In normal operations with STOVL aircraft, it is the vertical landing that poses the main problems with HGR, for whereas on STO the aircraft leaves its efflux behind, for landings the aircraft may arrive above its appointed landing site, create a cloud of hot gas and then proceed to descend into this. Clearly the dynamics of the entire landing trajectory are important, so our original rig (Fig. 5) incorporated means to raise or lower the model at any chosen speed or acceleration profile, at rates scaled to the jet velocities. A movable fan could be used to simulate ambient wind effects.

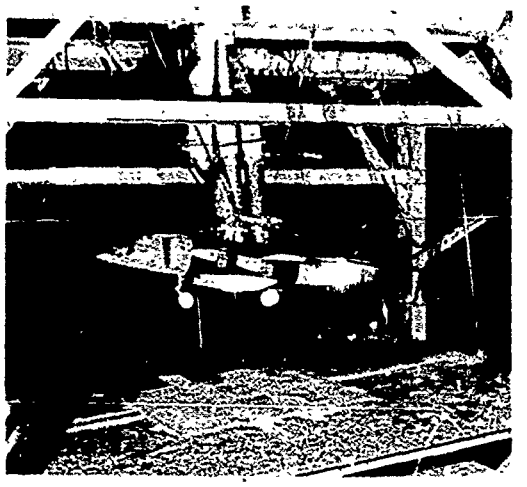

FIG. 5

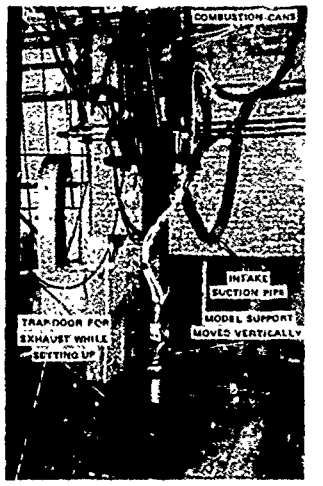

FIG. 6

With the aid of underfuselage strakes and other HGR features for all our configurations, we have found that hot gas recirculation (HGR) can be confined below a height of 10 feet (see Fig. 8). However, the details of such temperature versus height profiles depend on many variables, such as the nozzle array and the jet parameters, the strake array, the relationship of underbelly to air intake layout, and the ambient wind. The hot gas cloud is, of course, highly unsteady, so the temperatures encountered vary from one test to another. Consequently we repeat each test three times. With so many variables to investigate, both for suckdown and hot gas ingestion, even optimising the details of a few variants of a configuration takes a lot of work.

There is an important aspect of HGR testing which has been glossed over so far in this lecture. That is the question of proper thermodynamic scaling between the model simulation and the full scale situation. This will be discussed in the next section.

THERMODYNAMIC SCALING FOR HGR

It would be possible to devote an entire lecture to this topic alone, but that would be out of proportion in a presentation concerned mainly with testing techniques and facilities. On the other hand, it is a fact that for aircraft with high temperature jets, an inappropriate choice of scaling law could be quite misleading. Consequently it is worthwhile considering the reasoning and evidence behind the choice of particular scaling rules.

For many years the straightforward temperature scaling rule proposed by Abbott (Ref. 2) was accepted. This assumed that the temperature rise (above ambient) found in the air intake flow would be proportional to the temperature rise ejected into the field around the aircraft by the jet effluxes. With this rule, if the model jets were run at (say) half of the temperature excess to be used at full scale, then the temperature rise found in the model intake also would be half of the full scale value.

More recently, in discussions between Rolls-Royce at Bristol and British Aerospace at Kingston, it has been recognised that it is more logical to scale the intake temperature rise to the heat flux of the jets, rather than the temperature. For given pressure ratio, the excess-heat flux varies as excess temperature divided by the square root of absolute temperature (i.e. $\propto \theta_j / T_j^{\frac{1}{2}}$). The entrained secondary airflow depends on the jet momentum, which is independent of temperature. Hence when the flows are mixed, the final excess temperature is proportional to the excess-heat flux of the jets. Milford (3, 4) argued that the Abbott rule would apply only to situations where there is a direct flow of hot gas from jets to intake, but if this occurs the hot gas ingestion is so excessive that the aircraft is not viable. If hot gas recirculation is sufficiently indirect and restricted to permit a practical aircraft, any hot gas ingested will have mixed substantially with ambient air, and consequently the effects of buoyancy need to be included in the non-dimensional groups governing scaling.

Following this argument, he concluded that for any practical configuration, the ratio of intake temperature excess to jet temperature excess will not be a constant, but will fall with increasing jet absolute temperature:

$$\frac{\theta_i}{\theta_j} = k\left(\frac{T_j}{T_a}\right)^{-\frac{1}{2}} \qquad \ldots\ldots \quad (1)$$

where θ is the excess of temperature above ambient, and T is the absolute total temperature.

A substantial amount of work has been done towards establishing the limits of validity of this rule, and further work is in progress. The high variability and scatter always found in HGR testing (particularly with inclusion of ambient wind) makes it necessary to do a lot of testing to establish the trends.

Figure 7 illustrates typical results, for 6 different model configurations, in the form of graphs of the worst temperature excess ratio versus the ratio of absolute jet temperature. If the Cox and Abbott rule applied, all the graphs would be horizontal, whereas by the Milford rule they should have a slope of - 1/2. The experimental graphs all have slopes in the range - 1/2 to - 1.

FIG. 7

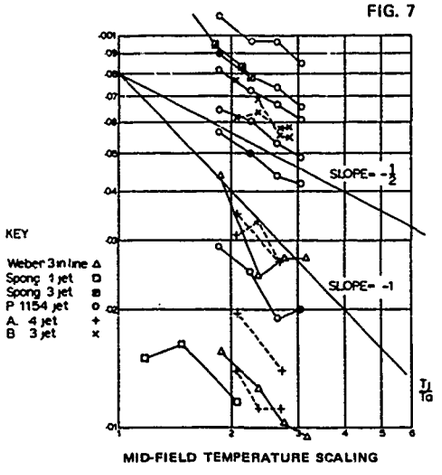

MID-FIELD TEMPERATURE SCALING

FIG. 8

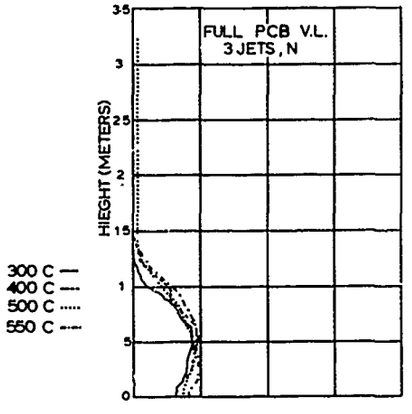

CORRECTED TEMPERATURE RISE(C)

So far, I conclude that for HGR experiments with acceptable configurations, the Milford scaling rule is roughly right, but it seems possible that eventually a more general rule may turn out to be:

$$\frac{\theta_i}{\theta_j} = k\left(\frac{T_j}{T_a}\right)^{-n} \qquad (2)$$

where n may range from 0.3 to 1.0 according to the extent of mixing with ambient air before ingestion. Work continues!

The scaling of time from model to full scale depends on the proposition that at "corresponding time" in the model and full scale sequences of events, the flow fields will be geometrically similar. This implies that the velocity distributions must be similar. To ensure that the influence of buoyancy is properly represented, the Cox number for model and full scale must be set the same:

$$C_o = \frac{R_e^2}{G_r}\left(\frac{T_j}{T_a}\right)^{-\frac{1}{2}} \quad . \quad . \quad . \quad . \quad . \quad (3)$$

where R_e = Reynolds' number and G_r = Grashof's number.

For any given scale of model, choosing a particular jet temperature leads to a particular jet velocity. If the model temperature is chosen less than full scale (as it usually is) then this leads to a jet velocity considerably less than full scale, and all the model velocities should be scaled similarly. This allows time for much more detailed measurements of the unsteady temperatures. If there are jets with different temperatures, they cannot both be scaled properly at once, so it is necessary to choose which one is the more significant - usually the front jets, for PCB configurations.

If the thermodynamic parameters of the model tests were properly scaled, the experimental recordings of intake temperature versus height can be factored (using Equation 2) to the equivalent full scale profiles, as shown in the typical results of Figure 8. For any given set of model data, the Milford rule predicts lower full scale HGR than the Cox rule. For a long time it has been clear that viable PCB powered vectored thrust configurations can be designed, and the research emphasis in the past few years has been centred on proving the efficiency of the most favoured configurations, which we may not show here!

MAJOR HOT GAS INGESTION FACILITY

Twenty-two years of work on the old rigs illustrated in Figure 5 and Figure 6 have given us an understanding of the basic principles of both suckdown forces and HGR, but as the biggest obstacles of ignorance are cleared away they are replaced by questions related to efficiency and to operating techniques. Now the questions are of this nature: "Given a certain aircraft configuration, with appropriate underfuselage devices, are there circumstances where wind from some angle would cause a serious loss of thrust?" or perhaps "Given a more or less vertical landing with partial PCB, would a small nozzles-aft movement in the last few feet of descent allow higher landing weight?"

The latter question, for example, poses the possibility that a small vectoring of the nozzles, or the aircraft as a whole, in the final second of descent may blow the hot gas cloud vigorously about, while gently shifting the aircraft. This sort of consideration raises the need for real-time motions of the aircraft model, relative to a fixed site over which an ambient wind may be blowing from any angle.

Another important consideration arises from the fact that it is the combined effects of suckdown force (and moments) together with thrust loss from HGR that will determine the maximum safe landing weight or the minimum PCB temperature. Consequently it is highly desirable that both effects shall be measurable on the same model and facility. Now in the past, these functions were separated because one needed high-q blowing (but not temperature) while the other involved temperature (but not high-q).

Our new combined facility (Figs. 9, 10) addresses all such problems in a very flexible way. The model aircraft can move in any trajectory 5 feet high by 12.5 feet long, on the ends of a pantograph linkage controlled by a remote cam. The aircraft may roll and pitch during that trajectory, and nozzle rotation in real time will be provided. The hot gas is provided at separately controlled temperatures to front and rear nozzles, using hydrogen fuelled combustors. Intake suction is provided. A large blower fan may be positioned at any angle from - 20 degrees to + 45 degrees to the axis of the facility. This facility has been commissioned, and is now engaged in vigorous research on our supersonic STOVL project.

REFERENCES

1. C.L. Bore: Harrier Aerodynamic Design: Air Intake. Aircraft Engineering, December 1969.

2. W.A. Abbott: Estimation of Intake Temperatures During V/STOL Operation from Model Tests. NGTE Note NT.600, March 1966.

3. C.M. Milford: Scaling Factors for Hot Gas Recirculation. BAe-KAD-N-GEN-2787, August 1981.

4. C.M. Milford: Further Consideration of Recirculation Temperature Scaling Laws. BAe-KAD-N-GEN-2844. June 1982.

5. M. Cox and W.A. Abbott: Studies of the Flow Fields Created by Single Vertical Jets Directed Downwards Upon a Horizontal Surface. NGTE Memo M.390, October 1964.

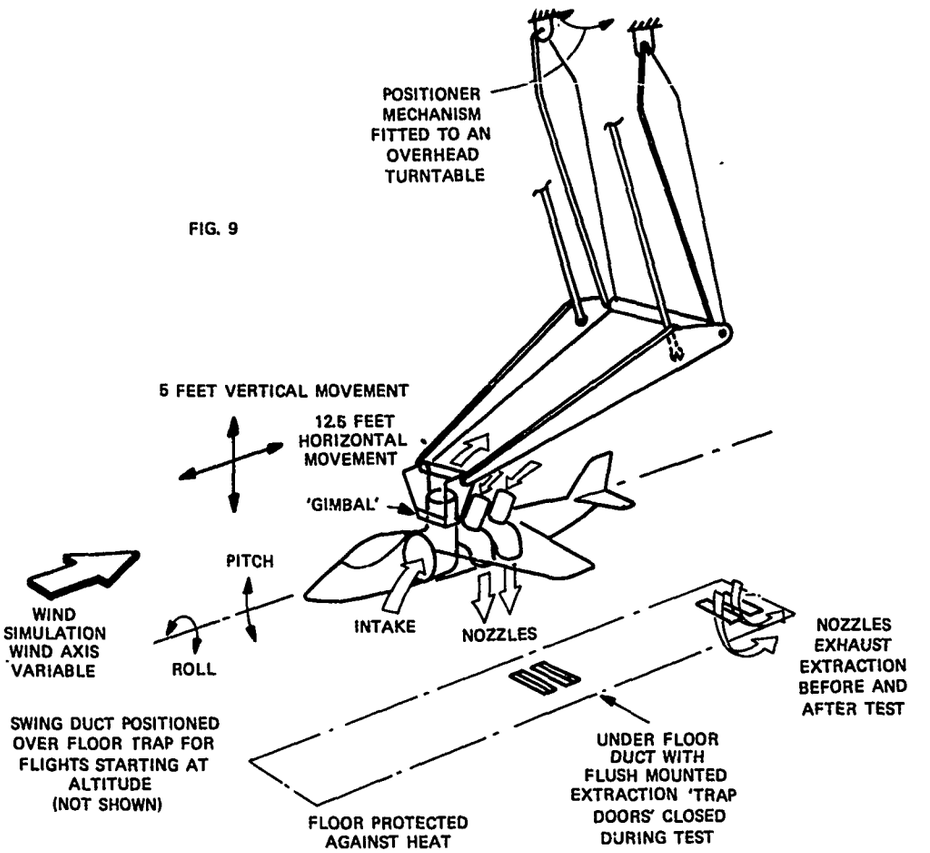
POSITIONER MECHANISM FITTED TO AN OVERHEAD TURNTABLE
5 FEET VERTICAL MOVEMENT
12.5 FEET HORIZONTAL MOVEMENT
'GIMBAL'
PITCH
WIND SIMULATION WIND AXIS VARIABLE
ROLL
INTAKE
NOZZLES
NOZZLES EXHAUST EXTRACTION BEFORE AND AFTER TEST
SWING DUCT POSITIONED OVER FLOOR TRAP FOR FLIGHTS STARTING AT ALTITUDE (NOT SHOWN)
UNDER FLOOR DUCT WITH FLUSH MOUNTED EXTRACTION 'TRAP DOORS' CLOSED DURING TEST
FLOOR PROTECTED AGAINST HEAT

FIG. 9

FIG. 10

AERODYNAMICS OF V/STOL AIRCRAFT

- PERFORMANCE ASSESSMENT -

BY

D. C. Leyland
Deputy Chief Aerodynamicist
British Aerospace PLC
Warton Division
Preston, Lancs PR4 1AX
England

1. INTRODUCTION

V/STOL aircraft designs encompass forms of powered lift varying from rotors, as for a helicopter, through propellers and ducted fans to jets. Consideration here will be restricted, however, to jet borne aircraft, since only that type has ever gone into production (the Harrier/AV8B family) and is the only variant in serious consideration for the highly attractive, but difficult to meet, requirement for a supersonic V/STOL aircraft.

The common feature is that jet thrust is employed to sustain lift at zero or low forward speed, though there is now the added attraction of the facility for using deflected thrust to enhance combat capability. Discussion here will therefore extend beyond the conventional V/STOL mode to cover combat performance assessment since improvement in that aspect has become one of the drivers in configuration design. The developments in figure 1 cover a range of more than 20 years, from the now dis-favoured lift engines to examples (the tilt nacelle and the 2-post vectored thrust) where nozzles are arranged at the trailing edge of the wing to give lift enhancement as well as thrust deflection in combat. The development of active control technology for unstable flight allows the necessary location with respect to c.g.

Performance calculation for V/STOL aircraft is really little different from that for conventional aircraft except that the lift and drag data sets have to include jet interference terms and with jet deflection to be taken into account the engine data has to allow separation of nozzle gross thrust and intake ram drag. The means for calculation of jet induced effects is still in a rudimentary state and there must be recourse to experimental data, either by examination of published data for similar configurations or by early testing of project models in a suitable wind tunnel. The latter procedure is to be recommended because a further feature that has to be taken into account is the influence of induced jet effects on the trim of the aircraft, primarily in transition from jet to wing-borne lift and in the effect on drag due to lift, and estimation methods are simply not available.

No attempt will be made here to provide sets of data from which V/STOL performance can be estimated; there is too wide a range of parameters to be considered. Rather, the various phases of flight will be considered and point made of items that require particular consideration in making a performance assessment.

2. PERFORMANCE REQUIREMENTS FOR VERTICAL OPERATION

2.1 General

The first and most obvious requirement for vertical take-off is an excess of vertical thrust over weight, that is, a vertical thrust/ weight ratio greater than 1. The question is how much greater? Allowance must be made for:

i) Margin for acceleration and manoeuvre
ii) Jet-induced lift losses
iii) Hot gas re-ingestion
iv) Reaction control bleed

2.2 Margin for Acceleration and Manoeuvre

Reference 1 states (for vertical landing):

Starting from a steady rate of descent of not greater than 4 ft/sec, sufficient height control power shall be available to produce upward vertical accelerations of not less than those specified in the table below, following an abrupt step input of the thrust magnitude control. In any case, the steady state thrust-to-weight ratio available, shall not be less than that specified in the table.

LEVEL	INCREMENTAL VERTICAL ACCELERATION - 'g'	T/W
1	0.10	1.05
2	0.05	1.02
3		1.01

The apparent inconsistency between the two columns is due to the specified starting condition of a steady descent, because vertical damping would provide some upward vertical acceleration even in the absence of excess of thrust over weight.

The Level 1 and Design condition (all systems operating) therefore demands an installed thrust/weight ratio of at least 1.05, or 5% excess thrust. In this context thrust means nozzle gross thrust less jet-induced lift losses.

2.3 Jet-Induced Lift Losses

2.3.1 Away from Ground

The jets emerging from the nozzles induce a downward (and inwards towards the jets) flow field about the aircraft as illustrated diagramatically in figure 2. In static conditions the flow causes downward forces, primarily flat plate drag on the wings. The lift loss is proportional to the nozzle gross thrust and is equivalent, typically, to 2-3% thrust. Clearly, because of convergence of flow towards the jets, nozzles situated under the wing entrain the greatest lift losses under static conditions, away from the ground.

There are theoretical methods being developed for predicting these losses but reference can generally be made to test data for a particular configuration.

2.3.2 Ground Effect on Jet-Induced Lift Losses

The presence of the ground destroys the downward momentum of the air entrained by the jets and a different flow pattern results. An understanding of the effects can be obtained by considering the extreme examples illustrated in figure 3.

Disc with central jet:

When a single jet of hot gas is directed onto a surface it spreads out laterally as a thin sheet in which the peak velocity decays rapidly as mixing occurs with the surrounding air. Eventually, the buoyancy forces created by the reduced density of the gases become sufficiently large to overcome the inertia forces and the edge of the jet sheet rises. The resulting flow pattern produces a ring vortex system under the disc; the reduced pressure around the vortex causes a suck-down effect.

Disc with peripheral jet:

The peripheral "curtain" of gases contains the cushion of high pressure air under the disc - the hovercraft principle. The resulting lift augments the direct lift due to the jet pressure and momentum. A partial approach is made to this condition if jet flow can be located at the trailing edge of a wing.

Fountain Flow

Nozzle grouping in practical V/STOL configurations results in a combination of the two basic effects, often with development of a so-called fountain between jets and the combination may be either favourable (cushion) or unfavourable (suck-down) compared with the free air losses. Very close to the ground the effects are dependent on jet configuration details (fig 4), or can be modified by use of suitable strakes under the fuselage, as has been accomplished for Harrier (fig 5). External stores are also likely to influence ground effects on jet induced lift losses.

Although a favourable ground cushion effect is obviously preferable to a suck-down effect it cannot be used to reduce the margin of excess thrust over weight for VTO because the thrust margin required must always be based on the worst case, that is, away from ground if a favourable cushion effect is present, close to the ground if a "suck down" is present.

2.3.3 Effect of Forward Speed

Increasing forward speed results in increasing jet-induced lift losses.

This can be reasoned from the fact that the jets entrain a downward velocity proportional to jet velocity V_J; the downwash angle induced is inversely proportional to forward velocity Vo but the resultant lift is proportional to the product of downwash angle and Vo^2. Consequently, it can be shown that:

$$\frac{\Delta L}{X_G} = k \frac{1}{\frac{\rho_J V_J^2}{\rho_o V_o^2}} \quad \text{(ref 2)}$$

The reasoning applies within the speed range where free stream momentum is small compared with jet momentum and little or no bending of the jets occurs. Beyond a certain point.

$$\frac{\rho_J V_J^2}{\rho_o V_o^2} = 4, \text{ typically,}$$

the increasingly large rearward bending of the jet plumes reduces the downwash and, as the parameter tends to zero, the losses reduce to zero, as shown in figure 6.

The effects of forward speed are not entirely unfavourable. Where there is a suck-down effect near the ground, forward speed reduces the effect, as shown in figure 7. Note here that increasing forward speed is shown on the X-scale in the opposite direction to that shown in the previous figure. The former presentation is more suitable for consideration of lift losses in forward flight, the latter for VSTOL.

Jet configuration also influences forward speed effects, a notable example being a 2-poster where jet flow is at the trailing edge of the wing and there is build up of induced lift (fig 8).

2.4 Hot Gas Re-Ingestion

There are two sources of re-ingestion, illustrated in figure 9.

The so-called 'bouyancy' effect arises from the fact that the gases issuing from a nozzle and impinging on the ground spread out laterally, eventually rise when the momentum is reduced sufficiently and re-circulate mixed with the ambient air. Being a "far field" effect the temperature rise at the intakes is time-dependent and quite small, reaching typically 5°C temperature rise after 30 seconds for a Pegasus under static ground running condition. This results in about 4% thrust loss. The effect increases with increasing height, up to a point, because increasing nozzle distance above the ground reduces the momentum of the gases flowing tangentially which means that they start to rise closer to the aircraft. As height is increased further the effect decays again and becomes negligible above about 30 feet above ground.

The 'hot gas fountain' effect occurs on multi-nozzle configurations when jet sheets spreading laterally meet on the ground between the nozzles and are deflected upwards to form hot gas fountains giving intense local heating effects. For a given configuration the mean temperature rise at the intakes is proportional to the excess temperature of the exhaust gases relative to ambient. A typical value of the temperature rise is 10% ($T_j - T_a$) or about 10°C from the "cold" forward nozzles on the Harrier, resulting in a thrust loss of about 8%. For 'hot' nozzles the thrust loss is clearly much greater and this is of concern in the development of plenum chamber burning (PCB), a form of reheat on the forward nozzles on the Pegasus engine, and more generally in future project studies where generally higher temperatures are seen necessary to produce the required thrust levels. Ingestion can also lead to engine surge through temperature distortion at the engine face. The whole subject is of major concern but discussion here is not appropriate.

Wind speed or aircraft speed on the ground obviously affect hot gas re-ingestion effects. Initially, forward speed reduces the fountain effects but increases buoyancy effects (with vertical nozzles), because the aeroplane is moving towards the rising front of hot gas. There is, therefore, a critical speed at which the effect is a maximum; above this speed the exhaust is blown backwards under the intakes and the effect falls rapidly to zero (figure 10). The speed for no re-ingestion can be quite low, say 50 knots, with consequent short landing distances, say 100m, and there could be much reduced constraints on design if STOL rather than STOVL could be an acceptable requirement.

2.5 Reaction Control Bleed

In jet-borne flight reaction controls are required for angular acceleration and trim. The thrust is normally supplied by H.P. compressor bleed air. The effect of compressor bleed is to increase turbine entry temperature and consequently to reduce thrust available, where T.E.T. limited. The design condition must allow maximum required simultaneous angular acceleration demands in pitch, roll and yaw plus trim demands in pitch at the most adverse c.,g. position and in roll/yaw at the crosswind limit, though a transient excess loss in thrust is now accepted and datum thrust loss defined for a so-called time-mean-bleed.

At zero forward speed in jet-borne flight an aeroplane is neutrally stable about all axes; both stiffness and damping forces are non-existent. Control-jet power must be incorporated to provide stability, to react out-of-trim moments and to provide angular acceleration for countering gust disturbances and for manoeuvring. A full dissertation on stability and control in jet-borne flight is beyond the scope of this lecture but some examples of out-of-trim moments that arise are of interest.

Jet-induced lift forces produce a nose-down moment on the Harrier due to reducing jet-induced downwash on the tail as it enters ground effect, noticable below about 4 metres (reference 4), and in the presence of a cross-wind the downward wing is subjected to a larger proportion of the jet induced lift loss and tends to drop.

Intake momentum drag in the presence of any cross-wind produces a destabilising yawing moment which can impose severe restrictions on aeroplanes with forward intakes. For practical reasons of available yaw reaction control power this moment can be opposed only up to moderate sideslip (cross-wind) angles; beyond the limit the aeroplanes yaws off uncontrollably, in a 'reverse weathercock' manoeuvre. With some forward speed, large rolling moments also result and this was the reason for augmenting the yaw and roll reaction control power during Hawker P1127/Kestrel/Harrier development (reference 3).

An example of the breakdown of reaction control requirements for a STOVL aircraft project design at the most critical flight conditions is shown in fig 11. It is to be noted that the trim requirements are generally larger than the basic handling (acceleration) requirements. There has been a lot of debate and confusion on the level of control required, with acceleration demands up to 2 rad/sec^2 quoted. That might be a total equivalent level, for countering trim as well as providing stability and manoeuvre; the basic acceleration requirement is inside 0.5 rad/sec^2 on all axes. In the case of fig 11, the assumptions were respectively 0.4, 0.25, and 0.15 rad/sec^2. The total thrust loss resulting from providing sufficient air bleed to satisfy the control requirements is in the order of 10%.

2.5 Thrust Margin for Vertical Operation

Typical values of thrust required to overcome jet-induced lift losses, hot gas re-ingestion and to provide sufficient allowance for acceleration and manoeuvre or full reaction control, for satisfactory VTOL, are shown in figure 12. The very high excess T/W required (in the region of 20%) is the reason why true vertical take-offs are rarely made operationally and "rolling verticals" or short taks-offs are used instead. In fact, the demand is so great that it is now common to project design for vertical land only - hence STOVL is the current acronym.

3. STOVL PERFORMANCE CONSIDERATIONS

3.1 Short Take-Off

If the thrust margin is inadequate for VTO or where operational considerations such as ground erosion prevent VTO, then a short take-off technique can be employed. STO can be divided into two categories:

Rolling Vertical Take-off, where the objective of the ground roll phase is to avoid hot gas or debris ingestion in the intakes. After a short ground roll the nozzles are rotated downwards (in about one second) and a near-vertical ascent can be made. The ground roll must be long enough to ensure that the critical speed for hot gas ingestion is passed and that increasing wing lift overcomes increasing jet-induced negative lift. This speed is as high as 50-60 knots for the Harrier. Due to the reducing lift loss and hot gas re-ingestion loss with reducing nozzle angle, an angle less than maximum gives optimum RVTO performance (figure 13).

Short Take-off, where a significant positive wing lift contribution (say 25% W) is required to make flight possible. Here, as in conventional take-off, ground roll distance increases with increasing unstick speed while airborne distance diminishes. However, with vectored thrust, there is the additional variable of nozzle angle. With increasing take-off weight increasing unstick speed is required, implying increased airborne drag and therefore increasing forward thrust, demanding a smaller nozzle deflection.

It is convenient to relate S.T.O. performance to the ratio of take-off weight ($W_{T/O}$) to maximum practical hover weight (W_H) and it is shown in reference 2 that S.T.O. performance can be presented non-dimensionally in the form:

$$\frac{S_G \delta}{\theta \, W_{T/O}} = f \left\{ \frac{W_{T/O}}{W_H} , \theta_J \right\}$$

$$\frac{S_A}{\sqrt{\theta}} \frac{\sqrt{\delta}}{W_{T/O}} = f \left\{ \frac{W_{T/O}}{W_H} , \theta_J \right\}$$

$$\frac{V_{U/S}}{\sqrt{W}} = f \left\{ \frac{W_{T/O}}{W_H} , \theta_J \right\}$$

In practice it is found (reference 2) that the nozzle angle/ unstick speed combination at which the average acceleration in the airborne phase becomes zero represents the optimum unstick conditions, yielding the smallest total (ground run + airborne) distance.

Examples of non-dimensional S.T.O. performance curves are given in figure 14 and a comparison with conventional take-off in figure 15. The take-off technique on Harrier is to slam to full throttle with nozzles aft to give initial acceleration and avoid the initial lift loss with increasing forward speed and as r.p.m. stabilises move the nozzle to 70° and then hold attitude constant. The acceleration is then such that the speed is near optimum and the speed must be controlled on attitude because unless there is a wind of 15 kts, the ASI does not register.

Ski-jump Take off

The ski-jump is a variant on a free (non-catapult) take-off from a carrier deck, which in turn is a variant on a short take-off, an aircraft such as the Harrier having sufficient thrust and the thrust deflection capability to achieve positive climb away from the deck length available. The notion of the ski-jump is that the aircraft can be launched in upwardly inclined flight path at a lower speed than from a flat deck. The acceptability of the manoeuvre relies on the aircraft accelerating sufficiently, during the semi-ballistic trajectory which follows, to reach normal launch speed by the time the flight path becomes horizontal.

The differences in performance assessment lie in the tolerances allowable on the height loss off the end of the deck or off the ski-jump. In a real-life situation, allowance must be made for the statistical mean of variations from nominal performance. For catapult launchers, a recognised minimum launch speed is that which gives an average height drop of 15 feet increased by 3 standard deviations (3) in launch speed (figure 16). This implies that only 1 in 1000 launches will in fact have a height drop of 15 feet. For Harrier, in a flat deck launch, it was found that there is then a 5 margin (or 1 in 3.6×10^6) on striking the sea, a satisfactory low probability of that catastrophe.

In consideration of ski-jumps, the variation of height drop with launch speed is very much steeper than for flat decks and a safety margin of 3 over the speed for 15 feet height drop is inappropriate. A margin of 5 over sea-strike was argued and gave a flight path, involving a minimal decay of vertical speed followed by a slightly climbing accelerating transition, that was acceptable to the development test pilot. Flight trials have led to some variations in definition to safety margins but similar principles need to be applied to any similar situation.

3.2 Short Landing

3.2.1 Airborne Phase

The use of jet lift introduces additional freedom in the selection of approach path and speed. Approach angle can be varied independently of approach speed by altering either nozzle angle (or ratio of lift thrust to propulsive thrust) or total thrust. Ref 3 quotes "glide-slope tracking by means of thrust modulation was more satisfactory than by means of nozzle angle modulation".

Maximum performance, that is minimum landing distance, demands minimum approach speed and maximum approach angle consistent with flare capability. These in turn require maximum usable aerodynamic lift and maximum usable jet lift, consistent with thrust/drag balance.

Figure 17 illustrates the balance of forces. The equations

$$W\sin\gamma - X_G \sin(\alpha - \delta') - (D + X_D) = 0$$

$$W\cos\gamma - X_G \cos(\alpha - \delta') - (L + \Delta L) = 0$$

combine to give

$$\left(\frac{D + X_D}{L + \Delta L}\right)\cos\gamma - \sin\gamma = \frac{X_G}{W}\left(\frac{D + X_D}{L}\right)\left[\cos(\alpha - \delta') - \sin(\alpha - \delta')\right]$$

which can be solved to yield approach angle and hence approach speed and airborne distance as a function of usable thrust/ weight ratio, as illustrated in figure of course, less than that available for S.T.O. because of the thrust margin required for control of the approach path and any overshoot.

A further reason for retaining a healthy thrust margin during final approach is that hot gas reingestion is likely to occur as the aeroplane approaches the ground, resulting in thrust loss and consequently lift loss if uncontrolled. A temperature rise of 15°C on short landings is quoted in reference 4.

3.2.2 Ground Roll

Ideally, during the ground roll vertical thrust should be 'killed' to give maximum wheel braking, and full reverse thrust used to increase the available deceleration. In practice this would demand a thrust vector variation of 180°, involving considerable design ingenuity and in any case the use of reverse thrust at low forward speeds is restricted by considerations of hot gas and debris ingestion. On the Harrier the 100° nozzle setting is prohibited at low forward speeds and at the higher speeds wheel braking is restricted by the necessity to retain directional control (tandem main undercarriage). Consequently the short landing distance is about 3 x short take-off distance at the same weight.

3.3 Vertical Landing

Adequate performance for a vertical landing essentially requires only that there be sufficient installed thrust to provide appropriate excess over weight and allow for control. The aircraft can be assumed of lower weight for landing than for take-off and hence there is the attraction of designing for STOVL, that is, short take-off accepted for a fully loaded aircraft and engine sizing dependent upon design for vertical land.

There can be constraints in design, however, in configuration layout and in engine choice. Fig 19 shows a possible RALS configuration, with engine by-pass flow switchable between a rear thrust nozzle or a lifting nozzle at the front of the aircraft. Choice of vertical nozzle location is fairly limited. Primary nozzles are located at the wing trailing edge, to enhance wing lift in combat, and, with the front nozzle located as far as possible as practicable, aircraft balance requires almost equal thrust front and rear. Hence, on a thrust balance plot, as in fig 20, there is a limited area that will satisfy total thrust and balance requirements.

In comparison with the thrust requirements on fig 20 is a by-pass-ratio/fan- pressure-ratio carpet for a possible engine. The thrust required could be achieved by increasing engine size but that would increase aircraft size (and cost). Turbine entry temperature increase does not help, but a possible solution is augmentation of the front nozzle thrust via some form of after-burn (plenum chamber burning). That, of course, leads to complication and to added weight, and the risk of problems related to intake hot gas re-ingestion is increased. In the event of detailed design of such an aircraft it may be necessary to accept an existing engine (or engines) and solutions would have to be found for front nozzle thrust augmentation.

4. TRANSITION-PERFORMANCE CONSIDERATIONS

The accelerating transition manoeuvre from jet-borne flight to aerodynamic lift involves a change of the thrust vector from upwards to forwards at a rate which allows aerodynamic lift to build up at the same rate as, or slightly higher than, jet lift decays. This manoeuvre should be made at constant incidence, accelerating slowly.

A typical nozzle angle and speed history in an accelerating transition is illustrated in figure 21. The range of possible settings for transition can be produced as in fig 22. For any new design early checks need to be made that transition, taking into account balance requirements, is possible.

The decelerating transition is a less precisely co-ordinated manoeuvre in the early stages because initially excess lift is being 'dumped' and the rate is not critical. The technique is to deflect the nozzles rapidly downwards and forwards at part throttle at a fairly high airspeed, increasing incidence to maintain height as speed reduces, then opening up the throttle(s) as maximum unstable incidence is approached.

5. CRUISE

In conventional flight VTOL aircraft generally become conventional aircraft, with performance evaluated conventionally. Some particular characteristics arise, however, because of the usually high level of installed non-afterburn thrust. The effects are seen in sfc and spillage drag curves (fig). In conventional (fighter) aircraft with T/W > 1 something like half the thrust is obtained by afterburning so that in cruise the thrust requirement demands sfc on the 'flat' part of the sfc curve. With the need to keep jet temperatures low for VTOL aircraft, afterburning is small or zero, and throttling for cruise gives sfc on the steeply rising part of the sfc curve. There is greater than usual care needed in determining and defining the low thrust sfc, and in establishing optimum cruise conditions. There is also consideration to be given in choice of engine in basic project design since the penalty on cruise fuel flow for a 'dry' engine can be significant.

The large throttling for cruise leads also to high spillage drag. If, for example, a dry engine is to equal an engine with 30% afterburn, the intake will be 30% greater. The reduction in A_0/A_c for cruise could give 60% increase in C_D spill which, applied to the larger capture area, gives twice the original spillage drag. There can be some compensation by increasing the frontal area of the intake cowl to better cancel pre-entry force but that has a penalty of its own in an increase in wave drag. As ever, in aircraft design, which compromise will you have?!

6. VECTORED THRUST AS A MANOEUVRING AID

In calculating the flight performance of vectored thrust aeroplanes some of the approximations used in conventional flight performance estimation are no longer valid. In particular, the assumption that thrust is aligned approximately with the flight path and that gross thrust and intake momentum drag act along the same 'thrust line' is not valid. Remember that only gross thrust can be vectored; intake momentum drag acts parallel to the flight path. The diagram of external forces is illustrated in figure 24.

One benefit of vectored thrust in an air combat situation stems from the ability to decelerate rapidly whilst applying extra (jet) lift, in turning flight, as illustrated in figure 25. The extra deceleration capability compared with conventional aeroplanes is due to the forward gross/thrust component with nozzles fully deflected (giving rearward thrust even if nozzle angle is 90°, due to incidence) and the sustained intake momentum drag due to the sustained intake mass flow. The extra lift is in the region of 1/2 to 3/4 'g' for an aeroplane such as the Harrier. Although gross thrust is typically 1.5 x W at high speed low altitude due to ram effects, up to half of this can be lost in jet-induced effects (figure 6).

The more general benefit of thrust vectoring is seen, for higher performance aircraft, in the way that turn rate can be increased, particularly attained turn rate at low speeds. A typical comparison of characteristics is shown in figure 26 for a projected STOVL aircraft. The aircraft is compared with a conventional fighter aircraft, as used in a combat simulator assessment of relative combat performance. The conventional aircraft has a larger wing and hence has greater attained performance compared with the STOVL aircraft with nozzles zero, but a lower sustained performance because of the resulting higher drag. With thrust deflected the STOVL aircraft more than matches the conventional aircraft, and particularly at low speed where the later stages of combat take place. There is a reduction in sustained turn rate at higher speeds, arising from the particular nozzle schedule chosen; development could well lead to different schedules, or acceptance of pilot over-ride.

Some results of the combat simulation study are shown in figure 27 and the clear advantage of thrust deflection is shown. There was an added benefit from pilot freedom of use of nozzle, allowing the possibility of partial thrust reversal whereas the auto-schedule was defined essentially to give max L/D.

7. JET LIFT ENHANCEMENT

Benefits on in-flight combat performance are clearly obtainable from thrust vectoring but a significant additional advantage can be obtained from arranging the nozzle exit so that wing lift is increased, a jet flap effect. The subject is dealt with in ref 5, where methods for calculating the effect are indicated, but the essentials of the development are worth repeating here.

Some configurations on which benefit can be obtained are shown in figure 28. The engine nacelle on wing has given most benefit, the wing root trailing edge location was that of the project used in the combat performance study in Section 6.

An example of a prediction is shown in figure 29 for a low speed tunnel model. The prediction is based on jet flap theory, with some, though surprisingly small, adjustment for the limited spanwise extent of the engine efflux; the effect is primarily a function of total jet momentum. More recent work has provided confirmation of the effect up to high subsonic speeds.

A particular configuration study had a layout in the style of figure 30 and resulting drag polars are shown in figure 13. The jet induced effect is significant only at higher C_L so that fullest benefit is seen on max C_L and hence in attained turn rate. Sustained turn rate is also improved, however, at low speed.

It is worth noting that the full benefit can be obtained only if the aircraft can be trimmed without major penalty. Figure 11 indicates how a foreplane configuration has the facility for balancing jet lift and induced effects by a positive lift load. A breakdown of lift components is shown in figure 33, with a 40% increase in lift for jet deflection being distributed between direct jet lift, jet induced lift and beneficial trim. The sort of increases in turn rate achieved for thrust deflection is shown in figure 34. The higher peak turn rate allows initial advantage to be obtained in combat and then firing opportunities tend to be achieved at lower speeds where the same turn rate as the opponent can be achieved at a lower speed, implying a smaller turn radius. Comparative assessments on a combat simulator are required to form judgements between different aircraft but some indication of advantage can be obtained by use of a combat correlation parameter (figure 35).

REFERENCES

1. USAF Mil. Spec MIL-F-83300
   Flying Qualities of Piloted V/STOL Aircraft

2. College of Aeronautics Short Course on Aircraft Performance Estimation, Paper 12
   Some Special Characteristics of the Performance of Vectored Thrust V/STOL Aircraft and Related Topics
   J. Q. Calkin and T. S. R. Jordon

3. AIAA Paper 71-773
   Harrier Development from the Flight Test Point of View
   J. F. Farley (H.S.A.)

4. NASA TN D 6791
   Flight Evaluation of a Vectored Thrust V/STOL Aeroplane during simulated instrument approaches using the Kestral (XV-6A) Airplane
   Morellod, Penson, Shanks, Culpepper

5. AGARD CP 285
   Jet-Wing Interaction to give improved combat performance
   A. Vint.

- AGARD CP 319
  Study of Combat Aircraft Manoeuvrability by Air to Air Combat Simulator
  A. G. Barnes

- Iowa State University Press
  Introduction to V/STOL Airplanes
  Dr. L. Kohlman

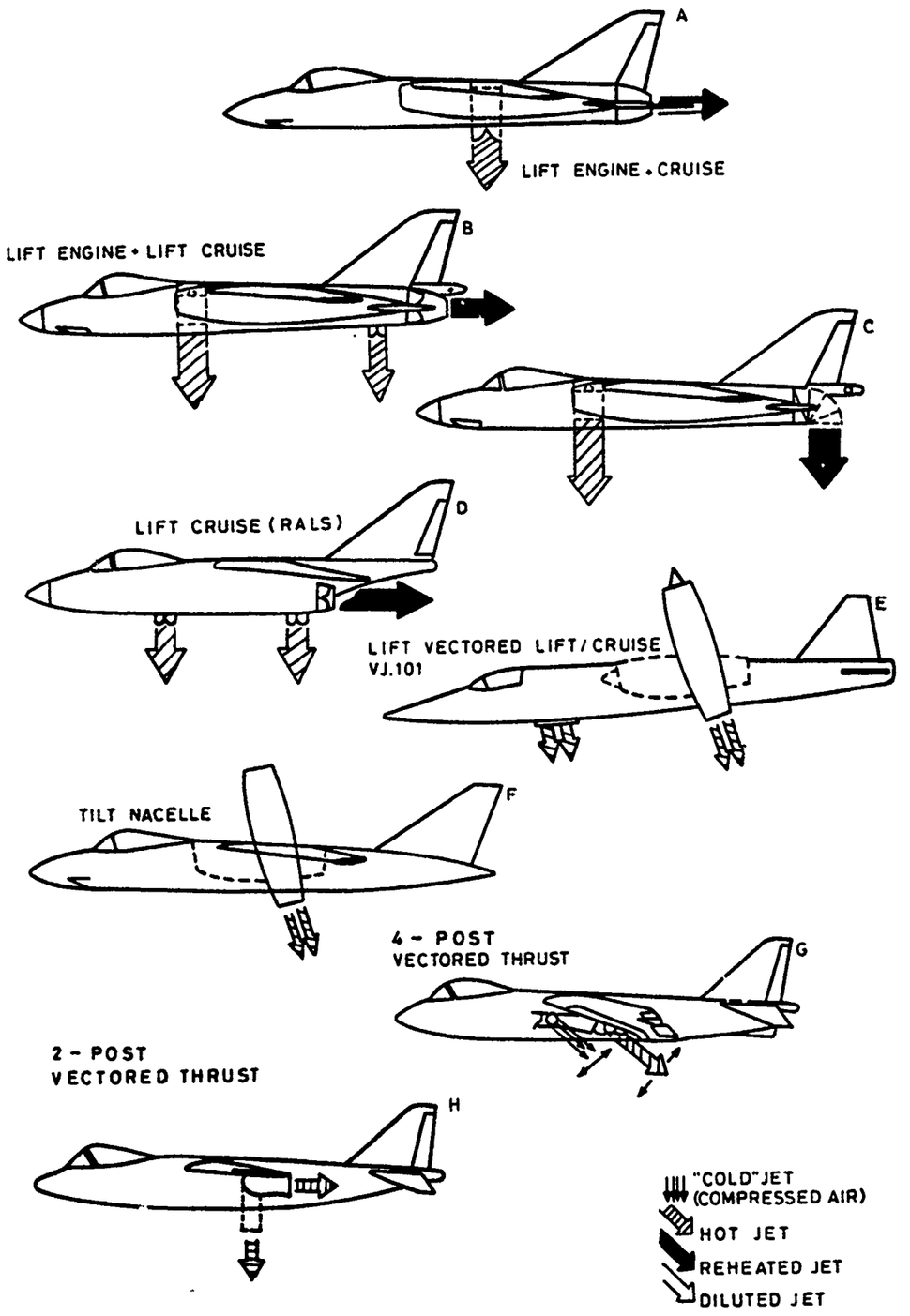

FIG. 1 V/STOL PROPULSION CONCEPTS

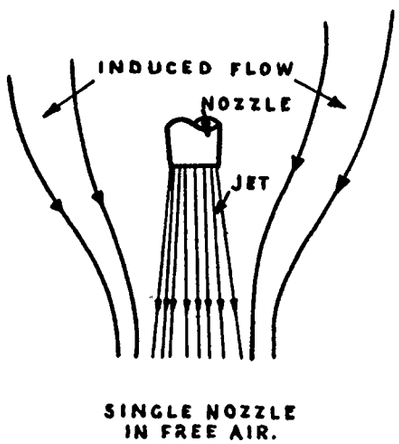

SINGLE NOZZLE
IN FREE AIR.

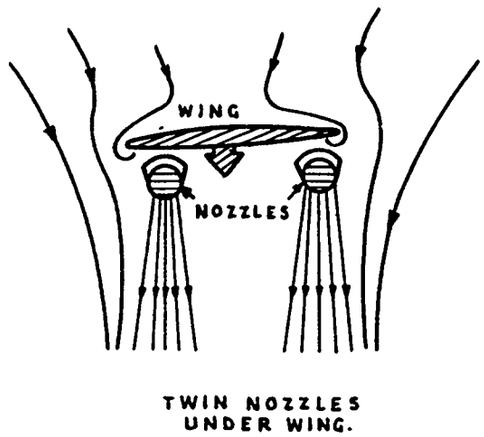

TWIN NOZZLES
UNDER WING.

FIG. 2

JET-INDUCED AIRFLOW INDUCING DOWNLOAD ON PLANFORM SURFACES
STATIC - AWAY FROM GROUND

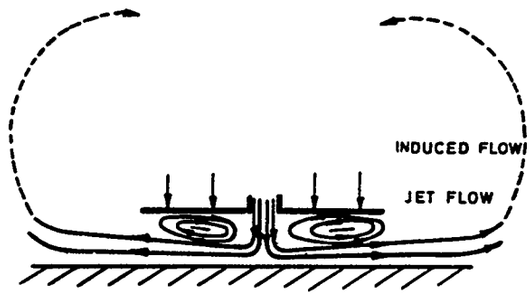

a) CENTRAL JET SUCK DOWN EFFECT

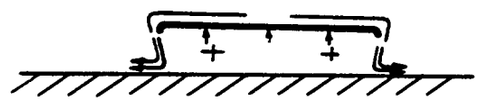

b) PERIPHERAL JET : CUSHION EFFECT

c) FOUNTAIN FLOW

FIG. 3 GROUND EFFECT ON JET INDUCED
LIFT LOSS (EXTREME CASES)

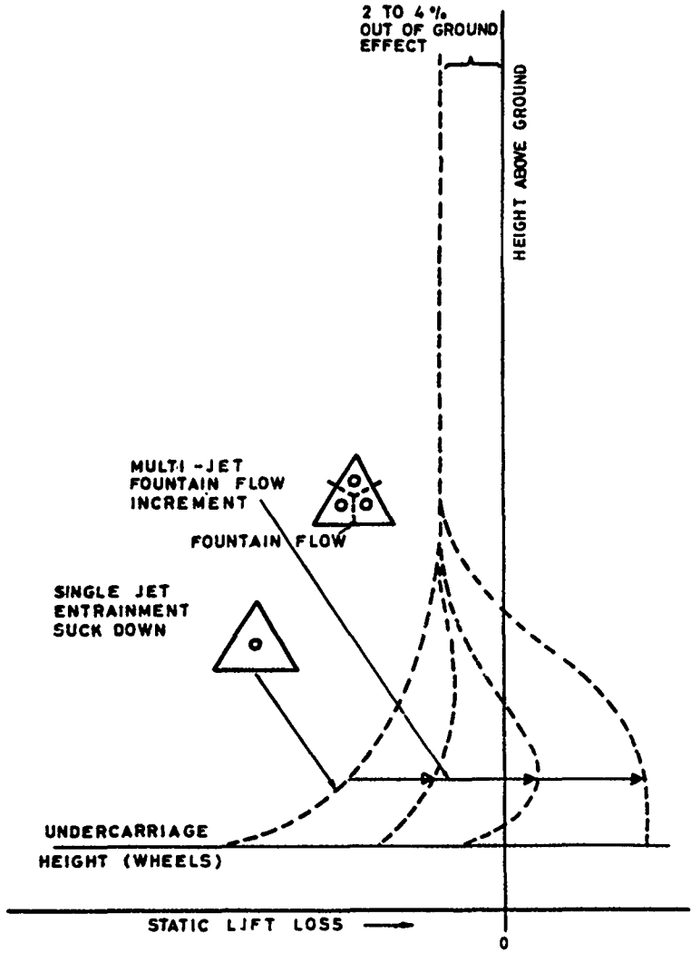

FIG. 4 JET INDUCED LIFT INCREMENT IN HOVER

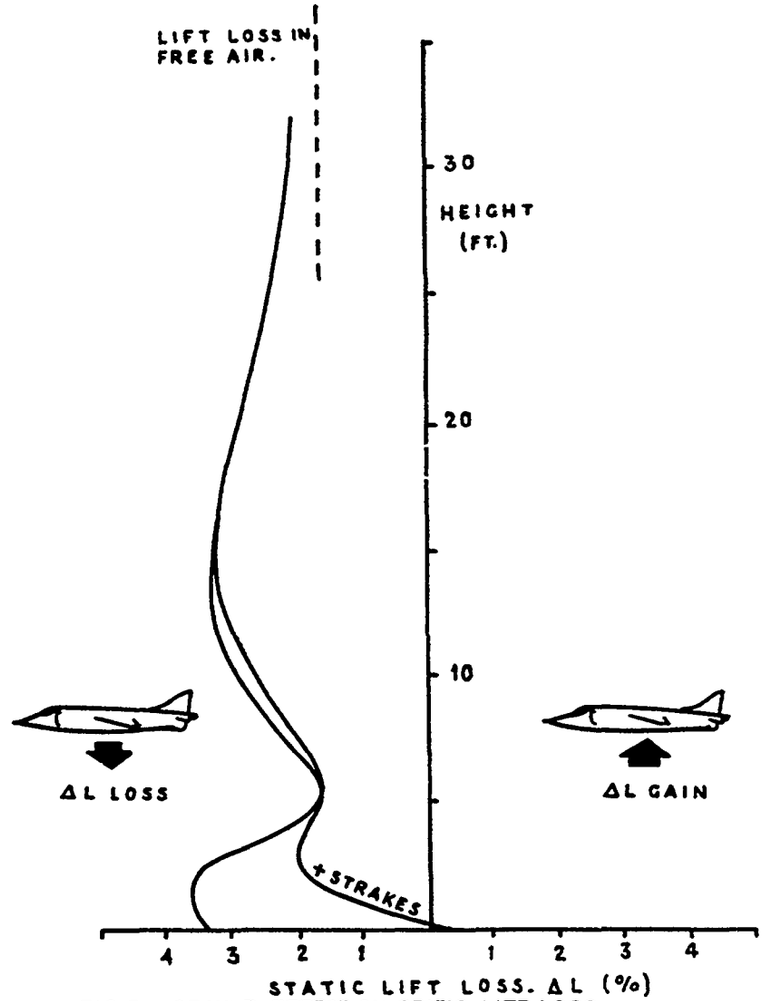

FIG.5 GROUND EFFECT ON STATIC LIFT LOSS
(HARRIER)

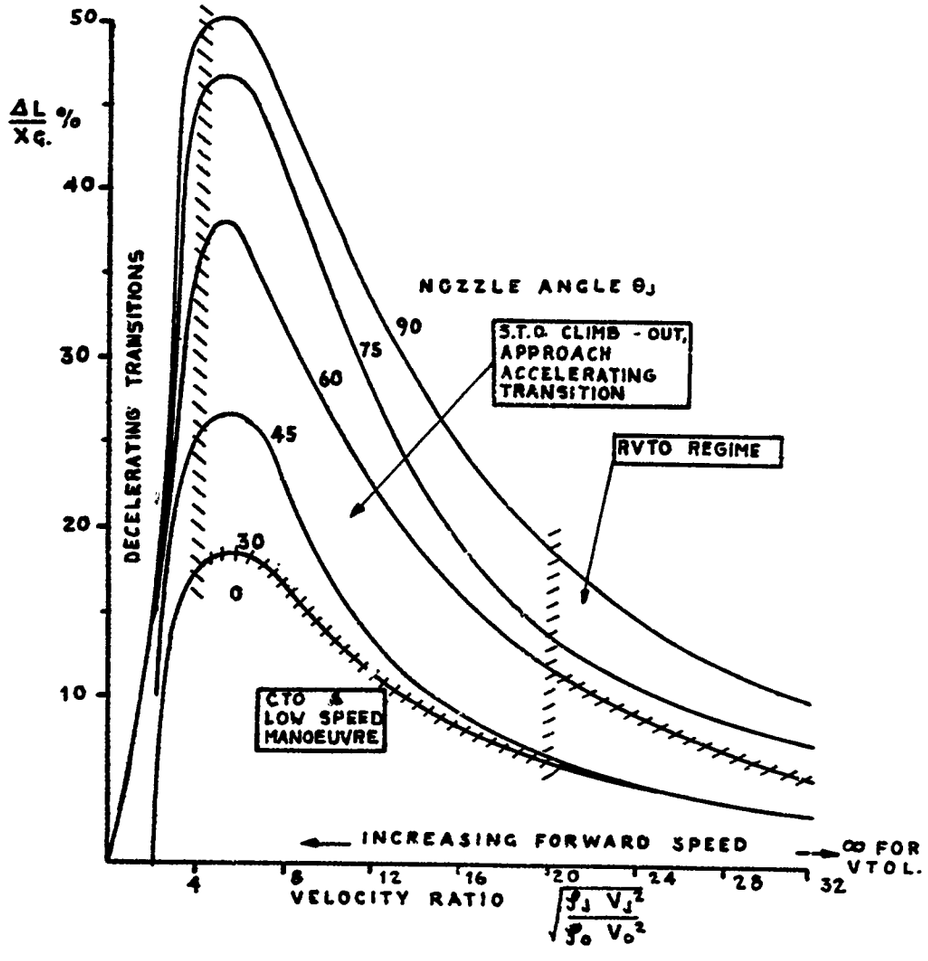

FIG. 6 LIFT LOSS IN FORWARD FLIGHT

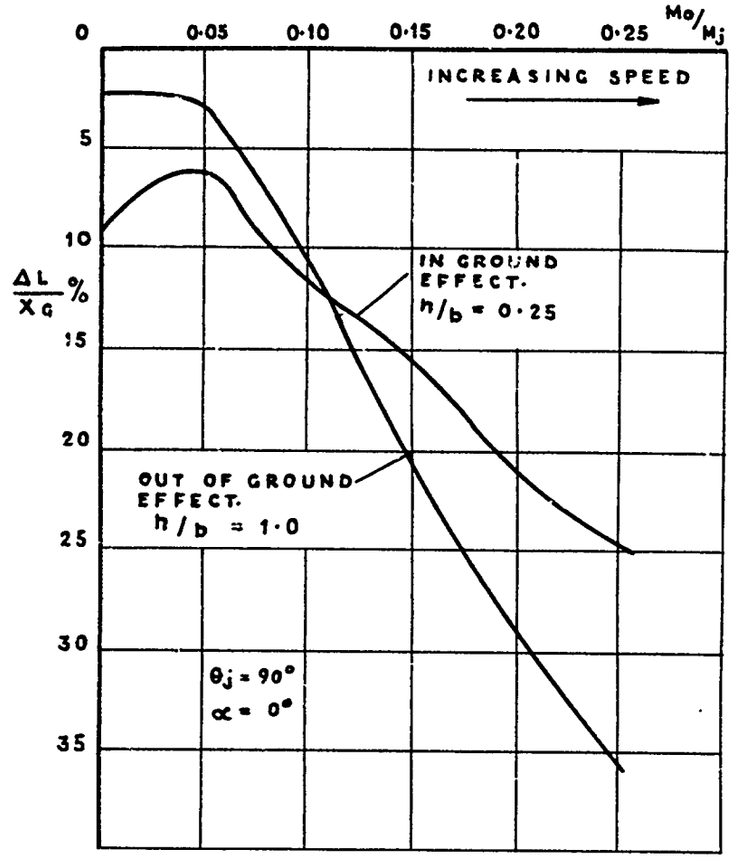

FIG. 7 THE EFFECT OF GROUND PROXIMITY ON LIFT LOSSES

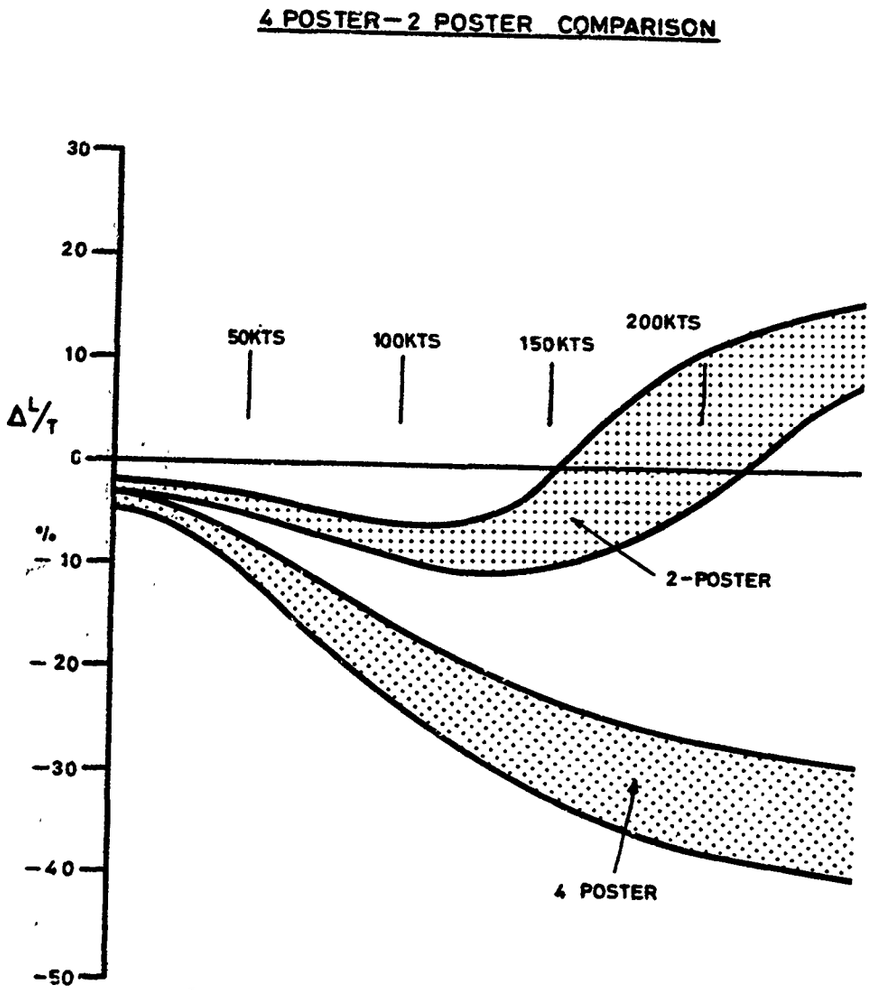

FIG. 8 JET INDUCED LIFT OUT OF GROUND EFFECT— $\theta j = 60° - 90°$.

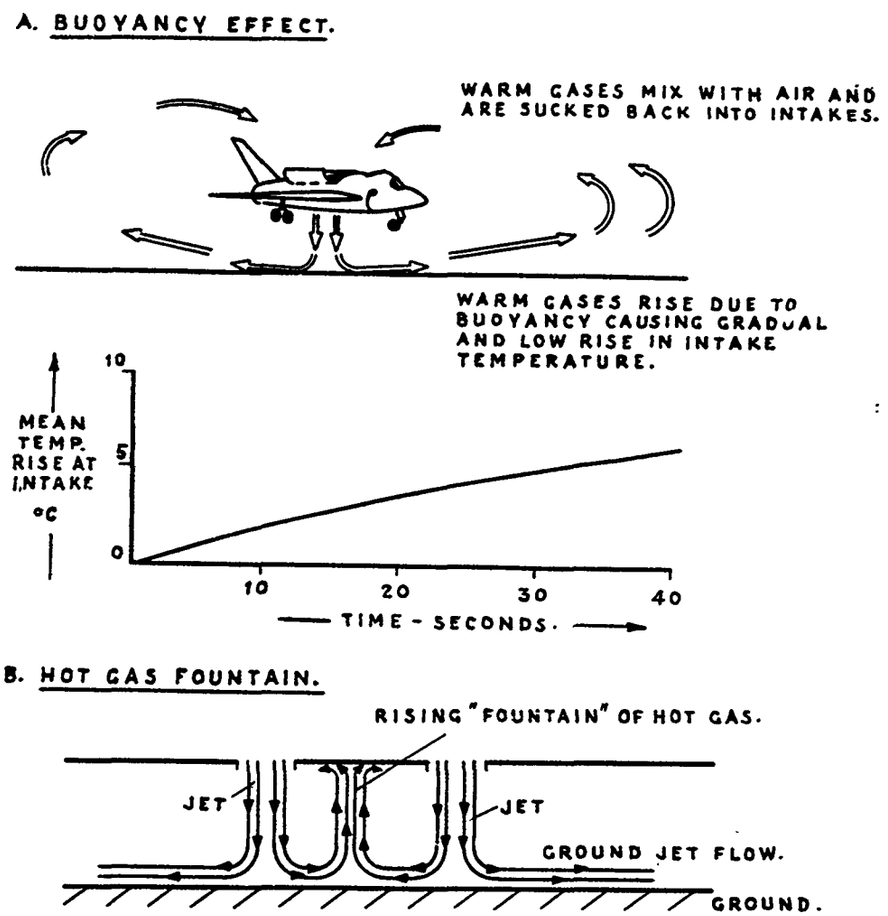

FIG.9 HOT GAS RE-INGESTION EFFECTS

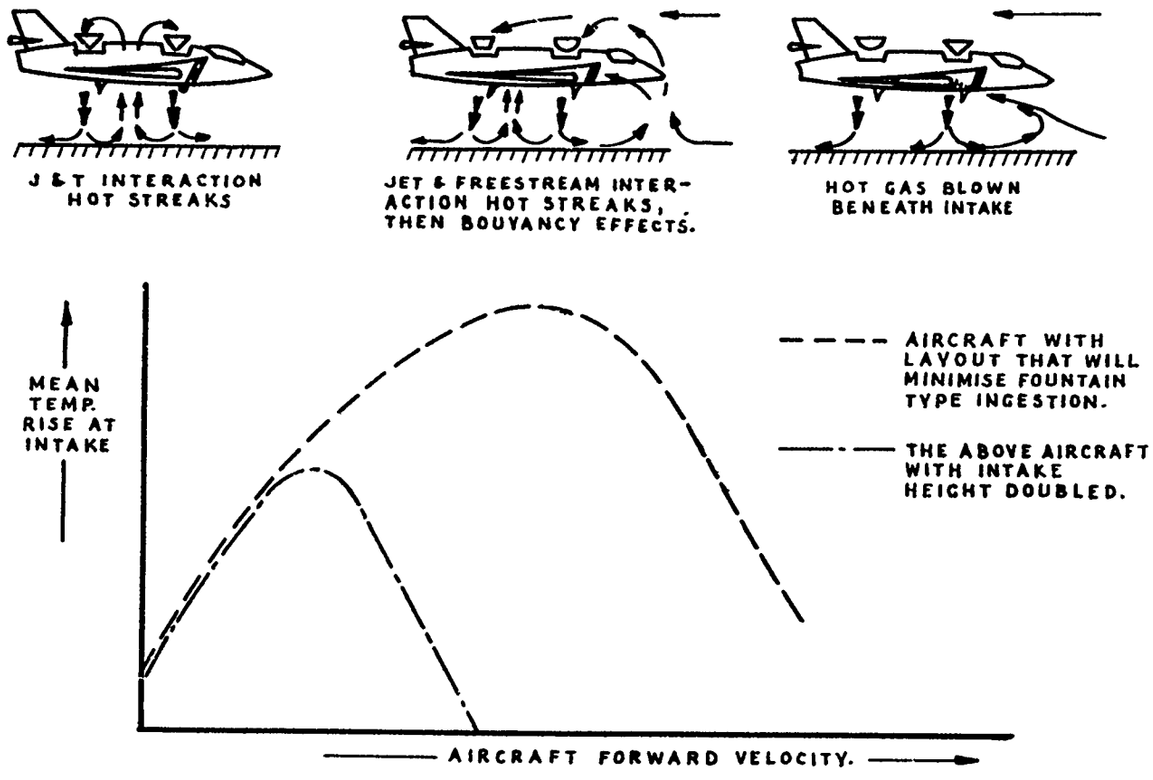

FIG.10 EFFECT OF FORWARD SPEED ON REINGESTION

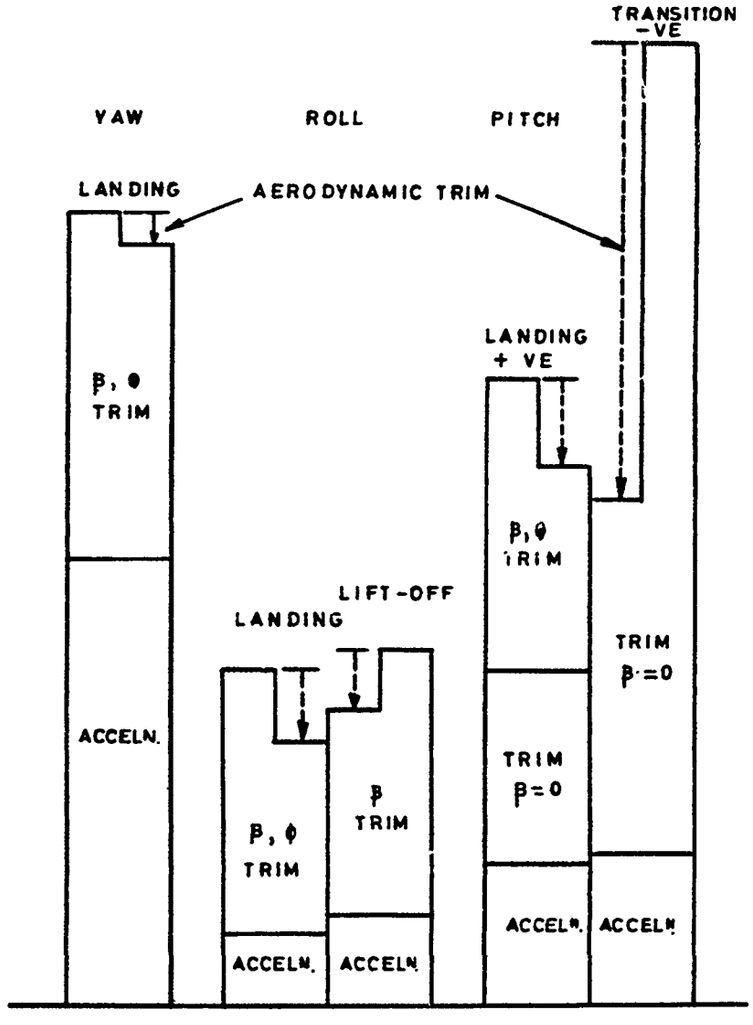

FIG. 11 REACTION CONTROL REQUIREMENTS

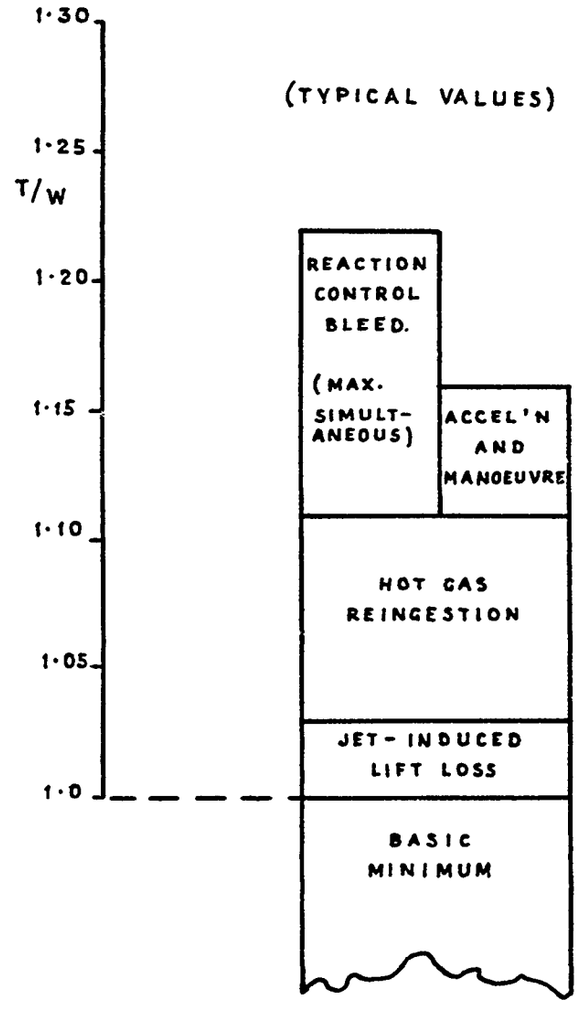

FIG. 12 THRUST-WEIGHT RATIO REQUIRED FOR V.T.O.L

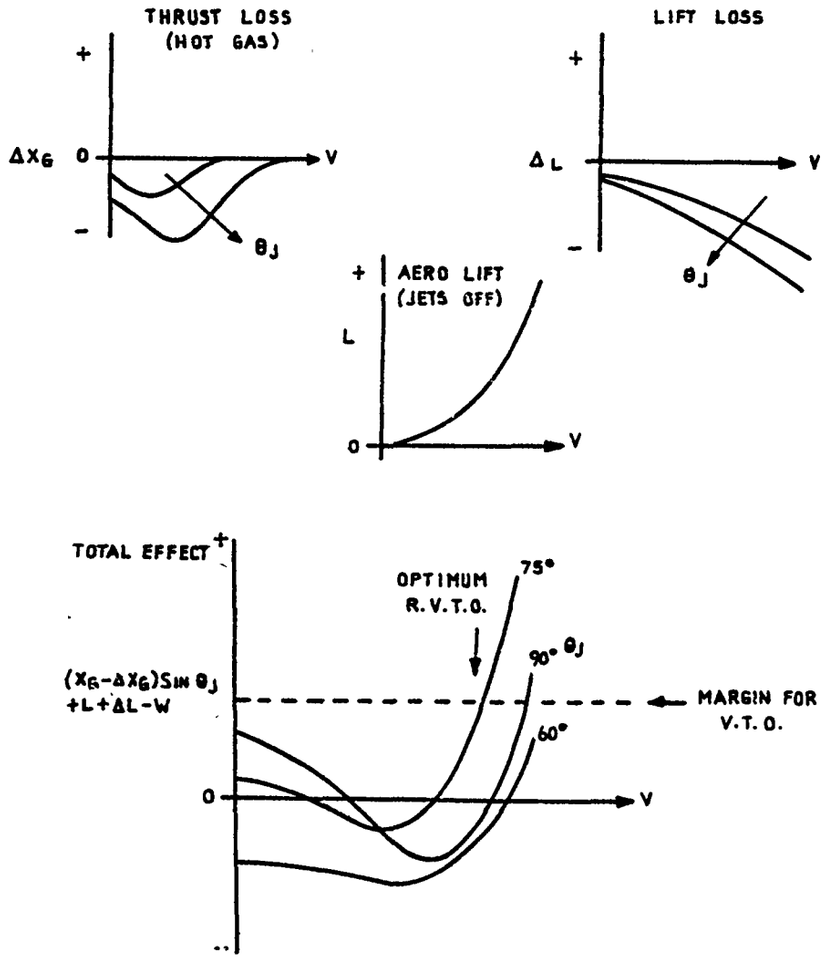

FIG. 13 ROLLING VERTICAL TAKE OFF EFFECTS OF FORWARD SPEED

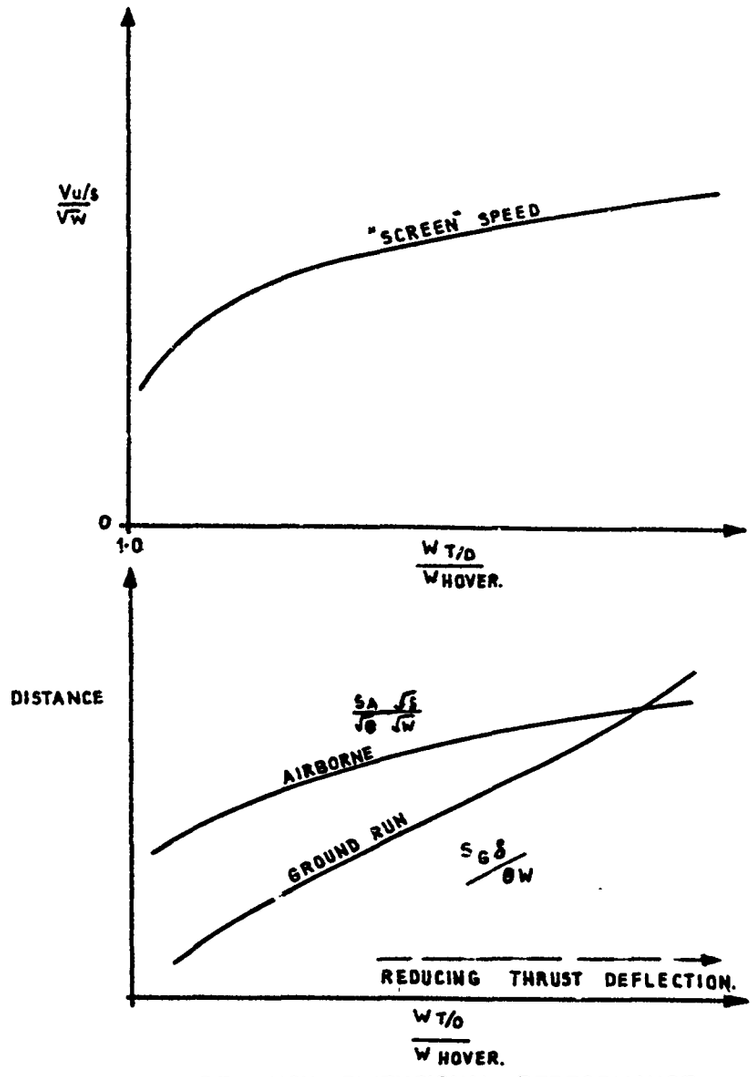

FIG. 14 S.T.O. NON-DIMENSIONAL PERFORMANCE SPEED AND DISTANCE

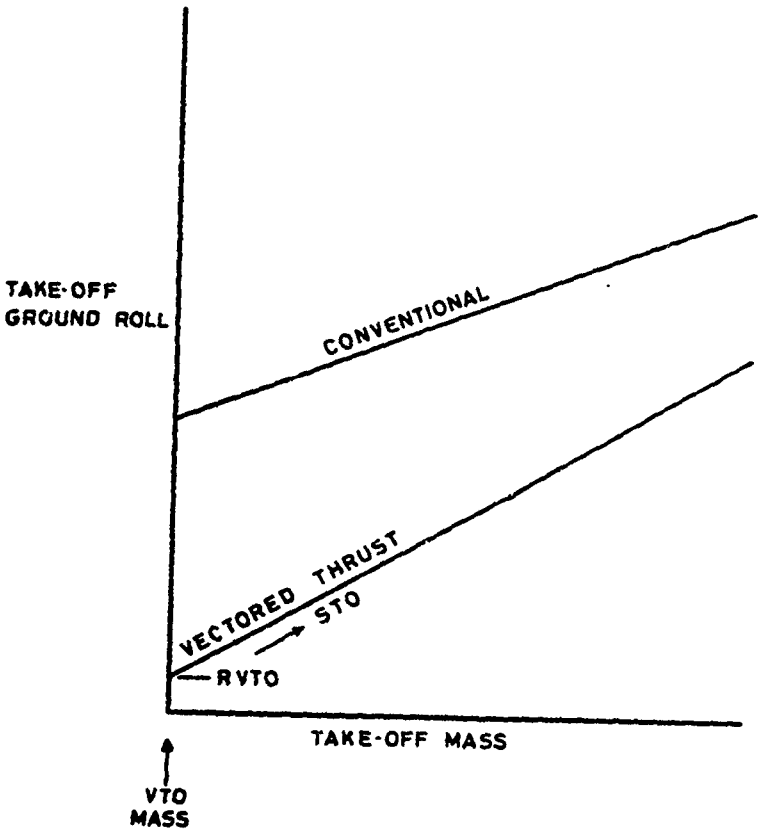

FIG. 15 DEFLECTED THRUST TAKE-OFF

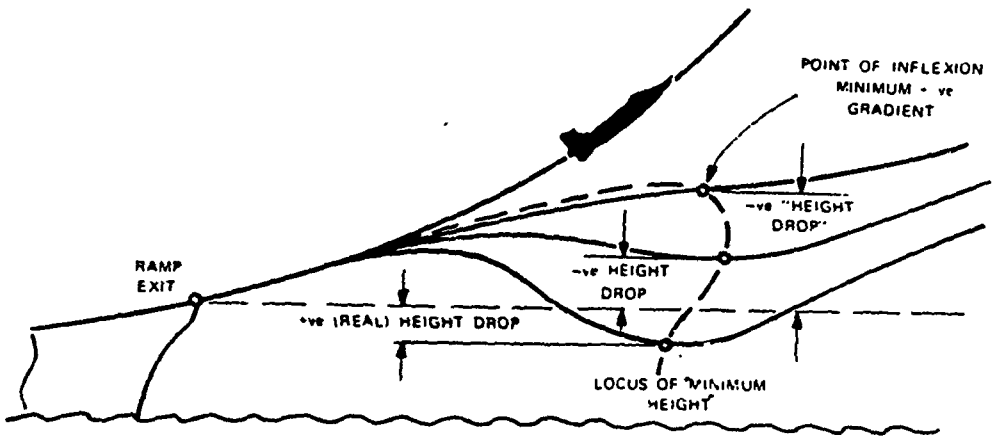

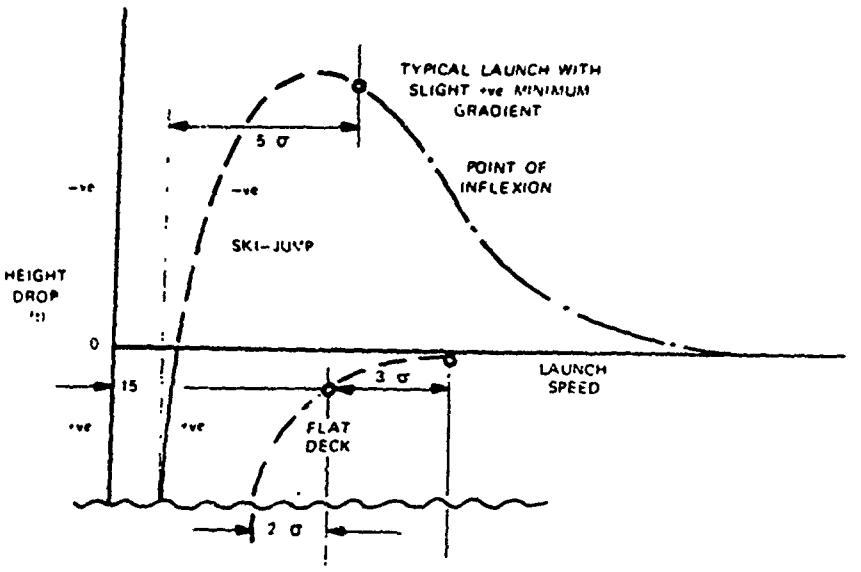

FIG. 16 DEFINITION OF HEIGHT DROP AND LAUNCH SPEED MARGINS FOR SKI-JUMP

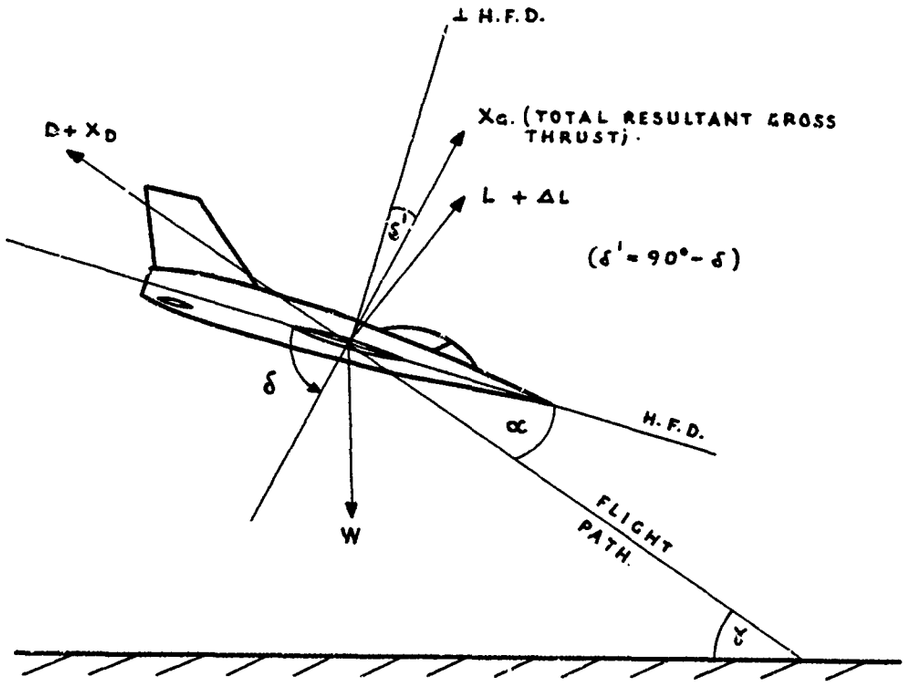

FIG.17 VECTORED THRUST APPROACH

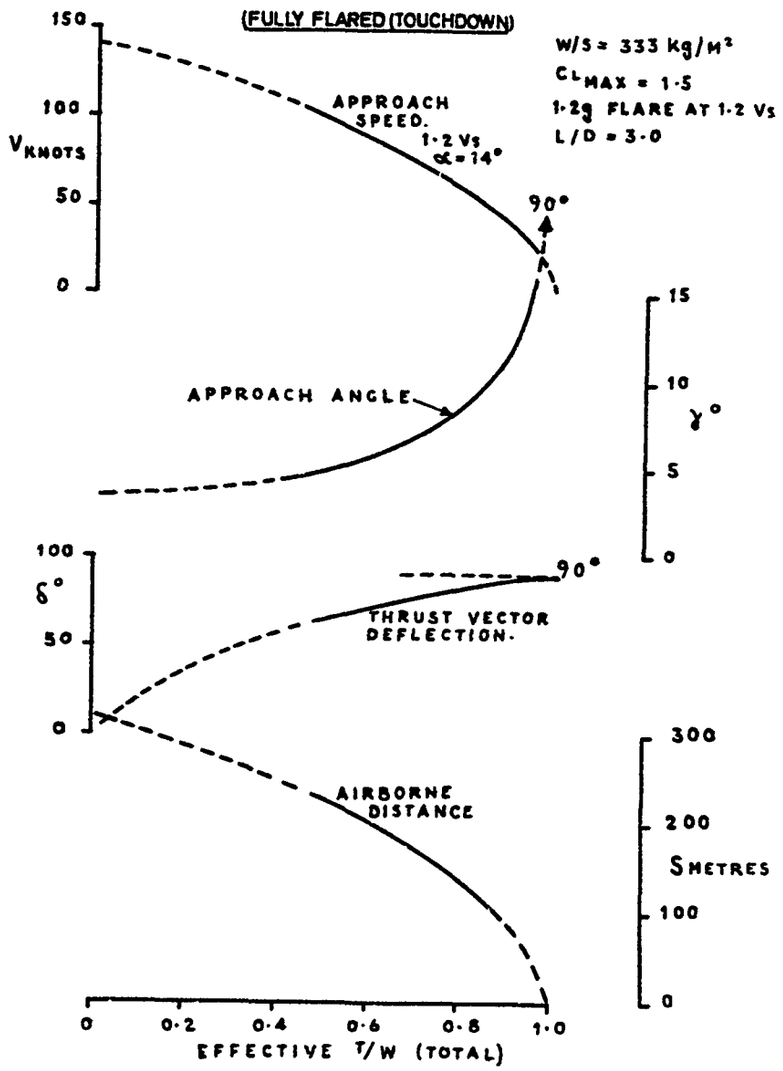

FIG.18 EFFECT OF VECTORED THRUST ON LANDING AIRBORNE DISTANCE FROM 15m

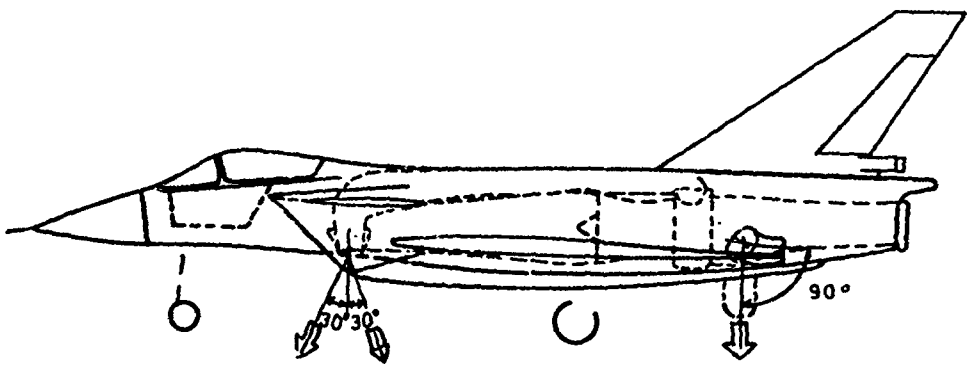

FIG. 19 REMOTELY AUGMENTED LIFT SYSTEM (RALS)

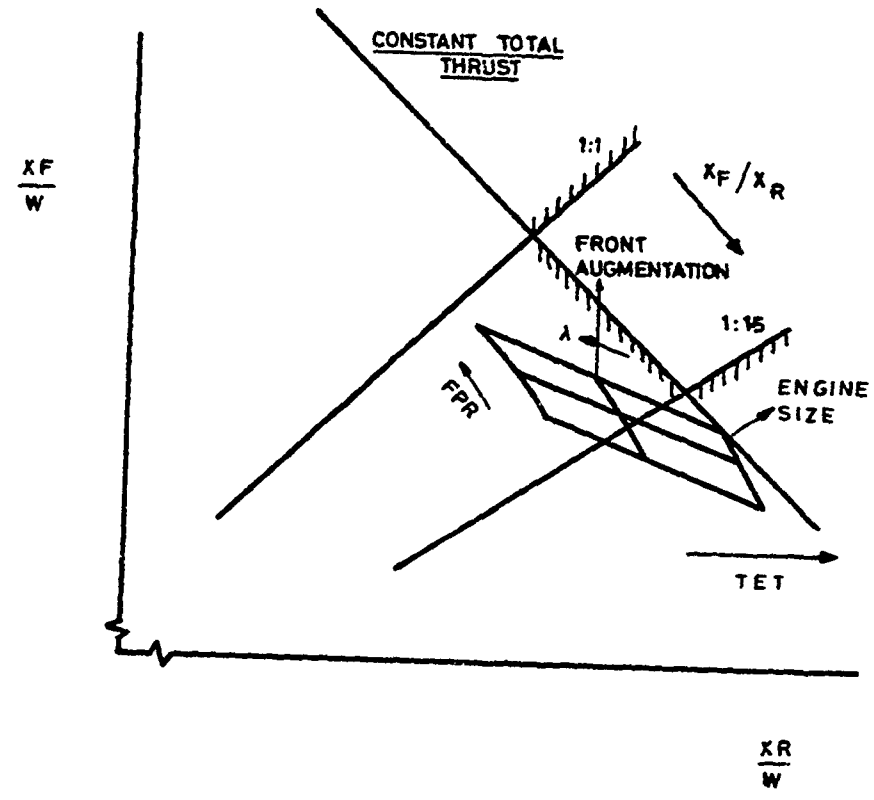

FIG. 20 BALANCE CHARACTERISTICS

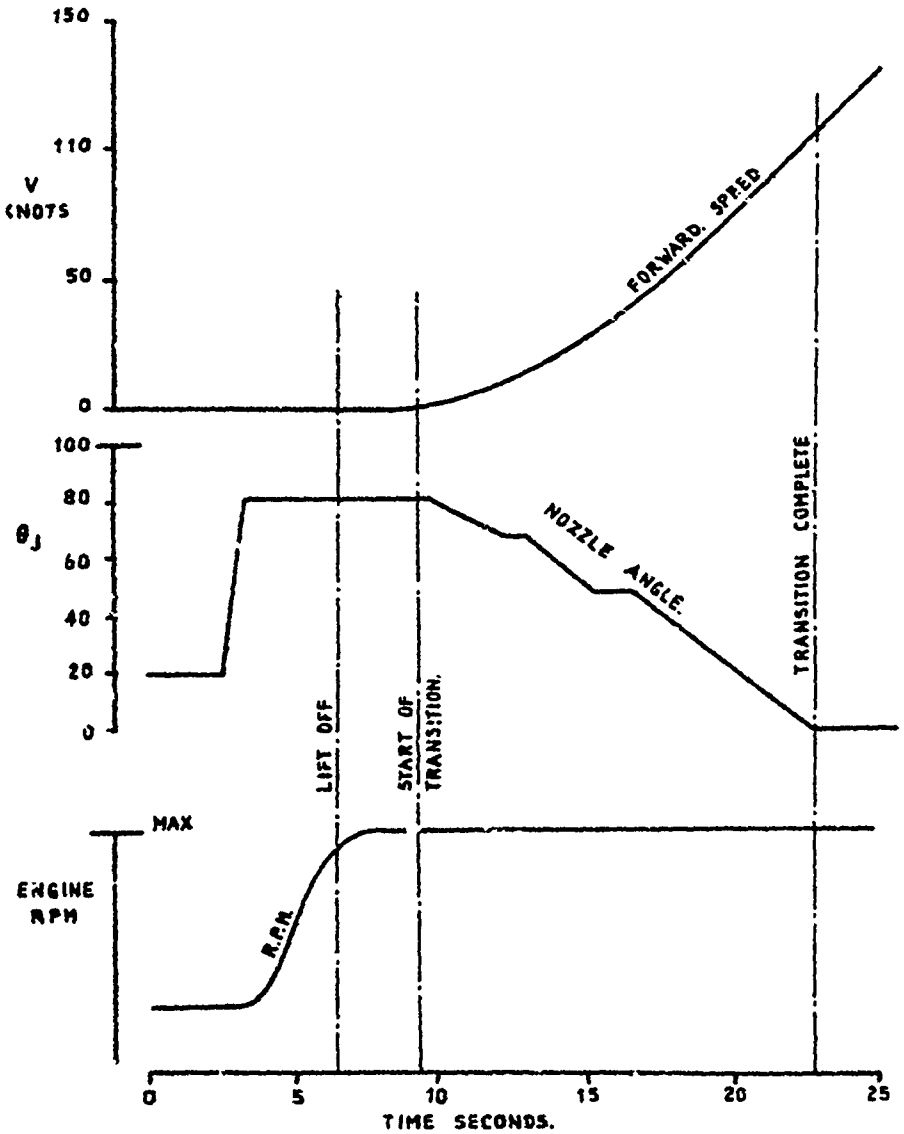

FIG. 21 ACCELERATING TRANSITION AFTER V.T.O. (KESTREL)

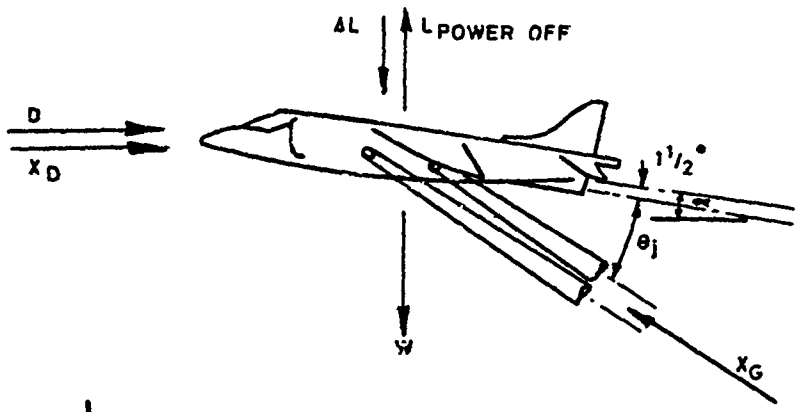

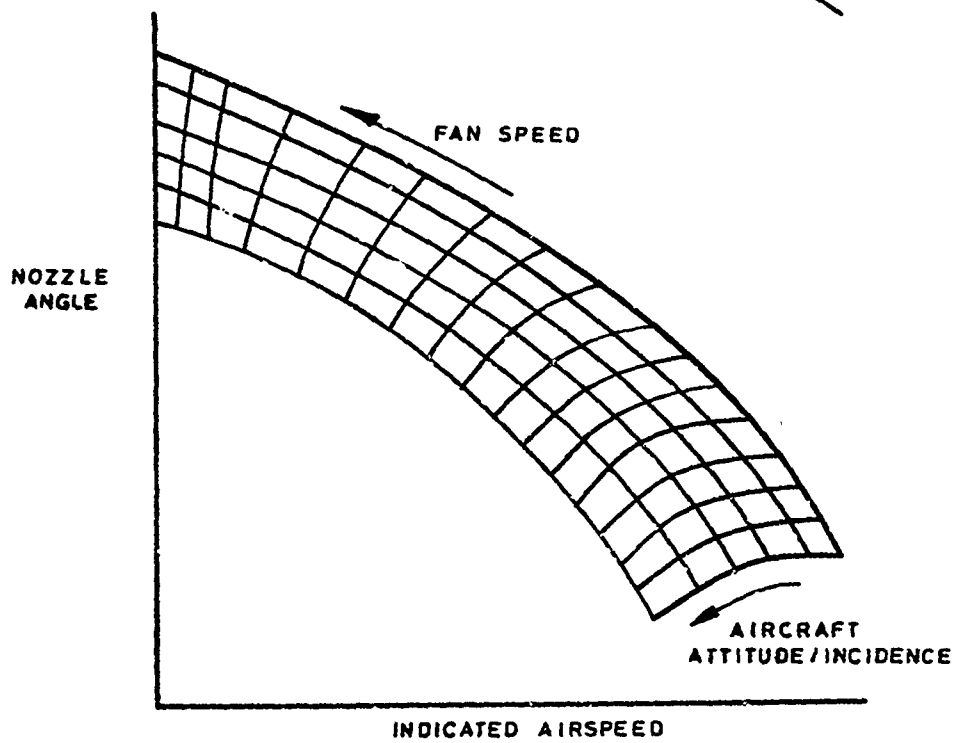

FIG. 22 SEMI - JETBORNE CARPET

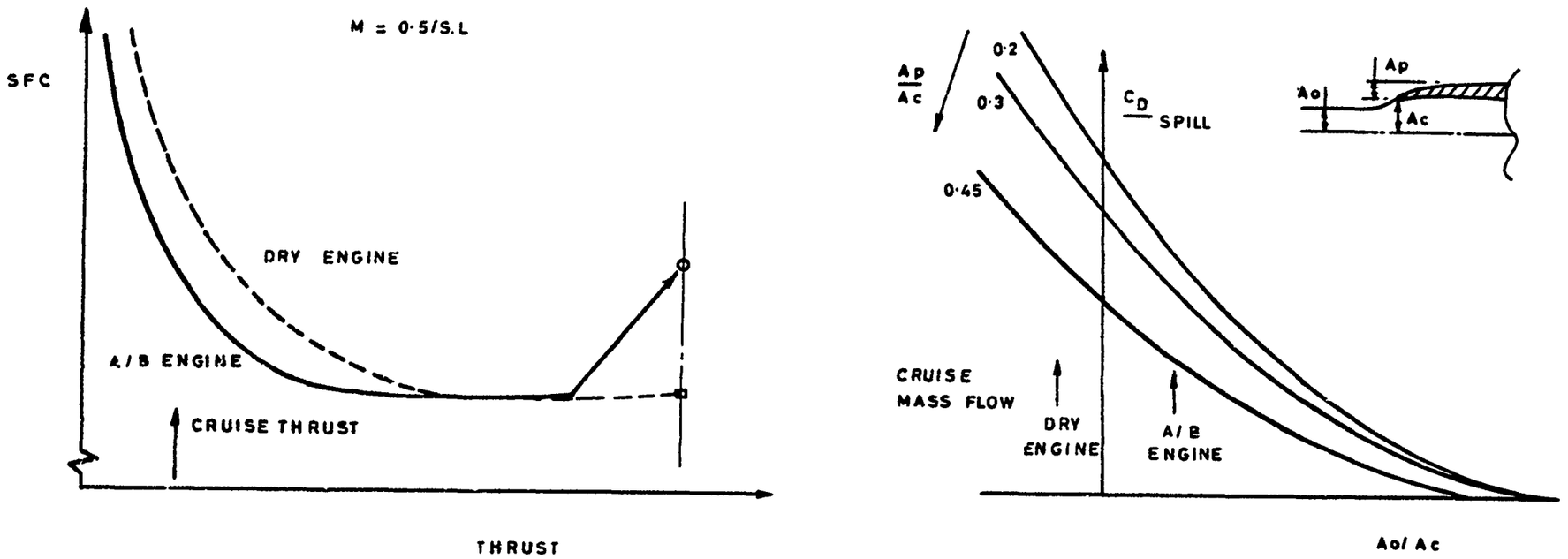

FIG. 23 EFFECT OF ENGINE SCALE ON CRUISE

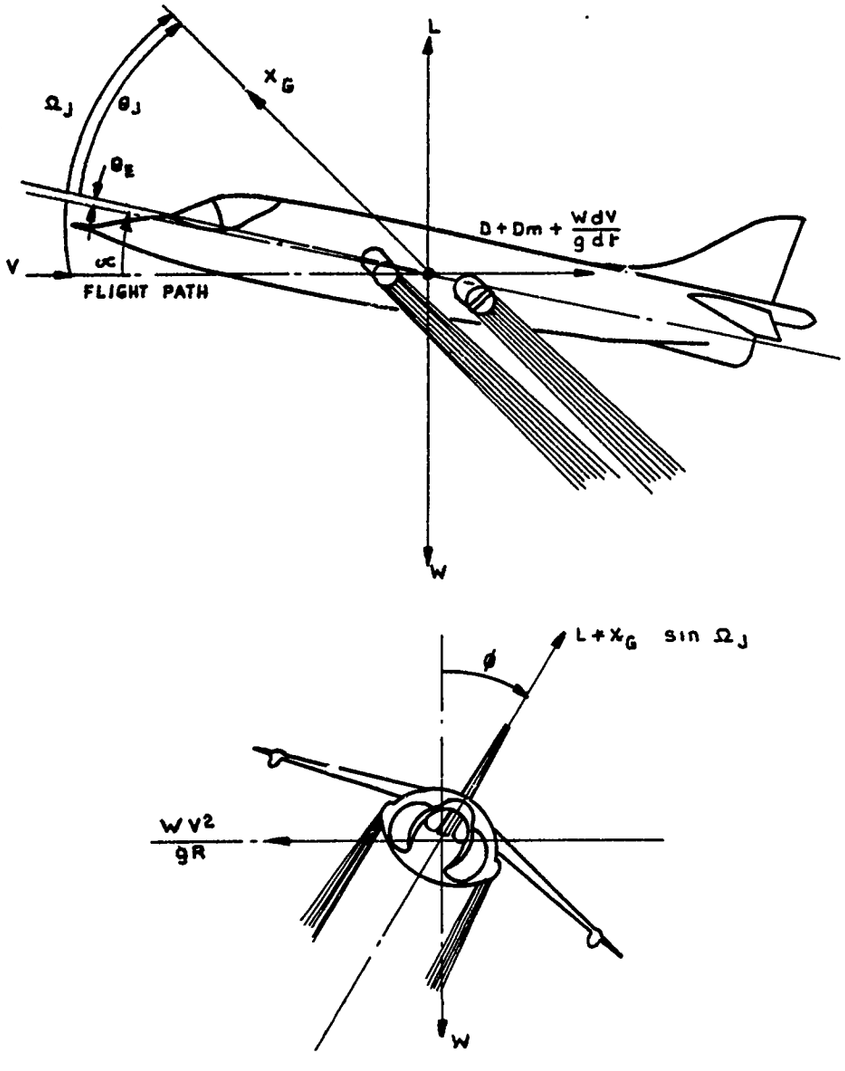

FIG. 24 TURNING TRACK FORCE DIAGRAM

LEVEL FLIGHT DECELERATING TURNS.

——— VECTORED THRUST AIRCRAFT (NOZZLES DOWN, MAXIMUM THRUST)

- - - - - CONVENTIONAL AIRCRAFT (WITH REHEAT)

— — — CONVENTIONAL AIRCRAFT (IDLING, WITH AIRBRAKE)

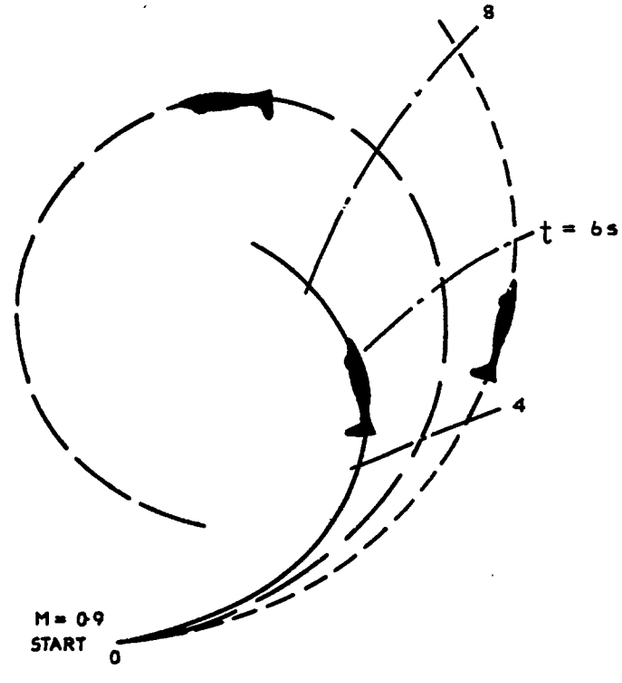

FIG. 25 TURNING TRACK PERFORMANCE

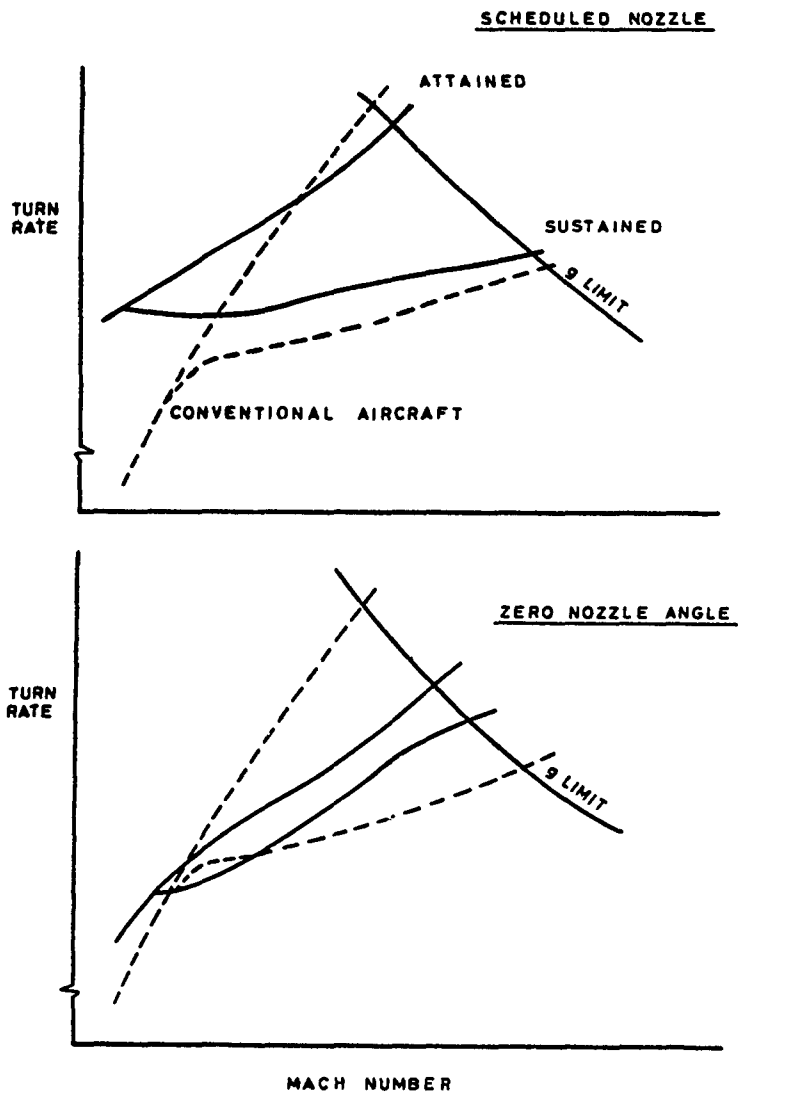

FIG. 26 COMBAT CHARACTERISTICS
THRUST VECTORING VERSUS CONVENTIONAL AIRCRAFT

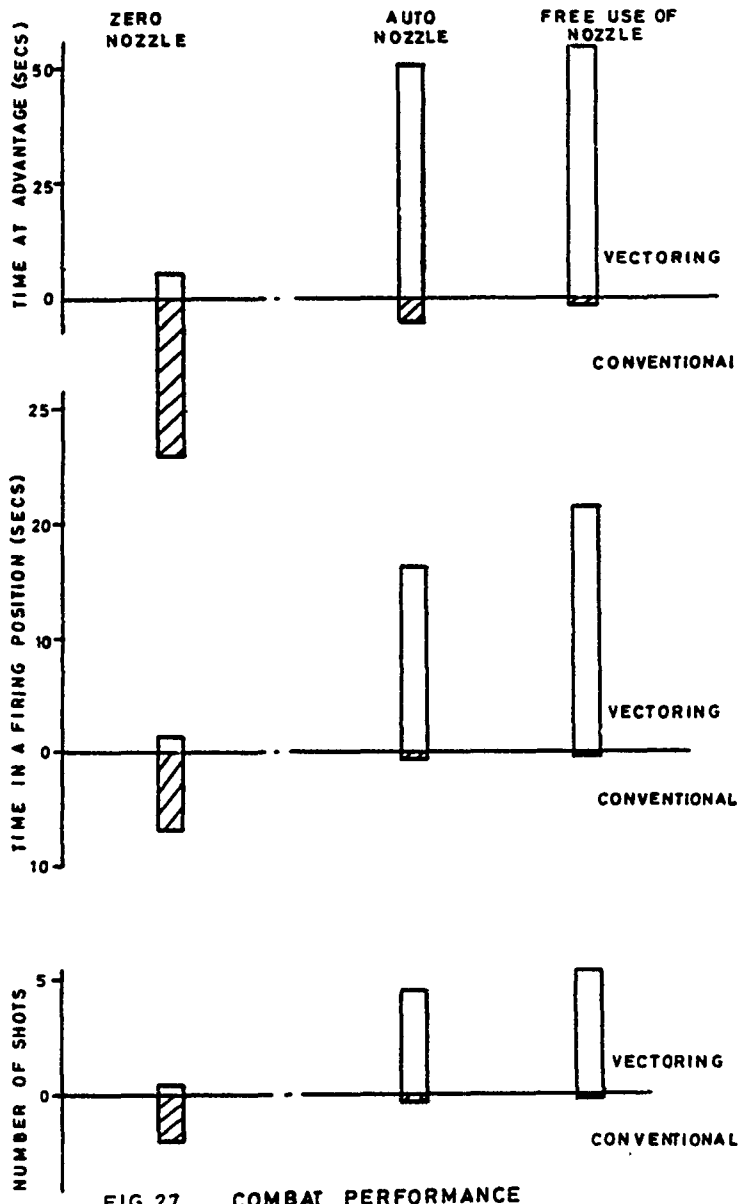

FIG.27 COMBAT PERFORMANCE
THRUST VECTORING Vs CONVENTIONAL

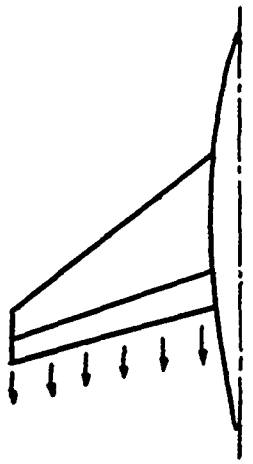

CONVENTIONAL FULL-SPAN BLOWN FLAP.

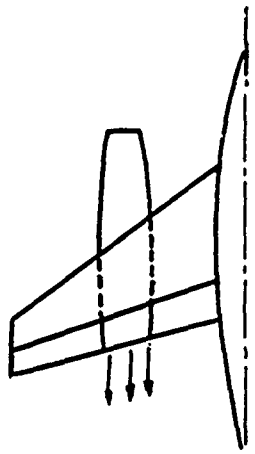

2. ENGINE NACELLE ON WING WITH JET EMERGING AT TRAILING EDGE

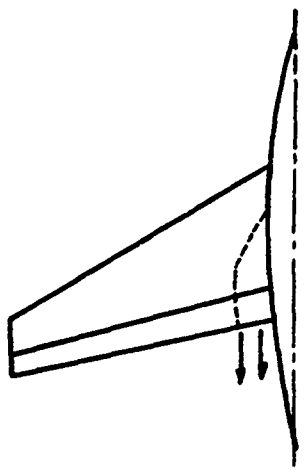

3. ENGINE EXHAUST DUCTED TO WING ROOT T/E

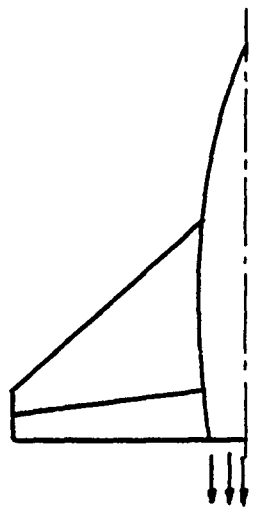

4. REAR ENGINE MOUNTING WITH WING T/E AND NOZZLE EXIT COINCIDENT.

FIG. 28

POSSIBLE CONFIGURATIONS TO TAKE BENEFIT OF BENEFICIAL JET-WING INTERACTION

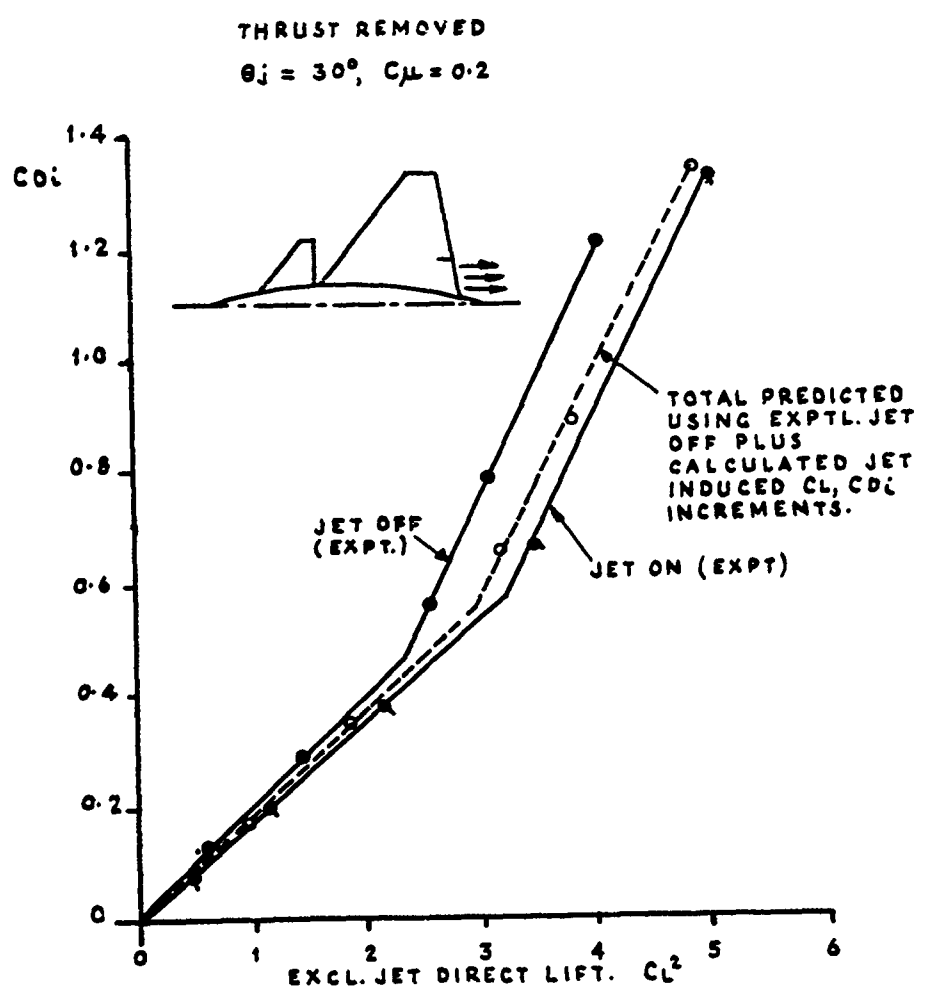

FIG. 29

COMPARISON OF PREDICTED AND MEASURED JET-INDUCED EFFECTS ON INDUCED DRAG POLAR

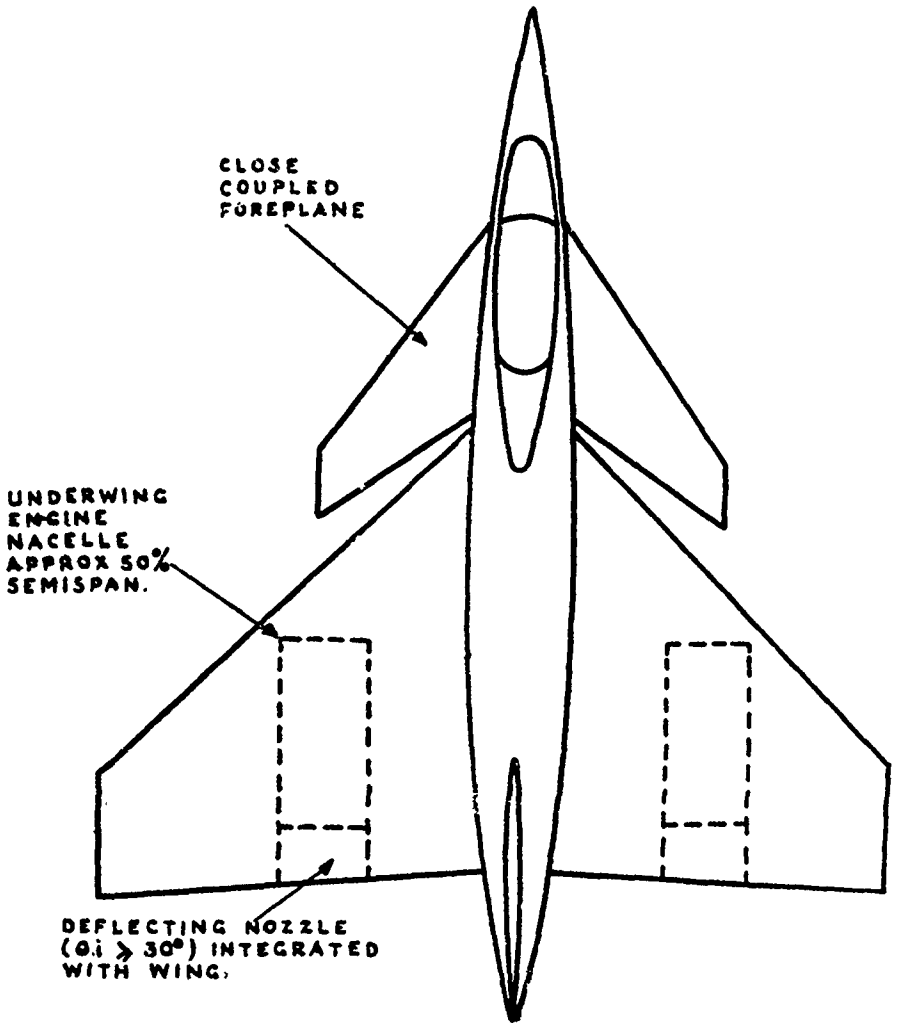

FIG. 30 CANARD CONFIGURATION FOR JET WING INTERACTION STUDIES

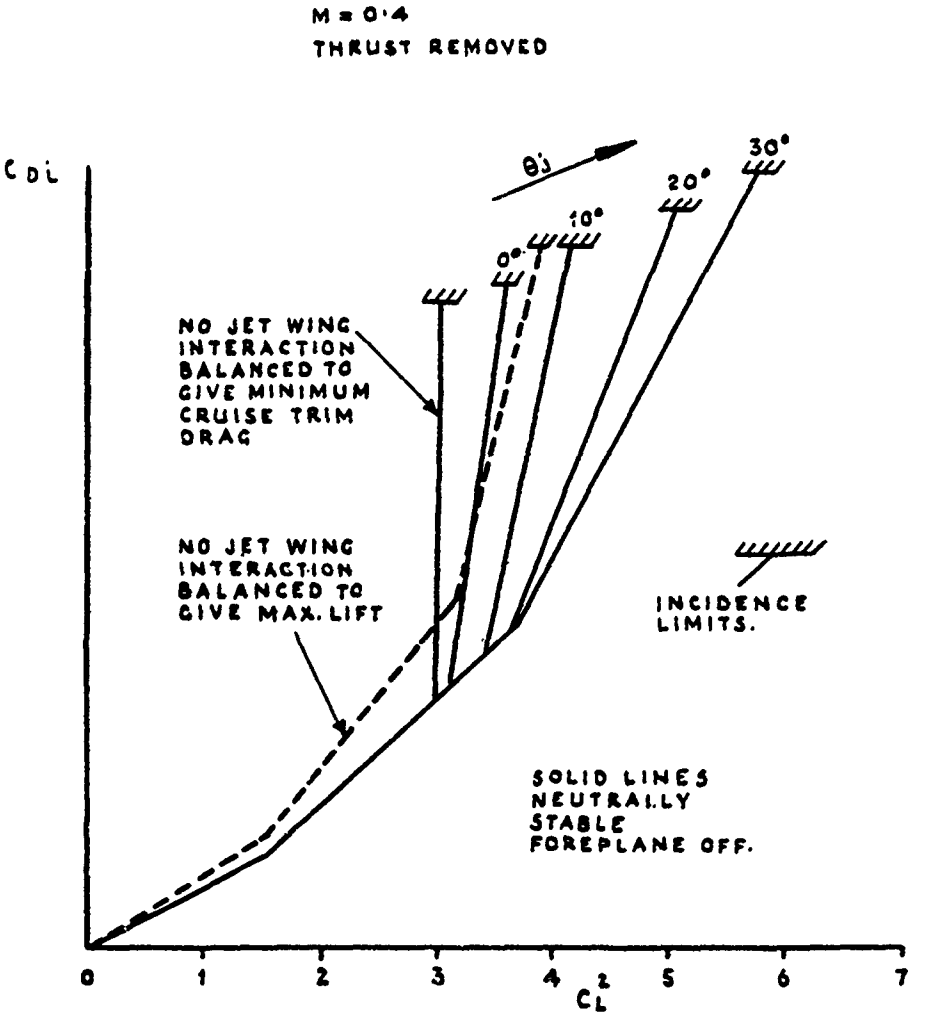

FIG. 31 PREDICTED TRIMMED INDUCED DRAG POLARS FOR CANARD CONFIGURATION WITH JET ENHANCEMENT

1. INCREMENTAL INDUCED EFFECTS ON WING

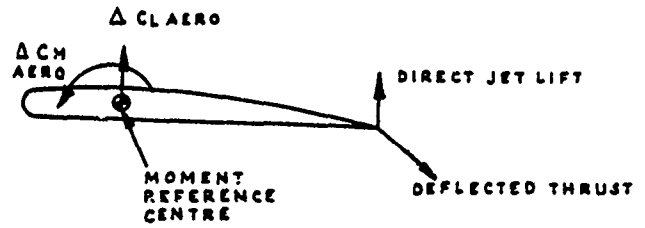

2. CONVENTIONAL AIRCRAFT REQUIREMENTS TO TRIM JET INDUCED EFFECTS

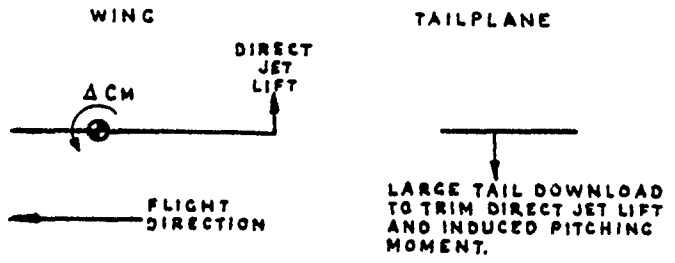

3. CANARD AIRCRAFT REQUIREMENTS TO TRIM JET INDUCED EFFECTS

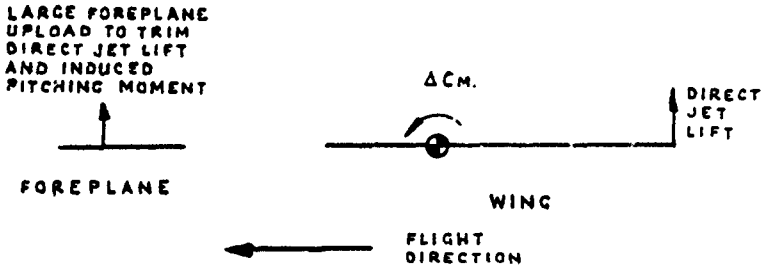

FIG. 32 TRIM CONSIDERATIONS WITH JET INDUCED EFFECTS

M = 0·4

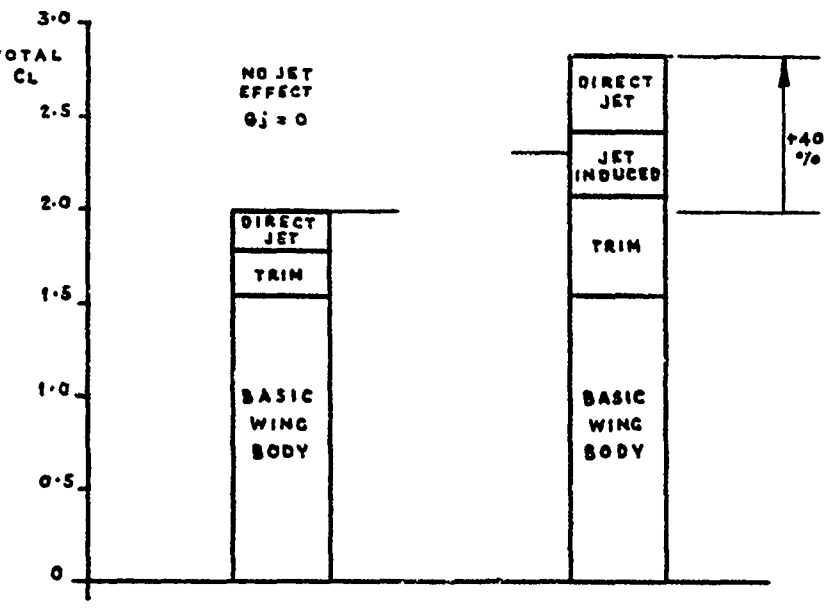

FIG. 33 BREAKDOWN OF EFFECT ON TOTAL LIFT OF JET WING INTERFERENCE

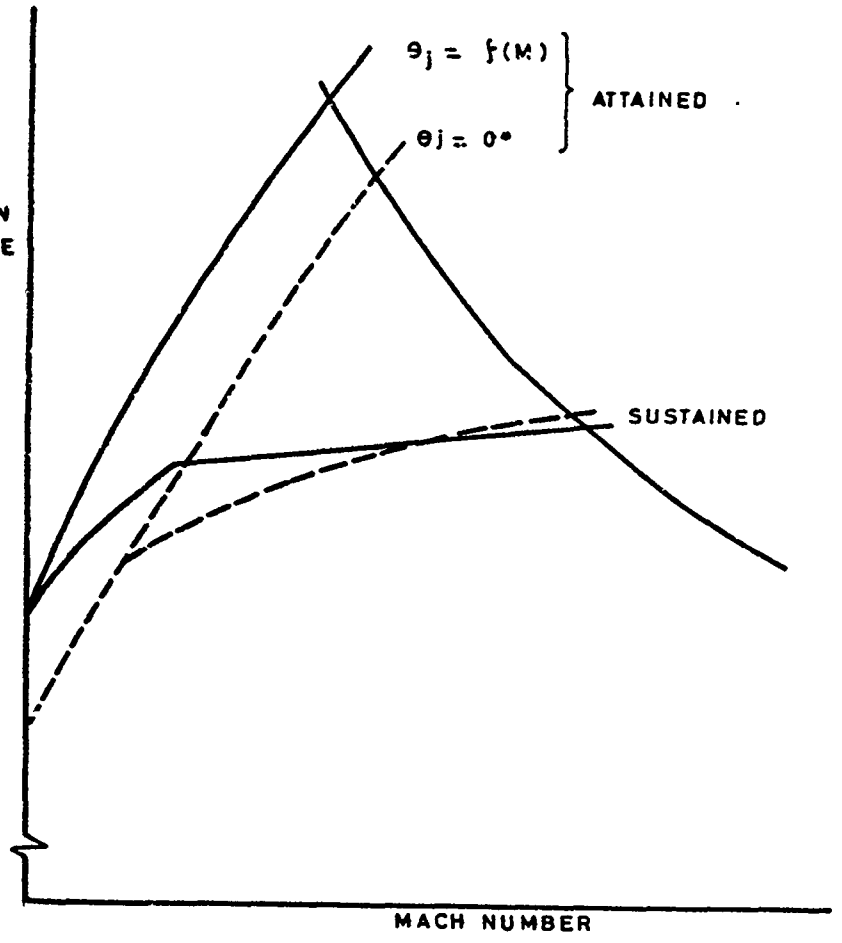

FIG. 34 EFFECT OF THRUST DEFLECTION WITH LIFT ENHANCEMENT ON COMBAT CHARACTERISTIC

$$C.C.P = S.E.P.^i \times S.T.R.^j \times A.T.R^k$$

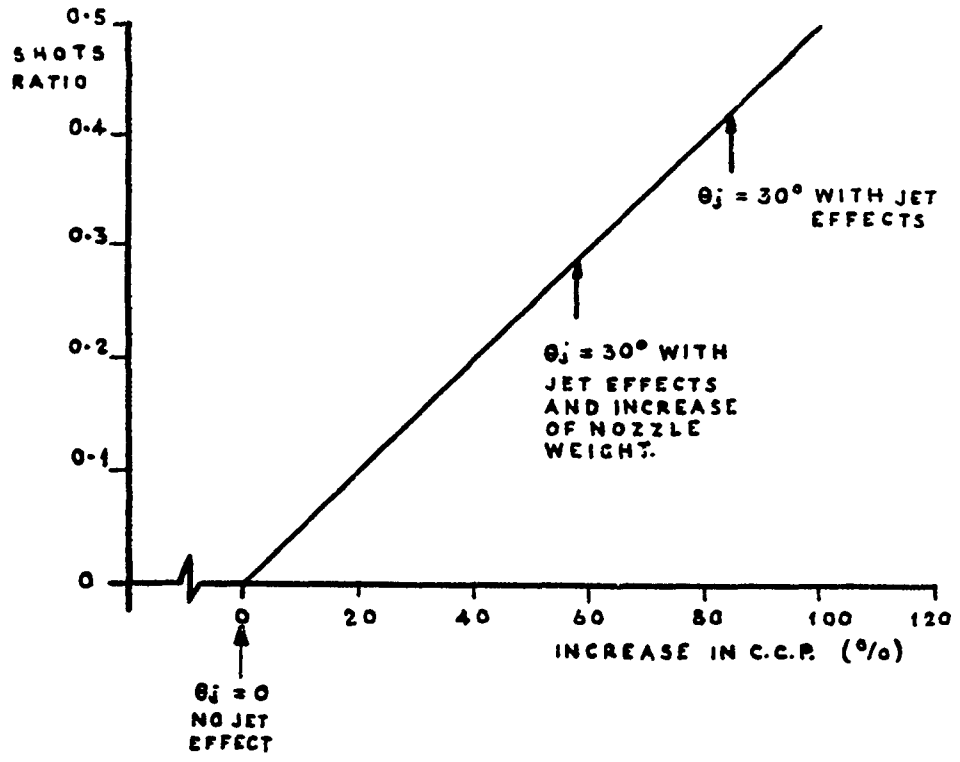

FIG. 35 PREDICTED EFFECT OF JET ENHANCEMENT ON COMBAT CORRELATION PARAMETER

ASSESSMENT OF AERODYNAMIC PERFORMANCE OF V/STOL AND STOVL FIGHTER AIRCRAFT

W. P. Nelms
NASA Ames Research Center, Moffett Field, California 94035, U.S.A.

SUMMARY

A summary of the research efforts in the United States to assess the aerodynamic performance of V/STOL and STOVL fighter/attack aircraft is presented. Emphasis will be on research programs at NASA Ames Research Center conducted jointly with the Department of Defense and Industry. Both small- and large-scale research programs are considered when aerodynamic and propulsion/airframe integration activities are discussed. The impact on aerodynamic performance of special configuration features that are related to the V/STOL requirement will be addressed.

1. INTRODUCTION

The Navy's desire for increased force dispersal and the possibility of runway denial that confronts the Air Force may dictate the need for V/STOL or STOVL aircraft in the future. Research is now underway in the United States to ensure the readiness of technology for development of this type of aircraft by the late 1990s. The focal point of this research is Ames Research Center, the NASA lead center for powered-lift aircraft. For this reason, this paper emphasizes V/STOL activities at Ames which are conducted jointly with the Department of Defense (DOD) and the Industry.

In particular, aerodynamic performance and propulsion/airframe integration for V/STOL and STOVL fighter aircraft will be addressed. This will include the impact on aerodynamic performance of special configuration features that are related to the V/STOL requirement. The important issues of propulsion systems, handling qualities and control, and ground effects are addressed in other lectures in this series and will not be covered here.

The paper will begin with a brief description of the V/STOL fighter configurations (Ref. 1) which are used in the research programs. Both twin and single engine concepts are considered. For convenience, the presentation will be divided into two parts, beginning with small-scale research programs and concluding with large-scale programs. Subjects that will be discussed in the small-scale area include configuration aerodynamics and propulsion/airframe integration. This latter topic includes in-flight thrust vectoring, top inlet studies, and propulsion simulation in wind-tunnel tests. Large-scale research items addressed are a large-scale twin engine fighter model, high angle-of-attack studies, and thrust augmenting ejector research.

2. V/STOL FIGHTER CONCEPTS

A number of V/STOL and STOVL fighter/attack aircraft concepts have been studied as part of a joint NASA Ames/Navy/Industry research program. These concepts have been described in a previous lecture (Ref. 1) which includes both twin and single engine configurations. Several small- and large-scale wind-tunnel models of these aircraft concepts have been fabricated and used in the research programs to assess aerodynamic performance. These models are representative of the actual aircraft defined in detailed systems studies and therefore go beyond "generic research models," since many of the uncertainties are configuration dependent. The objective is to develop an aerodynamic data base on a number of promising concepts and to ensure the readiness of technology for development of this type of aircraft. The following paragraphs give a brief review of the twin and single engine aircraft concepts.

The twin-engine concepts are shown in Fig. 1 and are described in Ref. 1. Additional information on these concepts is given in Refs. 2-7. A design (Refs. 1-3) by General Dynamics (E205) is shown at upper left in Fig. 1. Lift augmenting ejectors of the short-diffuser type (Alperin) are used for propulsive lift. These are located in four bays that are inboard of the engine nacelles. The design also features a vectored engine over the wing (VEO) lift improvement concept, strakes inboard of the nacelles, a canard, and a single vertical tail. At the upper right of Fig. 1, a design by Grumman is illustrated (Refs. 1, 2, and 4). This concept features a General Electric Remote Augmented Lift System (RALS) for propulsive lift (Ref. 1). Two aft-mounted General Electric Augmented Deflector Exhaust Nozzles (ADEN) (Ref. 1) at the wing trailing edge and dual forward burner/nozzles compose this propulsive lift system. A concept by Northrop is shown at lower left (Refs. 1, 2, and 5). Northrop also uses a RALS with two aft ADEN nozzles and a single burner/forward nozzle. This concept features two large wing-mounted afterbodies to provide internal volume for fuel, avionics and landing gear stowage, and to provide a mounting for the twin vertical tails. The additional internal volume is needed because of space requirements of the propulsive lift system.

The three concepts described are horizontal attitude takeoff and landing (HATOL) aircraft. The next two use a vertical attitude takeoff and landing (VATOL) scheme, or commonly referred to as "tail sitters." The lower center concept shown in Fig. 1 is another design by Northrop (Refs. 1, 2, and 6). Two turbojet engines with swiveling nozzles are used for propulsive lift while the aircraft is in the vertical attitude. This is a tailless design with wing leading edge extensions (LEX) and a top-mounted inlet system. The final concept at lower right of Fig. 1 is a configuration by Vought (Refs. 1, 2, and 7). Again, swiveling nozzles are used for vertical flight. Vought has used a side-mounted inlet design with canards. It should be noted that both VATOL concepts also have conventional/short takeoff and landing capability as depicted by the Vought design with an overload of stores.

The single engine concepts studied in Phase I of the joint Ames/Navy/Industry program are shown in Fig. 2. These were discussed in the previous lecture (Ref. 1) and are described in detail in Refs. 8-13. A design by General Dynamics (E7) is shown at upper left (Refs. 1, 8-10). Two thrust augmenting ejectors located longitudinally on each side of the fuselage in the wing root area provide the forward lift while a deflecting two-dimensional nozzle located on the underside of the fuselage provides the aft lift. The engine fan flow feeds the ejectors and the engine core flow is exited through the deflecting nozzle while in vertical flight. For forward flight, the ejectors are shut down and the fan flow exits through the aft axisymmetric nozzle. The core flow continues to be exhausted through the two-dimensional nozzle. This concept is a tailless design

that has the F16 forward fuselage and vertical tail. A design by Rockwell (Refs. 1, 8, and 11) is shown at the upper right of Fig. 2. This concept features spanwise-lift augmenting ejectors both forward and aft on the wing for propulsive lift. An alternate design has a forward ejector system that is rotated to a chordwise position. Both designs are tailless configurations with top-mounted inlet systems.

A "four-poster" concept developed by McDonnell Douglas is shown at the lower left of Fig. 2 (Refs. 1, 8, and 12). This concept uses a deflected thrust propulsive lift system with fan stream burning and it includes features such as side-mounted inlets and a canard. Finally, a concept developed by Vought is shown at lower right of Fig. 2 (Refs. 1, 8, and 13). A tandem fan propulsion system is used to provide propulsive lift in this highly integrated wing-canard design. This concept features a high degree of wing/body blending and the use of multiple control surfaces including forward ventral surfaces with two-axes of travel.

3. SMALL-SCALE RESEARCH

Research activities involving the use of small-scale models in both low- and high-speed wind tunnels is described. Generally, small-scale testing is conducted first to sort out any major configuration problems before large-scale models are constructed. Small-scale model research addresses two subjects that are closely related — configuration aerodynamics and airframe/propulsion integration.

3.1 Configuration Aerodynamics

The uncertainties that affect aerodynamic performance for the previously mentioned V/STOL fighter concepts will be described. The uncertainties associated with configuration characteristics driven by propulsive lift requirements will be emphasized. Next, the wind-tunnel models and tests will be described and then example results will be given.

3.1.1 Aerodynamic Uncertainties

In any new aircraft system, there are uncertainties in such discipline areas as propulsion, aerodynamics, structures, and avionics. For example, experience indicates that in the early phases of development, V/STOL aircraft are likely to exhibit stability, control, and flying-quality uncertainties in the takeoff/landing, hover, and transitional modes of flight. Ground effects such as suckdown and recirculation are important areas of concern. Operating from small, heaving ships in poor weather conditions will most assuredly present problems. There are uncertainties that relate to new propulsive lift concepts that must be explored. In other words, research is needed in many of the technical areas that are related to V/STOL aircraft development; however, the emphasis here is on identification of the uncertainties in aerodynamics. In particular, aerodynamic performance in the up-and-away flight mode will be emphasized in the section on configuration aerodynamics.

Therefore, a number of uncertainties that affect aerodynamic performance have been identified for each of the twin and single engine V/STOL fighter concepts in the joint Ames/Navy/Industry research program. These are briefly summarized in Figs. 3 through 11 for each of the concepts. Obviously there are many uncertainties that are common to all concepts and there are some that apply not only to V/STOL, but to CTOL aircraft as well. Those uncertainties that are uniquely associated with the V/STOL requirement are highlighted here.

General Dynamics. The General Dynamics' twin engine design is dictated by the incorporation of thrust augmenting ejectors for propulsive lift in the thick regions inboard of the nacelles. This results in an unusual wide-body type of configuration that is totally different from existing aircraft. The minimum drag, and particularly the supersonic wave drag, is of concern because of the large volumes required for the vertical lift system (Fig. 3). In other words, is this a reasonable transonic/supersonic fighter configuration and can the drag levels be predicted for this wide-body concept using existing methods?

Integration of the forward ejector bays, the outboard nacelles, and the canards results in a conceptual design that has a large amount of planform area that is located well forward on the aircraft. The question arises as to where the aerodynamic center is located for this type of configuration and its travel with Mach number. Can the design be configured with subsonic instability that is acceptable for a post-1995 fighter aircraft? Also, can existing techniques adequately predict the aerodynamic center location for this type of wide-body design?

For a maneuvering fighter aircraft, the maximum usable lift and the onset of wing buffeting are important considerations; both are uncertain for this type of configuration. The lateral-directional characteristics are uncertain for this unique wide-body concept since both the experimental data and the adequate prediction methods are lacking.

Grumman. In the Grumman RALS twin engine design we see a similar concern for minimum drag and, in particular, transonic wave drag that is associated with the added volume that is required by the propulsive lift system (Fig. 4). Again, there is an uncertainty of the aerodynamic performance that is associated with the unusual wide-body configuration.

Northrop (HATOL). The Northrop RALS twin engine design also shares the minimum drag and transonic wave drag uncertainties that are associated with the added propulsive lift system volume (Fig. 5). In this configuration, Northrop has attempted to gain back internal volume that is lost to the propulsive lift system by adding wing-mounted afterbodies. However, it is not clear whether these relatively large-volume bodies can be integrated into a reasonable transonic fighter configuration without undue drag penalties. If they can, this offers the designer many desirable options. Finally in the Northrop concept, the concern of the canard/wing interactions is evident; this applies to the prior two concepts as well. There are two reasons the canard is used on these propulsive lift concepts: one is to trim out the aft-deflected thrust with a positive-lift producing canard deflection; another is to improve the high angle-of-attack aerodynamic performance.

Northrop (VATOL). The Northrop twin-engine VATOL concept also has the concerns for transonic wave drag and aerodynamic center travel with Mach number (Fig. 6). In addition, this concept depends on the wing

leading-edge extension (LEX) for good high-angle-of-attack performance. The LEX affects the longitudinal aerodynamics, the vertical tail effectiveness, and the flow quality to the top-mounted inlet on this concept. Top-mounted inlets offer many advantages to V/STOL fighter aircraft. Reduced radar cross section and a clear undersurface for mounting stores and for easier mating to the arresting device, are advantages to this particular VATOL concept. A potential and significant advantage of top-mounted inlets to HATOL configurations is reduced ingestion of hot gases and debris during takeoff and landing. However, the effect of the airframe on this type of inlet system is of concern, particularly at the angles of attack for maneuvering.

Vought. Finally, the Vought twin-engine VATOL design exhibits many of the uncertainties already mentioned including minimum drag, wing/canard interactions, and buffet onset (Fig. 7).

Turning to the single engine concepts, a number of uncertainties that affect the aerodynamic performance of these aircraft have been identified in the joint Ames/Navy/Industry program.

General Dynamics. When the General Dynamics single engine design is considered, a number of the uncertainties that are a direct result of the requirements for propulsive lift are seen (see Fig. 8). There is a concern for minimum and transonic wave drag. Another concern is the large, forward fuselage vertical surface that forms the inboard ejector diffuser surface because of its effect on the lateral/directional stability of the configuration. This large, slab-sided area forward of the aircraft center of gravity is potentially destabilizing. Another concern is the limitation to the optimum wing design that is imposed by the necessity to incorporate the ejector lift system into the wing root area. Finally, the unique integration of the two-dimensional core nozzle with the underside of the fuselage creates an uncertainty in afterbody drag.

Rockwell. The successful incorporation of the spanwise-thrust augmenting ejector system into the wing is a major concern of the Rockwell single-engine concept (Fig. 9). The alternate configuration, in which the forward ejector is rotated 90°, may be a better design. In any event, the minimum drag of this concept is of concern because of the volume requirements of the propulsive-lift system. The top inlet uncertainties on this concept reaffirms the need for technology studies in these types of inlet systems. The uncertainty that is involved in the prediction of the aerodynamic performance of this design at high angle of attack applies to all of the concepts.

McDonnell Douglas. The deflected thrust propulsive lift concept used by McAir in their single engine V/STOL fighter design resulted in the use of a canard. This close-couple canard is responsible for some of the uncertainties (Fig. 10). The canard contribution to high angle-of-attack lateral/directional instability is a concern. Generally, close-coupled canards, especially with dihedral, tend to reduce directional stability which leads to a larger vertical tail. However, these effects are dependent on canard location and the location and type of vertical tail (single or twin tail). The reduction in longitudinal stability that is caused by the canard is a concern, but the addition of a horizontal tail could improve this situation. The three surface design is an option on this concept. Existing analytical and empirical techniques generally cannot be used to predict these canard effects accurately, because they are very configuration-dependent as a result of the aerodynamic interaction between the canard, the wing, and the other aircraft surfaces.

The deflected-thrust propulsive lift concept leads to other uncertainties, one of which includes the effect of large half-axisymmetric inlets on lateral/directional stability. Another uncertainty includes the nonlinearities in pitching moment characteristics that are caused by the forward location of the propulsion system. This engine location can also have an effect on the configuration drag. In fact, a major unknown on this concept is the subsonic and supersonic minimum drag. In addition, the propulsive flow effects on the aerodynamic performance of this design is an uncertainty, particularly at transonic speeds where the concern is the effect on drag. Also, the jet plume interference effect on the downstream aircraft surfaces is an unknown factor for this deflected-thrust concept.

Vought. The uncertainties of the Vought single engine, tandem fan design are outlined in Fig. 11. The aerodynamic performance of this concept is highly affected by the close-coupled canard in the wing plane, the highly swept strakes, and the high degree of wing/body blending. These characteristics combine to produce uncertainty in both the longitudinal and lateral/directional aerodynamics, particularly at the higher angles of attack. These same configuration features make available prediction methods questionable. Effectiveness of the multiple control surfaces on this design is uncertain, particularly the capability of the forward ventral surface with two-axes of travel in producing direct lift and direct side force. Finally, the minimum drag associated with the configuration volume for the tandem fan propulsion system is uncertain.

3.1.2 Wind Tunnel Models and Tests

Several of the contractors from Phase I of the joint NASA Ames/Navy/Industry research program were selected to fabricate wind-tunnel models in Phase II. These models are used to assess the aerodynamic performance and to investigate the aerodynamic uncertainties for the concepts from Phase I. Both twin- and single-engine models are included. These models are briefly described in this section together with a few comments about the wind-tunnel tests.

3.1.2.1 Twin-Engine Models

General Dynamics. In Phase II, General Dynamics built a wind-tunnel model to simulate the up-and-away flight configuration of their twin-engine design using thrust augmenting ejectors for propulsive lift (Configuration E205). This 9.4% scale model, which is sized for testing in the Ames Unitary and 12-Foot Wind Tunnels, is shown in Figs. 12 and 13. The model is built of high-strength steel to withstand the loads that are associated with high-angle-of-attack testing at transonic Mach numbers. It is a large model for testing at these speeds, and has a span of 1.07 m (42.01 in.) and a length of 1.57 m (61.86 in.). Additional dimensional data for the model are presented in Table 1.

This versatile model provides the following features: (1) variable wing leading-edge and trailing-edge flaps; (2) variable incidence canard with variable leading-edge and trailing-edge flaps; (3) variable longitudinal canard location; (4) alternative inboard strake shapes; (5) all-movable vertical tail; (6) wing-root bending moment gage; and (7) the ability for testing component buildup. The model has flow-through nacelles,

and the internal drag of these nacelles is determined during the tests using a precalibrated 20-tube rake mounted at the exit of each duct. A 6.25-cm (2.5-in.) high-capacity, six-component Task balance is sting-mounted internally in the model to measure the aerodynamic forces.

Northrop (HATOL). The 9.5% scale model fabricated by Northrop to simulate their twin-engine RALS concept is shown in Figs. 14 and 15. The model is sized for testing in the Ames Unitary and 12-Foot Wind Tunnels, and it has been designed to withstand the loads that are encountered at high angles of attack at transonic speeds. As is the case with the General Dynamics model previously described, the Northrop model is relatively large for testing at transonic-supersonic speeds. The HATOL model has a span of 0.95 m (37.14 in.) and an overall length of 1.52 m (59.84 in.). Table 2 gives additional dimensional data.

The following features are available on the model: (1) variable wing leading-edge and trailing-edge flaps, (2) variable incidence canard, (3) all-movable vertical tails, and (4) the ability for testing component buildup.

Northrop (VATOL). For Phase II, Northrop built a 9.5% scale model of their twin-engine VATOL configuration shown in Figs. 16 and 17. The model, which is sized for testing at subsonic through supersonic speeds in the Ames Unitary and 12-Foot Wind Tunnels, has been designed to withstand the loads at high angle of attack at transonic speeds. It has a 0.95-m (37.14-in.) span and an overall length of 1.50 m (58.91 in.). Additional dimensional data for the VATOL model are given in Table 3.

The Northrop model has the following features: (1) variable wing leading-edge and trailing-edge flaps, (2) alternative LEX size and LEX-off capability, (3) all-movable vertical tail, and (4) the ability for testing component buildup. In addition, each duct had 22 total pressure tubes and four static pressure orifices that are permanently mounted internally near the inlet throat to obtain initial data on the effects of the air-frame on the top-mounted inlet system. A precalibrated, 21-tube rake at the exit of each flow-through duct is used to determine the internal drag during the tests. A 5.08-cm (2-in.), high-capacity, six-component Task balance is sting-mounted internally in the model to measure the aerodynamic forces.

3.1.2.2 Single-Engine Models

General Dynamics. In Phase II, General Dynamics fabricated a wind-tunnel model to simulate the up-and-away flight configuration of their single-engine design which featured a combination of augmenting ejector/thrust deflection for propulsive lift (Configuration E7). This 11.1% scale model sized for testing in the Ames 11-Foot, 9- by 7-Foot, and 12-Foot Wind Tunnels is shown in Figs. 18 and 19. The model is constructed of high-strength steel to withstand the loads that are associated with high angle-of-attack testing at transonic speeds. This is a very large model for testing at these speeds. It has a wing reference area of 0.72 m^2 (7.79 ft^2), a span of 1.10 m (3.6 ft), and a length of 1.59 m (5.23 ft). Additional dimensional data for the model is given in Table 4.

This model has the following features: (1) a baseline wing with camber and twist and an alternate "plain" wing (no twist and camber), (2) variable trailing-edge flaps, (3) deflectable rudder, (4) missiles mounted on the wing tips or beneath the wings, (5) wing tip extensions, (6) wing-root bending moment gage and wing-tip accelerometer, and (7) the ability for testing component buildup. The model has a flow-through inlet system. The internal drag of this system is measured during the tests using two precalibrated rakes with total and static pressures — one rake at the exit of the two-dimensional nozzle and the other rake at the axisymmetric nozzle exit. A 6.35-cm (2.5-in.) high-capacity, six-component Task balance is sting-mounted internally in the model to measure the forces.

McDonnell Douglas. McDonnell Douglas (McAir) designed and fabricated a 9.2% scale wind-tunnel model of their deflected-thrust concept (configuration 279-3). The model (Fig. 20) is sized for testing in the Ames Unitary and 12-Foot Wind Tunnels. High-strength steel is used in the model construction to withstand high-angle-of-attack testing in these facilities. This versatile model can be tested in both a flow-through and a jet-effects mode. Figure 21 shows the flow through configuration which is supported by a sting that exits through the aft fuselage. The jet effects model is supported through the vertical tail. The model has a 1.01-m (3.30-ft) span and a length of 1.55 m (5.08 ft). Table 5 gives additional model information.

The following features are provided in this model: (1) variable wing leading-edge and trailing-edge flaps, (2) a remotely actuated, variable incidence canard, (3) two longitudinal wing locations, (4) a horizontal tail which allows three-surface testing, as well as canard- or aft-tail-alone testing, (5) deflectable rudder, (6) wing-root bending moment gage and wing-tip accelerometer, and (7) the ability for testing component buildup. On the flow-through model, the internal drag is measured during the tests by precalibrated rakes permanently mounted in the ducts. A 6.35-cm (2.5-in.) high-capacity, six-component Task balance is sting-mounted internally in the model to measure the aerodynamic forces.

On the jet-effects model, both cruise and fan-stream burning nozzle settings can be tested using high pressure air. A number of other items have been added to this jet effects model including (1) static pressure taps on the aft fuselage, at the wing root, and on the thermal ramps, (2) total pressure rakes for surveying the plume, and (3) additional nozzle ramp spacers to allow a parametric study of wake distance from the fuselage. In addition, a number of "dummy" sting components are available to allow determination of sting and sting-shroud interference during testing of the flow-through and jet-effects models.

3.1.2.3 Wind-Tunnel Tests

Tests of the twin- and single-engine V/STOL fighter models are primarily conducted in three Ames major facilities — the 11-Foot Transonic, the 9- by 7-Foot Supersonic, and the 12-Foot Pressure Wind Tunnels. (Northrop has also tested its twin-engine models and General Dynamics its single-engine model in their own 7- by 10-foot wind tunnels.) The tests in the Ames tunnels cover an overall Mach number range from 0.2 to 2.0 at a constant Reynolds number of 9.84×10^6/m (3.0×10^6/ft). Excursions in Reynolds number are made to determine the effect of this parameter at several Mach numbers.

In the 12-Foot Pressure Wind Tunnel, tests are conducted at Mach 0.2 and 0.4. Angle of attack is varied to 85° on a two segment support system, the first from approximately -5° to 45° and the second from approximately 35° to 85°. Angle of sideslip is varied from about -5° to 10°.

In the 11-Foot Transonic Wind Tunnel, the Mach number is continuously variable from 0.4 to 1.4. Angle of attack is varied from approximately -5° to 28°, and angle of sideslip from -4° to 10°. In the 9- by 7-Foot Supersonic Wind Tunnel, the Mach number range of 1.5 to 2.0 is covered in tests of these models with some excursions to Mach 2.5 for some configurations. Angle of attack is varied from -5° to 15° and angle of sideslip from -4° to 8°.

3.1.2.4 Test Plans

To date, the three twin-engine models have been tested in all three tunnels, and most of the results have been analyzed and reported. Extensive tests of the two single-engine models are planned for 1984 and 1985.

A number of other test activities are planned that relate to the General Dynamics E7 design. In addition to the above described one-ninth-scale force model tests, NASA Lewis has tested a one-third-scale, one-half-span model to study the ejector performance. (This will be described later in the ejector research section.) This model has now been converted by General Dynamics to a full-span powered model with a flowing inlet. Tests of this model are planned in the NASA Langley 4- by 7-Meter Tunnel to study the aircraft's transition characteristics. Also in progress is the construction of a 0.15-scale powered free-flight model to be tested at the NASA Langley 30- by 60-Foot Wind Tunnel in the summer of 1984. This test will begin to determine the control laws for the E7-flight-control system. A number of large-scale activities are also planned.

3.1.3 Example Results

A number of uncertainties that affect aerodynamic performance and are attributable to configuration features that relate to the V/STOL requirement have been identified. Many of these uncertainties have been investigated in the wind-tunnel test program just discussed. A few examples of the results from this test program that relate to these uncertainties will be briefly described. Again the discussion will be limited to the up-and-away flight mode. The results presented are taken from Refs. 14 through 22.

3.1.3.1 Minimum Drag

Among the major uncertainties that are associated with the V/STOL requirements for these future fighter aircraft are the minimum drag and transonic wave drag. These effects on aerodynamic performance were identified as concerns by all of the contractors in the present research program. The uncertainties are a result of the additional volume and surface area requirements associated with the propulsive lift system as compared to conventional takeoff and landing (CTOL) fighter aircraft. In addition, the ability to predict these drag characteristics for these unique configurations using existing techniques is a major uncertainty.

The minimum drag coefficients of the three twin-engine models versus Mach number are shown in Fig. 22. These are presented for a wind-tunnel test Reynolds number of 3×10^6/ft and are based upon the wing reference area of the respective models. A number of observations can be made about these data.

The minimum drag for these unusual types of configurations are predicted reasonably well at subsonic speeds. However, at supersonic speeds the minimum drag is both over and underpredicted on the General Dynamics and Northrop VATOL models (Refs. 16 and 21). Thus the experimental data base for these kinds of configurations shows the research needed to improve the prediction methods.

How do these drag characteristics compare to existing fighter aircraft? The subsonic minimum drag for several high-performance CTOL fighters is in the vicinity of a drag coefficient (CD) of 0.0200 (200 counts), and the supersonic drag level varies between 400 and 500 counts. Therefore, despite the additional volume and wetted area required for the propulsive lift system, these V/STOL configurations appear to have reasonable drag levels. In fact, the two Northrop designs appear to be on the low side, particularly at supersonic speeds.

The drag coefficients that are presented in Fig. 22 are based on the planform area of the wing with its leading and trailing edges extended to the fuselage centerline, a standard way of defining reference area. However, as noted in Ref. 19, this definition of reference area can lead to difficulties when comparing configurations which have much of their lift generated by surfaces other than the wings (canards, strakes, etc.). A more reasonable reference area has been found to be the total configuration planform area (Fig. 23 taken from Ref. 19). Here the lift curve for the E205 ejector configuration is apparently far superior to the Northrop HATOL and VATOL designs (left of figure), but essentially collapses onto the HATOL and VATOL curves when the total planform area is used (right of figure). The Northrop curves have also been reduced, but to a lesser degree. If these same area ratios are applied to the minimum drag data of Fig. 22, the resulting revised drag levels would be the ones that are shown in Fig. 24. On this basis, the differences in the minimum drag coefficients of the configurations are reduced, although the HATOL and VATOL supersonic levels are still lower. In fact, the experimental minimum drag of the Northrop HATOL design is worthy of note.

In an effort to gain additional internal volume to offset that lost to the propulsive lift system, Northrop uses two wing mounted afterbodies on their HATOL design. These bodies increase the volume by approximately 13% of the configuration total volume. The question, of course, is what do these afterbodies do to the configuration drag. The HATOL minimum drag in Fig. 22 shows several surprising findings. First, the very high experimental drag-rise Mach number (about 0.95) of this concept is unusual. It is much higher than predicted and higher than the other concepts. Also, the low level of the drag between Mach 1 and 1.4 as compared to the other concepts was an unexpected finding. Both of these results led to a number of repeat runs as a check of the data. The repeat runs gave exactly the same answers.

To further understand the minimum drag of the Northrop HATOL configuration, a component buildup test was performed (Refs. 14 and 20). Four of the eight different configuration combinations that were tested are shown in Fig. 25. This shows the relatively small drag increment (about 10 drag counts through the Mach range) that is associated with the afterbodies. This represents only about 4% of the total drag at Mach 1.1. Another

interesting finding in Fig. 25 is the large drag increment that is associated with the canards and vertical tails at subsonic speeds. By taking advantage of some of the other configuration combinations that were tested in the component buildup, a major portion of this increment was traced to an unfavorable interference of the canards on the vertical tails. This suggests an area for improvement during development of this configuration, such as the possibility of a slight repositioning of the vertical tails.

3.1.3.2 Wave Drag

Continuing the discussion of minimum drag, a major uncertainty is the transonic wave drag for these V/STOL fighter concepts because of the additional volume required by the propulsive lift system. This concern was identified by the contractors for all the concepts studied. The VATOL concepts should be less of a problem because they do not require as much volume for an onboard lift system as the HATOL configurations do.

To determine the penalty in wave drag for these V/STOL concepts, a comparison with existing fighter aircraft on an equal reference basis is in order. Such a comparison is shown in Fig. 26. Here the wave drag is defined as the drag coefficient increase from Mach 0.8 to 1.2. This is plotted versus the ratio of the maximum cross section area (adjusted for inlet capture area) to the square of the aircraft length. For reference, also shown on the plot is the wave drag of the Sears-Haack optimum body of revolution for a specified length and volume, and both 1.5 and 2.0 times this wave drag level. In all cases, the drag coefficient is based on the cross sectional area. Several existing fighter aircraft are represented by the open symbols and the present V/STOL model experimental results are denoted by the three solid symbols (NH = Northrop HATOL, NV = Northrop VATOL, GD = General Dynamics E205).

The wave drag of the HATOL is surprisingly low when it is compared to other fighter aircraft. The HATOL drag level is less than 1.5 times the Sears-Haack level. Again, it appears that the large afterbodies and their additional internal volume do not overly penalize the configuration in terms of wave drag.

The plot also shows the effect of proper area ruling on the E205 ejector concept. Although it has a wave drag higher than the HATOL concept, the E205 drag level is also less than 1.5 times the Sears-Haack drag level. It is interesting to note that the two designs that have considerable volume dedicated to the propulsive lift system (RALS and ejectors) have wave drag levels relative to the Sears-Haack body of less than 1.5 times when compared to a factor of about 1.7 for the Northrop VATOL configuration. In fact, the VATOL configuration has a wave drag that is almost equal to that of the E205 design.

In summary, these types of V/STOL concepts can be configured to give reasonable values of wave drag when compared to existing fighter aircraft, even when the additional volume requirements of the propulsive lift system are considered. As Fig. 26 shows, the V/STOL concepts have wave drag levels that are lower than those of many of the existing fighter aircraft that have been considered. This fact dispells one of the major uncertainties that is associated with these high performance V/STOL fighter concepts, at least for these twin-engine designs. This assessment for the single-engine concepts is awaiting wind-tunnel tests of the two models.

3.1.3.3 High Angle-of-Attack Aerodynamics

A number of the aerodynamic uncertainties concern the high angle-of-attack flight regime for these powered lift fighter concepts, and the ability to predict these characteristics by using existing techniques. To investigate these uncertainties, the models are typically tested to approximately 90° in the Ames 12-Foot Wind Tunnel and to approximately 25° at transonic speeds in the Ames 11-Foot Wind Tunnel.

An example of this is shown in Fig. 27. The GD ejector configuration (E205) was tested to an angle of attack of 85° at Mach number 0.2 in the Ames 12-Foot Wind Tunnel. These results (Refs. 14, 16, and 22) are shown for the model with all control settings at zero. To reach these high angles of attack, two sting support arrangements are used. This is indicated by the circular and square symbols, respectively, in the figure.

A prediction method (AEROX) developed at NASA Ames (Refs. 23 and 24) to rapidly estimate nonlinear aerodynamic characteristics to high angles of attack, was used for the estimates in Fig. 27. Although it did not always predict the absolute values of the various coefficients, the trends and slopes estimated by the program are good for this unique type of configuration. This is only one example, but it appears that this approach offers potential for aerodynamic predictions to angles of attack far beyond the capability of the computational methods presently used.

The measured angle-of-attack characteristics for the GD E205 model at the higher Mach numbers are shown in Fig. 28 (Refs. 14 and 16). The control surfaces are all set to zero deflection for this component buildup. Results for the subsonic and supersonic speeds are similar. The lift and drag of the body (BN), which includes the nacelles and the baseline inboard body-nacelle strakes, and the body-plus-vertical tail (BNV) are essentially identical. Even without the outboard wing panels, these configurations generate lift coefficients of at least 0.8 because of both the large lifting area of the wide body and nacelles, and the favorable interaction between the inboard strakes and the wide body and nacelles.

Addition of the wing (BNWV) results in increased lift coefficients as expected. Adding the canard (BNWVC), which increases the total planform area by 9.3%, further increases the lift coefficients to very high values at both Mach numbers, as a result of favorable canard-wing interactions. At $M = 0.9$, this increase in lift is about 35% at $\alpha = 20°$ angle of attack; at $M = 1.2$ it is about 23% for this same angle of attack. Or considering this another way, adding the canard at a lift coefficient of 1.3 reduces the drag coefficient about 34% at $M = 0.9$ and about 21% at $M = 1.2$. As these results demonstrate, this concept offers the combination of two technologies for improved high angle-of-attack aerodynamics — close coupled canards and strakes.

3.1.3.4 LEX Effects

One of the uncertainties that has been identified by Northrop for the VATOL design concerns the effectiveness of the wing leading edge extension (LEX). This surface affects the longitudinal aerodynamics, the

vertical tail effectiveness, and the flow quality to the top-mounted inlet on this concept. To explore this uncertainty, three sizes of LEXs were tested on the VATOL model (Fig. 16). These were the standard size, one approximately one-half this size (alternate), and with LEX-off. The measured longitudinal characteristics are compared in Fig. 29 for Mach numbers 0.6 and 0.9. These results, taken from Ref. 19, are based on the total model planform area to give a true comparison of these lift enhancing surfaces as previously described. The results show that at angles of attack above 10° at subsonic speeds, the standard LEX improves the lift (up to 15%) and the drag as compared to the LEX-off (up to 40%). There were no lift or drag benefits from the LEX at Mach number 1.2 (Ref. 19).

As shown in Fig. 29, the larger, standard LEX gives the greater benefits in lift and drag when it is compared to the smaller LEX. As an added note, studies of LEX effects on flow quality to the top inlet of the VATOL model show the larger LEX to give the better performance at the higher angles of attack. Reference 19 further indicates that a larger canard relative to the wing size gives greater benefits when it is compared to a smaller one. Therefore, these results suggest that the larger LEXs and larger canards produce greater improvements in lift and drag, but they are limited by the control power of the elevons. Finally, Ref. 19 indicates that the benefits of the VATOL LEX and the HATOL canard are comparable in overall magnitude.

3.1.3.5 Aerodynamic Center

A major uncertainty that has been identified for the E205 ejector configuration is the aerodynamic center (A. C.) location and travel with Mach number. This arises because the integration of the forward ejector bays, the outboard nacelles, and the canards results in a design with a large amount of planform area that is located well forward on the aircraft. Because of this, the concern is whether the configuration has an acceptable stability at subsonic speeds, and also whether the existing prediction techniques are appropriate in the design of a unique configuration as in the E205.

Figure 30 shows the A. C. location in terms of percent mean aerodynamic chord (MAC) for the ejector model as measured in the three wind tunnels (Refs. 14, 16, and 22). All control surfaces were set at zero deflection. Results for canard-on (open symbols) and canard-off (solid symbols) configurations are shown. The experimental data show a forward A. C. location of approximately 26% at subsonic speeds for the canard-on configuration. This instability level is probably considerably higher than is desired; however, modern control-system technology is becoming sufficiently mature so that allowances can be made for such instabilities (for example, the X-29A forward-swept-wing demonstrator aircraft is about 35% unstable). However, this instability level can be affected appreciably by canard longitudinal location and strake shape. This is demonstrated in Fig. 30 by the shaded area which indicates the experimental range of A. C. location travel that is obtained for various combinations of strake shape and canard location tested on the model.

Estimates of the A. C. location, obtained by using several prediction methods, are also shown in Fig. 30. The solid and dashed lines show the estimates made by General Dynamics for the canard-on and canard-off configurations. With exception of Mach number 0.95, the estimates agree well at subsonic speeds and up to approximately Mach number 1.2. Above this speed, the A. C. location is predicted to be farther aft on both configurations than the experimental results indicate. This difference is about 5% of the MAC for the canard-on configuration.

The long- and short-dashed curve in Fig. 30 is a prediction for the canard-on configuration that was obtained by using the Ames AEROX program. The results predicted by this method are within 4% of the MAC for these measured data. The predictions shown above met with varying success for this type of configuration. Also, the calculated and measured results shown in Fig. 30 are for the low-angle-of-attack attached-flow regime. The existing prediction methods are expected to be less reliable in the nonlinear regions at higher angles of attack.

To further amplify the A. C. location of the E205 configuration as it is affected by the canard longitudinal locations and the strake shapes tested, Fig. 31 (Ref. 22) is shown. These results are for Mach 0.2 in the Ames 12-Foot Wind Tunnel, and include the small center-of-gravity shifts on the aircraft that are caused by these surface variations (generally less than 0.5% MAC). The upper portion of the figure shows that moving the canard either forward or aft of the baseline position by 25% of the wing MAC (this movement was available on the model) changes the stability by about 5.5% MAC. Changing the strake size from the large (baseline) to the strake off reduces the instability by approximately 2%. Thus on this configuration, the canard variations tested have a greater effect on stability than do the strake variations tested.

The effects of these canard and strake variations on maximum-trimmed lift coefficients $(C_{L_T})MAX$, were estimated in Ref. 22 by using canard incidence and wing-flap test data. These results are shown in the lower portion of Fig. 31. The reduced instability of the aft canard location allows a 20% increase in maximum trimmed-lift coefficient over the baseline mid position. The lift is reduced by about this same percentage by moving the canard forward. Changing from the baseline strake to strake off increases the maximum-trimmed lift by about 9%. Thus, because of their respective influences on A. C. location, the canard changes have greater effect on maximum trimmed lift than do the strake changes.

3.1.3.6 Buffet Onset

In-flight thrust vectoring in combat is a possibility with any of the V/STOL fighter concepts because of the inherent thrust vectoring capability that already exists in the concept. A canard is generally used on these concepts to provide trim with a positive lift and to improve the high angle-of-attack performance of the wing. This leads to an uncertainty that affects the buffet onset characteristics of these types of configurations. To investigate this uncertainty, a wing-root bending moment gauge was installed in the left wing of the GD E205 ejector model to obtain an initial indication of the angle of attack for buffet onset at transonic speeds in the Ames 11-Foot Wind Tunnel. Some measured results (Refs. 14, 16, and 17) from these tests are shown in Fig. 32 with all control surface deflections set at zero. Canard-on (baseline mid-position) and canard-off experimental data are indicated by the circular and square symbols, respectively, and appear in the upper plot of Fig. 32. At subsonic speeds, the canard gives a slight increase in the angle of attack for the onset of buffeting (α_{BO}), but at the supersonic Mach number this trend is reversed. The predictions that are shown in Fig. 32 are obtained from Ref. 3, and are based on the correlation of results from tests of

similar configurations. The agreement at subsonic speeds is within a degree or so, but the prediction at Mach number 1.2 is approximately 4° lower than the experiment. The reversal in the effect of the canard with increasing supersonic Mach number is predicted. However, further research is needed to gain a better understanding of buffet-onset phenomena.

At the bottom of Fig. 32, measured data are shown for the three different longitudinal canard locations. At subsonic Mach numbers, the midposition (baseline) gives the higher buffet-onset angle of attack. At Mach number 1.2, there is a reversal in the effects of the canard location.

3.2 Airframe/Propulsion Integration

This section will briefly describe three research activities that relate to the airframe/propulsion integration characteristics of these high-performance V/STOL concepts. These include in-flight thrust vectoring, top inlets, and propulsion simulation in wind-tunnel testing.

3.2.1 In-Flight Thrust Vectoring

To expand the limited propulsion/airframe interaction data base on high-performance V/STOL aircraft concepts, a wind-tunnel research program was conducted at NASA Ames Research Center. The model (Fig. 33) is a one-eighth scale, twin-engine, V/STOL fighter concept developed to study various types of nozzles that are integrated into this type of configuration. The model geometry is based on the Grumman Design 623-family of configurations and is a forerunner of the RALS concept previously described in this paper and in Ref. 1. The nozzles considered in the study are a baseline circular convergent-divergent nozzle, an ADEN (Ref. 1) and an ALBEN (Asymmetric Load Balanced Exhaust Nozzle). The ALBEN, a CTOL derivative of the ADEN, features elliptical-throat and expansion-surface contours. Figure 34 shows the model with the ADEN installed on it. This nozzle on the wind-tunnel model can be tested in the cruise mode and in the thrust-deflection mode for in-flight maneuvering, but 90° thrust deflection is not available on this model.

The model includes the capability to measure forces and pressures. Extensive pressure instrumentation is installed on the wings and nacelles to isolate the propulsion-induced effects. The model is supported by twin vertical tails (Fig. 33), which also provide passage for high-pressure air for jet-effects testing. Tests were conducted in the Ames 11-Foot Transonic Wind Tunnel for Mach numbers from 0.4 to 1.4. Some of the results (Refs. 25-28) are summarized here.

The unvectored-ADEN and the ALBEN nozzles are competitive on a thrust-removed drag polar basis, an example of which is shown in Fig. 35 (see Ref. 26). Both of these nozzles show large performance gains, at all flight conditions, relative to the circular nozzle. For example, a typical cruise drag reduction of 50 counts (0.0050) at Mach 0.9 is shown in Fig. 35. However, some of this drag increment is due to the difficulty of integrating a circular nozzle exit with a straight wing trailing edge. The influence of thrust-vectoring for this ADEN (installed at the trailing-edge of the wing in the root area) travels very far upstream and spanwise nearly to the wing tip. This results in significant jet-induced lift as indicated by the example in Fig. 36 (Ref. 26) of the ADEN cruise lift build-up. This shows the jet-off aerodynamic lift, the jet-induced lift, and the jet lift itself.

When vectoring the ADEN, an optimum polar locus is formed by an envelope of points that cover a range of deflection angles. This means that deflection angle should be scheduled with angle of attack to achieve optimum performance. In general, larger thrust-vectoring advantages are measured as the subsonic Mach number is reduced. No vectoring benefits were found at supersonic speeds in this research program.

At a key Mach 0.9 cruise nozzle (nonafterburning) condition (CL = 0.3), a 40-count drag reduction is realized as the ADEN is vectored from 0° to 10° in Fig. 37 (Ref. 26). When this thrust vectoring payoff is combined with the previously described 50-count reduction of the cruise ADEN versus the circular nozzle, a 90-count reduction is achieved for the vectored ADEN over the baseline circular nozzle installation. This 90-count reduction represents 25% of the zero-lift drag for this V/STOL concept. Finally, at Mach 0.9 maneuver conditions, only moderate (about 10°) deflection angles of the ADEN combat (maximum afterburning) nozzle are expected to provide advantage, because larger deflections cause nozzle thrust losses and induced-drag penalties.

3.2.2 Top Inlet

In the previously described studies of V/STOL fighter/attack aircraft concepts, top-mounted air induction systems have been identified as a very promising and desirable design feature. This inlet location offers a number of significant advantages when compared with conventional locations, including (1) decreased ingestion of debris and hot gases during takeoff and landing, (2) reduction in radar cross section, and (3) improved weapons integration. However, there are a number of concerns with top-mounted inlets, including increased upper-surface local Mach number at the higher angles of attack because of flow expansion, particularly at the higher Mach numbers. Other concerns include possible ingestion of (1) distorted flows at high angle of attack, (2) vortices from a canard or wing leading-edge extension (strake), and (3) low-energy boundary layers. A major concern is the lack of aerodynamic data on these types of inlets at higher speeds on which to base aircraft design studies. Because of this and the desirable features of top-mounted inlets, a program, jointly sponsored by Ames and the David Taylor Naval Ship Research and Development Center (NSRDC), was initiated to develop an aerodynamic data base on this promising technology.

To explore top inlet performance, the previously described Northrop VATOL model (Fig. 17) was provided with additional components and instrumentation (Fig. 38). This included remotely controlled mass flow control plug assemblies, inlet flow-field instrumentation at the inlet face to measure flow pressures and direction, and steady state and dynamic pressure instrumentation located at the simulated engine compressor face.

The LEX on the wing is the key to the top inlet performance on the present VATOL concept. These surfaces produce a strong, counter-rotating vortex pair which effectively inhibits upper-fuselage flow separation by entraining high-energy free-stream air into the upper-fuselage region and by sweeping low-energy boundary layer air outward. Thus the LEX size is an important parameter to investigate, as well as other geometric features that affect the upper-inlet flow field. The following airframe variations were tested in the research

program: (1) LEX size and the absence of LEX, (2) wing leading-edge flap deflection, (3) canopy-on and canopy-off, and (4) canard integration and deflection. Tests were conducted in the Ames 11-Foot and 9- by 7-Foot Wind Tunnels over a Mach number range of 0.6 to 2.0. Angle of attack was varied to approximately 28° subsonically and to approximately 18° at the highest supersonic speeds. Angle of sideslip was varied up to 8° to 10°.

This research program generated extensive data on top-inlet flow field and engine-inlet performance characteristics at subsonic, transonic, and supersonic speeds. The significant findings from this wind-tunnel test program are presented in Refs. 29 through 34.

One example result is the summary of the measured distortion effects with angle of attack and angle of sideslip as shown in Fig. 39 (see Ref. 29). Distortion is defined here as the maximum minus the minimum pressure recovery at the compressor face divided by the average pressure recovery. In Fig. 39, distortion-limited operating envelopes are shown for Mach numbers 0.9 and 1.2 as a function of angle of attack and angle of sideslip. Both windward and leeward results are shown. The estimated airplane operating envelope and the wind-tunnel test envelope are outlined for both Mach numbers. The top figures are for a distortion level of less than 0.2 (cross hatching) and the bottom curves are for less than 0.15. In both cases, the white areas represent distortion values above these two levels. The higher distortion level ($\leq$0.2) is considered to be acceptable to the particular turbojet engine proposed for this design. As the results show, the top inlet provides good performance over the envelope tested particularly, at the lower Mach number. Some of the problem areas (indicated in Fig. 39), particularly at Mach number 1.2, were shown during the test to be associated with the wake that was generated by the LEX/fuselage intersection. Configuration tailoring in this region could substantially reduce or eliminate these problems.

To demonstrate the potential of this top inlet system, a comparison of pressure recovery with that of other fighter aircraft using more conventional inlet installations is shown in Fig. 40 (see Ref. 31). The comparison aircraft include the YF-16 with a fuselage-shielded inlet system, the YF-17 prototype with a wing-shielded inlet, and an advanced Northrop fighter configuration with side-mounted, two-dimensional external compression inlets with fixed, vertical ramps. The comparisons are shown at Mach numbers 0.9, 1.6, and 2.0. Note that the results reflect differences in inlet design and mission requirements and do not allow a precise comparison of the relative merits of the various systems. Rather, the comparisons serve only as an indication of the potential for the present VATOL top-inlet system.

A number of comments concerning the results in Fig. 40 are in order. In the cruise angle-of-attack range (α = 0 to ~3°), the top inlet system provides recoveries that are comparable to those of the other aircraft at all three Mach numbers. At the transonic speed (M = 0.9), the top inlet is competitive to the maximum α tested, 25°. At supersonic speeds, the top inlet performance deteriorates with angle of attack primarily because of the flow field expansion which increases local inlet Mach number and causes higher inlet shock losses. In contrast, the recoveries of the shielded inlet systems improve with angle of attack because of the flow-field precompression that is provided by the forebody and/or wings.

Because of load factor constraints, the angles of attack at supersonic speeds for fighter aircraft are typically limited to 15° and 10° at Mach 1.6 and 2.0, respectively. Figure 40 shows that at these conditions, the present top inlet system gives "adjusted" recoveries that are not significantly lower than those of the other systems. The "adjusted" curves reflect the performance that is obtainable if the previously mentioned low pressure wake regions that are generated by the LEX/fuselage juncture could be eliminated by minor configuration tailoring. Note that the present top inlet system has not undergone the many hours of developmental testing that each of the other systems in Fig. 40 has. The top inlet performance could be improved with similar development efforts.

In summary, considering both the distortion level envelopes and the recovery comparisons, the top inlet is considered a viable option for these V/STOL fighter aircraft. Additional research work is needed, but considering the stated advantages of top inlets for these types of aircraft, this research effort is expected to continue.

3.2.3 Propulsion Simulation

The V/STOL concepts previously described are characterized by closely coupled inlets, canards, wing, and nozzles. Because of the interactions of the aerodynamic and propulsive flows on these "close coupled" configurations, the conventional methods of wind-tunnel testing may not give the proper results. The conventional methods consist of testing two models, a flow-through and a jet-effects model, and then combining these results into overall aerodynamic performance. However, this technique will not measure the above mentioned interactions. Therefore, a new method of wind-tunnel testing fighter aircraft that uses compact multimission aircraft propulsion simulators (CMAPS) is being pursued jointly at Ames Research Center and at the U.S. Air Force Wright Aeronautical Laboratories. This development will allow simultaneous simulation of both inlet and nozzle flows on a wind-tunnel model.

The details of this new test technique have been described in another lecture in this series (Ref. 35). Thus, only a few comments will be given here. Figure 41 shows the components of the propulsion simulator program and Refs. 36 through 41 give additional information. The simulator (upper right) is powered by high pressure air that drives a single-stage turbine which in turn drives a four-stage axial flow compressor. The simulator is approximately four inches in diameter and approximately ten inches long. Other elements of the program in Fig. 41 are the simulator control system and the calibration laboratory which is being constructed at Ames. This facility will allow complete and accurate calibration of a model containing two simulators. Also shown at upper left is the first wind-tunnel model to be tested with two of these simulators installed in it.

This model has been tested in the flow-through and jet-effects modes, and this past year it was tested with propulsion simulators installed on it. The model, which is shown in the 11-Foot Transonic Wind Tunnel in Fig. 42, simulates a wing-canard, twin-engine, high-performance STOL fighter configuration with deflectable nonaxisymmetric exhaust nozzles. Both force and pressure data were obtained in the test. Two examples of the results that are shown here are taken from Ref. 41.

One purpose of the test was to explore the ability of the CMAPS to simulate full-scale engine conditions in terms of inlet mass flow ratio (MFR) and nozzle pressure ratio (NPR). During this first test, a conservative approach was taken, and the angle-of-attack/MFR combinations were selected so that the maximum distortion would not exceed 25% based on the results of the flow-through test. The intent was to reduce CMAPS blade stresses and to minimize the possibility of compressor stall. Also, a 1,000-psi limit was placed on the turbine drive air for this test.

The demonstrated MFR range of the CMAPS with the model baseline inlet is shown in Fig. 43. At Mach numbers less than 0.9, the CMAPS upper airflow set points were limited to less than the maximum possible by the distortion limit of 25%. Alternate inlets with different lower-lip configurations were not tested, but if they had been, they would have permitted operation at maximum airflow and higher angles of attack at Mach numbers below 0.9. The lower airflow set points were based on a selected turbofan cycle and were greater than the windmill airflow and, thus, fall within the CMAPS/MFR envelope.

The demonstrated NPR envelope of the CMAPS is shown in Fig. 44. This figure shows the maximum and minimum values of NPR that were set for each Mach number. The minimum NPR boundary is determined by the windmilling operation of the simulator. The maximum NPR boundary is determined by the 1,000-psi limit on turbine drive pressure. The flow-through model NPR operating line is shown for reference. It is seen that the CMAPS can easily simulate flow-through NPR values. The upper line, labeled Pt2/Pto = 1.0, indicates the approximate maximum NPR that could be achieved with this exhaust nozzle throat area with 100% inlet recovery, low distortion, and no turbine drive pressure restriction. The NPR range of the CMAPS is limited when compared with a jet-effects simulator. The maximum NPR for a jet effects simulator is limited only by the design pressure of the chamber inside the model. The minimum is NPR = 1.0, or jet off, which is lower than the CMAPS windmill NPR. However, both the NPR and airflow range of the CMAPS are sufficient to investigate the operating range of the existing engines and a majority of advanced cycle engines.

4. LARGE-SCALE RESEARCH

This section of the paper describes a number of research programs in which large-scale wind-tunnel models are used to address the aerodynamic performance and the propulsion/airframe integration aspects of V/STOL fighter aircraft. This research takes place at low speed and under static test conditions. Tests are typically conducted in the Ames 40- by 80-Foot Wind Tunnel and at the Ames Outdoor Aerodynamic Research Facility (OARF). The 80- by 120-Foot Wind Tunnel will become a part of this test complex in the near future.

As an example of the type of tests that are conducted in these facilities, a full-scale model of the AV-8B with a Pegasus engine is shown mounted in the Ames 40- by 80-Foot Wind Tunnel in Fig. 45. Tests were conducted at thrust levels of up to 16,500 lb at speeds approaching 180 knots. The nozzle deflection was limited to 65° because of model size relative to that of the test section. It is expected that operation of such a model in the Ames 80- by 120-Foot Test Section will not be as restrictive in thrust deflection. Figure 46 shows the same model at the OARF. Forces are measured by load cells that are located at the support attachment points.

The large-scale V/STOL fighter research activities that are summarized in this section include a twin-engine fighter model and tests, high angle-of-attack studies, and thrust-augmenting ejector research.

4.1 Twin-Engine Model

A large-scale wind-tunnel model of a twin-engine V/STOL fighter is described in this section. This model has been tested in the Ames 40- by 80-Foot Wind Tunnel and an example of the results is given.

4.1.1 Model Description

Many of the uncertainties that affect aerodynamic performance of V/STOL fighter aircraft exist at the hover- and low-speed transition conditions. Because of this, NASA Ames is conducting a research program that is centered around a large-scale wind-tunnel model of a twin-engine supersonic V/STOL fighter. The configuration selected for this research is the General Dynamics E205 configuration. This concept, described early in this paper, was derived in the Phase I studies of Ref. 3, and is further described in Ref. 1. The large-scale model currently does not have the ejector propulsive lift system installed, but rather is configured in a STOL fighter configuration. Figure 47 shows the model that is installed in the Ames 40- by 80-Foot Wind Tunnel and Fig. 48 gives the model geometry. The 7.28-m (23.9-ft) span model is equipped with close-coupled canards and an aft fuselage control (beaver tail) for pitch control. The canard, with leading- and trailing-edge flaps, can be mounted in three longitudinal positions to investigate canard/wing interference. The beaver tail is intended primarily as a takeoff and landing pitch trim device. Roll and secondary pitch control are provided by the outboard wing trailing-edge flaps (ailerons) which are normally set at a geometric angle that is close to those of the inboard wing flap (primary nozzle flap).

The model is powered by two General Electric J-97 turbojet engines, each producing 9,340-N (2,200-lb) thrust at a pressure ratio of 2.0. The engines are mounted in nacelles at 33% semispan. This provides a large strake area (inboard of the nacelles) for possible future integration of an ejector system to give the model VTOL capability. The nacelles are somewhat oversized in comparison to the E205 design to accommodate the J-97 engine. The model combines two propulsive-lift technologies, upper-surface blowing (USB) and spanwise blowing (SWB) to augment the lift over a wide angle-of-attack range. As shown in Fig. 49, the J-97 exhausts into a transition duct where 16% of the flow can be diverted to the SWB system to delay wing stall by augmenting the wing leading-edge vortex. The remaining 84% of the engine flow exhausts into a two-dimensional, half-wedge, convergent-divergent nozzle. This nozzle preturns the flow down 25°, and exhausts over the nozzle flap upper surface, providing exhaust vectoring capability from -10° to 40°. This propulsion system is an adaptation of the vectored engine-over wing (VEO-wing) concept developed by General Dynamics (Refs. 42 and 43).

The SWB exhausts at a 34° sweep-back angle, as measured in static tests, from a rectangular nozzle that is flush with the nacelle outer wall approximately 1.5 nozzle heights above the wing surface. When the model is

tested without SWB, this nozzle is covered and the two-dimensional USB nozzle area is increased to maintain the same overall exhaust area. The thrust characteristics and flow turning angles for each nacelle were measured at the Ames Static Test Facility. The results of these static tests and a complete propulsion system description are reported in Ref. 44.

4.1.2 Tests and Results

The model has undergone three investigations in the Ames 40- by 80-Foot Wind Tunnel and one investigation at the Ames Static Test Facility. During these studies, the characteristics of the flow surrounding the airframe, as well as overall aerodynamic force and moment characteristics, were investigated. The model was equipped to measure the surface pressure on the canard, wing, strake, and flaps as well as total pressure distributions in the propulsion system exhaust. The location of the surface taps can be seen as the dark lines on the port side of the model in Fig. 47. The surface of the wing was also instrumented to measure surface air temperature to study the environment to which the wing will be exposed by SWB.

A summary of the results of tests of this model are given in Refs. 45 through 47. Basic longitudinal characteristics are given in Ref. 45 for nozzle thrust vector angles (δ_T) of 40°, 18°, and -1°. An example is given in Fig. 50 for $\delta_T = 18°$, with SWB on and the canard in the aft position. Power strongly affects lift characteristics over the entire alpha range. The combination of USB and SWB generates maximum lift coefficients well in excess of four at high-thrust coefficients with gentle stall characteristics. The maximum lift generated is even higher for $\delta_T = 40°$ (Ref. 45). At $\alpha = 15°$, USB induces a 10% to 15% increase in lift. Spanwise blowing provides an additional 10% to 13% improvement in lift. Other significant findings are presented in Refs. 45 through 47.

4.2 High Alpha Research

A research program to study the high angle-of-attack aerodynamic performance of V/STOL fighter aircraft at low speed is being conducted at Ames Research Center using large-scale models. Of primary interest in this program is the use of vortex lift to enhance the high-lift aerodynamic characteristics and the ability to predict the resulting complex and interacting flows. This is of concern for fighter aircraft during maneuvering flight and is of additional concern for V/STOL fighter aircraft during transition flight. A brief description of one model and test will be given here as an example of the type of activity in this research program. The material presented is taken from Refs. 48 through 51.

4.2.1 Model Description

In this research program, a well-instrumented, large-scale powered model of a close-coupled canard-delta-wing V/STOL fighter configuration was tested in the Ames 40- by 80-Foot Wind Tunnel. It is a 0.4-scale model of a design that was developed by Vought in the studies of Ref. 7. The concept was briefly described earlier and was further described in the Ref. 1 paper. The model that is shown is installed in the 40- by 80-Foot Wind Tunnel (Fig. 51), and the model geometry is given in Fig. 52.

For these high angle-of-attack studies, a sting-type of support system is used (Fig. 51). The model is sting-mounted with the wing chordplane in a vertical position so that rotation of the wind-tunnel turntable allows testing through 90° angle of attack. Figure 53 indicates how both pitch and yaw are obtained. The 12-in. diam tip-driven fans provide inlet airflow and low-velocity exhausts. Adjustable control surfaces included canard incidence, canard trailing-edge flaps, and wing leading- and trailing-edge flaps. Force and moment data were measured by an internal six-component strain gauge balance. Approximately 500 pressures were measured to document the model surface and duct pressure distributions, and the power conditions. The model was tested to about 110° angle of attack, at several angles of sideslip, and at several power levels. Canard and flap variations were made, and canard-on and canard-off configurations were investigated. The results from the test are given in Refs. 48 through 51.

4.2.2 Tests and Results

An example of the high angle-of-attack longitudinal aerodynamic characteristics that were measured during the test is shown in Fig. 54 (Ref. 51). The power-removed results are for canard-on and canard-off configurations. The lift curves are nearly identical up to an angle of attack of 10°, beyond which the canard-on model achieves greater lift. Both configurations reach maximum lift at approximately 33° angle of attack. Although the canard adds only 15% more area over the wing reference area, a 34% increase in maximum lift is achieved.

An attempt was made to predict the above longitudinal aerodynamics in the high angle-of-attack regime, which is characterized by a complete absence of attached flow or attached vortex flow on the top-side of the lifting surfaces. To make these predictions, a flat-plate analogy was used which is described in Ref. 51. Figure 55 (see Ref. 51) gives the results of the predictions. With exception of the pitching moment, the estimates of the model longitudinal characteristics in the fully stalled angle-of-attack range were good.

4.3 Ejector Research

For several years, Ames Research Center has conducted research on thrust augmenting ejectors for application to powered-lift aircraft. The objective has been to evaluate the fluid dynamics of the ejector itself and to integrate it with the complete propulsive lift system. This has involved fundamental ejector development, small- and large-scale tests, and the application and development of prediction techniques. An important guideline in all of these programs is the ability to package the ejector system within the lines of the aircraft configuration. The research activities have included ejectors that are applicable to both the STOL and the V/STOL aircraft. The present discussion will be limited to a brief summary of several efforts that are related to V/STOL fighter aircraft. Reference 52 gives an excellent review of these research activities.

There are three types of ejectors that are considered for fighter aircraft that have a vertical flight capability (see Fig. 56). All three types have been used in several of the V/STOL fighter concepts described

in this paper and in Ref. 1. The research activities that are related to the "fuselage ejector" and the "short diffuser ejector" are summarized below. The "spanwise ejector" is the type of ejector that was used in the XFV-12A Thrust Augmentor Wing aircraft that was built and tested by Rockwell International.

4.3.1 Fuselage Ejector

The fuselage ejector was initially proposed by de Havilland Aircraft of Canada Ltd., and research has continued to be supported jointly by NASA and Canada. These efforts are summarized in Refs. 52-55. This type of ejector is considered for designs where part of the fuselage is used for one side of the diffuser with the other side provided by a retractable lower door as indicated by Fig. 56. An advantage of this ejector over the short-diffuser type and the spanwise types is mechanical simplicity, and possibly, flow stability because of the long diffuser.

The development of the fuselage ejector was first accomplished by component development and testing using laboratory models. Verification of the results from these component and small-scale tests is provided by the large-scale model shown in Fig. 57. This generic model is installed in the Ames 40- by 80-Foot Wind Tunnel and is powered by a J97 engine. The two ejector bays with the numerous spanwise ejector lobes are evident in the figure. Several wind-tunnel tests of this model have provided a valuable data base for treating induced effects and transition performance. These tests proved that there is a need to deflect the ejector thrust from the vertical position so that sufficient thrust could be provided for transition. An effective way to accomplish this is to swivel the primary nozzle lobes. Some initial testing has been done to evaluate this method.

The J97 powered model (Fig. 57) currently includes an improved method of swiveling the primary nozzle lobes for additional ejector thrust deflection (from vertical) and includes the redesign of the primary nozzles to improve mixing. Extensions to the research effort include continued development of the ejector itself and the capability to add rear thrust which can be varied in deflection, location, and jet shape. This simulated vectored core thrust was recently tested in combination with the ejectors in hovering tests at the OARF. The core thrust was vertically deflected near the rear of the model. Tests were conducted at heights of 12 ft and at the 2-ft wheel height above the ground. Future additions to the model include different wing planforms and airfoil shapes, as well as the possible addition of a canard. Alternate trailing-edge flaps will include both unblown and blown concepts.

As previously mentioned, a program is underway to incorporate the "fuselage ejector" concept together with a deflected thrust nozzle into the General Dynamics-E7 configuration. Among the several test activities in this program is an effort to further evaluate and develop the ejector system. To accomplish this, a one-third-scale, half-span powered model of the E7 configuration has been tested in the NASA Lewis 9- by 15-Foot Wind Tunnel. The model installed in the tunnel is shown in Fig. 58. The test was run with the tunnel sidewalls removed in an open test section configuration. The powered ejector lobes are evident in the figure. For this test, the inlet was faired over and the aft two-dimensional deflecting nozzle was not used. The Mach number was varied from zero (static tests) to 0.185, which is approximately the end of the transition speed for the concept. Angle of attack was varied from 0° to about 20° and a few sideslip runs were made. The outcome of the test was a verification of the ejector performance.

Another effort that relates to the E7 concept is the design and fabrication of a large-scale, engine-powered model for tests in the Ames 40- by 80-Foot Wind Tunnel in approximately three years. The objective of this program is to demonstrate the engine/airframe integration, including the incorporation of the "fuselage type" ejector system and the deflecting two-dimensional nozzle. This is a joint effort among many groups including NASA, the Canadian Government, General Dynamics, de Havilland, and Pratt and Whitney. Finally, a joint NASA Lewis/General Dynamics program to validate the propulsion system for an E7 technology demonstration aircraft (ducting, air collector, full-scale ejector, etc.) was begun in the Fall of 1983; the first tests are scheduled for the Spring of 1985.

4.3.2 Short Diffuser Ejector

The short diffuser ejector (Fig. 56) was developed by Flight Dynamics Research Corporation, and recent development work has been jointly sponsored by NASA and the Navy (Refs. 56 and 57). This chordwise ejector system is the concept that is used by General Dynamics (Ref. 3) in their twin-engine V/STOL fighter design (E205) that is described earlier in this paper and in Ref. 1. The ejector uses two sets of nozzles, a primary jet and a diffuser boundary layer control (BLC) nozzle as shown by Fig. 59. The purpose of the latter nozzle is to entrain the flow to the diffuser walls in the mixing section. In the current design, there is a flow split of 60% to the upper nozzles and 40% to the lower nozzles. An important part of the development of this ejector system has been to lower the upper nozzle envelope to minimize the "doors closed" length of the ejector while still maintaining the high augmentation ratio. The purpose of this is to package the ejector system within the inner wing/strake area of the E205 configuration during the up-and-away flight mode.

Up until recently, the majority of work on this ejector concept has included tests of small-scale models at low NPR. These tests indicated that an augmentation ratio of 2.1 is possible. Higher NPRs will reduce this value to something below 2.0. To investigate the performance of this ejector system as it is packaged in the E205 configuration, a 0.2-scale model will be tested in the Ames 7- by 10-Foot Wind Tunnel. This model is a semispan simulation of the E205 as shown in Fig. 60 and it is currently under construction at Ames; plans are to test it statically (approximately mid-1984) before it is tested in the 7- by 10-Foot Wind Tunnel.

4.3.3 Ejector Performance

Ames Research Center has studied the ejector for powered-lift applications for a number of years. A commonly used summary of ejector performance is presented in Fig. 61. Augmentation ratio, ϕ_I (ratio of ejector thrust to isentropic thrust of the primary nozzle), is shown versus a gross indication of the packaging capability of the ejector, $L/\bar{t}$. This is the ratio of ejector length to a given average nozzle size. Thus the objective in the research programs has been to move the performance and geometry of thrusting ejectors in hovering aircraft up, and to the left of, the plot in Fig. 61. A description of the various ejector concepts in the figure is given in Ref. 52. One important point that arises from this broad ejector research program

is that aircraft development should proceed only after a theoretical and experimental data base is accumulated on the ejector itself. This data base should include not only small-scale ejector and complete configuration wind-tunnel testing, but also full- or large-scale testing using "boiler plate" models of both aircraft components and complete configurations.

5. CONCLUDING REMARKS

A research effort in the United States to develop the technology for a V/STOL or STOVL fighter aircraft in the post-1995 time period has been summarized in this paper. Emphasis has been on aerodynamic performance and airframe/propulsion integration research programs that have been conducted at the Ames Research Center, the NASA lead center for powered lift aircraft. The activities summarized are, in the most part, joint NASA, Navy, and Industry programs, which represent the major V/STOL fighter aircraft efforts in the U.S. The research activities include both small- and large-scale wind-tunnel programs.

An effort has been made to focus on aerodynamic uncertainties that are associated with configuration features resulting from the V/STOL requirement. Example uncertainties are those related to minimum drag, wave drag, high angle-of-attack characteristics, and power-induced effects. An observation from this extensive research effort is that a majority of the aerodynamic and airframe/propulsion uncertainties are configuration-dependent and must be explored by use of wind-tunnel models that are representative of actual configurations as contrasted to "generic" models. This has been the direction of both the small- and large-scale research efforts at Ames.

6. REFERENCES

1. Nelms, W. P., and Anderson, S. B., "V/STOL Concepts in the United States – Past, Present, and Future." AGARD-FDP-VKI Lecture Series No. 7 on V/STOL Aerodynamics, von Karman Institute, Belgium, May 14-18, 1984.

2. Nelms, W. P., "Studies of Aerodynamic Technology for VSTOL Fighter/Attack Aircraft." AIAA Paper 78-1511, August 1978.

3. Lummus, J. R., "Study of Aerodynamic Technology for VSTOL Fighter/Attack Aircraft." NASA CR-152128, 1978.

4. Burhans, W. R., Crafa, V. J., Dannenhoffer, N. F., Dellamura, F. A., and Krepski, R. E., "Study of Aerodynamic Technology for VSTOL Fighter/Attack Aircraft." NASA CR-152129, 1978.

5. Brown, S. H., "Study of Aerodynamic Technology for VSTOL Fighter/Attack Aircraft – Horizontal Attitude Concept." NASA CR-152130, 1978.

6. Gerhardt, H. A., and Chen, W. S., "Study of Aerodynamic Technology for VSTOL Fighter/Attack Aircraft – Vertical Attitude Concept." NASA CR-152131, 1978.

7. Driggers, H. H., "Study of Aerodynamic Technology for VSTOL Fighter/Attack Aircraft." NASA CR-152132, 1978.

8. Nelms, W. P., and Durston, D. A., "Concept Definition and Aerodynamic Technology Studies for Single Engine VSTOL Fighter/Attack Aircraft." AIAA Paper 81-2647, December 1981.

9. Foley, W. H., Sheridan, A. E., and Smith, C. W., "Study of Aerodynamic Technology for Single-Cruise-Engine VSTOL Fighter/Attack Aircraft." NASA CR-166268, 1982.

10. Foley, W. H., "An Integrated Aerodynamic/Propulsive Design for a STOVL Fighter/Attack Aircraft." ICAS-82-1.6.2, 1982.

11. Mark, L., "Study of Aerodynamic Technology for Single-Cruise-Engine VSTOL Fighter/Attack Aircraft." NASA CR-166270, 1982.

12. Hess, J. R., and Bear, R. L., "Study of Aerodynamic Technology for Single-Cruise-Engine VSTOL Fighter/Attack Aircraft." NASA CR-166269, 1982.

13. Driggers, H. H., "Study of Aerodynamic Technology for Single-Cruise-Engine VSTOL Fighter/Attack Aircraft." NASA CR-166271, 1982.

14. Nelms, W. P., and Durston, D. A., "Preliminary Aerodynamic Characteristics of Several Advanced VSTOL Fighter/Attack Aircraft Concepts." SAE Paper No. 801178, October 1980.

15. Nelms, W. P., Durston, D. A., and Lummus, J. R., "Experimental Aerodynamic Characteristics of two VSTOL Fighter/Attack Aircraft Configurations at Mach Numbers from 0.4 to 1.4." NASA TM-81234, December 1980.

16. Lummus, J. R., Joyce, G. T., and O'Malley, C. D., "Analysis of Wind Tunnel Tests Results for a 9.39% Scale Model of a VSTOL Fighter/Attack Aircraft." NASA CR-152391, Vols. 1-4, January 1981.

17. Lummus, J. R., "Aerodynamic Characteristics of a VSTOL Fighter Configuration." AIAA Paper 81-1292, 1981.

18. Nelms, W. P., Durston, D. A., and Lummus, J. R., "Experimental Aerodynamic Characteristics of Two VSTOL Fighter/Attack Aircraft Configurations at Mach Numbers from 1.6 to 2.0." NASA TM-81286, May 1981.

19. Durston, D. A., and Smith, S. C., "Lift Enhancing Surfaces on Several Advanced VSTOL Fighter/Attack Aircraft Concepts." AIAA Paper 81-1675, August 1981.

20. Moore, W. A., "Wind Tunnel Data Analysis of the Northrop Horizontal Attitude VSTOL Fighter Configuration for Mach Numbers from 0.4 to 1.4." NASA CR-166277, 1982.

21. Moore, W. A., "Wind Tunnel Data Analysis of the Northrop Vertical Attitude VSTOL Fighter Configuration for Mach Numbers from 0.4 to 1.4." NASA CR-166278, 1982.

22. Durston, D. A., and Schreiner, J. A., "High Angle of Attack Aerodynamics of a Strake-Canard-Wing V/STOL Fighter Configuration." AIAA Paper 83-2510, October 1983.

23. Axelson, J. A., "Estimation of Transonic Aircraft Aerodynamics to High Angles of Attack." J. Aircraft, Vol. 14, June 1977, pp. 553-559.

24. Axelson, J. A., "AEROX — Computer Program for Transonic Aircraft Aerodynamics to High Angles of Attack, Vols. I, II, III." NASA TM X-73,208, 1977.

25. Schnell, W. C., and Ordonez, G. W., "Axisymmetric and Non-Axisymmetric Exhaust Jet Induced-Effects on a VSTOL Vehicle Design, Part I — Data Presentation." NASA CR-166146, 1981.

26. Schnell, W. C., "Axisymmetric and Non-Axisymmetric Exhaust Jet Induced-Effects on a VSTOL Vehicle Design, Part II, Analysis of Results." NASA CR-166365, 1982.

27. Schnell, W. C., and Ordonez, G. W., "Axisymmetric and Non-Axisymmetric Exhaust Jet Induced Effects on a VSTOL Vehicle Design, Part III, Experimental Technique." NASA CR-166147, 1981.

28. Smeltzer, D. B., and Levin, A. D., "Test Results from a Jet-Effects VSTOL Fighter Model with Vectoring Non-Axisymmetric Nozzles." NASA TM-81210, June 1980.

29. Smeltzer, D. B., Nelms, W. P., and Williams, T. L., "Airframe Effects on a Top-Mounted Inlet System for VSTOL Fighter Aircraft." AIAA Paper 81-2631, December 1981.

30. Smeltzer, D. B., Nelms, W. P., and Williams, T. L., "Airframe Effects on a Top-Mounted Fighter Inlet System." AIAA Paper 81-2631R, J. of Aircraft, Vol. 19, No. 12, December 1982.

31. Williams, T. L., Hunt, B. L., Smeltzer, D. B., and Nelms, W. P., "Top-Mounted Inlet System Feasibility for Transonic-Supersonic Fighter Aircraft." AGARD Fluid Dynamics Panel Symposium, May 1981.

32. Williams, T. L., Nelms, W. P., and Smeltzer, D. B., "Top-Mounted Inlet System Feasibility for Transonic-Supersonic Fighter Aircraft." NASA TM-81292, April 1981.

33. Durston, D. A., and Smeltzer, D. B., "Inlet and Airframe Compatibility for a V/STOL Fighter/Attack Aircraft with Top-Mounted Inlets." NASA TM-84252, June 1982.

34. Durston, D. A., and Smeltzer, D. B., "Inlet and Airframe Compatibility for a V/STOL Fighter/Attack Aircraft with Top-Mounted Inlets." ICAS Paper 82-4.2.2, Proceedings from 13th Congress of the International Council of the Aeronautical Sciences and AIAA Aircraft Systems and Technology Conference, Vol. 2, August 1982.

35. Koenig, D. G., "V/STOL Wind Tunnel Testing." AGARD-FDP-VKI Lecture Series No. 7 on V/STOL Aerodynamics, von Karman Institute, Belgium, May 14-18, 1984.

36. Eigemann, M. F., and Bailey, R. O., "Development of the Propulsion Simulator — A Test Tool Applicable to VSTOL Configurations." SAE Paper No. 770984, November 1977.

37. Bailey, R. O., Harper, M., and Janetta, T., "Evaluation of Turbo-Propulsion Simulators as a Testing Technique for Fighter Aircraft." AIAA Paper 79-1149, June 1979.

38. Bailey, R. O., Mraz, M., and Hiley, P., "The Design of a Wind Tunnel VSTOL Fighter Model Incorporating a Turbine Powered Engine Simulator." AIAA Paper 81-2635, December 1981.

39. Harper, M., "The Propulsion Simulator Calibration Laboratory at Ames Research Center." AIAA Paper 82-0574, March 1982.

40. Smith, S. C., "Determining Compressor Inlet Airflow in the Compact Multimission Aircraft Propulsion Simulators in Wind Tunnel Applications." AIAA Paper 83-1231, June 1983.

41. Bailey, R. O., Smith, S. C., and Gustie, J. B., "Propulsion Simulation Test Technique for V/STOL Configurations." SAE Paper 83-1427, October 1983.

42. Whitten, P. D., "An Experimental Investigation of Vectored-Engine-Over-Wing Powered Lift Concept." AFFDL-TR-7692, 1978.

43. Bradley, R. G., Jeffries, R. R., and Capone, F. J., "A Vectored-Engine-Over-Wing Propulsive Lift Concept." AIAA Paper 76-917, September 1976.

44. Harris, M. J., and Falarski, M. D., "Static Calibration of a Two-Dimensional Wedge Nozzle with Thrust Vectoring and Spanwise Blowing." NASA TM-81161, 1980.

45. Falarski, M. D., Whitten, P. D., and Harris, M. J., "Aerodynamic Characteristics of a Large-Scale Model of a Highly Maneuverable Supersonic V/STOL Fighter: STOL Configuration." AIAA 80-0234, January 1980.

46. Howell, G. A., Crosthwait, E. L., and White, M. C., "Evaluation of Pressure and Thermal Data from a Wind Tunnel Test of a Large-Scale, Powered, STOL Fighter Model." NASA CR-166170, June 1981.

47. Falarski, M., Dudley, M., and Howell, G., "Analysis of Data From a Wind Tunnel Investigation of a Large-Scale Model of a Highly Maneuverable Supersonic V/STOL Fighter: STOL Configuration." AIAA Paper 81-2620, December 1981.

48. Stoll, F., and Minter, E., "Large-Scale Wind Tunnel Tests of a Sting-Supported V/STOL Fighter Model at High Angles of Attack." AIAA Paper 81-2621, 1981.

49. Minter, E. A., and Yates, R. W., "Wind Tunnel Test of a 0.4-Scale Fighter Model at High Angles of Attack — Analysis of Pressure Data." NASA CR-166198, 1981.

50. Stoll, F., and Koenig, D. G., "Low Speed Wind Tunnel Measurements of a Canard Controlled Fighter Model Through High Angles of Attack." NASA TM-84403, 1983.

51. Stoll, F., and Koenig, D. G., "Large-Scale Wind-Tunnel Investigation of a Close-Coupled Canard-Delta-Wing Fighter Model Through High Angles of Attack." AIAA Paper 83-2554, October 1983.

52. Koenig, D., Stoll, F., and Aoyagi, K., "Application of Thrusting Ejectors to Tactical Aircraft Having Vertical Lift and Short-Field Capability." AIAA Paper 81-2629, December 1981.

53. Whittley, D. C., and Koenig, D. G., "Large Scale Model Tests of a New Technology V/STOL Concept." AIAA Paper 80-0233, 1980.

54. Garland, D. B., and Whittley, D. C., "Phase I and Wind Tunnel Tests of the J-97 Powered, External Augmentor V/STOL Model." NASA CR-152255, 1980.

55. Garland, D. B., and Harris, J. L., "Phase 2 and 3 Wind Tunnel Tests of the J-97 Powered, External Augmentor V/STOL Model." NASA CR-152380, 1980.

56. Alperin, Morton, and Wu, J. J., "Recent Development of a Jet Diffuser Ejector." AIAA Paper 80-0231, 1980.

57. Alperin, Morton, and Wu, J. J., "A Jet-Diffuser Ejector for a V/STOL Fighter." NASA CR-166161, 1981.

7. ACKNOWLEDGMENTS

The author wishes to acknowledge the contributions to this paper provided by Don Durston and Dave Koenig of the NASA Ames Research Center, and to the various Industry personnel involved in the contracted study activities.

TABLE 1. GEOMETRY OF GENERAL DYNAMICS E2O5 MODEL

Property	Wing	Horizontal canard (midposition)	Vertical tail
Airfoil			
Root	NACA 64A204	NACA 64A005	5.3% biconvex
Tip	NACA 64A204	NACA 64A003	4.0% biconvex
MAC, m (in.)	0.340 (13.40)	0.183 (7.20)	0.184 (7.26)
Aspect ratio	3.62	1.08[a]	1.27
Taper ratio	0.190	0.37	0.43
Root chord, m (in.)	0.495 (19.51)	0.249 (9.82)	0.245 (9.64)
Tip chord, m (in.)	0.094 (3.71)	0.092 (3.63)	0.105 (4.14)
Span, m (in.)	1.067 (42.01)	0.184 (7.26)[a]	0.222 (8.75)
Dihedral, deg	0	0	---
Incidence, deg	0	---	---
Twist (positive LE up at tip), deg	0	0	0
Hinge line			
B.L., m (in.)	---	0.228 (9.00)	0
F.S., m (in.) (coincident with 0.25 MAC)	---	0.620 (24.41)	1.252 (49.30)
W.L., m (in.)	---	0.396 (15.59)	0.403 (15.87)
Hinge-line sweep, deg	---	1.8	0
Leading-edge sweep, deg	40	45	47.5
Exposed area, m^2 (ft^2)	0.128 (1.374)	0.029 (0.308)[a]	0.039 (0.419)

Wing to centerline ref. area: 0.315 m^2 (3.39 ft^2)
Total planform ref. area: 0.671 m^2 (7.22 ft^2)
Body length: 153 m (60.10 in.)

[a]One panel.

Table 2. GEOMETRY OF NORTHROP HATOL MODEL

Property	Wing	Horizontal canard	Vertical tail
Airfoil			
Root	NACA 65A204	NACA 64A004	NACA 64A004
Tip	NACA 64A204	NACA 64A004	NACA 65A004
MAC, m (in.)	0.516 (20.33)	0.176 (6.91)	0.141 (5.56)
Aspect ratio	2.12	0.77[a]	1.31[a]
Taper ratio	0.18	0.27	0.31
Root chord, m (in.)	0.754 (29.68)	0.248 (9.79)	0.198 (7.79)
Tip chord, m (in.)	0.136 (5.34)	0.068 (2.66)	0.060 (2.38)
Span, m (in.)	0.943 (37.14)	0.122 (4.79)[a]	0.169 (6.65)
Dihedral, deg	-3	5	---
Incidence, deg	-0	---	---
Twist (positive LE up at tip), deg	-6	0	0
Hinge line			
B.L., m (in.)	---	0.128 (5.05)	0.163 (6.42)
F.S., m (in.) (coincident with 0.25 MAC)	---	0.654 (25.75)	1.42 (55.82)
W.L., m (in.)	---	0.053 (2.08)	0.061 (2.40)
Hinge-line sweep, deg	---	0	0
Leading-edge sweep, deg	50	60	42.5
Exposed area, m^2 (ft^2)	0.269 (2.90)	0.019 (0.206)[a]	0.022 (0.235)[a]

Wing to centerline ref. area: 0.419 m^2 (4.51 ft^2)
Total planform ref. area: 0.573 m^2 (6.17 ft^2)
Body length: 1.52 m (59.84 in.)

[a]One panel.

TABLE 3. GEOMETRY OF NORTHROP VATOL MODEL

Property	Wing	Vertical tail
Airfoil		
Root	NACA 65A204	NACA 65A004
Tip	NACA 64A204	NACA 64A004
MAC, m (in.)	0.516 (20.33)	0.155 (6.12)
Aspect ratio	2.12	1.10
Taper ratio	0.18	0.34
Root chord, m (in.)	0.754 (29.68)	0.215 (8.46)
Tip chord, m (in.)	0.136 (5.34)	0.072 (2.85)
Span, m (in.)	0.943 (37.14)	0.158 (6.22)
Dihedral, deg	-3	---
Incidence, deg	-0	---
Twist (positive LE up at tip), deg	-6	0
Hinge line		
B.L., m (in.)	---	0
F.S., m (in.) (coincident with 0.25 MAC)	---	1.273 (50.11)
W.L., m (in.)	---	0.054 (2.12)
Hinge-line sweep, deg	---	2.5
Leading-edge sweep, deg	50	50
Exposed area, m^2 (ft^2)	0.294 (3.16)	0.023 (0.244)

Wing to centerline ref. area: 0.419 m^2 (4.51 ft^2)
Total planform ref. area: 0.545 m^2 (5.87 ft^2)
Body length: 1.50 m (58.91 in.)

TABLE 4. GEOMETRY OF GENERAL DYNAMICS E7 MODEL

Property	Wing	Vertical tail
Airfoil		
Root	NACA 0004-63 (optimum supersonic camber — CL = 0.2 @ M = 1.6, C.P. @ 0.511 MAC)	5.3% biconvex
Tip	NACA 0004-63	3.0% biconvex
MAC, m (in.)	0.7978 (31.409)	0.2315 (9.116)
Aspect ratio	1.665	1.294
Taper ratio	0.115	0.437
Root chord, m (in.)	1.1827 (46.564)	0.3066 (12.069)
Tip chord, m (in.)	0.1357 (5.342)	0.1341 (5.278)
Span, m (in.)	1.0973 (43.200)	0.2850 (11.222)
Dihedral, deg	0	---
Incidence, deg	0	---
Twist (positive LE up at tip), deg	-5.7	---
Leading-edge sweep, deg	60	47.5
Trailing-edge sweep, deg	-10	25.9

Wing to centerline reference area: 0.7233 m^2 (7.786 ft^2)
Body length: 1.579 m (62.718 in.)

TABLE 5. GEOMETRY OF McDONNELL DOUGLAS 279-3 MODEL

Property	Wing (theoretical)	Canard (exposed)	Horizontal tail (exposed)	Vertical tail
Airfoil				
Root	64AX06.2 MOD	64A008	64A008	64A005
Tip	64AX04 MOD	64A003	64A003	64A003
MAC, m (in.)	0.3751 (14.768)	0.1678 (6.607)	0.1678 (6.607)	0.2223 (8.753)
Aspect ratio	3.00	3.00	3.00	1.20
Taper ratio	0.25	0.25	0.25	0.35
Root chord, m (in.)	0.5361 (21.108)	0.2397 (9.438)	0.2397 (9.438)	0.3057 (12.037)
Tip chord, m (in.)	0.1340 (5.277)	0.0599 (2.359)	0.0599 (2.359)	0.1070 (4.214)
Span, m (in.)	1.0049 (39.564)	0.4493 (17.688)	0.4493 (17.688)	0.2478 (9.756)
Dihedral, deg	-9	0	0	---
Incidence, deg	0	0	0	---
Twist (positive LE up at tip), deg	-4	0	0	---
Hinge line				
B.L., m (in.)	---	0.1072 (4.220)	0.0386 (1.520)	---
F.S., m (in.) (coincident with 0.25 MAC)	---	0.4984 (19.624)	1.3642 (53.708)	---
W.L., m (in.)	---	0.2734 (10.764)	0.2464 (9.700)	---
Hinge line sweep, deg	---	0	0	---
Leading-edge sweep, deg	45	50	50	45
Trailing-edge sweep, deg	11.3 (avg.)	21.4	21.4	11.2
Exposed area, m^2 (ft^2)	---	0.0674 (0.725)	0.0674 (0.725)	0.0511 (0.550)

Wing to centerline reference area: 0.3369 m^2 (3.626 ft^2)
Body length: 1.5486 m (60.968 in.)

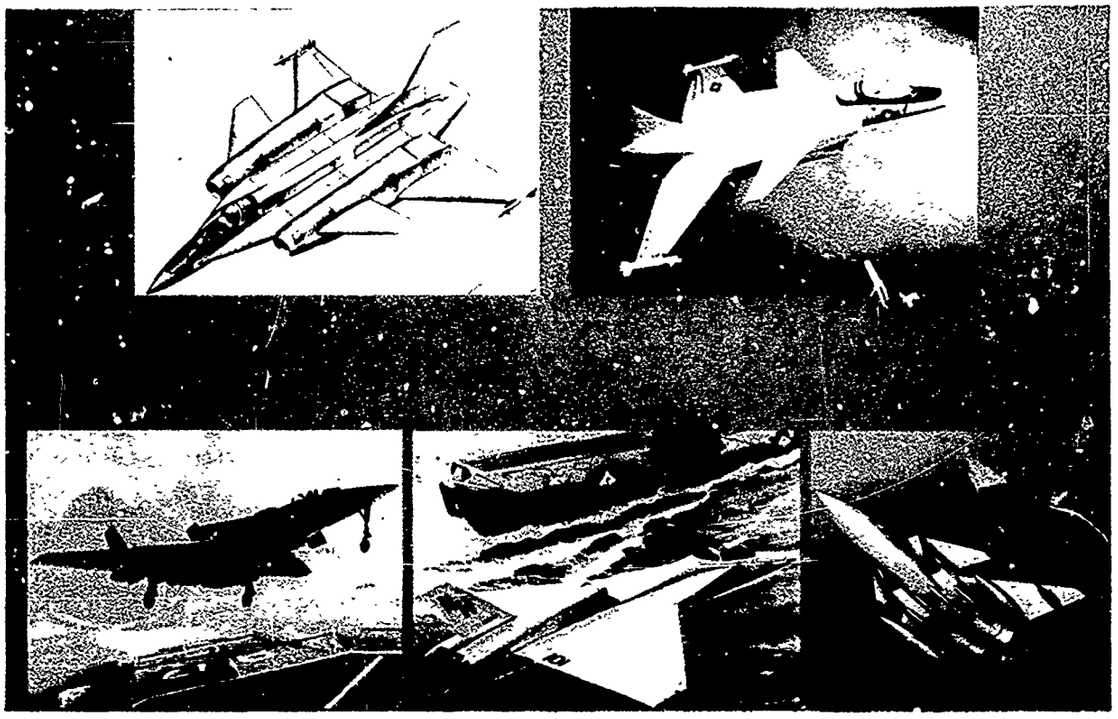

Figure 1. Twin-engine V/STOL fighter concepts.

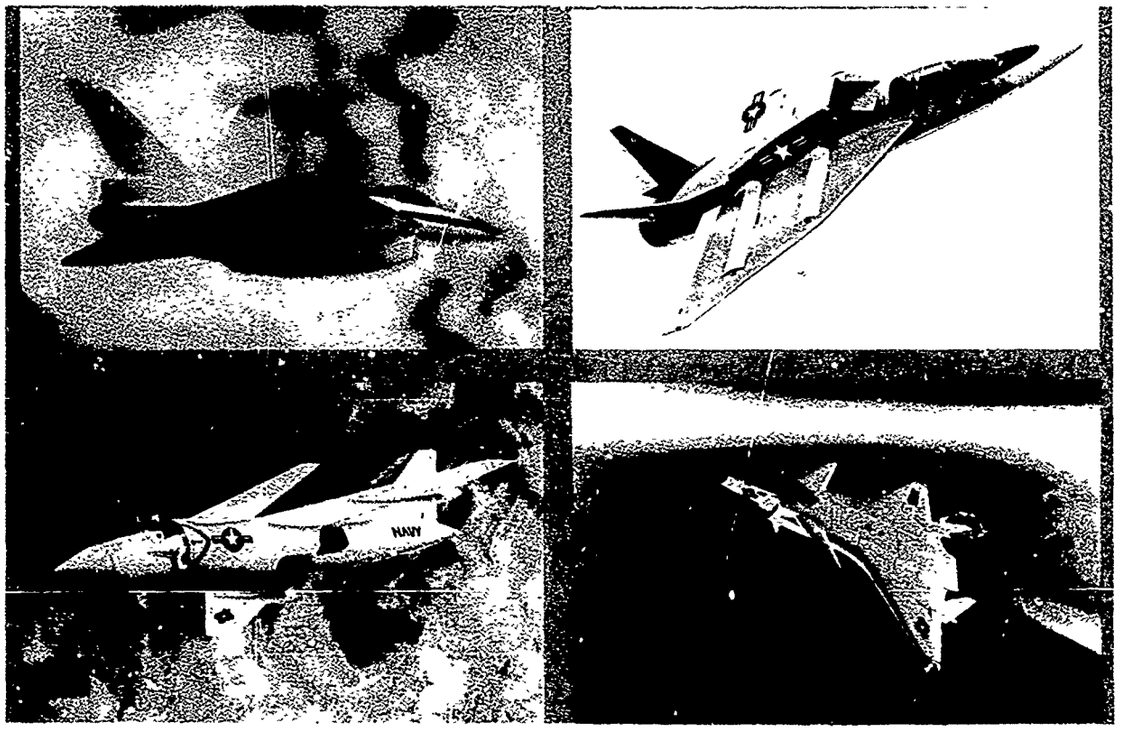

Figure 2. Single-engine V/STOL and STOVL fighter concepts.

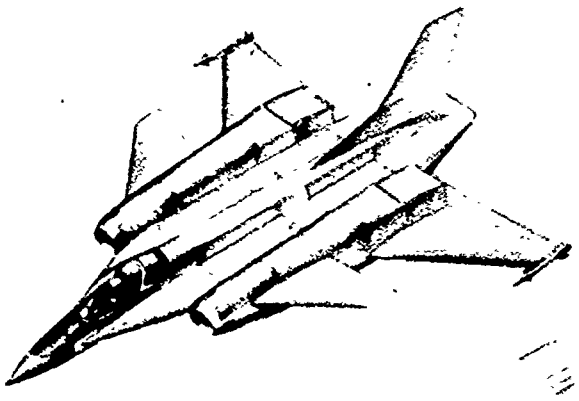

AERODYNAMIC UNCERTAINTIES

- MINIMUM DRAG
- A.C. LOCATION
- $C_{L_{max}}$ USABLE
- BUFFET ONSET
- LATERAL/DIRECTIONAL CHARACTERISTICS
- SUPERCIRCULATION
- WIDE-BODY CONFIGURATION AERODYNAMICS

Figure 3. Aerodynamic uncertainties of General Dynamics twin-engine concept.

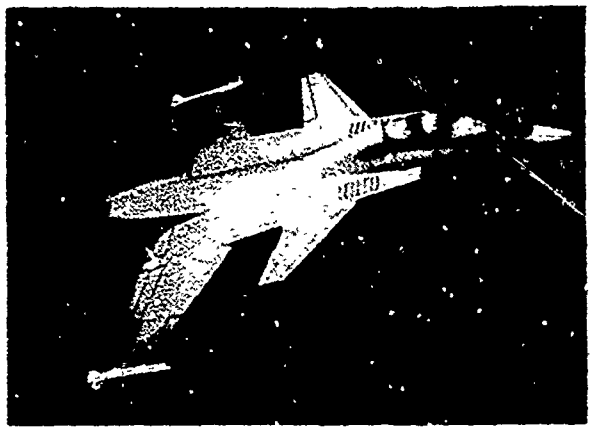

AERODYNAMIC UNCERTAINTIES

- SUPERCRITICAL, MULTI-ELEMENT WING AERODYNAMICS
- MINIMUM DRAG
- BUFFET ONSET
- WIDE-BODY CONFIGURATION AERODYNAMICS
- WING/CANARD INTERACTIONS
- HIGH α CHARACTERISTICS
- THRUST VECTORING/SUPERCIRCULATION

Figure 4. Aerodynamic uncertainties of Grumman twin-engine concept.

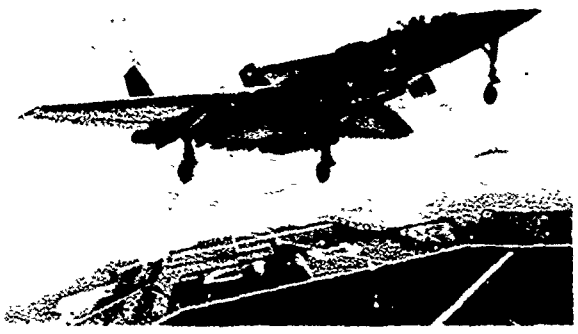

AERODYNAMIC UNCERTAINTIES

- MINIMUM DRAG
- CANARD EFFECT ON STABILITY AND A.C. LOCATION
- CANARD/WING FLAP COMBINATION FOR MINIMUM C_{D_L}
- CANARD EFFECT ON DIRECTIONAL CHARACTERISTICS
- TWIN AFTERBODY DRAG
- VECTORED THRUST FOR MANEUVER

Figure 5. Aerodynamic uncertainties of Northrop HATOL twin-engine concept.

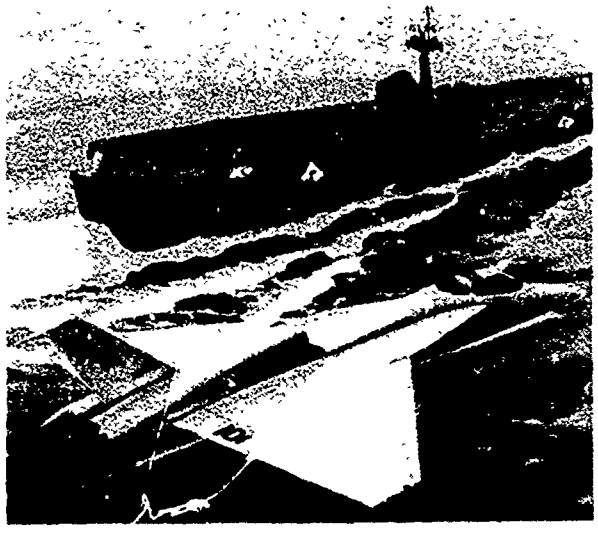

AERODYNAMIC UNCERTAINTIES

- MINIMUM DRAG
- LEX EFFECT AT HIGH α
- A.C. TRAVEL
- MANEUVER FLAPS FOR DRAG IMPROVEMENT AT $M > 1$
- TOP INLETS
- BUFFET ONSET
- INLET SPILLAGE EFFECTS

Figure 6. Aerodynamic uncertainties of Northrop VATOL twin-engine concept.

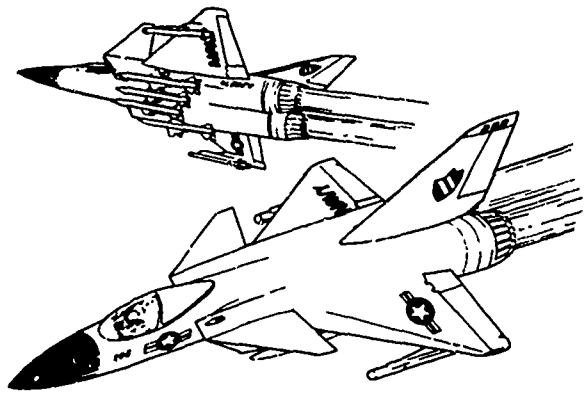

AERODYNAMIC UNCERTAINTIES

- TRANSITION AERODYNAMICS
- MINIMUM DRAG AND DRAG RISE
- VARIABLE CAMBER WING
- BUFFET ONSET
- WING/CANARD INTERACTIONS
- INLETS AT EXTREME α AND β

Figure 7. Aerodynamic uncertainties of Vought twin-engine concept.

AERODYNAMIC UNCERTAINTIES

- LATERAL/DIRECTIONAL CHARACTERISTICS
- WING CAMBER RESTRICTED BY EJECTOR
- WING PLANFORM EFFECTS
- AERODYNAMIC/EJECTOR INTERACTIONS
- TAILLESS CONFIGURATION AERODYNAMICS
- 2-D NOZZLE/FUSELAGE INTEGRATION
- MINIMUM DRAG

Figure 8. Aerodynamic uncertainties of General Dynamics single-engine concept.

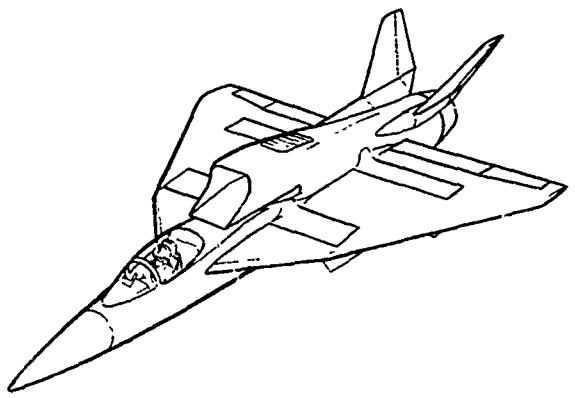

AERODYNAMIC UNCERTAINTIES

- MINIMUM DRAG
- DRAG DUE TO LIFT
- WING PLANFORM EFFECTS
- DRAG OF BLUNT WING TRAILING EDGES
- HIGH ANGLE-OF-ATTACK AERODYNAMICS
- TOP INLET
- WING-TIP MOUNTED VERTICAL TAILS

Figure 9. Aerodynamic uncertainties of Rockwell single-engine concept.

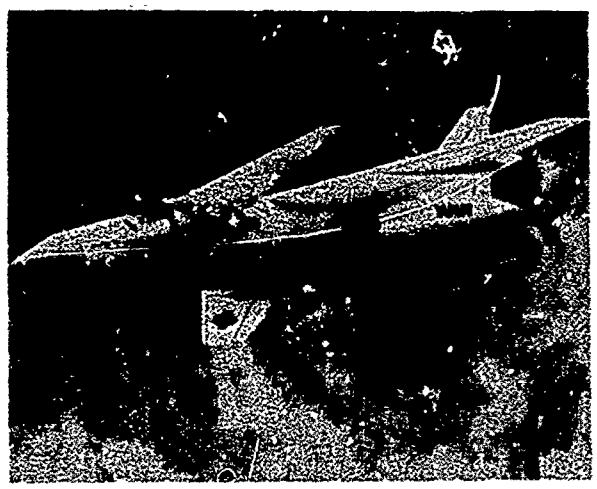

AERODYNAMIC UNCERTAINTIES

- CLOSE-COUPLED CANARD EFFECTS ON:
  - LATERAL/DIRECTIONAL CHARACTERISTICS
  - C_L AND Cm AT HIGH α
  - LONGITUDINAL STABILITY
- LARGE HALF-AXISYMMETRIC INLETS
- FORWARD LOCATION OF ENGINE
- MINIMUM DRAG
- PROPULSIVE FLOW EFFECTS ON AERODYNAMICS
- PREDICTION OF CANARD EFFECTS

Figure 10. Aerodynamic uncertainties of McDonnell-Douglas single-engine concept.

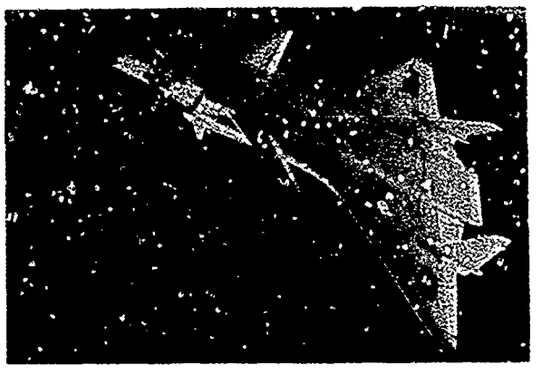

AERODYNAMIC UNCERTAINTIES

- STRAKE AND CANARD EFFECTS
- BLENDED WING BODY AERODYNAMICS
- MINIMUM DRAG
- LATERAL/DIRECTIONAL CHARACTERISTICS
- MULTIPLE CONTROL EFFECTIVENESS
- FORWARD TWO-AXES CONTROL SURFACE
- AERODYNAMIC PREDICTION METHODS

Figure 11. Aerodynamic uncertainties of Vought single-engine concept.

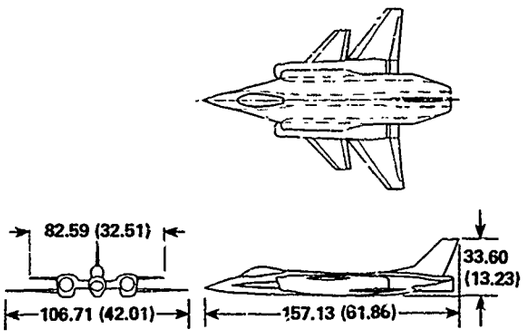

Figure 12. Wind-tunnel model of General Dynamics E205 configuration.

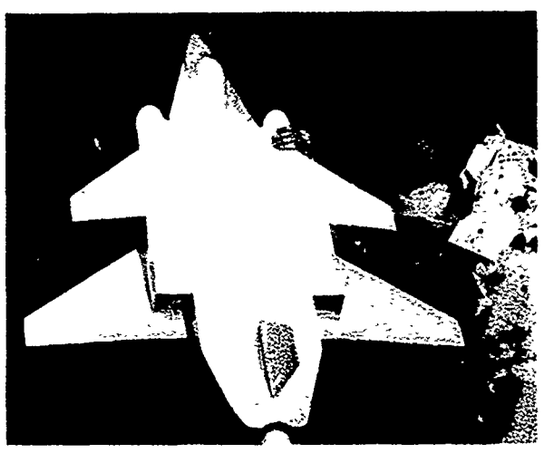

(a)

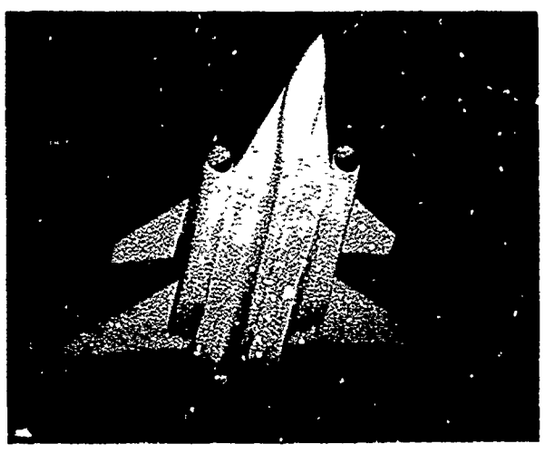

(b)

Figure 13. Model of General Dynamics E205 configuration in Ames 12-Foot Wind Tunnel.

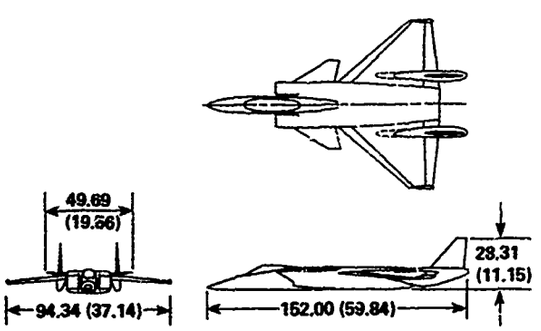

Figure 14. Wind-tunnel model of Northrop HATOL configuration.

(a)

(b)

Figure 15. Model of Northrop HATOL configuration in Ames 11-Foot Wind Tunnel.

(a)

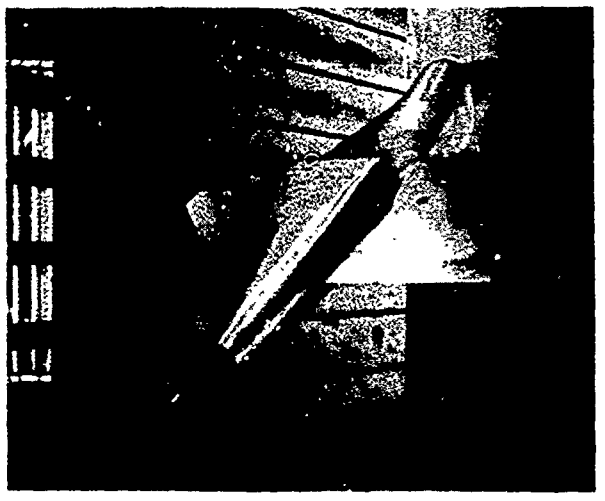

(b)

Figure 17. Model of Northrop VATOL configuration in Ames 11-Foot Wind Tunnel.

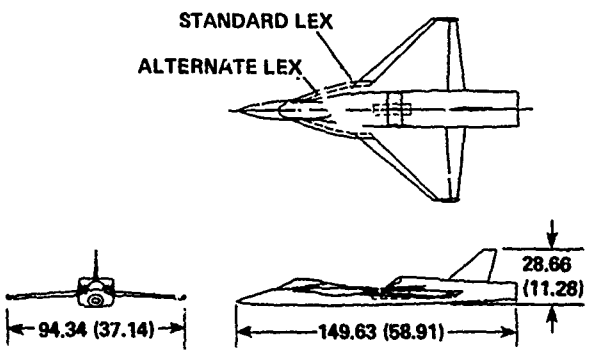

Figure 16. Wind-tunnel model of Northrop VATOL configuration.

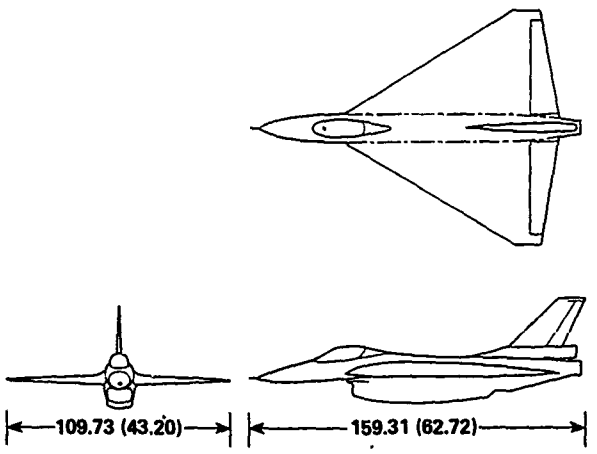

Figure 18. Wind-tunnel model of General Dynamics E7 configuration.

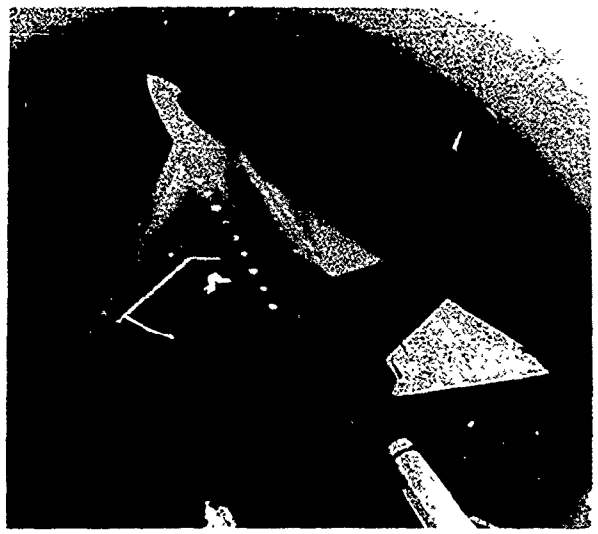

(a)

(b)

Figure 19. Model of General Dynamics E7 configuration in Ames 12-Foot Wind Tunnel.

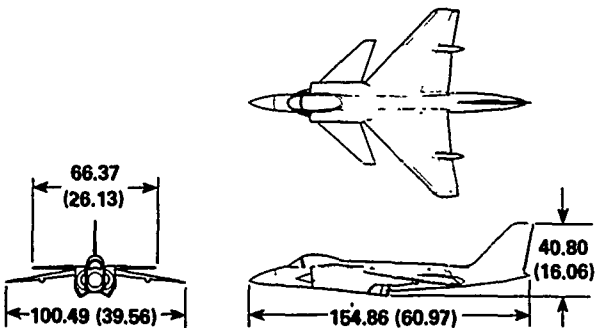

Figure 20. Wind-tunnel model of McAir 279 configuration.

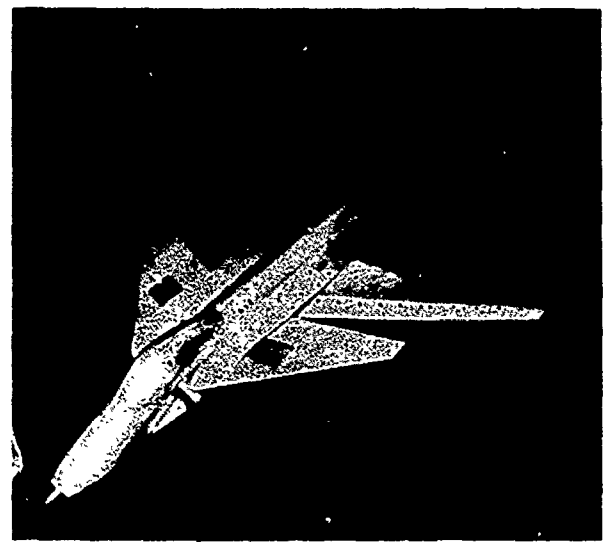

Figure 21. Model of the McAir 279 deflected thrust concept (flow-through configuration).

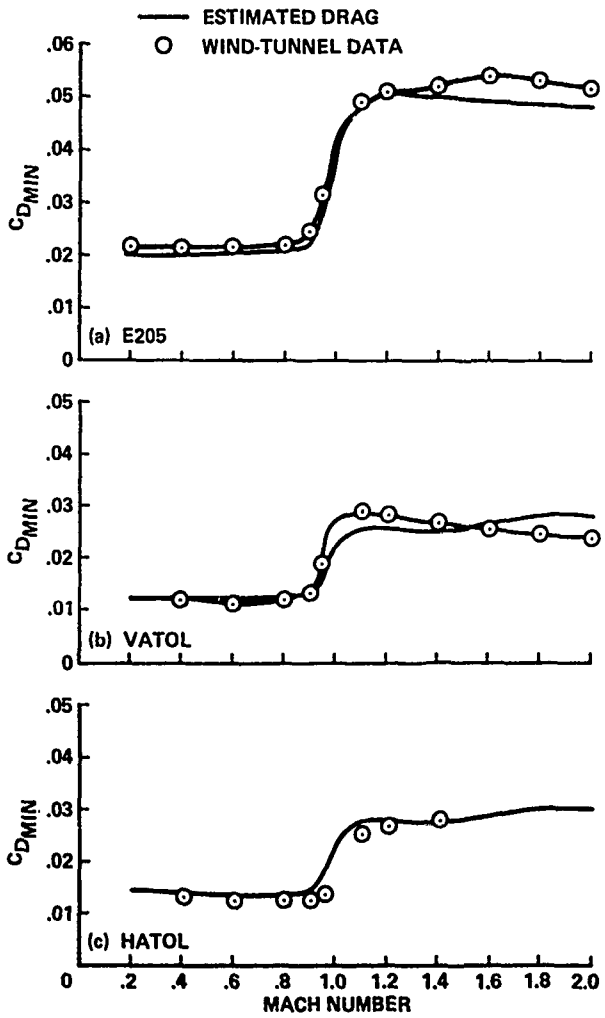

Figure 22. Minimum drag coefficients for the three twin-engine models based on wing reference area.

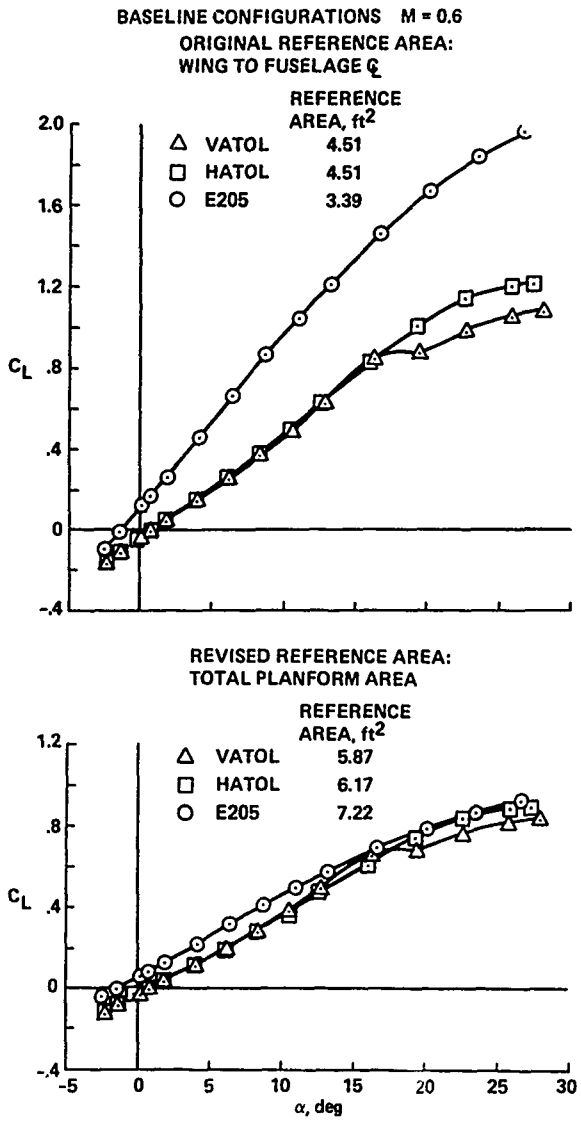

Figure 23. Reference area effects.

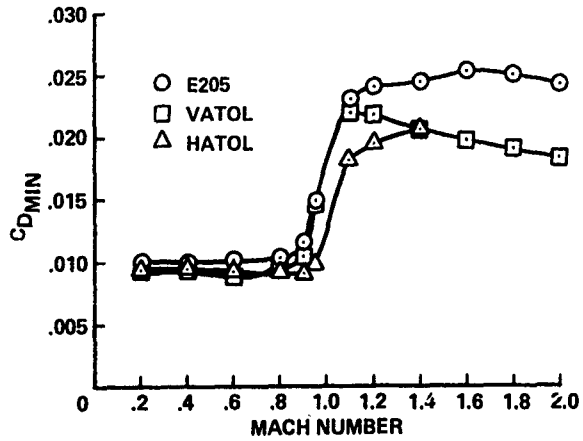

Figure 24. Minimum drag coefficients for the three twin-engine models based on total planform area.

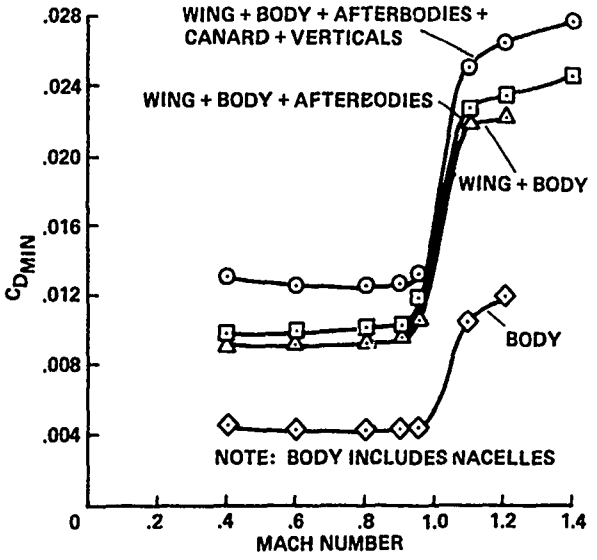

Figure 25. Minimum drag component buildup for the Northrop HATOL model.

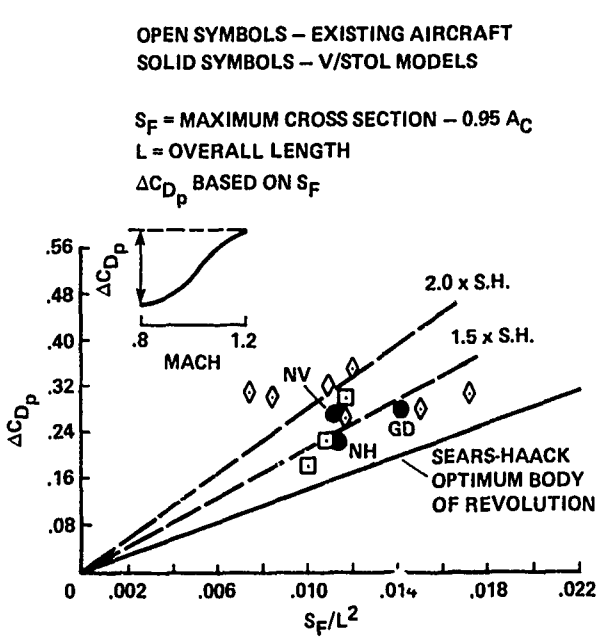

Figure 26. Wave drag comparison.

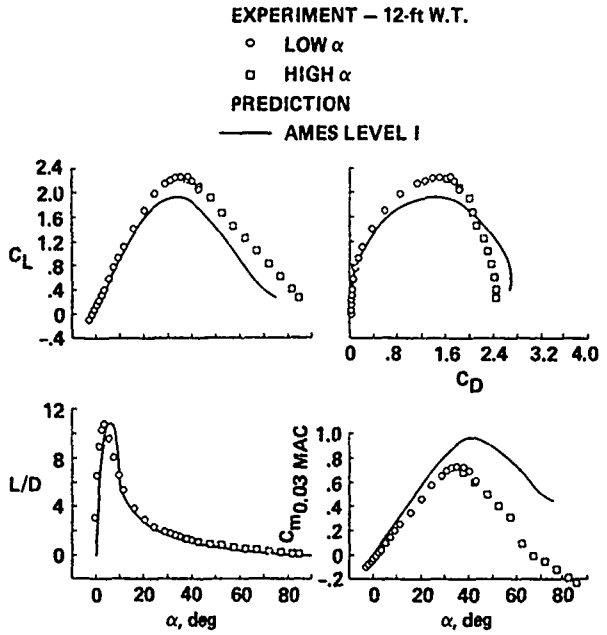

Figure 27. High angle-of-attack characteristics of the E205 model; M = 0.2.

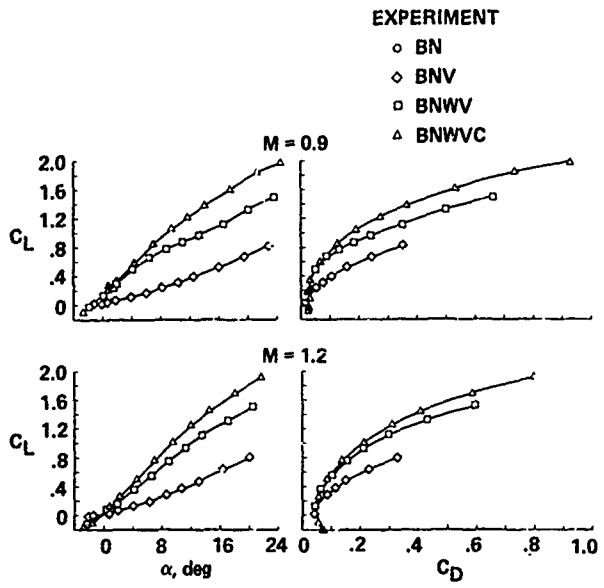

Figure 28. Component buildup for the E205 model.

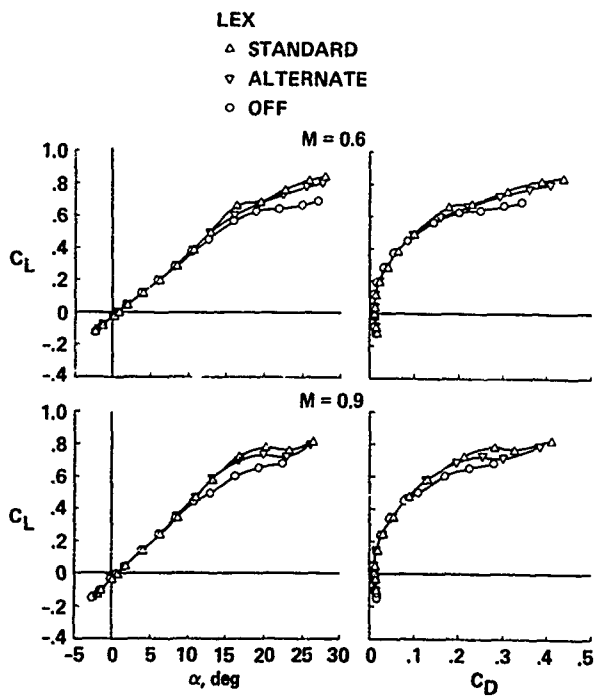

Figure 29. Effect of LEX size on VATOL model; based on total planform area.

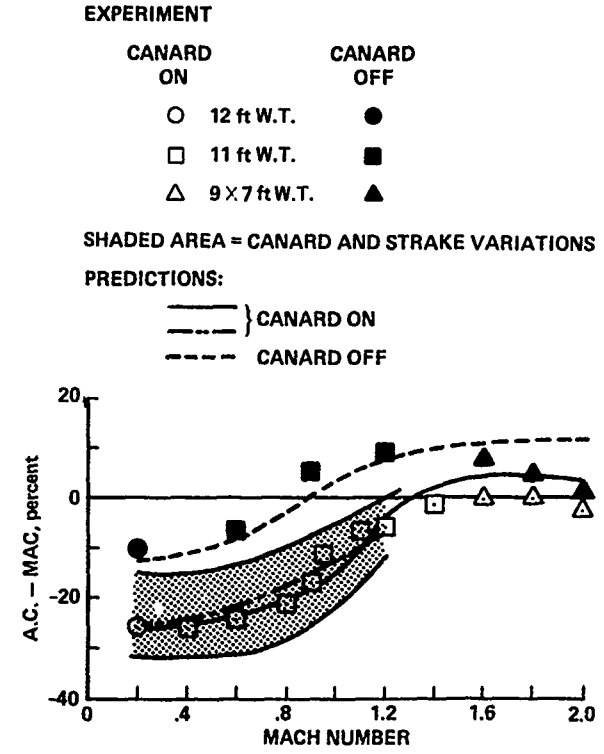

Figure 30. Aerodynamic center location for the Z205 model.

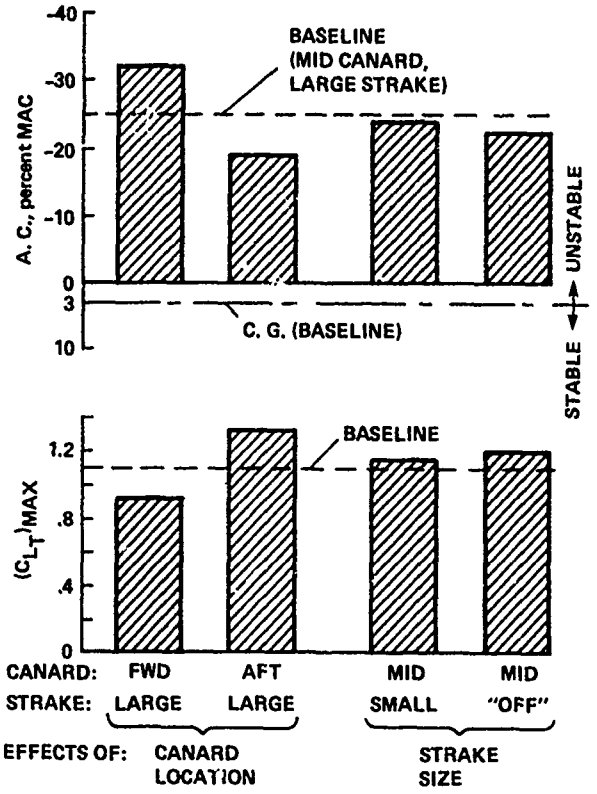

Figure 31. Effects of canard and strake variations on stability and maximum trimmed lift for the E205 model.

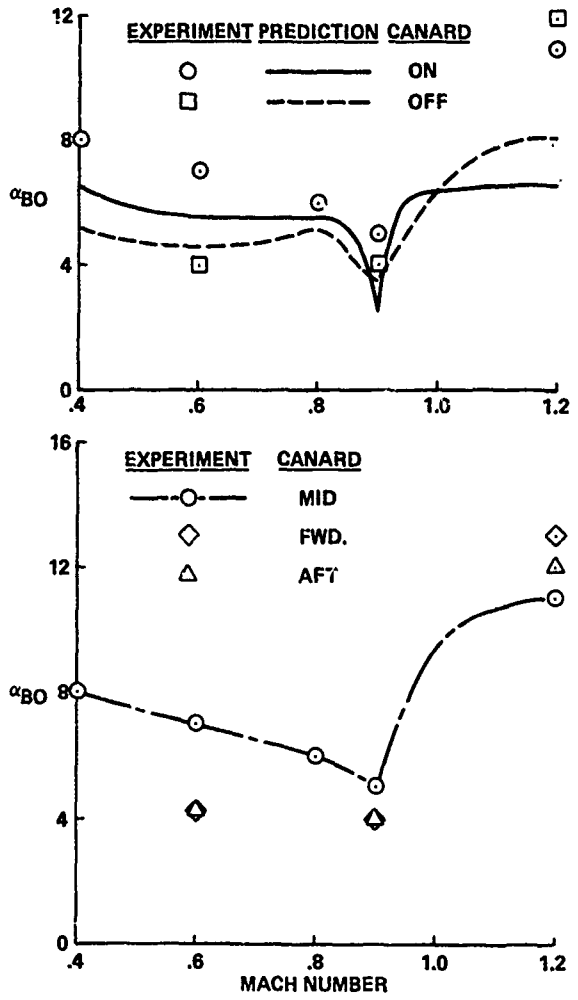

Figure 32. Buffet-onset angle of attack for the E205 model.

Figure 33. Grumman 623 model installed in the Ames 11-Foot Wind Tunnel.

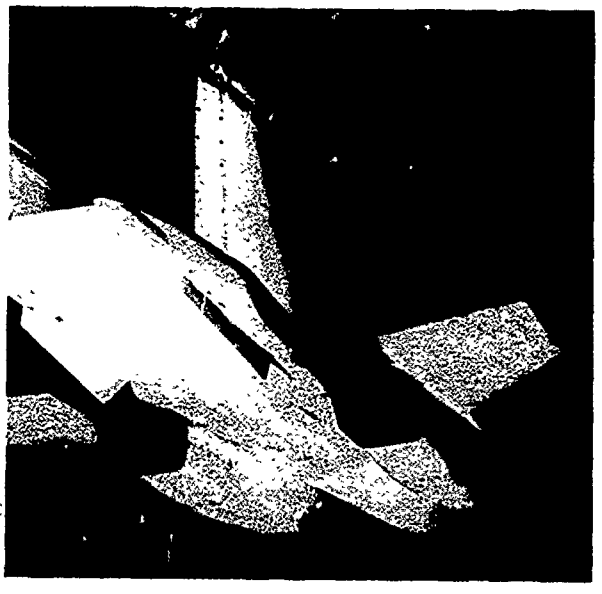

Figure 34. ADEN nozzles on the 623 model.

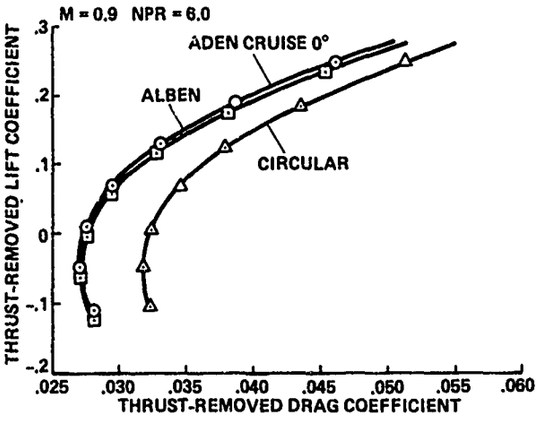

Figure 35. ADEN, ALBEN, and circular nozzle thrust-removed polar comparison.

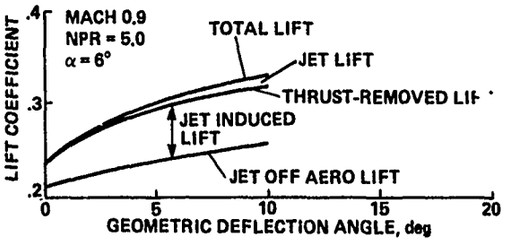

Figure 36. ADEN cruise lift component buildup.

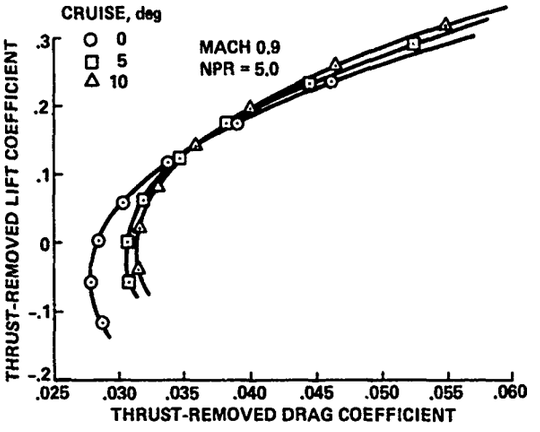

Figure 37. Effect of ADEN cruise vectoring.

(a) (b)

Figure 38. Northrop VATOL top inlet model in Ames 11-Foot Wind Tunnel.

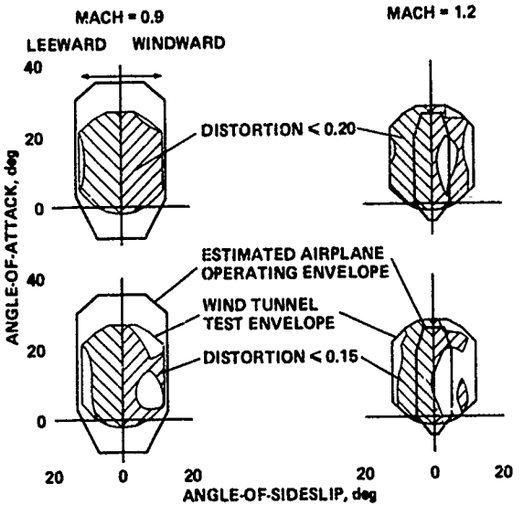

Figure 39. Distortion-limited operating envelopes for the VATOL configuration.

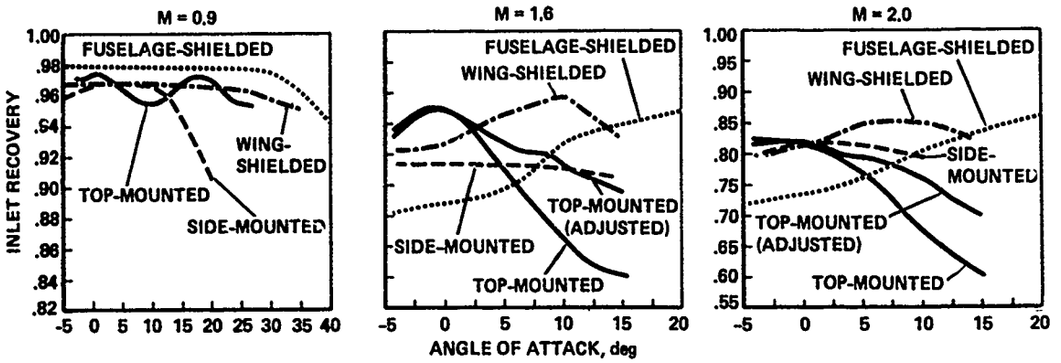

Figure 40. Comparison of inlet recoveries for the top and conventional inlet installations.

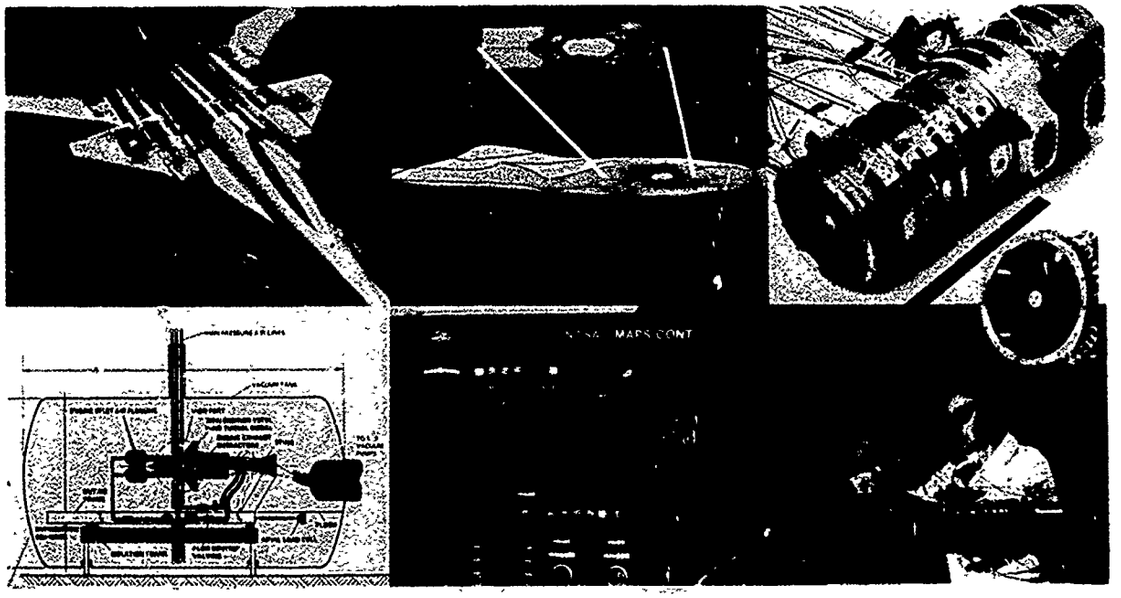

Figure 41. Elements of the propulsion simulator research program.

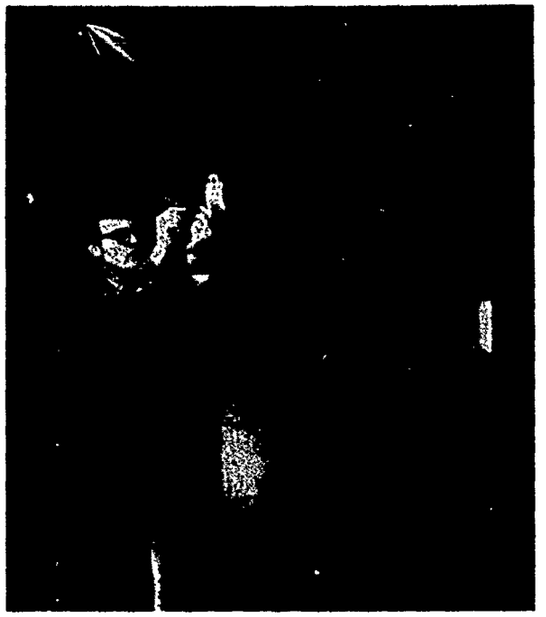

Figure 42. CMAPS model in Ames 11-Foot Wind Tunnel.

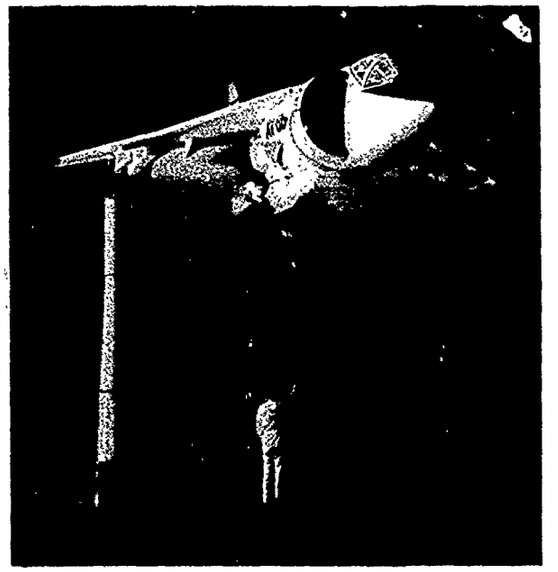

Figure 45. AV-8B in Ames 40- by 80-Foot Wind Tunnel.

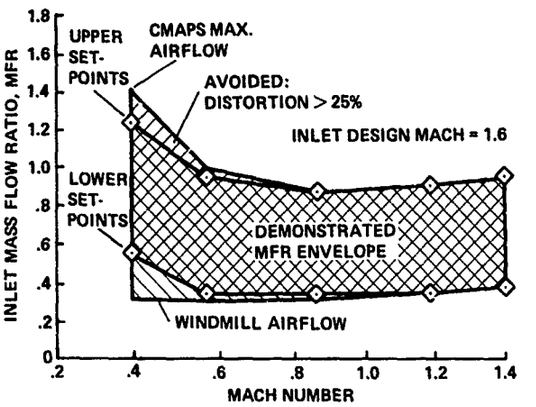

Figure 43. Demonstrated inlet mass flow ratio envelope.

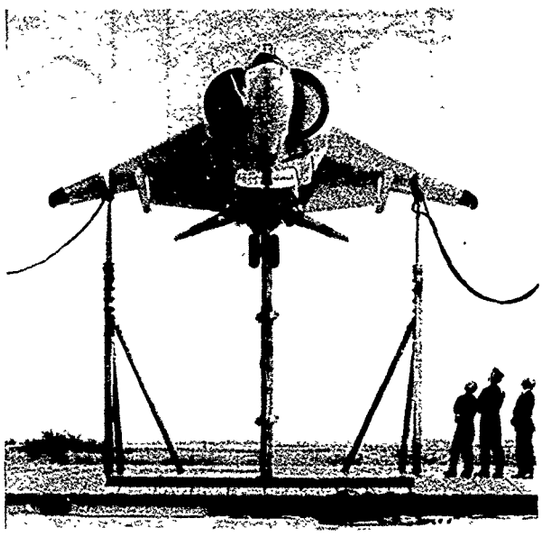

Figure 46. AV-8B on Ames Outdoor Aerodynamic Research Facility.

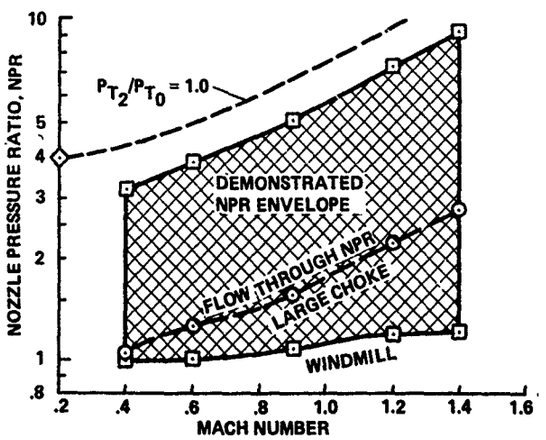

Figure 44. Demonstrated nozzle pressure ratio envelope.

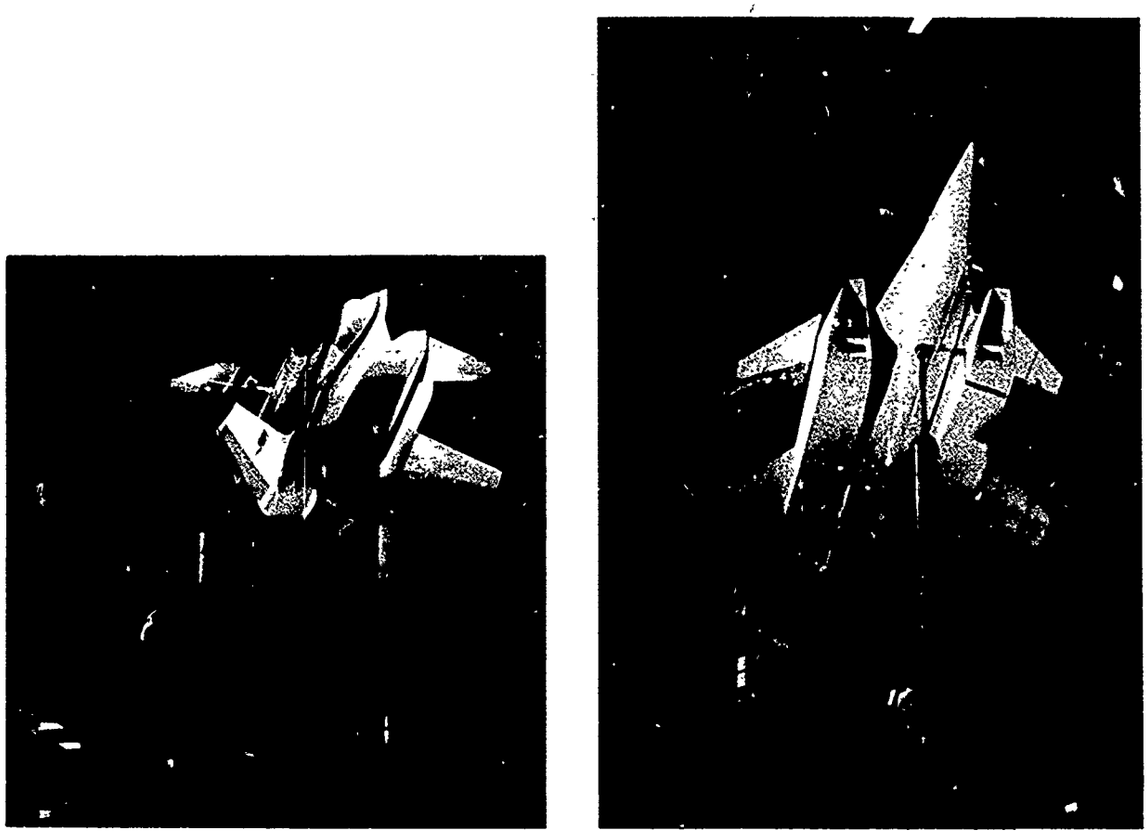

(a) (b)

Figure 47. Twin-engine V/STOL fighter model in Ames 40- by 80-Foot Wind Tunnel.

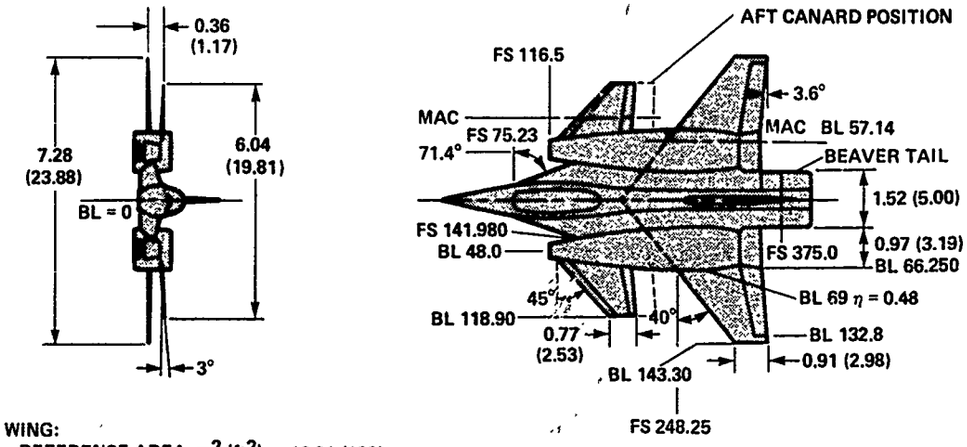

WING:	
REFERENCE AREA, m^2 (ft^2)	16.91 (182)
ASPECT RATIO	3.13
TAPER RATIO	0.243
AIRFOIL SECTION	64A204
GEOMETRIC TWIST	4°
MEAN AERO CHORD, m (ft)	2.61 (8.56)
CANARD:	
AREA, m^2 (ft^2)	3.53 (37.98)
CANARD AREA/WING AREA	0.208
ASPECT RATIO	2.07
TAPER RATIO	0.419
AIRFOIL SECTION	64A004
MEAN AERO CHORD, m (ft)	1.38 (4.52)

ALL DIMENSIONS IN m (ft)

Figure 48. Twin-engine V/STOL fighter model geometry.

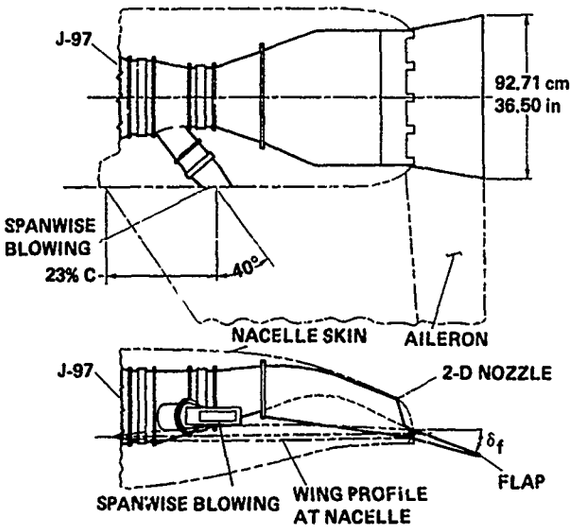

Figure 49. Twin-engine fighter model nozzle geometry.

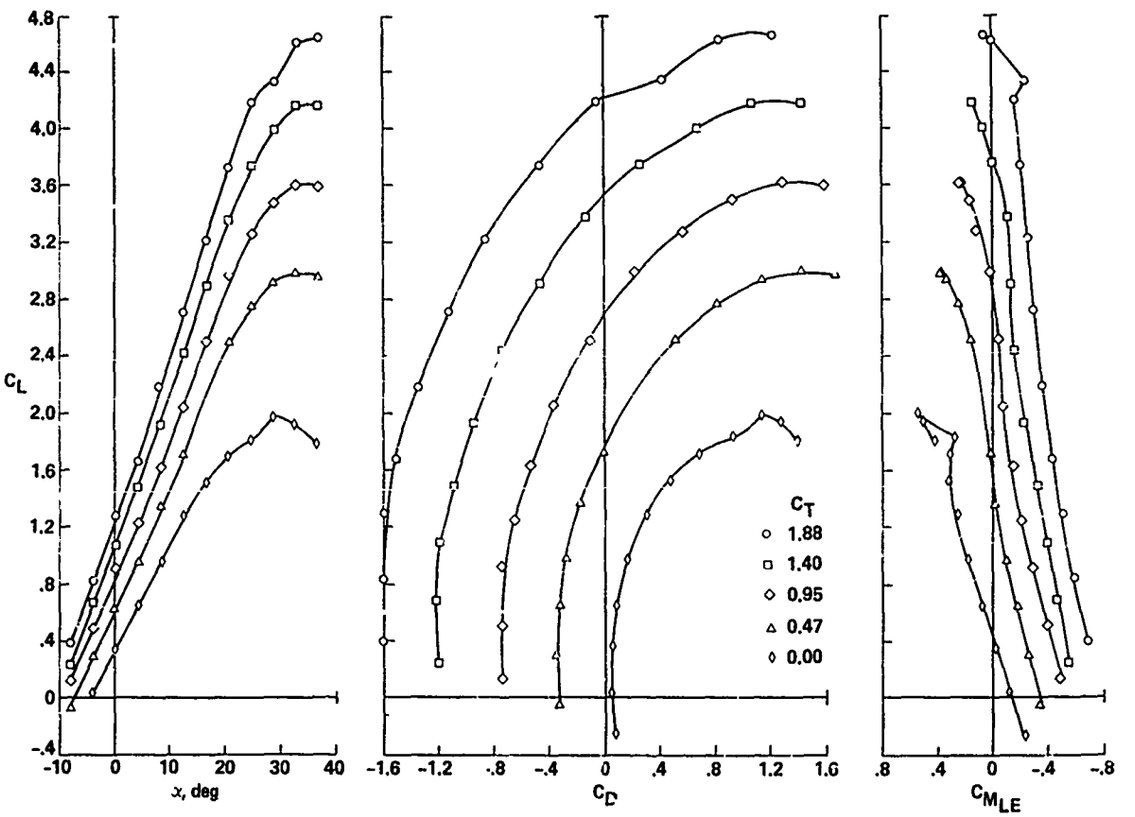

Figure 50. Longitudinal characteristics of the twin-engine fighter model with USB and SWB.

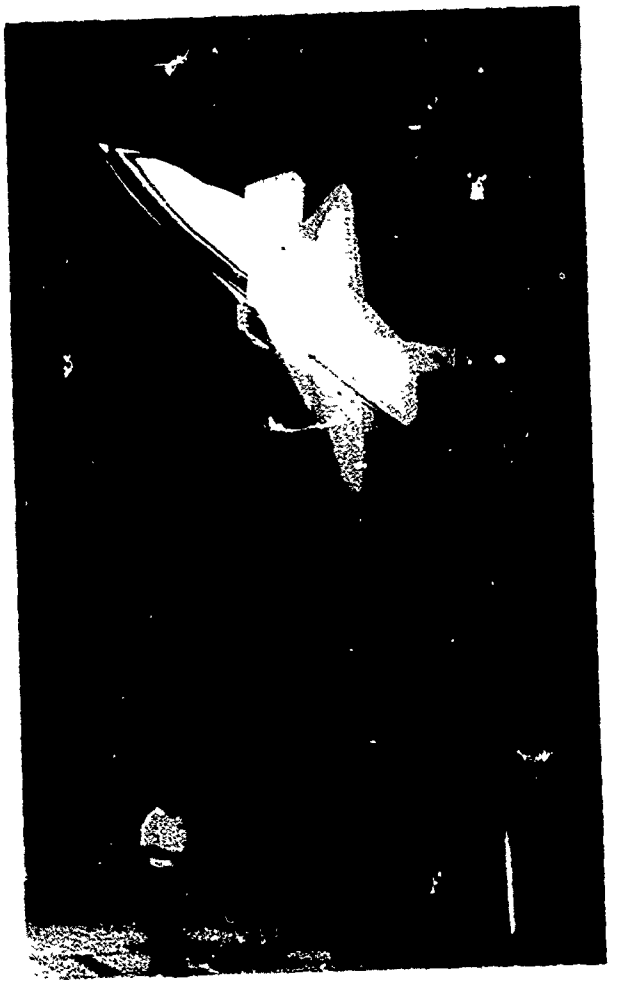

Figure 51. High angle-of-attack installation in the Ames 40- by 80-Foot Wind Tunnel.

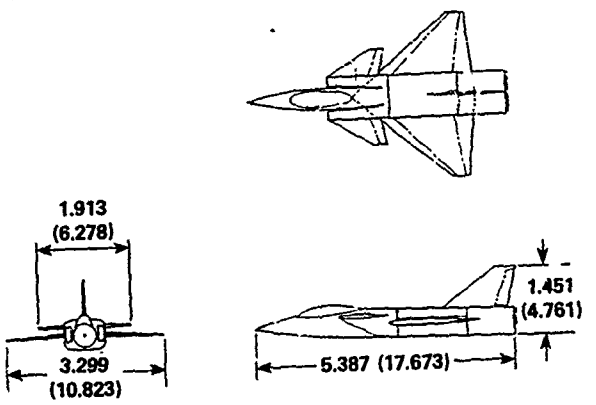

Figure 52. Geometry of the model of the Vought configuration.

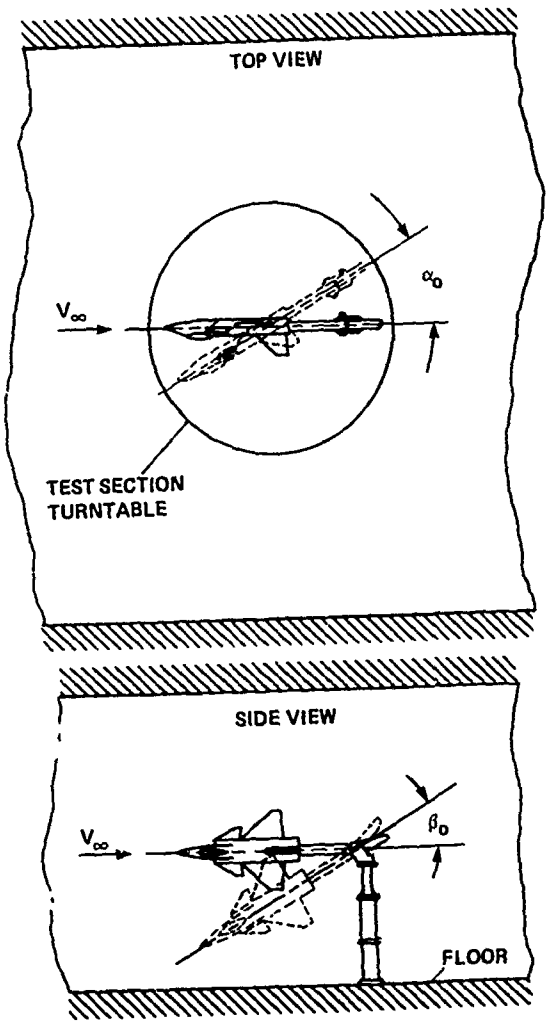

Figure 53. Pitch and yaw methods for high angle-of-attack testing in the Ames 40- by 80-Foot Wind Tunnel.

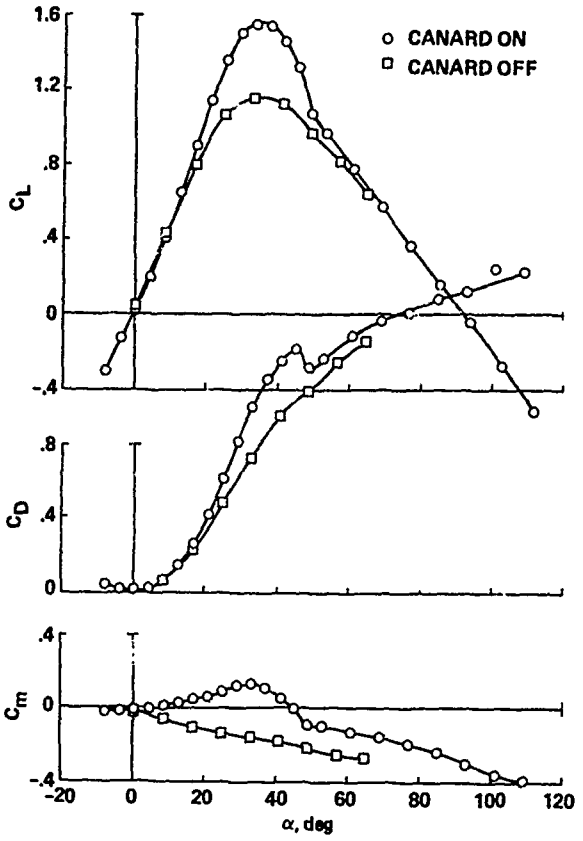

Figure 54. Low-speed, high angle-of-attack characteristics of the Vought model.

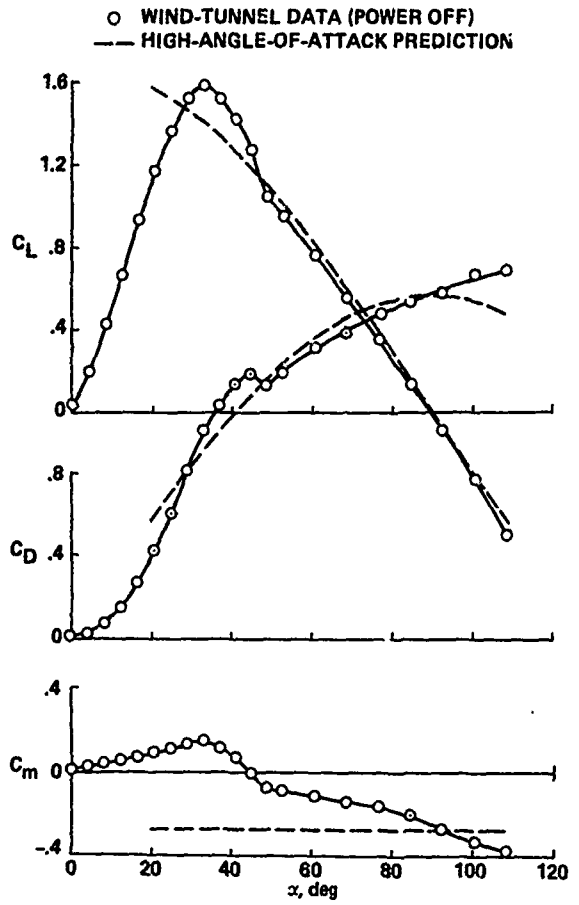

Figure 55. Prediction of high angle-of-attack characteristics of the Vought model.

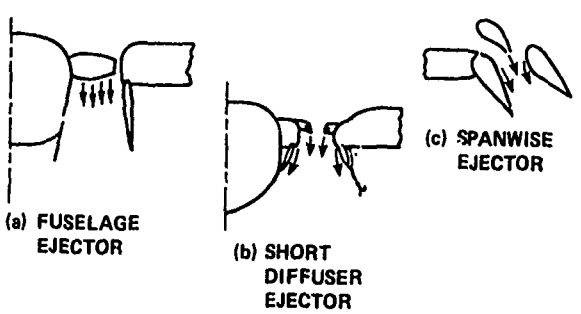

Figure 56. Thrusting ejector concepts for V/STOL aircraft having "V" capability.

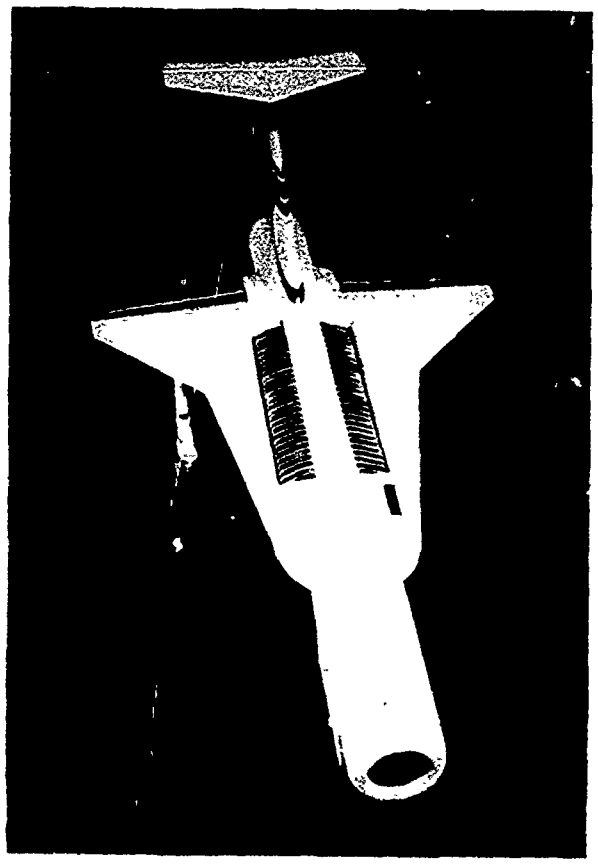

Figure 57. J97 powered ejector model in the Ames 40- by 80-Foot Wind Tunnel.

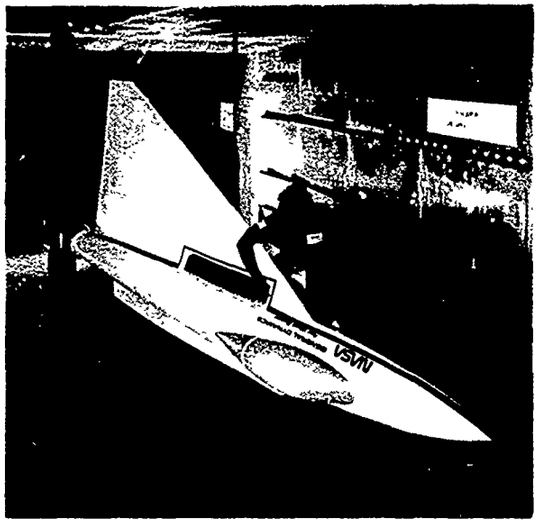

Figure 58. One-third-scale, powered ejector model of the E7 configuration in the Lewis 9- by 15-Foot Wind Tunnel.

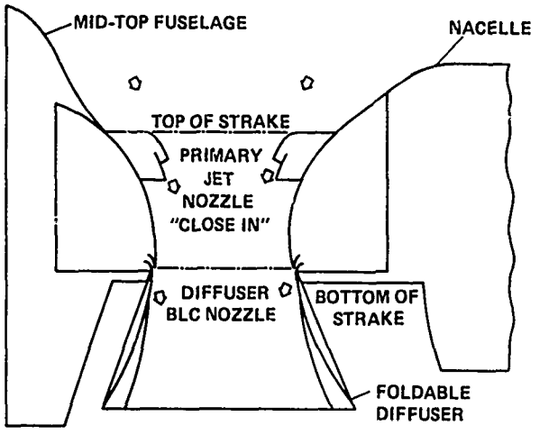

Figure 59. Short diffuser ejector.

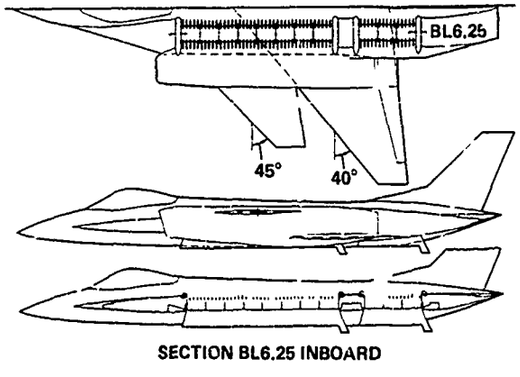

Figure 60. E205 semispan ejector model.

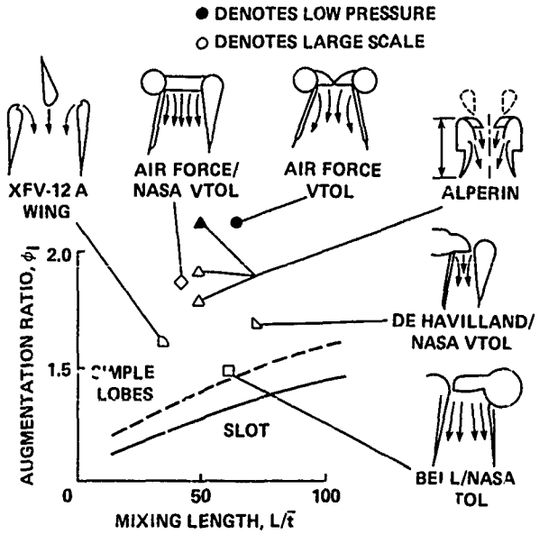

Figure 61. Summary of lift augmenting ejector performance.

NOTES ON SPECIAL FLIGHT ASPECTS, SUCH AS STO, SKI-JUMP AND ODM

C.L. Bore
Head of Research
British Aerospace Kingston

INTRODUCTION

Most of this course has considered the very early stages of V/STOL aircraft aerodynamics: the preliminary research, configuration choice and design. That is all very well, but there are several hundred V/STOL aircraft in service, and many more to come, and it is vital to define how these aircraft may be operated safely to the limits of their capability in a wide variety of circumstances. In the present context, many of the more significant aspects of this work can be illustrated by considering the formulation of STO performance, its extension to (flat) deck-launch and then ski-jump take-offs.

This field of aerodynamics differs in approach from that used in the purely predictive phases because it comes into action when there are aircaft in real service. Then one finds that engine performance (for example) now varies not only with ambient temperature and altitude, but also depends on whether water injection is used, the various short ratings, and details such as the intake pressure recovery factor and hot gas ingestion and the amount of high pressure bleed being used. Variability between diffent engines also has to be allowed for. In order to allow for such variables, those responsible have to reconcile numerous flight tests with wind tunnel tests by means of semi-empirical theories incorporating considerable detail.

Since the Operating Data Manuals (ODM) that result from this work are destined for use by flight planners and aircrew, one finds that many of the familiar aerodynamic terms are heavily disguised in terms of parameters closer to operational reality. Thus lift coefficient tends to vanish, and standardised aircraft weight (W/δ) appears on charts such as those related to standardised take-off distance ($S/\sqrt{\theta}$), where δ is relative pressure and θ is the relative ambient temperature. Again, the engine thrust often disappears, and the non-dimensional compressor speed comes in ($n/\sqrt{\theta}$).

The work that I will outline has been developed patiently by our Performance Evaluation Team under the guidance of Trevor Jordan, and this account is based on extracts from Reference 1, which forms part of Reference 2.

THRUST RATINGS

One of the guiding principles in all this type of work is first to establish the non-dimensional parameters which dominate the performance, and another is to relate these parameters back to other parameters which are readily observable in the cockpit or in the operational planning office. Now for jet-lift V/STOL aircraft, the engine thrust dominates the performance. As the entire thrust is vectorable, it is no longer so convenient to talk of "net thrust". Figure 1 shows that the "momentum drag" force acting upon the air intake acts in a direction appropriate to the oncoming flow (whether free stream or induced downdraught) and the forces acting in line with the nozzles correspond with the gross thrust. In the general case where reheat or PCB can be varied, we would need to take account of the front nozzle and rear nozzle forces separately, but for the Harrier the combined vector can be used. Thus whenever we use the term "thrust", it is the gross thrust (i.e. stream force) that is meant.

Since there are very large thrusts available at take-off, the accelerations available are high, and it is possible to get very substantial boosts of thrust (relative to maximum continuous) for the very short times needed. Thus for Pegasus engines we have:-

(a) Short Lift Rating, available for 15 seconds per flight (also wet)

(b) Normal Lift Rating, available for 2½ minutes per flight (also wet)

(c) Maximum Thust Rating, available for 15 minutes per flight

(d) Maximum continuous.

Of these, the highest rating is nearly 60% greater than maximum continuous. In order to avoid Turbine Entry Temperature limitations for short periods in high ambient conditions, both the Short Lift and Normal Lift ratings are available with water injection.

Figure 2 shows a chart which enables limiting engine condition to be assessed for given rating and manoeuvre (which demands reaction control bleed) and hence TET rise. It will be noted that there is an overall limit on $n/\sqrt{\theta}$. This is a measure of compressor blade Mach number which, if exceeded too much, may lead to surge.

FORCES IN PARTIALLY JET-BORNE FLIGHT

One difference from VTO conditions arises from the fact that the air intake efficiency varies with forward speed. Another arises from the fact that the jet induced downdraught leads to a change of both local effective incidence and downdraught dynamic pressure with forward speed, as we will see.

Experimental data show that (for jets at angles above 30 degrees) the induced downdraught dynamic pressure is proportional to the jet dynamic pressure:-

$$\left(\frac{\rho_o}{\rho_{std}}\right)^{\frac{1}{2}} V_{ind} \propto \left(\frac{\rho_j}{\rho_{std}}\right)^{\frac{1}{2}} V_j \quad \ldots\ldots (1)$$

When the forward speed is large enough relative to the induced velocities, it can be shown that:-

$$\Delta\alpha_{ind} = \frac{V_{ind}}{V_o} \propto \frac{V_j}{V_o}\left(\frac{\rho_j}{\rho_o}\right)^{\frac{1}{2}}$$

$$\propto \left(\frac{\rho_j V_j^2}{\rho_o V_o^2}\right)^{\frac{1}{2}} \quad \ldots\ldots (2)$$

The jet induced lift loss is given by

$$\Delta L = \frac{dC_L}{d\alpha} \cdot \Delta\alpha \cdot \tfrac{1}{2}\rho_o V_o^2 S$$

$$\propto \frac{dC_L}{d\alpha} S \rho_o V_o^2 \left(\frac{\rho_j V_j^2}{\rho_o V_o^2}\right)^{\frac{1}{2}} \quad \ldots\ldots (3)$$

But $X_j \triangleq \rho_j A_j V_j^2$

$$\therefore \frac{\Delta L}{X_j} \propto \frac{dC_L}{d\alpha} \frac{S}{A_j}\left(\frac{\rho_j V_j^2}{\rho_o V_o^2}\right)^{-\frac{1}{2}}$$

For a given aircraft $\frac{dC_L}{d\alpha}$, S, A_j are fixed, so:-

$$\frac{\Delta L}{X_j} \propto \left(\frac{\rho_j V_j^2}{\rho_o V_o^2}\right)^{-\frac{1}{2}} \quad \ldots\ldots (4)$$

Thus the primary variable for lift loss in forward flight is the ratio of jet "equivalent velocity" to free stream equivalent airspeed, i.e. V_{je}/V_e. It can be seen that $\Delta L/X_j$ increases with forward speed (in a way analogous to the normal acceleration due to a vertical gust). In the simplified treatment above, the effect of varying nozzle angle (θ_j) has been left aside.

Figure 3 shows a typical lift loss variation with V_{je}/V_e for a Harrier-type configuration. Clearly, within a certain range of jet velocity ratio and nozzle angle, Equation 4 is a good approximation. Four regimes can be identified, in which different mechanisms operate, and which apply to different flight conditions.

(a) $4 < \left(\frac{\rho_j V_j^2}{\rho_o V_o^2}\right) < 20$

$\theta_j > 30$ degrees

This is the range of V_{je}/V_e and θ_j for which the above discussion is appropriate. It applies to STO climb out, SL approach and accelerating transition.

(b) The same range of V_{je}/V_e

$\theta_j < 30$ degrees

Here some additional, more complex mechanisms become significant. This regime applies to CTO and to low speed turning with jet deflection.

(c) $\left(\frac{\rho_j V_j^2}{\rho_o V_o^2}\right) > 20$

all relevant θ_j (say $\theta_j > 60$ degrees)

This is the regime of VTOL and RVTOL. Power-off aerodynamic lift is small and it is convenient to regard the total aerodynamic lift (negative, of course) as the lift loss, rather than the change of lift.

(d) $\left(\frac{\rho_j V_j^2}{\rho_o V_o^2}\right) < 4$

all θ_j

This regime is where the free stream momentum gets large compared to the jet momentum and all lift losses must tend to zero as the parameter tends to zero. The physical mechanism is the increasingly large rearward bending of the jet plume. This range applies to decelerating transitions.

BALANCE OF FORCES IN PARTIALLY JET-BORNE FLIGHT

Having examined lift loss in forward flight, we can now consider the balance of forces in partially jet-borne flight (Fig. 4). In the case of the Harrier, the nozzle datum angle is set at 1½ degrees below the wing datum, so we find:-

$$L_o - \Delta L + X_j \sin(\alpha + \theta_j + 1\tfrac{1}{2}) = W \quad (5)$$

and

$$X_j \cos(\alpha + \theta_j + 1\tfrac{1}{2}) = D + X_D \quad (6)$$

Now L_o (i.e. lift with power off) and D will be functions of airspeed and incidence. The lift loss (Δ L) is a function of X_j, θ_j and airspeed, because the latter fixes V_{je}/V_e. X_j and X_o are obviously functions of compressor speed (n) and airspeed. Hence we have five variables: airspeed, incidence, rpm, and weight. Since we have two equations, if we fix the weight and any two of the other variables, the remaining two are determined. These relationships are illustrated in Figure 4 in a graph which is so-called the "semi-jetborne carpet". From later discussions you will see that this can be generalised for all weights and atmospheric conditions by replacing IAS by $(IAS/\sqrt{W})$ and rpm by (W/W_H).

SHORT TAKE-OFF

A short take-off is normally used when the weight is appreciably greater than that which can be achieved in a VTO, say by 10% or more. If an intermediate weight is to be taken off, the optimum procedure will be an RVTO, but of course there is nothing to stop an STO being performed even at weights below VTO weight. We can assume, however, that in any STO a significant aerodynamic contribution to lift is required. Figure 5 illustrates the terms used.

The performance problems are:-

(a) What unstick speed should be used?

(b) What are the ground run and the distance to 50 feet height for this unstick speed?

There is clearly a minimum speed below which the aircraft cannot leave the ground. As the unstick speed increases beyond this point, the air-borne distance will decrease from infinity in a roughly hyperbolic fashion, whilst the ground run will increase parabolically, and some intermediate speed will give a minimum combined distance to 50 feet. So far, we have left nozzle angle aside. First suppose that this angle is small, then with the high thrust/weight ratio there will be significant acceleration along the airborne path. Now suppose that we increase the nozzle angle and try again, then we will find that the unstick speed and minimum distance will decrease but the air-borne acceleration will reduce. Ultimately the speed at 50 feet will be the same as at unstick, and this is considered to mark the safe maximum for the angle θ_j.

THE TAKE-OFF WEIGHT RATIO

When rationalising VTO performance, it was found that the take-off weight ratio (W/W_H) was very useful for correlating flight test data and for preparing operating data. This is defined as the ratio of take-off weight to the hover weight which could be sustained at the same compressor rpm as used for take-off. Since hover weight is closely proportional to gross thrust, the <u>TOW ratio amounts to an inverse thrust/weight ratio</u>. The same parameter is found useful for STO correlations, as we will see.

The potential usefulness of this parameter seems fairly clear, for obviously the higher the ratio of weight/hover weight, the higher must be the unstick speed and hence both the ground and airborne runs. Also, considering the ground run, if we take W_H as (say) 95% of the installed thrust and neglect drag as secondary, then the acceleration (a) along the ground is proportional to W_H/W, and by Newtonian dynamics we have $V^2=2aS_g$, where S_g is the ground run.

Then we find

$$\frac{W}{W_H} V^2 = 1.9\, g\, S_g \quad . \quad . \quad . \quad . \quad . \quad (7)$$

To show that W/W_H is a valid parameter more generally requires a longer demonstration which will only be outlined here.

It can be shown that for STO conditions, the standardised optimum unstick speed ($V_u/\sqrt{\theta}$), the ground run (S_g/θ), and the air-borne distance ($S_a/\sqrt{\theta}$) are functions of non-dimensional engine speed ($n/\sqrt{\theta}$) and standardised weight (W/δ), where θ is the relative ambient temperature and δ is the relative ambient pressure. Since (X_j/δ) is a function ($n/\sqrt{\theta}$) and ($V/\sqrt{\theta}$) it follows that optimum speed and nozzle angle are functions of (W_H/δ) and (W/δ).

By considering the balance of forces along the flight path and normal to it, it can be shown that:

along path: $$X_{j/\delta} \cos(\theta_j + \alpha') = X_{D/\delta} + D/\delta + \frac{W}{\delta} \sin\gamma \quad . \quad . \quad . \quad (8)$$

normal to path: $$X_{j/\delta} \sin(\theta_j + \alpha') = \frac{W}{\delta} \cos\gamma + \Delta n \frac{W}{\delta} - L/\delta \quad . \quad . \quad . \quad (9)$$

Now for STO conditions the angle of climb γ is not more than 5 degrees, and hence remembering the constancy of the forces discussed above, Δn is virtually constant, and therefore the air-borne path is approximately circular.

If $n/\sqrt{\theta}$ is fixed then W_H/δ follows. If W/δ also is fixed then all terms in (8) are fixed and therefore the angle γ has a particular value. Therefore Δn has a particular value. If we start from those values of W_H/δ and W/δ and then change all forces in proportion, balance is maintained with virtually fixed γ and Δn. Hence at constant W/W_H, γ and Δn will remain fixed provided all other forces vary in proportion to W.

Now consider the aerodynamic terms L and D. It is implicit throughout that the mean incidence used is constant at its optimum or limiting value. It follows that L and D are proportional to V_e^2. Hence if L and D are to remain proportional to W, it follows that V_e must be varied proportional to $\sqrt{W}$.

It has already been shown that the lift loss in forward flight is represented by

$$\frac{\Delta L}{X_j} = f\left(\frac{\rho_j V_j^2}{\rho_\infty V_\infty^2}, \theta_j\right)$$

Now $X_j \doteq \rho_j A_j V_j^2$ and $L \propto \rho_\infty V_\infty^2$

$$\therefore \frac{\rho_j V_j^2}{\rho_\infty V_\infty^2} \propto \frac{X_j}{L}$$

Hence if W/W_H is maintained constant and $V_e/\sqrt{W}$ is constant, it follows that $\rho_j V_j^2/\rho_\infty V_\infty^2$ is fixed. Thus ΔL is also proportional to X_j and to W.

The remaining term is the momentum drag, X_D. A simplified argument suggests that with (W/W_H) and $(V_e/\sqrt{W})$ constant, X_D would be proportional to W. This is confirmed by detailed data charts.

From arguments such as those above, it can be shown that the optimum nozzle rotation speed, the ground run, and the airborne distance can all be standardised in terms of the aircraft weight and plotted as functions of the Take-Off Weight ratio W/W_H :-

$V_e/\sqrt{W}$ vs W/W_H . . . . . Figure 6

$(Sg/\theta)/(W/S)$ vs W/W_H . . . . . Figure 7

$S_a/\sqrt{\theta}/\sqrt{W/S}$ vs W/W_H . . . . . Figure 8

Clearly such charts incorporate allowance for both ambient temperature and ambient pressure (i.e. altitude) from the outset.

GROUND PROXIMITY EFFECTS

The treatment shown above is fairly general, and applies straightforwardly to flat-deck take-offs, but when first applied to STO over flat ground the calculated take-off distances were excessive, sometimes by up to 50%. The missing factor was found to be a substantial ground proximity effect - much larger than conventional wing tip vortex reflection effects. This is shown in Figure 9 where it can be seen that there can be substantial additional lift on the aircraft during STO, when close to the ground. The effect on STO distance is quite marked, because the aircraft experiences these increments for 50% of the time to 50 feet. When these increments of lift due to jet deflection close to the ground are incorporated, the non-dimensional approach outlined will cope with any sort of STO.

SKI-JUMP

It was in 1972 that Lt.Cdr. D.R. Taylor approached the company with his ideas on the advantages of launching vectored thrust aircraft in an upward trajectory at a much lower speed then possible from a flat deck (Fig. 10). This relied on the aircraft accelerating enough during the semi-ballistic trajectory to reach normal launch speed by the time that the flight path was horizontal. Hence the description of the Ski-Jump as "building a runway in the sky". Figure 10 illustrates the definition of "height drop", which had to be generalised to deal with ramp launches.

In order to extend the STO charts to cope with Ski-Jump, it was necessary to introduce two extra non-dimensional parameters. One was the equivalent launch speed for (say) 10 feet of height drop: $(V_{e,10}/\sqrt{W})$. This too was a function of (W/W_H).

The other parameter needed to collapse the information was found to be the nominal ramp angle, defined as

$$N_{orm} = \left(\gamma_s/\sqrt{\sigma}\right)\sqrt{W_H/W_{H\ datum}}$$

where σ (here alone, in this paper) signifies relative density. This ensures that (at given non-dimensional conditions) not only are all the forces (propulsion, aerodynamic and gravity) in proportion and therefore accelerations invariant, but also that the vertical velocity at launch is constant.

SKI-JUMP SAFETY MARGINS

Generalisation of the requirements for adequate safety margins for ski-jump was found to be necessary, and this generalisation reflected back on to the schemes for charting flat-deck launches.

It was found (see Fig. 11) that positive height drop varies far more steeply with variation of launch speed than for flat-deck launches, and there is thus less scatter margin between 15 feet drop and striking the sea (or land). It was concluded that to give sufficient safety, the nominal launch speed should be 5 standard deviations σ (i.e. 5σ) above the speed for sea strike. Setting this criterion resulted in a typical ski-jump trajectory in which the vertical component of velocity never goes far negative before the climbing accelerating transition takes over. This made the pilots far happier than they were for flat-deck launches.

In assessing the magnitude of the standard deviation to be used for the safety margin, account is taken of all the parameters which are likely to vary, such as fluctuating wind-over-deck, variation in angle of attack achieved, errors in weight, air temperature, hover performance etc. Variation in end-of-deck speed, however, needs separate consideration, because the main contribution to this comes from variation in nozzles down point - and that affects the airspeed required as well as that reached. Hence the standard deviation considered should be in the difference between (airspeed required) and (endspeed available).

FEEDBACK TO FLAT-DECK SAFETY MARGINS

In the HMS "Hermes" flat-deck trials (1979) all the variations mentioned above were thoroughly assessed. When all the variabilities were combined, it was found that a 5 σ margin called for launch speeds higher than those found satisfactory by the pilots. Taking into account the psychological facts - that pilots are not keen on large height drops or on taking regular emergency action, a two-pronged criterion was devised to fit the flight trials data:-

(a) A margin of 2.3 σ over the speed for 10 foot drop. This ensures that only 1 in 100 launches drops 10 feet, a level which indicates that emergency action may be taken.

(b) A margin of 4.1 σ over sea strike for a launch where emergency action is taken: that is power is increased to the next higher rating, and angle of attack is increased, both for 3 seconds after deck-end. Since only 1% of launches would reach this condition, the 4.1 σ margin is adequate to create the overall level of safety.

CONCLUDING REMARKS

It is hoped that the approaches illusrated have been sufficient to show how the extra parameters needed for V/STOL aerodynamics can be incorporated into the Operating Data Manuals. The sorts of procedures needed are not new, but the range of combinations of conditions is large, and the work involved is additional to that needed for conventional aircraft. For future advanced STOVL aircraft there will be even more parameters to include, such as different temperatures, velocities and thrusts for the front and rear jets, and allowances for hot gas re-ingestion. It all means a lot more work to do than most aerodynamicists are familiar with, but we are quite used to that, and we are well along the road.

REFERENCES

1. T.S.R. Jordan: Some Special Characteristics of the Performance of Vectored Thrust Jet V/STOL Aircraft. BAe-KAD-L-GEN-1932.

2. (Various): Short Course on Aircraft Performance. Cranfield Institute of Technology. March 1984.

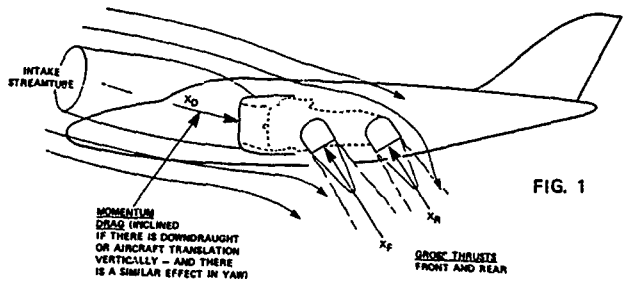

FIG. 1

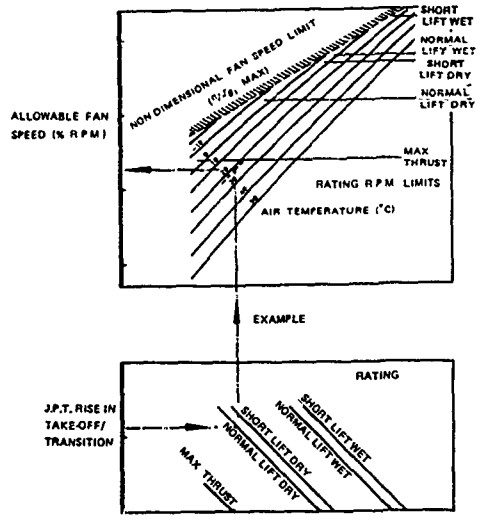

ENGINE OPERATING LIMITS
FIG. 2

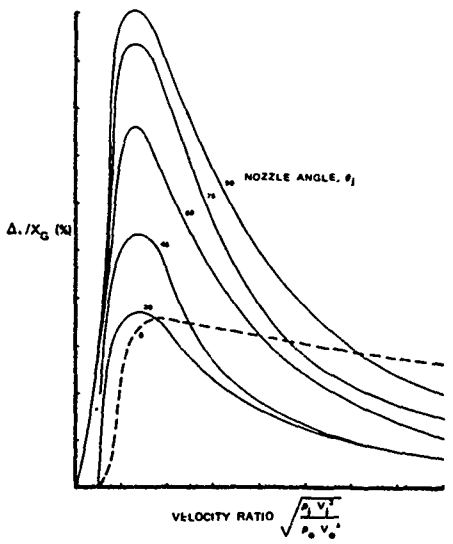

LIFT LOSS IN FORWARD FLIGHT
FIG. 3

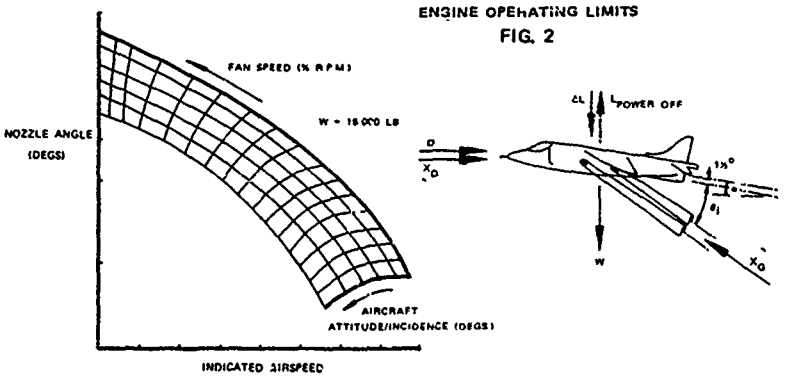

SEMI-JETBORNE CARPET FIG. 4

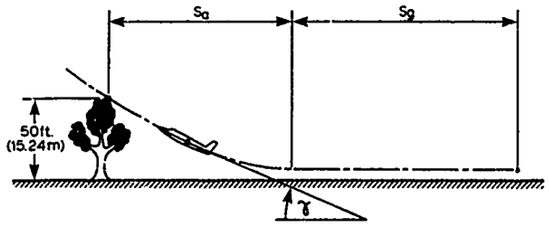

S.T.O. GEOMETRY FIG. 5

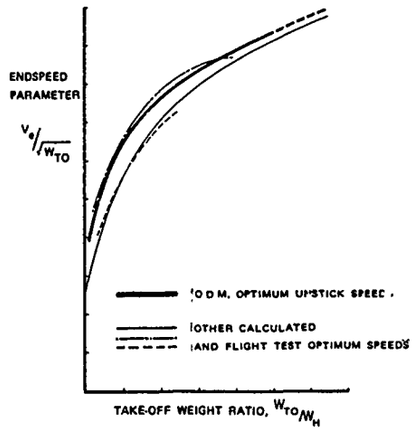

NON-DIMENSIONAL S.T.O. PERFORMANCE – END SPEED
FIG. 6

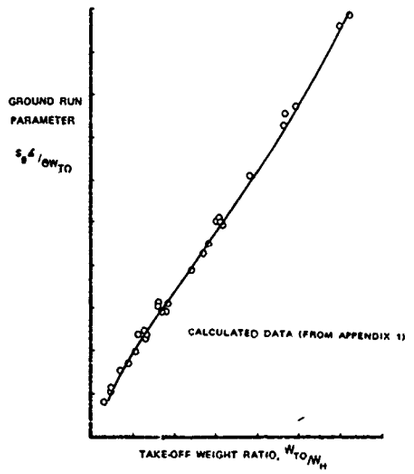

NON-DIMENSIONAL S.T.O. PERFORMANCE – GROUND RUN
FIG. 7

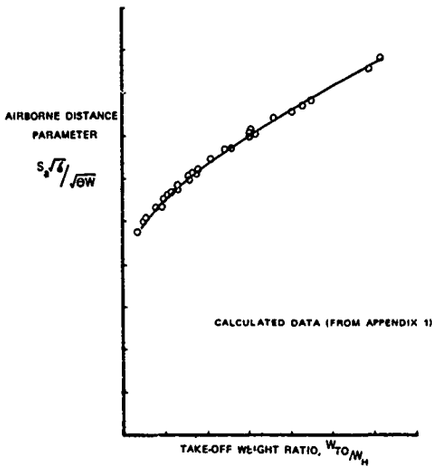

NON-DIMENSIONAL S.T.O. PERFORMANCE – AIRBORNE DISTANCE
FIG. 8

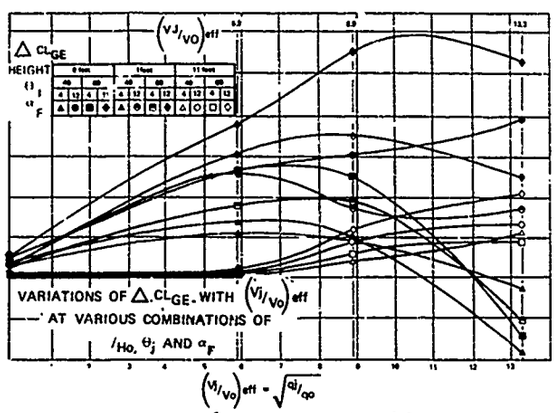

FIG. 9 GROUND PROXIMITY ΔC_L

FIG. 10

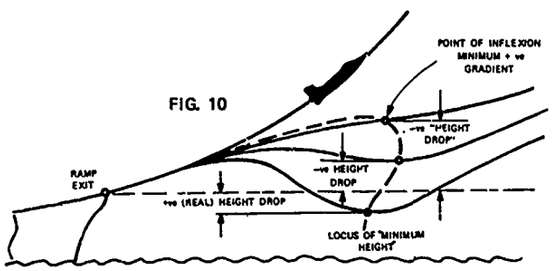

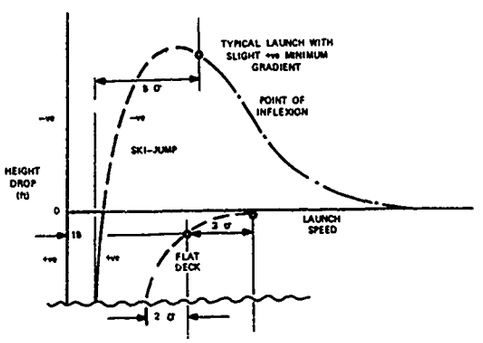

DEFINITION OF HEIGHT DROP AND
LAUNCH SPEED MARGINS FOR SKI-JUMP
FIG. 11

REPORT DOCUMENTATION PAGE			
1. Recipient's Reference	2. Originator's Reference AGARD-R-710	3. Further Reference ISBN 92-835-1472-6	4. Security Classification of Document UNCLASSIFIED

5. Originator	Advisory Group for Aerospace Research and Development North Atlantic Treaty Organization 7 rue Ancelle, 92200 Neuilly sur Seine, France
6. Title	SPECIAL COURSE ON V/STOL AERODYNAMICS
7. Presented at	the von Kármán Institute, Rhode-St-Genèse, Belgium 14–18 May 1984 and 4–8 June 1984 at NASA Ames Research Center, Moffett Field, CA, USA.

8. Author(s)/Editor(s)	9. Date
Various	April 1984
10. Author's/Editor's Address	**11. Pages**
Various	386

12. Distribution Statement	This document is distributed in accoradance with AGARD policies and regulations, which are outlined on the Outside Back Covers of all AGARD publications.

13. Keywords/Descriptors

Vertical take off aircraft	Aerodynamic characteristics
Short take off aircraft	Design criteria
Aerodynamics	Education

14. Abstract

The aim of the Special Course on V/STOL Aerodynamics was to outline and discuss the additional knowledge of aerodynamics needed to embark on the design of V/STOL aircraft. The influence of V/STOL features on wing design, layout considerations, engine and air intake considerations, effects of jet effluxes, wind tunnel and flight testing, manoeuvrability and control, performance assessment and special aspects of flight aerodynamics were discussed by nine lecturers at the course which was presented on 14–18 May 1984 at the von Kármán Institute, Belgium, and on 4–8 June 1984 at the NASA Ames Research Center, USA under the joint sponsorship of the Institute, NASA, and the Fluid Dynamics Panel of AGARD.